Development and clinical translation of virus-specific T cell therapies for treatment of life-threatening viral diseases.

Rachel Cooper

A thesis submitted to the College of Medicine, Veterinary and Life Sciences, University of Glasgow in fulfilment of the requirements for the degree of Doctor of Philosophy

July 2025

Institute of Infection, Immunity and Inflammation
College of Medical, Veterinary and Life Sciences
University of Glasgow

Abstract

Adoptive immunotherapy with virus-specific T cells (VST) has demonstrated clinical efficacy in restoring antiviral immunity in immunocompromised patients.

Epstein-Barr virus (EBV) is an extremely common herpesvirus (90% prevalence worldwide), that infects the majority of individuals during childhood or adolescence and thereafter establishes a lifelong latency in the host. In immunocompromised individuals, EBV can drive a malignant transformation of B cells due to the absence of circulating memory EBV-specific T cell surveillance. Transplant patients are particularly at risk of developing an aggressive EBV-induced lymphoma, and despite first line treatments the mortality rate remains high.

The Scottish National Blood Transfusion Service has been involved in adoptive EBV VST therapy of EBV-associated lymphomas for over 20 years. Initial EBV VST products were manufactured from healthy donor leukapheresis using repeated stimulations with EBV-infected lymphoblastoid cell lines to induce expansion of EBV-specific T cell clones. These therapies have treated over 200 patients with excellent safety and efficacy in tumour regression (>60% complete response rates). More recently, we developed a new manufacturing process by stimulating donor leukapheresis with EBV peptide pools, followed by isolation of responding memory EBV VST using cytokine capture selection, with further culture expansion. This study aimed to comprehensively compare EBV VST therapies manufactured from the two processes, with characterisation assays developed to assess quality, phenotype, functionality, migratory capacity and clonal repertoire of T cell products. Peptide-derived VST demonstrated enhanced degranulation and cytokine production to a broad range of EBV latent antigens, as well as a dominant central memory phenotype, which may improve persistence and targeted tumour clearance in patients. Moreover, the peptide process had clear benefits in terms of process biosafety, reduced culture duration and massively higher yield of patient doses.

Furthermore, the emergent severe acute respiratory syndrome coronavirus-2 (SARS-CoV-2) outbreak at the beginning of this study allowed us to investigate SARS-CoV-2 immune responses in individuals following natural resolution of primary infection. Natural killer cell frequency within peripheral blood mononuclear cells was significantly increased in individuals within 1-3 months convalescence compared to unexposed individuals. Convalescent donors had detectable CD4 and CD8 memory T cells populations to SARS-CoV-2 spike, nucleocapsid and membrane peptides whereas unexposed individuals showed no lymphocyte responses to the SARS-CoV-2

antigens. Interestingly, the frequency of SARS-CoV-2-specific T cells within the total T cell compartment decreased over time from symptoms resolution, indicating memory T cell responses of unvaccinated individuals after primary infection decline without antigen re-exposure. With detectable memory T cell populations, we were able to isolate SARS-CoV-2-specific T cells from donor blood using cytokine capture or T cell activation-induced marker selection. We further developed a culture protocol to rapidly expand a purified SARS-CoV-2 VST population with desirable central memory phenotype and broad SARS-CoV-2 antigen effector functionality. Given that disease severity has been associated with a reduced or dysfunctional T cell response, adoptive transfer of healthy donor SARS-CoV-2 VST may provide a potential treatment strategy. To this end, the peptide-mediated process developed for EBV was rapidly translated to manufacture an allogeneic bank of SARS-CoV-2 VST, with clinical products tested in a first-in-human trial for high-risk hospitalised patients.

The development and clinical manufacture of two T cell therapies targeting very different viral diseases required comprehensive analytical testing to understand the potential functional mechanisms of these cell products. The extensive suite of characterisation assays developed was used to build a profile for antigen-specific T cell therapies, in order to evaluate the optimal characteristics for clinical efficacy.

Table of Contents

List of Tables

List of Figures

Acknowledgements

Firstly, I owe the biggest thanks to my supervisors Dr Alasdair Fraser and Professor Gerry Graham, and third unofficial supervisor Professor John Campbell. I am extremely grateful to the three of you for all the support, guidance, opportunities and endless inspiration you have provided me both within this study and throughout the last 10 years. Al and John I hope you will enjoy this thesis on the best cells, and relinquish your criticisms on the colour scheme. I have appreciated so much your hilarity, mentorship and friendship over the years, top team assemble!

This thesis would not have been possible without Paul. I am immensely thankful for all the help you have given me; as if all the lab work, ideas, and boring yourself to death reading about T cells wasn't enough, you also looked after me when I was in my lowest of times. I am so glad I get to keep working (literally) beside my bestie, and continue to learn so much from you.

To all my amazing SNBTS colleagues, thank you for all the help and support every one of you has given me over the years. A special thanks to Stuart, Kay and Niall who poured over all my endless chapters, you provided me with such scientific wisdom with only limited merciless mocking! To Nik, Scott, stabby, Ang, Biff, David, Kayleigh, & Sid, you all feel like my hilarious crazy weird family instead of work mates by now.

A huge thanks to everyone at CRG who were so warm and welcoming to me through in Glasgow, I had such a fun time in your group! You were all such glorious people to work with; particularly Alan, Catherine and Chris you helped me in so many ways.

This work is also a testament to the many people who have been dedicated to this study, with particular appreciation to Dr Linda Smith, Dr Gwen Wilkie, Professor Marc Turner and Professor Mark Vickers. I am extremely grateful to the many collaborators who contributed to this study, with special thanks to Dr Catherine Sutherland and Dr Graeme Cowan for all the molecular training and bioinformatics analysis. Thanks also to Professor Jo Mountford and Dr Alison Thompson for their continued support and encouragement in personal development.

I am incredibly lucky to have such a large supportive family to help me through life. To Heather, Sam, Pete, Hazel & Philip, you all make me laugh and smile in different

ways, you are truly the best siblings a girl could hope for. With special thanks to Peter and Margaret Grossick who have been unfailingly generous to me and been my strength through everything. To my mum who always put her kids before herself and never let us believe we couldn't be anything we wanted to be; and my dad, the best of humans who is my ultimate inspiration for everything: this is dedicated to the two of you.

Finally to the most wonderful friends both old and new, you have shaped me into the person I am today. There are many close friends I want to thank for the role they played in my life, but most of all the three other halves to my whole: Lisa, Maia and Megan; you really saved me in recent years and forever inspire my heart and soul.

Author's Declaration

"I declare that, except where explicit reference is made to the contribution of others, that this dissertation is the result of my own work and has not been submitted for any other degree at the University of Glasgow or any other institution."

Printed Name: Rachel Cooper

Signature:

Abbreviations

ACD	Acid citrate dextrose
ACE	Angiotensin converting enzyme
ACT	Adoptive cell therapy
ADV	Adenovirus
AICD	Activation-induced cell death
AIM	Activation-induced marker
ANOVA	Analysis of variance
APC	Antigen-presenting cell
ARDS	Acute respiratory distress syndrome
ATMP	Advanced therapeutic medicinal product
BCR	B cell receptor
BKV	BK virus
BL	Burkitt lymphoma
CAEBV	Chronic active EBV infecion
CAR	Chimeric antigen receptor
CCD	COVID-19 convalescent donor
CCS	Cytokine capture selection
CD	Cluster of differentiation
cDNA	Complementary deoxyribonucleic acid
CDR	Complementary determinant region
cGMP	Current good manufacturing process
CHOP	Cyclophosphamide hydroxydaunorubicin oncovin prednisolone
CMV	Cytomegalovirus
CNS	Central nervous system
COVID-19	Coronavirus disease-2019
CP	Convalescent plasma
CRS	Cytokine release syndrome
CS	Closed system
CTL	Cytotoxic T lymphocyte
CTLA	Cytotoxic T lymphocyte-associated protein
DLBCL	Diffuse large B cell lymphoma
DC	DC
DLI	Donor lymphocyte infusion
DMSO	Dimethylsulphoxide
DN	Double negative T cell
DNA	Deoxyribonucleic acid
DP	Double positive T cell
EBER	EBV-encoded RNA
EBNA	Epstein-Barr nuclear antigen
EBV	Epstein-Barr virus

EDTA	Ethylenediaminetetraacetic acid
ELISPOT	Enzyme-linked immunospot
FACS	Flow activated cell sorting
FBS	Fetal bovine serum
FMO	Fluorescence minus one
FSC	Forward scatter
FVD	Fixable viability dye
GC	Gastric carcinoma
gDNA	Genomic deoxyribonucleic acid
gp	Glycoprotein
GMP	Good manufacturing process
G-Rex	Gas-permeable rapid expansion
GVHD	Graft versus host disease
HBV	Hepatitis B virus
HCV	Hepatitis C virus
HHV	Human herpes virus
HIV	Human immunodeficiency virus
HL	Hodgkin lymphoma
HLA	Human leukocyte antigen
HLH	Haemophagocytic lymphohistiocytosis
HSA	Human serum albumin
HSCT	Haematopoietic stem cell transplant
IAV	Influenza A virus
ICB	Immune checkpoint blockade
ICR	Intracellular cytokine release
IFN	Interferon
Ig	Immunoglobulin
IL	Interleukin
IM	Infectious mononucleosis
JCV	John Cunningham virus
LAG	Lymphocyte-activation gene
LCL	Lymphoblastoid cell line
LMP	Latent membrane protein
LNA	Locked nucleic acid
MFI	Median fluorescence intensity
MHC	Major histocompatibility complex
MHRA	Medicines and healthcare regulatory agency
MLR	Mixed lymphocyte reaction
MNC	Mononuclear cell
mRNA	Messenger ribonucleic acid
miRNA	Micro ribonucleic acid
MS	Multiple sclerosis
NGS	Next generation sequencing

NK	Natural killer cell
NKT	Natural killer T cell
NKTL	Natural killer T cell lymphoma
NPC	Nasopharyngeal carcinoma
NSP	Non-structural protein
nvCJD	New variant Creutzfeldt-Jakob disease
ORF	Open reading frame
PAMP	Pathogen-associated molecular pattern
PBMC	Peripheral blood mononuclear cell
PBS	Phosphate buffered saline
PCR	Polymerase chain reaction
PD	Programmed death
PLO	Primary lymphoid organ
PMA	Phorbol myristate acetate
Poly I:C	Polinosinic:polycytidylic acid
PRR	Pathogen recognition receptor
PTLD	Post-transplant lymphoproliferative disorder
QC	Quality control
RBC	Red blood cell
RBD	Receptor binding domain
RIS	Reduction of immunosuppression
RNA	Ribonucleic acid
RPMI	Roswell Park Memorial Institute medium
RT	Room temperature
SARS-CoV-2	Severe acute respiratory syndrome coronavirus-2
SEM	Standard error of the mean
SLE	Systemic lupus erythematosus
SLO	Secondary lymphoid organ
SNP	Single nucleotide polymorphism
SSC	Side scatter
SOT	Solid organ transplant
TCM	Central memory T cell
TCR	T cell receptor
TEM	Effector memory T cell
TEMRA	Terminal effector memory-RA T cell
Tfh	Follicular helper T cell
Th	Helper T cell
TIM	T cell immunoglobulin and mucin domain-containing protein
TLDA	Taqman low density array
TLR	Toll-like receptor
TNF	Tumour necrosis factor
Treg	Regulatory T cell
t-SNE	t-stochastic neighbour embedding

TAA	Tumour-associated antigen
VCA	Viral capsid antigen
VST	Virus-specific T cell
VV	Vaccinia virus
WBC	White blood cell

Chapter 1

Introduction

Chapter 1 – Introduction

1.1 Virus-specific T cells

Historically, the absence of a clear role for the thymus led to various suppositions such as that size did indeed matter: infant deaths during surgery were attributed to a large thymus thought to obstruct breathing, and prior to the 1950s doctors suggested irradiation to reduce thymus size. Initial investigations into the role of the thymus in leukaemia pathogenesis demonstrated that thymectomy could protect mice from development of lymphocytic leukaemia (Miller, 1959), though tangential observations uncovered an immunological role. Neonatal thymectomised mice had significant peripheral and tissue lymphopenia, increased susceptibility to viral infections and remarkably did not reject allogeneic skin grafts from different mice and even rat strains (Miller, 1961). Further experiments in chickens led to the discovery that humoral and cellular immunity were mediated by two distinct cell types: Thymus-derived 'T' cells and Bursa-derived 'B' cells (Cooper et al., 1965, Cooper et al., 1966). Fortunately for alliteration continuity, Miller repeated such findings in mice demonstrating bone marrow was the equivalent site of production of B cells, and that specific antigens were required to activate thymus-derived cells to coordinate antibody production (Miller and Mitchell, 1968).

Lymphocyte biology has long been at the forefront of immunology research, with six decades following their discovery leading to classification of an extensive set of different T cell subtypes. T cells are generally distinguished by expression of the major T cell receptor complex (Cluster of Differentiation 3 - CD3) and the principal co-receptors CD4 and CD8, with further classifications dependent on the stage within the T cell lifespan.

1.1.1 T cell development

As the major sites of lymphocyte development, the bone marrow and thymus are termed primary lymphoid organs. The thymus is populated by lymphoid progenitors originating from the bone marrow, which have potential to generate precursors of natural killer (NK) cells, dendritic cells (DC) and T cells. Early stages of T cell development require migration to and within distinct locations of the thymus

elegantly orchestrated by chemokine guidance, adhesion proteins, transcription factors and cytokine signalling. Upon migration and entry to the thymus via the cortical-medullary junction, the early progenitors interact with NOTCH1 ligand Delta1 expressed by thymic stromal cells which drives commitment towards the T cell lineage (Hosokawa and Rothenberg, 2021). These progenitors do not express CD4 or CD8 co-receptors and are thus termed double negative (DN) thymocytes. Upon thymus entry, DN thymocytes upregulate chemokine receptor CXCR4 which binds chemokine ligand CXCL12 expressed by cortical thymic epithelial cells to facilitate retention within the cortex. Here, thymocytes undergo early development and begin gene rearrangement of the T cell receptor (TCR) locus. TCR are heterodimeric complexes formed of two chains: either alpha (α) and beta (β) chains or gamma (γ) and delta (δ) chains. T cells expressing γδ-TCR, designated γδ-T cells represent a very small subset of the T cell compartment which are termed unconventional since they target cells for killing based recognition of stress signals expressed on the cell surface instead of via antigen-specific binding. Though development of γδ-T cells involves intricate mechanisms of selection by the thymus as elegantly reviewed in (Pellicci et al., 2020), this section will instead provide a brief overview of the development of conventional αβ-T cells.

Early development of DN thymocytes is categorised into four stages (DN1-4) of T cell lineage commitment, starting with DN1 thymocytes entry to the thymus as above. Initial rearrangements are made in the TCR-β chain in DN2 cells as they migrate towards the outer cortex (Kumar et al., 2018). A developmental checkpoint occurs at DN3, whereby cells which have failed to make successful β-chain rearrangements are arrested in the stage and soon die, whereas thymocytes that have rearranged a functional TCR-β chain progress to DN4 stage. Near the subcapsular region, assembly of a pre-TCR arrests further β-chain rearrangements and induces proliferation of the β-selected thymocytes. The DN4 cells then upregulate both CD4 and CD8, becoming double positive (DP) thymocytes and begin rearrangements of the α-chain locus. Successful α-chain rearrangements then allow low level expression of the αβ-TCR and CD3 complex on DP thymocytes. Thymic cortical epithelial cells or other medullary antigen-presenting cells (APC) then present peptides to the thymocytes through major histocompatibility complex (MHC) molecules in a complex at the cell surface termed peptide:MHC (pMHC). Any thymocytes with TCR unable to interact with pMHC undergo death by neglect apoptosis, whereas cells with TCR able to recognise

self-pMHC complexes receive survival signals, and therefore are positively selected for further maturation. Such positive selection interactions of the DP thymocyte with peptides bound to MHC class I or MHC class II determines development into a CD8 or CD4 single positive (SP) cell respectively. Furthermore, DP or SP thymocytes which recognise self-pMHC complexes with too high affinity undergo apoptosis, eliminating any potentially harmful self-reactive cells by negative selection. A small subset of CD4 SP cells that experience strong TCR interactions with self-pMHC undergo a selection for development into regulatory T cells (T_{reg}) which are crucial for mediating self-tolerance (Owen et al., 2019). Cells which have survived positive and negative selection then complete final stages of maturation in the medulla whereby SP cells upregulate sphingosine 1-phosphate receptor (S1PR) which promotes chemotaxis into the bloodstream. Mature thymocytes therefore exit the thymus and enter the blood as naïve T cells, so-called as they have not yet encountered their specific antigen. A more detailed account of the current understanding of mechanisms and mediators involved in thymus T cell development is comprehensively reviewed in Ashby and Hogquist (2024), though is out of scope of the present study.

1.1.2 Antigen presentation

Naïve T cells migrate through the circulation and home to secondary lymphoid organs (SLO) including the spleen, lymph nodes and mucosal-associated lymphoid tissues. Entry of naïve T cells into lymphoid tissues is regulated by coordinated expression of various chemokines and adhesion molecules such as lymphoid homing receptor CD62L, through which T cells can adhere to the vascular endothelium of SLO or inflamed sites, and migrate through the endothelial venule wall via diapedesis (Rahimi and Luster, 2018). In SLO, naïve T cells then interact with APC to initiate adaptive immune responses. DC, and other professional APC such as macrophages, and B cells, are vital for the uptake of antigens which are efficiently processed into peptide fragments and loaded onto MHC molecules for presentation (Pishesha et al., 2022). In this way, presentation of a wide range of foreign antigens or altered self-peptides allows for detection of infection or cancer respectively.

Intracellular or endogenous peptides are mainly presented on MHC-class I molecules, for which antigens must be processed into short peptides of approximately 8-10 amino acids for efficient binding inside the binding pocket. In contrast, MHC-class II molecules which have an open binding groove can bind longer peptides of ~13-25

amino acid residues and mostly present exogenous peptides (Wieczorek et al., 2017). Importantly, identification of the best peptide sequences for viral antigens or neoantigens through MHC binding predictions is crucial for the design of personalised adoptive antigen-specific T cell therapies (Zajonc, 2020).

1.1.3 T cell activation and antigen-specific T cell memory

As naïve T cells migrate through SLOs, they transiently bind to each APC they encounter allowing sampling of a large number of MHC molecules for their cognate antigenic peptide. In the rare event the naïve T cell TCR does match to its recognised pMHC complex, conformational changes in cell adhesion molecules stabilise binding between APC and T cell to facilitate differentiation into antigen-specific T cells (Dustin, 2008).

At least three types of signal are required to induce clonal expansion and differentiation of antigen-specific T cells. The first event to trigger T cell activation is engagement of TCR to pMHC along with either CD4 or CD8 co-receptor. In addition to this, co-stimulatory signals that promote T cell survival, and cytokines that signal differentiation into particular effector T cell subtypes are also essential. Co-stimulatory molecules are dependent on the MHC molecules, in humans termed the human leukocyte antigen (HLA) system. Therefore an individuals' HLA type determines which co-stimulatory molecules trigger survival signalling, with the most defined being B7 molecules expressed by APC (Chen and Flies, 2013). There are numerous T cell co-stimulatory receptors, with the most studied belonging to immunoglobulin (Ig) superfamily (including CD2, CD28, ICOS, and CD226); or tumour necrosis factor (TNF) superfamily (including CD27, CD30, CD137, and CD154). Upregulation of such receptors can be used as markers to identify antigen-specific activated T cells.

Upon activation, naïve T cells produce interleukin (IL)-2, along with a higher affinity IL-2 receptor which mediates re-entry to the cell cycle and rapid proliferation to induce clonal expansion (Abbas et al., 2018). Typically, proliferation and differentiation into effector T cells takes 4-5 days, contributing to the lag period usually seen in primary viral infections. Naïve T cells then differentiate into various CD4+ or CD8+ effector T cell subtypes, somewhat dependent on APC-secreted cytokines determining lineage fate. Differentiation causes cleavage of CD62L which

allows the activated T cells to exit to SLOs to the peripheral bloodstream, with subsequent changes in adhesion molecules directing the migration to inflamed tissue sites. Antigen-specific memory T cells which then re-encounter their cognate antigen in the periphery can then induce effector functions, initiated through TCR-pMHC binding and formation of an immunological synapse with the 'target' cell. Effector functions are largely determined by the molecules produced as discussed further in **section 1.3.1**. In terms of antiviral responses, CD4+ 'helper' T cells function primarily by secreting cytokines such as interferon-gamma (IFN-γ), TNF-α, and IL-2, which activate other immune pathways. Effector CD8+ 'cytotoxic' T cells elicit antiviral or antitumour responses through secretion of cytolytic enzymes that directly kill the target cell.

1.1.4 Approaches to treat viral infections with adoptive T cell therapies

Adoptive cell immunotherapy has long been explored in the treatment of both viral infections and cancers. Viral infection is a common complication following transplantation and dependent on the infection can rapidly become fatal without therapeutic intervention. Transplant patients have obvious risk of viral infection due to heavy iatrogenic immunosuppression they receive to prevent graft rejection, which correspondingly diminishes the ability to mount responses to invading pathogens. Even following tapering or cessation of immunosuppressive regimes, there is a significant delay in the recapitulation of the immune system post-transplant, and/or tolerance of an immature immune system suddenly exposed to active viral infection (Tomblyn et al., 2009, Leen et al., 2014). As such, transplant recipients can be at risk for severe viral complications even several years post-transplant. Since many viruses can hide latently and persist within the host throughout their lifespan, transplant patients are vulnerable to both primary infection by exogenous viruses (Boeckh et al., 2005) and reactivation of endogenous latent viruses. Due to their high incidence and disease severity, the most clinically serious viruses able to reactivate in immunocompromised patients are cytomegalovirus (CMV), Epstein-Barr virus (EBV), human herpes virus-6 (HHV-6), adenovirus (ADV), BK virus and JC virus (Barrett and Bollard, 2015) . Further complicating this is the link between some viruses with an increased risk of cancers, particularly CMV and EBV which are endemic worldwide (Smith and Khanna, 2017). While pharmacological antivirals can halt lytic viral replication usually through inhibition of viral replication enzymes, they impair the

development of long-term virus-specific T cell immunity and consequently disease relapse frequently occurs following termination of treatment. Therefore adoptive cellular immunotherapy was pioneered in the post-transplant setting as an approach to treat virus-driven diseases, though advances in this field have extended applications to reset immune responses in various viral, malignant, and even autoimmune disorders (Weber et al., 2020, Han et al., 2024).

Donor lymphocyte infusions (DLIs) are one of the earliest examples of adoptive immunotherapy (Barrett and Bollard, 2015). This approach utilised transplant donor peripheral blood, with the expectation that donor blood would contain an array of virus-specific memory T cells providing that the donor had prior exposure to the most common viruses. As such, since the transplant donor is already matched to the highest possible degree to the patient in question, this represented a resourceful strategy as prophylaxis alongside haematopoietic stem cell transplant (HSCT) to provide antiviral immunity. While DLI have demonstrated efficacy in controlling viral infections post-transplant, treatment was associated with high rates of infusion-related toxicity (Hromas et al., 1994, Papadopoulos et al., 1994, Heslop et al., 1994, Porter et al., 1999). It is estimated approximately 10% of peripheral circulating T cells are antigen-naïve dependent on age and antigen exposure, whereas antigen-specific T cells to any given virus are logs lower in number (Mackinnon et al., 1995, Bordignon et al., 1999). Therefore, the low frequency of virus-specific memory T cells is massively outnumbered by naïve alloreactive T cells able to target the host MHC and potentially induce life-threatening graft versus host disease (GVHD).

Approaches then focused on the removal or inactivation of potential alloreactive T cells within DLI to improve the safety of this therapy. For this strategy, numerous groups co-cultured the transplant recipient and donor blood to create a mixed lymphocyte reaction (MLR). Any donor T cells which were stimulated by the recipient APC would then upregulate T cell activation markers including CD25, CD69, CD137, and HLA-DR. Such alloreactive T cells expressing one or more of the above activation markers can be selectively depleted from DLI using cell selection techniques approved for clinical use such as: fluorescence-activated cell sorting; magnetic bead cell separation (van Dijk et al., 1999, Fehse et al., 2000, Hartwig et al., 2006, Wehler et al., 2007, Nonn et al., 2008, Albon et al., 2013); marker-directed immunotoxins (Mavroudis et al., 1996, Solomon et al., 2002, Amrolia et al., 2003, Samarasinghe et al.,

2010); or photodepletion (Chen et al., 2002, Guimond et al., 2002, Mielke et al., 2008, Bastien et al., 2010). While depletion methods can significantly reduce the numbers of alloreactive T cells to ~1-10% of all donor T cells depending on the depletion technique, even these small residual numbers were sufficient to induce clinical GVHD responses upon adoptive transfer in some cases (Solomon et al., 2005, Amrolia et al., 2006, Mielke et al., 2011). Furthermore, these studies highlighted the frequency of circulating memory T cells specific for numerous viruses are thresholds lower than that of CMV-specific and EBV-specific T cells which usually dominate the memory T cell compartment (Schulze Lammers et al., 2022). Consequently, high doses of T cells were required to confer protection against a large spectrum of viruses and even following allodepletion these doses would likely exceed the GVHD threshold of alloreactive T cells (Leen et al., 2014). Therefore, since the ratio of alloreactive T cells to viral reactive T cells was considered too high using allodepletion techniques, subsequent strategies aimed to isolate and expand highly-specific virus-specific T cells (VST) for therapy.

As a latent virus, CMV (which drives chronic infection and robust T cell memory responses in immunocompetent individuals) was the original candidate to test adoptive transfer VST therapy. Following assessment of functional efficacy in animal models, the first clinical study in humans was by transfer of donor CMV-specific VST to HSCT patients as prophylaxis (Riddell et al., 1992, Walter et al., 1995). For this, donor fibroblasts were infected with culture supernatant containing live CMV to establish feeder cell lines and further co-cultured with autologous peripheral blood mononuclear cells (PBMC). This allowed antigen presenting cells within the PBMC population to process CMV antigens released by the infected fibroblasts and present peptides in a class I / class II context to activate CMV antigen-specific T cells. After 7 to 14 days, limiting dilution cloning was used to isolate T cells with CMV-specific cytolytic activity and cells were further expanded for 3-10 weeks in culture with frequent re-stimulations using irradiated CMV-infected fibroblasts. The resultant polyclonal CMV-specific T cell isolates were administered intravenously to HSCT patients as four infusions given weekly. Monitoring of patient peripheral blood samples throughout the trial showed poor CMV-specific T cell killing pre-infusion, however adoptive transfer of CMV VST rapidly reconstituted CMV-specific immunity even after the first infusion, which amplified and persisted for up to 12 weeks post-infusion. This protected all recipients from CMV viremia and disease, which typically

has a high risk of rapidly causing significant morbidity/mortality in HSCT immunodeficient patients. Demonstration of clinical efficacy and safety of CMV-specific T cell adoptive transfer has been evidenced in several phase I/II clinical trials, with further testing in phase III trials ongoing (Walti et al., 2023). Moreover, significant advances in techniques have allowed optimisation of the manufacturing processes, resource quality, allogeneic matching, generated VST products, and therapy delivery (Neill and Peggs, 2021). Such approaches will be reviewed in more detail in **Section 1.3** and remains a focus of discussion throughout the present study. Importantly, the success of CMV-specific T cell immunotherapy motivated further interest in the use of other virus-specific T cells as treatment and prophylaxis for other chronic viral infections in immunocompromised patients. To this end, Epstein-Barr virus was a major candidate for targeting by adoptive T cell therapy since it is involved in several potentially fatal diseases.

1.2 Epstein-Barr virus (EBV)

Often described as an extremely "successful" virus, EBV establishes a persistent and usually asymptomatic infection in more than 90% of adults worldwide. As a member of the *gammaherpesviridae* family, its formal designation according to herpesvirus nomenclature is human herpesvirus-4 (HHV-4). Thought to have originated around 12 million years ago (Ehlers et al., 2010), EBV has indeed been successful for a virus by evolving mechanisms to hide latently in humans, whilst not being fatal for the majority of hosts. Increasingly however EBV has been found to be involved in or causative of numerous human pathologies and it is likely the full extent as to how the virus affects us in health and disease is still poorly understood. As the first human virus identified able to induce tumourigenesis, EBV has been associated with numerous malignancies including Burkitt lymphoma (BL), diffuse large B cell lymphoma (DLBCL), gastric carcinoma (GC), Hodgkin lymphoma (HL), nasopharyngeal carcinoma (NPC), natural killer cell/T cell lymphoma (NKTL), and post-transplant lymphoproliferative disorder (PTLD). EBV can also cause many non-malignant disorders including infectious mononucleosis (IM), chronic active EBV infection (CAEBV), haemophagocytic lymphohistiocytosis (HLH), acute cerebellar ataxia; and more recent convincing evidence suggests the virus is involved in numerous autoinflammatory diseases such as multiple sclerosis (MS) and systemic lupus erythematosus (SLE) (Damania et al., 2022). While even more pathologies have been suggested to be linked to EBV infection or immune responses against EBV (comprehensively reviewed in Zhang et al. (2021) and Huang et al. (2023)), the ubiquitous prevalence of the virus can make causality very difficult to prove, and as such evidence should be carefully validated in the understanding of clinical manifestations of this virus.

1.2.1 EBV structure

Like other members of the *herpesviridae* family, EBV is a DNA virus with a relatively large genome compared to other human viruses. The EBV virion consists of toroid-shaped protein core wrapped with DNA, surrounded by an icosahedral nucleocapsid, protein tegument and viral envelope with external glycoprotein spikes (Straus et al., 1993) as shown in **Figure 1.1**.

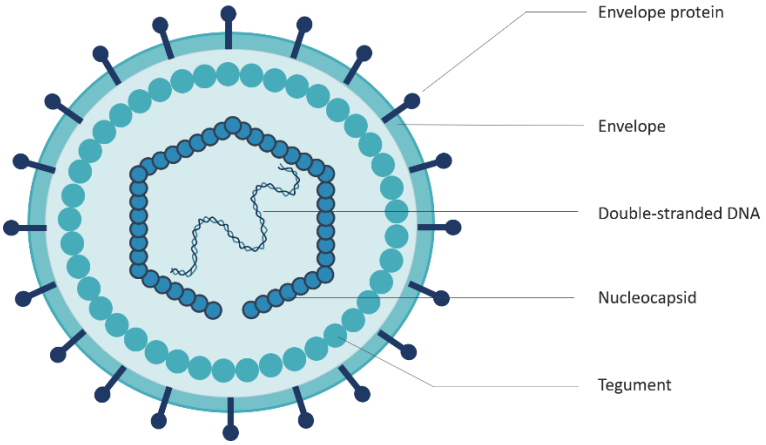

Figure 1.1 - EBV virion structure.

EBV is made up of a toroid protein core with viral double-stranded DNA and is encapsulated within an icosahedral nucleocapsid, protein tegument and outer virion lipid envelope.

The EBV genome is composed of linear, double-stranded DNA approximately 172 kilobase pairs in length. EBV was the first herpesvirus to be completely sequenced, with strain B95-8 sequence derived from an individual with infectious mononucleosis published in 1984 (Baer et al., 1984). Subsequently, the Raji strain sequence was used to create a putative wild-type strain sequence by filling in the blank of a 12kb deletion of the B95-8 strain (Raab-Traub et al., 1980, Parker et al., 1990, de Jesus et al., 2003).

Initially cloned and sequenced using EcoRI and BamHI restriction enzymes, open reading frames (ORF) were ordered according to fragment size (A-Z). Nomenclature of the open reading frames starts with the BamHI fragment, followed by L or R to indicate leftwards or rightward direction from the promoter, and finished with the frame number. For example, BALF2 encodes the second left reading frame of BamHI-A fragment. The 84 EBV ORFs encode lytic and latent genes, with the majority of these genes translated into functional proteins. Lytic genes are subdivided into immediate-early, early, and late genes, which are involved in viral replication and assembly named according to the BamHI nomenclature. Latency gene-encoded products are classified as Epstein-Barr nuclear antigens (EBNAs) or latent membrane proteins (LMPs). In addition, the genome encodes several non-coding functional RNAs including EBV-encoded RNAs (EBERs), and microRNAs. Both termini of the genome contain numerous tandem direct repeats that enable circularisation to form an episome within infected cells (Bankier et al., 1983).

1.2.2 EBV types

Following sequencing of different isolates worldwide, it is currently widely accepted that EBV is classified into two main genotypes: EBV type 1 and EBV type 2. Phylogenetic analysis suggests the two types have arisen from a recombination event between an earlier EBV strain probably with another *lymphocryptovirus* within the last 100,000 years (McGeoch, 2001). Main differences between the strains occur in the EBNA-2 locus, with 70% homology at the gene level and 53% at the protein level, with the two EBNA-2 types easily distinguished by serum immunoblotting (Dambaugh et al., 1984). Additionally the variation in EBNA-2 is associated with differences in EBNA-3A, EBNA-3B, EBNA-3C and EBNA-LP genes between the two strains (Sample et al., 1990). Type 1, first isolated from an infectious mononucleosis patient (B95-8), is the most prevalent type worldwide, predominantly in Europe, North America, South America and Asia. Type 2 conversely, first isolated from a Burkitt lymphoma patient (AG876) is considerably rarer and predominant within Africa, Alaska and Papua New Guinea (Zimber et al., 1986). Co-infection with both EBV-1 and EBV-2 have been reported (Lung et al., 1991, Smith et al., 2019), as well as intertypic recombinants expressing the type 1 EBNA-2 with type 2 EBNA-3 gene products (Midgley et al., 2000, Yao et al., 1996). Technological advances have allowed sequencing of EBV genomes from over 600 individuals worldwide with different diseases or otherwise healthy 'controls' to investigate geographical/ disease associations (Correia et al., 2018, Xue et al., 2021). Interestingly, EBV-2 isolates have been shown to have markedly lower levels of divergence across the genome, whereas EBV-1 genomes harboured higher diversity particularly in latency genes suggesting different evolutionary rates between the subtypes (Kaymaz et al., 2020). The most well-known EBV strains that have been isolated and sequenced are outlined in **Table 1.1.**

While the EBV type variation has not been directly associated with EBV diseases, one report found EBV-1 was more likely to cause infectious mononucleosis than EBV-2 (Crawford et al., 2006) though this was not corroborated in a similar study (Tierney et al., 2006). The most significant functional difference currently evidenced is the efficiency of EBV-1 to readily transform B cells into lymphoblastoid cell lines (LCL) *in vitro* compared to EBV-2 (Rickinson et al., 1987). While the exact mechanism of differential transforming ability between the strain types is unclear, type 1 EBNA-2 is

required for B cell entry to later stages of the cell replicative cycle (Gordon et al., 1986), whereas a sequence variation in type 2 EBNA-2 results in greater EBNA-2 inhibition by transcriptional repressor protein BS69 (Ponnusamy et al., 2019). Furthermore, type 2 strains have demonstrated greater efficiency to infect epithelial cells than type 1 strains through overexpression of lytic glycoprotein gp110 (Tsai et al., 2017). Therefore, downstream control of lytic and latent genes by EBNA-2 as a transcriptional regulator may influence tropism of infectivity between the two EBV types.

EBV Type	Strain	Origin	Disease	Source	Reference
1	EBV-WT	-	-	-	de Jesus et al. (2003)
1	B95-8	USA	IM	LCL	Baer et al. (1984)
1	Raji	Nigeria	BL	LCL	Parker et al. (1990)
1	Akata	Japan	BL	BL cell line	Lin et al. (2013)
1	Mutu	Kenya	BL	BL cell line	Lin et al. (2013)
1	Daudi	Kenya	BL	BL cell line	Correia et al. (2018)
1	C666-1	China	NPC	NPC biopsy	Cheung et al. (1998)
1	GD1	China	NPC	Saliva	Zeng et al. (2005)
1	GD2	China	NPC	NPC biopsy	Liu et al. (2011)
1	HKNPC1	Hong Kong	NPC	NPC biopsy	Kwok et al. (2012)
1	M81	Hong Kong	NPC	LCL	Tsai et al. (2013a)
1	HKNPC2-9	Hong Kong	NPC	NPC biopsy	Kwok et al. (2014)
1	K4123-Mi K4413-Mi	USA USA	Healthy donors	sLCL	Lei et al. (2013)
1	NA19114 NA19315 NA19384	Nigeria Kenya Kenya	Healthy donors	LCL	Santpere et al. (2014)
1	GC1	Korea	GC	GC cell line	Song et al. (2015)
1	YCCEL1	Korea	GC	GC cell line	Kanda et al. (2016)
1	60 strains	UK, USA, Germany, Africa, Australia, China, Japan, Hong Kong	BL, GC, HL, IM, NPC, PTLD	LCL, sLCL, NPC biopsy, saliva	Palser et al. (2015)
2	AG876	Ghana	BL	LCL	Dolan et al. (2006)
2	Jijoye	Nigeria	BL	BL cell line	Correia et al. (2018)
2	11 strains	Kenya, Nigeria, Papua New Guinea, Australia	BL, PTLD	sLCL	Palser et al. (2015)

Table 1.1 – Published EBV genomes.

Adapted from Young et al. (2016). *BL, Burkitt lymphoma; GC, gastric carcinoma; HL, Hodgkin lymphoma; IM, infectious mononucleosis; LCL, lymphoblastoid cell cline; NPC, nasopharyngeal carcinoma; PTLD, post-transplant lymphoproliferative disorder; sLCL, spontaneous lymphoblastoid cell line.*

1.2.3 EBV entry and replication

Numerous EBV glycoproteins (gp) are involved in the entry of EBV into different cell types. Entry into B cells is facilitated by gp350/220 binding to its receptors either CD21 or CD35 on the surface of B cells (Ogembo et al., 2013). This initial attachment initiates endocytosis of the virion into the cytosol. Further attachment of EBV gp42 with HLA class II on B cells results in a conformational change which allows the inner core machinery gp85/25 (also referred to as gHgL) and gp110 (also referred to as gB) to fuse to endocytic membranes. A recent study also demonstrated EBV was able to infect a subset of mature T cells that intrinsically expressed CD21 through a similar interaction with gp350 (Smith et al., 2020a), which may be the mechanism by which EBV can initiate the rarer T cell malignancies. Epithelial cells in contrast express low or undetectable levels of CD21, CD35 and HLA class II (Birkenbach et al., 1992). Attachment is instead thought to be mediated by complexes of gp85/25, gp110 and BMRF2/BDLF2 which bind with high affinity to various integrins expressed on epithelial cells (Xiao et al., 2008, Chesnokova et al., 2009). Without interaction with HLA class II, gp42 interferes with glycoprotein-integrin binding, inhibiting entry into epithelial cells (Sathiyamoorthy et al., 2016). Interestingly due to the binding of HLA class II with gp42, virions replicated within B cells have low expression of gp42 enabling efficient infection of epithelial cells. Conversely, in virions produced within epithelial cells, the low levels of gp42 would be unaffected without HLA class II associations with relative levels of gp42 increasing with a demonstrated efficient capacity to infect B cells (Borza and Hutt-Fletcher, 2002). As such, gp42 is considered a determinant of tropism for EBV to infect different cell types. Entry of EBV into epithelial cells has been demonstrated by direct membrane fusion (Miller and Hutt-Fletcher, 1992), lipid raft-dependent endocytosis and macropinocytosis (Wang et al., 2015). Further reports have shown EBV is capable of infecting other cell types such as monocytes (Savard et al., 2000), smooth muscle cells (Magg et al., 2018), and neurons (Jha et al., 2015), though the extent to which this occurs *in vivo* is unclear.

Following fusion, tegument proteins of the virus are dissolved allowing the capsid to be transported on microtubules to nuclear pores (Kieff, 1996). Subsequently released into the nucleus, the linear EBV genome circularises to form a covalently closed extrachromosomal episome wrapped in nucleosomes which can then proceed to lytic or latent states (Howley, 2022).

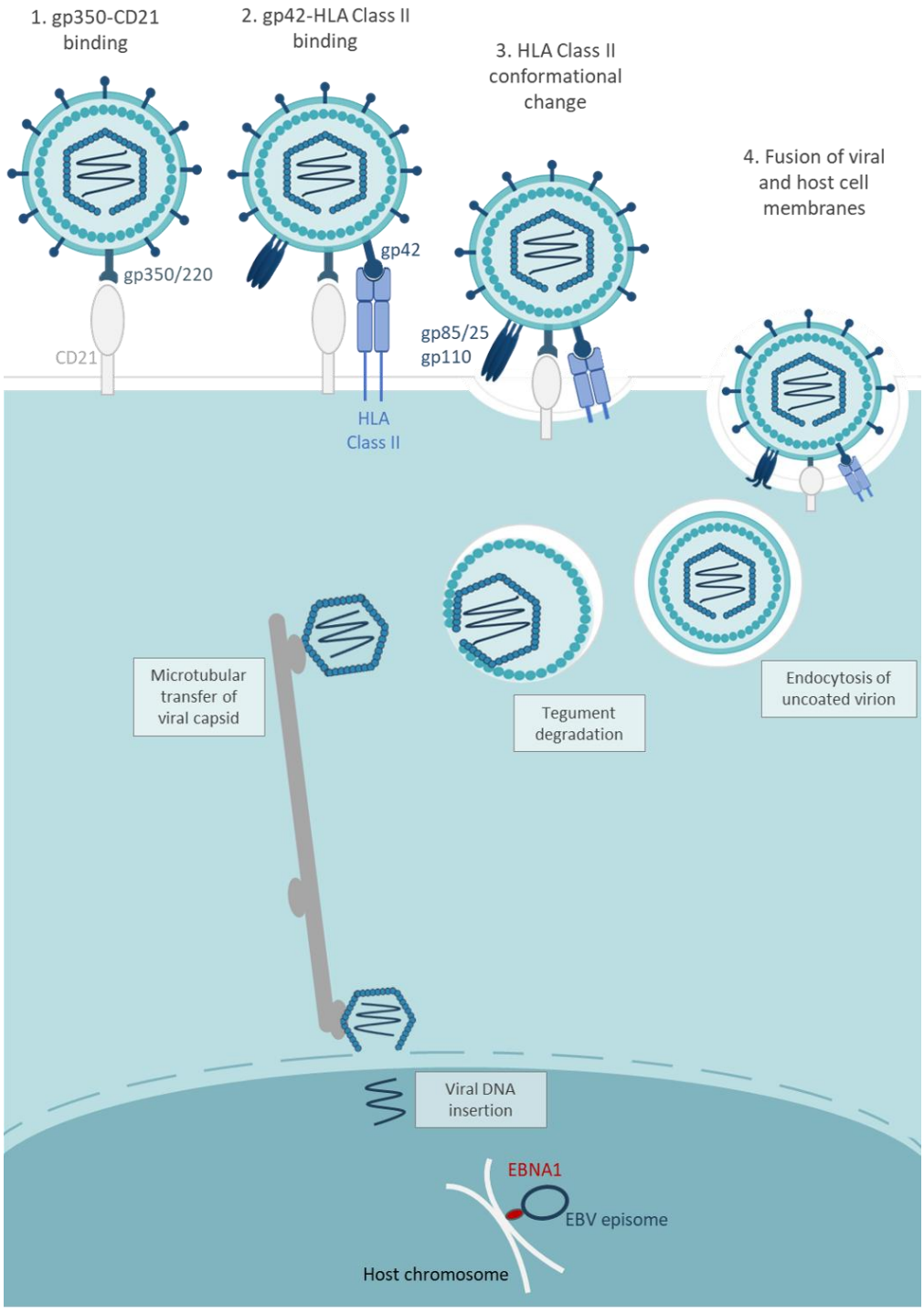

Figure 1.2 - EBV viral entry into B cells.

EBV glycoprotein gp350/220 binds to the host B cell membrane CD21 or CD35 receptor. Further attachment of EBV gp42 to HLA class II on the B cell surface results in a conformational change that induces fusion of the inner core machinery gp85/25 and gp110 to fuse to endocytic membranes of the host cell. The EBV virion is uncoated and endocytosed within the host cell facilitating tegument degradation. The viral capsid is released into the cytoplasm and transported via microtubular-mediated transport to the nuclear membrane. The linear EBV genome is then transported through nuclear membrane pores into the nucleus. EBV can then enter either lytic replication via induction of EBV immediate-early genes BRLF1 and BZLF1, or enter viral latency in which EBV nuclear antigen EBNA-1 tethers the EBV genome to host chromosomes resulting in circularisation an episome.

Adapted from (Damania and Pipas, 2009).

1.2.4 EBV primary infection

The majority of immunocompetent individuals acquire EBV during early childhood via salivary contact, of which infections are usually asymptomatic or mild illnesses (Hislop et al., 2007). If exposure is delayed until adolescence or adulthood, a heightened T cell response to EBV can cause IM, a usually self-limiting, benign lymphoproliferative disease (Leung et al., 2024). There are two main theories regarding primary infection; either EBV first infects epithelial cells in the oropharynx where it replicates and then spreads to nearby resting naïve B cells, or EBV directly infects tonsillar resting naïve B cells within Waldeyer's ring. Saliva contains EBV virions high in gp42 with a tropism for B cell infection (Jiang et al., 2006), which supports the former theory that the virus first replicates in a HLA class II negative epithelial cell. Conversely, a sensitive nested PCR method detected low levels of EBV in the blood of IM patients 3 weeks prior to symptom onset, at which high viral load was detected in both the blood and oral cavity, indicating B cells are the first cell type infected (Dunmire et al., 2015). While some infected B cells within the oropharynx then undergo lytic replication to produce infectious progeny, the majority become latent within memory B cells to evade immune surveillance (Kurth et al., 2000).

1.2.5 EBV lytic replication

Co-ordinated regulation of EBV lytic replication is required for viral spread from cell-to-cell and host-to-host, with a 100-1000-fold amplification of EBV DNA within 24 hours of lytic induction (Hammerschmidt and Sugden, 1988, Nagaraju et al., 2019). Lytic phase EBV-infected cells have rarely been detected *in vivo,* likely due to efficient host T cell responses against lytic antigens (Steven et al., 1997). Lytic EBV has been reported in oropharyngeal epithelial cells (Steven et al., 1997, Pegtel et al., 2004) and tonsillar plasma cells (Laichalk and Thorley-Lawson, 2005), allowing virion shedding into the saliva. Since lytic replication was only detected in antibody-secreting B cells but not in other B cell populations within the tonsils, it indicated lytic replication only occurs when infected naïve B cells differentiate to plasma cells (Crawford and Ando, 1986, Laichalk and Thorley-Lawson, 2005). In this way, the EBV lytic cycle is primarily induced by B cell differentiation, though can also be triggered by stressors, immune suppression and local hypoxia (Kenney and Mertz, 2014). The temporal sequence of the EBV lytic cycle is classified into expression of viral immediate-early, early, and late genes. Functions of lytic and latent genes are outlined in **Table 1.2**.

ORF	Gene Product	Function
Immediate-Early Lytic		
BZLF1	Zta, ZEBRA	Lytic cycle transactivator, oriLyt binding, regulate viral replication
BRLF1	Rta, R	Lytic cycle transactivator
Early Lytic		
BALF2	EA	DNA replication, ssDNA-binding protein, early antigen
BALF5		DNA replication, DNA polymerase
BBLF2/3		DNA replication, spliced primase helicase complex component
BBLF4		DNA replication, helicase homolog
BKRF3		DNA replication, uracil DNA glycosylase
BMRF1	DPAP	DNA replication, DNA polymerase accessory protein, mismatch repair core
BSLF1		DNA replication, primase homolog
BMLF1	Mta, SM	DNA replication, mRNA export factor, late lytic gene transactivator
BGLF4		DNA binding, EBV protein kinase, virion assembly
BALF1		Immune evasion, BCL2 homolog anti-apoptosis
BCRF1	vIL-10	Immune evasion, IL-10 homolog B cell proliferation, inhibit IFN-γ release
BARF1		Immune evasion, decoy receptor to scavenge CSF-1
BDLF3	gp150	Immune evasion, downregulate HLA expression
BGLF5		Immune evasion, downregulate HLA expression
BILF1		Immune evasion, downregulate HLA expression
BNLF2A		Immune evasion, downregulate HLA expression
Late Lytic		
BBRF1		Capsid protein, portal protein for DNA insertion
BVRF1		Capsid protein, portal protein for DNA retention
BALF3		Capsid protein, terminase component to cleave DNA concatemers
BDRF1		Capsid protein, terminase component to cleave DNA concatemers
BGRF1		Capsid protein, terminase component to cleave DNA concatemers
BFLF1	UL32	Capsid protein, mediates DNA packaging into capsids
BFRF1A		Capsid protein, mediates DNA packaging into capsids
BCLF1	MCP	Capsid protein, major capsid protein
BDLF1	TRX2, mCP	Capsid protein, triplex capsid protein 2, minor capsid protein
BFRF3	SCP, VCA-p18	Capsid protein, small capsid protein, viral capsid antigen-p18
BORF1	TRX1, mCPBP	Capsid protein, triplex capsid protein 1, minor capsid-binding protein
BFLF2		Capsid protein, nuclear egress complex component
BBLF1	MyrP	Tegument protein, myristoylated protein
BDLF2		Tegument protein
BGLF1		Tegument protein
BGLF2	MyrPBP	Tegument protein, myristoylated protein binding protein

BGLF4		Tegument protein, protein kinase
BKRF3		Tegument protein
BLRF2		Tegument protein
BNRF1	MTP	Tegument protein, major tegument protein, EBV translocation to nucleus
BOLF1	LTPBP	Tegument protein, large tegument protein binding protein
BPLF1	LTP	Tegument protein, large tegument protein, suppress TLR signalling
BRRF2		Tegument protein
BSRF1	PalmP	Tegument protein, palmitoylated protein
BVRF1		Tegument protein, portal plug
BALF4	g110, gB	Envelope glycoprotein, attachment and fusion
BDLF2	BDLF2	Envelope glycoprotein, attachment and fusion
BILF2	gp78	Envelope glycoprotein, unknown function
BKRF2	gp25, gL	Envelope glycoprotein, attachment and fusion
BLLF1a/b	gp350/220	Envelope glycoprotein, attachment and fusion
BMRF2	BMRF2	Envelope glycoprotein, attachment and fusion
BXLF2	gp85, gH	Envelope glycoprotein, attachment and fusion
BZLF2	gp42	Envelope glycoprotein, attachment and fusion, immune evasion
BBRF3	gp44, gM	Envelope glycoprotein, assembly and release
BLRF1	gN	Envelope glycoprotein, assembly and release
Latency		
BKRF1	EBNA1	Survival, episomal maintenance and tethering to host chromosomes, viral DNA replication, latent gene transactivator, immune evasion through interference with MHC presentation
BYRF1	EBNA2	Transformation, latent and cellular gene transactivator
BERF1	EBNA3A	Transformation, suppress B cell apoptosis, promote oncogenesis
BERF2	EBNA3B	Survival, tumour suppressor gene to regulate EBNA3A & 3C
BERF3/4	EBNA3C	Transformation, suppress B cell apoptosis and promote oncogenesis
BWRF1	EBNALP	Transformation, latent gene transactivator
BHRF1	BHRF1	Immune evasion, BCL2 homolog anti-apoptosis
BNLF1	LMP1	Survival & transformation, CD40 homologue promote B cell differentiation, TNFR signalling, suppress apoptosis, promote oncogenesis
BNRF1	LMP2A	Survival & transformation, BCR homologue promote B cell differentiation, suppress apoptosis, promote oncogenesis
BNRF1	LMP2B	Survival, tumour suppressor gene regulate LMP1 & 2A
EBER1/2	EBER RNAs	Non-coding RNAs,
BART1	BART miRNAs	Latent gene transactivator microRNAs, immune evasion
BHRF1	BHRF1 miRNAs	Latent gene transactivator, immune evasion

Table 1.2 - EBV gene functions.
Adapted from Hutt-Fletcher (2015) and Murata (2018).

Immediate-early genes BZLF1 and BRLF1 are considered molecular switches between the latent and lytic phases of the EBV lifecycle. Expression of BZLF1 has been shown to be the first EBV gene upregulated upon stimulation of the B cell receptor (BCR), indicating the mechanism of B cell differentiation by turning on the EBV lytic switch (Bryant and Farrell, 2002, Ye et al., 2010). Encoding transcription factors, BZLF1 and BRLF1 function to activate their own and each other's promoters (Zp and Rp respectively), as well as other early lytic genes required for viral DNA replication. BZLF1 protein also binds directly to the viral genome at the origin of lytic replication, termed oriLyt (Hammerschmidt and Sugden, 1988); and interacts with some of the core replication proteins thought to promote formation of the replication complex.

Early lytic genes drive viral genome replication. Viral DNA synthesis is mediated by core replication complex components BALF2, BALF5, BBLF2/3, BBLF4, BKRF3, BMRF1 and BSLF1. Replication compartments formed within the nucleus from BMRF1 proteins allow segmentation of viral DNA synthesis from host DNA and histones (Sugimoto et al., 2011, Chiu et al., 2013). This causes a honeycomb-like morphology of the nucleus, with EBV replication compartments occupying approximately 30% of the nuclear volume during lytic amplification (Nagaraju et al., 2019). Furthermore, mRNA transporter BMLF1 protein mediates synthesised DNA processing and translation essential for infectious virion production (Thompson et al., 2016, Verma et al., 2016). Other early genes are indirectly involved in promoting EBV replication, through mechanisms including suppression of B cell apoptosis (BHRF1, BALF1); activation of B cell proliferation (BCRF1), and inhibition of pro-inflammatory cytokine signalling (BCRF1, BARF1).

Late genes encode proteins required for virion assembly and have been functionally classified due to their ability to be transcribed in the absence of viral DNA synthesis. First, viral nucleocapsids are pre-formed from viral capsid proteins assembled in the nucleus. There are four structural capsid proteins: major capsid protein (MCP), minor capsid protein (mCP), small capsid protein (SCP), and minor capsid protein-binding protein; encoded by BCLF1, BDLF1, BFRF3, and BORF1 respectively. The capsid is formed of 12 penton and 150 hexon molecule complexes of MCP (Liu et al., 2020). Triplex complexes of SCP, mCP and mCPBP connect MCP hexons at distal tips assembling an icosahedral structure. Since lytic EBV replication produces long concatemers, the DNA must be processed and cleaved into linear genome units by

viral terminase complex proteins BALF3, BDRF1, and BGRF1 (Bloss and Sugden, 1994, Chiu et al., 2014). The linear genomes are then packaged into the preformed capsids through portal complexes BBRF1 and BVRF1 (Sheaffer et al., 2001, Lebedev et al., 2007) mediated by packaging proteins BFLF1 and BFRF1A (Pavlova et al., 2013).

Packaged nucleocapsids then bud through the nuclear membrane and are coated with the viral tegument. As well as being a major structural component, tegument protein BPLF1 also catalyses toll-like receptor (TLR) signalling intermediates, causing suppression of the TLR cascade as a mechanism of innate immune evasion (van Gent et al., 2014). Two further glycoproteins gM and gN, encoded by BBRF3 and BLRF2 respectively, form complexes to mediate exocytosis of tegumented virions. Newly assembled virions within cytoplasmic vesicles are then released into extracellular space via exocytosis.

1.2.6 EBV latency states

While lytic replication proceeds in a small subset of oropharyngeal cells following primary infection to allow production of infectious progeny, the majority of infected B cells are thought to enter viral latency states. Several genes are associated with EBV latency including EBNA-1, EBNA-2, EBNA-3A/B/C, EBNA-LP, LMP1, LMP-2A/B, BHRF1, as well as EBV-encoded RNAs (EBERs) and numerous microRNAs (Howley, 2022). Differential expression of these genes characterizes distinct latency states which are associated with different clinical pathologies as detailed in **Table 1.3**.

Latency Type	Latency Genes								Associated Disorders
	EBERs	EBNA1	EBNA2	EBNA3 A/B/C	EBNA LP	LMP1	LMP2 A/B	BHRF1	
0	+	-	-	-	-	-	-	-	
I	+	+	-	-	-	-	-	?	BL, GC
II	+	+	-	-	-	+	+	?	HL, NPC, NKTCL
III	+	+	+	+	+	+	+	+	IM, PTLD, AIDS-associated lymphoma

Table 1.3 - EBV latency type gene expression and associated disorders.

Adapated from Massini, Simer & Hohaus (2009). *AIDS, acquired immunodeficiency syndrome; BL, Burkitt Lymphoma; EBER, Epstein-Barr virus-encoded ribonucleic acid; EBNA, Epstein-Barr virus nuclear antigen; GC, gastric carcinoma; HL, Hodgkin lymphoma; IM, infectious mononucleosis; NKTCL, NK T cell lymphoma, NPC, nasopharyngeal carcinoma; NPC, nasopharyngeal carcinoma; PTLD, post-transplant lymphoproliferative disorder.*

A model for EBV latency originally proposed by Thorley-Lawson and Gross suggests EBV exploits the B cell differentiation pathway by switching between different latency programs as shown in **Figure 1.3** to persist within the B cell compartment (Thorley-Lawson and Gross, 2004). Briefly, preferential infection of resting naïve B cells expressing all of the latency-associated genes (Latency III) promotes proliferation into activated B cell blasts as observed in IM and lymphomas in immunocompromised individuals. Since this profile of expressing all latency genes is very immunogenic, development of EBV lymphoblasts in immunocompetent individuals is readily controlled by host EBV-specific T cells. Blasts then migrate to lymphoid follicles and clonally expand within the germinal centre, resulting in a switch to a restricted latent gene expression profile (Latency II). Of these latency II genes, LMP-1 and LMP-2A are homologues for B cell stimulatory proteins CD40 and BCR respectively. Through mimicry of foreign antigen B cell activation, this induces immunoglobulin gene rearrangements by somatic hypermutation and isotype switching, causing the blasts to differentiate into memory B cells. EBV-infected memory B cells then enter the peripheral blood which becomes the site of persistence and downregulate expression of all latency genes (Latency 0) to evade T cell detection. Infected memory B cells may later divide, returning to the germinal centre and upregulating EBNA-1 to allow a template of the viral DNA to be transferred to daughter B cells (Latency I), though as a normal feature of memory B cell homeostasis this is considered distinct from viral-driven lytic replication. Instead, lytic replication is thought to occur when infected memory B cells terminally differentiate into plasma cells, with resultant progeny virions able to infect nearby naïve B cells or epithelial cells.

Supporting this model of colonisation of the B cell compartment as the reservoir for EBV persistence, ablative chemotherapy prior to HSCT removing host B cells but not epithelial cells has been shown to eradicate EBV from the body (Gratama et al., 1990). Furthermore, individuals with X-linked agammaglobulinaemia who lack mature B cells have no evidence of EBV infection or cellular immunity to EBV throughout their lifespan (Faulkner et al., 1999). Conversely, in individuals with X-linked hyperimmunoglobulin M syndrome that cannot form germinal centres and lack classical class-switched IgD-/CD27+ memory B cells, EBV was detected in non-classical germinal centre-independent IgD+/CD27+ memory B cells (Conacher et al., 2005). Furthermore, studies of IM patients reported lack of EBV+ cells within

germinal centres, but detected large numbers of EBV+ blasts in extrafollicular locations (Niedobitek et al., 1992, Kurth et al., 2000). Therefore, some studies do not support this model of EBV latent persistence through the germinal centre reaction, however it is worth noting these reports are from patients with more rare clinical pathologies and therefore may reflect non-physiological settings forcing an atypical route of EBV infection.

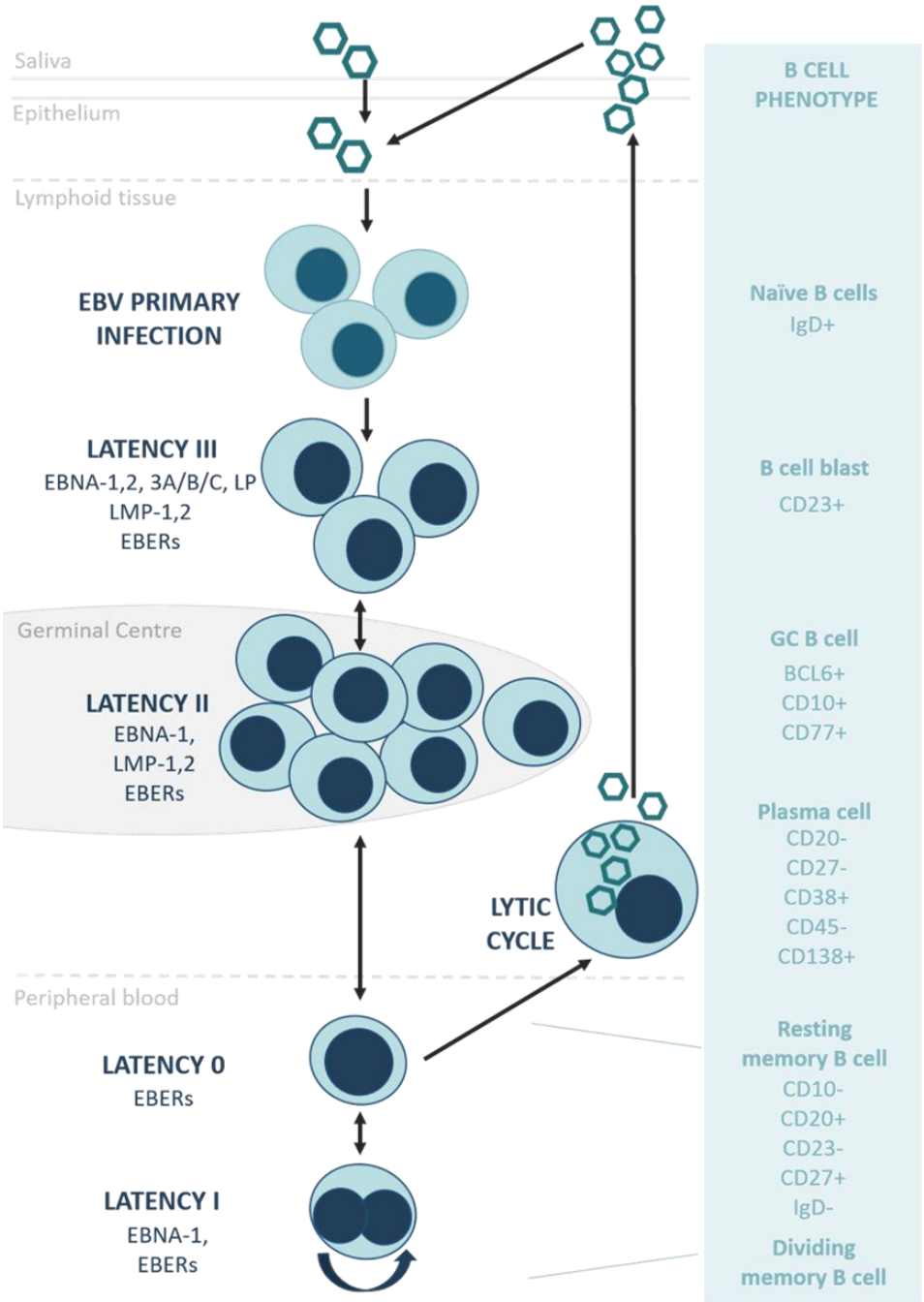

Figure 1.3 - Model of EBV latency programs in B cells.

Adapted from Andrei et al. (2019) and Howley (2022).

Although the exact mechanism and sites of latency within different health and disease contexts are not completely understood, the roles of latency genes have been extensively characterised. Initially, following primary infection of B cells, the BamHI W promoter (Wp) drives transcription of EBNA-LP and EBNA-2 (Mrozek-Gorska et al., 2019). Co-activation of EBNA-LP and EBNA-2 then regulate transcription of numerous viral and host cellular genes. Transactivation by EBNA-2 targets viral promoters BamHI C promoter (Cp) which drives upregulation of EBNA-1, EBNA-3A, EBNA-3B, EBNA-3C and BHRF1. EBNA-2 also transactivates the LMP1 promoter (LMP1p) responsible for LMP1 expression which is essential for B cell transformation. In addition, EBNA-2 also transcribes several cellular promoters including those of c-Myc, CD21 and CD23.

Only expressed in the latency III program, both EBNA-3A and EBNA-3C act to inhibit the tumour suppressor proteins p14 and p16 through epigenetic modification (Skalska et al., 2010). Expression of EBNA-3A and EBNA-3C were essential for the establishment and maintenance of LCL growth *in vitro*, indicating these genes are required for the cellular transformational capacity driven by EBV (Maruo et al., 2011). Furthermore, EBNA-3A and EBNA-3C have been shown to epigenetically regulate pro-apoptotic protein BCL-2 interacting mediator of cell death (Bim) (Paschos et al., 2009), which drives the c-Myc over-expression of infected lymphoblasts during BL pathogenesis (Bristol et al., 2024). Latent expression of BHRF1 encoding a BCL homologue further potentiates anti-apoptosis and immune evasion functions (Kelly et al., 2009). Although the EBNA-3 genes constitute a gene family, generation of recombinant viral mutants demonstrated that EBNA-3B was dispensable for B cell immortalisation (Tomkinson and Kieff, 1992) in contrast to EBNA-3A and EBNA-3C that were requisite for viral oncogenesis (Tomkinson et al., 1993). Infection with EBNA-3B knockout EBV resulted in aggressive tumour formation in humanised mouse models, and screening of DLBCL, HL and BL human biopsies identified EBNA-3B silencing mutations (White et al., 2012). Furthermore, the infected B cells had significantly reduced secretion of T cell chemoattractant CXCL10 with concordant lack of T cell recruitment to EBNA-3B KO tumours, however this could be partially rescued by addition of CXCL10. Evidence of this gene having tumour suppression functionality was the first to be described for a tumour virus, and may represent an evolutionary adaptation to limit lymphoproliferative mortality to the host (Allday et al., 2015). Given that T cell interactions are essential for the germinal centre reaction,

and that EBNA-3B downregulates several genes upon entry to the germinal centre, it is further postulated EBNA-3B could be involved in switching to the latency II program (White et al., 2010).

EBV induces expression of three latent membrane proteins (LMPs) in latency III or latency II cells: LMP-1, LMP-2A, and LMP-2B. These proteins are expressed at the cell surface and within intracellular perinuclear regions (Lynch et al., 2002). Differentiation of germinal centre B cells into memory B cells usually requires CD40 activation by co-stimulatory molecule CD154 expressed on antigen-specific T cells. As a homologue of CD40, LMP-1 protein mimics cellular CD40 signal transduction in an antigen-independent manner, causing activation of multiple TNF receptor family intracellular signalling pathways. Constitutively expressed in variable forms of both the lytic and latent lifecycle, LMP-1 has diverse cellular functions to induce proliferation, survival, immune evasion and angiogenesis (Kieser and Sterz, 2015). Similarly, LMP-2A is a homologue of the B cell receptor (BCR) and mimics BCR-mediated signal transduction required for memory B cell development. Conversely, LMP-2B is an isoform of LMP-2A but lacks the amino terminal domain required for intracellular signalling. Instead LMP-2B has been shown to negatively regulate LMP2A expression and function by preventing the switch from latent to lytic cycles in Akata cell lines (Rechsteiner et al., 2008). Both LMP-2A and LMP-2B have been extensively mutated within the EBV genome indicating they are not essential for viral latency (Howley, 2022). Concordantly, the LMP-2 proteins have been found to be dispensable to B cell transformation, though normal expression provides a significant growth advantage (Mancao and Hammerschmidt, 2007, Zhang et al., 2023). Expression of LMP-1 however has been shown to be critical for transformation of B cells *in vitro (Dirmeier et al., 2003)*, and inducing tumour formation in animal models (Kulwichit et al., 1998, Zhang et al., 2012, Zhang et al., 2023). As such, LMP-1 is considered the principal EBV oncogene. All three proteins have also been detected in epithelial cell tumours (Smatti et al., 2018, Lin et al., 2018) indicating other oncogenic roles not associated with BCR mimicry.

As the only gene expressed in all latency states except latency 0, EBNA-1 is essential for EBV persistence. Through direct binding to the viral episome at the origin of plasmid, termed oriP, EBNA-1 serves to tether viral DNA to the host chromosomes and enables their segregation during the S-phase of cellular mitosis. This is mediated

by modular structure of the EBNA-1 protein which contains several oriP DNA binding sites in the C-terminal domain, and positively charged amino acid sequences in the N-terminal domain required for chromosome binding (Kanda et al., 2013). Recombinant viral mutants lacking the EBNA-1 gene were still able to immortalise B cells, however at very low frequency of several thousand-fold less efficiency of wild type EBV (Humme et al., 2003). Since EBNA-1 maintains EBV genomes as circular episomes, lack of EBNA-1 resulted in EBV genomic integration into host chromosomes, however the ability to stably express all viral latent proteins required for transformation was substantially limited. Furthermore, EBNA-1 mutants induced B cell growth similar to WT EBV at initial days post-infection, but by day 8 expression of EBNA-2 and MYC protein were significantly reduced and consequently the transformed cells did not survive past 2 weeks post-infection (Pich et al., 2019). Therefore, while EBNA-1 is not required for initial B cell transformation, it is critical for the continued maintenance of EBV latency. Additionally, glycine-alanine repeat sequences within the structure of EBNA-1 reduces translational efficiency which then interferes with EBNA-1 peptide presentation by MHC class I molecules (Apcher et al., 2010). This results in weak recognition of EBNA-1 by cytotoxic CD8+ T cells and as such allows EBNA-1 to mediate immune evasion in the more restricted latency states.

Two small nuclear non-coding RNA molecules EBER1 and EBER2 are highly expressed in all EBV-infected cells at each stage of lytic or latent cycle, with approximately 5 million EBER transcript copies per cell (Lerner et al., 1981). As such, in situ hybridization of EBERs is currently the most sensitive technique to detect EBV infection in tissues (AbuSalah et al., 2020). Although abundantly expressed and shown to be confined to the nucleus (Fok et al., 2006), EBER functions remain incompletely defined. Studies investigating EBER knockout mutants have generated conflicting results, with reports demonstrating EBER expression was essential for transformation (Yajima et al., 2005, Wu et al., 2007), and others showing no differences between mutants and wild type EBV (Gregorovic et al., 2015, Pich et al., 2019), though this may reflect different EBV cell lines used. Knockdown of EBER2 in B cells with type II EBV latency was shown to prevent binding of transcription factor PAX5 to terminal repeats of the latent EBV genome, with downstream upregulation of LMP expression (Lee et al., 2015). EBER knockouts however had equivalent LMP protein expression to wild type EBV (Pich et al., 2019), indicating potential roles as

guides for viral genome transcription can be carried out by other factors in absence of functional EBERs.

While the majority of EBV latent proteins are highly immunogenic, viral microRNAs (miRNAs) can regulate viral and cellular gene expression without stimulating the host immune response. Currently 44 mature EBV miRNAs have been detected in EBV-infected cells, encoded by BART1 and BHRF1 clusters. While numerous EBV miRNA targets have been identified, the cooperative regulation by miRNAs make it difficult to study individual miRNA functions. BART1 miRNAs have been shown to be downregulated in replicating cells and co-operatively prevent expression of IE lytic gene BZLF1 thereby maintaining EBV latency (Lin et al., 2015). BHRF1 cluster mutants failed to facilitate LCL transformation *in vitro*, thought to be due to BHRF1-encoded miRNA acting on promoters of EBNA-LP and LMP1 genes to maintain latency (Poling et al., 2017). Furthermore, EBV miRNAs can inhibit T cell recognition and killing of infected cells through downregulation and/or inhibition of promoters for genes involved in peptide presentation, demonstrating direct mechanisms by which miRNAs contribute to EBV immune evasion (Albanese et al., 2016).

Roles of the many EBV lytic and latency genes have been well defined, though how EBV mediates lifelong latency with limited morbidity in the vast majority of the population is incompletely understood. It is clear that epigenetic regulation, through numerous post-translation modification mechanisms, is critical in the co-ordinated control of viral and cellular gene product expression (Murata et al., 2021), as well as efficient hijacking of B cell metabolic pathways to orchestrate transition between latency programs and lytic reactivation (Müller-Durovic et al., 2024). It is also likely EBV has evolved mechanisms that utilise host innate and immune responses to maintain viral latency, which may be key to uncovering the aberrant host to immune interactions that lead to pathologies.

1.2.7 Immune responses to EBV infection and reactivation

Like other viral infections, induction of the innate immune response to EBV is triggered by intracellular pathogen recognition receptors (PRRs) capable of identifying various pathogen-associated molecular patterns (PAMPs) within the viral genome or transcribed gene products. An important PRR for double stranded RNA detection is RIG-I, which has been shown to recognise an RNA-polymerase III-

transcribed EBER RNA intermediate during lytic replication and initiate a type I interferon response (Ablasser et al., 2009, Duan et al., 2015). Additionally, a major PRR for DNA viruses is interferon-γ-inducible protein-16 (IFI16) which activates the inflammasome within the cytoplasm of infected cells. Lytic EBV replication is rapidly detected by IFI16, and IFI16 co-localisation with the EBV genome in latently-infected cells is a key mediator in the switch from latent to lytic reactivation (Ansari et al., 2013, Pisano et al., 2017). Furthermore, recognition of the EBV genome and induction of innate responses by numerous Toll-like receptors (TLRs) has been reported including TLR2, TLR3, TLR7 and TLR9 (Gaudreault et al., 2007, Iwakiri et al., 2009, Fiola et al., 2010, van Gent et al., 2014, Zheng et al., 2014).

Upon inflammatory induction, key mediators of the innate cellular response include NK cells, invariant natural killer-T cells (iNKT), and γδ-T cells. Primary EBV infection induces a significant NK cell expansion which can lyse lytically infected cells, with the magnitude of NK cell response linked to disease severity of IM in numerous studies (Azzi et al., 2014, Williams et al., 2005, Balfour et al., 2013). EBV lymphoproliferative disorders have been reported in patients with inherited disorders specifically resulting in NK cell deficiency or abrogated NK cell responses, indicating NK cells are critical for EBV infection control (Parolini et al., 2000, van Montfrans et al., 2012, Orange, 2013, Salzer et al., 2013). Significant expansions of activated γδ-T cells have also been reported following EBV primary infection (Fujishima et al., 2007, Hassan et al., 1991, Farnault et al., 2013, Zhong et al., 2017). As a subset of unconventional T cells, γδ-T cells can elicit killing of viral-infected and cancer cells in an MHC-independent manner, instead recognising various molecules related to cellular stress, metabolic dysfunction or inflammation. Expansion of γδ-T cells expressing the Vγ9Vδ2 receptor with strong EBV responses have been detected in approximately half of the general population, while the other half combat primary infection with NK cells alone; with no demographic or clinical factor currently identified to explain this polymorphism (Djaoud et al., 2017). Studies *in vitro* have demonstrated Vγ9Vδ2 T cells can recognise isopentenyl pyrophosphate (IPP) secreted by EBV+ cell lines, a phospho-antigen synthesised by stressed or transformed cells, though it is unclear if this is the mechanism of recognition during primary infection *in vivo*. Moreover, this Vγ9Vδ2 T cell population elicited significantly enhanced effector functionality to Daudi and Akata cell lines than other EBV-infected targets. This is thought to be due to polymorphisms in the Daudi and Akata genome that lack β2-microglobulin causing

downregulation of MHC class I molecules, therefore preventing MHC class I-specific inhibitory receptor triggering on γδ-T cells. This highlights fundamental differences in immune mediators between EBV strains, which may underpin the varied pathogenesis of EBV-associated diseases. Invariant NKT cells are a further subset of unconventional T cells able to induce cytotoxicity without peptide recognition. Patients with EBV-associated HL and NPC have been shown to have depleted frequency and functionally impaired iNKT, which suggests this subtype plays a role in the continued regulation of EBV reactivation as well as primary infection response (Yuling et al., 2009, Chung et al., 2013).

Adaptive immunity to EBV is mediated by both humoral and cellular responses. Following primary infection, antibodies are generated against a wide range of EBV lytic antigens (Hinderer et al., 1999, Zeng et al., 1997, Sugimoto et al., 2011) including: p18 viral capsid antigen (VCA) (BFRF3 gene); p23 VCA (BLRF2 gene); p125 membrane protein (BALF4 gene); p143 tegument protein (BNRF1 gene); p150 capsid protein (BCLF1 gene); DNA polymerase accessory protein (BMRF1 gene), DNA polymerase (BALF5 gene); early antigen (BALF2 gene); and ZEBRA (BZLF1 gene). Antibodies against EBV latent antigens are largely absent or undetectable in healthy carriers, except for EBNA-1 IgG which are detected throughout the host lifespan (Meij et al., 1999, Paramita et al., 2011). This highlights effective evasive strategies of EBV during latency stages to prevent development of latency-specific memory B cells. Clinical diagnostics are usually based on serum IgM and IgG levels against EBV VCA and EBNA-1. Anti-VCA IgM appear early in infection, usually disappearing after 4-6 weeks, and anti-VCA IgG peak 2-4 weeks post-infection before contraction but persist through the host lifespan. Antibodies against EBNA-1 however aren't detected in early stages, instead appearing a couple of months post-infection. Therefore, the presence of VCA IgM or IgG with absence of EBNA-1 IgG diagnoses a current or recent primary infection (Howley, 2022). Eventually, the serology profile reaches that of a healthy carrier: IgM anti-VCA-, IgG anti-VCA+, IgG anti-EBNA1+, IgG anti-EBNA2low/- which is stable long-term (Guerrero-Ramos et al., 2014). Antibodies against EBV envelope glycoproteins gH/gL, gp42 and gp350 able to neutralize infection of B cells and epithelial cells have also been reported in serum of healthy donor adults, which may be important for long-term control of EBV reactivations (Bu et al., 2019).

Although host EBV-specific CD8+ T cells are unable to eradicate the virus from the body, they are able to lyse EBV-infected cells recognised by presentation of viral antigen on the surface of infected cells by MHC class I molecules (Klein, 1994). The most robust CD8+ T cell responses upon primary infection are mounted against immediate-early and early lytic genes, though the response broadens to late and latent antigens with persistent infection (Hislop et al., 2002, Woodberry et al., 2005). A large amount of work has been done to define T cell responses during primary infection, though the majority of studies investigate symptomatic IM patients as these are easily identified as newly infected with EBV. Extremely high expansions of CD8+ cells specific to EBV lytic antigens have been reported in these patients, at 1-40% of the total CD8+ compartment (Catalina et al., 2001, Hislop et al., 2002, Pudney et al., 2005, Abbott et al., 2013). However, since IM represents an atypical pathology, it likely does not reflect T cell responses for the vast majority who acquire EBV in early childhood without symptomatic presentation. There have been a number of longitudinal studies that have tracked EBV-seronegative individuals through seroconversion to investigate T cell responses to asymptomatic primary infection. Two studies in children demonstrated very limited expansion of EBV-specific T cells and total CD8+ numbers over the course of asymptomatic primary infection, even with high EBV viral load (Silins et al., 2001, Jayasooriya et al., 2015). A further study in university students identified several individuals undergoing silent infection, with viral load as high as seen in IM patients, but with no changes to overall T cell compartment and a low frequency of EBV-specific T cells detected (Abbott et al., 2017). These results suggest only very small numbers of EBV-specific T cells are sufficient to both control EBV primary infection and develop into robust memory T cell responses without driving a substantial pathological response.

T cell responses in long-term healthy carriers are largely directed to the EBNA-3 antigens, although studies usually use LCLs to stimulate polyclonal T cell expansion *in vitro* which may bias the antigen-specific responses and therefore may not fully represent the frequencies within peripheral circulation (Murray et al., 1992). Nonetheless, there is a clear hierarchy of antigens that generate T cell responses, with EBNA-3 family as immunodominant and to a lesser extent EBNA-2 and LMP2, whereas EBNA-1 and LMP-1 have weak T cell responses. While the antigen specificity is also influenced by HLA type, the weak immune response to EBNA-1 and LMPs likely reflects an immune evasion strategy by which EBV is able to hide during the relevant

latency programs. Though EBV-specific T cell responses contract after primary infection, continued regulation of EBV-infected cells is attributed to a significant fraction (0.1-3%) of the circulating CD8+ memory T cell pool which is stable over the host lifespan (Hislop et al, 2007). The only virus that exceeds this memory T cell response in humans is CMV. Conversely, EBV-specific CD4+ T cell responses are approximately 10-fold lower than that of CD8+ T cells, and with specificity more broadly distributed across IE, E and L lytic antigens as well as the different latent antigens (Leen et al., 2001, Amyes et al., 2003, Long et al., 2011, Ning et al., 2011). The increased breadth of the EBV-specific CD4+ T cell response is thought to reflect the large range of antigens released by infected cells and processed by antigen-presenting cells, as well as antigen presentation by infected B cells themselves (Leung et al., 2013, Howley, 2022). Memory EBV-specific CD4+ T cells with a polyclonal repertoire are maintained throughout the host lifespan, with multifunctional effector responses through classic Th1 production of interferon-gamma (IFN-γ), tumour necrosis factor-alpha (TNF-α), and interleukin-2 (IL-2), primed ready to induce CD4 helper functions (Long et al., 2011, Ning et al., 2011, Cárdenas Sierra et al., 2014). There have also been reports of CD4+ T cells with capacity to directly lyse EBV-infected cells, so-called cytotoxic CD4+ T cells, though it is not known to what extent they play a role in the natural *in vivo* response to the virus (Long et al., 2005, Haigh et al., 2008, Choi et al., 2018).

1.2.8 Role of EBV in lymphoma

As previously discussed, EBV can be involved in a wide range of clinical conditions. EBV-associated diseases are broadly categorised into those of active lytic infection, autoimmune disorders, and malignancies (Damania et al., 2022, Huang et al., 2023). The role of EBV in epithelial cancers is out of scope of the current review which will focus on EBV lymphoproliferations, however pathogenesis of EBV+ epithelial transformations is comprehensively discussed by Low et al. (2023). How EBV is involved in autoimmune disorders is less clearly understood, though an interesting review by (Robinson et al., 2024) considers the current evidence and mechanistic theories. While clinical manifestations are clearly diverse; the diagnosis and classification of disease are largely determined by germinal centre expression of EBV lytic and/or latent antigens. Importantly, the EBV antigen expression as well as host immune responses are key in determining the optimal approaches for therapy.

For example, expression of the minimal spectrum of EBV latent antigens is considered the most difficult to treat because such associated lymphomas can develop in relatively immunocompetent individuals. It is suggested EBV-associated Burkitt lymphoma (BL) and Hodgkin lymphoma (HL) may arise from germinal centre B cells with latency I or II profile respectively, which get stuck in the cell cycle transition and consequently become malignant. The exact mechanism for this is currently unknown in HL, but it is inferred that high protein expression of LMP1 and LMP2 observed in all Reed-Sternberg cells (a clinical feature of HL) are involved in oncogenic transformation (Massini et al., 2009, Shannon-Lowe and Rickinson, 2019). EBV+ BL most frequently occurs in sub-Saharan Africa in regions endemic for malaria, where the higher number of germinal centre B cells responding to malaria may permit increased opportunity for chromosomal translocations within the c-myc oncogene (Münz, 2023). Consequent overexpression of c-myc is the major determinant of a highly proliferative BL phenotype, though EBV microRNAs expressed in latency I may drive enhanced anti-apoptotic signals increasing the potential for malignant transformation (Vereide et al., 2014). Furthermore, diffuse large B cell lymphoma (DBLCL) is the most common high-grade non-Hodgkin lymphoma globally, of which ~10% are EBV+ tumours. EBV+ DLBCL is usually of latency type II within relatively immune competent individuals, although can present with latency III in elderly or more immunocompromised individuals (Bourbon et al., 2021). The interaction between DLBCL and EBV is still poorly understood, though mutations in EBNA-3B have been identified in some cases (White et al., 2012). As a tumour suppressor gene, this may lead to increased risk of lymphoma development. EBV infection can also induce many different types of highly aggressive NK cell or T cell lymphomas usually of type II latency, though factors resulting in an NK cell/ T cell reservoir for viral persistence in these rarer cases are still largely unclear (Damania et al., 2022).

Why T cell immunity fails to control latency I or II tumour growth in these otherwise immunocompetent individuals is not fully understood, though clearly any arising tumours restricted to these few subdominant EBV antigens would have a competitive advantage through evasion of immune surveillance. Despite this, LMP-specific T cells are frequently detected in the blood of patients with latency II tumours (Chapman et al., 2001), though they can be at reduced frequency compared to healthy carriers. Numerous HLA alleles are associated with risk for the different EBV-associated malignancies, with implication that mutations in genes within the MHC region may

contribute to antigen-specific 'holes' in the T cell repertoire of such individuals (Taylor et al., 2015). The tumour microenvironment (TME) is also thought to play a major role in pathogenesis of these lymphomas. Particularly in HL patients, mechanisms have been observed whereby the TME inhibits immune infiltration (Chetaille et al., 2009, Barros et al., 2012), or recruits immunomodulatory cells which drive an immunosuppressive TME (Morales et al., 2014).

Conversely, tumours expressing the numerous type III latency EBV antigens are highly immunogenic, generally susceptible to T cell control, and therefore typically only develop to severe lymphomas in those with a compromised immune system.

1.2.9 Post-transplant lymphoproliferative disorder (PTLD)

As mentioned above, EBV can induce severe immunoblastic lymphoproliferations in immunocompromised individuals. Transplant patients are particularly at risk of developing EBV-induced PTLD since they are iatrogenically immunosuppressed to prevent graft rejection. Without the protective memory EBV-specific CD8+ T cell response, a primary infection or reactivation of EBV can rapidly develop into serious pathologies.

As an umbrella term for a spectrum of lymphoproliferative diseases developed following transplant, recent World Health Organisation (WHO) and International Consensus Classification (ICC) identifies six subclasses of PTLD characterised into two major types: non-destructive and destructive (Alaggio et al., 2022, Campo et al., 2022). Non-destructive PTLDs are further sub-classified into plasmacytic hyperplasia, infectious mononucleosis-like PTLD and florid follicular hyperplasia. These are non-malignant polyclonal lymphoproliferations with preserved lymph node architecture and are typically readily treated by reduction in immune suppression. Destructive PTLDs are more aggressive, and are subcategorised into polymorphic PTLD, monomorphic PTLD and classic Hodgkin lymphoma (cHL) PTLD dependent on lesion morphology and clonality. The different categories of PTLD and current typical clinical management is outlined in Table 1.4.

Lesion Type	EBV+ PTLD Category	Clonality	Typical Treatment
Non-destructive	Plasmacytic hyperplasia	Polyclonal	Most likely to respond to RIS or surgery.
	IM-like	Polyclonal	
	Florid follicular hyperplasia	Polyclonal	
Destructive	Polymorphic	Polyclonal	May respond to RIS. Often requires rituximab with or without chemotherapy.
	Monomorphic (DLBCL, BL, T cell/ NK-cell lymphomas)	Monoclonal	May respond to rituximab alone. May require multi-agent chemotherapy.
	Classic HL	Monoclonal	Requires multi-agent chemotherapy.

Table 1.4 - Classification of EBV+ post-transplant lymphoproliferative disorders.

Adapted from El-Mallawany and Rouce (2024). *BL, Burkitt lymphoma; DLBCL, diffuse large B cell lymphoma; HL, Hodgkin lymphoma; IM, infectious mononucleosis; PTLD, post-transplant lymphoproliferative disorder; RIS, reduced immunosuppression.*

Data from various transplant registries indicates overall incidence of PTLD varies between 1-25% following solid organ transplant (SOT) (Peters et al., 2018, Allen and Preiksaitis, 2019, Mark et al., 2024, Tajima et al., 2024) and between 1-16% following HSCT (Dierickx and Habermann, 2018, Fujimoto et al., 2019, Lee et al., 2021, Lindsay et al., 2021). These varied ranges are dependent on a multitude of risk factors including: donor and recipient EBV serostatus, transplant type, immunosuppression conditioning regimen, recipient age, degree of HLA-mismatch between donor and recipient, and development of GVHD.

The most significant risk for developing PTLD is in EBV-seronegative patients receiving an allograft from an EBV-seropositive donor and as such is more common in children (Kinzel et al., 2022). Paediatric EBV-seronegative patients have >70-fold increased risk of developing PTLD compared to that of EBV-seropositive children or adults (Cockfield, 2001, Dharnidharka et al., 2012). Interestingly reports have demonstrated maternal transfer of EBV-specific antibodies to infants which may protect against infection, however maternal antibody levels have found to decay within 6 months (Reynaldi et al., 2016). Therefore, it is suggested that EBV-seropositive donors <6 months old should be considered seronegative, since the serostatus of these donors doesn't reflect natural infection and have demonstrated negligible transmission of EBV to seronegative recipients (Mabilangan et al., 2020, Preiksaitis et al., 2024). This is an important exception when stratifying risk and donor selection for infant transplants, which are already so limited by size-matching constraints. Presence of other chronic viral infections such as cytomegalovirus and

hepatitis C are also risk factors for PTLD development (Lim et al, 2006). The type and intensity of immunosuppression post-transplant are independent risk factors, though assessment of particular immunosuppressive agents is challenging due to the common use of combination regimens. Regimes that include immunosuppressive agents that act against T cells confer a higher risk for EBV+ PTLD development, including T cell depleting antibodies and anti-thymocyte globulin (Landgren et al., 2009, Hoegh-Petersen et al., 2011, Asleh et al., 2019, Fujimoto et al., 2019, Salas et al., 2020). In addition, increased risk of developing EBV+ PTLD has been associated with homozygous expression of HLA-A1 in both the transplant recipient (Kinch et al., 2016) and organ donor (Zaffiri et al., 2020).

PTLD arising in SOT recipients are typically of recipient origin, although in EBV-naïve recipients the virus is acquired from the EBV-seropositive allograft (Swinnen et al, 2008). Tumours expressing type III latency are invariably of B-cell origin and develop in the first year post-transplant. The incidence of PTLD following SOT varies by the transplanted organ, with intestinal or pancreas transplants associated with highest risk (L'Huillier et al., 2019, Tajima et al., 2024).

PTLD developing after HSCT usually results from transplant donor B cells and appears within the first 6–12 months post-transplant, when profound deficiencies of host EBV-specific T cells are seen. In PTLD patients resulting from HSCT transplantation, significantly higher incidence was associated with pre-conditioning regimens involving total body irradiation as opposed to those without, as well as having an HSCT graft from a non-HLA-matched sibling donor (Kinzel et al., 2022).

1.2.10 Current treatments for EBV+ PTLD

Currently the first-line therapy for PTLD is reduction of immunosuppression (RIS), which allows partial restoration of the host EBV-specific T cell functionality. This therapy can be successful in some cases, though is limited by the subsequent potential risk of inducing graft rejection. Reduced immunosuppression is most effective in non-destructive early lesions, which may regress with RIS alone (Tsai et al., 2001). Use of RIS as a strategy for PTLD following SOT has been associated with 37% complete remission rate, a 17% relapse rate, and 32% incidence of graft rejection (Reshef et al., 2011). Therefore, if complete remission is not achieved within 2-4 weeks of RIS, or if disease progression or graft rejection occurs within this

window, other treatment strategies must be employed (Zaffiri et al., 2020). Furthermore, for PTLD following HSCT, RIS may not be possible to due high risk of fatal GVHD (Al Hamed et al., 2020), and rarely results in sufficient recovery of EBV-specific immunity to eradicate PTLD (Clerico et al., 2022).

Secondary lines of treatment usually involve singular or combinatorial use of anti-CD20 monoclonal antibody rituximab and chemotherapy regimens. Rituximab has demonstrated effective depletion of CD20+ B cells and as such can be used as a therapy for CD20+ PTLD. A large multicentre phase II trial of 148 CD20+ PTLD patients demonstrated 25% patients had sustained complete responses to rituximab monotherapy, and a further 37% achieved complete response with rituximab and subsequent chemotherapy (Trappe et al., 2017). A recent long-term study of real-world cohort patients receiving rituximab monotherapy out-with a trial setting demonstrated 38% complete response rate, with 87.5% of these patients sustaining disease-specific survival at 5 years follow-up (González-Barca et al., 2021). If complete response is not achieved with rituximab alone, current guidelines recommend four cycles of CHOP-21 chemotherapy (cyclophosphamide, doxorubicin, vincristine, and prednisone every 21 days) to clear any further malignant cells. Though combined rituximab with CHOP (R-CHOP) can be an effective therapy for CD20+ PTLD, chemotherapy is associated with significant toxicities, with a recent trial reporting 53% patients had CHOP-induced toxicity including grade 3/4 infections and acute renal failure (Zimmermann et al., 2022). Furthermore, while CD20+ PTLD represents ~75% of all PTLD cases (Orjuela et al., 2011, Zimmermann and Trappe, 2013), patients with CD20- PTLD or who are relapsed/refractory to R-CHOP have no current effective treatments (Atallah-Yunes et al., 2023). Surgery or radiotherapy can be utilised for the removal of localised PTLD tumours, though such cases are rare (Rossignol et al., 2015, Orlandi et al., 2021).

Despite the current treatment options, mortality remains estimated at 30-50% due to complications of treatment and refractory disease, with significantly higher rates in PTLD patients with extra-lymphatic involvement, older patients and those with established GVHD (Styczynski et al., 2013, Kinzel et al., 2022). Importantly, while novel therapeutics are being explored, there is a paucity of late-stage clinical trials due to PTLD rarity and massive disease heterogeneity. Moreover, randomised controlled trialling of investigational therapies against established standard of care is

unethical due to the aggressive nature and high fatality of the disease, therefore introducing improvements in treatment efficacy is very challenging.

1.2.11 Treatment of EBV+ PTLD with EBV VST

Immunotherapy using VST was first clinically used as prophylaxis or treatment of EBV-positive PTLD in the mid-1990s within the HSCT transplant setting (Rooney et al., 1995, Rooney et al., 1998, Gustafsson et al., 2000). For this initial strategy, blood was taken from the HSCT transplant donor to generate EBV VST *ex vivo,* which were then administered to the transplant patient as VST infusions. However, for PTLD patients resulting from SOT, EBV VST cannot be derived from the organ donor since there is generally no donor blood available. Therefore, EBV VST generated from the patient themselves were also investigated as an approach to treat PTLD in SOT recipients (Haque et al., 1998, Khanna et al., 1999, Savoldo et al., 2006). Patient-derived, or autologous cell therapies have the clear benefit of reduced risk of immune reactions or rejection when delivered back to the patient as compared to donor-derived allogeneic cell therapies. While autologous EBV VST therapy demonstrated tumour regression in some patients, the timescale to generate patient-specific EBV VST after diagnosis severely limited the potential delivery of this therapy, with many patients dying before infusion. Furthermore, the lengthy manufacture of autologous VST does not allow for the potential of this cell therapy as a prophylaxis, and high costs to generate patient-specific cells is impractical for scalable PTLD management. Additionally, it is more difficult or can be impossible to produce EBV VST from EBV-seronegative individuals, and who are consequently at higher risk of developing PTLD following a transplant. Finally it can be very challenging to isolate and expand T cells from patients who have undergone iatrogenic immunosuppression. Therefore in the early 2000s several groups developed cell banks of EBV VST derived from “third-party” otherwise healthy donors (i.e. not the transplant patient or recipient). Such allogeneic cell therapies could be manufactured and cryopreserved for long-term storage in liquid nitrogen, therefore allowing therapy delivery in an “off-the-shelf” manner rapidly following PTLD diagnosis. By making VST banks from a range of donors with wide-ranging HLA types, allogeneic cells with the best HLA match could be selected for each patient and thereby minimise risk of immune reaction to therapy.

The first multicentre phase 2 trial for administration of third party EBV VST to treat PTLD after SOT showed overall patient response rates of 64% and 52% at 5 weeks

and 6 months, respectively (Haque et al., 2007). Since then, other clinical studies have replicated successful results of safety and efficacy using third-party donor EBV VST for the treatment of relapsed or refractory PTLD as outlined in **Table 1.5**.

Reference	EBV+ PTLD Patients				Manufacturing Approach	Responses			TSAE
	Total	HSCT	SOT	NT		CR	PR	ORR	
Sun et al. (2002a)	2	0	2	0	LCL *ex vivo* expansion	1	1	75%	None
Haque et al. (2007)	33	2	31	0	LCL *ex vivo* expansion	14	3	52%	None
Barker et al. (2010)	2	2	0	0	LCL *ex vivo* expansion	2	0	100%	None
Uhlin et al. (2012)	1	0	0	0	Multimer selection BMLF1 & LMP2	1	0	100%	None
Vickers et al. (2014)	10	6	4	0	LCL *ex vivo* expansion	8	1	80%	None
Gallot et al. (2014)	11	9	0	2	LCL *ex vivo* expansion	3	1	44%	None
Chiou et al. (2018)	10	0	10	0	LCL *ex vivo* expansion	8	1	100%	None
Mika et al. (2019)	1	1	0	0	LCL *ex vivo* expansion	1	0	100%	None
Kazi et al. (2019)	59	28	20	11	LCL *ex vivo* expansion	23	12	59%	None
Prockop et al. (2020)	46	33	13	0	LCL *ex vivo* expansion	21	8	63%	1 GVHD
Jiang et al. (2022)	3	3	0	0	EBV consensus peptides stimulation & CD137 selection	3	0	100%	None
Bonifacius et al. (2023)	24	14	5	5	EBNA1 & EBV consensus peptides stimulation & IFN-γ selection	14	2	60%	None
Mahadeo et al. (2024)	43	14	29	0	LCL *ex vivo* expansion	12	10	51%	None
Wistinghausen et al. (2024)	15	0	15	0	LMP1 & LMP2-transduced LCL *ex vivo* expansion	4	4	53%	1 grade III CRS

Table 1.5 – Clinical studies using third-party EBV VST therapy of relapsed/refractory EBV+ PTLD

CR, complete response; CRS, cytokine release storm; GVHD, graft versus host disease; HSCT, haematopoietic stem cell transplant; LCL, lymphoblastoid cell line; NT, non-transplant; ORR, overall response rate; PR, partial response; SOT, solid organ transplant; TSAE, treatment-associated serious adverse event.

1.2.12 Methods to generate EBV VST

The initial method developed to generate EBV VST was by co-culture of EBV-immortalised LCL that express a wide range of EBV latent and lytic cycle proteins, with the same donor PBMC. Repeated stimulation allows presentation of EBV antigens expressed on LCL to T cells within the PBMC population, driving *ex vivo* expansion of EBV-specific clones. Conventionally this requires 6-12 week long stimulations with irradiated LCL (to prevent LCL outgrowth in culture) to induce EBV VST expansion into clinically relevant numbers. Once characterisation and functional evaluation is complete and when cultures are deemed sufficiently purified and specific for EBV, the products can be formulated into patient bagged doses and cryopreserved for long term storage in liquid nitrogen cell banks. The Scottish National Blood Transfusion Service (SNBTS) have generated two EBV VST banks using the LCL method. The first bank was made from 135 local Scottish donors and used to treat 74 patients in initial clinical studies (Haque et al., 1998, Haque et al., 2001, Haque et al., 2002, Wilkie et al., 2004, Wynn et al., 2005, Haque et al., 2007, Haque et al., 2010). Following regulatory changes to white blood cell products due to the new variant Creutzfeldt-Jakob disease (nvCJD) outbreak in the UK, a second bank was made from 25 New Zealand donors at low risk of nvCJD. This bank is still in clinical use and has been issued to >100 relapsed or refractory PTLD patients under a Medicines and Healthcare Regulatory Agency (MHRA) 'Specials' license (Vickers et al., 2014, Chiou et al., 2018, Kazi et al., 2019).

As can be seen in **Table 1.5**, the LCL *ex vivo* expansion method is still widely used as the approach to manufacture EBV VST for adoptive transfer therapy. However, this method requires lengthy and complex cell culture and carries the risk of using a live virus in the supernatant to establish LCL lines. Therefore, other methods and techniques have been developed to manufacture antigen-specific T cells for therapeutic use. Other approaches for the derivation of EBV-specific T cells include DC antigen presentation with *ex vivo* expansion (Gerdemann et al., 2013, Withers et al., 2017), multimer selection (Uhlin et al., 2012) and cytokine capture selection (CCS) (Moosmann et al., 2010, Icheva et al., 2013).

DC or other artificial APC can be loaded with peptides from the desired viral antigens, and used to present these antigens to relevant T cells for *ex vivo* expansion (Ngo et al., 2014). While similar conceptually to the LCL *ex vivo* expansion process, use of non-

infected or non-tumour cells as APC allows complete customisation of peptides, therefore making antigen-specific T cell products refined to individual peptide targets. This ability to tailor to antigens of choice has substantially progressed the development of T cell products specific to multiple viruses (Vasileiou et al., 2020). Adoptive transfer of multi-virus T cells offers a different approach by prophylactic administration to prevent the most common post-transplant viral infections (Dadwal et al., 2024).

Multimer selection allows isolation of HLA-epitope specific T cells from a mixed blood cell source of an EBV-seropositive donor. While this is a rapid manufacturing method, it is restricted by HLA type and can be difficult in donors with low frequency of the particular epitope-specific T cells (Bollard and Heslop, 2016). Also, since currently multimers are mainly available for HLA class I antigens, lack of HLA class II multimers and hence inability to isolate CD4+ antigen-specific T cells may have consequences on therapeutic efficacy (discussed further in **Section 1.3.1**).

Cytokine capture selection is another isolation methodology using peptides to stimulate PBMC from a seropositive donor (Campbell, 2003, Campbell et al., 2011). The functionally responsive antigen-specific memory T cells then secrete antiviral effector cytokines such as IFN-γ. These cytokine-secreting T cells can then be isolated by magnetic column enrichment. This method allows rapid purification of VST and a simpler isolation protocol through being unrestricted to HLA type. This approach also has the benefit in only selecting functionally active T cells capable of producing antiviral effector responses and therefore limits the potential for isolating functionally exhausted T cells in the cell product. SNBTS recently developed this technique to generate third party EBV VST for therapy using class I and class II-restricted peptide pools covering sequences for 15 different EBV lytic and latent antigens. A post-selection culture process was then optimised to expand the EBV-specific T cells isolated by CCS for up to 3 weeks to make clinically relevant numbers for therapy. Due to successful process optimisation and translation, a third bank of EBV VST was manufactured to GMP standards at SNBTS and has since been approved for clinical use in relapsed/refractory on a Specials compassionate use basis. Since the LCL and CCS approaches to EBV VST manufacture differ so much in methodology, it was the basis of this thesis to comprehensively compare processes and products in terms of factors important to adoptive cell therapy for PTLD patients.

1.3 Understanding what makes a good T cell therapy

Advances in approaches for cell therapy manufacture should always be considered against the potential improvements to safety and efficacy of the product. Following successful trials showing safety of VST products, a key focus of investigation is to elucidate how the infused cells contribute to clinical outcome in some patients, but not in others. It is tempting to speculate that clinical outcome is largely dictated by heterogeneous disease and clinical management of PTLD patients, however the T cell products should also be explored as a differential factor. To compare therapies, a broad range of assays should be utilised to characterise cell status, health, function and purity, as well investigating fundamental aspects of T cell biology. This section will focus on understanding what makes an effective T cell therapy in the context of allogeneic adoptive transfer for viral driven and/or cancerous diseases.

1.3.1 Roles of helper and cytotoxic T cells in adoptive transfer for viral diseases

Antigen-specific T cells are broadly classified into CD4+ helper T cells and CD8+ cytotoxic T cells. CD4+ T helper (Th) cells are then further categorised into Th subpopulations based on the effector cytokines they secrete. Currently, major CD4 subtypes include: Th1- important for intracellular antiviral and antibacterial immunity, Th2 - important for allergy responses and extracellular helminth infections; Th17 which mediate various antibacterial and antifungal responses and follicular helper (Tfh) cells which are important for maturation of B cell responses. Furthermore, regulatory T cells (Treg) also express CD4 and are crucial in controlling the immune response and mediating tolerance to self-antigens. A comprehensive analysis of the roles of different CD4 T cell subsets is reviewed in (Ruterbusch et al., 2020), however the present study will focus on cytotoxic CD8+ and CD4 Th1 cells which drive antiviral and antitumour responses.

The main role of cytotoxic CD8+ antigen-specific T cells is to directly lyse target virally-infected cells or tumour cells. Following antigen-MHC recognition by cognate TCR, CD8+ T cells secrete granules containing cytotoxic enzymes perforin and granzymes, a process known as degranulation. Perforin is a pore-forming protein creating holes in the target cell membrane, which then allows granzymes to enter the target cell and trigger it for apoptosis. In this way, CD8+ T cells elicit highly specific

target lysis by killing the cell from the inside and limiting damage to neighbouring cells. Both CD8+ and Th1 CD4+ T cells are defined by their effector functionality to secrete pro-inflammatory cytokines IFN-γ, TNF-α and IL-2.

For the purposes of adoptive cell transfer to treat viral infections and/or tumours, it is clear that cytotoxic immune cells are crucial to effectively kill the targeted pathogenic cells. While CD4+ T cells have proven crucial to the support and survival of memory CD8+ virus-specific T cells in natural host responses (Novy et al., 2007), it is unclear whether CD4+ T cells are required to maintain clinical responses in adoptive T cell therapies.

An initial study of gene-marked allogeneic EBV VST adoptively transferred to HSCT patients demonstrated both CD4+ and CD8+ populations of the infused T cells persisted and expanded in vivo up to 11 months (Heslop et al., 1996). In another study of VST adoptive transfer after HSCT, CMV-specific CD8+ T cell clones demonstrated poor persistence without additional CD4+ CMV-specific T cell helper responses (Peggs et al., 2003). Furthermore, in the SNBTS phase II trial testing third-party EBV VST for refractory PTLD patients, a significantly higher number of patients had clinical responses lasting at least 6 months when infused with lines with a higher percentage of CD4+ T cells as compared to those containing <1% CD4+ T cells (Haque et al., 2007). These results loosely correlate a clinical benefit with the presence of CD4+ cells within adoptive T cell products, though without direct comparisons in trials the effect of CD4:CD8 content is hard to delineate. Interestingly, even cases where EBV VST products predominantly composed of CD4+ T cells (>50%), rather than CD8+ T cells, these have produced similarly effective clinical responses to the usual CD8-skewed T cell products (Leen et al., 2013, Prockop et al., 2020). No statistical correlations between CD4 to CD8 ratio were seen in these studies, though this was likely limited by small and heterogeneous patient cohorts. Whether the clinical responses seen in these cases was still principally driven by the few CD8+ T cells present in the products that then expanded *in vivo*, or whether the large numbers of infused CD4+ T cells indirectly mediated tumour killing is unclear. There is also the possibility that CD4+ T cells within these products were able to directly lyse target cells themselves as the lesser defined population of cytotoxic CD4+ T cells. While the exact roles by which adoptive transferred T cells elicit efficacious and prolonged tumour remission is still poorly understood, it is crucial to

comprehensively characterise the effector roles and capacities of CD4+ and CD8+ populations present in T cell products to track correlates of clinical responses.

1.3.2 T cell memory and adoptive T cell persistence

Increasingly in the field of T cell immunotherapy, clinical outcomes have been limited by recurrence relapse of the tumour a significant time after initial treatment. Central memory T cells have an established heightened capacity for proliferation compared to effector T cells which are further down the differentiation process. Therefore, it is often conjectured that central memory T cells would be the most desirable for adoptive transfer therapy due to the increased ability for clonal expansion and consequently longer persistence in the patient, therefore potentially preventing relapse. Supporting this model, adoptive transfer of CMV-specific T cells demonstrated improved survival and expansion *in vivo* following adoptive transfer to CMV+ macaques when derived from enriched central memory than effector memory cells (Berger et al., 2008). Improved engraftment and tumour response was also seen using central memory-derived CMV-specific T cells transferred into immunodeficient mouse models when compared to effector memory-derived cells (Wang et al., 2011). Another study demonstrated that sorted central memory antigen-specific T cells adoptively transferred to a melanoma mouse model had 3 log-fold higher expansion in the circulation at 21 days post-infusion than non-sorted controls (Kueberuwa et al., 2017). In addition, the high proliferative capacity of central memory T cells also resulted in enhanced tumour clearance in melanoma transgenic mice compared to effector T cells which were far less successful in controlling large tumours (Klebanoff et al., 2005).

While persistence of adoptive T cell therapies can be difficult to track in human trials, one clinical study used a retroviral vector to gene-mark EBV-specific T cells prior to allogeneic transfer to HSCT patients for prophylaxis of PTLD (Heslop et al., 2010). Gene-marked T cells were detected in 18/26 patients at 7 years post-infusion, with these cells maintaining anti-EBV functionality in LCL co-culture assays. While characterisation of the lines prior to infusion indicated 10-20% cells had central memory phenotype, the long-term persistence *in vivo* and sustained clinical responses indicate even a small number is sufficient to enter the memory pool and provide long-lived protection. Therefore, phenotypic characterisation needs to be

utilised to characterise central memory and effector populations in therapeutic T cell products to provide insights on potential functional persistence in patients.

1.3.3 T cell trafficking, migration and infiltration

Adoptive transfer of cellular therapies relies on the ability of the administered cells to reach and function within sites of disease. T cells, and lymphocytes in general, have sophisticated migratory mechanisms that are integral to their development, trafficking between peripheral blood and lymphoid organs, as well as extravasation into inflammatory tissue. These migratory and surveillance mechanisms are facilitated by expression of chemokine ligands and receptors.

Chemokines are a family of chemotactic cytokines that are secreted at sites of inflammation, wound healing and tumour formation. They are recognised by chemokine receptors expressed on both innate and adaptive immune cells, thereby facilitating the migration of cells to sites of infection or injury and orchestrating the immune response and/or modulatory mechanisms. Chemokine ligands are classified into four subfamilies (CC, CXC, XC and CX3C) according to location of cysteine residues within their sequence (Murphy et al., 2000), which are crucial in forming the overall quaternary structure and ligand binding affinity to corresponding chemokine receptors. Chemokine receptors are 7-transmembrane G-protein coupled receptors (GPCRs) also classified into subfamilies based on the structure of the ligands they bind, with an additional family called ‘atypical’ chemokine receptors (ACKR) which are silent due to their inability to couple G proteins. In this way ACKRs are thought to modulate the signalling activating of nearby chemokine receptors by scavenging available chemokine, transporting chemokine through a polarised cell, and/or forming multimers with other chemokine receptors (Bonecchi and Graham, 2016).

Chemokine ligand binding to receptor in most cases is not exclusive, as many chemokine receptors have high promiscuity of ligands they bind and equally chemokine ligands often bind multiple receptors. In addition, chemokine biology becomes very complex due to a multitude of factors which influence chemokine-induced intracellular signalling pathways including: ligand binding affinity, cell type on which the chemokine receptor is expressed, potential formation of homo- or hetero-multimeric receptor structures, different G or other proteins, post-translational modifications and whether surrounding tissue is inflammatory or in

homeostasis (Hughes and Nibbs, 2018). Overall, the high degree of complexity of parameters allows for an extremely sophisticated, time-coordinated and networked immune response.

In context of the present study, it is clear infused EBV VST must be able to reach disease site(s) and sufficiently infiltrate into the PTLD tumour in order to achieve a clinical response. However not all PTLD patients achieve responses with EBV VST, therefore differential ability of the infused T cells to localise to the tumours should be considered. While clinical studies able to track transferred EBV VST within the patient between blood and tissues are lacking, we can infer potential chemotactic axes involved by investigating other EBV+ lymphomas. Such tumours have been reported to exhibit differential expression of chemokines and chemokine receptors dependent on EBV latency, which contribute to the overall tumour microenvironment and likely mediate the evasion of immune cell recruitment.

For example, Reed-Sternberg cells of EBV+ HL tumours have been found to secrete chemokine ligands CCL17 (van den Berg et al., 1999, Beck et al., 2001) and CCL22 (Maggio et al., 2002). The receptor for these ligands (CCR4) is expressed on T helper cells and regulatory T cells, and absent on effector cytotoxic CD8+ T cells, indicating a mechanism by which the tumour microenvironment simultaneously attracts immunomodulatory cells and evades anti-tumour responses (Marshall et al., 2004). Chimeric Antigen Receptor (CAR) T cells genetically modified to express CCR4 were found to show enhanced migration to HL tumour cells *in vitro* and improved migration to CD30+ engrafted tumours in SCID mice (Di Stasi et al., 2009).

In EBV+ Burkitt lymphoma biopsies, tumour cells were found to have barely detectable expression of CCL17 compared to EBV+ LCL which had a high protein level of CCL17 (Kanamori et al., 2004). Expression of CCL17 was found to be induced by EBNA-LP in EBV-infected cell lines, and as such could be a further mechanism by which EBV latency III tumours do not evade T cell infiltration in immunocompetent individuals. In contrast, EBV+ BL lines secreted significantly higher concentrations of CCL3 and CCL22 compared to both EBV-uninfected B cells, and EBV+ latency III tumour cells (Miyauchi et al., 2011). High specific expression of these chemokines by BL tumours has been suggested as a potential EBV-induced immunosuppressive pro-tumour strategy through recruitment and retention of regulatory T cells to the

tumour site. In addition, high expression of CCR1 but negligible levels of CCR2, CCR3 and CCR5 have been observed in EBV+ LCLs and rare EBV latency III-expressing BL tumours as compared BL tumours expressing EBV latency I or II antigen profiles (Zvejniece et al., 2022). This suggests one or more of the EBV latency III genes induces B cell expression of CCR1, contributing to the immunogenic profile of EBV latency III cells. Furthermore, since the numerous chemokine ligands of CCR1 are abundantly secreted in SLO, potential migration of EBV+ latency III B cells to SLO may be involved in the disease pathogenesis and/or immune cell clearance of tumours in these locations.

The human CCR5 receptor has famously been associated with HIV-1 entry into T cells following the observation that individuals with a 32-base pair loss-of-function deletion in the CCR5 gene ($CCR5^{\Delta 32}$) renders these individuals resistant to HIV infection (Gupta et al., 2019). Though only reported in a relatively small cohort study (Bogunia-Kubik et al., 2007), the $CCR5^{\Delta 32}$ mutation significantly correlated with fewer carriers exhibiting EBV reactivation post-HSCT (2/17 patients), compared to much higher incidence of EBV reactivation in those lacking the mutation (34/75 patients). Further to this, CCL3 and CCL4 (ligands of CCR5) have been found to be significantly upregulated in PTLD patient tumour cells induced by EBV LMP1, with markedly higher CCL3 concentration in patient plasma (Tsai et al., 2013b).

Better understanding of the chemokine and receptor profile of manufactured EBV VST and target tumour cells may provide insight to mechanism by which adoptively transferred cells can elicit a profound anti-tumour response in PTLD patients. Additionally, specific upregulated chemokine ligands in other EBV+ tumours could be targeted using EBV VST with modified expression of particular chemokine receptors.

1.3.4 T cell clonal repertoire

Effective T cell responses to combat infection or malignant growth depend upon a highly diverse TCR repertoire able to recognise a wide range of antigens. Following T cell development in the thymus, the TCR repertoire is shaped by natural selective pressures and gradual immune senescence throughout the aging process (Porciello et al., 2022). In terms of chronic viral infections, repeated stimulation by different antigens as well as viral evasion mechanisms can select specific T cell clones for expansion, resulting in refinement of the TCR repertoire. Arguably it is likely the

presence and expansion of particular clonotypes that underpins the differences of T cell-mediated immunity between those able to naturally resolve infection versus individuals that progress to severe disease. Therefore, it is fundamental within the immunotherapy field to be able to analyse the TCR repertoire of immunocompetent and immunodeficient individuals and monitor longitudinal T cell dynamics upon disease pathogenesis and/or therapeutic interventions.

Significant advances in sequencing and computational techniques in recent years have enabled analysis of the highly diverse and complex TCR repertoire. Since the complementary determinant region 3 (CDR3) of the TCRβ chain is unique to each clonal population, deep sequencing of this region can be used both to track specific T cell populations as well as measure T cell clonal diversity (Joshi et al., 2022). Obtained CDR3 sequences can be analysed by various bioinformatics algorithms to: match to known epitopes uploaded to TCR databases, measure sequence similarity to indicate shared pMHC specificity, and calculate entropy indices of diversity to measure the number of unique TCRs and their abundance within a repertoire (Chiffelle et al., 2020). High-throughput bulk TCRβ sequencing has been validated to detect an individual TCR clonotype within a polyclonal T cell population with a limit of detection of about 1 in 100,000 (i.e. 0.001%) allowing sensitive recognition of rare clones (Robins et al., 2012). Such applications can be utilised to both monitor host T cells to any given antigen(s) in the context of health and disease and to track infused T cells incorporation into the patient immune repertoire.

One study investigating transfer of autologous tumour-specific T cells to treat metastatic melanoma observed persistence of adoptive T cells at 40 days post-infusion in 10/10 (100%) patients receiving polyclonal products, however only 2/10 (18%) receiving monoclonal products (Chapuis et al., 2017). The enhanced persistence in polyclonal T cell populations was also associated with more patients achieving complete responses, indicating diverse clonal T cell populations expand more effectively in the patient repertoire for continued tumour remission. In a more recent study, Keller et al. (2019) used NGS to sequence the TCRβ chain to track a multi-virus VST product (targeting ADV, CMV, and EBV) delivered to immunocompromised HSCT patients. Though difficult to draw conclusions from a small cohort and differential viral diseases, higher T cell clonal diversity was associated with greater control of CMV viremia. This may suggest broad coverage of T

cell clones is beneficial for effective reconstitution of the patient repertoire and to prevent viral epitope or development of tumour escape clones. Furthermore, a positive correlation between repertoire diversity of autologous EBV VST therapy and long-term survival was observed in EBV+ NPC patients (Wang et al., 2021). A case study of an HSCT patient also showed increasing numbers of different CD4+ and CD8+ clonotypes in the peripheral blood up to 4 months following allogeneic EBV VST transfer with concurrent decline of EBV viremia, indicating reconstitution of diverse clones contribute to control of the viral reactivation (Lin et al., 2013).

While these studies have indicated more clonally diverse T cell products have induced better therapeutic responses, it is likely the importance of clonal diversity is highly dependent on the disease context and immune evasion mechanisms by the particular virus/tumour. Therefore, TCR repertoire analysis should be utilised to build up a more complete understanding of how clonal diversity impacts on T cell therapy efficacy for different diseases. In the case of EBV-driven PTLD, it is also vital to characterise the dominant clonotypes required to target EBV+ latency III tumours in immunocompromised patients.

1.3.5 T cell inhibition and exhaustion

Following inflammatory signalling, activated T cells need to be downregulated once a pathogenic challenge has been overcome. Furthermore, whilst peptide-MHC complex stimulation efficiently orchestrates targeted inflammatory responses against malignant or pathogen-infected cells, responses must be tightly regulated to prevent inappropriate triggering of T cells causing bystander damage. Therefore, the immune system has evolved various mechanisms to keep T cell responses in check, namely the upregulation of immune inhibitory receptors (otherwise known as immune checkpoints) induced by chronic antigenic stimulation or inflammation. From current understanding, the most commonly recognised inhibitory receptors upregulated in activated T cells include cytotoxic T-lymphocyte-associated protein 4 (CTLA-4), lymphocyte-activation gene 3 protein (LAG-3), programmed cell death protein 1 (PD-1), T cell immunoglobulin and mucin domain-containing protein 3 (TIM-3) and T cell immunoreceptor with Ig and ITIM domains (TIGIT).

LAG-3, also classified as CD223, is a transmembrane glycoprotein that binds canonical ligand MHC-class II, and has been suggested to bind additional ligands including

galectin-3 (Gal-3)(Kouo et al., 2015), fibrinogen-like protein 1 (FGL1)(Wang et al., 2019), liver and lymph node sinusoidal endothelial cell C-type lectin (LSECtin)(Xu et al., 2014), α-synuclein preformed fibrils (α-syn PFF) and the TCR-CD3 complex. The cytoplasmic tail of LAG-3 contains highly conserved EP, KIEELE and FxxL amino acid sequences which exert inhibitory functions. The EP motif induces local acidification of the cytosol as well as sequestering of Zn^{2+} cations which causes tyrosine kinase p56 (Lck) dissociation from CD4 or CD8 co-receptors, which prevents zeta-chain-associated protein kinase (ZAP) 70 phosphorylation and ultimately limits TCR signalling (Guy et al., 2022). While an initial study indicated KIEELE was essential for blocking IL-2 production thereby inhibiting T cell proliferation (Workman et al., 2002), a later study that deleted the KIEELE motif did not corroborate this finding (Maeda et al., 2019). Consequently, the role of the KIEELE motif, as well as the FxxL motif, is still undefined (Aggarwal et al., 2023). The LAG-3 pathway is terminated by the cleavage of the extracellular domain of LAG-3 by A disintegrin and metalloproteinase domain-containing proteins (ADAM) 10 and 17. The resultant product of LAG-3 shedding, soluble LAG-3 (sLAG-3) has been explored as potential biomarker of immune responses in the cancer setting, though there are conflicting reports on whether this leads to a better or worse prognosis (Li et al., 2018, Pan et al., 2023, Malinga et al., 2022, Ueda et al., 2024).

TIM-3 was first identified as an inhibitory receptor that regulates IFN-γ-producing T cells (Monney et al., 2002). However, it has also been shown to be expressed on regulatory T cells (Gao et al., 2012), NK cells (Ndhlovu et al., 2012), mast cells (Phong et al., 2015), macrophages, DC (Anderson et al., 2007), and B cells (Bod et al., 2023). As the name suggests, TIM-3 consists of an extracellular immunoglobulin variable domain and mucin stalk, and a transmembrane domain and cytoplasmic tail to transmit intracellular signalling. Ligands for TIM-3 including galectin-9 (Gal-9), phosphatidylserine (PtdSer), high mobility group box-1 (HMGB-1) and carcinoembryonic antigen-related cell adhesion molecule-1 (CEACAM-1); binding at different regions of the immunoglobulin domain to induce inhibitory functions (Wolf et al., 2020). In resting cells, TIM-3 resides within the cell membrane, and upon TCR stimulation is recruited to the immunological synapse (Clayton et al., 2014). Although inhibitory signalling motifs have not been fully elucidated, it is indicated that two tyrosine residues within the cytoplasmic tail (Tyr256 and Tyr263) mediate interactions with HLA-B-associated transcript-3 (BAT-3) which functions to recruit

Lck (Rangachari et al., 2012). Upon ligand binding, phosphorylation of Tyr256 and Tyr263 causes BAT-3 to dissociate from the TIM-3 cytoplasmic tail, thereby inhibiting Lck promotion of TCR signalling (Clayton et al., 2014). Furthermore, Src family tyrosine kinase (Src-FYN) also binds the cytoplasmic tail at the same region as BAT-3, and is thought to potentiate inhibitory signalling through competition of TIM-3 (Lee et al., 2011). TIM-3 can also be cleaved into soluble form (sTIM-3), which is again thought to be a regulatory mechanism of the inhibitory pathway (Möller-Hackbarth et al., 2013).

TIGIT also consists of an extracellular immunoglobulin variable region, a transmembrane domain, and cytoplasmic tail which contains immunoreceptor tyrosine-based inhibitory (ITIM) and immunoreceptor tail tyrosine (ITT) motifs important for modulatory mechanisms (Yu et al., 2009). TIGIT is mainly expressed on lymphocytes including activated T cells, regulatory T cells, NK cells (Stanietsky et al., 2009), and B cells (Xiao et al., 2020b); although recent data suggests TIGIT can be upregulated on innate immune cells in different disease contexts (Brauneck et al., 2022, Yamada et al., 2023). Few ligands have thus far been identified to bind TIGIT, including highest affinity to poliovirus receptor (PVR, also classified as CD155); and with lower affinities to PVR ligands 2 (CD112) and 3 (CD113). In T cells, TIGIT is thought to exert inhibitory effects by competitively binding shared ligands with co-stimulatory molecule CD226 (Jantz-Naeem et al., 2023). When bound to its associated ligands CD155 or CD122, CD226 activates to bind lymphocyte function-associated antigen-1 (LFA-1) (Shibuya et al., 1999), an integrin that facilitates T cell priming, migration and cytotoxicity (Gérard et al., 2021). Competitive ligand binding by TIGIT, as well as ability to directly bind CD226 in *cis*, prevents CD226 homodimerisation thereby inhibiting T cell co-stimulatory functions (Johnston et al., 2014). While intrinsic mechanisms of the ITIM and ITT motifs to deliver inhibitory signals within NK cells have been identified, T cells with TIGIT forms mutated at these motifs induced inhibitory effects similar to TIGIT WT indicating this domain is not essential for T cell inhibition (Banta et al., 2022).

CTLA-4 is another inhibitory receptor with characteristic immunoglobulin variable-like domain. As the name suggests it was discovered on cytotoxic T lymphocytes (Brunet et al., 1987), and is well-known to suppress immune responses through expression on activated T cells and regulatory T cells (Read et al., 2006, Jain et al.,

2010). However, further reports of expression on NK cells (Lougaris et al., 2018, Stojanovic et al., 2014) and B cells (Yang et al., 2021), suggest CTLA-4 can also play a mediatory role on lymphocytes other than T cells. The inhibitory role on conventional T cells is mediated through competitive binding of CTLA-4 ligands to T cell co-stimulatory receptor CD28 (Krummel and Allison, 1995). As described previously, following TCR-pMHC binding, co-stimulation through CD28 is required to fully activate T cells. Binding of CD28 to B7 molecules CD80 or CD86 expressed on APCs induces T cell production of anti-apoptotic protein Bcl-X (Boise et al., 1995) and T cell proliferation cytokine IL-2 (June et al., 1987) to promote antigen-specific T cell expansion. On naïve T cells CTLA-4 is sequestered within intracellular clathrin-coated vesicles and is rapidly trafficked to the cell membrane upon T cell activation (Lindsten et al., 1993). The extracellular domain of CTLA-4 has higher affinity to CD80 and CD86 than that of CD28 and therefore can out-compete CD28 in co-stimulatory functions (Collins et al., 2002). Additionally, phosphorylation of the intracellular YVKM motif in the cytoplasmic tail of CTLA-4 induces recruitment of SH2-containing inositol 5'-phosphatase-2 (SHIP-2). While the direct role of SHIP2 in CTLA-4 signalling is not fully understood, it is thought to induce dephosphorylation of the CD3 zeta chain and linkers for activation of T cells (LAT) to inhibit TCR-complex activation. Although numerous mechanisms for CTLA-4 intracellular signalling on downstream pathways have been suggested, repeatedly-tested chimera experiments have demonstrated CTLA-4-deficient T cells have the standard resting phenotype rather than a hyperactivated phenotype (Bachmann et al., 2001, Homann et al., 2006, Read et al., 2006, Chikuma and Bluestone, 2007, Friedline et al., 2009, Tai et al., 2012). Even under challenge with various viral stimuli, CTLA-4-deficient and wildtype T cells had identical TCR repertoire selection, antigen-induced clonal expansion, memory formation, effector functionality and maintained secondary responses (Homann et al., 2006). This has caused debate as to the role and importance of CTLA-4 intracellular signalling, with evidence suggesting that CTLA-4 primarily elicits T cell inhibition in a cell-extrinsic manner (Walker, 2017).

Programmed death-1 (PD-1), also known as CD279, similarly contains an extracellular immunoglobulin variable-like domain, transmembrane domain, and cytoplasmic domain containing two tyrosine signalling motifs (ITIM, and immunoreceptor tyrosine-based switch motif (ITSM)) that mediate inhibitory functions. Initially discovered to be preferentially expressed on apoptotic cells (Ishida

et al., 1992), subsequent studies by the same group found PD-1 expression was induced through antigen-stimulated signalling on T cells and B cells (Agata et al., 1996). Though constitutively expressed on DN thymocytes during TCR rearrangements (Nishimura et al., 1996), inducible expression of PD-1 following activation has been reported on T cells, B cells, NKT cells, monocytes and DC. PD-1 binds two known ligands, PD-L1 and PD-L2, further members of the B7 family. PD-L1 is broadly expressed on many haematopoietic, non-haematopoietic, and malignant cell types, and is dependent on the inflammatory milieu for regulation (Boussiotis, 2016). PD-L2 has three-fold higher affinity for binding PD-1 compared to PD-L1 (Butte et al., 2007) and expression is limited to B cells, DC, macrophages and mast cells (Bardhan et al., 2016). Following T cell activation, PD-1 interactions with its ligands cause phosphorylation of the intracellular tyrosine motifs which induces recruitment of SHIP-2, with mutagenesis studies suggesting the ITSM motif is essential for inhibitory effects to the BCR (Okazaki et al., 2001) or TCR (Chemnitz et al., 2004). Engagement of SHIP-2 proximal to TCR-CD3 complexes inhibits major mediators of TCR signalling including CD3-zeta (CD3ζ), protein kinase-C-theta (PKC-θ) and ZAP70.

Signalling initiated by the different inhibitory receptors often overlaps with the same pathways, and therefore co-expression of these receptors can have an accumulative inhibitory effect. For example, CTLA-4 and PD-1 can both induce modulatory functions through inhibition of serine/threonine kinase Akt through targeting of different upstream mediators (Parry et al., 2005). Additionally, LAG-3 and TIM-3 can both cause dissociation of Lck from the CD4 and CD8 co-receptors to dampen downstream TCR signalling. While synergy in inhibitory pathways has been suggested as a potential redundancy mechanism, it is more likely the repertoire of negative regulators is vital to ensure a fine-tuned modulation of T cells to balance between infection/cancer control and development of autoimmunity disorders (Schnell et al., 2020).

Due to the presence of alternative inhibitory receptors able to act by synergistic and disparate mechanisms, inhibitory receptors have been likened to operate by ‘volume control’, whereby overall inhibitory effect is dependent on the cumulative strength of inhibitory signals relative to activation signals within a certain timeframe (Rumpret et al., 2020). Several immune checkpoint blockade (ICB) monotherapies have been

tested in late-stage trials for various cancers as reviewed in (Coschi and Juergens, 2023), however trials using combination ICBs have shown improved anti-tumour responses (Curigliano et al., 2021, Tawbi et al., 2022, Madariaga et al., 2023, Bishnoi et al., 2024). With combination therapies targeting multiple stimulatory/inhibitory receptors as well as the tumour microenvironment, it may be possible to reverse aspects of T cell exhaustion and regain endogenous effector T cell functionality (Schnell et al., 2020, Giles et al., 2023).

The T cell exhaustion phenotype was first described in mice infected with chronic lymphocytic choriomeningitis virus (LCMV). This study identified activated T cells that persisted in the host but were unable to elicit effector functions, which the authors described as "Sisyphean CD8 T cells, engaged in a continual and ineffective effort much like the Greek king Sisyphus" (Zajac et al., 1998). A hierarchical model of T cell differentiation has been proposed, whereby at early stages of exhaustion loss of IL-2 production dampens T cell proliferative capacity, and at later stages, cells lose degranulative capacity, ability to produce TNF-α and finally IFN-γ (Wherry and Ahmed, 2004). Given the consequences of a loss of functionality, it is crucial to assess stages of T cell differentiation/exhaustion to determine whether a T cell therapy has sufficient capacity to induce therapeutic effector responses. To this end, expression of numerous inhibitory receptors coincident with functional assays should be investigated to profile exhaustion status of T cell therapies (Blank et al., 2019).

1.3.6 Factors important to T cell therapy manufacture

Alongside more advanced characterisation to assess the quality of cell therapies, there is continuous drive to improve the bioprocess manufacture of cellular products. Clinical manufacture of allogeneic T cell therapies requires generation protocols that are optimised for safety, quality, scalability, expense, and duration of production. All resources, materials, and processes must also be compliant to current Good Manufacturing Practice (GMP) standards as per the relevant UK regulatory body for production of Advanced Therapeutic Medicinal Products (ATMP).

A major limiting factor for the generation of T cell therapies to treat viral infections is the requirement of large cell numbers for the treatment, usually around 1-2x10^7 cells/kg for a patient dose, with several doses needed per regimen. In attempts to scale manufacture, bioreactors have been developed that provide mechanical stirring

and medium/ gas exchange to maximise cell proliferation in culture. While bioreactors have successfully cultured non-specific T cells, antigen-specific T cells have proven difficult to grow in these devices (Foster et al., 2004, Hollyman et al., 2009). Such failures are attributed to the inability of antigen-specific T cells to consistently adapt in moving cultures, as well as the requirement of close interactions with APC to drive clonal outgrowth which is limited in large-scale bioreactor systems (Ganeeva et al., 2022). More recently, gas-permeable rapid expansion (G-Rex) culture vessels have been developed by Wilson-Wolf which significantly improve T cell expansion compared to standard culture flasks, as such currently dominate the market in T cell therapy production (Gagliardi et al., 2019, Gotti et al., 2022). In the G-Rex flasks, cells rest on a large surface area silicone gas-permeable membrane at the base of the flask. This allows improved gas exchange and a greater volume of culture medium than the restricted depth in standard flasks, therefore providing more nutrients to the cells as well as diluting waste metabolites (Forget et al., 2016). Additionally, since the G-Rex flask is positioned vertically, the majority of media can be removed and replaced without disrupting the cells at the bottom of the flask. The G-Rex has been shown to expand cell populations from approximately $5x10^5$ cells/cm^2 to $30x10^6$ cells/cm^2 in 1 to 10 days of culture without the need for splitting or medium replacement. Therefore, these flasks facilitate a simplified protocol with fewer cell manipulations, thereby improving the consistency of cell populations between cultures, limiting contamination risk, limiting T cell exhaustion due to excessive passaging. Advances in selection and culture systems have also resulted in improved integration of closed-process manufacture between platforms, which is vital for complex generation protocols.

While the consideration of production costs in development of these salvage therapies for patients with no other treatment options is distasteful, it is of course crucial for the viability of adoptive cell therapy development. With state-of-the-art technology and advanced biology techniques come equivocally high costs for incorporation into cell therapy manufacturing. All materials and consumables used must be tested, validated and approved for clinical cell manufacture, and any final formulations validated for human administration. In addition to price of materials for the actual manufacture, there are considerable costs associated with use of clean room facilities, requirement for specialist translational and production scientists, and of the breadth of QC testing required for release of the final products for clinical use.

If, after years of development a cell therapy product is successfully manufactured, the cost of testing through clinical trials can be prohibitively expensive. Such challenges mean that very few ATMPs have been successfully translated from bench to bedside, often referred to as the "valley of death" in the cell therapy field (De Luca and Cossu, 2023). To recoup the costs of development and manufacture, companies demand very high starting prices for these therapies, usually in the region of £50,000 to £500,000 per patient treatment (Sainatham et al., 2024). Such prices can then restrict access to therapy between different healthcare systems, insurance and regional boards. Crucially, cell therapy manufacturing processes should be carefully refined to reduce costs and maximise cell yields, thereby driving down patient treatment prices. Therefore, in addition to comparison of our EBV VST products on the basis of quality and functional characterisation, the manufacturing processes will also be compared in cost-effectiveness to deliver multiple patient treatments.

1.4 Aims of thesis

It was the overall aim of this thesis to comprehensively profile virus-specific T cell therapies developed at SNBTS to characterise product identity, quality, and functionality. Manufacturing and characterisation processes were also evaluated in terms of safety, practicality and potential therapeutic benefits.

Principal Areas of Investigation:

(A) Molecular and Phenotypic Analysis

Initial aims were to undertake a deep molecular and phenotypic analysis to compare EBV VST products derived from both LCL and peptide stimulation. Using flow cytometry and TaqMAN qPCR, VST were assessed for expression of lymphocyte markers, T cell memory markers, chemokine receptors, differentiation transcripts and senescence markers both at rest and upon antigen recall.

(C) TCR Repertoire Analysis

Due to differential antigenic stimulation, it was hypothesised there may be disparities in clonal selection, diversity and EBV specificity between T cells generated using the LCL versus CCS method. LCLs classically express mainly latent viral epitopes, whereas

EBV VST derived from LCL stimulation have been found by other groups to respond to epitopes predominantly on EBNA-3A, B and C proteins. Use of an EBV consensus peptide pool by the CCS method may generate T cells with different dominant responses. Therefore, bulk next-generation sequencing of TCRβ chain was used to dissect the clonal repertoire present in LCL-derived and CCS-derived VST products. Assessment of TCR clones and repertoire diversity allowed comparisons between the manufacturing processes, as well as evaluation of donor variation. In addition, identification of epitope-specific clones within products may indicate product suitability to target other EBV-related disorders where viral antigen expression is limited to subdominant proteins.

(C) Functional Analysis

Following the genetic and transcriptional profile, key factors involved in VST response were determined through T cell functional assays. To assess effector functions, T cells were tested in viral challenge assays to measure expression of degranulation markers, antiviral cytokines and T cell activation markers. Furthermore, ability to recognise and lyse infected target cells was evaluated using dose-escalation cytotoxicity assays. Products were also analysed for specificity to individual viral antigens, as well as off-target responses using the relevant functional assays.

(D) Translation of Methods

Using the manufacturing, phenotyping and functional assays developed in this study for EBV VST, it became an additional aim to test application of these methods to other virus-specific T cell products. Investigation of the translation of both generation and characterisation methods to different VST therapies allowed evaluation of the developed and validated protocols.

Chapter 2

Materials & Methods

Chapter 2 – Materials & Methods

2.1 General solutions and reagents

Frequently used solutions throughout these studies and their composition are detailed in **Table 2.1**.

Solution	Components	Concentration	Supplier
PE Buffer	Dulbecco's phosphate buffered saline (DPBS)		Gibco
	Ultrapure EDTA	[2.5mM]	Invitrogen
PEA Buffer	Dulbecco's phosphate buffered saline (DPBS)		Gibco
	Ultrapure EDTA	[2.5mM]	Invitrogen
	Human serum albumin (HSA)	[0.5%]	CSL Behrin
CS6.66 Freezing Solution	CryoStor CS10 freezing medium (10% DMSO)	[66.6%]	Stem Cell Technologies
	Plasma-Lyte 148 buffer	[33.3%]	Baxter Healthcare

Table 2.1 - List of general solutions and their composition.

All fluorescently conjugated antibodies used for flow cytometry assays are listed with clone and manufacturer details in **Table 2.2**.

Marker	Clone	Conjugate	Surface or Intracellular	Supplier
Annexin V	A5	BV421	Surface	BioLegend
CCR1	KF10B29	APC	Surface	BioLegend
CCR2	K036C2	BV421	Surface	BioLegend
CCR3	5E8	PE	Surface	BioLegend
CCR4	L291H4	BV421	Surface	BioLegend
CCR5	J418F1	BV421	Surface	BioLegend
CCR6	G034E3	PE	Surface	BioLegend
CCR7	G043H7	FITC	Surface	BioLegend
CD2	REA972	PE-Vio770	Surface	Miltenyi Biotec
CD3	BW264/56	PE	Surface	Miltenyi Biotec
CD3	REA613	FITC	Surface	Miltenyi Biotec
CD38	REA572	PE-Vio770	Surface	Miltenyi Biotec
CD39	REA739	PE-Vio770	Surface	Miltenyi Biotec
CD4	VIT4	PerCP-Vio700	Surface	Miltenyi Biotec
CD4	VIT4	PE-Vio770	Surface	Miltenyi Biotec
CD4	VIT4	APC	Surface	Miltenyi Biotec
CD8	REA734	VioGreen	Surface	Miltenyi Biotec

CD8	SK1	Alexa Fluor700	Intracellular	BioLegend
CD14	REA599	FITC	Surface	Miltenyi Biotec
CD16	REA423	APC	Surface	Miltenyi Biotec
CD19	REA675	PerCP-Vio700	Surface	Miltenyi Biotec
CD45	REA747	VioBlue	Surface	Miltenyi Biotec
CD45RA	T6D11	VioBlue	Surface	Miltenyi Biotec
CD45RO	UCHL1	PerCP-Vio700	Surface	Miltenyi Biotec
CD45RO	UCHL1	APC	Surface	Miltenyi Biotec
CD56	AF12-7H3	APC	Surface	Miltenyi Biotec
CD62L	145/15	FITC	Surface	Miltenyi Biotec
CD62L	145/15	VioBlue	Surface	Miltenyi Biotec
CD107a	REA792	PE	Intracellular	Miltenyi Biotec
CD137	REA765	APC	Intracellular	Miltenyi Biotec
CD154	REA238	PE	Intracellular	Miltenyi Biotec
CD154	REA238	APC	Intracellular	Miltenyi Biotec
CXCR3	G025H7	FITC	Surface	BioLegend
CXCR4	12G5	PE	Surface	BioLegend
CXCR5	J252D4	BV421	Surface	BioLegend
CXCR6	K041ES	APC	Surface	BioLegend
DRAQ7	N/A	APC-Cy7	Surface	BioLegend
Granzyme B	REA226	FITC	Intracellular	Miltenyi Biotec
Granzyme B	GB11	BV510	Intracellular	BioLegend
HLA-DR	REA805	VioBlue	Surface	Miltenyi Biotec
IFN-γ	4S.B3	eFluor450	Intracellular	eBioscience
IFN-γ	REA600	VioBlue	Intracellular	Miltenyi Biotec
IL-2	MQ1-17H12	PE-Cy7	Intracellular	BioLegend
LAG-3	11C365	BV421	Surface	BioLegend
NKG2C	REA205	FITC	Surface	Miltenyi Biotec
NKG2D	1D11	BV421	Surface	BD Biosciences
PD-1	REA1165	PE	Surface	Miltenyi Biotec
Perforin	dG9	BV711	Intracellular	BioLegend
PKH67	N/A	FITC	Surface	Sigma-Aldrich
TCR-αβ	REA652	PE	Surface	Miltenyi Biotec
TCR-γδ	REA591	APC	Surface	Miltenyi Biotec
TIM-3	F38-2E2	VioBright-FITC	Surface	Miltenyi Biotec
TNF-α	Mab11	PE	Intracellular	BioLegend
TNF-α	cA2	FITC	Intracellular	Miltenyi Biotec

Table 2.2 - Flow cytometry antibody details.

2.2 Generation of EBV VST

2.2.1 Donors

EBV VST lines were generated from donor material using both the LCL repeated stimulation method and peptide-mediated IFN-γ cytokine capture selection (CCS) and expansion method as detailed below. Source material for the LCL process manufacture was leukapheresis units from New Zealand regular blood donors (NZ

code, for therapeutic use due to low risk of CJD) which were supplied cryopreserved by the New Zealand Blood Service and transported to SNBTS Aberdeen for liquid nitrogen storage until clean room manufacture.

For the peptide-mediated generation process, source material was either buffy coats from regular blood donors supplied by SNBTS (for development phase) or donor leukapheresis supplied by SNBTS Clinical Apheresis Unit (for manufacturing phase). Manufacture for this process was from fresh material (within 72 hours of donation) at SNBTS Jack Copland Centre.

All donors were fully consented for use under sample governance 17~16. Donors were of known ABO and Rhesus blood groups, and pre-screened for EBV sero-positivity. Donors were also required to screen negative for antibodies against hepatitis B virus (HBV), hepatitis C virus (HCV), human immunodeficiency virus (HIV), and human T-lymphotropic virus type I (HTLV1); as well as HLA-typed to choose a panel of donors that allowed maximal coverage of the population.

2.2.2 HLA typing

Peripheral blood samples were sent to SNBTS Haematology & Immunology labs at Royal Infirmary Edinburgh for HLA typing. Following extraction of DNA, HLA genotyping of donors was undertaken for HLA-A, B and DRB1 loci using Lifecodes HLA eRES SSO Typing kits (Immucor Inc, USA).

2.2.3 EBV peptides

EBV Consensus Peptivator peptide pools (Miltenyi Biotec) were used to isolate EBV VST by cytokine capture selection (see **2.2.5**) and to test for functional reactivity of EBV VST products. These peptide pools consist of 43 MHC Class I and II-restricted peptides covering 15 EBV proteins: LMP1, LMP2A, EBNA1, EBNA2, EBNA3, EBNA4, EBNA6, BALF2, BRLF1, BMLF1, BMRF1, BNRF1, BZLF1, BLLF1, BXLF2. Peptides were 15-mer sequences with 11 amino acid overlap.

2.2.4 Generation of EBV VST by LCL stimulation

Originally, EBV VST were manufactured by the Aberdeen SNBTS team from New Zealand donors using the LCL repeated stimulation method as outlined in (Vickers et

al., 2014). New Zealand donors were utilised due to the similar HLA distribution in the population, but with no risk of CJD present in the UK population. Briefly, an aliquot of frozen donor leukapheresis was thawed and infected with EBV B958 supernatant, and cultured for 4-8 weeks until established into LCL. LCL were then irradiated (40 Gy) and co-cultured with remaining autologous donor leukapheresis to allow antigen presentation from LCL to mononuclear cells (MNC). Cells were co-cultured at an initial ratio of [40:1] MNC to LCL, and at day 10 and weekly thereafter re-stimulated at [4:1] VST to LCL. Cultures were maintained in RPMI containing fetal bovine serum (FBS) [20%] and IL-2 [20 IU/mL] at a density of $1x10^6$ cells/mL for approximately 2 months. Cultures were tested routinely after 6 stimulation rounds for a minimal specificity in a 4 hour chromium release cytotoxicity assay as described in (Wilkie et al., 2004), and upon satisfactory results (>10% specific target killing) were cryopreserved in HBSS containing HSA [10%] and DMSO [10%], at 50 or $150x10^6$ cells per bag for paediatric or adult doses respectively, and stored in vapour-phase liquid nitrogen. Final product samples were required to pass bacterial, mycoplasma, viral and endoxotoxin testing as negative or not detected to be permitted for clinical use. Final product samples at harvest were also immunophenotyped for CD3, CD4, CD8, CD19, CD56, and viability (using 7-AAD) with a criteria of <2% CD19+ cells and >80% viability. This EBV VST bank was released for clinical use as an ATMP under an MHRA 'Specials' license since 2011.

2.2.5 Generation of EBV VST by IFN-γ CCS & expansion

A next-generation EBV VST bank was developed and manufactured by our group using a peptide-mediated IFN-γ selection & expansion method from UK donor leukapheresis. For this process, EBV sero-positive donors were pre-screened for T cell cytokine responses to EBV consensus peptides using flow cytometric intracellular cytokine assay whereby a minimum criterion >0.08% CD3+/ IFNγ+ was required for a donor to be taken forward to manufacture. Selected donors then gave a leukapheresis donation via the SNBTS Clinical Apheresis Unit, which was transferred fresh to SNBTS Jack Copland Centre for clean room manufacture. Leukapheresis product was volume adjusted with acid citrate dextrose (ACD-A) (Fresenius Kabi) and set up for cytokine capture selection (CCS) enrichment on the CliniMACS Prodigy automated cell processor (Miltenyi Biotec) to isolate IFNγ+ T cells responsive to EBV peptide stimulation. The CCS programme was set to run overnight with a 4 hour

antigen stimulation period followed by CCS labelling and selection as per manufacturer's instructions. Non-target cells were then irradiated (40Gy) and co-cultured with IFNγ+ target cells to allow continued co-stimulation by APC in culture without outgrowth of these non-target cells. Co-cultures were set up in G-Rex100M-CS (closed-system) flasks in GMP TexMACS serum-free medium (Miltenyi Biotec) supplemented with GMP-grade IL-2 [200 IU/mL] (GE Healthcare) and expanded for 17-18 days. At culture harvest, cells were washed and counted using EBV VST Trucount assay as outlined in **2.4.3**. VST were then cryopreserved at $150x10^6$ cells/bag in [2:1] formulation of Plasma-Lyte 148 (Baxter Healthcare Ltd) to CryoStor10 (BioLife Solutions). Formulated bags were controlled rate frozen and stored in nitrogen vapour-phase tanks. Final product samples were required as above to pass bacterial, mycoplasma, viral and endotoxin testing as negative or not detected to allow for clinical use.

2.3 Generation of SARS-CoV-2 VST

2.3.1 Donors

COVID-19 Convalescent Donors (CCD) were recruited from the local Scottish population through the SNBTS Convalescent Plasma Program to donate peripheral blood buffy coats for this study under sample governances 20~02 and 19~11. CCD were eligible to donate if they had a confirmed positive SARS-CoV-2 PCR test and were a minimum of 28 days after resolution of infection symptoms, as well as fulfilling the current criteria for whole blood donation. Uninfected Donors (UD - adults confirmed as having no evidence of COVID-19 symptoms at time of donation) were used to compare initial phenotyping and SARS-CoV-2 antigen T cell responses with CCD. All samples and donations were provided through informed consent.

2.3.2 SARS-CoV-2 peptides

SARS-CoV-2 Peptivator peptide pools (Miltenyi Biotec) containing 15-mer sequences with 11 amino acids overlap were used for VST isolation and subsequent VST reactivity responses.

Initial research and development to isolate SARS-CoV-2 VST was done using manually mixed research-grade peptivators for $Spike^{WT}$, Nucleocapsid and Membrane (SC2-

SNM) antigens. Research-grade peptides were reconstituted according to manufacturer's instructions in DMSO/sterile water for injection mix (Miltenyi Biotec). In January 2021 a GMP-grade peptide pool was released covering selected immunodominant regions of Spike, Nucleocapsid, Membrane and Envelope proteins (SC2-Select) and therefore manufacturing of the SARS-CoV-2 VST bank proceeded using SC2-Select. GMP-grade peptides were reconstituted according to manufacturer's instructions in sterile water for injection. Comparisons between SC2-SNM and SC2-Select for VST isolation are made in Chapter 6. **Table 2.3** shows a full list of SARS-CoV-2 peptivators used for VST isolation and their sequence coverage.

SARS-CoV-2 Peptivator	GenBank Protein ID	Sequence coverage
Spike^{WT}	QHD43416.1	Immunodominant regions: aa 304-338, 421-475, 492-519, 683-707, 741-770, 785-802, 885–1273
Nucleocapsid	QHD43423.2	Complete sequence
Membrane	QHD43419.1	Complete sequence
Select	Not stated	Immunodominant regions (9-22aa length) of Spike^{WT}, Nucleocapsid, Membrane, Envelope and non-structural proteins (63x MHC class I-restricted and 25x MHC class II-restricted)

Table 2.3 - SARS-CoV-2 Peptivators used for VST isolation.

All peptivator pools were supplied by Miltenyi Biotec and reconstituted to stock concentration of [0.6nmol/mL] as per manufacturer's instructions.

As SARS-CoV-2 variants evolved over the course of the pandemic, new peptides manufactured for variants of concern were released. Where possible (depending on dates of VST production), final product SARS-CoV-2 VST were tested for reactivity to these escape mutant peptides. A full list of SARS-CoV-2 peptivators used for final product VST reactivity testing is detailed in **Table 2.4**.

SARS-CoV-2 Peptivator	GenBank Protein ID	Sequence coverage
Spike^{WT}	QHD43416.1	Immunodominant regions: aa 304-338, 421-475, 492-519, 683-707, 741-770, 785-802, 885–1273
Spike S1	QHD43416.1	N-terminal S1 domain of Spike: aa 1-692
Spike$^{\alpha}$		B.1.1.7 lineage (alpha variant) covering mutations: deletion 69, deletion 70, deletion 144, N501Y, A570D, D614G, P681H, T716I, S982A, D1118H

Spike$^{\beta}$		B.1.351 lineage (beta variant) covering mutations: D80A, D215G, 242 deletion, 243 deletion, 244 deletion, K417N, E484K, N501Y, D614G, A701V
Spike$^{\delta}$		B.1.617.2 lineage (delta variant) covering mutations: T19R, G142D, E156G, deletion 157, deletion 158, L452R, T478K, D614G, P681R, and D950N
Spike^{o}		B.1.1.529/BA.1 lineage (omicron variant) covering mutations: A67V, H69 deletion, V70 deletion, T95I, G142D, V143 deletion, Y144 deletion, Y145 deletion, N211 deletion, L212I, insertion 214EPE, G339D, S371L, S373P, S375F, K417N, N440K, G446S, S477N, T478K, E484A, Q493R, G496S, Q498R, N501Y, Y505H, T547K, D614G, H655Y, N679K, P681H, N764K, D796Y, N856K, Q954H, N969K, L981F
Nucleocapsid	QHD43423.2	Complete sequence
Membrane	QHD43419.1	Complete sequence
Select	Not stated	Immunodominant regions (9-22aa length) of Spike^{WT}, Nucleocapsid, Membrane, Envelope and non-structural proteins (63x MHC class I-restricted and 25x MHC class II-restricted)

Table 2.4 - SARS-CoV-2 Peptivators used for VST reactivity testing.

All peptivator pools were supplied by Miltenyi Biotec and reconstituted to stock concentration of [0.6nmol/mL] as per manufacturer's instructions.

2.3.3 CCD buffy coat PBMC isolation

CCD Buffy coats were used in both initial development of SARS-CoV-2 VST generation protocol (n=15) and later to screen for donors with minimum SARS-CoV-2 VST responses for use in full-scale manufacturing (n=108). Buffy coats were diluted [1:3] with PBS and added to tubes containing Ficoll-Paque (GE Healthcare). Tubes were centrifuged at 450g for 40 minutes and the resulting buffy layer extracted and washed. Isolated PBMC were then washed twice in PBS and counted for WBC concentration using DxH520 haemoanalyser.

2.3.4 CCD leukapheresis collection

Donors screened for using PBMC Screening assay in **2.7.2** with ≥0.08% CD3+/IFN-γ+ cells in response to SC2-Select peptide stimulation were recruited for full-scale bank manufacture to donate leukapheresis starting source material. Development VST lines were initially generated using commercially acquired leukapheresis from USA

donors (n=4) (Key Biologics) and GMP banked VST were manufactured using leukapheresis from UK donors (n=9) via SNBTS Clinical Apheresis Unit at Edinburgh Royal Infirmary. Leukaphereses were collected via standard 5L Optia process and suspended in ACD-A for use within 24-72 hours of collection.

2.3.5 Isolation of SARS-CoV-2 VST by manual IFN-γ CCS

Buffy coat PBMC or leukapheresis were plated at $5x10^6$ WBC/mL/cm^2 in standard corning plates and incubated overnight (16-18 hours) at 37°C, 5% CO_2. The following morning, plates were stimulated with either SC2-SNM or SC2-Select peptides at [0.3nmol/mL] for 6 hours at 37°C, 5% CO_2. Plates were subsequently harvested, washed, and counted using the MACSQuant10 analyser. Cells were then labelled with IFN-γ Catch Reagent (Miltenyi Biotec) at [100µL/ 10^7 cells] and incubated on ice for 5 minutes. Cells were then diluted in TexMACS [100µL/ 10^6 cells] and incubated with gentle rotation at 37°C for 45 minutes. Tubes were then diluted [1:1] with cold PEA buffer to end the cytokine secretion reaction. Cell were washed and labelled with IFN-γ-PE-conjugated antibody on ice for 10 minutes. Cells were washed and finally labelled with anti-PE microbeads for 15 minutes at 4°C. Following labelling, cells were washed and a small pre-sort sample taken. Remaining suspension was run through magnetic LS columns, whereby unbound cells were collected as the non-target fraction and magnetically bound IFN-γ+ cells were collected as the target fraction. Following isolation, each pre-sort, non-target and target fraction was counted using MACSQuant10 and small sample was stained with the T cell memory phenotype panel in section **2.5.6** to analyse sorted populations.

2.3.6 Isolation of SARS-CoV-2 VST by manual TNF-α CCS

For comparison studies against VST isolation using IFN-γ CCS (the only commercially available GMP-grade CE-marked kit to isolate VST), SARS-CoV-2 VST were also isolated using a manual TNF-α CCS approach. For this plating, stimulation and CCS isolation was as per protocol for manual IFN-γ CCS isolation outlined in **2.3.5** except using TNF-α Catch Reagent and TNF-α-PE-conjugated antibody (both Miltenyi Biotec).

2.3.7 Isolation of SARS-CoV-2 VST by manual CD154 bead sort

As a further comparison to VST isolation using cytokine capture selections in **2.3.5** and **2.3.6,** SARS-CoV-2 VST were also isolated using expression of T cell activation marker CD154. To this end, PBMC were plated and stimulated with peptides as per **2.3.5.** Prior to incubation, CD40 blocking antibody (Miltenyi Biotec) was added to cell suspension at [1µg/mL] to prevent CD154 downregulation on T cells induced during the stimulation by CD40+ APC interactions. Cells were then incubated for 6 hours at 37°C, 5% CO_2. Following stimulation, plates were harvested, washed, and counted using the MACSQuant10 analyser. Cells were subsequently re-suspended in cold PEA buffer [40µL/ 10^7 cells] and labelled with CD154-biotin-conjugated antibody (Miltenyi Biotec) at [10µL/ 10^7 cells] at 4°C for 15 minutes. Cells were subsequently washed, pellets re-suspended in cold PEA buffer [80µL/ 10^7 cells] and labelled with anti-Biotin microbeads (Miltenyi Biotec) at [20µL/ 10^7 cells] at 4°C for 15 minutes. Labelled cells were then washed and run through magnetic LS columns to sort into unbound negative fraction and magnetically bound CD154+ target fraction. As above, samples from pre-sort, negative and target fractions were counted and phenotyped for analysis.

2.3.8 Isolation of SARS-CoV-2 VST by automated IFN-γ CCS

For full-scale development and manufacture of SARS-CoV-2 VST bank, VST were isolated using a fully automated, closed-system IFN-γ CCS programme on CliniMACS Prodigy cell processor. To this end, leukapheresis material was counted using DxH 520 haemoanalyser and $2x10^9$ WBC taken for Prodigy isolation. Cells were diluted in ACD-A at $1x10^7$ WBC/mL and added via closed heat seal to tubing set TS500 (Miltenyi Biotec) alongside required reagents for IFN-γ CCS programme: CliniMACS IFN-γ CCS kit, GMP-grade SC2-Select Peptivator, GMP-grade TexMACS medium, CliniMACS EDTA buffer (all Miltenyi Biotec) supplemented with HSA [0.5%] and saline (Baxter) supplemented with HSA [2.5%]. CCS was run overnight with delay to stimulation as per automated programme (stimulation incubation time 5 hours) and negative fraction and target fractions collected the following morning. Samples from the non-target and target fractions were counted using SARS-CoV-2 Trucount assay (see section **2.4.4**) on BD Lyric QC flow cytometer and phenotyped to analyse the sorted populations.

2.3.9 SARS-CoV-2 VST culture optimisation

Non-target cells from the IFN-γ CCS assay were irradiated at 40 Gy and used as feeders for the IFN-γ+ target cells. Cultures were initially seeded at either 1×10^7 total cells per cm^2 (200–400 non-targets: 1 target), or 3×10^6 total cells per cm^2 (100 non-targets: 1 target) in G-Rex culture vessels (Wilson Wolf). Cells were cultured in GMP-grade TexMACS medium, and supplemented to determine culture optima using [200 IU/mL] IL-2 (GE Healthcare), [155 IU/ml] IL-7 (Miltenyi Biotech), [2%] human AB Serum (SNBTS) or [2%] human platelet lysate (nLiven, Sexton Biotechnologies). As nLiven is not fully European GMP-compliant it was replaced with pathogen-inactivated, xeno-protein-free GMP-compliant T-Liven (Sexton Biotech) for the scale up demonstrator VST products from leukapheresis. Cells were cultured for up to 28 days with feeds every 3 to 4 days and cultures split as necessary to maintain a density of 0.5 to 3×10^6 T cells/cm2. At day 14, VST cultures from six donors were split to test feeder re-stimulation, where thawed irradiated non-target cells were added to cultured VSTs at (10 non targets: 1 VST) alongside a control culture with no feeder re-stimulation. Samples were taken every 3 to 4 days for immunophenotyping with the lymphocyte panel as per **2.5.5**.

2.3.10 Validation of SARS-CoV-2 VST culture expansion protocol

From results of optimisation experiments in Chapter 4, SARS-CoV-2 VST culture expansion was validated for development and bank manufacture as follows. Briefly, cultures were seeded at 3×10^6 total cells per cm^2 (100 non-targets: 1 target) in closed-system G-Rex flasks in culture medium (GMP-grade TexMACS medium supplemented with [200 IU/mL] IL-2 and [2%] GMP-grade T-Liven). Cells were cultured for 14 days with feeds and splits at day 7 and 11 to maintain density of 1-$3x10^6$ cells/cm^2. At day 14, cells were harvested, washed with saline supplemented with [2.5%] HSA and counted by TruCount (section **2.4.4**) on BD Lyric flow cytometer. Samples were taken for phenotyping and VST reactivation responses using DC intracellular cytokine assay in section **2.7.5**. Remaining VST were formulated at either $1x10^7$ cells/mL in CS6.66 freezing solution into either vials (1mL/cryovial) or dose bags (15mL/cryobag) and cryopreserved for long-term storage in LN_2.

2.4 Cell enumeration

2.4.1 Haemoanalyser counts

Starting source material PBMC or raw leukapheresis was counted using standard Sysmex or DxH520 haemoanalysers. Counts were made on neat cell suspension samples (unless haemoanalyser count was out of range) to minimise potential error by dilution. As basic flow analysers, concentrations of WBC, RBC, and granulocyte per µL were obtained on the basis of size and scatter properties (done by automated gating and analysis).

2.4.2 Flow cytometry counts

Use of a flow cytometry-based counting method allows more accurate enumeration of cultured cells which may have different shape/size to be accurately detected by automatic haemoanalysers. Furthermore, flow-based counting allows the ability to add in stains or antibodies to count particular cell populations. We utilised the BD Trucount™ tubes as a CE-certified counting method used in clinical diagnostic labs.

2.4.3 EBV VST Trucount

EBV VST in process controls and final product samples were enumerated using a Trucount assay. For this, 100µL cell suspension was added to a BD Trucount™ Absolute Counting Tube (BD Biosciences) and diluted with 500µL PE buffer. Viability dye DRAQ7 (1µL) was then added, ready for immediate acquisition on BD Canto or BD Lyric flow cytometers. Cell concentration was calculated as per **2.4.5**.

2.4.4 SARS-CoV-2 VST Trucount

SARS-CoV-2 VST in process controls and final product samples were enumerated using a similar Trucount assay as in **2.4.3**. The assays was slightly modified however to since the SARS-CoV-2 VST expansion process was a shorter duration (14 days) than EBV VST (18-20 days) which for some poor expansion lines resulted in residual RBCs present at harvest. Therefore, CD45 staining was incorporated as the most stable lymphocyte marker to ensure only lymphocytes were counted for final dosing formulation. To this end, 100µL cell suspension was added to a BD Trucount™ Absolute Counting Tube and diluted with 500µL PE buffer as above. Cells were then labelled with CD45-VioBlue antibody (Miltenyi Biotec) and incubated at RT for 5 minutes. Viability dye DRAQ7 (1µL) was then added, ready for immediate acquisition

on BD Canto or BD Lyric flow cytometers. Cell concentration was calculated as per **2.4.5.**

2.4.5 Trucount concentration calculation

Trucount templates were gated as shown in **Figure 2.1**. Briefly, Trucount beads were gated on the basis of FSC/SSC properties. Cells were gated to exclude debris only on the basis of FSC/SSC properties, and subsequently gated on viable cells.

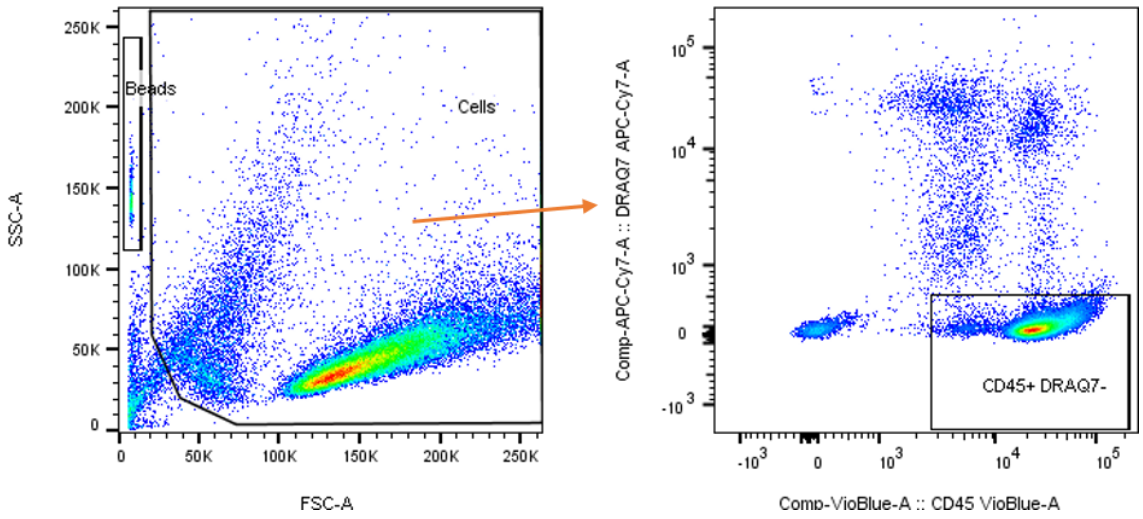

Figure 2.1 – Flow cytometry Trucount gating strategy.

To enumerate viable cell concentration using Trucount assays, analyses were initially gated on all cells and Trucount beads on the basis of forward and side scatter properties. Cells were then sequentially gated for viable cells: DRAQ7- cells for EBV VST; of CD45+ DRAQ7- for SARS-CoV-2 VST.

Cell concentration was then enumerated using the following calculation:

$$[\text{Cell count per uL}] = \frac{\text{No. of viable cell events}}{\text{No. of bead events}} \times \frac{\text{No. of beads per test (LOT specific)}}{\text{Test volume (uL)}}$$

2.5 Surface marker flow cytometry assays

Flow cytometry was used to characterise and phenotype populations present in cell samples. Samples were either stained with surface markers and analysed as fresh material, or subject to intracellular staining using cell fixation protocols as described in **2.7**.

2.5.1 Surface marker staining

Fresh or thawed VST were assessed for surface marker immunophenotyping of the multicolour flow cytometry panels outlined in **Table 2.5**. To this end, $2x10^6$ cell samples were washed in PEA buffer and centrifuged at 300g for 5 minutes. Cells were re-suspended in 100µL PEA buffer and incubated at RT for 3 minutes with 5µL Fc Receptor blocking reagent to prevent non-specific binding. Antibody cocktails as according to the flow cytometry panels in **Table 2.5** were added with relevant FMO controls and incubated at 4°C for 20 minutes. Samples were washed in PE buffer and centrifuged at 300g for 5 minutes. Cells were then re-suspended in 200µL PE buffer with 1µL dead cell stain DRAQ7 added prior to acquisition. Samples were acquired on MACSQuant10 Analyzer (Miltenyi Biotec)or LSR Fortessa (BD Bioscienses) recording 80,000 events.

Panel	VioBlue	VioGreen	FITC	PE	PerCP-Vio700	PE-Vio770	APC
Lineage	HLA-DR	—	CD14	CD3	CD19	CD38	CD16
Lymphocyte	NKG2D	CD8	NKG2C	TCR-αβ	CD4	CD2	TCR-γδ
T Cell Memory	CD45RA	CD8	CD62L	CD3	CD45RO	CD4	CD56
T Cell Exhaustion	LAG-3	CD8	TIM-3	PD-1	—	CD39	CD4

Table 2.5 - Surface marker flow assays multicolour antibody panels.

For full details of antibodies used in flow cytometry panels refer to **Table 2.2**.

2.5.2 Thawing of cryopreserved VST for flow cytometry assays

Cryopreserved samples of EBV VST, SARS-CoV-2 VST, bulk CD3+ and PBMC were kept for long term storage in liquid nitrogen tanks for assays where combined batched testing was optimal. To reconstitute cells, vials or bags were thawed in a water bath at 37°C until there were no visible crystals, and transferred to fresh conical tube. Samples were then slowly and gently diluted 1 in 10 with RT TexMACS medium. Tubes were then centrifuged at 275g for 8 minutes (acceleration 3, deceleration 3) and supernatant removed. Cells were re-suspended in fresh TexMACS medium and either taken directly for phenotyping analysis, or rested overnight prior to use in functional assays.

2.5.3 Initial gating strategy

All flow cytometry analyses were subject to an initial gating strategy to gate on either lymphocytes for starting material or all cells for final product material (debris exclusion) on the basis of FSC/SSC properties. It was crucial for final product material to have an unbiased all cells gate to ensure any impurities/ contaminating cells in the products could be identified and quantified. This population was sequentially gated on singlets (doublet exclusion) using FSC-A vs FSC-H, and finally gating on viable cells (dead cell exclusion) by negative expression of dead cell dye (DRAQ7 or FVD eFluor780).

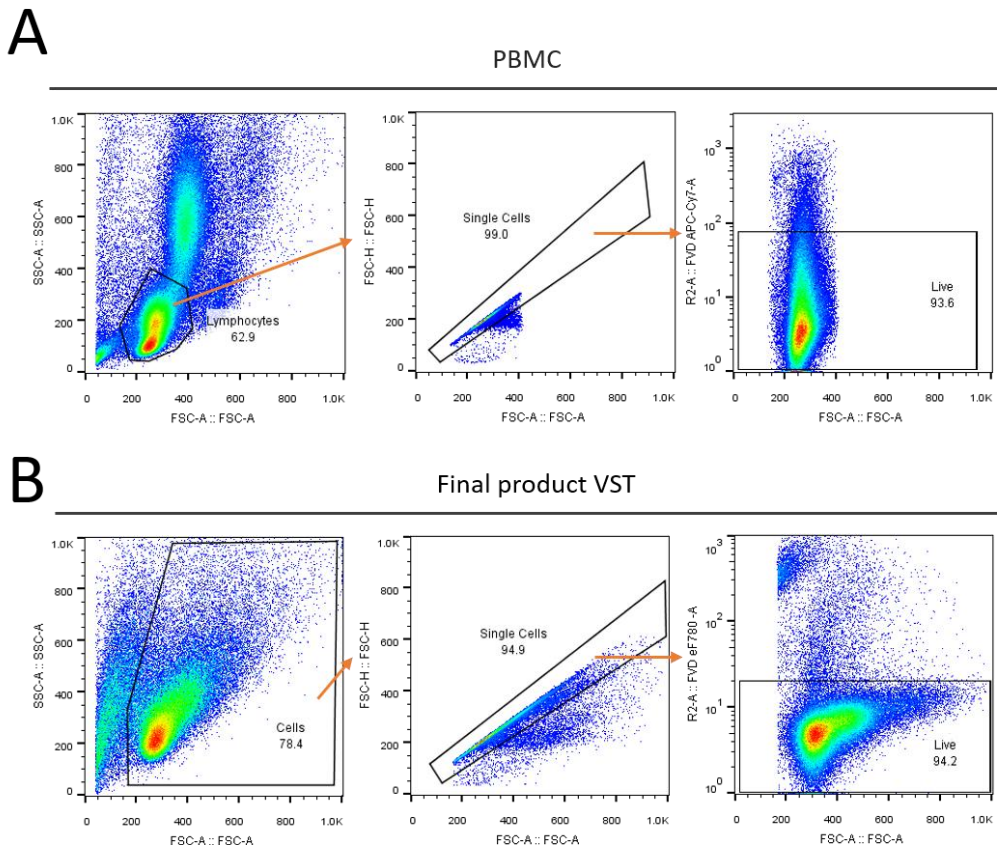

Figure 2.2 - Flow cytometry initial gating strategy.
All flow analyses were subject to initial gating to select either **(A)** lymphocytes in the starting material PBMC or **(B)** all cells for VST final products; and sequentially gated on singlets and live cells.

2.5.4 Lineage gating strategy

SARS-CoV-2 buffy coat-derived PBMC were analysed for WBC lineage markers as shown in **Table 2.5**. Viable singlet lymphocytes were gated as above, followed by gating as CD3+ T cells, CD14+ monocytes, CD16+ NK cells and CD19+ B cells.

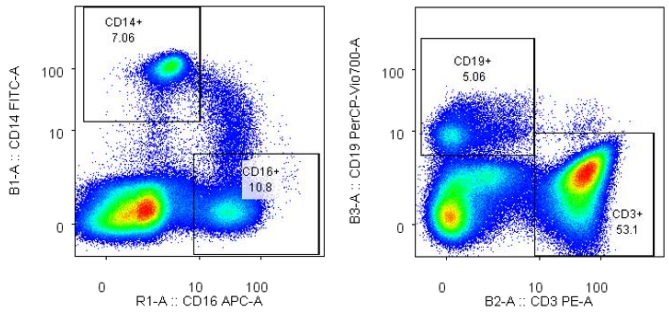

Figure 2.3 - Flow cytometry lineage gating strategy.
PBMC stained with the lineage flow cytometry panel were pre-gated on lymphocytes/ singlets/ live cells, followed by gating on CD3+ T cells, CD14+ monocytes, CD16+ NK cells and CD19+ B cells.

2.5.5 Lymphocyte gating strategy

Final product SARS-CoV-2 VST were analysed for lymphocyte markers as shown in **Table 2.5.** Viable singlet lymphocytes were gated as above, followed by analysis of expression of CD2+ T cells, TCRαβ+ T cells and TCRγδ+ T cells. Expression of NKG2C and NKG2D was also quantified to assess expression of these receptors on final product VST.

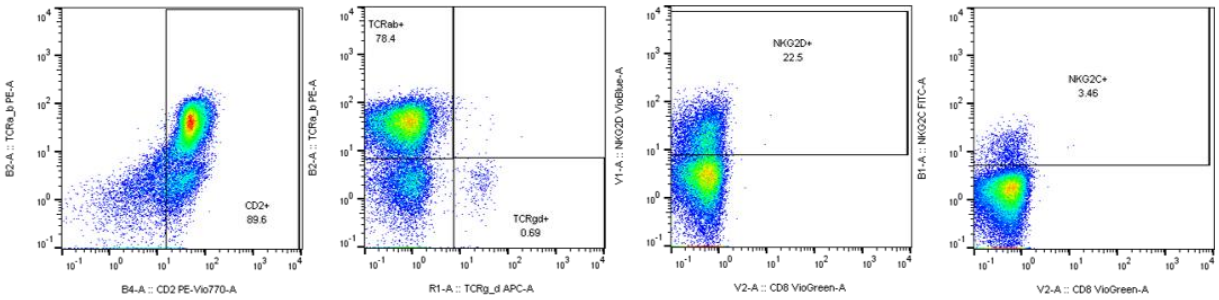

Figure 2.4 - Flow cytometry lymphocyte gating strategy.

VST stained with the lymphocytes flow cytometry panel were pre-gated on lymphocytes/ singlets/ live cells, followed by gating for CD2+ cells, TCRαβ+ cells, TCRγδ+ cells, NKG2D+ cells, and NKG2C+ cells. All gates were placed based on FMO controls.

2.5.6 T cell memory gating strategy

Source material, sorted target cells, and final products were analysed for T cell memory as per **Table 2.5**. Viable cells were initially assessed for frequency of T cells (CD3+/CD56-), NKT cells (CD3+/CD56+), NK cells (CD3-/CD56+) and B cells (CD19+). T cells were gated into subtypes: CD8 (CD8+/CD4-), CD4 (CD4+/CD8-), DP (CD4+/CD8+) and DN (CD4-/CD8-). Both CD4+ and CD8+ cells were then gated for subpopulations: naïve T cells (TNaive: CD62L+/CD45RA+), central memory T cells (TCM: CD62L+/CD45RO+), effector memory T cells (TEM: CD62L-/CD45RO+), terminal differentiated T cells (TEMRA: CD62L-/CD45RA+).

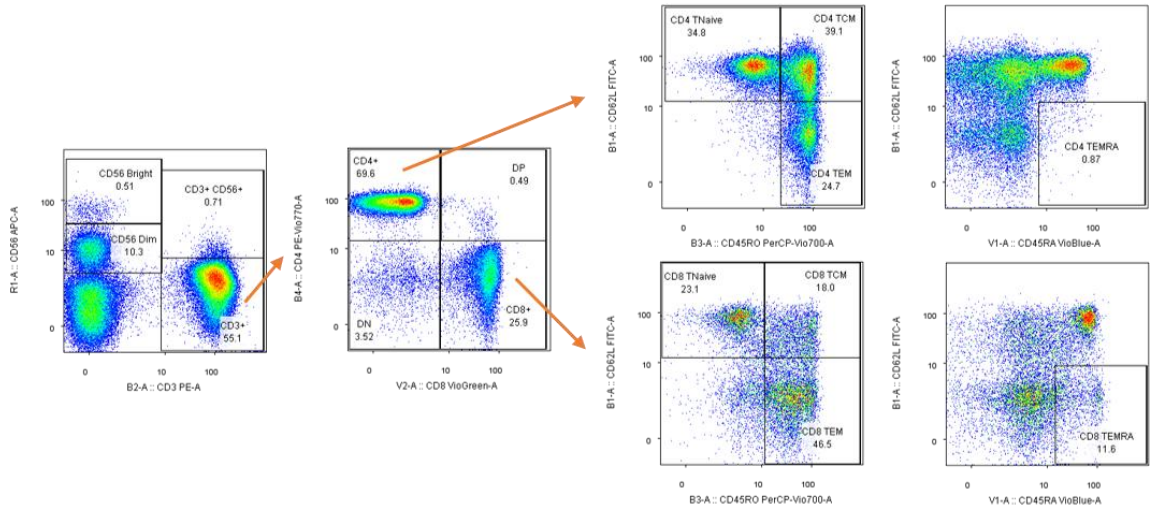

Figure 2.5 - Flow cytometry T cell memory gating strategy.
T cell memory phenotyping using exemplar PBMC identified the following populations: NK cells (CD3-/CD56+), NKT cells (CD3+/ CD56+), CD4 T Cells (CD3+/ CD4+) and CD8 T cells (CD3+/ CD8+). Both CD4 and CD8 T cells were sequentially gated for memory subpopulations as follows: TNaive (CD62L+/ CD45RA+), TCM (CD62L+/CD45RO+), TEM (CD62L-/CD45RO+) and TEMRA (CD62L-/CD45RA+).

2.5.7 T cell exhaustion gating strategy

Final product EBV VST and SARS-CoV-2 VST were analysed for T cell exhaustion as shown in **Table 2.5**. Viable cells were gated into CD4+ and CD8+ T cells, followed by gating to assess the frequency of single or co-expressing T cell activation/inhibitory markers: LAG-3, PD-1 and TIM-3.

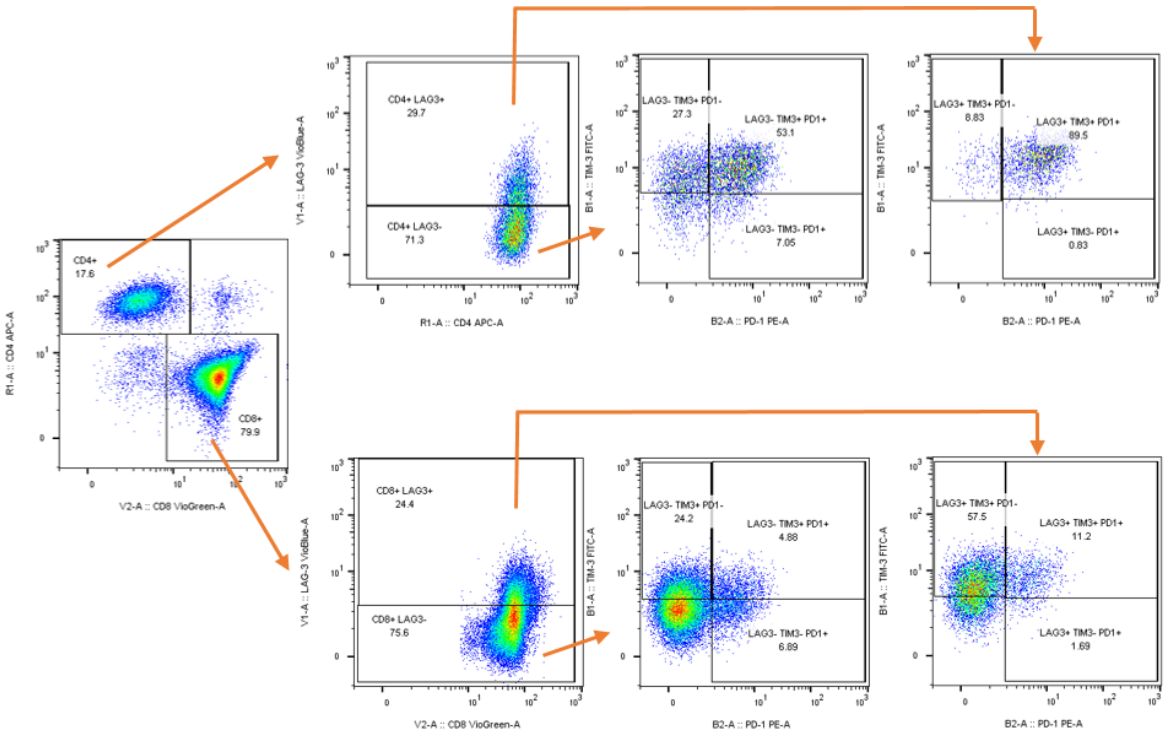

Figure 2.6 - Flow cytometry T cell exhaustion gating strategy.

VST stained with the lymphocyte flow cytometry panel were pre-gated on lymphocytes/ singlets/ live cells, followed by gating on CD4+ or CD8+ T cells. Both CD4 and CD8 compartments were

then analysed for single, dual or triple expression of markers LAG-3, PD-1 and TIM-3. All gates were set according to FMO controls.

2.6 Chemokine receptor flow cytometry assays

2.6.1 Chemokine receptor surface staining

Fresh or thawed VST samples were counted and $1.2x10^7$ viable cells taken for immediate chemokine receptor surface staining. Samples were centrifuged at 300g for 5 minutes. Pellets were then re-suspended in 600µL PEA buffer + 30µL Fc Receptor blocking reagent and incubated at RT for 3 minutes. T cell subtype antibodies were initially added: CD4 PE-Vio770 (12µL) and CD8 VioGreen (12µL); and cell suspension then aliquoted into 12x FACS tubes at 50µL per tube ($1x10^6$ per tube). Single chemokine receptor antibodies (all BioLegend) were added per tube as detailed in **Table 2.6**, with an FMO control containing CD4/CD8 staining only.

Tube	Antibodies added		
1 – FMO Control	CD8 VioGreen	CD4 PE-Vio770	—
2 – CCR1	CD8 VioGreen	CD4 PE-Vio770	CCR1 APC
3 – CCR2	CD8 VioGreen	CD4 PE-Vio770	CCR2 BV421
4 – CCR3	CD8 VioGreen	CD4 PE-Vio770	CCR3 PE
5 – CCR4	CD8 VioGreen	CD4 PE-Vio770	CCR4 BV421
6 – CCR5	CD8 VioGreen	CD4 PE-Vio770	CCR5 BV421
7 – CCR6	CD8 VioGreen	CD4 PE-Vio770	CCR6 PE
8 – CCR7	CD8 VioGreen	CD4 PE-Vio770	CCR7 FITC
9 – CXCR3	CD8 VioGreen	CD4 PE-Vio770	CXCR3 FITC
10 – CXCR4	CD8 VioGreen	CD4 PE-Vio770	CXCR4 PE
11 – CXCR5	CD8 VioGreen	CD4 PE-Vio770	CXCR5 BV421
12 – CXCR6	CD8 VioGreen	CD4 PE-Vio770	CXCR6 APC

Table 2.6 - Chemokine receptor antibody cocktails.

Tubes were incubated at 4°C for 20 minutes, and fixable viability dye (FVD, Invitrogen) working solution (500µL PE buffer + 0.5µL FVD eF780 per tube) added for a further 15 minutes at 4°C. Tubes were then washed with PE buffer, centrifuged

at 300g for 5 minutes, and re-suspended in 200µL/test PE buffer and ran on either BD LSR II or BD Canto flow cytometers at 80,000 events recorded.

2.6.2 Chemokine receptor intracellular staining

For development of the chemokine receptor profiling assay, chemokine receptors were also tested for expression by intracellular staining in case of potential intracellular receptor trafficking. For this, thawed VST were stained with CD8 VioGreen and CD4 PE-Vio770 as per **Table 2.6** at 4°C for 20 minutes, and FVD working solution added for a further 15 minutes at 4°C. Tubes were then washed with PE buffer, centrifuged at 300g for 5 minutes, and re-suspended in 500µL/test BD Cytofix/Cytoperm solution [1X] (BD Biosciences) at 4°C for 20 minutes. Tubes were washed with BD Perm Wash, centrifuged, and re-suspend in 100µL/test BD Perm Wash (BD Biosciences) with individual chemokine receptor antibodies as per **Table 2.6** added at 4°C for 20 minutes. Finally, cells were washed with PE buffer, centrifuged and re-suspended in 200µL/test PE buffer and run on BD Canto flow cytometer recording 80,000 events. Direct comparisons were made between samples only surface stained versus intracellular stained for chemokine receptor antibodies (n=8 donors).

2.6.3 CCL2 uptake assay

Fresh or thawed VST samples were also taken to assess uptake of fluorescently labelled chemokine CCL2. To this end, cells were plated in a 96-well plate at $1x10^6$/200uL/well in 2x wells for CCL2 uptake (TexMACS medium + fluorescent CCL2 APC [25nM]) vs plated control (TexMACS medium only). Plates were incubated at 37°C, 5% CO_2 for 1 hour, with CD4 and CD8 antibodies as above added for the final 20 minutes of incubation. Wells were subsequently harvested into tubes and washed with PE buffer. FVD working solution was added for 15 minutes at 4°C and tubes then centrifuged and re-suspended in PE buffer for flow cytometer acquisition as above.

2.6.4 Chemokine receptor gating strategy

Analysis of flow cytometry files was performed using FlowJo version 10.6.2 (TreeStar Inc). All analyses were subject to an initial gating strategy as shown in **Figure 2.2** in which debris and doublets were excluded on the basis of forward and scatter

properties, and subsequently gated on live cells (FVD negative). Live cells were then gated on CD4+ T cells or CD8+ T cells. Gates for acquisition of chemokine receptor/ CCL2 expression were then placed according to FMO controls as shown in **Figure 2.7** for PBMC. Populations were then quantified using percentages corrected to FMO controls.

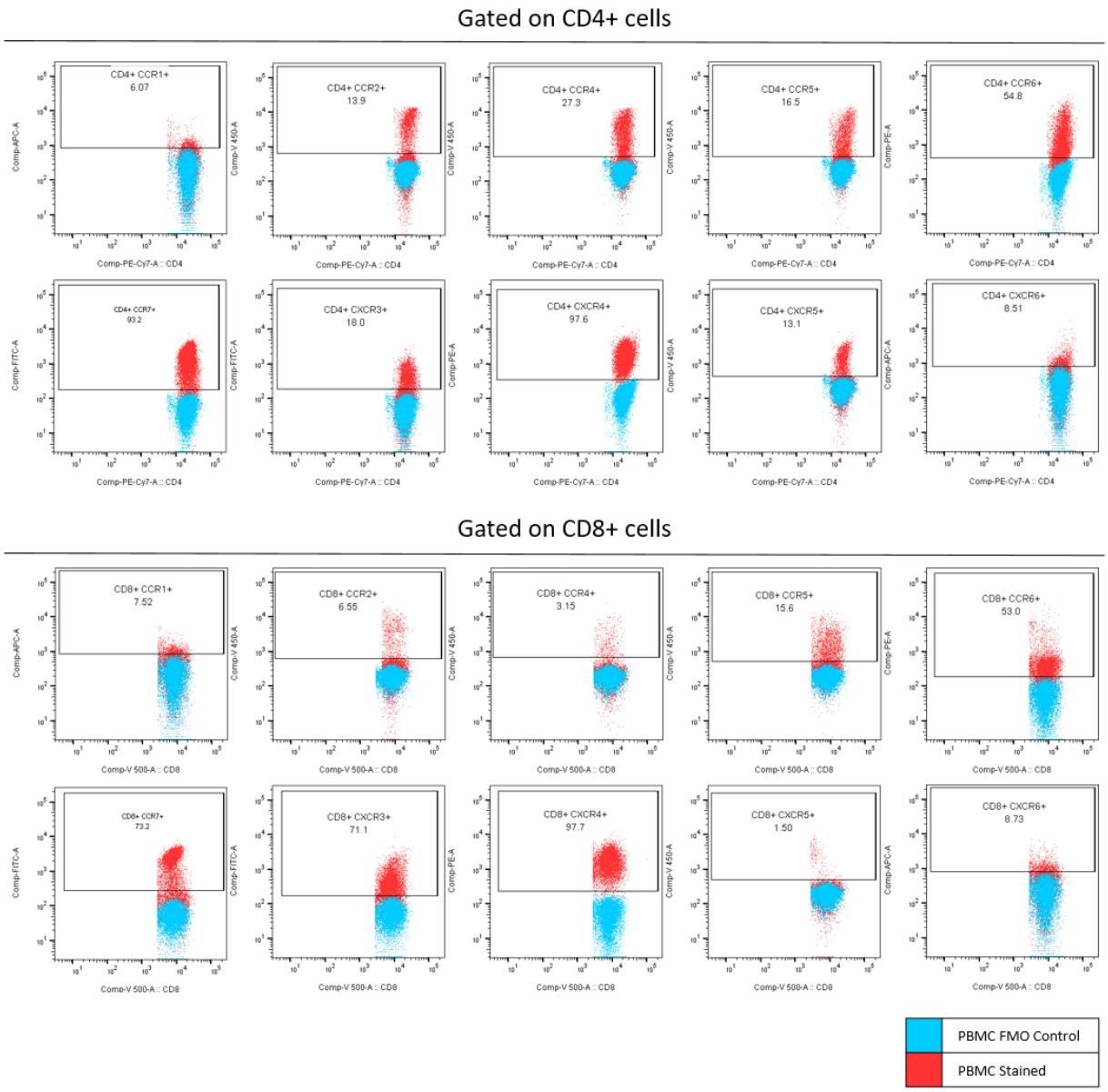

Figure 2.7 – Flow cytometry chemokine receptor gating strategy.

All flow cytometric analyses were subject to a sequential gating strategy of Cells/ Singlets/ Live to exclude debris, doublets and dead cells respectively. Live cells were then gated on either CD4+ or CD8+ cells and gates for chemokine receptors were then placed according to FMO controls. Exemplar staining for chemokine receptors CCR1, CCR2, CCR3, CCR4, CCR5, CCR6, CCR7, CXCR3, CXCR4, CXCR5 & CXCR6 are shown for stained PBMCs (red) in comparison to PBMC FMO controls (blue).

2.7 Intracellular cytokine release flow cytometry assays

Flow cytometric intracellular cytokine release (ICR) assays were used to test functional responses of initial starting material T cell responses for donor screening, final product reactivity for both EBV VST and SARS-CoV-2 VST, and patient monitoring following SARS-CoV-2 VST infusion in the Phase I trial. Each assay involved an initial antigen stimulation followed by an intracellular staining protocol which are detailed below.

2.7.1 PBMC EBV peptide screening

Buffy coat-derived PBMCs or raw leukapheresis material were counted using DhX 520 haemoanalyser and plated in TexMACS medium in a 24-well plate at $5x10^6$ WBC/mL/well for the following treatments: negative control, PMA/ionomycin positive control, and GMP EBV Peptivator consensus (Miltenyi Biotec). All peptide pools were used at [0.3nmol/mL], and cell activation cocktail (BioLegend) added to the positive control well at [1X]. Cells were stimulated for a total of 5 hours at 37 °C, 5% CO_2; with Brefeldin A (BioLegend) added at [5µg/mL] for the final 3 hours. Harvested wells were then stained with PBMC Screen A intracellular antibody panels as per **Table 2.8**.

2.7.2 PBMC SARS-CoV-2 peptide screening

Buffy coat-derived PBMCs or raw leukapheresis material were counted using DhX 520 haemoanalyser and plated in TexMACS medium in a 24-well plate at $5x10^6$ WBC/mL per well with treatments: negative control, PMA/ionomycin positive control, Spike, Nucleocapsid, Membrane, Spike + Nucleocapsid + Membrane combined (SNM), and GMP SARS-CoV-2 Peptivator Select (Select). All peptide pools were used at [0.3nmol/mL], and cell activation cocktail (BioLegend) added to the positive control well at [1X]. Since SARS-CoV-2 peptides were reconstituted in DMSO/water to improve dissolution of more hydrophobic regions, the negative control well contained DMSO/water at the same volume as the peptide wells. Cells were stimulated for a total of 5 hours at 37 °C, 5% CO_2; with Brefeldin A (BioLegend) added at [5µg/mL] for the final 3 hours. Harvested wells were then stained with PBMC Screen A & PBMC Screen B intracellular antibody panels as per **Table 2.8**.

2.7.3 EBV VST degranulation ICR assay

Fresh or thawed EBV VST lines were counted using TruCount assay and plated in a 48-well plate in TexMACS medium at 2.5x10^6 cells/mL/well. Plates were set up to test the following conditions: individual EBV antigen pepmixes BARF1, BMLF1, BMRF1, BRLF1, BZLF1, EBNA1, EBNA2, EBNA3A, EBNA3B, EBNA3C, EBNALP, gp350/340, LMP1, LMP2 (all JPT); EBV consensus peptides (Miltenyi Biotec), positive control (PMA/ionomycin) and negative control (no antigen). Prior to antigen stimulation, degranulation marker antibody CD107a PE was added to all wells at 2µL/well to allow staining throughout stimulation due to transient expression of this marker. Peptides were then added to respective wells as above at [1µg/mL] for JPT pepmixes or [0.3 nmol/mL] for Miltenyi Peptivators. Cells were stimulated for a total of 5 hours at 37 °C, 5% CO_2; with Brefeldin A (BioLegend) added at [5µg/mL] for the final 3 hours. Harvested wells were then stained with EBV VST intracellular antibody panel as per **Table 2.8**.

2.7.4 Generation of autologous DC for VST reactivation testing

Monocyte-derived DC (DC) were generated from freshly isolated CD14+ monocytes. Briefly, monocytes were isolated from PMBC or leukapheresis using anti-CD14 microbeads (Miltenyi Biotech) as per manufacturer's instructions, resulting in highly purified (>90%) monocyte isolates. Cells were cultured at 37°C, 5% CO_2 for 6 days in RPMI (Life Technologies) supplemented with [5%] AB serum, [2mM] Glutamax (Sigma-Aldrich), [20ng/mL] GM-CSF, and [15ng/mL] IL-4 (both Miltenyi Biotech). Media was replaced on days 2 and 4 of culture. After 6 days, cells were harvested using [1X] TrypLE (Life Technologies), counted and frozen in CryoStor10 freezing medium (Stem Cell Technologies) until required for VST stimulation.

2.7.5 SARS-CoV-2 VST + DC co-culture ICR assay

Final product SARS-CoV-2 VST lines were also assessed for functional reactivity using the ICR, however since these lines were highly CD4-skewed autologous DCs were added to allow antigen presentation. The day prior to VST harvest, autologous immature cryopreserved DC (refer to **2.7.4**) were thawed and loaded with peptides [0.3nmol/mL] for 6 hours at 37°C, 5% CO_2. All assays were tested with basic treatments: Spike WT, Nucleocapsid, Membrane, SNM, SARS-CoV-2 Select, positive

control (PMA/ionomycin) and negative control (DMSO/water). Where enough VST and DC were available, additional peptide stimulations included escape antigens Spike-alpha (B1.1.7 lineage), Spike-beta (B1.351 lineage), Spike-gamma (P.1 lineage), Spike-delta (B.1.617.2 lineage) and Spike-omicron (B1.1.529/BA.1 lineage); and non-SARS peptides Adenovirus Hexon 5, EBV consensus, CMV pp65, and GAD65 (all Miltenyi Biotech).

Poly I:C [20µg/mL] and PGE2 [1µg/mL] were added overnight to induce DC maturation. The following morning, DC were counted, phenotyped for maturity, and co-cultured with SARS-CoV-2 VST at [5 VST : 1 DC] in TexMACS medium in a 48-well plate at $2.5x10^5$ DC + $1.25x10^6$ VST per well. Cells were stimulated for a total of 5 hours at 37 °C, 5% CO_2; with Brefeldin A (BioLegend) added at [5µg/mL] for the final 3 hours. Harvested wells were then stained with SARS-CoV-2 VST intracellular antibody panel as per **Table 2.8**.

2.7.6 SARS-CoV-2 VST + LCL vaccinia virus co-culture ICR assay

To assess SARS-CoV-2 VST responses to naturally processed SARS-CoV-2 antigen expressing cells we developed a collaboration with Professor Tao Dong's group in Oxford, who had established a vaccinia-based vector system for transfection of target cells with SARS-CoV-2 antigens. Their assay used autologous LCL infected with recombinant vaccinia virus (VV) constructs expressing SARS-CoV-2 antigens. Vaccinia virus constructs were generated as outlined in (Yin et al., 2023). Briefly, a plasmid containing Wuhan strain SARS-CoV-2 spike gene was modified with a C-terminal FLAG epitope to allow tag tracing without interference to extracellular binding domains and to remove a homologous early transcription termination signal. Plasmids were further modified to incorporate gene mutations present in alpha, delta, and omicron Spike variants, as well as nucleocapsid and membrane proteins. Vaccinia virus vectors expressing Zika pre-membrane protein (prM) were also generated as specificity controls. Plasmids were then cloned and transfected in HEK293T cells, and purified by plaque selection. DNA isolated from VVs was then used to infect EBV LCL to allow LCL HLA-mediated surface presentation of naturally processed SARS-CoV-2 or Zika prM proteins. SARS-CoV-2 VST were then co-cultured at [1:1] with the following LCL conditions: VV spike WT, VV spike delta, VV spike omicron, VV nucleocapsid, VV membrane, VV zika prM. Co-culture wells with VST + LCL stimulated with SARS-CoV-2 peptide pools (Miltenyi Biotec, as per **Table 2.4**) were included as

peptide response controls: spike WT, nucleocapsid and membrane. Co-cultures were then incubated at 37 °C, 5% CO_2 for 6 hours and stained with Oxford cytokine panel as outlined in **Table 2.7**. We supplied all target LCL, antigens and VST cells, and the experimental work was undertaken in Oxford by Prof Dong's team who supplied the resulting data for analysis.

Panel	BV421	Aqua	BV711	AF488	PE	PerCP-V700	PE-Cy7	APC	APC-H7
Oxford SC-2 VST	CD8	Viability	CD4	IFN-γ	CD107a	CD4	IL-2	TNF-α	CCL4

Table 2.7 - Oxford SARS-CoV-2 VST flow cytometry antibody panel.

2.7.7 Intracellular cytokine staining

Following antigenic stimulations detailed in sections **2.7.1** to **2.7.6**, wells were harvested into FACS tubes and centrifuged at 300g for 5 minutes. Supernatants were removed, tubes washed with PEA buffer and centrifuged again at 300g for 5 minutes. Supernatants were then removed and cells re-suspended in 100µL PEA buffer + 5µL FcR blocking reagent at RT for 3 minutes to block unspecific antibody binding. Antibody cocktails were made up for surface markers (white) as outlined in **Table 2.8** and added to tubes for 20 minutes incubation at 4°C. Tubes were then washed with PEA buffer and centrifuged at 300g for 5 minutes. Cells were then re-suspended in 500µL PE buffer + 0.5µL Fixable Viability Dye (FVD) eFluor780 per tube and incubated at 4°C for 30 minutes. Tubes were then washed with PE buffer, centrifuged at 300g for 5 minutes, re-suspended in 500µL Cytofix/Cytoperm solution [1X] (BD Biosciences) and incubated at 4°C for 20 minutes. Tubes were washed with Perm wash [1X] (BD Biosciences) and centrifuged at 300g for 5 minutes. Antibody cocktails for intracellular markers (blue) as outlined in **Table 2.8** were made up in Perm wash [1X] at antibody cocktail + 100µL Perm wash per test. Cells were then re-suspended in 100µL intracellular antibody cocktail/ Perm wash per test and incubated at 4°C for 20 minutes. Finally tubes were washed with Perm wash, centrifuged at 300g for 5 minutes, and re-suspended in 200µL PE buffer for acquisition on flow cytometer.

Panel	VB	VG	BV711	FITC	PE	PerCP-V700	PE-Cy7	AF700	APC
Screen A	IFN-γ	CD8	—	CD3	TNF-α	CD45RO	IL-2	—	CD56

Screen B	HLA-DR	CD8	—	Gr B	CD154	CD4	CD38	—	CD137
EBV VST	IFN-γ	Gr B	Perf	TNF-α	CD107a	CD4	IL-2	CD8	CD154
SC2 VST	IFN-γ	CD8	—	TNF-α	CD3	CD4	IL-2	—	CD154

Table 2.8 - Intracellular flow cytometry antibody panels.
Surface marker antibodies are shaded white and intracellular marker antibodies shaded blue.

EBV PBMC screening, and final product EBV VST degranulation ICR assays were analysed using a Fortessa LSR flow cytometer (BD Biosciences) recording up to 100,000 events. All research and development samples for SARS-CoV-2 PBMC and VST assays were run on a MACSQuant10 Analyser (Miltenyi Biotec) within a derogated containment level III laboratory due to unknown risk at the time of potentially infectious material. For both EBV VST and SARS-CoV-2 clinical-grade GMP-manufactured VST generated in clean room for the banks, assays were run on a Lyric flow cytometer (BD Biosciences) managed under QC qualification.

2.7.8 ICR assay gating strategy

All flow cytometric analyses were subject to initial cell/ singlet/ viable cell gating as shown in **Figure 2.2**. All intracellular flow cytometry assays were then pre-gated on CD4+ or CD8+ T cells, and then analysed for cytokine or activation marker expression. For this, intracellular cytokine or activation marker gates were set according to the no antigen negative control, and acquisition of marker in peptide stimulations quantified as percentage frequency as according to the gating strategy outlined in **Figure 2.8**. Multifunctional T cells were classified as T cells with co-expression of two or more cytokine or activation markers.

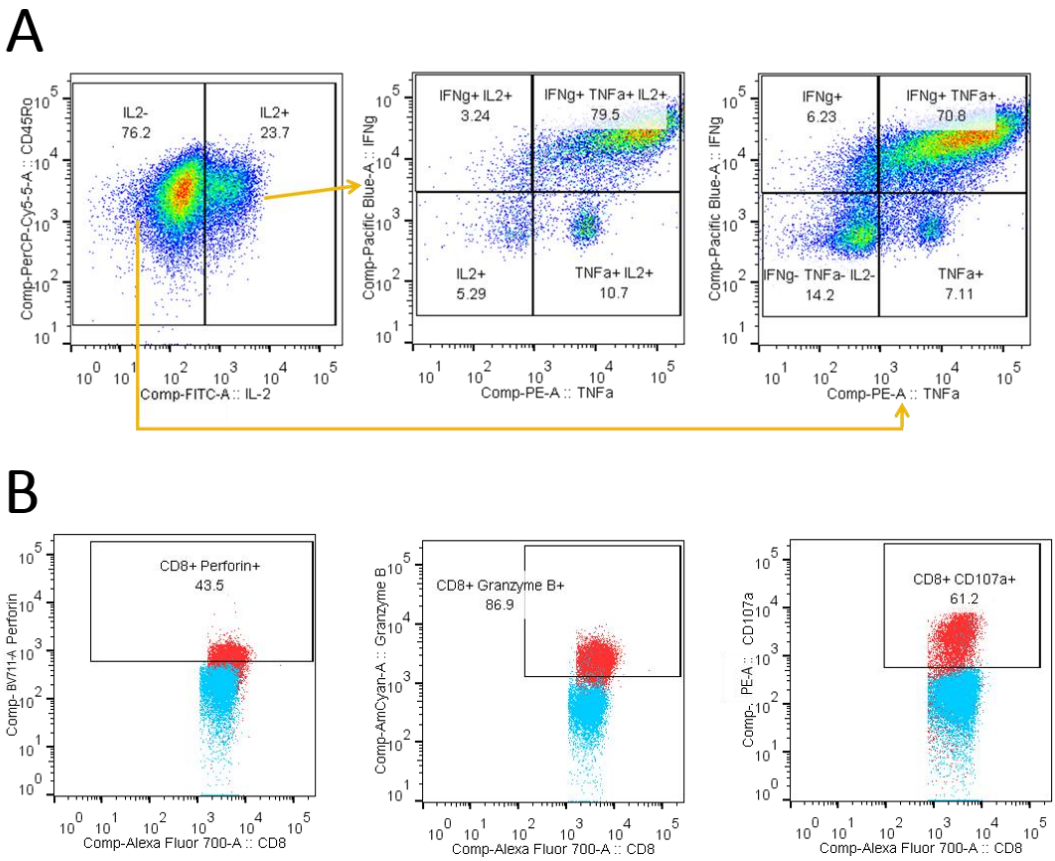

Figure 2.8 - Flow cytometry intracellular cytokine release and degranulation gating strategy. All analyses were subject to a sequential gating strategy of Cells/ Singlets/ Live to exclude debris, doublets and dead cells respectively. **(A)** For intracellular cytokine release analysis of antigen stimulated conditions, viable cells were gated on either all CD3+ T cells, CD4+ T cells or CD8+ T cells, and then analysed for positive expression of cytokines IFN-γ, TNF-α or IL-2 normalised to the negative control (no antigen stimulation) tube. To quantify co-expression of these three cytokines, the relevant T cell population was first gated on IL-2 positive or negative cells, with each IL-2 population then quantified for co-expression of IFN-γ and TNF-α. **(B)** For degranulation analysis in response to antigen stimulation (red), gated CD3+ T cells, CD4+ T cells or CD8+ T cells were quantified for positive expression of degranulation markers perforin, granzyme B and CD107a according to the negative control (no antigen stimulation, blue) tube.

2.8 Cytotoxicity assays

2.8.1 EBV VST cytotoxicity assay

To assess potency, cryopreserved EBV VST lines were thawed and rested overnight in TexMACS medium at 37°C, 5% CO_2 and tested tangentially in a flow cytometric-based cytotoxicity assay within the same month (using same batch reagents and LCL targets where possible).

HLA-matched and mismatched target LCL lines were labelled with PKH67 membrane dye (Sigma Aldrich) as per manufacturer's guidelines then added to a 96-well plate in triplicate wells per condition in TexMACS medium. LCL were cultured with EBV VST

at the following effector to target [E:T] of 1:1, 5:1, 10:1 and 20:1; LCL only and T cell only were used as controls. Each well was plated at a final density of $1.1x10^6$ total cells (target + effector) per well to ensure staining was consistent between different co-culture ratios. After incubation for 5 hours at 37°C, 5% CO_2 cells were harvested and washed twice in Annexin V binding buffer (BioLegend) and labelled with Annexin V-BV421 at 4°C for 30 minutes. Plates were then washed in Annexin V binding buffer, centrifuged and wells re-suspended in PE buffer and DRAQ7 dead cell dye (both BioLegend). Plates were run with up to 100,000 events acquired on MACSQuant10 Analyser (Miltenyi Biotec).

2.8.2 EBV VST CD4+ sorted cytotoxicity assay

To assess if the CD4+ T cell component within EBV VST lines had cytotoxic capacity, lines were sorted to highly enrich the CD4 cells and run in the cytotoxicity assay as before. To this end, EBV VST lines with higher CD4 content were thawed and rested overnight in TexMACS medium at 37°C, 5% CO_2. The following morning, cells were counted and stained with the CD4 sorting panel at 4°C for 20 minutes. Cells were then washed and input to a standard Tyto cartridge and sorted for CD4+ CD3+ cells using the MACSQuant Tyto cell sorter (Miltenyi Biotec). Sorted fractions were collected and analysed for purity and cell count using the MACSQuant10 Analyser (Miltenyi Biotec).

Unsorted, CD4+ sorted and CD4 non-target fractions were then all plated in a 96-well plate in TexMACS medium. Autologous EBV LCL and K562 (EBV negative cell line) were used as targets, co-cultured with the EBV VST at the following effector to target [E:T] ratios of 1:1, 5:1, 10:1 and targets only. Plates were then incubated for 5 hours at 37°C, 5% CO_2 and stained for Annexin V and DRAQ7 as detailed in **2.8.1**.

2.8.3 EBV VST cytotoxicity assay data analysis

Unlike all aforementioned flow cytometry analyses, this assay did not utilise the initial gating strategy in **2.5.3** to exclude dead cells since this was the output measure. Instead, cells were gated on positive expression of PKH67 to show only LCLs, and then analysed for Annexin V and DRAQ7 co-expression. Cytotoxicity was quantified as early apoptotic events (Annexin V+ /DRAQ7-) or late apoptotic/necrotic events (Annexin V+/DRAQ7+) to gate a total 'dead' population as per **Figure 2.9**. The frequency of total dead cells was normalised to LCL only wells to calculate the

percentage specific lysis at each [E:T] ratio. Evaluation of overall cytotoxic potency to compare between different VST lines was made by calculating the area under the curve of specific lysis over all [E:T] ratios from HLA-matched LCL targets.

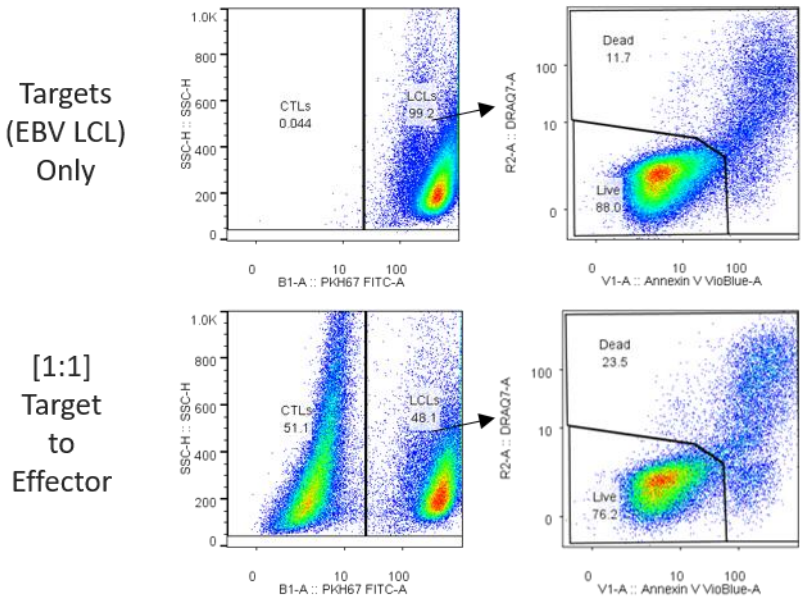

Figure 2.9 - Flow cytometry EBV VST cytotoxicity gating strategy.

PKH67-labelled target cells (EBV LCL) were co-cultured with effector EBV VST at multiple ratios for 5 hours and subsequently stained with apoptosis/ dead cell markers Annexin V and DRAQ7. For gating, all events were initially gated on PKH67+ cells (target LCL) or PHK67- cells (EBV VST). PKH67+ target LCL were then gated to analyse the total live cells (Annexin V-/ DRAQ7-), and total dead cells (Annexin V single positive, DRAQ7 single positive, and Annexin V+/ DRAQ7+). Each target to effector ratio (bottom panels) were normalised to the baseline percentage dead cells in target only control samples (top panel) to measure the specific lysis induced by addition of EBV VST to target LCL.

2.8.4 SARS-CoV-2 VST cytotoxicity assay

Without appropriate SARS-CoV-2 infected cell lines to utilise in a cytotoxicity assay, we generated autologous EBV LCL which could then be loaded with SARS-CoV-2 peptides to act as target cells for a killing assay. For this, LCL were generated by Epstein-Barr virus transformation as described previously, and maintained in RPMI 1640 medium supplemented with [10%] FBS (R10) for 6-8 weeks in culture. Prior to the cytotoxicity assay, LCL were labelled with [0.5µM] carboxyfluorescein succcindimidyl ester (CFSE, ThermoFisher) and loaded with [1µM] SARS-CoV-2 peptides at 37°C for 1 hour. LCL were then washed, counted and co-cultured with SARS-CoV-2 VST at the following effector to target [E:T] ratios 1:1, 2:1, 4:1, 8:1, and targets only. Unloaded LCL co-cultures with VST at the same [E:T] were included as

controls. Plates were then incubated for 6 hours at 37°C, 5% CO_2 and stained with CD19-BV421 (BioLegend) and dead cell dye 7-AAD (eBioscience). Samples were then run on Attune NxT flow cytometer (software v3.2.1). This assay was performed by Yanchun Peng (Senior Research Associate) in the collaborating lab of Prof Dong at University of Oxford.

2.8.5 SARS-CoV-2 VST cytotoxicity assay data analysis

As above, the initial gating strategy was not applied to cytotoxicity assay analysis. Instead, cells were gated on CD19+ CFSE+ cells to show only LCL, and then quantified for 7AAD+ dead LCLs. The percentage specific lysis at each [E:T] ratio was calculated by correction to the no-peptide controls with the same [E:T] ratio.

2.9 Mixed lymphocyte reaction immunogenicity testing

Cryopreserved samples were sent to Alcyomics Ltd as part of a collaborative project assessing potential immunogenicity of cell therapies, initiated through the Northern Alliance Advanced Therapy Centres (NAATC). Alcyomics Skimune® assays used healthy volunteer (HV) blood samples and skin biopsies to test the immunogenicity of SARS-CoV-2 VST. Mixed lymphocytes reactions (MLR) were set up using irradiated HV PBMC with either SARS-CoV-2 donor VST or SARS-CoV-2 donor PBMC (positive control). MLR were co-cultured at [1:1] HV PBMC: SARS-CoV-2 donor VST or PBMC. After 7 days, samples were taken for assessment of T cell proliferation, cytokine luminex, and MLR cells further co-cultured with HV skin biopsies for GVHD testing. Each SARS-CoV-2 donor was tested against n=3 HV in triplicate wells, with minimal or no HLA matches.

2.9.1 T cell proliferation assay

Following 7 day MLR cultures, tritiated thymidine was added to each well for 16-18 hours. Cells were then harvested onto a filter mat and counted using a β-scintillation counter to assess for [3H]-Thymidine uptake.

2.9.2 Cytokine multiplex

Culture supernatants were analysed using MSD Multi-Spot Proinflammatory panel 1 V-Plex kit (Meso Scale Diagnostics) following manufacturer's instructions.

Biomarkers included were IFN-γ, IL-1β, IL-2, IL-4, IL-6, IL-8, IL-10, IL-12p70, IL-13 and TNF-α.

2.9.3 Histology & GVHD analysis

For the Skimune® assays, negative controls consisted of co-culture of HV PBMC and HV autologous skin, and HV skin in medium only. The positive control was HV skin incubated with SARS-CoV-2 donor PBMC. The assay endpoint was histopathological damage observed in the skin tissue caused by exposure to the PBMC or VST. For this, $1x10^6$ MLR cells were harvested and co-cultured with HV skin for a further 3 days. Co-cultures were then formalin fixed, paraffin embedded, section and H&E stained. This was measured as skin grades (grades I to IV) according to the severity of the skin tissue damage observed as shown in **Figure 2.10**, adapted from (Lerner et al., 1974).

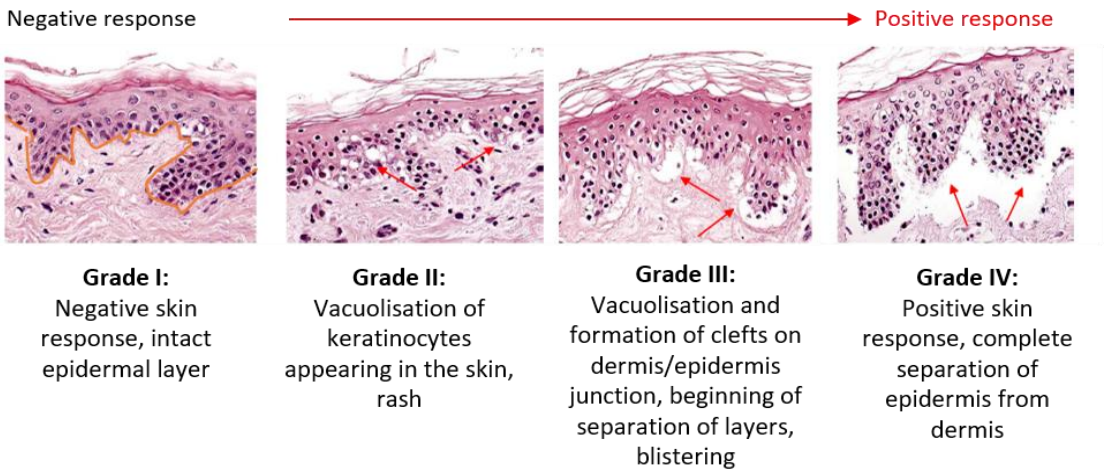

Figure 2.10 - GVHD histology grading.

Skin MLR culture histology was analysed for GVHD grading. Grade I was considered negative, with intact upper keratinocyte layer. Grade II refers to vacuolisation of the epidermis. Grade III shows severe damage of the epidermis layer, with initial separation of the epidermis and dermis layers. Grade IV refers to severe damage, with complete separation of the epidermis and dermis layer. Grade II or higher was regarded as a positive response.

2.10 Taqman low density arrays

2.10.1 RNA extraction

Cryopreserved EBV-VST products derived from both the LCL method and IFN-γ CCS method were thawed, and total RNA extracted using Qiagen RNAeasy columns with DNASe incubation for elimination of genomic DNA.

2.10.2 cDNA synthesis

For use in Taqman arrays, cDNA was synthesised from total RNA using SuperScript VILO reverse transcription kit (Invitrogen).

2.10.3 TLDA qPCR

Target cell cDNA [40ng] was diluted and mixed 1:1 with TaqMan Fast Advanced MasterMix and loaded onto a customized 384-well TaqMan Low Density Array (TLDA) card (Applied Biosystems) measuring a number of chemokine receptor, cytokine, transcription factors, senescence and CD marker genes. TLDA cards were run on an ABI Viia7 Real-time PCR System (Applied Biosystems).

2.10.4 TLDA analysis

Relative quantification of gene expression changes was determined using the $2^{-\Delta\Delta CT}$ as described in (Livak and Schmittgen, 2001). All genes from each sample were calculated for $2^{-\Delta\Delta CT}$ in relation to RPLPO housekeeper and normalised against naïve CD3+/CD62L+/CD45RO- T cells isolated from buffy coats (n=6) using FACS sorting.

2.11 TCR Repertoire Analysis

2.11.1 RNA extraction

T cell TCR repertoire was assessed through another collaboration established with Dr Graeme Cowan's group at the School of Biological Sciences, University of Edinburgh. Samples were taken from EBV VST & SARS-CoV-2 VST final products, and bulk T cells isolated using CD3 microbeads from matched donor PBMC as diversity controls. Samples were distributed into PCR tubes at $5x10^6$ cells/tube and centrifuged at 500g for 5 minutes to pellet. Supernatant was aspirated and pellets stored at -40°C. RNA was subsequently extracted from thawed pellets using Quick-RNA MiniPrep Plus Kit (Zymo Research) according to manufacturer's guidelines, with 15 minutes DNAse treatment at RT to minimize genomic DNA contamination. RNA was eluted into 30µL nuclease-free water.

2.11.2 cDNA synthesis for TCR-β amplification

Synthesis of cDNA was optimised for TCRβ amplification and performed using the protocol outlined (Smith et al., 2020b) in which RNA was first added to BC1R primer [20μM] and incubated for 2 minutes at 72°C followed by 3 minutes at 42°C. Reactions were then set up for cDNA synthesis by incubating the RNA mix above with the following mastermix: [10μM] SmartNNN primer, [10mM] dNTP mix, [20mM] DTT, [100U/μL] SMARTscribe reverse transcriptase, [40U/μL] RNAse inhibitor and [5X] First strand buffer. The SMARTNNN primer allows cDNA synthesis with 5' template switching and introduction of a unique molecular identifier to quantify cDNA molecules that have entered amplification and therefore prevent PCR amplification bias. Samples were incubated at 42°C for 45 minutes, followed by 70°C for 10 minutes to terminate the reaction. Samples were finally incubated with [5U/μL] Uracyl DNA Glycosylase at 37°C for 10 minutes to prevent exchange of unique molecular identifier sequences during subsequent amplification steps.

2.11.3 TCR-β amplicon generation

Following cDNA synthesis, two rounds of PCR amplification were set up to generate TCR-β variable region amplicons using nested TCR-βeta primers, Illumina-tagged indexed forward primers with SMART oligo sequence and Illumina-tagged reverse primers within the TCR constant region to ensure both forward and reverse indexing. Briefly, the first amplification was set up by adding 2μL cDNA used fresh from above to the following mastermix: [10μM] Smart_stepout 1 primer, [10μM] BC2R primer, [2X] Phusion Flash high fidelity mastermix and nuclease-free water. Samples were incubated at 98°C for 2 minutes; followed by 18 amplification cycles at 98°C for 5 seconds, 68°C for 10 seconds and 72°C for 15 seconds. Samples were then incubated at 72°C for 4 minutes for final elongation. The second amplification was set up by adding 2μL of the first PCR product to the following mastermix: [10μM] P7-SMART-Index, [10μM] P5-BCJ primer, [2X] Phusion Flash high fidelity mastermix and nuclease-free water. All primers used were custom generated DNA oligomers from IDT as detailed in **Table 2.9**. Second PCR products were then assessed for purified TCR-β amplification using gel electrophoresis against DNA ladder for size comparison, and then stored at -20°C prior to product pooling and purification using Monarch PCR Gel Extraction Kit (New England BioLabs) as per manufacturer's instructions.

Step	Primer	Application	Sequence
cDNA Synthesis	BC1R	cDNA synthesis	CAGTATCTGGAGTCATTGA
cDNA Synthesis	SMART-NNN	Template switch	AAGCAGUGGTAUCAACGCAGAGUNNNNUNNNNUNNNNUCTTrG$_{(3)}$
PCR 1	Smart_stepout1	Nested forward 1	CACTCTATCCGACAAGCAGTGGTATCAACGCAG
PCR 1	BC2R	Nested reverse 1	TGCTTCTGATGGCTCAAACAC
PCR 2	P7-SMART-Index	Forward	CAAGCAGAAGACGGCATACGAGATXXXXXXGGCGAAGCAGTGGTATCAACG CAGAGT
PCR 2	P5-BCJ	Reverse	AATGATACGGCGACCACCGAGATCTACACACACSTTKTTCAGGTCCTC
Sequencing	TCR_read1	Read 1	CGAG+ATCTACAC+ACACSTTKTTC+AGGTCCTC
Sequencing	TCR_read2	Read 2	GGCGAAGCAGTG+GTATCAACGCAGAGT
Sequencing	TCR&BCR Index	Read Index	ACTCTGCGTTGATACCACTGCTTCGCC

Table 2.9 - Primers used for TCR repertoire sample preparation and sequencing.

2.11.4 TCR-β next generation sequencing

Purified PCR product libraries were assessed for quality and concentration using Nanodrop and submitted to GeneWiz for next generation sequencing. Submitted libraries were further QC analysed by GeneWiz for quality and concentration using Qubit assay and band size using TapeStation automated electrophoresis. Libraries were then sequenced on an Illumina MiSeq nano platform using custom read primers TCR_read 1, TCR_read2 and TCR&BCR Index with LNA modifications (**Table 2.9**).

2.11.5 Repertoire sequencing analysis

All sequencing analysis was performed by collaborating bioinformatics PhD student Catherine Sutherland. Paired reads were initially assembled from FASTQs with PEAR v0.9.6. UMI processing, error correction and VDJ assignment were carried out using RTCR v0.5.1 (Mamedov et al., 2013). Custom Python scripts were used to process the RTCR output with statistical analyses performed using the SciPy packages (Virtanen et al., 2020). Sequences sharing the same CDR3 were considered to form a single clonotype. For comparisons of diversity, repertoires were downsampled to the same number of UMIs. To identify TCR sequences of known specificity, CDR3s were queried against the down sampled Immune Epitope Database (IEDB) (Fleri et al., 2017) (accessed 13/12/2021) using TCRMatch v0.1.1(Chronister et al., 2021) and against

VDJdb (Bagaev et al., 2020) (accessed 04/02/2022) by manual query. In both cases, only exact amino acid CDR3 matches were counted. Gliph2 was used to identify enriched amino acid motifs in the CDR3 region (Huang et al., 2020b). Clonal networks were visualised using Gephi v0.9 (Bastian et al., 2009).

2.12 Oncogene array testing

2.12.1 gDNA extraction

To determine whether there were any harmful mutational changes in the T cells during the culture and expansion period, we tested start material and final product VST for a panel of oncogenes using a multiparameter panel. This testing was supplied by the Cancer Genetics section of the Oxford Regional Genetics Labs. Genomic (gDNA) was prepared from leukapheresis PBMC and SARS-CoV-2 VST final products using PureLink™ Genomic DNA mini kit (Invitrogen) as according to manufacturer's instructions. Briefly, samples were pelleted and re-suspend in PBS containing Proteinase K [2mg/mL] and RNAse A [2mg/mL] and incubated at RT for 2 minutes. Samples were then diluted in PureLink™ Genomic lysis/binding buffer and incubated at 55°C for 10 minutes to induce protein digestion. Ethanol was then added, and lysates run through a spin column with multiple washes to elute the purified genomic DNA. Due to ethical restrictions, oncogene genetic testing could only be made on commercial material, therefore COVID-19 convalescent donor commercial leukapheresis from USA donors (Key Biologics) bought for translational development of the SARS-CoV-2 manufacturing process were used as representative material for the SARS-CoV-2 VST bank.

2.12.2 Oncogene array

Samples were sent to an accredited lab for testing in a single nucleotide polymorphism (SNP) array for 50 cancer associated genes. To test oncogenic potential induced by the SARS-CoV-2 isolation and expansion protocol, the frequency of SNP in oncogenes outlined in **Table 2.10** were compared between the leukapheresis starting material and the SARS-CoV-2 VST final product (to ensure analysis not affected by herited SNPs already present in the donor). Parallel sequencing using a targeted hotspot strategy (Ion AmpliSeq cancer hotspot v2) was used to identify >95% variants in the listed genes. Analytical sensitivity was based on

coverage to a minimum depth of 500x, with sensitivity of the assay (% mutant detectable in VST gDNA in a background of starting source leukapheresis gDNA) between 5-10%. The oncogene array assay and analysis was performed by Oxford Molecular Haematology lab John Radcliffe Hospital.

ABL1	BRAF	EGFR	FGFR1	GNAS	IDH2	KRAS	NPM1	PTPN11	SMO
AKT1	CDH1	ERBB2	FGFR2	GNAQ	JAK2	MET	NRAS	RB1	SRC
ALK	CDKN2A	ERBB4	FGFR3	HNF1A	JAK3	MLH1	PDGFRA	RET	STK11
APC	CSF1R	EZH2	FLT3	HRAS	KDR	MPL	PIK3CA	SMAD4	TP53
ATM	CTNNB1	FBXW7	GNA11	IDH1	KIT	NOTCH1	PTEN	SMARCB1	VHL

Table 2.10 - Genes tested in oncogene array

2.13 Statistical analysis

Statistical analyses were performed using Prism v9.4.1 (GraphPad) with specific tests detailed within figure legends. Each cohort dataset outlined below assumed normal data distribution of residuals in quantile-quantile plots.

2.13.1 Comparison of LCL- versus peptide-derived EBV VST

For analysis of LCL-derived EBV VST versus peptide-derived EBV VST in Chapter 3, the two groups were compared for individual parameters such as final product viability using unpaired t-tests where $p<0.05$ was considered statistically significant. For analyses within datasets with multiple parameters such as phenotypic analysis of different populations, or reactivity to different antigen conditions, the two groups were compared using unpaired two-tailed t-tests corrected for multiple comparisons (Holm-Šídák test) where $p<0.05$ was considered statistically significant. Correlations between functional marker expression and EBV VST line cytotoxicity were tested using computed Pearson correlation coefficients where $p<0.05$ was considered statistically significant with confidence intervals of 95%.

2.13.2 Comparison of healthy donor versus COVID-19 convalescent donors

For analysis of healthy donor versus COVID-19 convalescent donor PBMC populations and peptide responses in Chapter 4, the two groups were compared using unpaired two-tailed t-tests with Holm-Šídák test for multiple comparisons. Response

comparisons between the three individual SARS-CoV-2 peptides (spike, nucleocapsid and membrane) were tested using repeated-measures one-way analysis of variance (ANOVA) with the Geisser-Greenhouse correction to assume equal variability of differences within donor lines. Correlation between intra-donor frequency of populations compared to other baseline characteristics were tested using computed Pearson correlation coefficients with confidence intervals of 95%. Intra-donor tests of optimised culture conditions effect on phenotype and functional parameters were made using paired two-tailed t-tests corrected for multiple comparisons with Holm-Šídák method.

2.13.3 Comparison of IFN-γ-, TNF-α- and CD154-isolated SARS-CoV-2 VST

For analysis of IFN-γ-isolated, TNF-α-isolated and CD154-isolated SARS-CoV-2 VST in Chapter 5, intradonor comparisons for multiple parameters were tested using repeated measures one-way ANOVA, or two-way ANOVA for two categorical variables, with the Geisser-Greenhouse correction to assume equal variability of differences within donor lines. Correlation between intra-donor frequency of isolation marker subpopulations and donor characteristics were made using Pearson correlation coefficients with confidence intervals of 95%. Comparisons of CD4+ gated cells and CD8+ gated cells for functional responses were tested using paired two-tailed t-tests corrected for multiple comparisons with Holm-Šídák method.

2.13.4 Comparison of development versus banked SARS-CoV-2 VST

For comparison of manual-isolated versus Prodigy-isolated SARS-CoV-2 VST in Chapter 6, comparisons were made unpaired t-tests with Holm-Šídák method for multiple comparison correction. Correlations of banked SARS-CoV-2 VST expansion and phenotypic/ functional parameters were performed using Pearson correlation coefficients with confidence intervals of 95%. For analyses within datasets with multiple parameters such as phenotypic analysis of different cell populations, or reactivity to different antigen conditions, the two groups were compared using paired or unpaired two-tailed t-tests where relevant and corrected for multiple comparisons (Holm-Šídák test) with $p<0.05$ was considered statistically significant.

Chapter 3

Comparison of LCL versus peptide generation of EBV-VST for therapy

Chapter 3 – Comparison of LCL versus peptide generation of EBV-VST for therapy.

3.1 Introduction and aims

Adoptive transfer of donor T cells has been utilised as an immunotherapy for EBV-driven PTLD patients for over twenty years. This chapter focuses on the history of EBV T cell therapy and addresses methodological/technological advancements made to improve manufacture and delivery of this clinical cellular therapy.

VST were first successfully used in the mid-1990s to prevent or treat EBV-positive PTLD in patients who had received allogeneic HSCT (Rooney et al., 1995, Rooney et al., 1998, Heslop et al., 1996, Gustafsson et al., 2000). Note that at this time (and still commonly within the field) this cell therapy is referred to as 'CTL' for cytotoxic lymphocytes. However since generated products were not necessarily enriched for CD8+ T cells and could contain a substantial CD4+ component, nomenclature in this thesis will refer to the cells as VST. In these pilot studies, EBV VST were isolated from the HSCT donor since many patients would have already received cells from this matched individual. For this strategy, a leukapheresis donation from the transplant donor would be taken at the time of transplant to manufacture EBV VST which would then either be frozen and stored for potential use upon the transplant recipient developing PTLD, or given as a preventative prophylaxis. This approach however is largely not applicable for patients with PTLD resulting from SOT whereby the transplant donor is usually deceased and therefore there is no donor blood available. This is also an extremely expensive approach to therapy manufacture since development of PTLD only occurs in a subset of transplant recipients, with the prevalence being dependent on numerous risk factors including transplant type, immunosuppressive regimen, and EBV sero-status of both the transplant donor and recipient. Furthermore, it is prohibitively more challenging to make EBV VST from EBV-naïve transplant donors.

In such cases, autologous EBV VST have demonstrated success in driving regression of tumours (Haque et al., 1998, Khanna et al., 1999, Savoldo et al., 2006). However the major drawback of autologous treatment with this therapy is the extensive time required to generate EBV VST, as using the original published method the manufacturing process takes 3 to 4 months. Although a variable malignant disorder

dependent on site of tumour, PTLD is generally a fast-growing tumour and therefore if blood samples are taken from the patient at time of diagnosis, due to the period of EBV VST generation the disease often proves fatal before a full dose of autologous EBV VST are ready to be administered. In addition, autologous T cell lines derived from EBV-associated lymphoma patients have been found to grow slower than lines derived from healthy donors, with requirement for more frequent mitogenic stimulation (Bollard et al., 2004). This is not surprising given these patients are either naturally immunocompromised individuals or iatrogenically immunosuppressed for transplant. As such, autologous VST generation may not be easily translated or even practicable for many PTLD patients, although Savoldo and colleagues reported the feasibility of generating suitable EBV VST lines from 33/35 (94%) SOT patients in their study (Savoldo et al., 2006). Irrespective of the potential to generate autologous lines, since manufacture of EBV VST requires a leukapheresis starting source material to provide sufficient cells to make a therapeutically relevant T cell dose, collection of such a large blood volume from a PTLD patient may be detrimental to the patient's health and worsen disease progression. Therefore, numerous groups have investigated generation of EBV VST from 'third-party' allogeneic donors to assess the safety and practicality of manufacturing cryopreserved EBV VST banks for rapid 'off the shelf' delivery to PTLD patients on the basis of partial human leukocyte antigen (HLA) matching.

Initial studies delivering allogeneic EBV VST to PTLD patients by Professor Dorothy Crawford's group at the University of Edinburgh proved safe and efficacious and subsequently the SNBTS formed a collaboration to manufacture an allogeneic cryopreserved EBV VST bank for clinical use. The standard method for this manufacture was via repeated stimulation of EBV-specific T cell clones with an autologous EBV+ LCL allowing antigen presentation to drive expansion. SNBTS manufactured two EBV VST (generation 1 and 2) banks using this process and have recently manufactured a generation 3 bank with the newly developed methodology outlined in this chapter. The full history of the clinical use and scientific characterisation of EBV VST generated by SNBTS is detailed in **Table 3.1**.

Clinical Papers							
EBV VST Bank	**Date**	**Reference**	**Total Patients**	**HSCT Patients**	**SOT Patients**	**Response Rate**	**Additional Information**
Gen 1	2001	Haque *et al*. Transplantation.	1	0	1	100%	Liver transplant patient 18 months old
	2002	Haque *et al*. Lancet.	8	1	7	50%	4 paediatric, 4 adults with early polyclonal hyperplastic PTLD
	2005	Wynn *et al*. Lancet Oncol.	1	1	0	100%	6 year old girl with CNS lymphoma
	2007	Gandhi *et al*. Am J Transplant.	3	0	3	67%	3 adults with aggressive advanced monoclonal PTLD
	2007	Haque *et al*. Blood.	33	2	31	52%	10 paediatric, 21 adults
	2010	Haque *et al*. Transplantation.	32	NA	NA	NA	Long-term follow up of patients from 2007 paper
Gen 2	2014	Vickers *et al*. Br J Haematol.	12	6	6	72.70%	8 paediatric, 4 adults
	2016	Naik *et al*. J Allergy Clin Immunol.	5	0	0	25%	Primary immunodeficiency disorder patients
	2018	Chiou *et al*. Pediatr Transplant.	11	0	11	85.70%	Paediatric long-term survival (up to 5 years)
	2019	Kasi *et al*. haematologica.	59	28	20	59%	Long-term survival (up to 6 years)

Scientific Papers					
EBV VST Bank	**Date**	**Reference**	**Characterisation**	**No. Lines Tested**	**Additional Information**
Gen 1	2004	Wilkie *et al*. J of Immunotherapy.	Expansion, Phenotype, Cytotoxicity	135	Tests effect of irradiating final product on cytotoxicity
	2009	McAulay *et al*. J of Immunology.	Antigen specificity, TCR spectratyping	24	Compares antigen specificity of lines infused in 2007 paper with clinical outcome
	2009	Vanhouette *et al*. Immunology.	Phenotype, TCR clonality, Degranulation, Cytokines	12	Tests clonality after each stimulation and mechanisms of killing
Gen 2	2021	Cooper *et al*. Clin Exp Immunol.	Expansion, Phenotype, Cytokines	6	Tests effect of flask, reagents, stimulation intensity and cell number on outcome
Gen 3	2024	Cooper *et al*. Front Immunol.	Expansion, Phenotype, TCR Clonality, Cytokines, Cytotoxicity, Degranulation, Antigen specificity	18	Tests generation 2 vs generation 3 bank exemplar lines

Table 3.1 - Publications of allogeneic EBV VST manufactured by SNBTS.

In the first generation EBV VST bank, 135 donor T cell lines were generated by weekly stimulation by LCL co-culture and tested after each stimulation for cytotoxicity against autologous LCL versus non-specific K562 target cells (Wilkie et al., 2004). Following four stimulations the cytotoxicity against autologous LCL was generally high (30-50% lysis), however this was at comparable levels with cytotoxicity against K562 lines (40-70% lysis) indicating a non-specific killing response. This high level of killing against K562 lines may reflect a considerable population of NK cells, NKT cells, and/or γδ-T cells able to mediate unrestricted killing still present in cultures at earlier stimulation rounds, as indicated by the % CD56+ cells dropping from ~40% to <5% between one to four stimulations. Moreover, CD8+ T cells can elicit MHC-I-independent killing of tumour cells through activating receptor natural killer group 2 member D (NKG2D)-mediated cytotoxicity (Lerner et al., 2023). Therefore, agnostically activated CD8+ T cells earlier in culture may be driving a NKG2D-mediated cytotoxicity against tumour markers expressed on K562 cells, which are subsequently selected out during ongoing culture due to repeated antigen exposure driving an outgrowth of EBV-specific T cells. The majority of lines required 8-11 stimulations to generate T cells with specific cytotoxic response against the autologous LCL (>40% lysis) with negligible non-specific K562 killing (<20% lysis), following which cells were cryopreserved for therapy. Of the 135 donor lines generated, 107 passed the specific cytotoxicity release criteria for clinical use as allogeneic treatments, with the remaining 28 lines showing high killing of non-specific target cells.

This cell therapy was first used to treat an 18 month old combined liver and small bowel transplant patient who developed PTLD 9 months following transplantation (Haque et al., 2001). The patient was EBV seronegative prior to transplantation, however had positive IgG and IgM response to EBV viral capsid antigen upon diagnosis indicating a primary EBV infection. Though the EBV sero-status of the organ donor was unknown, it is likely EBV infection was contracted from the graft itself since PTLD primarily developed in the transplanted small bowel and lymph nodes. It is not uncommon for paediatric patients to be infected by the graft itself considering young children may not have encountered the virus and hence have not developed immunity, whereas transplant donors cannot always be chosen on the basis of EBV sero-status considering the prevalence is so high within the general population. Initially, the patient was withdrawn from immunosuppression (tacrolimus and

azathioprine) and treated with antiviral drug ganciclovir, immunoglobulin and corticosteroids. However this did not deter PTLD progression, and the patient exhibited symptoms of intestinal graft rejection meaning tacrolimus had to be restarted. While reduction in immunosuppression is still a first line modulation for PTLD, this case highlights the fine balancing act between allowing the host's natural immunity to control PTLD tumours versus the inherent risk of graft rejection. The patient was then treated with a single infusion of EBV VST with 2 HLA class I-restricted matches and 1 class II-restricted match at $1x10^6$ cells/kg dosage. Within a week of EBV VST infusion, EBV viral load reduced to undetectable levels, PTLD tumours had regressed and the patient went into complete remission with no evidence of GVHD or infusion-related toxicity.

Following efficacy and safety in this case study, an initial UK-wide phase I trial was carried out testing this 1st generation EBV VST bank in 8 patients (Haque et al., 2002). Two patients died rapidly from other causes after receiving only one or two EBV VST infusions, however EBV viral load had decreased following VST infusion suggesting some clinical effect. As discussed previously, PTLD is frequently an aggressive disease especially when involving multiple sites and consequently it is not uncommon in EBV VST trials for patients to die prior to receiving any or the full regimen of infusions. This can make evaluation of therapeutic efficacy and response rates challenging where there is debate amongst different trials, centres and/or clinicians on whether to include or exclude these patients from analysis. Of the 6 patients who received full EBV VST treatments: 3 had complete responses and went into remission; 1 had a partial response after two infusions and then declined further treatment with a PTLD resurgence 8 months later; and 2 patients did not respond to EBV VST infusions and died of progressive disease. No obvious factors such as degree of HLA matching between donor and patient, VST phenotype or *in vitro* cytotoxicity was found to correlate with clinical response in this small study. Importantly all infusions were well tolerated with no indications of toxicity or GVHD. A further publication reported the use of this bank to treat three patients with aggressive advanced monoclonal PTLD following SOT, with 2/3 patients responsive to EBV VST therapy (Gandhi et al., 2007). Interestingly, this paper demonstrated peaks in the systemic EBV viral load one hour following each VST infusion in all patients which was found to be of the tumour wild type virus origin (and not caused by B95.8 strain contamination of the EBV VST products) suggesting a transient release of EBV virions from lysed tumour

cells following VST infusion. Although one patient died from progressive PTLD-induced respiratory failure within 11 days of therapy, this study was the first to report visualisation of male donor infused VST within the female patient tumour during autopsy visualisation, demonstrating the infused VST had migrated to PTLD site and infiltrated within the B cell lymphoma. Therefore, it was indicated this patient may have responded to EBV VST if treated earlier in disease course and received the full dosing regimen.

A further case study reported the first effective treatment of an EBV+ brain tumour with EBV VST (Wynn et al., 2005). This case was an 8 year old non-transplant but immunocompromised patient with a primary central nervous system (CNS) EBV+ B cell lymphoma and high EBV viral load within the cerebrospinal fluid (CSF). The patient was initially treated with antiviral drugs and rituximab for four weeks, however the clinical condition deteriorated leading to a coma. The patient then received seven EBV VST infusions weekly, with neurological improvement seen by the third infusion when the patient regained consciousness and CSF EBV viral load dropped below levels of detection. Several months later the patient received a HSCT transplant from an EBV+ donor, leading to an EBV viral load resurgence in the CSF three months later. A further two infusions of EBV VST and rituximab was administered which rapidly regressed the tumour and EBV load, and the patient remained in long-term remission. Importantly, this study demonstrated the entry of activated VST into the brain with therapeutic effect, whereas rituximab has limited efficacy in CNS lymphomas due to poor penetrance of the blood brain barrier (Bromberg et al., 2019).

EBV VST from this 1st generation bank then went on to be used in the first phase 2 worldwide clinical trial using allogeneic EBV VST for treatment of PTLD. This multicentre trial treated 33 EBV+ PTLD patients of ranging age, transplant type and PTLD site who had failed to respond to conventional treatments (Haque et al., 2007). This trial reported an overall response rate of 64% at 5 weeks and 52% at 6 months following EBV VST therapy. In one monitored patient infused T cells were still detected up to 6 months following administration. Interestingly, this trial found a positive association with patient response and the percentage of CD4+ T cells within the EBV VST products, whereby lines with <1%, 1-4.9%, or >5% CD4+ T cells had patient response rates at 6 months following treatment of 18% (n=12), 56% (n=9)

and 83% (n=12) respectively. In addition, this trial demonstrated better patient outcomes with increasing number of HLA matches between the patient and EBV VST donor. A long-term follow up study of the patients who had a complete response at 6 months in the initial trial, showed that 86% had survived and were still in complete remission after 4 to 9 years, whereas only one patient had a PTLD relapse (Haque et al., 2010). Non-responder patients at 6 months all went on to receive further PTLD treatments, but survival rate was <40% within a year following VST treatment.

Although this first generation EBV VST bank demonstrated an impressive safety profile, after 2005 cell banks developed in Europe in the context of research laboratories had to be abandoned since they were not manufactured according to Good Manufacturing Practice (GMP) principles. Therefore SNBTS undertook to manufacture a new GMP-compliant bank with funding from the Wellcome Trust. This was awarded a 'Specials' license by the UK Medical Healthcare Regulatory Authority (MHRA) in 2012 to supply EBV VST as an ATMP (Vickers et al., 2014). This second generation EBV VST bank was derived entirely from New Zealand healthy donors to minimise the risk of transmission of nvCJD. Due to the nvCJD outbreak in the UK in the 1980s and 90s, concerns were raised over transmissibility to blood products particularly with high leukocyte content (Regan and Taylor, 2002). To choose a panel of donors with maximal HLA coverage of class I and class II matches, simulations were made using HLA typing of 304 patients on the East of Scotland renal transplant waiting list and 200 New Zealand platelet apheresis donors. This analysis found that 25 well-selected donors covered 85% of the patient population, however increasing panel size beyond this did not significantly increase coverage. Therefore, the new bank was made from 25 donors and manufactured as described previously. This report (Vickers et al., 2014) highlighted the operation of the second generation EBV VST bank, showing that within the first 21 months post-licensure 37 patient enquiries were received. Of these enquiries, thirteen patients died before EBV VST could be delivered, with a mean time of 6 days between enquiry through the initial patient request form and patient death. The authors noted delays to shipment were caused primarily by authorisation of treatment funding, as well as pre-testing cytotoxicity of the chosen best HLA match EBV VST line against PHA stimulated blasts derived from the patient blood samples to check for non-specific killing. To date (March 2025) SNBTS still supply EBV VST from this second generation bank, however as of 2010 this pre-infusion cytotoxicity assay using patient cells is no longer carried out to

minimise delays to treatment. Although this report was not a formal measure of therapy efficacy, of the patients infused at the time of study 72.7% had a complete response. Of the non-responding patients, two had non-haematopoietic sarcoma-like tumours. Sarcomas are known to be able to down-regulate HLA expression (Berghuis et al., 2009), and may also differ in antigen expression compared to PTLD tumours thereby potentially limiting LCL-derived EBV VST to target these tumours. A further two patients who did not respond to EBV VST infusion did not have any HLA class II matches, which may further support the theory that CD4+ T cells within EBV VST products improve anti-PTLD responses. This study also reported the first patient to have side effects from infusion with EBV VST from either the first or second generation EBV VST banks, where the patient developed a rash within a day following VST infusion. This was thought to be a possible skin GVHD and resolved within 24 hours following topical steroid and tacrolimus administration. At this time, other centres had also reported a few cases of mild transient skin GVHD following third party banked EBV VST (Doubrovina et al., 2012) and multi-virus VST (Leen et al., 2013) infusions indicating this was a possible side effect in some cases. However the overall risk to benefit ratio for these advanced disease patients highlights the relative safety of this therapy.

Lines from this second generation bank were also tested within the setting of patients with primary immunodeficiency disorders (PID) requiring HSCT that resulted in severe viral infections (Naik et al., 2016). In this multicentre study, SNBTS EBV VST were delivered to 4 paediatric PID patients following development of EBV lymphoproliferative disease, with only one patient responding to EBV VST therapy indicating the greater challenge in viral clearance within this patient group.

A further study focusing on paediatric SOT patients refractory to conventional treatments demonstrated 80% complete response rate up to 5 years post VST therapy with no cases of GVHD or toxicities (Chiou et al., 2018). In this study, all non-responding patients had late-onset PTLD (development of PTLD more than 12 months following transplantation) which may indicate that the poor response to VST therapy reflects differing overall disease initiation, progression and prognosis as well as tumour cell antigen expression and immunogenicity of this patient group (Bollard et al., 2012).

The most recent long term follow-up study of 59 PTLD patients who received EBV VST from the second generation bank demonstrated overall response rate of 59%, with two cases of mild cutaneous GVHD noted (Kazi et al., 2019). Lower response rates were associated with HSCT patients (46%) compared to SOT (75%) or non-transplant (64%) PTLD patients which likely reflects the poor clinical status and disseminated disease in HSCT PTLD patients. Interestingly, clinical response was higher in patients with PTLD in the CNS (67%) compared to patients without CNS disease (54%). However, this was likely biased by a higher number of CNS PTLD patients recruited earlier within the disease course due to unsuitability of first line treatment rituximab for this cohort. Association of improved response rates in patients receiving EBV VST with higher numbers of HLA class I and class II matches further supported the original observation of HLA matching correlating with efficacy by Haque and colleagues (2007).

More recently, several optimisation approaches were made to improve the LCL manufacturing process in terms of cell product quality as well as conformation with current GMP (cGMP) regulations (Cooper et al., 2021). The manufacturing protocol was improved by reducing the LCL to T cell stimulation ratio from 5:1 to 1:1 as the number of LCL is often a limiting factor in how many T cells can be co-cultured at each stimulation round. This ratio also has effects such as increasing functionality of final product T cell antiviral cytokine production. In addition, culture expansion, phenotype and functionality of T cells was maintained when cultured in a xeno- and serum-free GMP-compliant culture medium thereby reducing risk of potential product contamination. Culture expansion was also significantly improved using gas-permeable rapid expansion (G-Rex, Wilson Wolf LLC, USA) culture vessels compared to standard culture flasks (traditionally grown in T75 open cap flasks). The base of G-Rex flasks has a silicone membrane resulting in a larger surface area for gas exchange than standard flask caps and the larger culture volume means that nutrients last longer necessitating less frequent medium exchanges. Due to the faster growth of VST under these improved conditions, cells reached the same level of EBV VST purity and specificity after an optimised 3-4 stimulation round protocol in G-Rex flasks as compared to 6-9 stimulation rounds necessary in standard flasks. Therefore, this has obvious advantages associated with a shorter culture duration including improved cell health, reduced risk of contamination from extensive manipulation steps and reduced resource consumption of staff and facility time. Furthermore, G-Rex flasks

are also supplied as fully closed-system for GMP manufacture further reducing potential for introduction of a contaminant.

While considerable enhancements were made to modernise the LCL-derived EBV VST manufacturing process to cGMP standard, this approach still had challenges in terms of clinical manufacture, predominantly in the biosafety aspects of using live virus to generate LCL, long cultures to transform LCL lines, and the requirement of repeated LCL stimulation of T cells to make VST lines with sufficient specificity for EBV. Other techniques have been developed to isolate antigen-specific T cells including cytokine capture selection (CCS) first described by (Campbell, 2003). This technique was applied to the isolation of cytomegalovirus VST based on secretion of cytokines released in response to stimulation with CMV peptides (Rauser et al., 2004) and/or CMV lysate (Campbell et al., 2011). EBV VST have since been isolated from donor blood stimulated with EBV peptide pools followed by selection of interferon-gamma (IFN-γ)-secreting VST (Moosmann et al., 2010, Icheva et al., 2013, Kállay et al., 2018). This method provides a rapid isolation to administration approach (<36 hours), but the low frequency of circulating EBV VST (~0.1-1% of total T cells) yields sub-optimally low numbers of IFN-γ+ target cells, restricting the dosing regimen. Protocols to generate cytomegalovirus VST have combined IFN-γ direct selection with a short culture to expand selected cells to clinically relevant numbers (Hammer et al., 2005, Brestrich et al., 2009, Kim et al., 2018).

Therefore, it was the aim of my Masters project in 2015 to investigate proof-of-principle studies to isolate EBV VST from healthy blood donors using cytokine capture selection and combine this with a post-isolation culture system to assess ability to expand the IFN-γ+ target cells to clinically relevant numbers. The pilot research-scale tests using donor buffy coats indicated a substantial T cell expansion and development quickly progressed to process translation and full-scale clean room manufacture of a GMP-compliant 3rd generation EBV VST bank in my years as a research scientist following this. With multiple donor lines manufactured using this new process, it became the aim of my PhD to comprehensively characterise EBV VST derived from the peptide CCS process compared to previous LCL-derived EBV VST. For this comparative study, cryopreserved lines from the second-generation EBV VST bank (LCL-derived) versus the third-generation EBV VST bank (peptide-derived) were assessed for numerous parameters including product yield, phenotype, quality,

functionality, specificity and clonal diversity to evaluate the process and products for optimal T cell therapy (Cooper et al., 2024). In addition, since we have clinical response data for 102 patients treated with the second generation EBV VST bank from a recent audit, a secondary aim was to investigate any potential associations of clinical efficacy with product characteristics to understand what makes a desirable T cell profile for treating PTLD.

3.2 Generation of EBV VST by peptide-mediated cytokine isolation

Treatment of EBV-induced lymphomas with therapeutic allogeneic EBV VST relies upon a fast, safe, and efficient manufacturing process that generates potent targeted products to ensure optimal patient responses and safety. The standard method in this field uses LCL as APC to drive differentiation of naïve T cells into EBV VST over numerous stimulation rounds. We investigated a new technique (**Figure 3.1**) to isolate the small pool of memory VST within peripheral blood of EBV seropositive donors using IFN-γ capture selection. Since this selection process isolates a small number of target cells (~$1x10^6$) as shown later in this section, we then developed and optimized a subsequent culture expansion process. Briefly, the IFN-γ+ target cells are co-cultured with non-target mononuclear cells from the leukapheresis isolation (irradiated to prevent outgrowth) to provide cell density support in culture, continued antigen presentation from the peptide-primed APC and co-stimulatory signaling. Cells are cultured for 18 days in closed-system G-Rex100M-CS flasks in TexMACS medium supplemented with IL-2 [200 IU/mL] to drive T cell expansion. Cells are harvested following 18 days expansion and formulated into patient doses for cryopreservation and long-term liquid nitrogen storage.

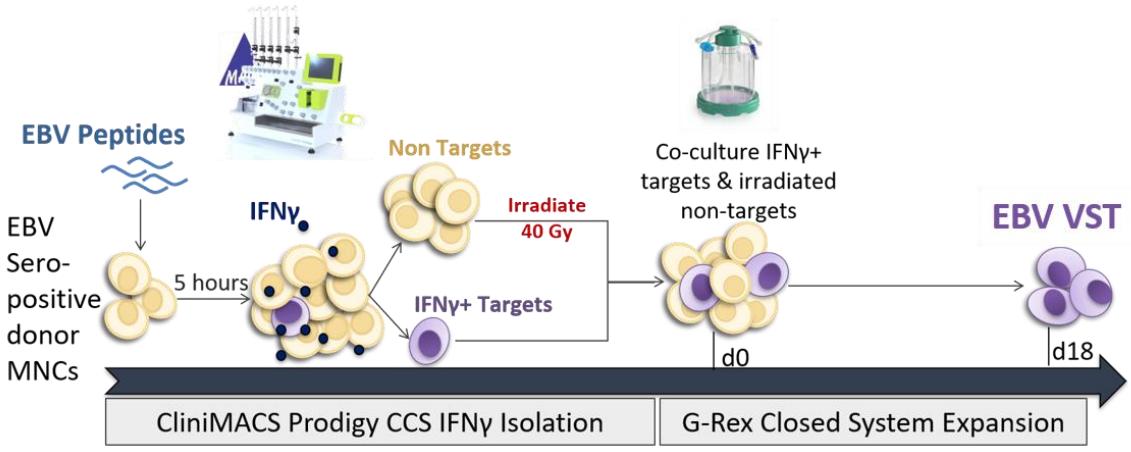

Figure 3.1 - EBV VST generation by peptide-mediated IFN-γ isolation and expansion.

The 3rd generation EBV VST bank manufactured by SNBTS was made using peptide-mediated IFN-γ isolation and expansion. For this, EBV sero-positive donor leukapheresis starting material was stimulated with GMP-compliant EBV consensus peptides (15-mer peptide pools with 11 amino acid overlap covering MHC class I and class II-restricted sequences of 15 lytic and latent EBV antigens) for 5 hours. Reactive IFN-γ-secreting memory EBV VST were then selected using a clinical grade IFN-γ capture system to isolate IFN-γ+ target cells through a magnetic column. All stimulation and isolation steps were carried using an automated closed-process CliniMACS Prodigy processor. The non-target cells from the isolation were then irradiated at 40 Gy and co-cultured back with the IFN-γ+ target cells to provide continued co-stimulatory signalling and feeder

support in culture for the first several days before irradiated cells died off. Co-cultures were seeded in G-Rex closed-system flasks in TexMACS medium with IL-2 supplementation for up to 18-19 days with medium additions at 1-2 times per week. At day 18 or 19, cells were harvested, washed and cryopreserved in CryoStor10: PlasmaLyte [2:1] freezing solution in bagged doses at $1.5x10^8$ cells/dose and controlled rate frozen for long term storage in liquid nitrogen vapour phase tanks.

3.2.1 Screening donors for EBV peptide T cell responses

For full-scale process translation, leukapheresis material from EBV sero-positive donors were acquired commercially from Key Biologics, USA and shipped fresh within 48-96 hours of apheresis collection. A total of seven Key Biologics leukapheresis USA donor runs (coded as EBVUSAD) were carried out to understand the kinetics of full-scale isolations and cultures, whereby $2x10^9$ WBC per run were set up for a Prodigy CCS isolation. In tandem with the CCS isolation, MNC samples were taken to stimulate with the EBV peptides to quantify T cell responses using an intracellular cytokine screening assay. For the screen, flow cytometric analyses were gated on lymphocytes/singlets/live cells, followed by sub-gating on CD8+/IFN-γ+ cells where the IFN-γ+ gate was set according to a no antigen control as per **2.7.1**. Although donors were selected based on confirmed IgG-positive serum antibody titre to EBV VCA, T cell responses in these donors to the EBV consensus peptides were variable. **Figure 3.2A** left panels shows exemplar flow cytometry plots of EBV peptide screen responses for donor EBVUSAD1 with a significant memory pool of CD8+/IFN-γ+ cells (0.28% of total live lymphocytes) as compared to donor KBL6 where CD8+/IFN-γ+ cells were barely detectable (0.014% of total live lymphocytes). Following the Prodigy CCS isolation, small samples of the target cells were taken for enumeration and phenotypic analysis by flow cytometry (**Figure 3.2A** right panels). As can be seen, donor EBVUSAD1 had a distinct lymphocyte population surrounded by debris and some monocytes, which when gated had 87.9% viability, whereas lymphocytes within the target fraction of donor EBVUSAD6 were only 0.71% viable. It was hypothesised the lack of detectable CD8+/IFN-γ+ cells in donor EBVUSAD6 at screen was predictive of negligible live lymphocytes isolated in the IFN-γ CCS assay. To investigate this further, the mean frequency of CD8+/IFN-γ+ cells at EBV peptide screen is shown for all seven donors in **Figure 3.2B**. The donor frequency of CD8+/IFN-γ+ cells at EBV peptide screen was tested for correlation with the viable cell count of IFN-γ+ target cells isolated by Prodigy CCS (**Figure 3.2C**). Although not statistically significant ($p=0.0547$, $R^2=0.555$), there was a trend of higher number of isolated live target cells with the higher frequency of peptide-reactive IFN-γ+ cells at screen. Both donors EBVUSAD3 and EBVUSAD6 which had 0.02% and 0.014%

CD8+/IFN-γ+ cells at screen respectively, isolated <5x10^5 viable cells. From these results, we decided to implement a minimum criterion of ≥0.1% CD8+/IFN-γ+ cells at EBV peptide screen for a donor to be taken forward with CCS isolation.

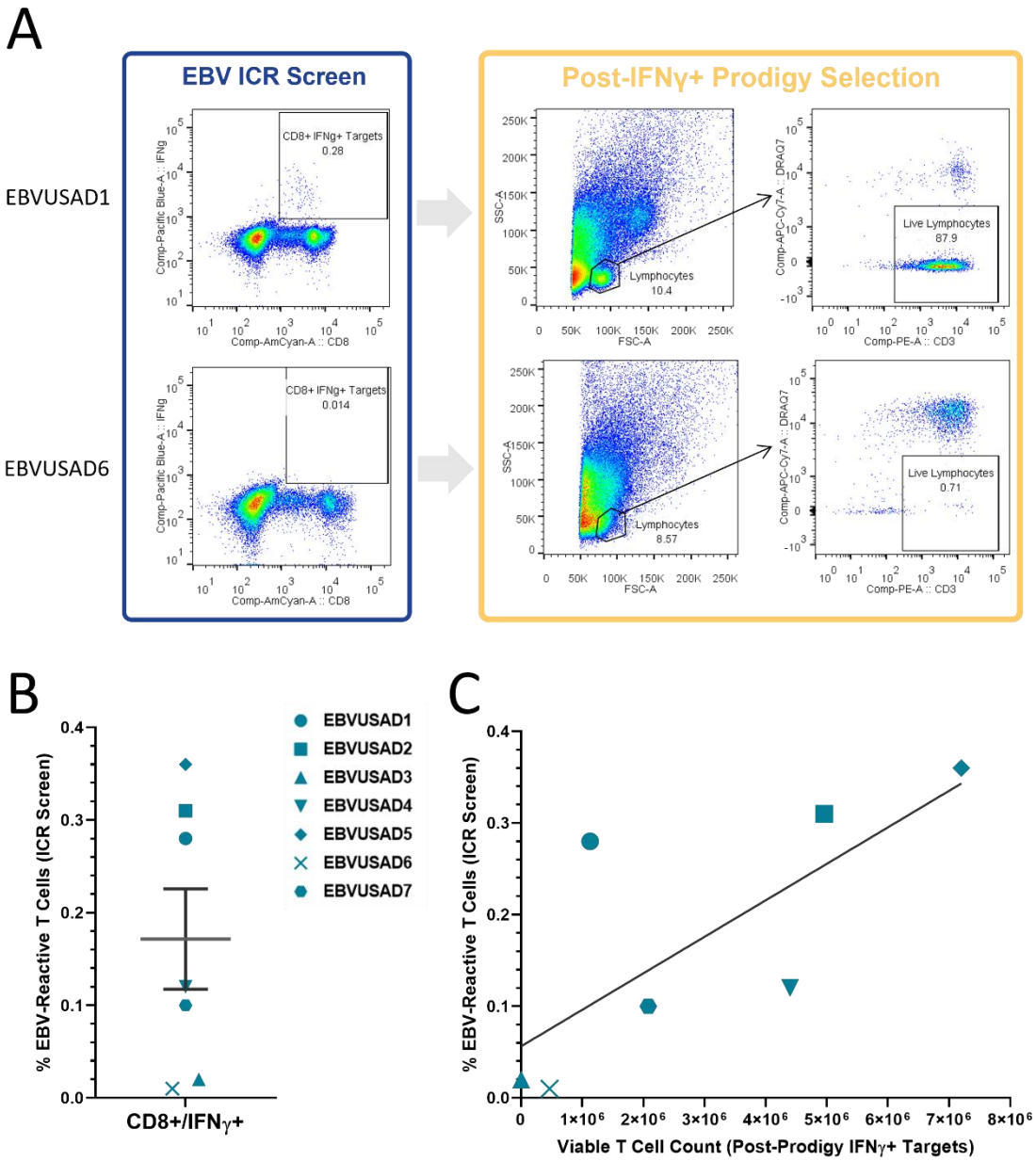

Figure 3.2 - EBV peptide T cell responses in seropositive donors and IFN-γ isolation.

Full-scale translation of the peptide CCS selection process utilised commercial leukapheresis starting material from EBV sero-positive donors EBVUSAD1-7. **(A)** Representative flow cytometry analysis shows EBV peptide screen T cell responses of donors EBVUSAD1 and EBVUSAD6 in the left panels where peptide reactive cells were gated as CD8+/IFN-γ+ cells normalised to no antigen negative controls. Flow analysis of the corresponding donor Prodigy CCS isolated IFN-γ+ cells in the right panels show initial gating of the lymphocyte population, followed by sequential gating of viable lymphocytes using dead cell stain DRAQ7. **(B)** The mean ± SEM frequency of CD8+/IFN-γ+ cells in EBV peptide screen assay is shown for all donors (n=7). **(C)** The donor frequency CD8+/IFN-γ+ cells showed no significant correlation with total number of isolated viable Prodigy CCS IFN-γ+ target cells. Statistical analysis was done by generating Pearson correlation coefficients, where $p<0.05$ was considered significant.

3.2.2 Isolated EBV peptide-specific T cells expand in culture

All target cells were set up in co-cultures with irradiated non-target cells at [1:300-600] to provide co-stimulatory signals and initial density support. Counts were taken twice weekly using Trucount tubes with addition of DRAQ7 to enumerate the total number of viable cells. The growth curves for all EBVUSA donor cultures are shown in **Figure 3.3A,** where the day 0 count is only the IFN-γ target cells and does not include the additional irradiated non-target cells. Isolation of cells from donors EBVUSAD3 and EBVUSAD6 resulted in less than $5x10^5$ target cells which subsequently failed to expand during the culture period between day 11 to 15. Interestingly, these two cultures show an initial peak in cell numbers at day 7, however this likely reflects that the irradiated non-target cells added at the start of co-culture have begun to die off between day 7 to 11 in this culture process. The fold expansion between day 0 target cells and day 18 or 19 harvested cells (**Figure 3.3B)** shows the five donors which had good growth expanded between 500-4000x fold over the culture period.

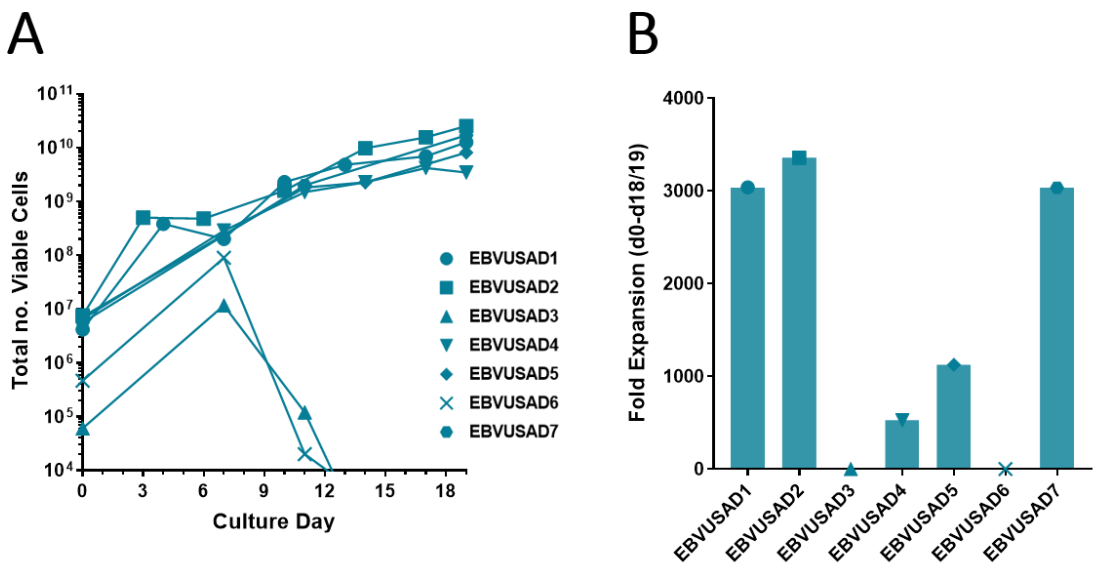

Figure 3.3 - Peptide EBV VST process full-scale translation culture expansion.

Following Prodigy CCS isolation, IFN-γ+ target cells were co-cultured with irradiated non-target cells and cultured in G-Rex100M closed system flasks in GMP TexMACS medium supplemented with IL-2 [200 IU/mL] for up to 19 days. **(A)** The total number of viable cells over the culture period is shown for each donor line. **(B)** The fold expansion between day 0 and day 18/19 harvest is shown for each donor line.

Since there was a clear observation in EBVUSAD3 and EBVUSAD6 showing lack of detectable IFN-γ+ cells at the screening point, negligible viable target cells isolated and failure to yield any EBV VST in culture; it was decided to utilise the EBV peptide T cell response from the ICR assay as a pre-screen donor selection criterion. Peripheral

blood samples from prospective EBV seropositive donors were tested and only donors with sufficient EBV T cell responses were recruited for inclusion in manufacture of the EBV VST bank. This therefore prevented non-eligible donors from going through apheresis collection, as well as reducing potential manufacturing failures.

3.2.3 Expansion of CD8+ central and effector memory cells

Basic phenotypic analysis was performed throughout culture to investigate changes in different population dynamics. For the lymphocyte surface phenotype panel, cells were initially gated on mononuclear cells/singlets/live cells, followed by gating of CD3-/CD56+ NK cells, CD3+/CD56+ NKT cells and CD3+/CD56- T cells. T cells were then gated into CD4+ T cells or CD8+ T cells, and each subtype further divided by T cell differentiation status: CD62L+/ CD45RA+ naïve T cells (TNaive), CD62L+/CD45RO+ central memory T cells (TCM), CD62L-/CD45RO+ effector memory T cells (TEM), and CD62L-/CD45RA+ terminally differentiated effector memory RA+ T cells (TEMRA). Representative t-stochastic neighbour embedding (t-SNE) dimensionality reduction analysis of these populations within the mixed blood leukapheresis starting source material of donor EBVUSAD1 is shown in **Figure 3.4A**. This analysis was then used to track changes in population frequencies from the IFN-γ CCS process and throughout culture expansion as shown for representative donor EBVUSAD1 (**Figure 3.4B**). As can be seen, the non-target cells from isolation are comparable to the leukapheresis lymphocyte population compositions as would be expected from the residual cells remaining following the CCS process. The IFN-γ+ target cells however were largely composed of CD8 TEM and CD8 TEMRA cells, with a small population of CD4 TCM & TEM cells indicating a significant enrichment of antigen-experienced T cells, with negligible contaminating NK cells or naïve T cells. Over the culture period there was substantial expansion of the CD8 central memory T cell population which composed the majority of day 18 harvested cells, with small populations of CD4 and CD8 effector memory T cells. This indicates that while the selection process isolated highly activated T cells nearing terminal differentiation, the culture process drives an outgrowth of central memory CD8+ cells, while still supporting expansion of CD4 effector memory cells which may be beneficial for allogeneic VST therapy persistence.

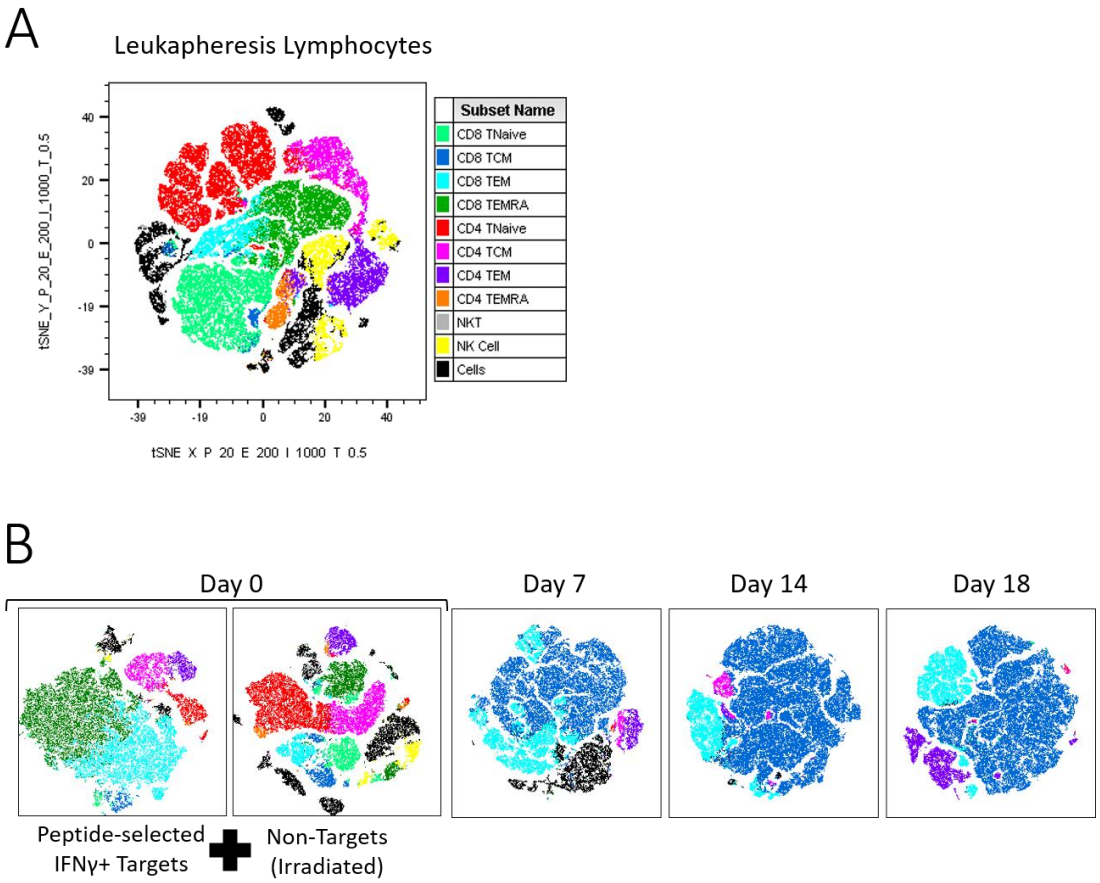

Figure 3.4 - Phenotypic analysis of populations throughout the peptide process expansion.

Flow cytometric surface marker phenotyping using t-stochastic neighbour embedding (t-SNE) dimensionality reduction analysis. **(A)** Exemplar leukapheresis starting material of EBVUSAD1 identified the following lymphocyte populations: NK cells (CD3-/CD56+), NKT cells (CD3+/ CD56+), CD4 T Cells (CD3+/ CD4+) and CD8 T cells (CD3+/ CD8+). Both CD4 T cells and CD8 T cells were then sequentially gated for T cell memory subpopulations: TNaive (CD62L+/ CD45RA+), TCM (CD62L+/CD45RO+), TEM (CD62L-/CD45RO+) and TEMRA (CD62L-/CD45RA+). **(B)** Dynamics of these gated populations were shown from co-culture set up at day 0 to day 18 of culture.

3.2.4 Expansion of peptide-specific effector T cells

To measure EBV specificity, samples were taken throughout the culture period to test functional recall to EBV consensus peptide pools (**Figure 3.5**). For this, cells were stimulated as per the screen assay with peptides for 5 hours and assessed for induction of antiviral cytokines IFN-γ, TNF-α and IL-2 compared to no antigen negative controls. Flow cytometry analysis was used to gate into populations with singular cytokine expression, dual cytokine expression or triple cytokine expression as per gating strategy outlined in **Figure 2.8**.

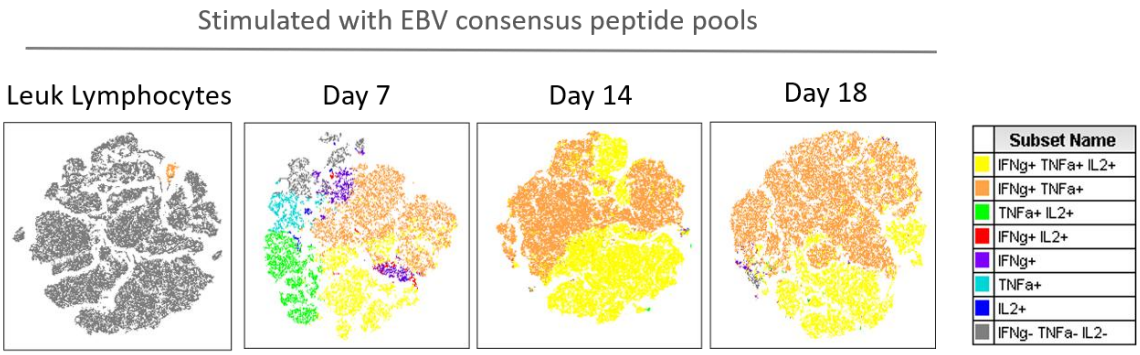

Figure 3.5 - Functional analysis of populations throughout the peptide culture expansion.

Flow cytometric intracellular cytokine staining using t-SNE dimensionality reduction analysis. The functional cytokine reactivity to 5 hour stimulation with EBV consensus peptide pools is shown for representative donor EBVUSAD1 at the leukapheresis screen pre-isolation (left panel), and at days 7, 14 and 18 of the culture process. Cytokine sub-populations were gated into triple positive (IFN-γ+/TNF-α+/IL-2+); dual positive (IFN-γ+/TNF-α+), (IFN-γ+/IL-2+), (TNF-α+/IL-2+); single positive (IFN-γ+), (TNF-α+), (IL-2+); and cytokine null (IFN-γ-/TNF-α-/IL-2-).

The small pool of memory EBV VST identified at screening (leuk lymphocytes panel) is dual positive for IFN-γ+/TNF-α+ expression. Following Prodigy CCS isolation and culture initiation, at day 7 there is a relative mix of different cytokine subpopulations reactive to EBV peptide recall. By days 14-18 there was outgrowth of the IFN-γ+/TNF-α+ dual positive and IFN-γ+/TNF-α+/IL-2+ triple positive T cell populations. Since IFN-γ+/TNF-α+/IL-2+ triple positive T cells were mainly found within the central memory population (Cooper et al., 2021), whereby IL-2 secretion mediates the high proliferative capacity of central memory cells in addition to the effector cytokines IFN-γ and TNF-α, this functional cytokine profile data supports the phenotypic outgrowth of TCM observed in **Figure 3.4**. Note, since the number of target cells from Prodigy CCS was limited (~10^6 cells), and the cells had just undergone antigenic stimulation for the isolation, cells could not be tested for functional reactivity at this time-point. Importantly this assay demonstrated the resultant T cells had high functional specificity to EBV peptides.

3.2.5 Bank manufacture of EBV VST using peptide-mediated process

Following successful process translation, a campaign of clean room manufacture generated EBV VST lines for clinical bank use from five UK donors. For this, donors were recruited through the clinical apheresis unit (CAU) at Royal Infirmary Edinburgh, where regular platelet donors with SNBTS viral testing history were selected on the basis of EBV sero-positivity and HLA coverage.

Prospective donors then provided peripheral blood samples which were tested for T cell responses to EBV peptides using the ICR screen assay developed in section **3.2.1**. From this screening assay, 11/17 (64.7%) EBV sero-positive donors had sufficient (>0.1%) T cell responses to EBV peptides for VST manufacture (**Figure 3.6A)**. The number of final product doses for all EBVUSA translational and EBVUK bank manufacturing runs are shown in **Figure 3.6B**, with no significant correlation seen between frequency of EBV peptide-reactive CD3+/IFN-γ+ cells at screen and final product dose yield (**Figure 3.6C**).

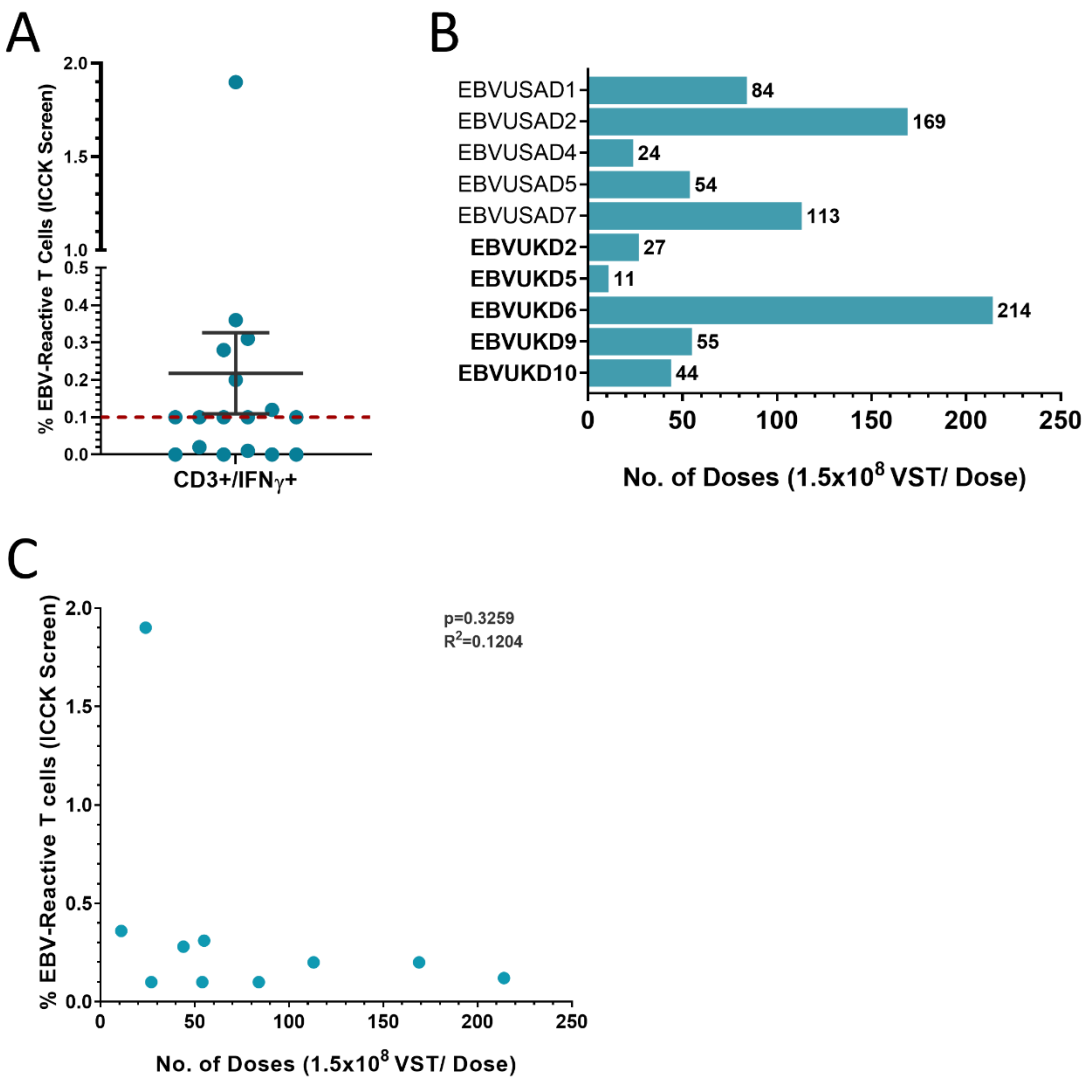

Figure 3.6 - Peptide-derived EBV VST donor screen and final product dose yield.

Screen and manufacture of peptide-derived EBV VST is shown for full-scale GMP translational lines (EBVUSA donors) and clean room banked lines (EBVUK donors highlighted in bold). **(A)** Initial ICCK screen identified 11/17 EBV sero-positive donors with sufficient T cell responses to EBV peptide stimulation. The red dotted line represents the minimum criterion of CD3+/ IFN-γ+ cells ≥0.1% for donor eligibility to manufacture. **(B)** The number of final product doses generated at $1.5x10^8$ cells/dose is shown for all manufactured donor lines. **(C)** No correlation was observed between frequency of EBV-reactive CD3+/ IFN-γ+ cells at screen and final product doses manufactured. Statistical analysis was done by generating Pearson correlation coefficients, where $p<0.05$ was considered significant.

Three process validation runs (EBVUKD2, EBVUKD5, EBVUKD6) and two clinical runs (EBVUKD9, EBVUKD10) from UK donors were performed, therefore making five clean room manufactured EBV VST lines. **Table 3.2** outlines EBVUK banked VST donor demographics including sex, age, HLA type, EBV viral capsid antigen (VCA) IgG serum antibody titre (U/mL) and the percentage of EBV VST reactive to peptides at initial ICCK screen.

Donor Code	Sex	Age	Blood Group	HLA								EBV VCA IgG (U/mL)	VST Screen (%CD3+/ IFNγ+)
				A*	A*	B*	B*	C*	C*	DRB1*	DRB1*		
EBVUKD2	M	65	O+	02:01	03:01	35:01	40:01	03:01	04:01	07:01	15:01	151	0.20%
EBVUKD5	M	51	O-	01:01	03:01	07:01	08:01	07:01	07:01	03:01	13:01	74	0.10%
EBVUKD6	M	40	O+	02:01	02:01	08:01	27:01	01:01	07:01	01:01	03:01	128	1.90%
EBVUKD9	M	61	O+	24:02	30:02	18:01	39:06	05:01	07:02	03:01	15:01	750	0.20%
EBVUKD10	M	53	O+	01:01	03:01	07:02	51:01	07:02	14:02	07:01	15:01	750	0.10%

Table 3.2 - Peptide EBV VST banked donor demographics.

3.2.6 Peptide EBV VST bank characterisation testing

Samples of final product harvested cells were taken for quality control (QC) testing to assess product identity and purity. Minimum criteria were set for product release, including viability ≥80%, CD3+ T cell ≥90% and CD3-/CD56+ NK cells ≤10%. All final products had >95% viability (**Figure 3.7A**), with negligible NK cells (**Figure 3.7B**). Some lines expanded a small CD3+/CD56+ NKT cell population (**Figure 3.7C**), however since these are still fundamentally T cells this was not an exclusion criterion for the product. All lines were highly purified for CD3+ T cells >97% (**Figure 3.7D**), and skewed to CD8+ T cells with small CD4+ populations (**Figure 3.7E**). Characterisation of T cell memory (**Figure 3.7F**) demonstrated negligible naïve or terminal differentiated effector memory RA (TEMRA) T cells; with most donors having an equal split of central memory (TCM) and effector memory (TEM) T cells.

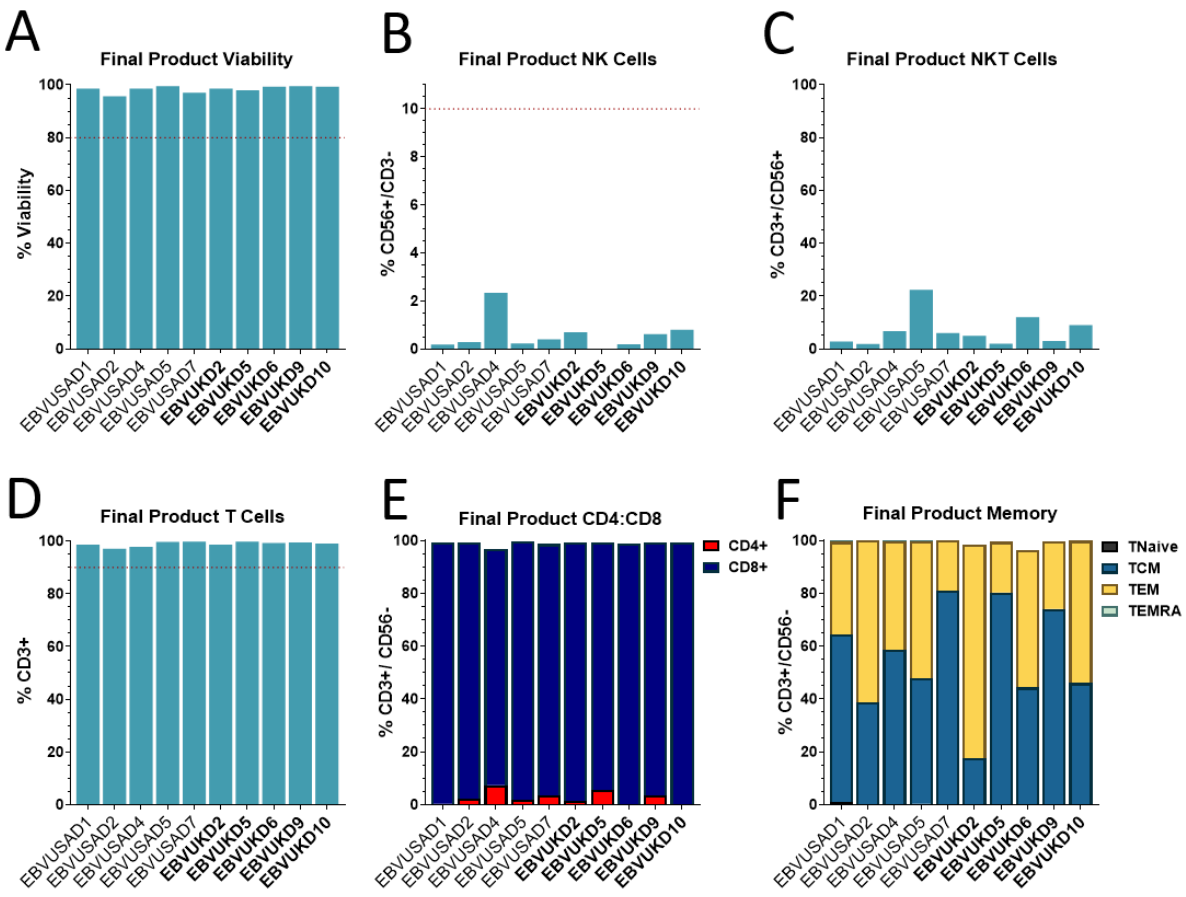

Figure 3.7 - Peptide-derived EBV VST final product phenotype.

Final product phenotypic characterisation of peptide-derived EBV VST is shown for full-scale GMP translational lines (EBVUSA donors) and clean room banked lines (EBVUK donors highlighted in bold). Total gated live lymphocytes were quantified for the percentage **(A)** viability (DRAQ7-), **(B)** NK cells (CD56+/CD3-), **(C)** NKT cells (CD3+/CD56+), and **(D)** T cells (CD3+). Within the gated CD3+ population, T cells were further subdivided for **(E)** CD4 to CD8 content, and **(F)** T cell memory subpopulations: TNaive (CD62L+/ CD45RA+), TCM (CD62L+/CD45RO+), TEM (CD62L-/CD45RO+) and TEMRA (CD62L-/CD45RA+). Red dotted lines indicate a criterion for therapy, whereby final product viability ≥80%, NK cells ≤10% and T cells ≥90% for product release.

Final product samples were also tested using a panel of QC assays for functionality and EBV specificity using the antigen recall assay. As described previously, harvested cells were stimulated with EBV consensus peptides and compared to non-antigen negative controls for 5 hours and further assessed for production of antiviral cytokines by intracellular flow cytometry staining. As can be seen, all lines had high expression of IFN-γ (**Figure 3.8A**) and TNF-α (**Figure 3.8B**) reactive to EBV peptide stimulation indicating high EBV specificity and ability to induce effector functionality upon antigen recognition.

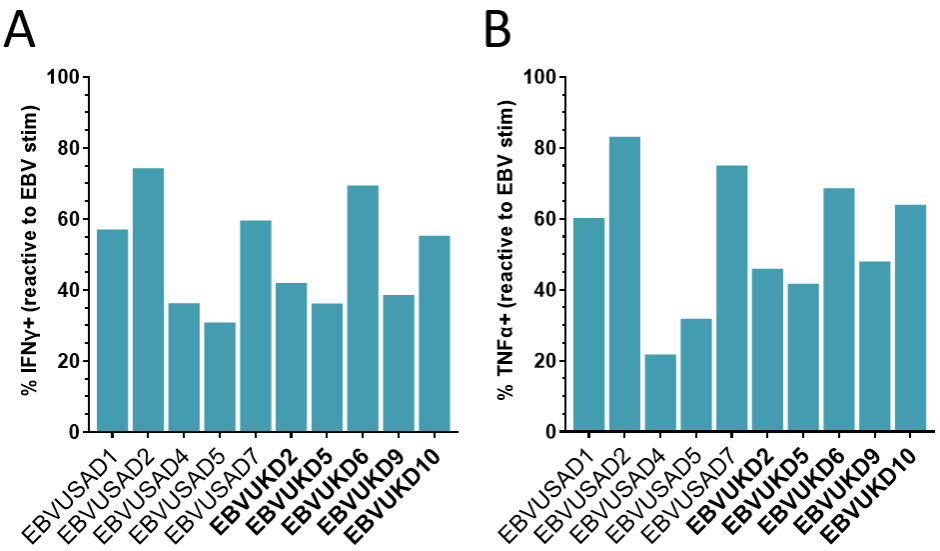

Figure 3.8 - Peptide-derived EBV VST final product function.

Final product functional characterisation of peptide-derived EBV VST is shown for full-scale GMP translational lines (EBVUSA donors) and clean room banked lines (EBVUK donors highlighted in bold). Harvested cells were stimulated with EBV peptides compared to negative no antigen controls and assessed for reactivity by quantifying the percentage **(A)** IFN-γ+ and **(B)** TNF-α+ cells.

Altogether this data shows the peptide manufacturing process successfully generated five clean room EBV VST lines highly enriched for cytotoxic T cells, with high functional specificity towards EBV peptides. All products passed the release criteria and most lines had high yields demonstrating a robust process for EBV VST manufacture.

3.3 Comparison of LCL-derived versus peptide-derived EBV VST

After successful manufacture of a new EBV VST bank using the peptide-mediated cytokine selection and expansion process, it was a major aim of this PhD to compare EBV VST products generated using both the peptide and original LCL process. Since SNBTS have a wealth of clinical data demonstrating efficacy of LCL-derived EBV VST products, it was crucial to ensure products made using the new peptide process were comparable to LCL-derived EBV VST to predict this therapy would also be safe and effective in PTLD patients. To allow the most accurate comparison, all subsequent assays were done using cryopreserved and thawed EBV VST samples from the second generation LCL-derived bank versus the third-generation peptide-derived bank.

3.3.1 Comparison of LCL and peptide manufacturing processes

A comparison of the two manufacturing processes to generate EBV VST is shown in **Figure 3.9** . As detailed previously, the LCL process uses EBV B95-8 strain supernatant to infect donor B cells causing transformation into LCL lines (**Figure 3.9A)**. Since B cells can present antigen including endogenous EBV antigens, the LCL are irradiated and subsequently co-cultured with remaining donor leukapheresis, driving the differentiation of EBV-specific T cells, where 6-9 stimulation rounds are usually required in manufacture to generate a pure population of EBV VST final products.

For the peptide-mediated method, leukaphereses from EBV sero-positive donors are stimulated with peptide pools (15-mers with 11 amino acid overlap) covering 15 lytic and latent MHC class I- and class II- restricted EBV protein sequences (**Figure 3.9B**). Memory EBV-specific T cells reactive to EBV peptides are then isolated using IFN-γ capture selection, and target cells are subsequently expanded for 3 weeks in culture.

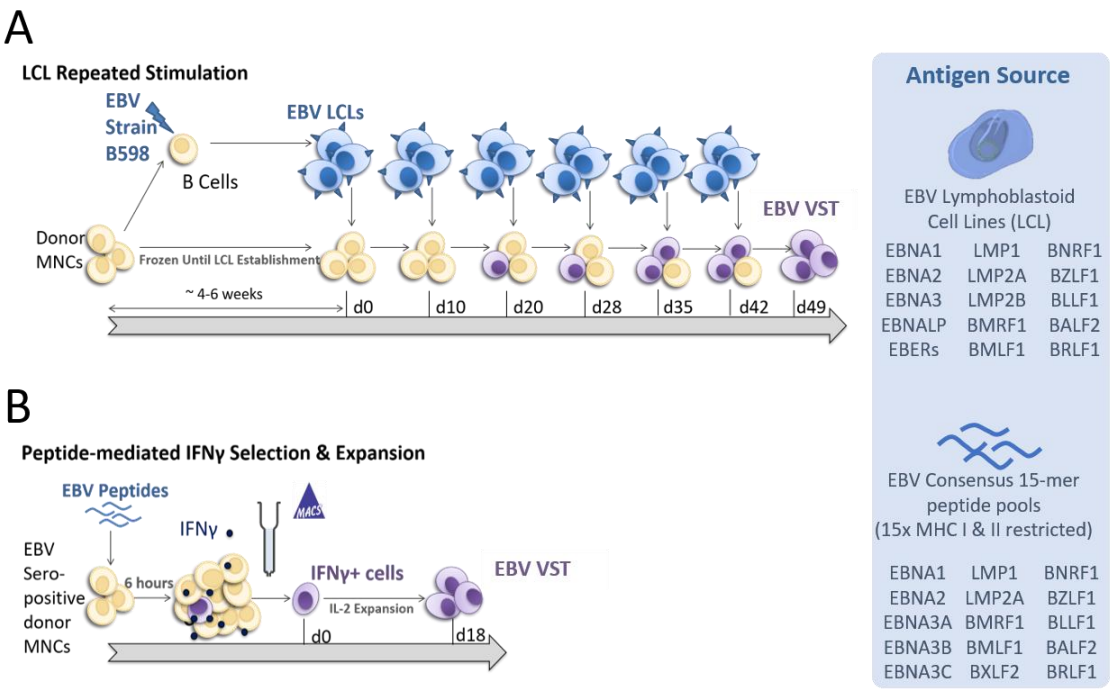

Figure 3.9 - EBV VST generation processes comparison.

(A) In the traditional LCL repeated stimulation process a portion of the donor mononuclear cells (MNC) are cultured in medium containing EBV strain B598 supernatant for four to six weeks to induce transformation of B cells into EBV-transformed lymphoblastoid cell lines (LCL) which express EBV antigens: EBNA1, EBNA2, EBNA3A, EBNA3B, EBNA3C, EBNALP, LMP1, LMP2A, LMP2B, BMRF1, BMLF1, BNRF1, BZLF1, BLLF1, BALF2, BRLF1 and EBERs. These LCL are cryopreserved and thawed for co-culture with the remaining thawed donor MNCs over multiple stimulation rounds to allow EBV antigen presentation to T cells resulting in a pure EBV VST product after six to nine stimulation rounds. **(B)** For the peptide-mediated IFN-γ selection & expansion process MNC from EBV sero-positive donors are stimulated for 4 hours with EBV consensus overlapping peptide pools covering MHC restricted sequences for EBV antigens: EBNA1, EBNA2, EBNA3A, EBNA3B, EBNA3C, LMP1, LMP2A, BMRF1, BMLF1, BNRF1, BZLF1, BLLF1, BALF2, BRLF1. Antigen-specific EBV memory T cells are isolated using IFN-γ cytokine capture selection. Non-targets from the selection are irradiated and co-cultured alongside the IFN-γ targets to provide co-stimulatory support and T cell expansion resulting in a pure EBV VST product in 18-19 days.

The major differences between the two methods in terms of processing and bank manufacture are outlined in **Table 3.3**. Donors for each bank were healthy apheresis donors, recruited through the New Zealand Blood Transfusion Service for the LCL-derived bank to provide similar HLA types to the Scottish population at time of nvCJD risk in the UK, versus through SNBTS for the peptide-derived bank. Leukapheresis from the New Zealand donors was cryopreserved and shipped to SNBTS Aberdeen as a frozen starting material for EBV VST generation, whereas starting material for the peptide-derived bank was required to be fresh for the Prodigy IFN-γ CCS isolation.

B95-8 viral supernatant was used as the live EBV source to infect and establish LCL lines for each New Zealand donor, and therefore the lines may have been variable in their antigen expression and density between donors. The peptide pools used for

peptide selection were standardised between donors, however since the peptides are HLA-restricted, this likely drove variation in presentation between donors with differential HLA alleles. The process duration was significantly longer taking 10-16 weeks for the LCL process as compared to 19-20 days for the peptide process. Culture medium for the LCL process contained fetal bovine serum, whereas the peptide-derived VST were grown in a GMP-grade xeno-free, serum-free medium. Cells were grown in standard open cap T25 and T75 flasks for the LCL process as compared to closed-system rapid expansion G-Rex100M-CS flasks for the peptide process. Finally, cells were frozen in human serum albumin with DMSO [10%] in Origen CryoStore bags into both adult and paediatric doses dependent on cell numbers at harvest for the LCL process. Since yield was generally high for the peptide process all bags were frozen down as adult doses ($1.5x10^8$ cells per dose) with the protocol for administration to give the volume required from the bag per kg body weight. These doses were cryopreserved in PlasmaLyte with CryoStor10 at a final DMSO concentration of [6.66%] in Miltenyi CryoMACS50 bags.

PROCESS	LCL REPEATED STIMULATION	PEPTIDE SELECTION & EXPANSION
DONORS NATIONALITY	New Zealand	UK
STARTING MATERIAL	Frozen Leukapheresis	Fresh Leukapheresis
ANTIGEN SOURCE	Donor-specific LCL (live virus)	HLA-restricted peptide pools
PROCESS DURATION	10-16 weeks (4-6 weeks LCL culture + 6-10 weeks VST culture)	19-20 days (1 day isolation + 18-19 days VST culture).
VST CULTURE MEDIUM	RPMI 1640 medium + fetal bovine serum [20%] + L-glutamine [2mM] + IL-2 [20 IU/mL]	GMP TexMACS medium + GMP IL-2 [200 IU/mL]
CULTURE VESSELS	Corning T25 & T75 flasks	Closed-system G-Rex100MCS flasks
FEEDS	Every 2-3 days throughout	Days 0, 7, 10 or 11, 13 or 14
FREEZING SOLUTION	Human serum albumin + DMSO [10%]	CryoStor10 + PlasmaLyte [2:1] (DMSO [6.66%])
FREEZING CONTAINER	Origen CryoStore bags + cryovials for QC & stability testing	CryoMACS50 bags
BAGGED DOSES	Adult $1.5x10^8$ cells/bag ($1x10^7$ cells/mL x15mL) Paediatric $5x10^7$ cells/bag ($3.33x10^6$ cells/mL x15mL)	$1.5x10^8$ cells/bag ($1x10^7$ cells/mL x15mL)

Table 3.3 - Differences in EBV VST manufacturing processes.

3.3.2 Improved yield and viability of EBV VST derived from peptide process

Clinical manufacture of cell therapies requires a fast, scalable, simplified and cost-effective generation protocol to be able to deliver treatments to patients. In an autologous setting it can provide multiple doses to the same donor and as an allogeneic product it can provide a bank of material for treatment of a large number of suitable recipients. Since the LCL and peptide processes differ in generation approach, with multiple rounds of LCL co-culture leading to differentiation of naïve T cells and/or expansion of EBV memory subpopulations within the starting source leukapheresis versus an initial isolation of a subset of EBV memory cells followed by expansion respectively, comparison of the overall fold expansion of cells over the culture period is not relevant. The final product cell count actually cryopreserved per manufacturing run however provides the best means to compare yields between the two processes. As shown in **Figure 3.10A**, the peptide processes generated a significantly increased ($p<0.0001$) number of final product viable cells yielding a mean=93±24 doses from a single donor manufacturing run as compared to the LCL process (mean=9±1 doses).

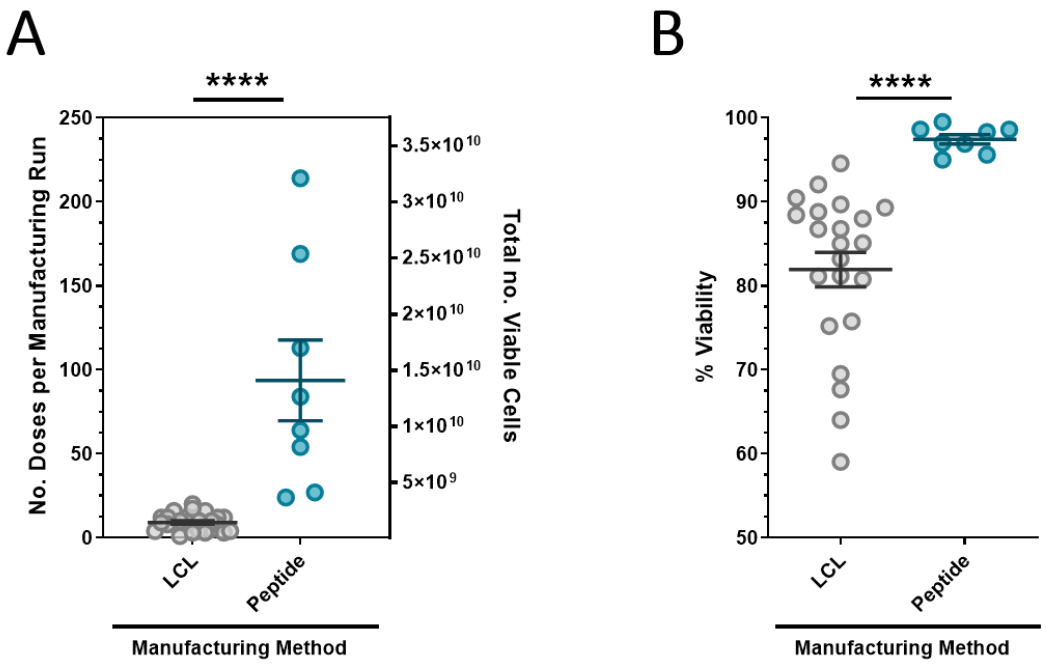

Figure 3.10 - Comparison of LCL-derived and peptide-derived EBV VST yield and viability.

Manufacturing methods were compared for final product viability and cell yield at day of harvest prior to characterisation between LCL-derived (n=22) and peptide-derived (n=8) EBV VST. **(A)** Yield measured by number of adult patient doses ($1.5x10^8$ cells per dose) per manufacturing run

on left y-axis and total number of viable cells on right y-axis. **(B)** Viability was measured as percentage of cells negative by dead cell dyes (7-AAD for LCL manufacturing process and DRAQ7 for peptide manufacturing process). Data is represented as mean ± SEM and statistical analysis performed using unpaired t-tests where ****p≤0.0001.

Furthermore, the percentage of viable cells in final products was significantly higher ($p<0.0001$) in peptide-derived compared to LCL-derived VST (**Figure 3.10B**). This difference likely reflects the shorter culture duration of the peptide process, whereas the LCL process has longer culture and frequent antigenic stimulation which may drive T cell activation-induced cell death (AICD).

3.3.3 Increased central memory phenotype in peptide-derived EBV VST

To understand differences in cell identity, purity and phenotype, EBV VST products from the two processes were compared using a wide range of lymphocyte and T cell lineage and activation markers to comprehensively characterise the products. After gating on live singlet cells, both LCL-derived and peptide-derived products were highly enriched for CD3+ T cells, each containing a varied sub-population of CD3+/CD56+ NKT cells (**Figure 3.11A**). From a regulatory perspective, cell therapy products should have contaminating cells quantified and given a strict limit prior to product release. The peptide process isolated T cells based on IFN-γ secretion and since this is also a major cytokine secreted by NK cells there is potential to co-isolate activated NK cells. Given that NK cells function in an MHC-unrestricted manner, we sought to minimise potential off-target effects by establishing a release criterion for the peptide process of ≤10% CD56+/CD3- NK cells. Since the LCL process co-cultures uses irradiated LCL for antigenic stimulation, it is possible there could be some surviving B cells in final products. Though the cells are irradiated and therefore unable to proliferate, to ensure product safety the criteria for product release was set to ≤2% CD19+ B cells. As can be seen, final products from both processes contained negligible levels of NK cells or B cells (**Figure 3.11A**). Both processes generated T cell content which was highly enriched for CD8 T cells, however some donors from the LCL-derived process also contained a substantial CD4 population (**Figure 3.11B**). Both processes generated negligible DP or DN T cells.

T cell memory profiling using surface markers (CD62L/CD45RA/CD45RO) within both CD8+ (**Figure 3.11C**) and CD4+ (**Figure 3.11D**) compartments revealed a significantly higher percentage of central memory T cells (TCM) in the peptide-

derived VST. LCL-derived VST had significantly higher frequencies of effector memory (TEM) and terminal effector compared to peptide-derived in both CD8+ and CD4+ compartments, indicating VST generated by the LCL process are more differentiated with a concomitantly reduced proliferative potential.

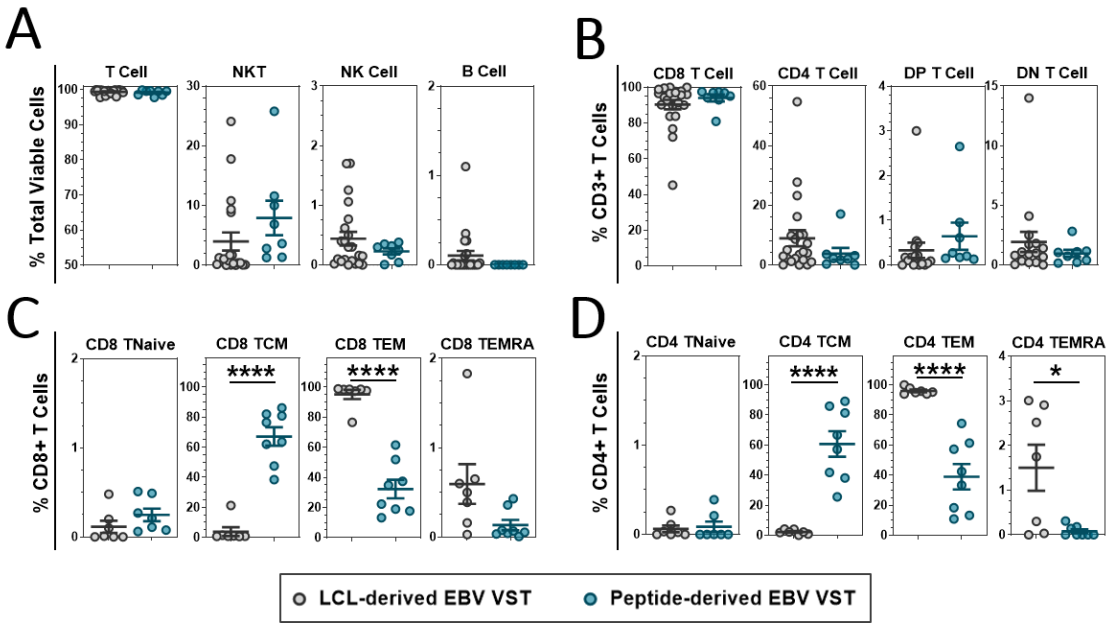

Figure 3.11 - Comparison of LCL-derived and peptide-derived EBV VST lymphocyte phenotype.

Phenotyping products compared lymphocyte populations between LCL-derived (n=22) and peptide-derived (n=8) EBV VST. **(A)** Gated on the total viable cells, analyses were quantified for T cells (CD3+), NKT cells (CD3+/CD56+), NK cells (CD3-/CD56+) and B cells (CD19+). **(B)** Gated CD3+ T cells were then sequentially gated for T cell subtypes: CD8 T cells (CD8+/CD4-), CD4 T cells (CD4+/CD8-), double positive (DP) T cells (CD4+/CD8+) and double negative (DN) T cells (CD4-/CD8-). Within the **(C)** CD8 or **(D)** CD4 compartments, T cells were assessed for differentiation status as follows: naïve T cells (CD62L+/CD45RA+/CD45RO-), central memory T cells TCM (CD62L+/CD45RA-/CD45RO+), effector memory T cells TEM (CD62L-/CD45RA-/CD45RO+) and terminal effector memory RA T cells TEMRA (CD62L-/CD45RA+/CD45RO-). All data is represented as mean ± SEM. Statistical analysis was done using unpaired t-tests where *p≤0.05, **p≤0.01, ***p≤0.001.and ****p≤0.0001.

3.3.4 Varied chemokine receptor profile between LCL- and peptide-derived EBV VST

Administration of EBV VST are delivered to PTLD patients intravenously, therefore it is crucial the transferred T cells have the capacity to migrate to the PTLD tumour site(s) for effector functionality. To assess differences in T cell migratory potential, cells from each manufacturing approach were profiled for expression of key inflammatory chemokine receptors. Comparison at the transcriptional level using

Taqman Low Density Array (TLDA) as described in **section 2.10** revealed LCL-derived VST had significantly higher expression of CXCR6 than peptide-derived VST (**Figure 3.12A**). While there were no significant differences between groups for the other markers tested in the array, TLDA analysis indicated VST derived from both methods had high expression of CCR2 and CCR5.

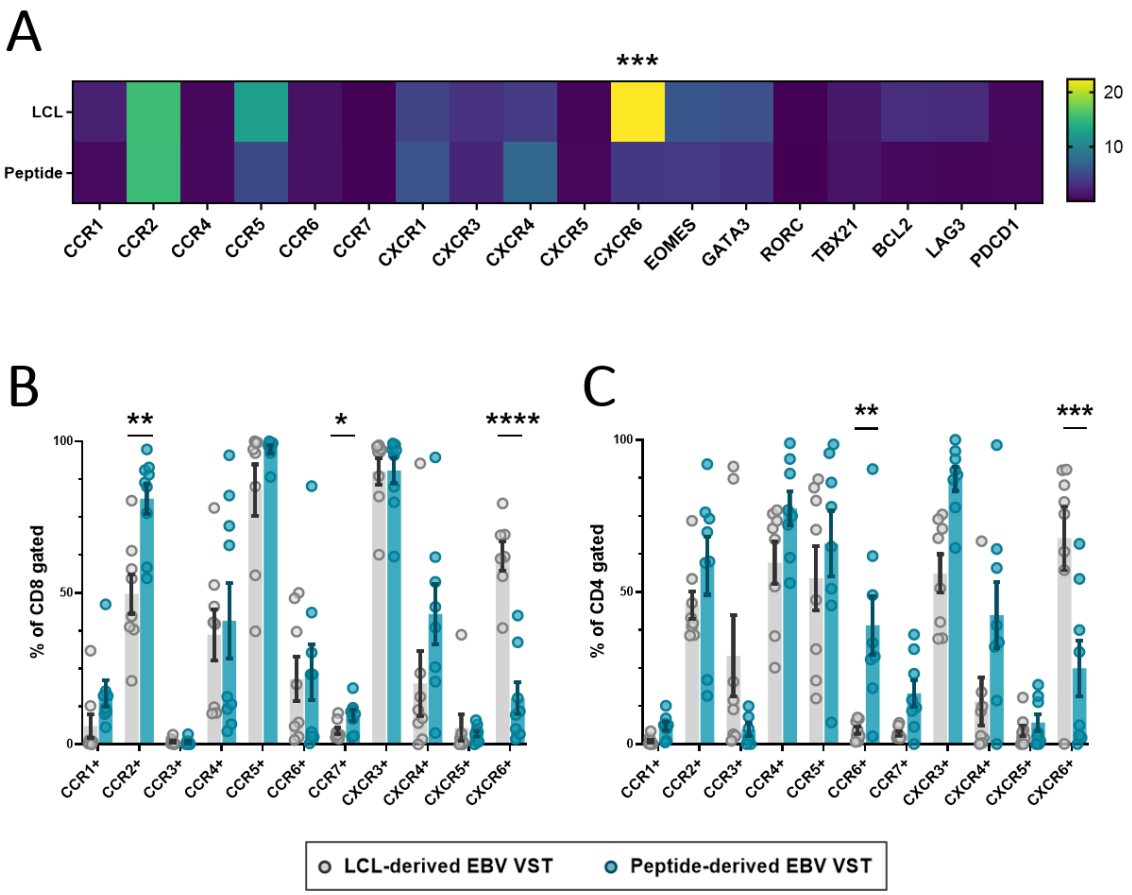

Figure 3.12 - Comparison of LCL-derived and peptide-derived EBV VST chemokine receptors.

LCL-derived and peptide-derived EBV VST were compared for chemokine receptor expression. **(A)** Expression of CC- and CXC- chemokine receptors, transcription factors and inhibitory receptors was measured at the transcriptional level using Taqman Low Density Array (TLDA). ΔΔCT values were calculated using housekeeper gene RPLPO of VST normalised to CD3+/CD62L+/CD45RO- naive T cells isolated from buffy coat PBMC (n=6). Data is represented as mean ΔΔCT for each group. **(B-C)** Chemokine receptor expression was also assessed at the protein level using flow cytometry to quantify chemokine receptor expression within the CD8 and CD4 compartments respectively. All data is represented as mean ± SEM. Statistical analysis was done using unpaired t-tests (Holm-Šídák for multiple comparisons) with *p≤0.05, **p≤0.01, ***p≤0.001.and ****p≤0.0001.

Flow cytometry characterisation was also used to assess chemokine receptor expression at the protein level as described in **section 2.6**. For this analysis, cryopreserved VST were thawed, washed and labelled for CD4 and CD8 and for the following chemokine receptors: CCR1, CCR2, CCR3, CCR4, CCR5, CCR6, CCR7, CXCR3, CXCR4, CXCR5 and CXCR6 individually. For analysis, cells were initially gated on

viable singlet cells, and then into CD4+ or CD8+ T cells for expression of each individual chemokine receptor within each compartment. Chemokine receptor labelling indicated CD8+ cells in LCL-derived VST had significantly lower expression of CCR2 and CCR7, but higher expression of CXCR6 compared to peptide-derived EBV VST (**Figure 3.12B**). The CD4+ cell expression of CXCR6 was significantly increased in LCL-derived VST, as well as significantly lower expression of CCR6 than peptide-derived EBV VST (**Figure 3.12C**). Since differences between the groups in antibody detected expression of CCR2, CCR7 and CCR6 was only seen in either CD8 or CD4 compartments, the lack of differences in these receptors seen by TLDA may reflect the inability to distinguish between T cell subpopulations using this array. Since both TLDA and flow cytometry results showed an increased expression of CXCR6 in LCL-derived EBV VST, this indicates a sustained significant difference of this receptor at the transcriptional and protein level.

The flow cytometric analysis of chemokine receptors was performed on thawed, rested VST products, however it was also of interest to investigate changes in chemokine receptor expression upon viral challenge. To test this, intra-donor assays were set up as shown in **Figure 3.13A** where an EBV VST vial was thawed, and following a wash step, a sample of cells were taken for immediate analysis (0 hours), and the remaining cells were cultured for 5 hours in TexMACS medium with EBV peptide pools to stimulate antigen recall. A 5 hour culture in TexMACS medium only was included as a negative control. Samples were then taken from each (5h negative control and 5h EBV stim) for chemokine receptor labelling as before. For representative donor EBVUKD6, the intra-donor 5 hour culture time-point samples showed a decrease in expression of CCR2 and CXCR3, and an increase in CXCR4 and CXCR6 compared to the 0h rest sample. However since the 5 hour EBV stimulation and 5 hour negative control were equivalent in expression of all markers, these changes were likely an effect of culturing the thawed cells rather than induced by antigenic re-challenge. The same results were replicated between three other EBV donor VST lines (data not shown), and therefore it was decided to perform all remainder chemokine receptor profiling by flow cytometry on cells at rest since 5 hour stimulation did not demonstrate any antigen-specific chemokine receptor modulation.

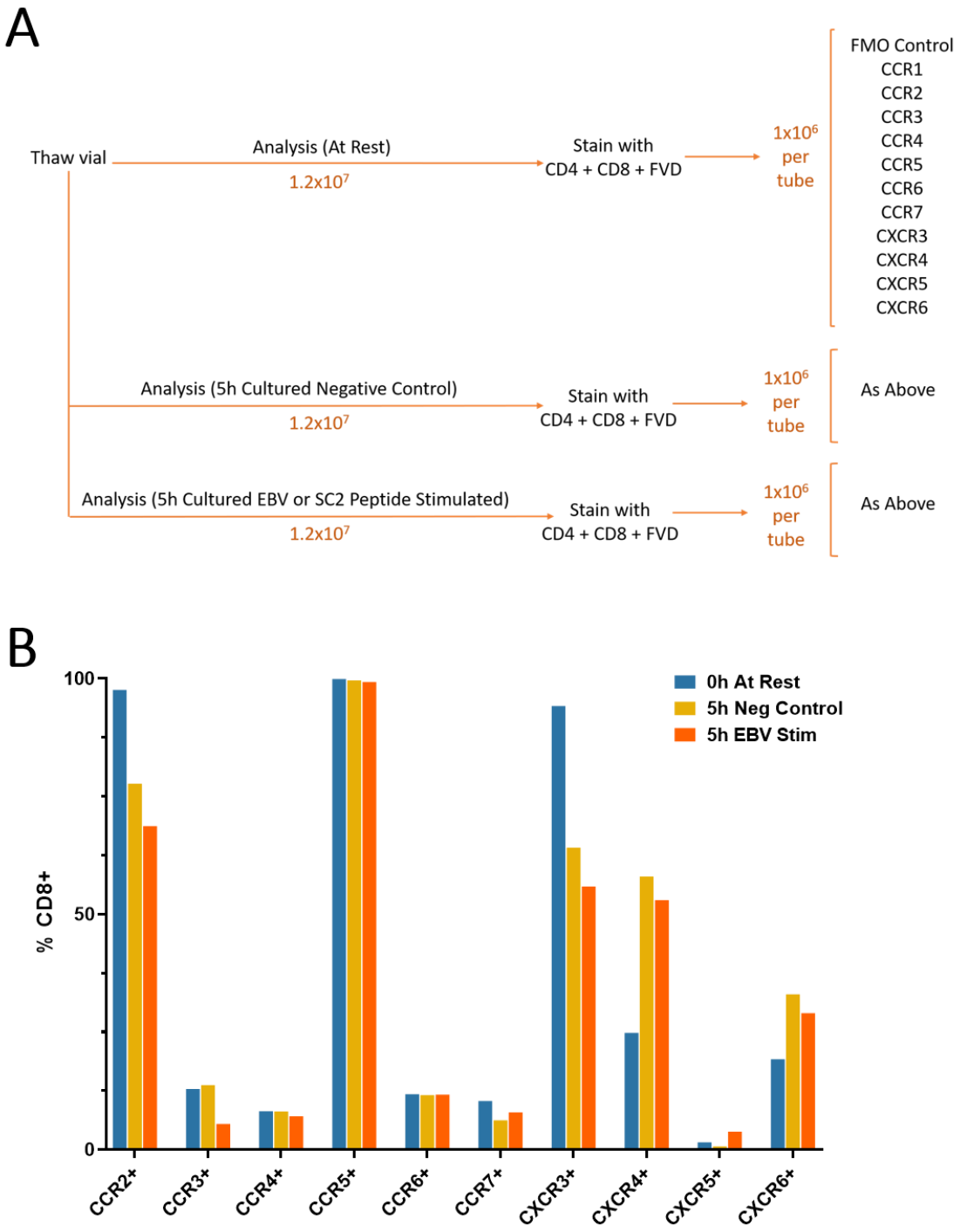

Figure 3.13 - Chemokine receptor expression at rest versus challenge.

EBV VST were tested for changes in chemokine receptor expression at rest versus with viral challenge. **(A)** To this end, a donor EBV VST vial was thawed, washed and a sample taken for immediate (0h, at rest) staining of CD4, CD8, fixable viability dye (FVD) and chemokine receptors. The remaining thawed cells were cultured for 5 hours in TexMACS medium with addition of EBV peptide pools for antigen re-challenge versus a negative (no antigen) culture control. **(B)** The percentage of CD8+ gated cells positive for chemokine receptors are shown for representative donor EBVUKD6 at 0h rest, 5h culture negative control and 5h EBV peptide stimulation.

3.3.5 Reduced expression of exhaustion markers in peptide-derived EBV VST

EBV VST final products were also assessed for expression of T cell activation/ inhibitory markers: PD-1, Tim-3 and Lag-3 by flow cytometry as outlined in **section 2.5.7**. While there were no significant differences between the two groups in CD8+ cells there was a consistent trend to lower expression of all exhaustion markers in peptide-generated VST (**Figure 3.14A**). The LCL-derived CD4+ cells had a significantly higher percentage of Lag3+ and PD1+/Tim3+/Lag3+ triple positive populations (**Figure 3.14B**). While singular expression of Lag3+ suggests a highly activated state, co-expression of numerous inhibitory markers is more indicative of true T cell exhaustion (Baessler and Vignali, 2024), therefore suggesting 20-30% of CD4+ T cells expanded in the LCL process had exhaustion phenotype. Since presence of CD4+ T cells in EBV VST therapy has been indicated to increase adoptively transferred T cell persistence, a higher degree of CD4+ T cell exhaustion in LCL-derived EBV VST may ultimately limit the longevity of support for CD8+ T cell function in these products.

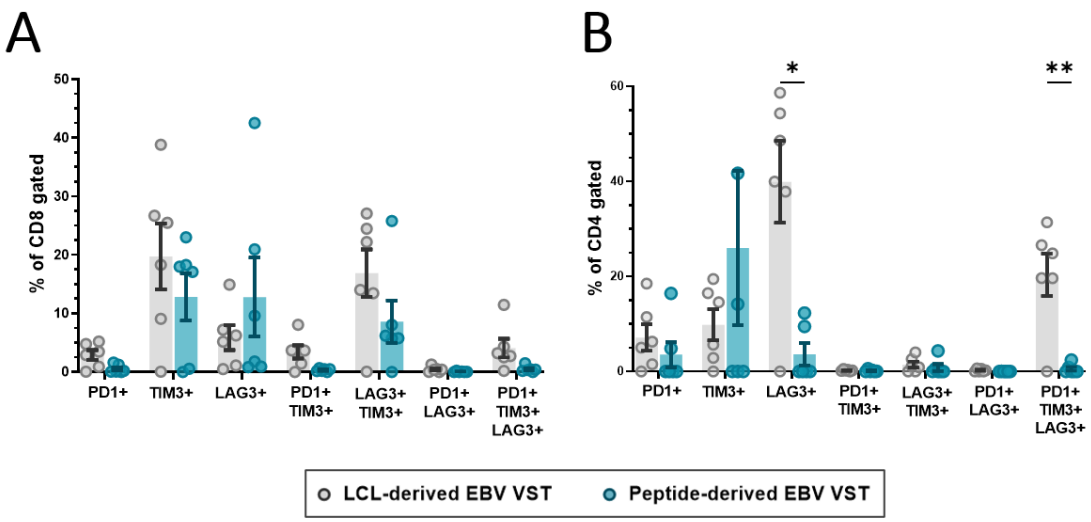

Figure 3.14 - Comparison of LCL-derived and peptide-derived EBV VST exhaustion.

Final product VST were assessed for T cell exhaustion through singular and co-expression of markers PD-1, TIM-3 and LAG-3. Exhaustion marker expression within the **(A)** CD8 compartment and **(B)** CD4 compartment was compared between LCL-derived (n=6) and peptide-derived (n=6) EBV VST groups. All data is represented as mean ± SEM. Statistical analysis was done using unpaired t-tests (Holm-Šídák for multiple comparisons) with *p≤0.05 and **p≤0.01.

3.3.6 Increased antiviral cytokine secretion in peptide-derived EBV VST

As a measure of effector functionality, EBV VST were tested in a stimulation assay to assess intracellular cytokine release as outlined in **section 2.7.3**. To this end, EBV VST were thawed, washed and plated in TexMACS medium, with addition of EBV consensus peptivator to measure overall EBV reactivity and PMA/ionomycin to measure maximal T cell functional capacity. Treatments were incubated for 5 hours with a no antigen negative control, followed by surface staining for T cell markers and intracellular cytokines IFN-γ, TNF-α and IL-2. Representative flow cytometry analysis of donor EBVUKD6 VST shows the induced expression of these cytokines within viable CD3+ cells upon stimulation with EBV peptide pools (VST + EBV consensus peptides) as compared to the negative control no antigen (VST only) and positive control VST + PMA/ionomycin (**Figure 3.15A**).

To assess co-expression of multiple cytokines, flow cytometry analyses were gated based on multiple of singular expression of IFN-γ, TNF-α and/or IL-2 as outlined in **Figure 2.8**, corrected to negative controls. As shown in **Figure 3.15B**, the percentage IFN-γ+/TNF-α+ cells was significantly higher in peptide-derived VST ($p<0.0001$), whereas LCL-derived VST contained a significantly larger proportion ($p<0.0001$) of cytokine-null (IFN-γ/TNF-α-/IL-2-) cells upon EBV recall. Furthermore, the percentage of IFN-γ+/TNF-α+/IL-2+ cells in response to PMA/ionomycin was significantly higher ($p=0.00024$) in peptide-derived EBV VST indicating a more potent antiviral cytokine capacity as compared to LCL-derived EBV VST (**Figure 3.15C**). Since the cytokine null population is negligible in both groups upon PMA/ionomycin stimulation, this indicates the EBV VST products generated do have functional capacity to secrete these cytokines. This implies the large cytokine null population in LCL-derived VST is not simply just a result of functional exhaustion. Instead, this may indicate the LCL-derived VST have specificity to other antigens expressed by LCL that are not included in the EBV consensus peptide pools used in recall testing, or further specificity to non-EBV epitopes.

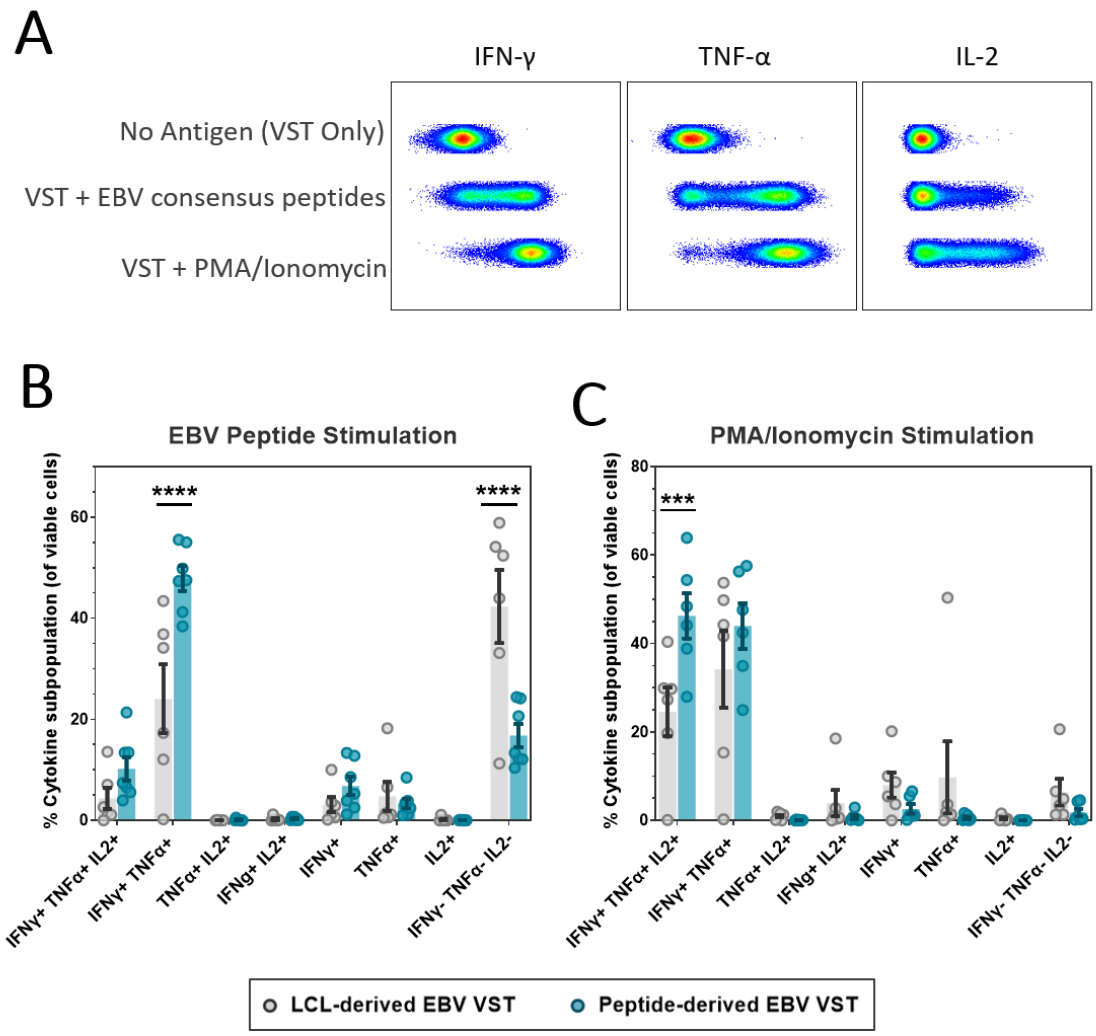

Figure 3.15 - Comparison of LCL-derived and peptide-derived EBV VST antiviral cytokines.

LCL-derived and peptide-derived EBV VST were compared for antiviral cytokine production upon stimulation. **(A)** Representative intra-donor flow cytometry analysis shows intracellular expression of antiviral cytokines IFN-γ, TNF-α and IL-2 following 5 hours stimulation with negative control no antigen (VST only), EBV consensus peptide stimulation (VST + EBV consensus peptides) or positive control (VST + PMA/ionomycin). The percentage of cytokine single expressing or co-expressing subpopulations were compared between LCL-derived (n=6) and peptide-derived (n=6) EBV VST reactive to **(B)** EBV peptide stimulation and **(C)** PMA/Ionomycin stimulation. All data is represented as mean ± SEM. Statistical analysis was done using unpaired t-tests (Holm-Šídák for multiple comparisons) with ***p≤0.001.and ****p≤0.0001.

3.3.7 Enhanced degranulation effector functionality in peptide-derived EBV VST

Since generated EBV VST derived from both manufacturing methods were composed mostly of cytotoxic CD8+ T cells, lines were also assessed for CD107-mediated degranulation responses upon stimulation. As per the cytokine release assay above, VST were thawed, washed and plated in TexMACS for a 5 hour stimulation in the following conditions: no antigen negative control, EBV consensus peptides, and PMA/ionomycin positive control. Representative flow cytometry analysis of donor

EBVUKD6 VST shows the changes in intracellular expression of these markers upon stimulation with EBV peptides or PMA/ionomycin as compared to the no antigen negative control (**Figure 3.16A**). Comparisons between groups were made on the basis of percentage of CD107a+ T cells corrected to negative controls, whereas since granzyme B and perforin labelling gave a broader expression profile these markers were assessed for median fluorescence intensity (MFI) corrected to the negative control (cMFI) as outlined in **Figure 2.8**. Peptide-derived EBV VST had a significantly increased population of CD107a+ CD8 T cells (**Figure 3.16B**) as compared to LCL-derived VST upon EBV peptide recall. Interestingly, peptide-derived VST also had a significantly higher population of CD107a+ CD4+ T cells whereas LCL-derived lines had negligible CD107a expression on CD4 T cells (**Figure 3.16C**). This may indicate peptide-derived CD4 VST have cytotoxic as well as helper functionality. While peptide-derived EBV VST trended towards higher cMFI of both granzyme B (**Figure 3.16D**) and perforin (**Figure 3.16E**) in comparison to LCL-derived, this was not statistically significant.

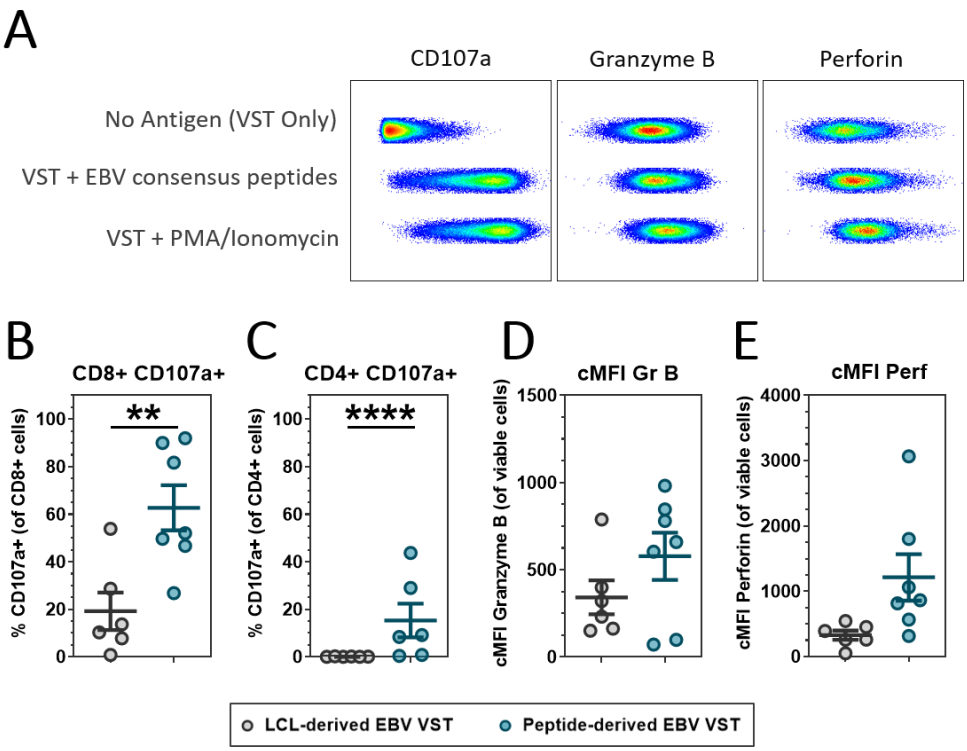

Figure 3.16 - Comparison of LCL-derived and peptide-derived EBV VST degranulation. LCL-derived and peptide-derived EBV VST were compared for antiviral cytokine production upon stimulation. **(A)** Representative intra-donor flow cytometry analysis shows intracellular expression of degranulation markers CD107a, granzyme B and perforin following 5 hours stimulation with negative control no antigen (VST only), EBV consensus peptide stimulation (VST + EBV consensus peptides) or positive control (VST + PMA/ionomycin). Comparisons between LCL-derived (n=6) and peptide-derived (n=6) EBV VST reactive to EBV peptide were made for **(B)** the percentage of CD107a+ CD8+ T cells, **(C)** the percentage of CD107a+ CD4+ T cells, **(D)** cMFi Granzyme B and **(E)** cMFI perforin. All data is represented as mean ± SEM. Statistical analysis was done using unpaired t-tests with **p≤0.01.and ****p≤0.0001.

3.3.8 Peptide-derived EBV VST demonstrate higher reactivity to EBNA antigens

Since the antigen source used in the two manufacturing processes was different, in addition to evaluating overall responses using EBV consensus peptides described above, (see **Figure 3.9**), EBV VST were also investigated for specificity to individual EBV antigens. To test this, EBV VST lines were thawed, washed and plated in TexMACS medium, then treated with JPT PepMix™ peptide pools for the following EBV antigens: BARF1, BMLF1, BMRF1, BRLF1, BZLF1, EBNA-LP, EBNA1, EBNA2, EBNA3A, EBNA3B, EBNA3C, LMP1, LMP2 and gp350/340. JPT PepMix™ peptide pools were 15-mers with 11 amino acid overlap, spanning entire antigen sequences allowing HLA-independent evaluation of responses. Cells were stimulated with the with JPT PepMix™ peptide pools for 5 hours including negative (no antigen) and positive (PMA/ionomycin) controls as according to **section 2.7.3**. Following stimulation cells were surface stained with CD4 and CD8 antibodies, followed by intracellular staining of T cell effector molecules: CD107a, CD154, IFN-γ, IL-2 and TNF-α. Flow cytometry analyses initially gated on viable singlet cells followed by gating in CD4+ and CD8+ cells. The CD4 and CD8 compartments were then assessed for peptide-induced expression of the effector molecules compared to negative controls.

Epitope sequences as well as peptide length of different antigens have differential binding capacity to MHC proteins, and therefore antigen processing can confer varied immunogenicity between CD4 and CD8 T cells. Therefore, analysis was performed to compare EBV antigen-specific responses between CD4 and CD8 T cells. To choose the best effector molecule to allow an unbiased comparison between CD4 and CD8 activation in this assay, four EBV VST lines which had equivalent CD4:CD8 ratio were quantified for the frequency of CD4+ or CD8+ T cells positive for effector molecule production by PMA/ionomycin as an antigen-independent T cell stimulus (Godoy-Ramirez et al., 2004). Comparison of effector molecules produced by PMA/ionomycin stimulation between CD4+ and CD8+ VST are shown in **Figure 3.17**. The percentage of CD107a+ cells was significantly higher ($p= 0.010206$) in CD8+ gated cells as compared to CD4+ gated cells, as might be expected since CD107a is a marker of T cell degranulation classically mediated by cytotoxic CD8+ T cells (Betts et al., 2003, Rubio et al., 2003, Aktas et al., 2009). Similarly, activation-induced CD154 expression was significantly increased on CD4+ gated cells than CD8+ gated cells, which again may be

expected as CD154 in primarily involved in priming of activated CD4 T cells (Graf et al., 1995, Mackey et al., 1998, Cron, 2003). The antiviral cytokines IFN-γ, IL-2 and TNF-α however have non-significant differences in activation-induced expression between CD4+ and CD8+ T cells. Since the frequency of IFN-γ+ cells between CD4+ and CD8+ T cells was more consistent than that of IL-2 and TNF-α which were more variable between the four intra-donor comparisons, IFN-γ expression was used going forward to compare antigen reactivity of VST CD4 and CD8 compartments.

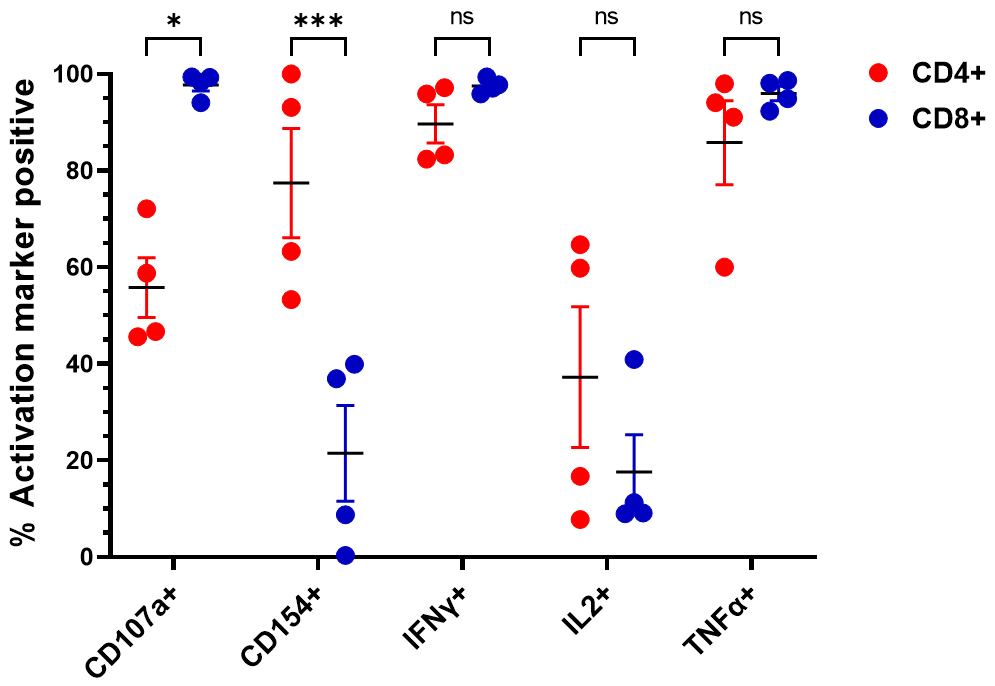

Figure 3.17 - Comparison of CD4 and CD8 T cell effector molecule production.

EBV VST lines with nearly equivalent CD4:CD8 ratio (ranging 40-60% of each population, n=4) were compared for effector molecule production by CD4+ or CD8+ gated T cells in response to PMA/ionomycin. All data is represented as mean ± SEM. Statistical analysis was done using paired t-tests to compare intra-donor CD4 versus CD8 effector responses where *p≤0.05 and ***p≤0.001.

Representative flow cytometry analysis of donor EBVUKD6 VST shows different reactivity to individual antigens between CD4+ and CD8+ gated T cells (**Figure 3.18A**). Reactivity of CD8+ T cells demonstrated a conserved antigen reactivity mainly to BZLF1, EBNALP, EBNA3A and EBNA3C between LCL and peptide-derived VST. Peptide-derived VST however had significantly higher CD8+ reactivity to EBNA3A ($p<0.0001$) compared to LCL-derived EBV VST (**Figure 3.18B**).

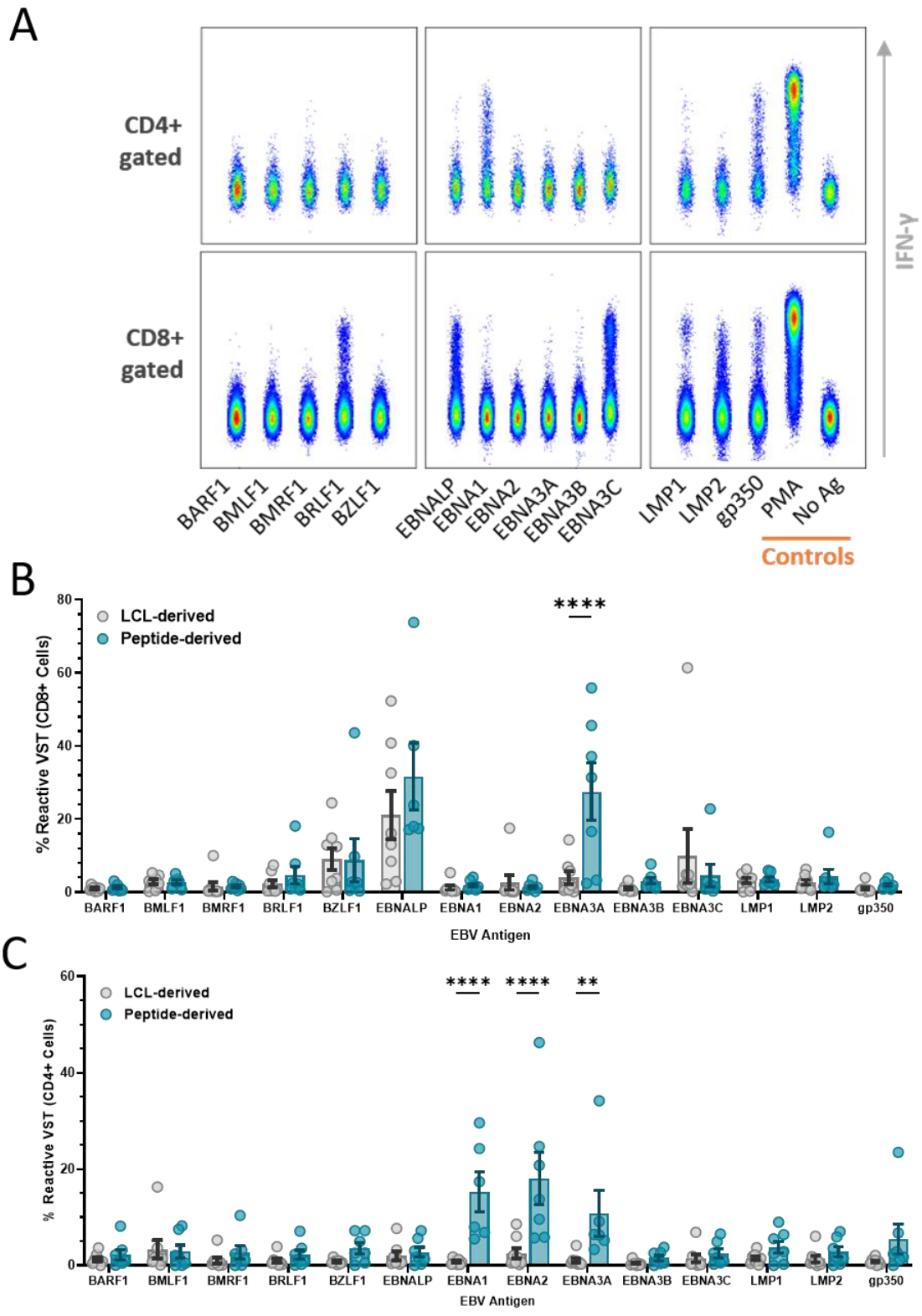

Figure 3.18 - Comparison of LCL-derived and peptide-derived EBV VST antigen reactivity.

EBV VST were assessed for antigen specificity by stimulation with individual EBV antigen pepmix pools followed by intracellular staining of reactive antigen-specific VST with effector markers. **(A)** Flow cytometric analysis of representative EBV VST donor EBVUKD6 shows IFN-γ+ reactive VST to EBV antigens, with positive control (PMA) and negative control (no ag). Individual antigen specificity was compared between the LCL-derived (n=8) and peptide-derived (n=7) EBV VST groups within **(B)** the CD8+ and **(C)** CD4+ compartments. Data is represented as mean ± SEM and statistical analysis was done using unpaired t-tests (Holm-Šídák for multiple comparisons) with **p≤0.01, and ****p≤0.0001.

Peptide-derived EBV VST also had significantly higher CD4+ cell reactivity compared to LCL-derived EBV VST for antigens EBNA1, EBNA2, and EBNA3A (**Figure 3.18C**).

The overall EBV VST reactivity of total viable cells not segregated into CD4 and CD8 compartments (**Figure 3.19**) demonstrated targeting towards EBNA antigens was significantly higher in peptide-derived than LCL-derived VST.

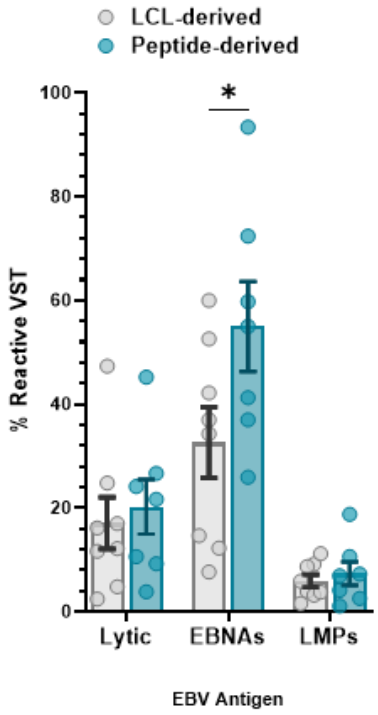

Figure 3.19 - Comparison of LCL-derived and peptide-derived EBV VST total antigen reactivity.

Total viable cells reactivity between LCL-derived (n=8) and peptide-derived (n=7) EBV VST were compared between lytic antigens (BARF1, BMLF1, BMRF1, BRLF1, BZLF1, gp350), EBNAs (EBNALP, EBNA1, EBNA2, EBNA3A, EBNA3B, EBNA3C) and LMPs (LMP1, LMP2). Data is represented as mean ± SEM and statistical analysis was done using unpaired t-tests (Holm-Šídák for multiple comparisons) with *p≤0.05.

3.3.9 Equivalent cytotoxic functionality of peptide- and LCL-derived EBV VST

As the gold standard assay for CD8+ T cell effector functionality, EBV VST generated by the two methods were assessed for cytotoxicity against EBV-infected target cells. For both first and second generation SNBTS EBV VST banks made by LCL stimulation, the final product functionality assay was to measure specific lysis to autologous LCL as infected targets (used to generate the lines) as LCL have EBV antigen expression

consistent with PTLD tumours. Since our EBV VST are given as an allogeneic therapy based on best HLA match between donor VST and patient, it was decided the most representative way to assess EBV VST in a cytotoxicity assay was to use best HLA-matched LCL as the target cells. To investigate this, LCL-derived (n=6) and peptide-derived (n=6) EBV VST were compared for specific lysis against both HLA-matched and HLA-mismatched EBV-presenting LCL targets with VST at increasing target to effector ratios. The number of HLA class I, class II and total matches between EBV VST lines and allogeneic LCL targets used in the study are outlined in **Table 3.4**. All cytotoxicity assays were performed within a two week period using the same reagents, and where possible the same donor LCL lines (whilst still allowing the maximal and minimal number of matches for HLA-matched and mismatched targets respectively) within the same day to minimise inter-assay variation.

	HLA-mismatched targets			HLA-matched targets		
VST Line	No. class I matches	No. class II matches	No. total matches	No. class I matches	No. class II matches	No. total matches
NZ200	0	0	0	4	2	6
NZ294	0	0	0	3	2	5
NZ026	0	0	0	3	2	5
NZ666	0	0	0	5	2	7
NZ806	0	0	0	3	2	5
NZ873	0	0	0	4	2	6
EBVUSAD1	0	0	0	5	2	7
EBVUSAD2	0	0	0	3	2	5
EBVUSAD4	0	0	0	3	2	5
EBVUSAD7	0	0	0	3	2	5
EBVUKD6	0	0	0	3	2	5
EBVUKD9	0	0	0	4	2	6

Table 3.4 - HLA matching between EBV VST and target cells for cytotoxicity assays.

Each EBV VST line was co-cultured with HLA-mismatched and matched targets in triplicate wells for the following target (LCL) to effector (VST) ratios: 0.1:1, 1:1, 1:5, 1:10, 1:20, and target only controls (**Figure 3.20A**). Following 6 hours co-culture, plates were stained with apoptosis marker annexin-V and dead cell stain DRAQ7. To

analyse target killing induced by VST, LCL pre-stained with PKH67 were gated and assessed for annexin V and/or DRAQ7 positive expression as % dead cells as shown for target only controls (top panels) and [1:1] target to effector ratio (bottom panels) in **Figure 3.20B**. Specific lysis at each ratio was normalised to baseline target cell death from target only controls (**Figure 3.20C, left graph**). The area under the curve (AUC) of HLA-matched target specific lysis was then calculated for a given VST product to allow a normalised comparison of cytotoxic ability and a single-figure value for cytotoxicity across a range of E:T ratios (**Figure 3.20C, right graph**). To this end, both LCL- and peptide-derived EBV VST demonstrated comparable cytotoxicity against infected targets (**Figure 3.20D**). To investigate if cytotoxic efficacy was dictated by HLA matching, each VST line cytotoxicity AUC was tested for correlation with the number of (**Figure 3.20E**) class I matches or (**Figure 3.20F**) total class I+II matches between EBV VST and allogeneic HLA targets. While there was a positive trend in increasing cytotoxicity with more HLA matches, no significant correlations were seen which may be due to the small sample number as well as the small range of number of HLA matches.

Though cytotoxicity assays against infected or tumour cells lines are considered the gold standard assay for determining potency in CD8+ T cell therapies, these assays are not optimal for ATMP QC testing due to complex assay set up, non-standardized donor target cells, and potentially use of infected target cell lines which for EBV requires use of a biological containment level 2 controlled laboratory for segregation. Therefore as part of this cytotoxicity assay study, in tandem each EBV VST upon was also set up for a degranulation + cytokine release assay against EBV consensus peptides as described in sections **3.3.6**-**3.3.7** to investigate if any of these activation markers correlated with cytotoxic potency. As can be seen, the percentage of granzyme B+ (**Figure 3.21A**), perforin+ (**Figure 3.21B**), or CD107a+ (**Figure 3.21C**) cells in response to EBV peptide stimulation did not show a significant correlation with cytotoxicity against EBV-infected target cells. The percentage of multifunctional IFN-γ+/TNF-α+ cells reactive to EBV peptide stimulation however demonstrated significant positive correlation ($p=0.008$) with the EBV cytotoxicity against EBV-infected target cells (**Figure 3.21D**). Therefore, we incorporated the percentage of IFN-γ+/TNF-α+ cells to EBV consensus peptides as a surrogate marker of LCL cytotoxicity for QC functionality testing of the peptide-derived EBV VST clinical bank manufacture.

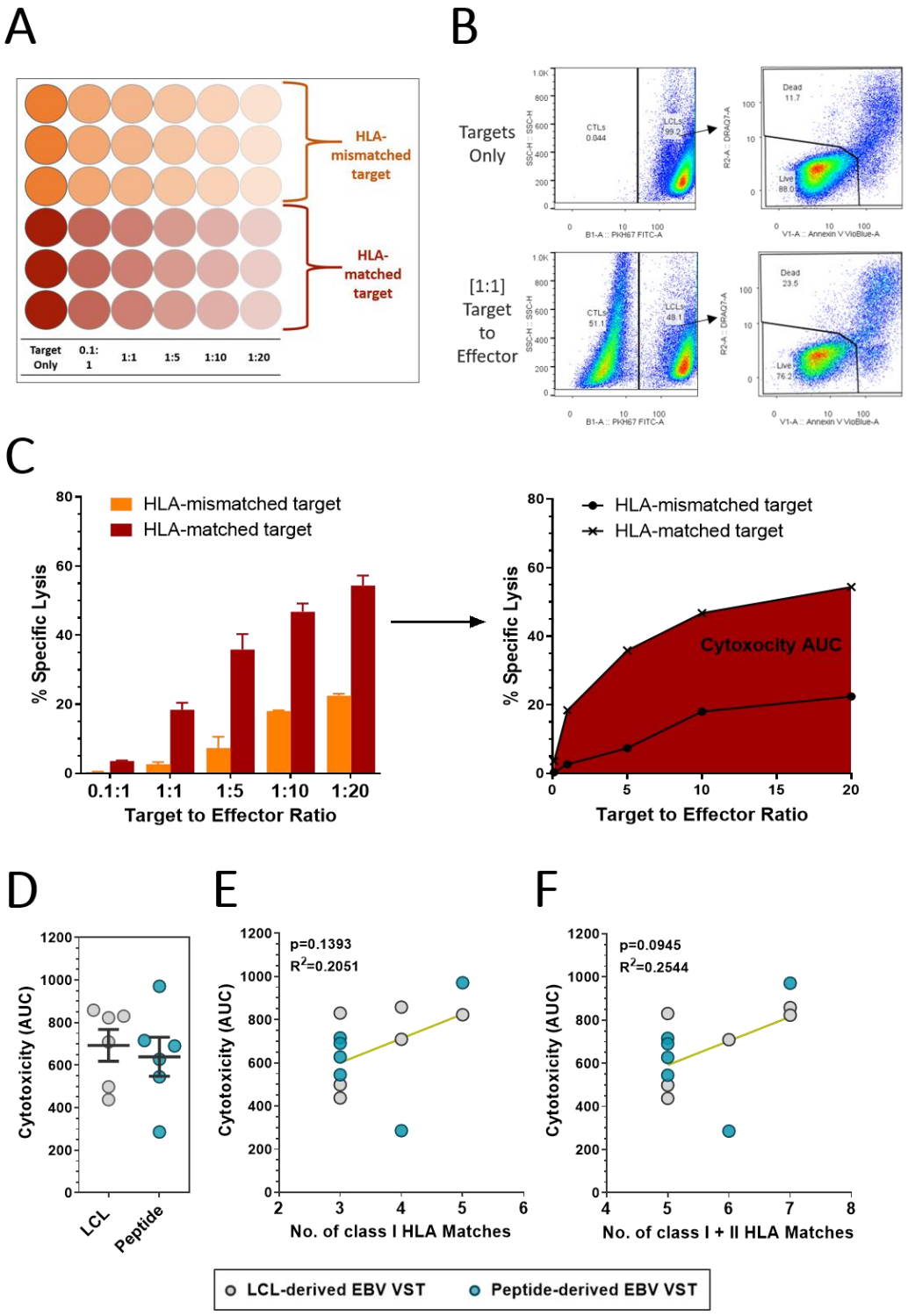

Figure 3.20 - Comparison of LCL-derived and peptide-derived EBV VST cytotoxicity.

LCL-derived and peptide-derived EBV VST was compared for cytotoxicity. **(A)** HLA-matched and mismatched EBV-infected cells (LCL) were used as targets over numerous target to effector ratios. **(B)** Cytotoxicity was measured as the percentage PKH67-labelled target cells positive for expression of annexin-V and/or DRAQ7. **(C)** Specific lysis of targets was quantified at each T:E ratio normalised to baseline death in target cell controls, and the area under the curve (AUC) of specific lysis of HLA-matched targets over all T:E ratios was calculated as a single value of overall cytotoxicity. **(D)** Overall cytotoxicity was compared between LCL-derived (n=6) and peptide-derived (n=6) EBV VST lines. Data is represented as mean ± SEM and statistical analysis was done by an unpaired t-test. Correlations were tested between cytotoxicity of EBV VST and **(E)** the number of class I and **(F)** total class I+II matches. Statistical analysis was done by generating Pearson correlation coefficients, where $p<0.05$ was considered significant.

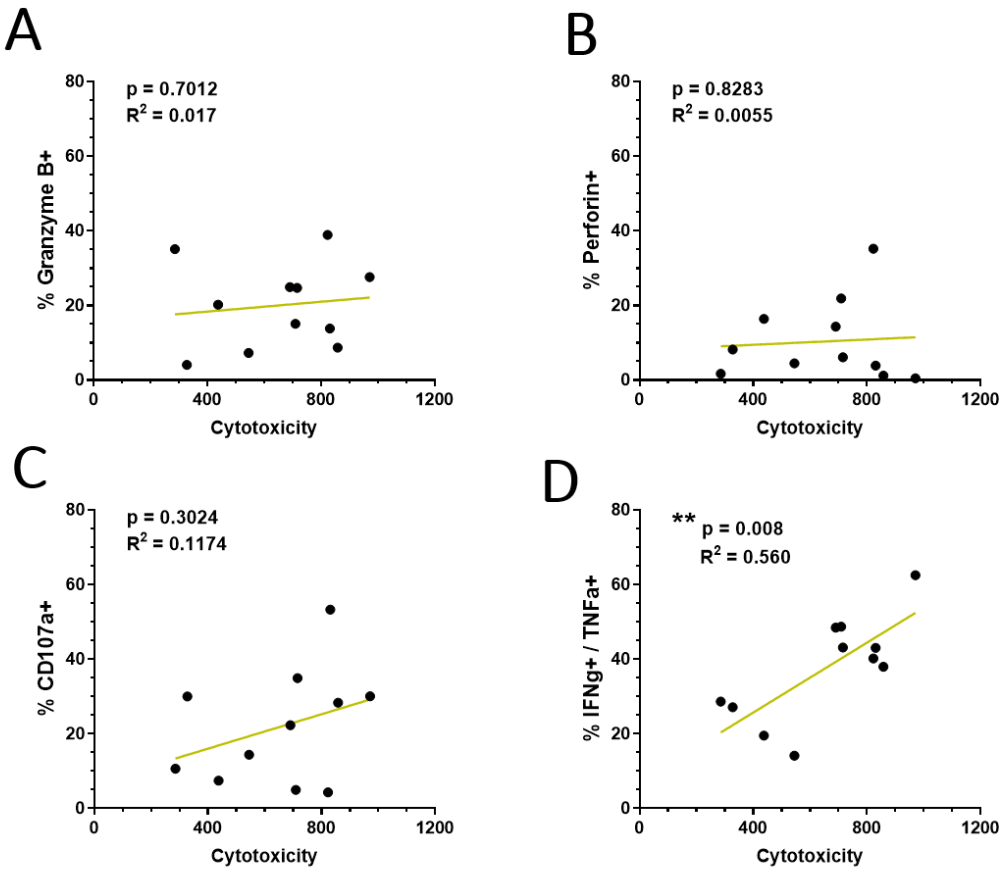

Figure 3.21 - VST cytotoxicity by EBV-infected targets versus activation by EBV peptides.

EBV VST lines (both LCL-derived and peptide-derived) were assessed for correlations between cytotoxicity against EBV-infected target cells and percentage of **(A)** Granzyme B+, **(B)** Perforin+, **(C)** CD107a+ and **(D)** IFN-γ+/TNF-α+ VST response to EBV peptide stimulation. Correlations were tested using computed Pearson correlation coefficients where $p<0.05$ was considered statistically significant. Each data point represents an individual donor EBV VST line (n=11), donor NZ873 was not included due to insufficient cells to run a cytotoxicity assay and intracellular cytokine release assay in tandem.

3.3.10 EBV VST contain cytotoxic CD4+ T cells

The majority of EBV VST lines generated by both LCL and peptide processes are largely skewed to CD8+ T cells, however some donor lines expand a significant CD4+ T cell population. One study reported association of better patient responses to EBV VST with higher CD4 content (Haque et al., 2007) and authors suggested this was due to the ability of helper CD4 T cells to activate transferred CD8+ T cells as well as provide pro-inflammatory signalling in the recipient. There is however also accumulating evidence of CD4+ T cells with MHC class II-restricted cytotoxic capacity, particularly within the context of viral infections (Cenerenti et al., 2022), and therefore it was hypothesised that CD4+ T cells within VST products could mediate direct target killing. To this end, EBV VST lines with sizeable CD4+ populations were sorted for CD4+ T cells and tested in a cytotoxicity assay against matched target LCL and compared to unsorted VST. Both unsorted and CD4-sorted VST were also co-

cultured with K562 as EBV- HLA unmatched control target cells. As previously, target LCL and K562 were pre-labelled with PKH67, then co-cultured with VST at [1:1] and [1:10] target to effector ratios for 6 hours, and subsequently stained with CD4/CD8 antibodies, annexin V, and DRAQ7 dead cell dye. Representative flow cytometry analysis is shown in **Figure 3.22A**. Analyses were first gated into PKH67- and PKH67+ populations (left plots). The PKH67- VST population was then quantified for CD4:CD8 ratio (middle plots). The PKH67+ target cells within each co-culture were then quantified for percentage of dead cells (annexin V+/ DRAQ7+, right plots).

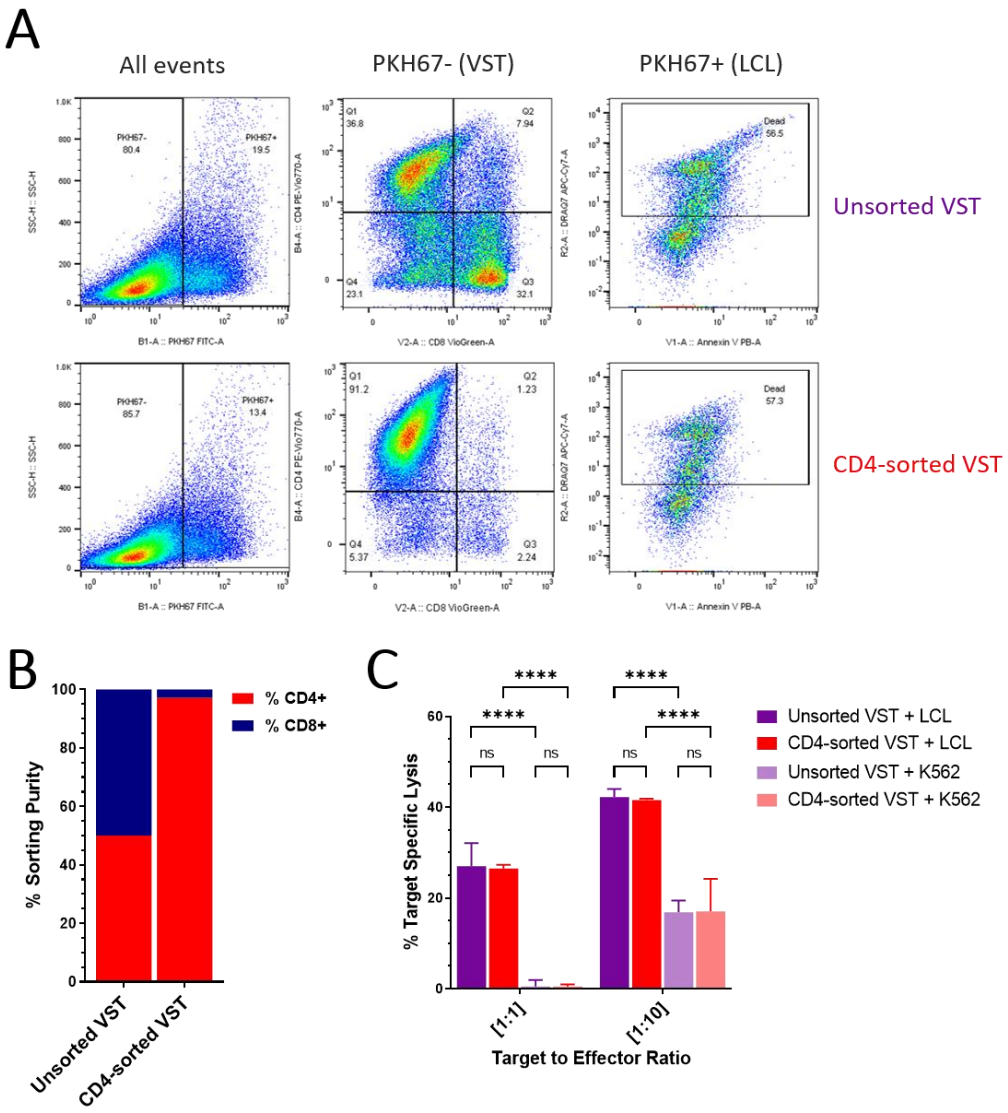

Figure 3.22 - EBV VST CD4-sorted cytotoxicity assay.

CD4-sorted and unsorted EBV VST were compared for cytotoxicity against target cells (HLA-matched EBV+ LCL and K562 EBV- controls). **(A)** Representative flow cytometry analysis shows gating of VST versus targets based on PKH67 expression (left plots). PKH67- VST were then quantified for the frequency of CD4+ and CD8+ T cells (middle plots). PKH67+ targets were assessed for % dead cells through positive expression of annexin V and/or DRAQ7 (right plots). Comparisons were made between co-cultures of targets with unsorted VST (top panel) versus CD4-sorted VST (bottom panel) **(B)** Unsorted and CD4-sorted VST were quantified for CD4+ T cell purity. **(C)** Specific lysis of targets was calculated at each T:E ratio normalised to baseline death in

target cell only controls. Comparisons were made between groups to assess the cytotoxic capacity of unsorted VST versus CD4-sorted VST, as well as specific killing of LCL versus K562 targets.

Specific lysis was calculated as the percentage of dead target cells at each target to effector ratio corrected to the baseline cell death in target only control wells. The level of enrichment of CD4+ cells through the use of a MACSQuant Tyto cell sorter is shown in **Figure 3.22B** whereby unsorted donor EBVOX1 contained equivalent CD4+ and CD8+ populations, whereas sorted cells were high purified (>95%) for CD4+ T cells. The percentage target specific lysis was then compared between unsorted and CD4-sorted VST co-cultures (**Figure 3.22C**). Killing of target LCL was equivalent between the CD4-enriched VST and unsorted VST at ~40% specific lysis at 1:10 target to effector ratio. Lysis of target K562 cells was significantly lower ($p<0.0001$) than LCL in both CD4-sorted and non-sorted VST at both co-culture ratios indicating the lysis of LCL was induced by antigen-specific recognition. Altogether this data suggests the enriched CD4-sorted VST had comparable ability to lyse target LCL to the mixed CD4/CD8 unsorted EBV VST which may indicate direct cytotoxic effector functionality of CD4+ EBV VST. It cannot be ruled out however that the specific lysis of LCL targets in the CD4-sorted VST was mediated by the residual CD8+ T cells in the enriched fraction, though given the frequency of CD8+ T cells was 2-3% of the total population it would be unlikely the numbers present would be sufficient to elicit equivalent specific killing as the unsorted VST. To investigate this further, future assays could look to further enrich CD4+ VST to a very high purity to ensure residual CD8+ T cells aren't compensating the killing functionality.

3.3.11 EBV VST are oligoclonal and express known EBV-specific sequences

In addition to evaluation of phenotypic characterisation and functional capacity to specific antigens, we wanted to determine the range of clones present within generated products to understand the T cell receptor (TCR) clonal repertoire diversity of T cell therapies, as this impacts on the potential breadth of response to PTLD. To assess clonal composition, EBV VST were sequenced for the TCR-β chain using a protocol adapted for unbiased bulk TCR sequencing of T cells expanded in a malaria infection model (Smith et al., 2020b). To get sufficient material for next generation sequencing, cDNA was synthesised using a protocol optimised for TCR-β amplification (Mamedov et al., 2013). For this, two rounds of PCR amplification were set up to generate TCR-β variable region amplicons using nested TCR-β primers,

Illumina-tagged indexed forward primers with SMART oligo sequence, and Illumina-tagged reverse primers within the TCR constant region to ensure both forward and reverse indexing. Initially the protocol was optimised for 18 cycles of amplification in the first PCR, followed by 12 cycles of amplification in the second PCR. Second PCR products were assessed for TCR-β purity using gel electrophoresis against a DNA ladder for expected band size 575bp as shown in **Figure 3.23A**. During initial assay development, purified bands could be seen for EBV VST final product samples (samples 1-2 and 5-14 in **Figure 3.23A**), whereas samples of the peptide-derived Prodigy IFN-γ isolated target cells (3-4 in **Figure 3.23A**) failed to show bands. The IFN-γ isolated target samples were included in this TCR sequencing study with the aim of understanding if the peptide culture process induces expansion or selection of particular clones between initial isolation and final VST product. However, since even at full-scale the Prodigy IFN-γ capture selection only isolates ~1-5x10^6 cells, very few target cells could be taken for TCR sequencing analysis (~1-5x10^5 cells), and therefore the lack of TCR amplification in these samples likely reflects low cell numbers. Therefore, attempts were made to optimise the TCR-β amplification of these lower quality IFN-γ isolated target samples by testing the primary PCR reaction at 18 cycles, 22 cycles and 25 cycles, and the secondary PCR reaction at 12 cycles, 18 cycles and 25 cycles. The only combination that showed optimised TCR-β amplification of IFN-γ isolated target samples was increasing the first PCR to 25 cycles as shown in **Figure 3.23B** where faint bands can be detected in samples 17, 18, 19 and 22 that had 25 (blue lines) as compared to 18 (orange lines) PCR1 cycles. Therefore, all TCR sequencing samples were run at the optimised 25 cycles for the primary PCR reaction. No differences were seen after changing the number of cycles for secondary PCR reaction which was run as the standard 12 cycles. All PCR products were purified using a gel extraction kit and assessed for quality and concentration using a Nanodrop. Purified PCR products were then submitted to Genewiz for sequencing on an Illumina MiSeq nano-platform using custom read TCR primers and a read index primer. All sequencing analysis was then performed by collaborating bioinformatics PhD student Catherine Sutherland, to pair reads with TCR VDJ assignment and match complementary determining region-3 (CDR3) amino acid sequences to known TCR epitope databases. In-depth details of sequencing analysis and software/ databases used is outlined in **section 2.11.5**.

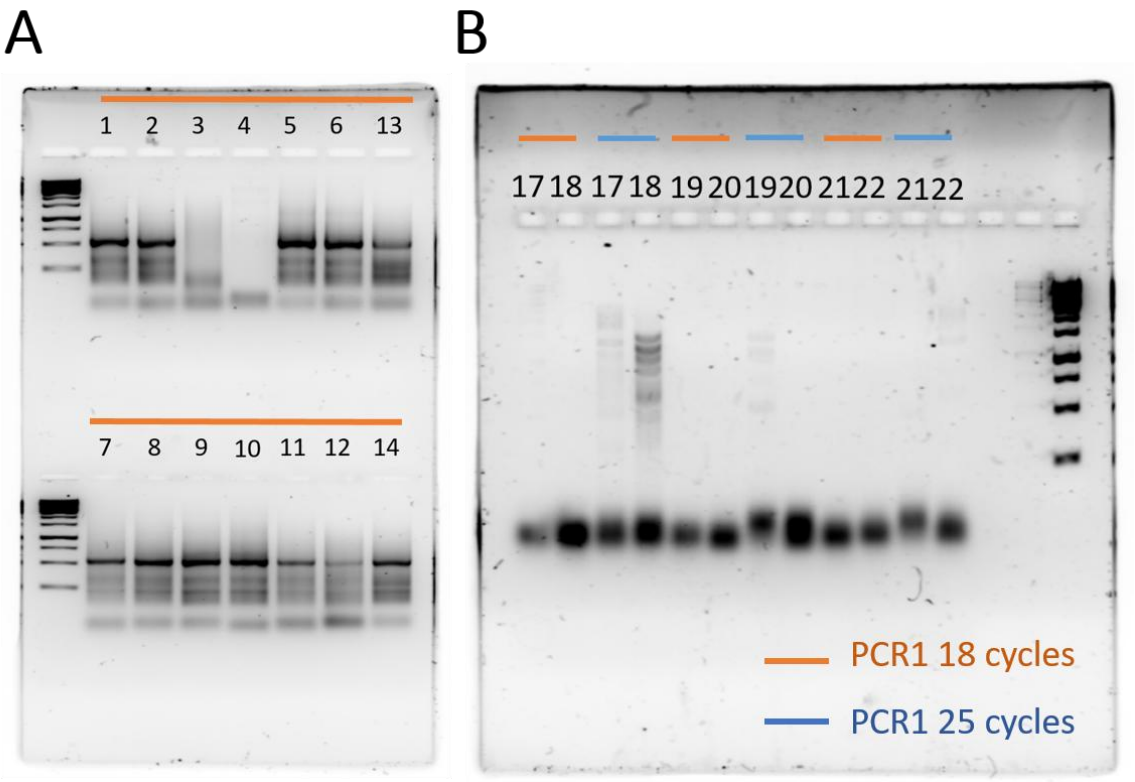

Figure 3.23 - TCRβ amplification optimisation.

Samples were amplified for TCRβ variable region using two rounds of PCR and assessed for TCRβ purity using gel electrophoresis. **(A)** Initial amplicons were generated using 18 cycles of amplification in the first PCR, where samples 1-2 and 5-14 were EBV VST final products and samples 3-4 were peptide-derived IFN-γ isolated target samples which failed to show a purified band at ~575bp. **(B)** Comparisons were made to test 18 cycles versus 25 cycles of amplification in the first PCR to optimise band detection of lower quality samples where samples 17-22 were all peptide-derived IFN-γ isolated target samples.

To assess differences in clonal diversity between EBV VST lines, T cell clonotypes were defined by sharing of the same CDR3 amino acid sequence and the proportion of each T cell product occupied by the top N number of clonotypes was quantified (**Figure 3.24**). Bulk T cells from donors were used as controls and showed highly diverse TCR repertoires, containing thousands of small clones. In contrast, EBV VST derived by either LCL or peptides were oligoclonal with individual repertoires dominated by either a single clonotype or between 10-100 clonotypes. As can be seen, one donor within each LCL-derived and peptide-derived groups generated EBV VST products with over 80% of the repertoire occupied by a top one clonotype, indicating monoclonal targeting of a single epitope.

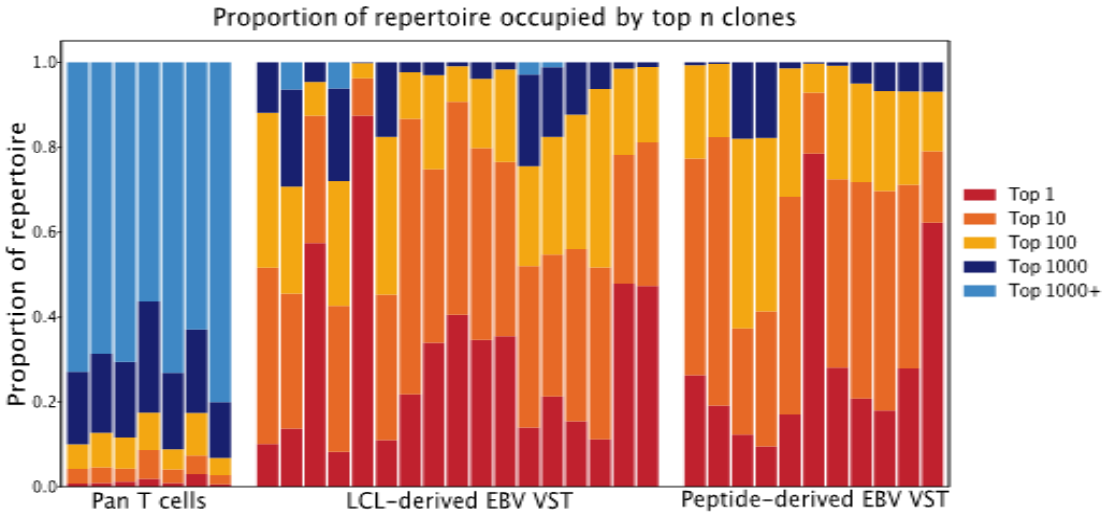

Figure 3.24 - Comparison LCL-derived and peptide-derived EBV VST TCR repertoire composition.

Comparison of TCRβ clonal repertoire composition between of LCL-derived EBV VST lines (n=18) and peptide-derived EBV VST lines (n=11). Stacked bars represent the proportion of the TCR repertoire occupied by the top n clones in that repertoire, where each bar represents a different donor. Pan T cells from unmatched donors (n=7) were used as bulk T cell diversity controls.

The overall clonotype count outlined in **Figure 3.25A** demonstrated a significantly smaller number ($p<0.0001$) of clonotypes present in both LCL-derived and peptide-derived VST as compared to bulk T cell controls. While peptide-derived VST indicated a more restricted clonotype count than LCL-derived VST, this was not statistically significant. The likelihood of a unique CDR3 sequence occuring by chance in the repertoire, or its generation probability (Pgen), was significantly lower in peptide-derived compared to both LCL-derived VST or bulk T cells (**Figure 3.25B**).

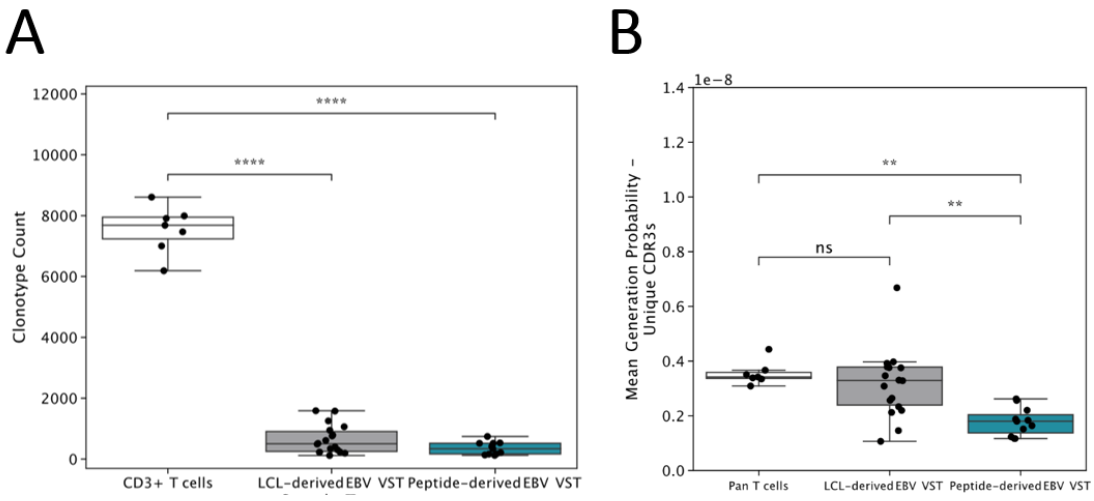

Figure 3.25 - Comparison LCL-derived and peptide-derived EBV VST clonotype count.

(A) Clonotype counts for UMI size matched repertoires (9542 UMIs) were compared between LCL-derived (n=18) and peptide-derived VST (n=11) and bulk T cells (n=7). Groups were compared using one-way ANOVA and Tukey's post-hoc test. **(B)** Generation probabilities for unique CDR3 sequences from each repertoire were calculated using OLGA. CDR3 sequences with a generation probability of 0 were excluded. Groups were compared using Kruskal-Wallis with Dunn's post-hoc test.

To assess the epitope specificities of EBV VST clonotypes, databases of known TCR: antigen binding were used to match the CDR3 sequences against previously recorded TCR epitopes. For this two TCR databases were queried: the Immune Epitope Database (IEDB) TCRMatch (Chronister et al., 2021) and VDJdb (Bagaev et al., 2020), where only exact matches to CDR3 amino acid sequences were included. As shown in **Figure 3.26** a greater proportion of the repertoire in peptide-derived VST comprised sequences annotated as EBV-specific compared with LCL-derived VST and bulk T cells, though no statistical significance was seen between the groups. Sequences with a wide range of other known antigen-specificities were also identified including influenza A and SARS-CoV-2, however EBV-specific sequences comprised the greatest proportion of VST in both the IEDB (**Figure 3.26A**) and VDJdb (**Figure 3.26B**) databases. Interestingly SARS-CoV-2 was second to EBV in the proportion of matches, however the EBV VST material used in this study was generated prior to emergence of SARS-CoV-2.

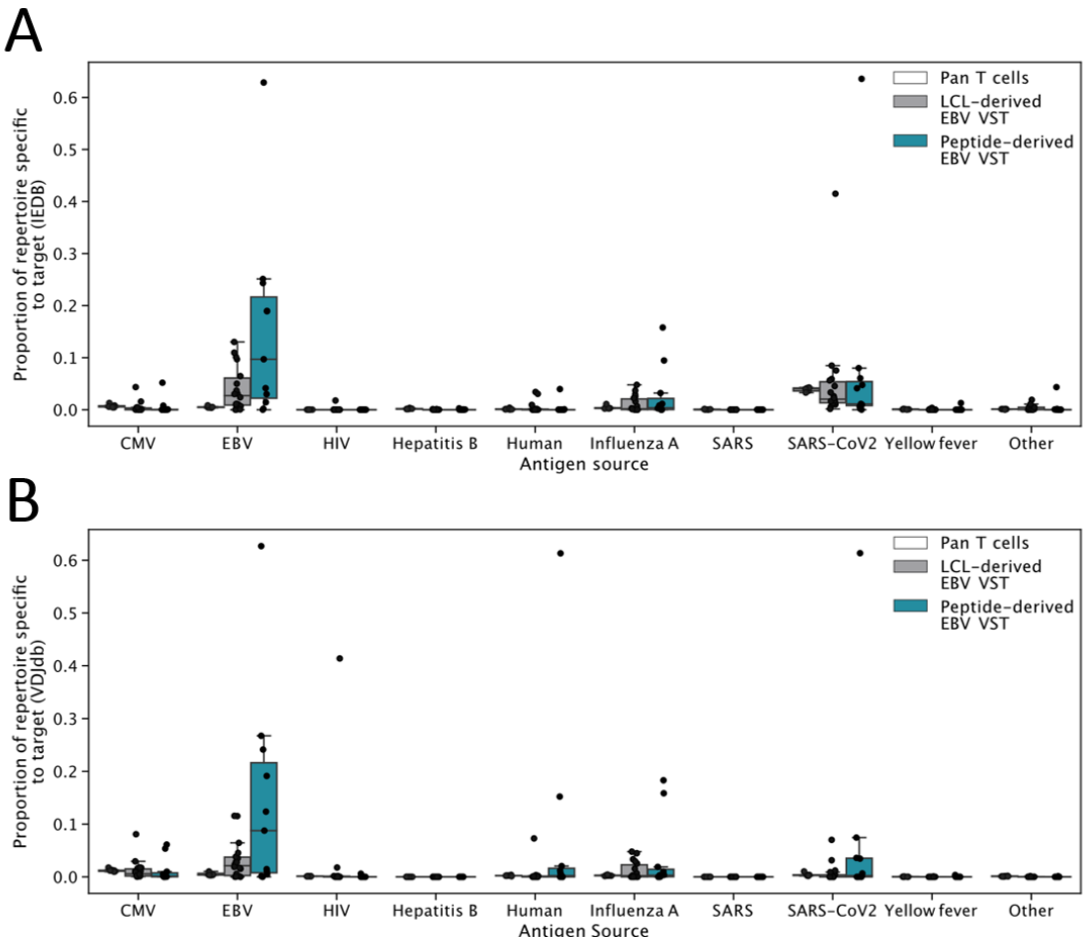

Figure 3.26 - Comparison LCL-derived and peptide-derived EBV VST viral specificity.

EBV VST TCR clonotype sequences were annotated with a wide range of antigen specificities by exact CDR3 amino acid match to recorded TCR: epitope entries in TCR databases **(A)** IEDB and **(B)** VDJdb. Groups were compared using Kruskal-Wallis with Dunn's post hoc test.

CDR3 amino acid sequences were further assessed for matches to individual EBV gene epitope sequences within the VDJdb (**Figure 3.27**). Using this database TCR matching, both peptide-derived and LCL-derived EBV VST had highest matched sequences to BMLF1 as compared to the sequences for other epitopes present within the database: BRLF1, BZLF1, EBNA3A, EBNA3B, EBNA4, LMP1, and LMP2A. No significant differences of EBV antigen specificity were seen between LCL-derived or peptide-derived EBV VST groups.

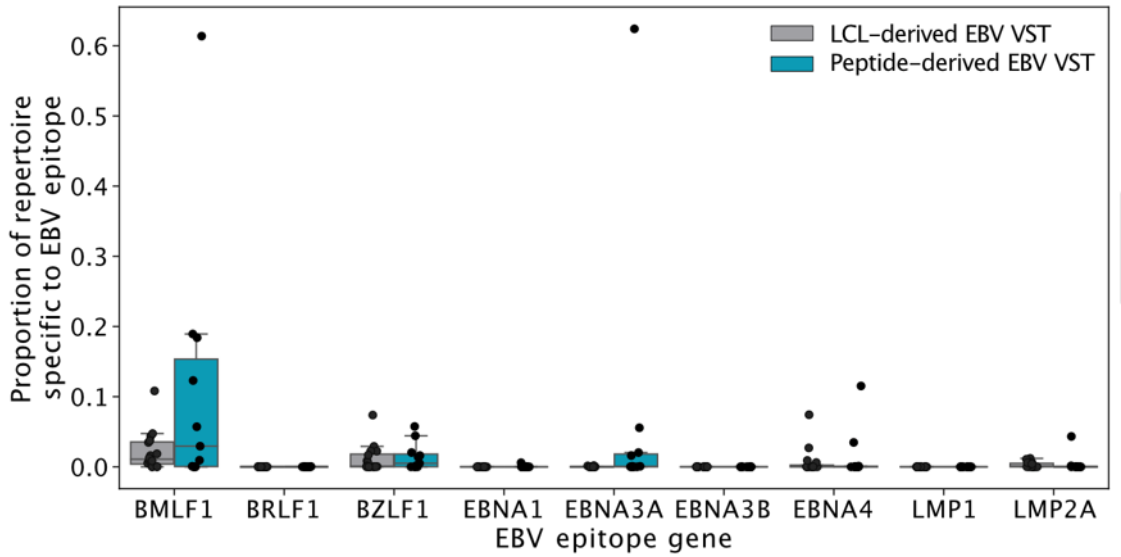

Figure 3.27 - Comparison LCL-derived and peptide-derived EBV VST EBV antigen specificity.

EBV VST TCR clonotype sequences were annotated with EBV antigen specificities. Proportion of each VST repertoire with an EBV-specific CDR3 match in the VDJdb database, split by epitope gene. Groups were compared using unpaired t-tests (Bonferroni correction for multiple comparisons).

Public (or shared) T cell responses to EBV have previously been observed in individuals with varying HLA types (Huisman et al., 2022). This study identified 97 public CDR3 sequences from EBV-specific T cells expanded following peptide-MHC tetramer binding and isolation that were present in more than one individual. Therefore to explore such responses in EBV VST, matching was tested against the 97 public sequences for EBV: BMLF1-GLC A*02 (9 sequences); BRLF1-YVL A*02 (9 sequences); BZLF1-RAK B*08 (24 sequences); EBNA3A-FLR B*08 (7 sequences); EBNA3A-QAK B*08 (15 sequences); EBNA3A-RPP B*07 (3 sequences); EBNA3C-LLD A*02 (1 sequence); LMP2-CLG A*02 (5 sequences); and LMP2-FLY A*02 (24 sequences). We identified 58 matched sequences, with 41 present in more than one sample (**Figure 3.28**). The most shared CDR3 sequences were specific to the BMLF1 and LMP2 antigens found in 16/29 and 14/29 of all EBV VST lines respectively. These

public CDR3 sequences were of low abundance in individual repertoires, suggesting the majority of expanded responses are private to the donor.

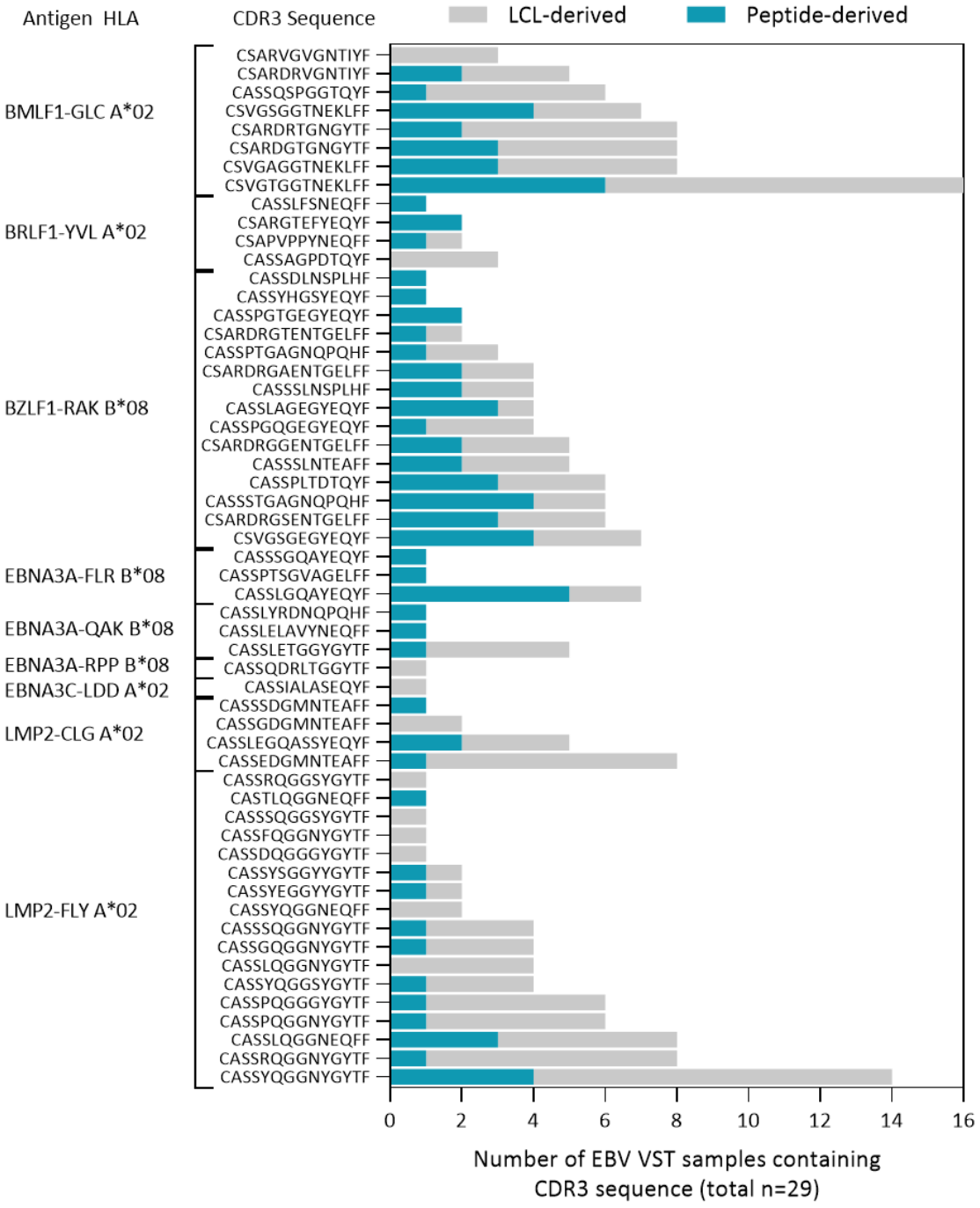

Figure 3.28 - Comparison LCL-derived and peptide-derived EBV VST public EBV CDR3 sequences.
CDR3 sequences from both LCL-derived and peptide-derived EBV VST were matched against previously identified public EBV-specific sequences by (Huisman et al., 2022). Bars represent the number of all EBV VST donor lines (n=29) which contained the public EBV CDR3 sequence colour coded to LCL-derived (grey, n=18) and peptide-derived (teal, n=11) VST. Samples were downsized to match the smallest EBV VST sample (31,233 UMIs).

Altogether the TCR sequencing data indicates EBV VST manufactured using both methods generate an oligoclonal T cell product, with substantial variation in CDR3 clonotypes between different donors.

3.4 Discussion

Adoptive transfer of allogeneic EBV VST for treatment of post-transplant EBV-induced lymphoma has been one of the pioneering T cell therapies to demonstrate clinical success. As technologies for antigen-specific T cell therapies advance in the field, characterisation is essential to understand the effects of different T cell generation methodologies. This chapter was focused on the comparison of EBV VST generated using standard LCL stimulation versus the more recent peptide-mediated selection and expansion using comprehensive profiling of phenotype, functionality, specificity and clonal composition.

Generation of EBV VST has conventionally used EBV transformed LCL to drive expansion of EBV VST due to their strong antigen-presenting capacity and expression of co-stimulatory molecules. We have previously described establishment of EBV VST banks manufactured by LCL stimulation (Wilkie et al., 2004, Vickers et al., 2014) which has demonstrated long-term clinical efficacy in refractory or relapsed PTLD patients in multiple follow-up studies (Haque et al., 2007, Haque et al., 2010, Chiou et al., 2018, Kazi et al., 2019).

A potential issue with the LCL process involves the biosafety risk around culture of LCL, which may continue to shed live EBV during expansion. While formalin fixation of LCL has been used to reduce biosafety risk (Hammer et al., 2007), serial passage of LCL is associated with accumulation of non-silent mutations which could induce non-specific T cell responses (Tan et al., 2018). We introduced an alternative approach using EBV peptide pools for antigenic stimulation. Interestingly, although donors for this process were selected on the basis of EBV sero-positivity, our developed screening assay identified only 11/17 donors that had detectable T cell responses to EBV peptide pools. This may reflect the peptide sequences and/or HLA restriction of the EBV consensus peptide pools used, however given these peptides cover highly immunogenic EBV antigen epitopes and the HLA alleles within this donor group, the majority of donors would be expected to have specific T cells to these antigens. Another potential factor determining responsiveness may be donor age, since our

banked donors averaged 54 (range 40-65 years). Multiple population studies have reported that despite the frequency of tetramer+ EBV-specific T cells increasing with age, the frequency of IFN-γ-producing tetramer+ EBV specific T cells significantly decreases in older individuals (Ouyang et al., 2003, Khan et al., 2004). While numerous parameters can influence immune senescence, the dynamics of T cell expansions/contractions with age has been found to be largely dependent on persistent viral infections, particularly CMV (Khan et al., 2002, Sansoni et al., 2008, Lanfermeijer et al., 2021). Furthermore, although frequency of the T cell repertoire specific to CMV/EBV increases with age, the number of varying CMV clonotypes decreases, indicating a clonal refinement with age (Britanova et al., 2016). Therefore, older individuals may have selected out particular EBV antigen-specific T cell clones with less coverage of sequences utilised in the EBV consensus peptide pools. To generate allogeneic immune cell therapies, it is generally a good risk strategy to recruit active donors that already regularly donate blood products and as such have tracked viral and medical history. In this instance we already had data from numerous apheresis donors, allowing identification of a pool of donors known to be EBV sero-positive, whilst negative for mandatory blood-borne pathogens and from there selected donors with ranging HLA types. Given that apheresis collection is generally a 2-3 hour process, choosing regular apheresis donors may introduce accidental bias to a more aged population able to commit to the required time. While this is largely an anecdotal observation in this small cohort, it raises a potentially important issue for the strategy of donor selection as the T cell therapy field expands.

Through combination of the peptide-induced IFN-γ selection of EBV VST followed by expansion using an entirely closed-system process and GMP-compliant reagents, we identified several practical advantages including reduced process manipulations, reduced hands-on time and shorter culture duration (see **Table 3.5**). Reducing the number of total manufacturing steps minimises risk to introduction of contaminants and affords benefits in terms of reducing staff hands-on time and clean-room facility costs, while automation also standardises processing for robust product manufacture. Additionally, we showed significantly improved viability in peptide-derived VST in comparison to LCL-derived VST which likely reflects the shorter culture duration. We also participated in a multicentre collaborative study run by Utrecht University and the Dutch Medicines Evaluation Board Despite to use a developed framework to estimate the cost to manufacture of cell therapies, comparing both EBV VST

manufacturing processes (Ten Ham et al., 2020, Ten Ham et al., 2021). Despite a high upfront cost of the peptide-mediated process, the ten-fold increase in treatment doses produced results in a more cost-effective manufacturing process compared to LCL manufacture. Moreover, the peptide process is a readily translatable platform to generate T cells targeting other antigens or viruses (Cooper et al., 2020).

METHOD	ADVANTAGES	DISADVANTAGES
LCL Repeated Stimulation	• Established clinical response rate (60-90%). • VST recognise a broad range of EBV latent and lytic peptides. • Can derive VST from EBV seropositive and seronegative donors. • Low upfront reagents/ materials cost per manufacturing run (~£3,615). However low yield (mean=9 doses) gives a higher final cost per dose (£401).	• Long protocol duration (8-12 weeks), higher facility cost. • VST yield is limited by availability of high numbers of LCLs. • VST contain a smaller central memory T cell pool. • Multiple stimulation rounds entail many culture manipulations, higher personnel and facility cost. • Biosafety risk with use of live virus in LCL establishment.
Peptide-mediated IFN-γ Selection & Expansion	• Shorter protocol duration (18 days), reduced facility cost. • All closed-process isolation and culture. • Improved viability and degranulation/ cytokine effector capacity. • Significantly greater yield per manufacturing process. • Can tailor process to a particular EBV antigen/ peptide mix. • Minimal manipulations, reduced personnel cost.	• VST are restricted to recognition of consensus EBV peptide pools. • Restricted to EBV-seropositive donors for manufacturing. • IFN-γ selection protocol can isolate NK / NKT cells => require stringent final product release criteria. • High upfront reagents/ materials cost per manufacturing run (~£22,000). However high yield (mean=84 doses) gives a low final cost per dose (£262).

Table 3.5 - Evaluation of EBV VST manufacturing processes.

EBV VST from both processes demonstrated a highly enriched T cell product containing a majority of CD8+ cells with a small population of CD4+ cells. Importantly, peptide-derived VST were significantly skewed towards central memory. Conversely LCL-derived VST were more differentiated to effector memory, which may reflect repeated antigenic stimulation. Given the increased proliferation capacity of central

memory T cells, this may suggest peptide-derived VST will persist longer upon adoptive transfer (López-Cantillo et al., 2022). Tracking of gene-marked cytomegalovirus VST from purified central memory versus effector memory populations adoptively transferred to non-human primate macaques demonstrated persistence of TCM clones up to 344 days, whereas TEM clones failed to persist >7 days post-infusion (Berger et al., 2008). Similarly, tumour-specific CD8+ cells skewed to TCM phenotype exhibited enhanced tumour clearance compared to TEM in adoptive transfer experiments in mice (Gattinoni et al., 2005) suggesting these T cells may be optimal for adoptive immunotherapy.

EBV lymphomas are commonly diffuse with extranodal involvement in numerous sites including kidney, liver, lung, spleen, gastrointestinal tract and central nervous system (Al-Mansour et al., 2013). It is therefore crucial that peripherally infused EBV VST can migrate and infiltrate within these sites in a tumour-targeted manner. Chemokine receptor expression was largely consistent in both EBV VST products, however peptide-derived VST had significantly higher levels of CCR2 and CCR7. The CCR2 ligand CCL2 has been reported to be upregulated in EBV+ lymphoma lines (Miyauchi et al., 2011), therefore higher CCR2 expression indicates an increased capacity for peptide VST to migrate to and infiltrate within the tumour microenvironment (Viola et al., 2012). High expression of CXCR6 on LCL-derived VST is consistent with a previous study (Parsonage et al., 2012) where CXCL16 secretion from EBV+ nasopharyngeal carcinoma recruited CXCR6^{high} T cells to the tumour site. While a genome-wide association study identified a positive correlation between LCL CXCL16 expression and EBV copy number (Houldcroft et al., 2014), it is not known if CXCR6 is required for effective trafficking of VST to EBV PTLD sites, or infiltration within the tumour through cellular contact and adhesion mechanisms (Chia et al., 2023). Since EBV+ lymphomas secrete high quantities of CCL3, CCL4, CCL22 and CXCL10 compared to EBV- lymphoma lines (Miyauchi et al., 2011), the high expression of cognate receptors CCR5, CCR4 and CXCR3 on both EBV VST groups may indicate complementary/alternate axes of migratory mechanisms. To assess if any of these chemokine receptors are fundamental for chemokine-mediated migration towards PTLD tumours, transwell assays could be set up to track migration of EBV VST towards LCL with and without selective chemokine receptor antagonists. For example, small compound inhibitor ML339 has been found to selectively inhibit CXCR6 and could be used to understand whether the CXCL16-CXCR6 axis induces

recruitment of EBV VST towards different EBV+ tumour cells (Peddibhotla et al., 2020). Generation of chemokine receptor knockout mice could also be made to investigate EBV VST trafficking, though due to the complementary or scavenging roles of some receptors dependent on ligand(s), it is complex to isolate any single mechanism in a biologically relevant context. Furthermore, it would be interesting to assess ability of generated EBV VST to infiltrate diffuse as compared to solid tumours, however it is challenging with human viruses to develop animal models that recapitulate the viral-induced cell transformation and consequent tumour microenvironment. A recent study reported humanised HLA-A2 transgenic NSG mice injected with EBV B95-8 and subsequently treated with immunosuppressive drug tacrolimus attenuated T cell responses, and consequently induced higher blood/ splenic EBV viral load and tumour burden (Caduff et al., 2020). Induced lymphomas had higher transcriptional expression of EBNA-2, LMP-1 and LMP-2, though transcript levels of other EBV latency III genes were not reported. The induced lymphoproliferations were also associated with high serum levels of CD30 and IL-2, hallmark PTLD biomarkers (Haque et al., 2011, Hinrichs et al., 2011, Vase et al., 2015), indicating this may be suitable to model immune-specific aspects of PTLD visualisation of localisation and invasion of adoptively-transferred T cells into lymphomas.

In terms of functionality upon antigen recall, peptide-derived VST had increased CD107a expression and higher frequency of multifunctional cytokine-producing populations indicating these cells have enhanced degranulation and co-stimulatory effector functions. Functional cytokine reactivity to individual EBV antigens demonstrated peptide-derived VST had significantly higher EBNA3A responses than LCL-derived VST. Interestingly, peptide-derived VST showed high final product reactivity to EBNA-LP despite this peptide not being in the original EBV consensus peptides used for CCS isolation. This suggests there is either cross-reactivity in the consensus peptides used for isolation, or the pepmixes used in final product evaluation of specificity. Analysis of the amino acid sequence of EBNA-LP revealed high sequence homology between aa466-479 “RPRPPARSLREWLL" and peptides in the consensus pool (personal correspondence, Miltenyi Biotec) which may indicate the peptide stimulation for CCS isolated and expanded cross-reactive T cell clones to EBNA-LP.

Furthermore, while CD4+ T cells within peptide-derived VST had functional reactivity particularly to EBNA1, EBNA2 and EBNA3A; LCL-derived VST CD4+ T cells had negligible reactivity to any of the EBV antigens tested. This observation is further supported by LCL-derived VST CD4+ T cells showing significantly higher co-expression of T cell inhibitory markers. Altogether these findings suggest up to a quarter of CD4+ cells expanded using the LCL process exhibit a T cell exhaustion profile with limited capacity to proliferate and release effector cytokines likely due to the repeated antigenic stimulation of this method. Peptide-derived VST however demonstrated considerable Th1 cytokine production upon antigen recall as well as expression of CD107a on a proportion of CD4+ T cells indicating potential capacity to degranulate. Investigating this further, peptide-derived VST lines sorted for CD4+ T cells showed equivalent cytotoxicity against HLA-matched LCL as the unsorted VST line controls (with ~50:50 CD4 to CD8 ratio). This suggests some peptide-derived VST CD4 T cells can directly induce killing of infected target cells. Cytotoxic CD4+ T cells have been observed in the context of some cancers and viral infections (Oh and Fong, 2021, Cenerenti et al., 2022, Malyshkina et al., 2023). In a large cohort study taking longitudinal samples of individuals before and after infectious mononucleosis (n=143), Granzyme B+ CD8 T cells are maintained up to two years following symptoms, whereas many individuals had a surge of Granzyme B+ CD4 T cells within the first 50 days of symptoms indicating CD4+ cells may have important cytolytic roles in primary EBV infection (Balfour et al., 2013). Other groups generating LCL-derived EBV VST have reported cytotoxic CD4 clones with killing targeted towards specific EBNA1, EBNA2, and EBNA3A epitopes using *in vitro* assays (Long et al., 2005). CD4 cytotoxicity was found to be MHC Class II-restricted and not mediated through Fas-ligand cytolytic pathways against both LCL (Sun et al., 2002b) and LMP1+ lymphomas (Choi et al., 2018). Instead CD4 cytotoxicity was dependent on granule exocytosis mechanisms, though granulysin has been suggested as the main mediator of CD4 cytolysis with lack of classical perforin or granzyme B expression (Sun et al., 2002b). Furthermore, multimer-isolated and expanded BHRF1-specific CD4+ T cell clones demonstrated HLA-DR*04:01-dependent BHRF1-restricted cytotoxicity of LCL targets (Landais et al., 2004). Although there is clear cytotoxic capacity, it is unknown in a therapeutic context if CD4+ EBV VST provide purely a helper role to CD8+ T cells, directly elicit killing of EBV infected cells or deliver mixed functionality. Likely this question is highly variable between cases, being largely

dependent on the disease, infected cell antigen presentation, patient to donor HLA matching, and therapeutic EBV VST line clone composition.

The overall cytotoxicity against HLA-matched LCL targets was equivalent between LCL-derived and peptide-derived EBV VST. Since LCL-derived VST have already demonstrated anti-tumour efficacy in patient clinical studies, it was vital to ensure peptide-derived VST had ability to recognise sequences presented by actual virus-infected cells in addition to the peptides they were generated against prior to their clinical use. These *in vitro* assays showed a trend whereby increasing numbers of HLA matches between VST and LCL was linked to increased cytotoxicity, as has been reported in improved patient outcomes with closer HLA matching (Haque et al., 2007, Kazi et al., 2019). Interestingly, cytotoxicity against EBV-infected target cells positively correlated with the percentage of IFN-γ+/TNF-α+ cells reactive to EBV peptides. This peptide antigen recall assay could therefore be used in a regulatory context to provide a suitable Quality Control as a surrogate assay to replace cytotoxicity assays which require culture of virus-infected target cells (Fraser et al., 2024). Furthermore, use of EBV peptides to measure functional response should ensure a more standardised assay to compare inter-donor VST line potency as compared to cytotoxicity against allogeneic LCL with differential HLA matching.

Analysis of the TCRβ repertoire showed substantial variation in clonotype size between VST, with certain isolates dominated by individual CDR3 sequences. In some products a large proportion of the repertoire was confirmed to contain sequences which are known to be EBV-specific in public databases. Many previously identified EBV-specific public CDR3 sequences were also identified although these were present at very low frequencies in most VST. However, matching is limited only to CDR3 sequences covering BMLF1, BRLF1, BZLF1, EBNA3A, EBNA3C and LMP2 antigens as identified previously as public EBV-specific clones (Huisman et al., 2022), and therefore matching is underestimated due to lack of other EBV antigen sequences in such databases. The mean generation probability of sequences is also reduced in EBV VST compared with bulk T cells, suggesting that TCRs were not present purely by chance but appear to have been actively selected. The majority of the repertoire in EBV VST is comprised of a restricted number of highly expanded clonotypes, which are less commonly occurring and represent private EBV responses in the donor individuals.

Repertoire comparison between the differentially generated products demonstrated that both groups had comparable absolute number of clonotypes however peptide-derived samples had lower generation probability than LCL-derived VST indicating the presence of more targeted cells using the peptide process. The repertoire of peptide-derived VST had a higher proportion of EBV-specific sequences (from public databases) than LCL-derived VST, possibly reflecting the different antigen sources used between the two methods. It is likely there is a significant overlap in the EBV consensus peptides used for stimulation and those used in the pMHC multimer experiments that contribute to TCR:epitope database curation. The range and density of antigens presented by LCL are likely to be more diverse and vary according to donor and HLA type (Arvey et al., 2012), potentially leading to greater inter-batch variability and more limited overlap with epitopes present in online databases.

Interestingly, EBV VST from both processes had a small proportion of the repertoire that matched to influenza A virus (IAV) and severe acute respiratory syndrome coronavirus 2 (SARS-CoV-2) sequences. All sequenced EBV VST were manufactured prior to 2019 therefore the annotation of SARS-CoV-2 specific sequences found in this study may represent cross-reactivity with pre-existing immunity to other human coronaviruses (McNaughton et al., 2022) or sequence homology in some EBV, IAV and SARS-CoV-2 epitopes as reported in other samples from unexposed individuals (Mateus et al., 2020).

While EBV VST from both groups had contained CDR3 sequences matching the majority of public EBV-specific epitopes, the proportion of each VST repertoire specific for each antigen was low. Using TCR database matching, antigen specificity was highest towards BMLF1. This data contradicts the functional reactivity to specific EBV antigen peptides which demonstrated EBV VST from both processes were mainly targeted towards EBNALP, EBNA3A, EBNA3C and BZLF1 antigens. Comparison between the two techniques to evaluate antigen specificity is limited to the HLA-restricted EBV-specific epitope sequences uploaded to public TCR databases, whereas the JPT Pepmixes used for functional reactivity testing were protein-spanning overlapping peptides allowing HLA-independent assessment of antigen-specific response. Furthermore, JPT peptides cover sequences for the following antigens which have no CDR3 sequences currently uploaded to the VDJdb database: BARF1, BMRF1, EBNALP, EBNA2, EBNA3C and gp350/340. To this end it is hypothesised

TCRβ sequencing is underestimating true antigen (and overall EBV) specificity of the EBV VST products. It is also not impossible that conserved sequences between EBV epitopes could facilitate cross-reactive T cell responses as has been reported for $BMLF1_{280}$ epitope-specific T cells harbouring cross-reactive responses to $BRLF1_{190}$ and $LMP2_{329}$ peptides (Cornberg et al., 2010). Use of multimers to bind and/or sort epitope-specific T cells in combination with the above antigen functional reactivity assay could be used to investigate potential cross-reactivity of clones within our EBV VST products. However, care should be taken for such analyses following demonstration of TCR transduced cells having ability to bind the specific tetramer but without a cytokine response to the peptide antigen, and conversely other transduced cells with high avidity for peptide recognition but unable to bind the specific tetramer (Lyons et al., 2006, Melenhorst et al., 2008, Wooldridge et al., 2009). This highlights the complexity of evaluating antigen specificity, and ideally a toolbox of techniques should be utilised to greater understand clones present in T cell immunotherapies. While the current study focussed on TCRβ sequencing and antigen functional reactivity, the wide range of donor HLA types within our banks would have made purchase of HLA-restricted EBV antigen multimers prohibitively expensive to allow practical utilisation of this technique.

This study had numerous limitations. Precautions were taken to ensure as close a comparison as possible, such as completing entire assays within a restricted timeframe and by a single operator, use of identical LOT reagents, use of the same donor target cells where appropriate in cytotoxicity assays; however numerous parameters limit the ability of direct comparison. Namely, EBV VST products from the two processes were made from different donors incorporating HLA differences as well as geographical discrepancy (New Zealand versus UK) where cellular immunity may be influenced by differential EBV strains, environmental pressures and/or exposure to discrete pathogens. In addition, all assays were performed on post-thaw cells to best replicate the product administered to a patient. The relative date of each bank manufacture and the consequent length of storage in liquid nitrogen storage was significantly different between banks: NZ LCL bank was generated 2010-2014 (10-13 years cryopreservation) and the UK peptide-derived bank was generated 2019-2022 (1-4 years cryopreservation). While prolonged storage might be expected to affect product functionality, it should be noted that even some of the earliest NZ VST lines had extremely functional responses in these assays. This maintenance of

quality has been independently monitored in the SNBTS facility through a comprehensive stability programme, and furthermore these stored products are still used clinically with curative responses in patients. Nonetheless, regardless of duration spent in liquid nitrogen storage, the alternate times of manufacture ultimately introduces many other different parameters such as cryopreservation solutions, reagents for culture and washing of cells, plastics and consumables, and techniques for basic lab procedures such as cell counts. All such variables may influence the differences seen in cell expansion, phenotype and function; and therefore comparisons made do not distinguish the LCL method and peptide method as techniques but encompass the whole manufacturing processes incorporated around them. It was suggested during an MHRA guidance meeting to do intra-donor manufacture in tandem between LCL and peptide method, but using identical starting source, cGMP reagents, flasks, consumables, operators, and analytical techniques. While such experiments would allow a true comparison, we are no longer able to perform LCL manufacture due to restrictions regarding introduction of live virus within our new clean room facility.

3.5 Chapter summary

This study describes the development and implementation of a new manufacturing process to generate EBV VST for clinical use with significant benefits in terms of product yield, cost-effectiveness and closed/ automated processing compared to the historical process. EBV VST products derived from the new peptide process were comprehensively characterised in comparison to our previous LCL-derived EBV VST which have a well-established patient safety and efficacy profile. While clonal diversity and cytotoxicity was comparable, peptide-derived EBV VST demonstrated enhanced degranulation, cytokine production to a broad range of EBV latent antigens and had a dominant central / effector memory status which may improve persistence and targeted tumour clearance in EBV post-transplant lymphoma patients. All data from this comparison study was compiled for a dossier to apply for licensure of the peptide-derived EBV VST therapy which was subsequently approved by the MHRA for clinical use in 2023. The efficacy of these EBV VST products will be followed as they continue to be supplied on a compassionate basis under ‘Specials’ licence to patients world-wide.

Chapter 4

Detection & Isolation of SARS-CoV-2 VST

Chapter 4 – Detection & isolation of SARS-CoV-2 VST

A brief foreword.

I started my PhD in October 2019. The aims then were entirely for the EBV VST comparison study covered in Chapter 3, with lofty aspirations to engineer EBV VST with a chemokine receptor in attempt to improve infiltration into solid tumours. This part of the project unfortunately never came to fruition. I remember at the end of 2019 it was prophesised the world was due some kind of global disaster, the more cynical among us predicting the start of World War 3 due to widespread political angst at the time. With the major 1918 Spanish flu pandemic 100 years prior, the outbreak of SARS-CoV-2 in 2019 has caused the widest infectious global health emergency of the 21st century. While for most people this led to a year or more of working from home and social distancing, researchers within the natural sciences all came together to focus on uncovering all aspects of SARS-CoV-2 virology, disease pathology, immune response, diagnostic testing and discovery of treatments. At SNBTS we had a unique opportunity to study COVID-19 immunity with the translational capacity to explore therapy development. I had a two week lock down before commencing work on testing donor blood for SARS-CoV-2 T cell responses with the aim to make a SARS-CoV-2-specific T cell therapy. This was certainly the busiest phase of my PhD and involved long hours of lone working until more lab members could return to work. As I write this four years later, like many who experienced personal loss and crisis from the pandemic and fallout thereafter, I find myself trying to forget these years as much as possible. On the whole the world has very much gotten "back to normal", but as it happens the concept of "new normal" in fact denotes that life has never felt more different. Regardless, I feel incredibly fortunate to be one of the few PhD students that came out of lockdown with more data than I knew what to do with, not to mention thankful in many ways to be kept sane through the opportunity to work and for the rewarding feeling to contribute during this dark time. I never did make banana bread or attempt a jigsaw, but here instead are three chapters covering my research in chronological order of "the COVID years" (inevitably a chapter title in many later memoirs of my generation); that will hopefully be useful in our ongoing understanding of this disease, and how we address investigation of immune response and potential of immunotherapy for future viruses.

4.1 Introduction and aims

4.1.1 Coronavirus outbreak

Severe acute respiratory syndrome coronavirus 2 (SARS-CoV-2) is reported to have emerged in Wuhan within the Hubei province of China in December 2019 (Zhou et al., 2020b, Wu et al., 2020). As a highly contagious novel respiratory virus emerging at the height of international travel to date, global spread was extremely rapid despite initial measures put in place for containment. Due to the relatively high morbidity and mortality rates of the resulting coronavirus disease 2019 (COVID-19), this disease was declared a public health emergency by the World Health Organisation (WHO) on March 11th, 2020.

4.1.2 SARS-CoV-2 origin

While the origin of SARS-CoV-2 is still debated at present, evidence suggests it is likely to have resulted from natural zoonotic transmission to humans. Numerous animals have found to be carriers and reservoirs for SARS-CoV-2 virus including bats, cats, ferrets, mink, pangolins and rabbits (Li et al, 2021), indicating their potential as the host reservoir. Genomic analysis showed that *Rhinolophus affinis* bat betacoronavirus RaTG13 had greatest similarity to SARS-CoV-2 (~96% sequence homology, (Zhou et al., 2020b)), however it diverges in sequence for the spike receptor binding domain (RBD) indicating weaker binding affinity to human angiotensin converting enzyme 2 (ACE2) (Wan et al., 2020b) . Numerous pangolin coronaviruses however have high sequence homology in the spike RBD residues (Lam et al., 2020) indicating a closer vector, yet mortality was rapid in these infected pangolins and therefore they are not likely to be a long-term reservoir species for SARS-CoV-2 (Xiao et al., 2020a). The current favoured hypothesis is that SARS-CoV-2 was transmitted from bats as intermediate hosts, to pangolins and then to humans, with natural selection of the spike protein for optimal ACE2 binding occurring as a natural evolutionary process either within pangolins or through human to human transmission (Andersen et al., 2020, Cascella et al., 2024). In addition, SARS-CoV-2 contains a polybasic cleavage site with a leading proline insertion (PRRAR) at the junction of S1 and S2 subunits of spike protein, which in turn allow effective cleavage by furin and addition of O-linked glycans (Walls et al., 2020). These features are

unique to SARS-CoV-2 and equivalent polybasic cleavage sites have not been observed in related sarbecoviruses to date.

The significance of these polybasic cleavage sites has been investigated experimentally in other viruses. More efficient cleavage of the MERS-CoV spike protein conferred ability of transmission of MERS-CoV from bats to humans (Menachery et al., 2020). Insertion of a furin cleavage site at the S1-S2 junction in SARS-CoV-1 enhanced cell-to-cell fusion however did not correspond with any change in infectivity (Follis et al., 2006). In avian influenza viruses, acquisition of polybasic cleavage sites within the hemagglutinin protein converts low pathogenicity strains to highly pathogenic strains (Nao et al., 2017). While the role in SARS-CoV-2 remains unclear, it suggests that these polybasic cleavage sites of spike protein may impact upon transmissibility and/or pathogenesis. Furthermore, O-linked glycosylation is hypothesised to create a mucin-like domain that can act as a shield and confer immune evasion mechanisms as seen in numerous other viruses (Bagdonaite and Wandall, 2018). Altogether these key features of sequence and protein structure likely offer evolutionary advantages with the consequence of improved transmission and/or pathogenesis, and therefore may explain why SARS-CoV-2 unlike previous betacoronavirus outbreaks escalated from localised epidemics to a global pandemic.

The theory that SARS-CoV-2 could have been leaked from a lab in Wuhan has gained considerable attention, likely due to the political landscape at the onset of the pandemic, with some reports suggesting the genetic structure of SARS-CoV-2 cannot rule out a laboratory origin. The primary evidence against this theory is that collective attempts worldwide to culture SARS-CoV-2 in cell lines over the last four years have consistently shown that serial passage induces deletion of the furin cleavage site in the spike gene (Hoffmann et al., 2020a, Lau et al., 2020, Hale, 2021, Johnson et al., 2021, Lamers et al., 2021). Had SARS-CoV-2 been propagated in a lab prior to the pandemic outbreak, it would be expected that this furin cleavage site would have been deleted. However this site is intact in early isolates of SARS-CoV-2. Interesting insights from two recent editorials have suggested the only evidence which could prove a lab leak hypothesis would be actual laboratory records of handing the original or very closely related Wuhan strain (Alwine et al., 2023). Without such evidence this theory can only be disproved through long term

phylogenetic studies to track patterns in sequence evolution, similar to debunked theory that HIV was introduced through polio vaccine batch (The Lancet, 2023).

4.1.3 SARS-CoV-2 structure

Both SARS-CoV-1 and SARS-CoV-2 belong to a subgenus of betacoronavirus known as sarbecovirus (Kirtipal et al., 2020). Like other coronaviruses, SARS-CoV-2 is a positive-sense single-strand RNA virus. SARS-CoV-2 was first established in both human airway epithelial cell cultures (Zhu et al., 2020) and African green monkey kidney epithelial 'vero' cells (Kim et al., 2020b) allowing isolation for RNA extraction. Next Generation Sequencing revealed a 28-30kb genome encoding four structural proteins (**Figure 4.1**): spike (S), membrane (M), nucleocapsid (N) and envelope (E), as well as several non-structural and accessory proteins (Kim et al., 2020a).

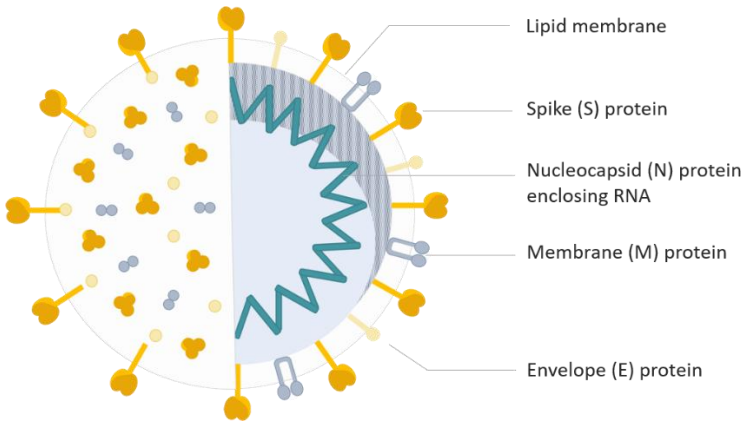

Figure 4.1 - SARS-CoV-2 virion structure.
SARS-CoV-2 is made up of structural proteins: envelope (E), membrane (M) and spike (S); and viral ssRNA is encapsulated within nucleocapsid (N) protein.

4.1.4 SARS-CoV-2 entry and replication

The spike protein is located on the outer virion surface, and composed of the S1 (amino-terminal) and S2 (carboxyl-terminal) subunits. The RBD of the S1 subunit can bind the human ACE2 receptor expressed on the host cell surface (Song et al., 2018, Jiang et al., 2020) and is the principal receptor for SARS-CoV-2 entry into human target cells. Numerous other adhesion molecules and co-receptors have been implicated in aiding viral entry including C-type lectins, CD26, CD147, integrins, heparin sulfate, neuropilin-1, sialic acid and vimentin; however at present none have been shown to support viral infection in the absence of the obligate receptor ACE2 (Eslami et al., 2022). Initial viral attachment is followed by priming whereby furin

proteases cleave at the S1-S2 junction to conformationally separate the S1 and S2 subunits (Vankadari, 2020, Essalmani et al., 2022). This exposes an S2 subunit site which is further cleaved primarily by host transmembrane serine protease 2 (TMPRSS2) in nasal/ airway epithelial cells (Hoffmann et al., 2020b) or cathepsin L (CTSL) in cells where TMPRSS2 is absent (Zhao et al., 2022b). This results in full dissociation of the S1 & S2 subunits, and conformation transition of the S2 subunit to reveal a short 19 amino acid segment called the fusion peptide (FP) which binds to the host cell transmembrane and ultimately fuses the virus and cell membranes together (Papa et al., 2021). The formation of a fusion pore allows insertion of viral genomic RNA (gRNA) into the host cell cytosol for uncoating and subsequent replication (**Figure 4.2**) (Jackson et al., 2022).

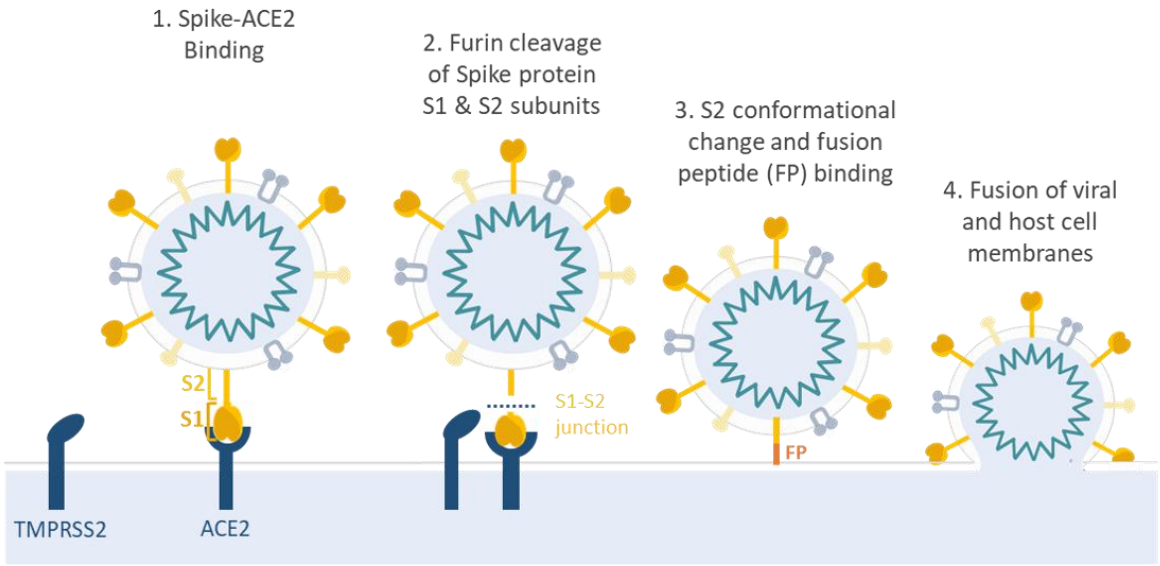

Figure 4.2 - SARS-CoV-2 viral entry mechanisms.

SARS-CoV-2 Spike protein subunit 1 (S1) binds to the host cell membrane ACE2 receptor. Host cell transmembrane serine protease (TEMPRS2) then cleaves spike at the S1-S2 junction to fully dissociate S1 and S2 subunits. This causes a conformation change in S1 subunit to expose the fusion peptide (FP) which fuses the host cell membrane allowing viral-host membrane fusion and viral RNA entry into the cytosol. Adapted from (Lamers and Haagmans, 2022) & (Le et al., 2023).

Following viral entry, the positive-sense gRNA recruits host ribosomes to translate Open Reading Frames (ORF) 1a and 1b which encode non-structural proteins (NSP)

all involved in replication and transcription (

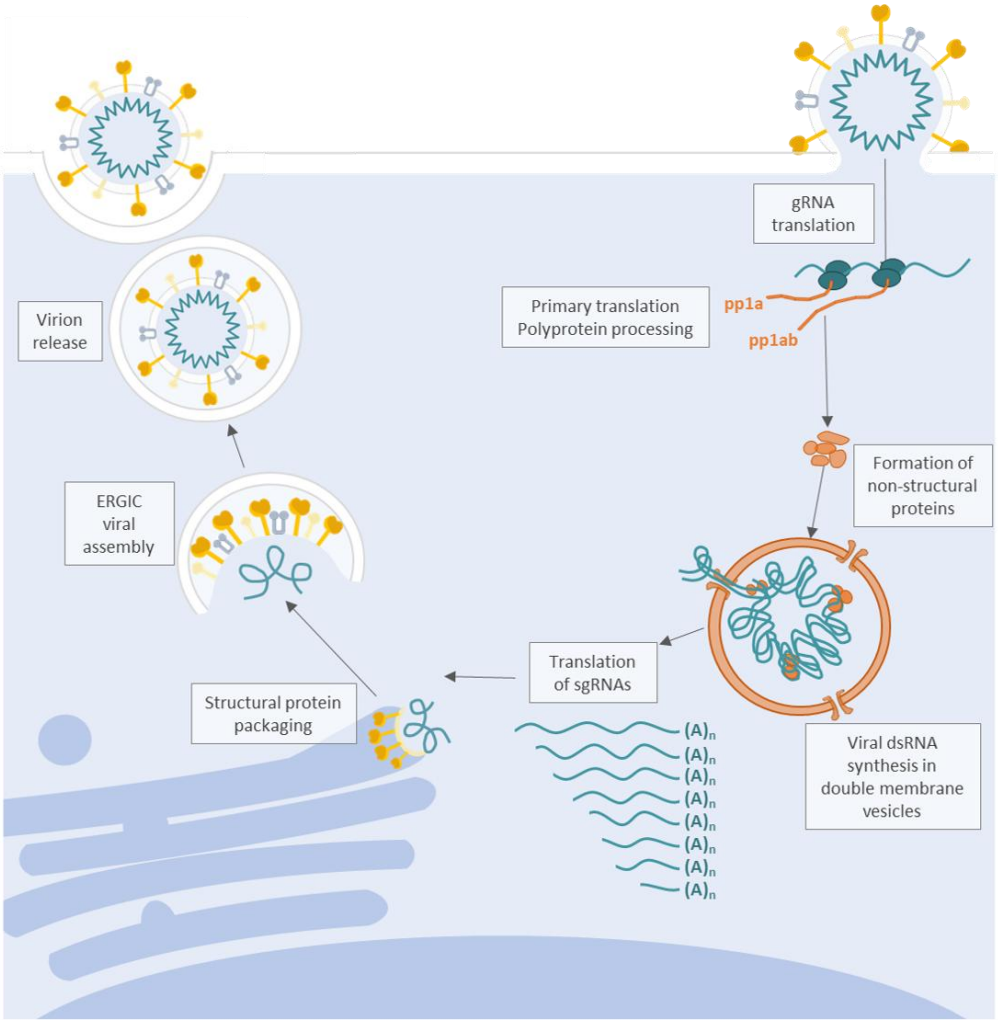

Figure 4.3) and constitute around 75% of the total SARS-CoV-2 genome (Wu et al., 2020). Initial rapid release of nsp1 shuts down translation of host mRNA, which prevents cellular antiviral defence mechanisms including induction of type I interferon signalling (Thoms et al., 2020). Furthermore nsp3, nsp4 and nsp6 induce remodelling of the host endoplasmic reticulum to form double membrane vesicles (DMV), a hallmark motif of positive-strand RNA virus infection which can be visualised by electron microscopy (Angelini et al., 2013, Cortese et al., 2020). These vesicles act as replication organelles which both organize viral RNA synthesis, and shield the double-stranded RNA intermediates from detection by cytoplasmic PRR or TLR present on local innate immune cells (Malone et al., 2022). Therefore SARS-CoV-2 demonstrates efficient initial strategies to evade innate immune responses and permit viral RNA synthesis. In addition, tomographic imaging has revealed nsp3 as a major constituent of a hexameric pore complex that spans DMV membranes which have been implicated in export of RNA to the cytosol (Wolff et al., 2020, Klein et al., 2020). Structures resembling the nucleocapsid protein were detected on the cytosolic

side of the DMV pore complex, suggesting direct RNA encapsidation as it exits the DMV (Wolff et al., 2020). The other non-structural proteins assemble into replication-transcription complexes, which act within DMV to initiate RNA replication primarily driven by nsp7, nsp8, nsp12, nsp13, nsp14 and nsp15 (**Figure 4.4**). This begins with replication of a full length antigenome gRNA to serve as a template, which directs synthesis of both further gRNA, as well as a nested set of subgenomic RNAs (sgRNA) of ORFs 2-9 encoding accessory proteins and structural proteins. Canonical transcription of eight sgRNA allows translation within the endoplasmic reticulum to be packaged into progeny virions.

For assembly, viral RNA is coated with nucleocapsid proteins in the cytosol, which traffics to endoplasmic reticulum-golgi intermediate compartments (ERGIC) which are decorated with spike, membrane and envelope proteins (Hartenian et al., 2020). This newly formed virion then traffics to the Golgi apparatus for post-translational modification, including glycosylation to aid in viral attachment which is also thought to shield epitopes from the neutralizing antibody response (Watanabe et al., 2020, V'Kovski et al., 2021). While most enveloped viruses then egress via the biosynthetic secretory pathway, SARS-CoV-2 virions were found to exit the cell within deacidified lysosomes (Ghosh et al., 2020). At present it is unclear why SARS-CoV-2 hijacks lysosomes for extracellular release, however since a primary role of acidified lysosomes is intracellular pathogen degradation, SARS-CoV-2 disruption of lysosomal exocytosis is suggested as a strategy to evade immune clearance (Liang et al., 2022).

Coronaviruses have evolved mechanisms to limit the transcriptional error associated with RNA viruses, whereby the mutational rate of most RNA viruses usually limit a genome size to ~15kb before such a deleterious mutation is accumulated that it would lead to collapse of the species (Sanjuán et al., 2010, Smith et al., 2014).

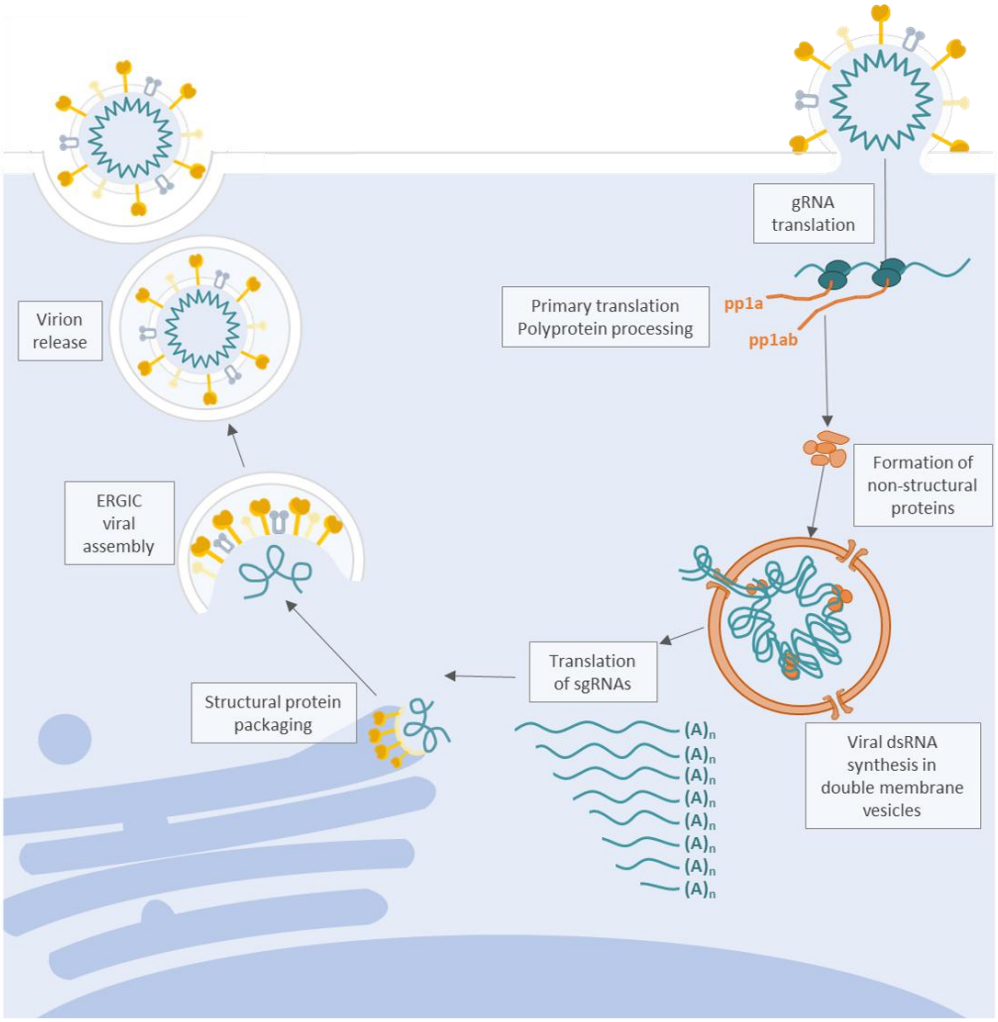

Figure 4.3 - SARS-CoV-2 viral replication.

SARS-CoV-2 viral gRNA undergoes initial translation to recruit host cell ribosomes and transcribe of template RNAs. SARS-CoV-2 genome encoded polypeptides are translated to form non-structural proteins involved in viral replication, transcription and host immune evasion roles; including double stranded RNA (dsRNA) processing, formation of double membrane vesicles and translation of subgenomic-RNAs (sgRNA). Translated structural proteins and accessory proteins are packaged for transit through the endoplasmic reticulum golgi apparatus intermediate compartments (ERGIC). Assembled virions are then released out of the cell via exocytosis. Adapted from (Jackson et al., 2022, Lamers and Haagmans, 2022, Malone et al., 2022)

Through acquisition of proteins in the replication transcription complex that increase replication fidelity, coronaviruses have an improved ability to preserve genetic integrity increasing the survival of the species as a whole. All stages are tightly regulated including: template unwinding by nsp13; proofreading by nsp10, nsp12, nsp13 and nsp14; and RNA capping by nsp10, nsp13, nsp14, and nsp16 (Malone et al., 2022). In addition, nsp15 is an endoribonuclease which shortens the poly-uridine sequences at the 5' end of negative-strand RNA, to evade recognition by PRR MDA5 to again hinder the host innate type I interferon response (Hackbart et al., 2020). While a multitude of evolved mechanisms to regulate viral replication and immune evasion have been discovered, there are likely still numerous other functions by which SARS-CoV-2 has such successful transmissibility and ultimately progression of infection.

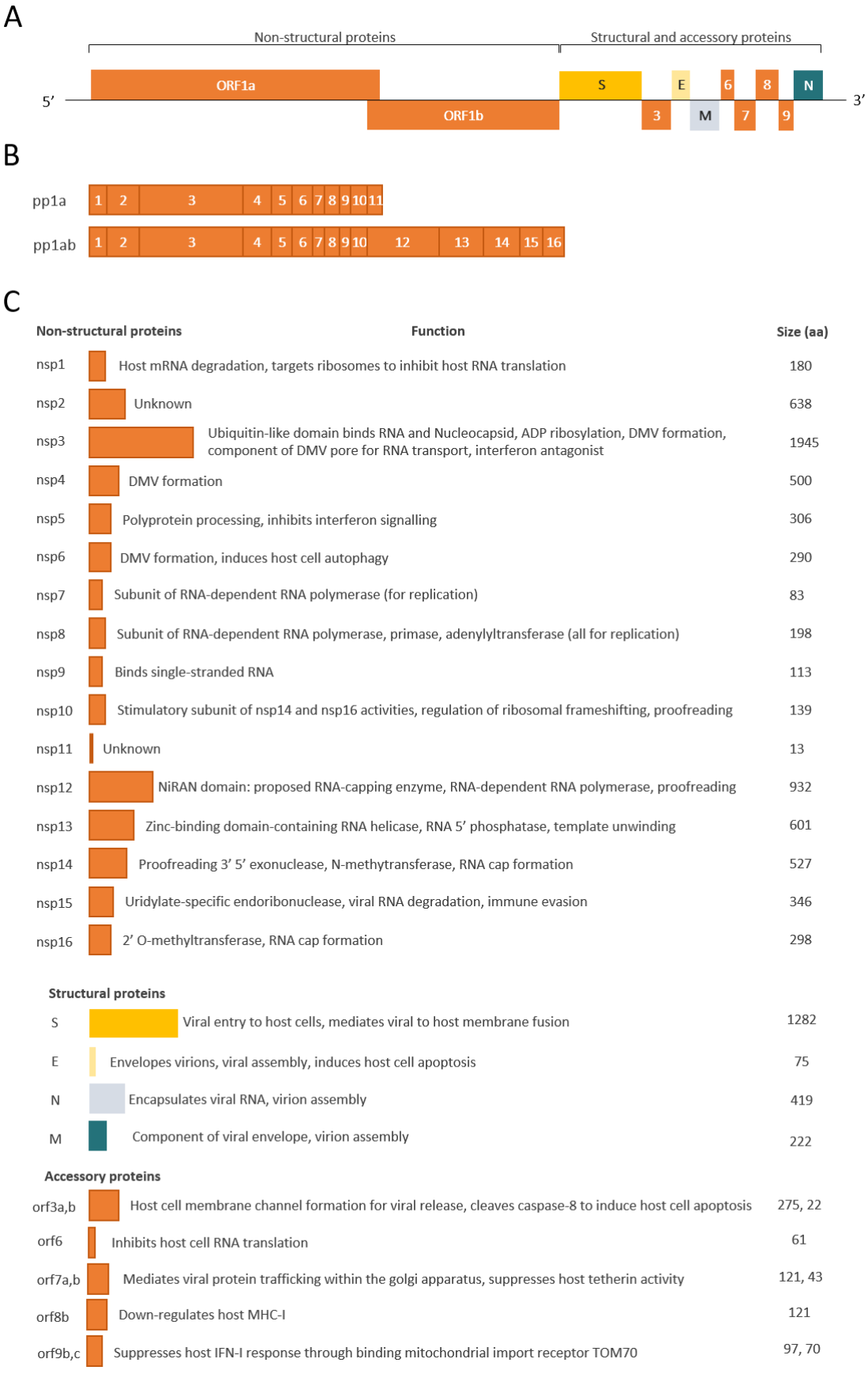

Figure 4.4 - SARS-CoV-2 genome and protein functions.

(A) SARS-CoV-2 genome structure. **(B)** ORF1a & 1b polypeptide sequence of non-structural proteins. **(C)** SARS-CoV-2 non-structural, structural and accessory proteins functions. Adapted from (Arya et al., 2021, Bai et al., 2022, V'Kovski et al., 2021, Yang and Rao, 2021).

4.1.5 SARS-CoV-2 infection and pathogenesis

Like most respiratory viruses, SARS-CoV-2 is transmitted via respiratory droplets or aerosols, whereby infected individuals can shed viral particles even prior to symptom onset by just exhalation (He et al., 2020). Initial infection of SARS-CoV-2 takes place within nasal mucosa cells or respiratory epithelial cells of the nose and upper respiratory tract (Parasher, 2021). Here the virus propagates, with a median incubation period of 4-5 days, during which individuals are highly infectious (Lauer et al., 2020, Li et al., 2020). Viral load peaks at symptom onset, where viral spread along ciliated cells of the conducting airways can cause the most common symptom (at least of the initial strain) of coughing, as well as sneezing, fever and fatigue (Sims et al., 2005, Hoffmann et al., 2020b). A strong host innate interferon response, as seen in children, can sufficiently restrict viral replication at this stage with very mild clinical manifestation (Yoshida et al., 2022), whereas impaired type I interferon responses were associated with disease progression (Hadjadj et al., 2020).

If the virus is not cleared by the aforementioned innate immune responses, infection can spread to the lower respiratory tract and ultimately the lung alveolar cells, also known as pneumocytes. Both *in vitro* data and animal models indicate SARS-CoV-2 primarily infects alveolar type 2 (AT2) cells (Hou et al., 2020, Salahudeen et al., 2020, Youk et al., 2020, Ziegler et al., 2020), however alveolar type 1 (AT1) cells can also be infected (Ziegler et al., 2020). While AT1 cells cover the 95% of the alveolar surface area and are responsible for gas exchange, AT2 cells secrete surfactants which lubricate the lung and help to reduce alveolar surface tension during respiration (Zhao et al., 2022a). Infected pneumocytes respond by secreting an array of pro-inflammatory cytokines including CCL2, CCL3, CXCL10, IFN-β, IFN-γ, IL-1, IL-6, IL-8, IL-12 and TNF-α (García, 2020). This acts to recruit immune cells such as neutrophils and T cells to the lung to kill virally infected cells, and in doing so contributes to inflammatory-induced lung injury. With immune-mediated apoptosis of the virally-infected lung cells causing release of newly made virions to infect neighbouring cells, it should be appreciated clearance of infection from the lungs requires an army of immune cells to initiate a fine-tuned coordinated attack.

Persistent inflammation-induced injury can lead to pulmonary pneumonia or acute respiratory distress syndrome (ARDS) in severe cases of COVID-19. Viral or inflammatory-induced death of both lung endothelial cells and epithelial cells

contributes to increased lung vascular permeability which impairs lung function and manifests as decreased blood oxygenation (Wang et al., 2020a, Zhou et al., 2020a). Histological examination of lung tissue of COVID-19 ARDS patients reveal diffuse alveolar damage (DAD) as a common pathology, whereby injury of the alveolar epithelial lining leads to leakage of plasma into the alveoli (Carsana et al., 2020, Menter et al., 2020). This is characterised by dying pneumocytes, intra-alveolar and interstitial oedema, formation of hyaline membranes and AT2 cell hyperplasia as they attempt to regenerate the alveoli. Hyaline membranes are made from fibrin-rich aggregates to seal the alveoli away from fluid accumulation, however this also restricts gas exchange. This formation of fibrin aggregates can also produce fibrin thrombi, which have been observed in the small arteries and veins of severe COVID-19 patients (Cui et al., 2020, Klok et al., 2020, Lodigiani et al., 2020, Tang et al., 2020, Wichmann et al., 2020). Presence of fibrin thrombi, elevated levels of D-dimers produced upon fibrin degradation, and low platelet counts have been associated with severe or fatal outcomes of COVID-19 (Al-Samkari et al., 2020, Grasselli et al., 2020, Lippi et al., 2020, Zhou et al., 2020a). Furthermore, highly elevated plasminogen activator inhibitor 1 (PAI-1), an inhibitor of the fibrinolysis pathway, in the serum and lungs correlated to COVID-19 disease severity (Kang et al., 2020, Lopez-Castaneda et al., 2021, Zuo et al., 2021, Toomer et al., 2023). This increased inhibition of fibrin degradation, combined with overactivation of coagulation contribute to a dysregulated pro-thrombotic state which can then lead to pulmonary embolisms or complications in other organs such as arterial thrombosis, myocardial infarctions or ischemic strokes (Cascella et al., 2024).

Multisystem disease or multi-organ failure has been reported in severe and critical cases of COVID-19. It is hypothesised the broad expression of ACE2 and TMPRSS2 across tissue types could in part explain the wide-ranging clinical manifestations of COVID-19 (Zou et al., 2020, Prato et al., 2024). ACE2 is a key regulator of the Renin Angiotensin Aldosterone System (RAAS) in humans which acts to cleave Angiotensin I and Angiotensin II. Breakdown of these vasoconstrictive hormones is crucial to modulate blood pressure and osmolarity. Expressed in many tissues throughout the body including heart, kidney, lungs, respiratory tract and intestinal tract, gallbladder and testis (Hikmet et al., 2020), ACE2 regulation provides many protective roles particularly within the cardiovascular and renal system. Additionally, since Angiotensin II has pro-apoptotic and pro-fibrotic actions on lung epithelial cells (Li et

al., 2008, Simões e Silva et al., 2013, Samavati and Uhal, 2020), as well as macrophage activation and pro-inflammatory cytokine release (Gopallawa and Uhal, 2014, Banu et al., 2020); its degradation by ACE2 has a direct role in the prevention of lung injury and cytokine storm. Although SARS-CoV-2 spike receptor binding does not overlap with the ACE2 catalytic domain, viral entry has been shown to downregulate ACE2 expression in the lung (Kuba et al., 2005, Yamaguchi et al., 2021, Lu et al., 2022) and gut (Triana et al., 2021), and therefore hypothesised as the likely mechanism by which SARS-CoV-2 induces cell invasion and pathogenesis.

4.1.6 COVID-19 clinical classification

In the majority of individuals, SARS-CoV-2 infection is asymptomatic or causes mild illness, however approximately 20% of cases progress to severe disease. As of March 2024, the latest National Health Institute update classifies the clinical spectrum of SARS-CoV-2 infection into five categories as outlined in **Table 4.1**.

Disease Category	Criteria
Asymptomatic or pre-symptomatic infection	Individuals with positive virologic test for SARS-CoV-2 but no symptoms consistent with COVID-19.
Mild illness	Individuals with any of the following symptoms: fever, cough, sore throat, fatigue, headache, muscle pain, nausea, vomiting, diarrhoea, loss of taste, loss of smell.
Moderate illness	Individuals with evidence of lower respiratory disease by clinical assessment or chest imaging, and an oxygen saturation measured by pulse oximetry (SpO_2) ≥94% on room air at sea level.
Severe illness	Individuals with SpO_2 <94% on room air at sea level, a ratio of arterial partial pressure of oxygen to fraction of inspired oxygen (PaO2 /FiO2) <300 mm Hg, respiratory rate >30 breaths/min, or lung infiltrates >50%.
Critical illness	Individuals with respiratory failure, septic shock, or multi-organ dysfunction.

Table 4.1 - Clinical spectrum of SARS-CoV-2 infection and disease.
Adapted from (NIH, Accessed March 2024.).

While there has been vast and rapid progress to attempt to elucidate disease pathogenesis, there is still very limited understanding of how the immune response to infection is dysregulated in patients with severe disease.

4.1.7 Immune response to SARS-CoV-2: the turbulence after the storm

Given that SARS-CoV-2 infection, disease pathogenesis and immune response are intrinsically linked, some key immune mechanisms have previously been described. It is important however to understand the plethora of immune mediators involved and how dysregulation contributes to the central factor of COVID-19 disease severity: the cytokine storm. Whether the elevated levels of cytokines released during COVID-19 are actually considered a 'cytokine storm' is still debated (Mehta and Fajgenbaum, 2021), this is discussed in more detail in Chapter 7, however it is undeniable that systemic elevation of certain inflammatory cytokines are a prognostic factor of SARS-CoV-2 disease pathogenesis.

As discussed earlier, innate immune sensing of SARS-CoV-2 RNA within infected cells is initiated by PRRs and TLRs including MDA5 (Yin et al., 2021, Sampaio et al., 2021), TLR2 (Zheng et al., 2021),TLR3 (Mukherjee et al., 2021), TLR7(Jangra et al., 2021), TLR8 (Campbell et al., 2021), triggering signalling cascades of cytokines in response to ligation, particularly type I/ III interferons and various chemokines. While it is unclear which are the first innate immune cells to traffic to the infected site, the initiation of IFN-I and chemokine secretion induces recruitment of DC, monocytes, macrophages, neutrophils, and NK cells; which further secrete chemokines to recruit adaptive immune cells to the lungs.

Cytokine driven recruitment and activation of B cells is crucial to initiate an effective humoral response against SARS-CoV-2. Following primary exposure, most individuals seroconvert within 7-14 days, with SARS-CoV-2-specific antibodies persisting up to several weeks following viral clearance. The spike protein RBD is particularly immunogenic, and neutralising anti-RBD IgG can potently inhibit virus entry by blocking spike/ACE2 interactions (Ju et al., 2020, To et al., 2020, Dispinseri et al., 2021). Some early studies reported that individuals with cross-reactive antibodies to other coronaviruses had significantly earlier, elevated and pro-longed antibody responses and surprisingly a more severe clinical course. This was suggested as a mechanism of antibody-dependent enhancement (ADE) in which the cross-reactive antibodies failed to neutralise SARS-CoV-2, or even potentiated entry to Fc receptor-II positive cells. While there have been reports of spike neutralising antibodies able to induce ADE using *in vitro* assays (Liu et al., 2021b, Wang et al., 2022), isolated

infection-enhancing antibodies provided protection against SARS-CoV-2 infection using *in vivo* mouse and non-human primate models (Li et al., 2021). Although evidence of naturally occurring ADE in human SARS-CoV-2 infection is difficult to investigate clinically, at present the lack of clinical reports and animal model results would suggest that ADE is a rare phenomenon of *in vivo* infection or vaccine response (Yang and Xu, 2022, Nakayama and Shioda, 2023). Longevity and memory of antibody response to primary infection of SARS-CoV-2 will be addressed further in the discussion of this chapter, and following variant re-exposure or vaccines discussed further in Chapter 7.

Emerging evidence at the start and throughout the pandemic indicated COVID-19 severity was correlated with lymphopenia, where patients with progressive disease have been reported to have reduced numbers of peripheral blood T cells and NK cells (Chen et al., 2020, Liu et al., 2021a, Wan et al., 2020a, Wang et al., 2020c). Severe disease also features accumulation of naïve and/or exhausted memory T cells which have been associated with a systemic hyperinflammatory responses and poorer prognosis (Diao et al., 2020, García, 2020, Zhou et al., 2020c, Zheng et al., 2020b, Zheng et al., 2020a). Accordingly, protection in those able to clear the infection naturally is associated with strong CD4 and CD8 T cell responses to spike, nucleocapsid and membrane proteins of the virus (Cao, 2020, Manjili et al., 2020, Tay et al., 2020, Thieme et al., 2020). T cell responses to SARS-CoV-2 and their role in protection against disease are reviewed in more depth in Chapters 6 & 7.

A quote from (Altmann D, ISCT conference): “immunology is impossible to comprehend; they invent a new cell type, factor or pathway every few days”. To date this has never been more apt as the study of SARS-CoV-2 immunology, particularly during initial phases of the pandemic when funding was paused and publishing was prioritised toCOVID-19 research. Many groups contributed to study the immunopathology of COVID-19, however often labs have a niche focus on a particular cell type, assay, model, technology or access to particular sample(s) which limits the ability to understand how all these observations fit together. Although it is difficult to create a full picture, there are numerous excellent reviews of SARS-CoV-2 immunology including (Brodin, 2021, Lamers and Haagmans, 2022, Tay et al., 2020, Yang et al., 2020, Zhu et al., 2023). The wealth of reports identifying different immune cell irregularities in COVID-19 was out of the scope of the current review, however a

general overview of consistently observed key immunological features of severe COVID-19 is summarised in **Figure 4.5**.

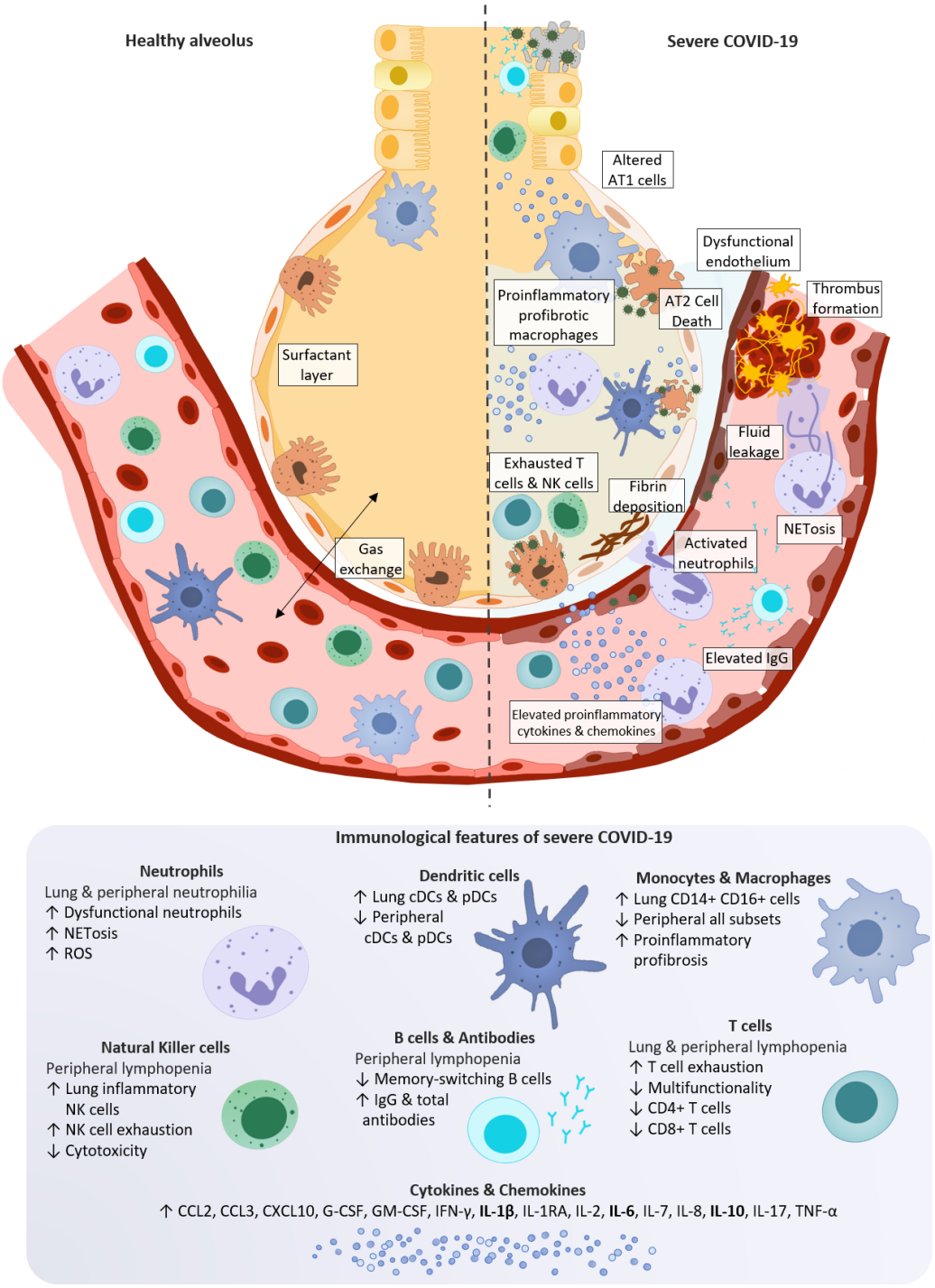

Figure 4.5 - Immunological features of severe COVID-19.

Severe COVID-19 pathogenesis in the lung and systemic immunological characteristics. Healthy alveoli are formed of pneumocytes: alveolar type 1 (AT1) cells which mediate gas exchange, alveolar type 2 (AT2) cells which produce surfactant. SARS-CoV-2 primarily infects AT2 cells causing AT2 cell death, with severe COVID-19 alveoli lacking protective surfactant layer. Viral damage of surrounding AT1 cells, fibroblasts and vascular endothelial cells induces a dysfunctional inflamed endothelium with gap formation and fluid leakage into the alveolus, impairing respiration and gas exchange. Infected cells secrete chemokines and cytokines which recruit innate immune cells such as neutrophils, macrophages, DC and platelets; which initiate type I interferon signalling and coagulation pathways. Deposition of fibrin forms hyaline membranes, and activated platelets

and neutrophils forming neutrophil extracellular traps (NETs) promotes further fibrosis and thrombosis formation. Inappropriate hyperinflammatory response of elevated lung and systemic cytokines is associated with innate and adaptive immune cell dysfunction. Immune irregularities of neutrophil, dendritic cell (DC), monocytes/macrophages, natural killer (NK) cells, B cells and antibodies, and T cell responses, as well as elevated inflammatory cytokines are consistently evidenced across reports in severe COVID-19. Adapted from (Lamers and Haagmans, 2022, Rovito et al., 2022, Schultze and Aschenbrenner, 2021, Yang et al., 2020).

Understanding of the dynamics between innate and adaptive immunity to SARS-CoV-2, and why it goes wrong in some individuals but not others is at present poorly understood, however numerous mechanisms have been associated from SARS-CoV-1 research. A mouse model of SARS-CoV-1 lethal infection showed Type 1 IFN signalling in the lungs within 6-24 hours post-infection was initiated by plasmacytoid DC and alveolar macrophages. This induced infiltration of inflammatory monocytes and macrophages that secreted high levels of IL-6, IL-1β, TNF-α and CCL2. At 6 days post infection, virus-specific T cells in the lungs had elevated expression of apoptosis markers which was rescued by neutralization of TNF-α indicating a direct or indirect mechanism by which TNF-α dampens the T cell response (Channappanavar et al., 2016). Interestingly this group and others demonstrated a delayed initiation of Type 1 IFN signalling caused inflammatory monocyte-macrophage accumulation, elevated proinflammatory cytokine levels, impaired T cell responses and resultant severe disease. Early Type 1 IFN signalling at 6-12 hours post-infection (prior to peak virus titres) had a protective effect in preventing lung immunopathology and mortality, indicating delayed expression of Type-1 IFN induces an inappropriate excessive inflammatory response (Haagmans et al., 2004, Kumaki et al., 2011, Channappanavar et al., 2016). Correspondingly, SARS-CoV-2 patients with critical disease have consistently been found to have significantly elevated levels of CCL2, IL-6, IL-10, and TNF-α which inversely correlated with low CD4 and CD8 counts (Chen et al., 2020, Diao et al., 2020, Hadjadj et al., 2020, Huang et al., 2020a, Lucas et al., 2020, Ronit et al., 2021), which again may suggest these pro-inflammatory cytokines promote T cell apoptosis thereby dampening the adaptive immune response. Elucidation of causative mechanisms in immune failure rather than effect or associations will be crucial to identifying targets for therapeutic intervention. With our current understanding of the science, the key areas for therapy targeting viral damage to prevent host hyperinflammatory intrinsic disease progression include: viral entry and replication, initiation of interferon signalling and lymphocyte dysfunction.

4.1.8 Chapter Aims

At the time of undertaking this study (April to June 2020), with no vaccines or treatments yet available there was clear clinical need for effective treatments for high risk COVID-19 patients. With accumulating literature demonstrating a dysregulated T cell response in severe COVID-19 patients, and protective SARS-CoV-2 T cell memory associated with efficient viral clearance, it was hypothesised that adoptive transfer of healthy donor virus-specific T cell (VST) immunity may be an effective treatment approach.

Adoptive transfer of VST has been used since the early 1990s to treat chronic refractory viral infections or reactivations in immunocompromised patients (Houghtelin & Bollard, 2017), and at SNBTS, we have proven clinical efficacy and safety data from treatment of over 200 patients with allogeneic HLA-matched Epstein-Barr VST in cases of refractory EBV-driven lymphoma post-transplant (Haque et al, 2007; Kazi et al, 2019). Just prior to the pandemic, we had completed development of a new platform to isolate EBV VST using Cytokine Capture Selection (CCS), with an optimised post-expansion protocol as outlined in Chapter 3. Since this process detects and isolates antigen-specific T cells on the basis of response to stimulation with peptides, it can be theoretically translated to investigate T cell responses to any antigen of choice. During the first wave of the pandemic, SNBTS was recruiting COVID-19 convalescent individuals to donate plasma as part of the national Convalescent Plasma (CP) programme to investigate CP as a potential therapeutic for COVID-19. As part of this process, we were also able to consent and recruit a cohort of COVID-19 convalescent donors to donate peripheral blood leukocytes from buffy coats to investigate the SARS-CoV-2 antigen specific T cell responses. The opportunity to study peripheral blood donated from individuals who were able to naturally clear their infection allows for the characterisation of T cells involved in protective immunity. To study antigen-specific responses we had access to peptide pools covering the SARS-CoV-2 spike, nucleocapsid and membrane proteins that were rapidly manufactured in early 2020 by Miltenyi Biotec. Since at this stage we did not know the exact pathogen classification of SARS-CoV-2 and potential for transmission by blood cells, all work was carried out within a derogated category III laboratory, with all handling of cells including flow cytometry labelling carried out within a Class II microbial safety cabinet, acquired on a quarantined flow cytometer. At collection,

samples were also sent to the National Microbiology Reference Unit within SNBTS for EuroImmun IgG testing which allowed us to compare SARS-CoV-2 T cell responses to antibody levels. In addition, peripheral blood cells from each donor were cryopreserved on day of collection for retrospective HLA typing by the SNBTS Histocompabitility and Immunogenetics (H&I) team. This study was testament to a huge collaborative effort between SNBTS departments to provide all supporting data to the T cell findings, and donor services teams who coordinated blood collections during these risky times. Particular recognition is made to the SNBTS clinical lead Dr Sharon Zahra who recruited, consented the donors and provided the relevant and appropriate details from their clinical records; as well as the principal study leads Professor John Campbell and Dr Alasdair Fraser who quickly conceptualised and secured approval/ funding for the research study.

The aim of this chapter was to analyse the peripheral blood cell compartments of COVID-19 convalescent donors in comparison to uninfected donor controls and investigate the detection of SARS-CoV-2 antigen-specific T cells using an intracellular cytokine flow cytometry assay. Furthermore, we wanted to determine if SARS-CoV-2-specific T cells could be isolated by cytokine capture selection and subsequently expanded in culture in order to develop a potential T cell therapy for COVID-19.

4.2 Detection of SARS-CoV-2 VST

To investigate the immune responses in individuals who naturally recovered from infection with the first wave SARS-CoV-2 wild type strain, we obtained peripheral blood buffy coats collected from COVID-19 convalescent donors (CCD, n=15) within the local Scottish population between April to June 2020. Donors were 23 to 58 years old (median 49 years) and evenly split by sex (7 female, 8 male). Diagnosis and resolution of infection were confirmed by SARS-CoV-2 PCR, with donations collected between 34 and 56 days after resolution of symptoms (see **Table 4.2** for infection details). In all cases, donors exhibited mild symptoms of COVID-19 infection and did not require hospital treatment. Uninfected donors (UD, n=17) with no evidence of COVID-19 symptoms or positive PCR testing during this period were used as comparison controls.

4.2.1 Differences in immune subsets after COVID convalescence

In the early months following SARS-CoV-2 outbreak, initial studies from Wuhan patient cohorts reported distinct changes in circulating immune cell subsets between healthy donors and patients with progressive disease. In particular, lymphopenia and reduced frequencies and overall number of CD4 T cells, CD8 T cells and NK cells in peripheral blood were consistently associated with severe COVID-19 in numerous studies (Chen et al., 2020, Zheng et al., 2020b, Qin et al., 2020, García, 2020).

As there were fewer reports of immune subsets in asymptomatic or mild disease convalescent donors during that time, we phenotyped PBMC from CCD in comparison to UD to determine any differences in lymphocyte populations. PBMC were isolated from buffy coats using standard Ficoll gradient centrifugation and immediately analysed using the lymphocyte and lineage flow cytometric panels outlined in **Figure 2.3** and **Figure 2.4**. Gating on all cells, singlets and viable cells sequentially, the mean percentage of monocytes, NKT cells and T cells were similar between CCD and UD **(Figure 4.6).** The mean percentage of T cells with an activated phenotype (HLA-DR+/CD38+), reported as elevated in other studies with moderate to severe disease, were not found to be significantly different between UD and CCD in this cohort of donors. NK cell frequencies were significantly elevated ($p = 0.0073$) in CCD compared to UD, and the mean percentage of B cells in CCD was significantly lower than in UD ($p=0.0003$).

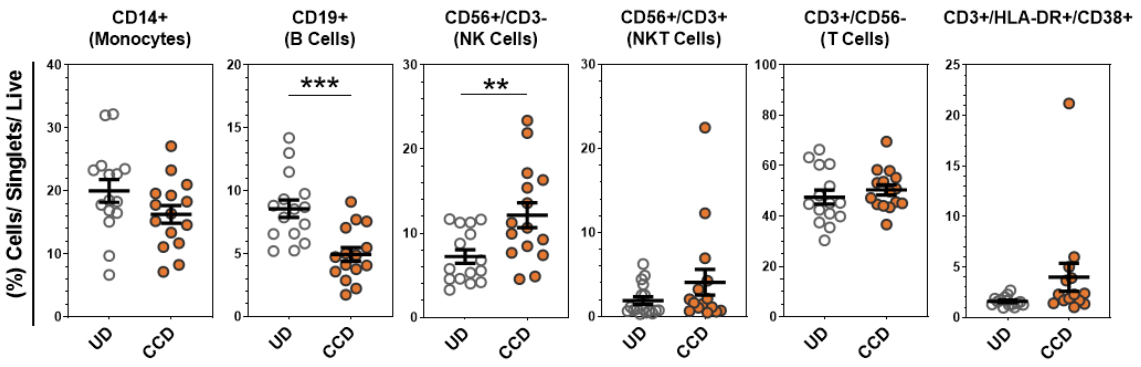

Figure 4.6 - Analysis of leukocyte subsets in CCD PBMCs.

Buffy coat-derived PBMCs from COVID-19 convalescent donors (CCD, n=15) and uninfected donors (UD, n=17) were assessed for leukocyte subsets by flow cytometry. Data is represented as mean ± SEM. Statistical analysis to compare CCD and UD groups was done by unpaired t-tests with Holm-Sidak correction for multiple comparisons where $p<0.05$ was considered statistically significant. **$p \leq 0.01$ and ***$p \leq 0.001$.

To investigate the distinct B cell and NK cell frequencies in CCD PBMC, correlations were tested with potentially linked donor parameters **(Figure 4.7)**. In this study, age did not correlate with **(A)** NK cell or **(B)** B cell levels in CCD, though a significant correlation (Pearson correlation p=0.04, r=0.524) was identified between percentage of **(C)** B cells and SARS-CoV-2 antibody content.

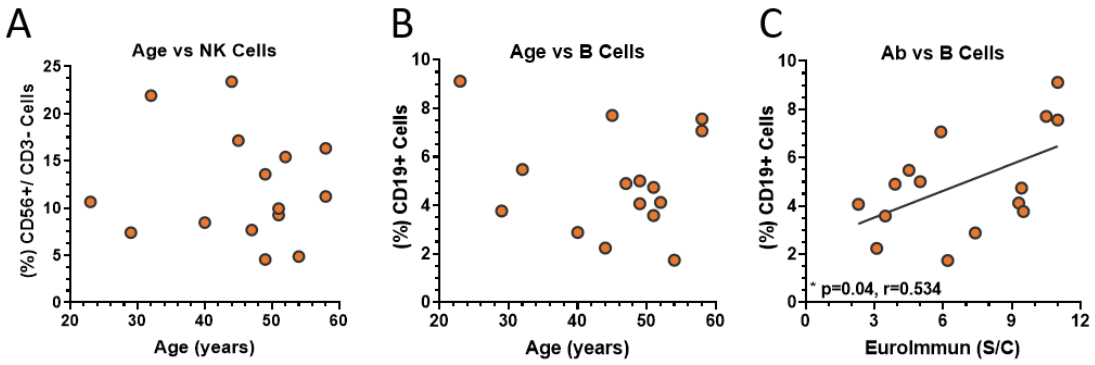

Figure 4.7 – CCD PBMC NK cell and B cell correlations.

Pearson correlation tests of CCD parameters were used to investigate the relation between **(A)** percentage NK cells (CD56+/CD3-) and donor age, **(B)** percentage B cells (CD19+) and donor age, and **(C)** percentage B cells (CD19+) and SARS-CoV-2 serum antibody content (EuroImmun S/C). Statistical analysis was done by generating Pearson correlation coefficients, where $p<0.05$ was considered significant.

Within the T cell compartment **(Figure 4.8)** the percentage of CD4+ and CD8+ T cells, as well as DN and DP T cells remained unchanged between CCD and UD (**A**). In addition, analysis of co-expression of T cell memory markers CD62L, CD45RO, and CD45RA revealed no difference in CD4 and CD8 memory subpopulations between UD and CCD for either CD4+ T cells (**B**) or CD8+ T cells (**C**).

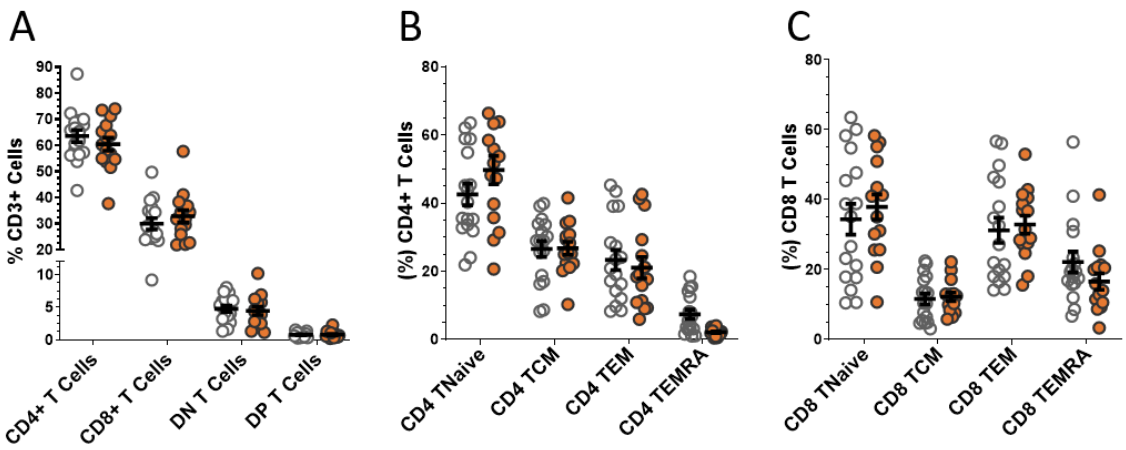

Figure 4.8 - Analysis of T cell subpopulations in CCD PBMCs.

Buffy coat-derived PBMC from CCD (n=15) and UD (n=17) as above were analysed for **(A)** basic T cell subsets, and T cell memory subpopulations further quantified for **(B)** CD4+ T cells and **(C)** CD8+ T cells. Data is represented as mean ± SEM. Significance was determined by unpaired t-test with Holm-Sidak correction for multiple comparisons. DN double negative (CD4−/CD8−), DP double positive (CD4+/CD8+), TNaive (CD62L+/CD45RA+/CD45RO−), TCM central memory (CD62L+/CD45RA−/CD45RO+), TEM effector memory (CD62L−/CD45RA−/CD45RO+), TEMRA terminal effector memory CD45RA revertant (CD62L−/CD45RA+/CD45RO−).

4.2.2 Optimisation of cytokine assay to detect SARS-CoV-2 responses

As outlined previously (**section 2.7.1**), an intracellular cytokine flow cytometric assay was developed to detect EBV VST in donor peripheral blood by stimulation with EBV consensus peptide pools. Research-grade SARS-CoV-2 individual peptide pools combining spike, nucleocapsid and membrane proteins became available by April 2020, allowing testing of these peptides to detect antigen-specific responses within donor peripheral blood. Since these peptide pools covered sequences of hydrophobic regions that are relatively insoluble (as outlined in **section 2.3.2**), reconstitution of the lyophilised peptides in DMSO was recommended with subsequent dilution in water. Initial correspondence from the peptide supplier indicated sterile 0.2µm filters may get blocked when filtering if reconstituted peptides are not completely dissolved. Since sterile filtration is required for downstream isolation of SARS-CoV-2 VST, intra-donor comparative stimulation assays were set up to test the effect of filtration on VST cytokine responses. Additionally, since CCD buffy coats were generally released by SNBTS Blood Dispatch in the early afternoon, the 5-hour peptide stimulation with subsequent surface and intracellular staining protocol developed for EBV VST was practically and logistically challenging. Therefore initial experiments also tested peptide stimulation for 5 hours versus 16 hours as suggested as the window for cytokine secretion for VST (Campbell, 2003). To test these parameters, PBMC freshly

isolated from each donor buffy coat (n=3) were plated in medium at $5x10^6$ WBC/mL/well of a 24-well plate ($2.5x10^6$ WBC/cm^2) in the conditions as shown in **Figure 4.9A**.

Following stimulations, wells were harvested and stained with the intracellular cytokine flow cytometry panel as outlined in **Table 2.8**. For analysis, viable CD3+ cells were gated and assessed for expression of IFN-γ (frequency was calculated by normalising to the negative control). Unfiltered peptides (clear circles) and filtered peptides (black diamonds) were comparable in % CD3+/IFN-γ+ PBMC for each individual peptide and the pooled peptides together (**Figure 4.9B**), indicating sterile filtration did not block passage of peptide pools through the filter. No significant difference in the frequency of CD3+/IFN-γ+ PBMC was observed between 5-hour (black square) and 16-hour (clear triangle) peptide stimulations (**Figure 4.9C**), demonstrating antigen-specific T cells could be detected at both these time-points. Therefore for subsequent CCD PBMC screening assays, peptides were sterile filtered prior to use and cells were stimulated for 16 hours with peptides to allow an overnight incubation. This was advantageous in that buffy coats could be pre-screened for a minimum SARS-CoV-2 VST detection level (≥0.08% CD3+/IFN-γ+ PBMCs responsive to S+N+M stimulation) prior to potential isolation of SARS-CoV-2 VSTs by cytokine capture selection. Additionally, since both intracellular cytokine and cytokine capture selection assay require a minimal 5-hour stimulation followed by 2-3 hour labelling protocols, the two cannot easily be done in tandem by one operator. Therefore the finalised workstream for a CCD buffy coat was basic phenotyping, CD14+ monocyte isolation (for downstream analysis), peptide screening plate set up, and CCS plate set up on day 0. Peptides could then be added to the screening plate at the end of day 0 for an overnight 16-hour incubation, with intracellular staining and flow analysis the following morning (day 1). During this time, the CCS plate was stimulated with peptides for 5 hours, and a go/ no go point prior to the CCS labelling and selection dependent on VST detection (**Figure 4.10**).

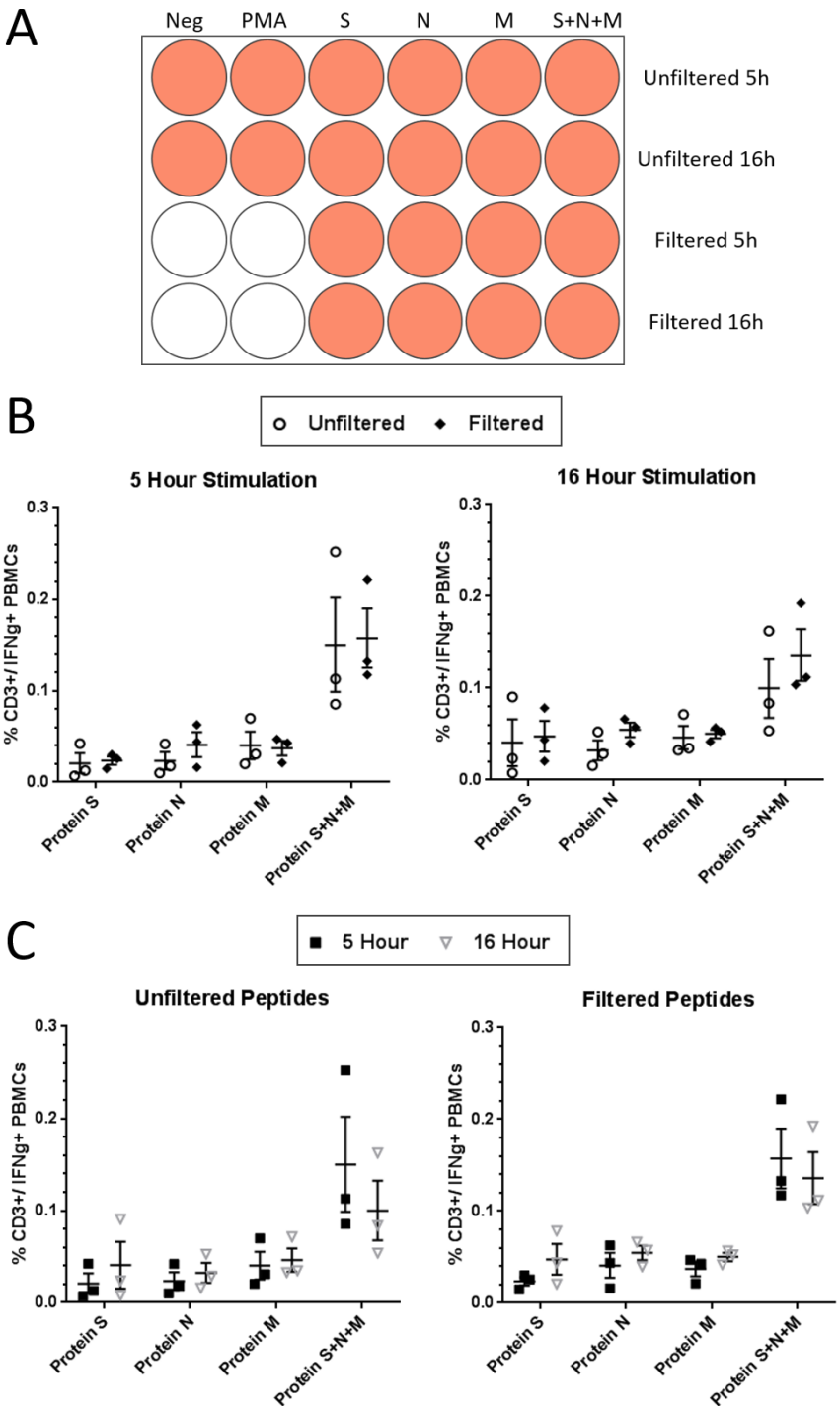

Figure 4.9 - SARS-CoV-2 peptide optimisation for VST detection.

SARS-CoV-2 peptide pools covering sequences for individual proteins spike (S), nucleocapsid (N), membrane (M), and the three pooled together (S+N+M) were used to stimulate PBMC from CCD buffy coats for detection of antigen-specific T cell responses. **(A)** PBMCs from each donor (n=3) were plated to test the following conditions: unfiltered peptides for 5 hour stimulation; unfiltered peptides for 16 hour stimulation; filtered peptides for 5 hour stimulation; and filtered peptides for 16 hours stimulation. Negative and positive controls (DMSO/water and PMA/ionomycin, respectively) were included for both 5 and 16 hour stimulation (however these do not require filtration). **(B)** No significant differences in percentage CD3+/IFN-γ+ PBMC were seen between unfiltered or filtered peptide pools. **(C)** No significant differences in percentage CD3+/IFN-γ+ PBMC were seen following 5 hour versus 16 hour peptide stimulations. Data is represented as mean ± SEM. Statistical analysis was performed using paired t-tests using the Holm-Šídák method for multiple comparisons where $p<0.05$ was considered statistically significant.

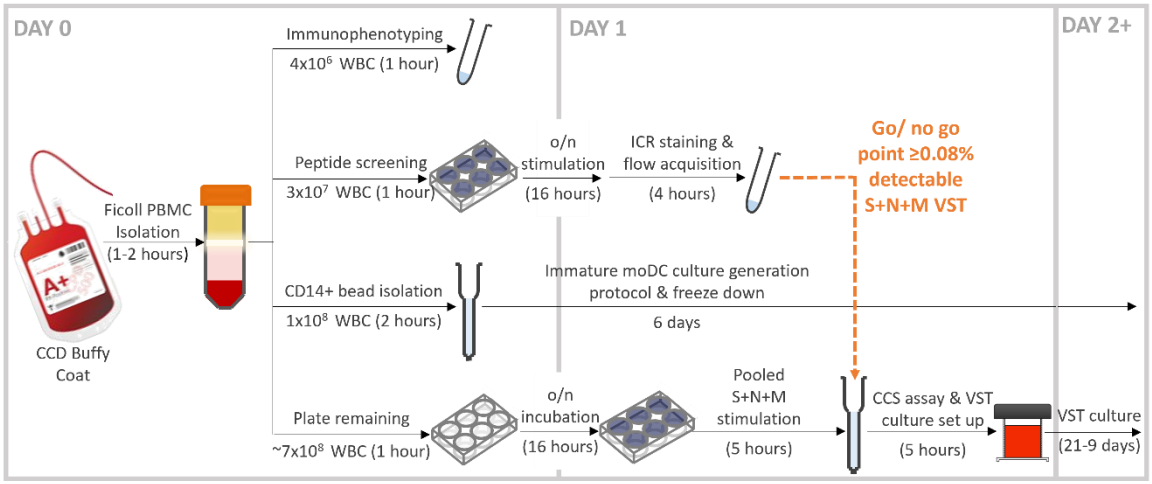

Figure 4.10 - CCD buffy coat experimental workstream.

Upon arrival of CCD buffy coats, PBMCs were isolated and divided up for immunophenotyping, peptide screening plate setup, CD14+ monocyte bead isolation and CCS plate set up on day 0. SARS-CoV-2 were added to the peptide screening plate at end of day for an overnight 16 hour stimulation, with subsequent intracellular staining and sample acquisition the following morning. Also on the morning of day 1, the CCS plate was stimulated with S+N+M peptides for 5 hours. If VST were detectable (≥0.08%) in screening assay, CCS assay & culture set up could proceed.

All CD14+ cell isolation, DC culture, freezing and DC phenotyping was performed by Dr Paul Burgoyne at SNBTS.

4.2.3 SARS-CoV-2 VST are detectable in CCD PBMC population

Using the optimised peptide stimulation and ICR staining protocol (**4.2.2**), PBMC from both CCD (n=15) and UD (n=17) buffy coats were screened for SARS-CoV-2 peptide responses. To this end, PBMC were stimulated with individual antigen peptide pools (spike, nucleocapsid or membrane) as well as the three pools combined (S+N+M). Following stimulation, cells were labelled with T cell and NK cell surface markers (CD3, CD4, CD8, CD56); intracellular cytokines (IFN-γ, TNF-α, IL-2) and activation markers (CD137, CD154) by multi-parameter flow cytometry. Representative flow analysis for exemplar UD and CCD stimulated with combined peptide pools, with gating applied from a negative control, showing the main markers with detectable responses (IFN-γ, TNF-α and CD154) is presented in **Figure 4.11A**. The frequency of SARS-CoV-2 VSTs in CCD calculated as CD3+/IFN-γ+ PBMCs positively correlated (Pearson correlation p=0.0381, r=0.5391) with SARS-CoV-2 antibody level (**Figure 4.11B**). Interestingly, the percentage of SARS-CoV-2 VST in CCD was found to decline significantly over time (Pearson correlation p=0.0021, r=0.6275) (**Figure 4.11C**). The mean percentage of CD3+/IFN-γ+ cells, CD3+/TNF-α+ cells and CD4+/CD154+ cells was higher in CCD compared to UD for stimulation with each individual peptide pool and for the combined peptide pools (**Figure 4.11D**).

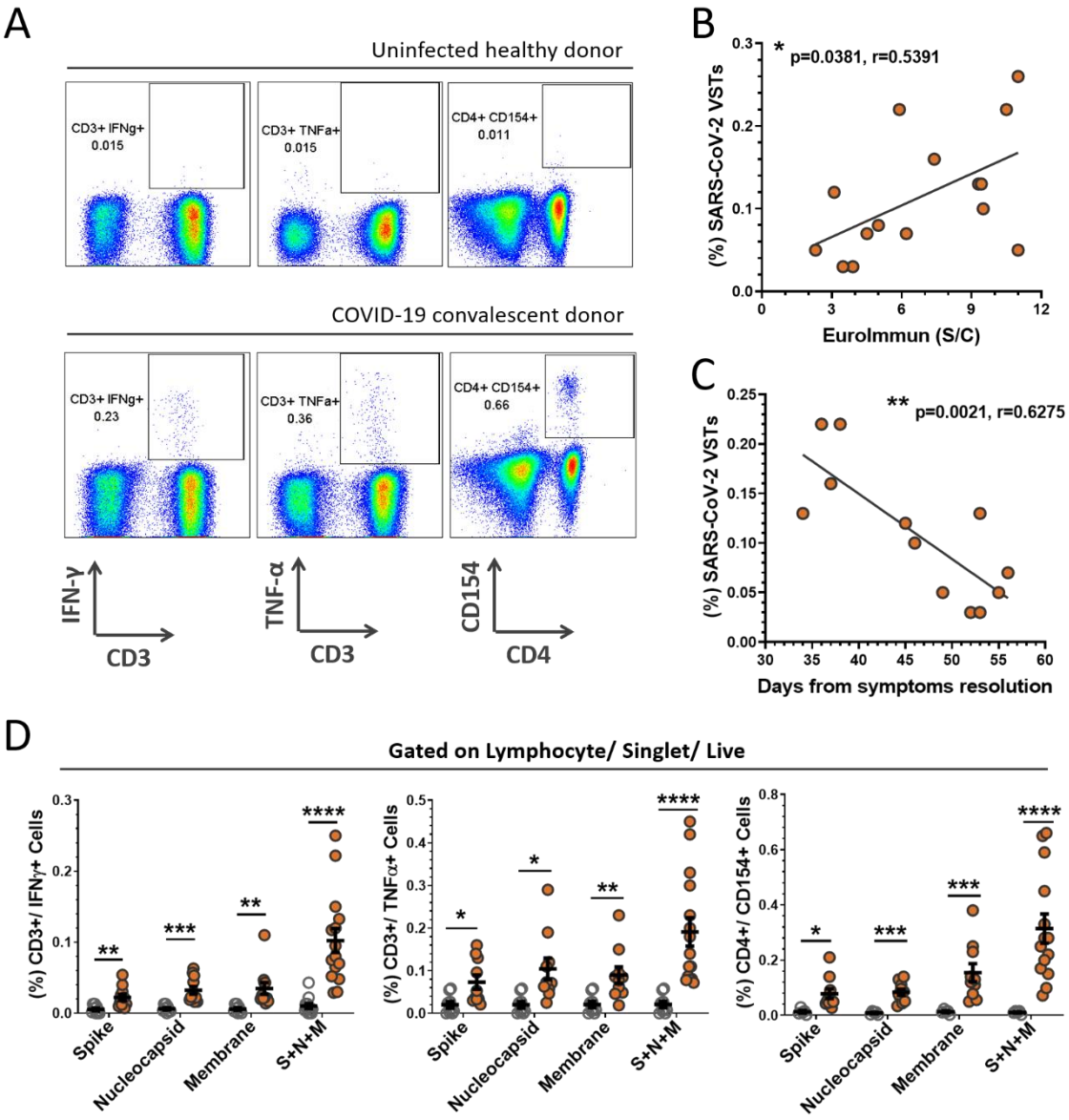

Figure 4.11 - PBMC responses to SARS-CoV-2 peptides.

PBMCs derived from buffy coats were incubated with SARS-CoV-2 peptides (Spike + Nucleocapsid + Membrane) for 5 hours and corrected against a no antigen control well for induced expression of cytokines and activation markers. **(A)** Representation of flow cytometric analysis from a healthy uninfected donor (UD, clear circles) and COVID-19 convalescent donor (CCD), note all flow analyses were gated on lymphocytes/ singlets / live cells and subsequently quantified for percentage CD3+/IFN-γ+ cells, CD3+/TNF-α+ cells and CD4+/CD154+ cells (see **Figure 2.8** for gating strategy). The percentage of SARS-CoV-2 VSTs in the CCD PBMC population (i.e. CD3+/IFN-γ+ cells reactive to pooled S+N+M peptides) significantly correlated with **(B)** antibody titre at donation (p=0.0381, r=0.5391) and **(C)** days from resolution of symptoms to donation (p=0.0021, r=0.6275). Calculation was performed using Pearson correlation coefficient. EuroImmun serum content assay for SARS-CoV-2 antibody titre was performed by SNBTS NMRU. **(D)** Mean percentages of CD3+/IFN-γ+ cells, CD3+/TNF-α+ cells and CD4+/CD154+ cells for individual and pooled peptides compared between HD (n=17, clear circles) and CCD (n=15, orange circles). Data is represented as mean ± SEM. Statistical significance was determined using unpaired t-tests corrected for multiple comparisons using the Holm-Šídák method where *p≤0.05, **p≤0.01, ***p≤0.001 and ****p≤0.0001.

Donor information including blood group, HLA type, days from COVID-19 symptoms onset to resolution, days from symptoms resolution to donation, SARS-CoV-2 antibody level, and the percentage of SARS-CoV-2 VST detected using the intracellular cytokine pre-screen assay is collated in **Table 4.2**.

Donor Code	Blood Group	HLA Type						Days from symptoms onset to resolution	Days from symptoms resolution to donation	Antibody level	% SARS-CoV-2 VST
		Ax	Ay	Bx	By	DRB1x	DRB1y				
C19BC1	O pos	31:01	32:01	35:01	51:01	01:01	13:01	8	38	10.5	0.22
C19BC2	O pos	01:01	68:01	51:01	57:01	07:01	14:01	10	36	5.9	0.22
C19BC3	A pos	*						-	34	9.3	0.13
C19BC4	O pos	03:01	26:01	07:02	38:01	15:01	16:01	13	45	3.1	0.12
C19BC5	O pos	03:01	32:01	07:02	27:03	08:01	13:01	14	52	3.9	0.03
C19BC6	A neg	01:01	01:01	08:01	08:01	03:01	07:01	14	55	2.3	0.05
C19BC7	O pos	*						14	56	6.2	0.07
C19BC8	B pos	02:01	11:01	07:02	56:01	01:01	08:01	10	46	9.5	0.10
C19BC9	O neg	02:01	11:01	18:01	44:02	01:01	15:01	18	37	7.4	0.16
C19BC10	O pos	**						-	-	11	0.05
C19BC11	B neg	01:01	26:01	08:01	44:02	03:01	04:01	7	49	11	0.26
C19BC12	A pos	02:01	24:02	35:01	44:02	04:01	04:04	7	53	9.42	0.13
C19BC13	O pos	*						-	-	5	0.08
C19BC14	O pos	02:01	02:01	NT	NT	04:04	15:01	-	-	4.51	0.07
C19BC15	O neg	03:01	29:02	44:03	57:01	07:01	15:01	13	53	3.48	0.03

Table 4.2 - Baseline characteristics and immune response of CCD.

Donor information for the COVID-19 convalescent donors (CCD, n=15) investigated in this study includes: blood group, HLA type, number of days from COVID-19 symptoms onset to resolution of symptoms, number of days from symptoms resolution to buffy coat donation, SARS-CoV-2 antibody level, and percentage SARS-CoV-2 VST detected in pre-screen assay. Antibody level refers to Euroimmun assay values (>1.1 = positive). Percentage SARS-CoV-2 VST refers to the percentage CD3+/IFN-γ+ cells responding to combined S+N+M peptides.
* Not consented for HLA typing.
** No sample taken for HLA typing.
NT: Not tested as insufficient DNA to type locus.
All clinical donor information (blood group, symptoms, dates of infection, resolution) was collected by SNBTS lead clinician Dr Sharon Zahra.
Following cDNA preparation from isolated PBMCs, HLA-genotyping was performed by SNBTS H&I laboratory for HLA-A, B and DRB1 loci using Lifecodes HLA eRES SSO Typing kits (Immucor Inc).
EuroImmun serum content assay for SARS-CoV-2 antibody titre was done by SNBTS NMRU.

CCD T cell IFN-γ, TNF-α and CD154 responses to individual peptide pools (n=10) were compared using RM one-way ANOVA to determine whether there was a preferential response to particular SARS-CoV-2 antigens. While the mean percentage of CD3+/IFN-γ+ cells and CD3+/TNF-α+ cells was comparable between the three peptide pools, the CD4+/CD154+ response was significantly higher (p=0.042) to membrane peptides than to nucleocapsid peptides. Altogether, these data indicate there was no consistent preferential T cell cytokine response to one particular SARS-CoV-2 antigen (**Figure 4.12**).

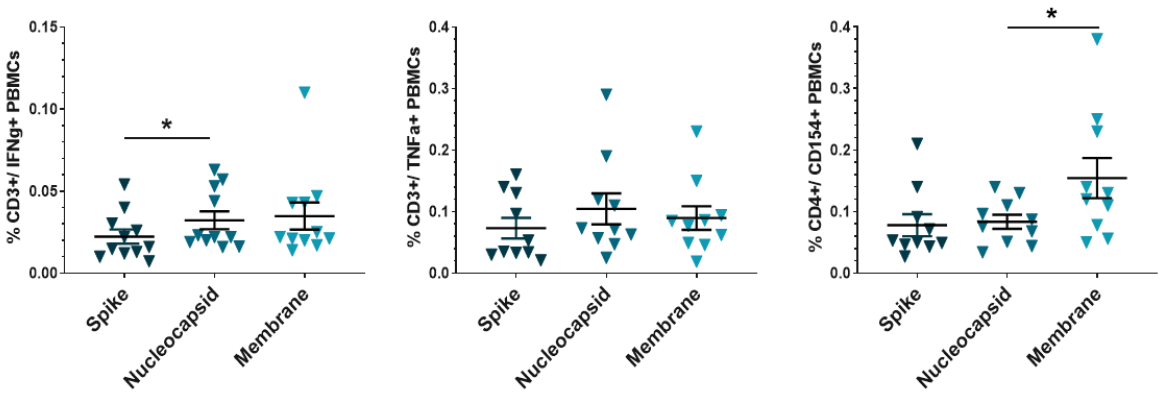

Figure 4.12 - SARS-CoV-2 individual antigen response comparison.

Mean percentages of CD3+/IFN-γ+ cells, CD3+/TNF-α+ cells and CD4+/CD154+ cells were compared for response to individual peptide pools: spike, nucleocapsid and membrane in CCD (n=10). Data is represented as mean ± SEM. Comparisons between the three antigens were made using RM one-way ANOVA with Geisser-Greenhouse correction where *p≤0.05, **p≤0.01, p≤0.001 and **** p≤ 0.0001.

Further dissection of the CCD cytokine response to SARS-CoV-2 peptide pools by gating on the Th, CTL and NK cell lymphocyte subsets indicates the IFN-γ response is primarily by CD4+ T cells (**Figure 4.13A**). The mean percentage of CD4+/IFN-γ+ PBMC was significantly higher than either CD8+/IFN-γ+ or CD56+/IFN-γ+ cells for each individual peptide pool and combined peptide pools. The percentage of CD8+/IFN-γ+ cells was significantly increased over CD56+/IFN-γ+ cells. Conversely the TNF-α response to pooled peptides demonstrated significantly higher CD56+/TNF-α+ cells than CD8+/TNF-α+ cells (**Figure 4.13B**).

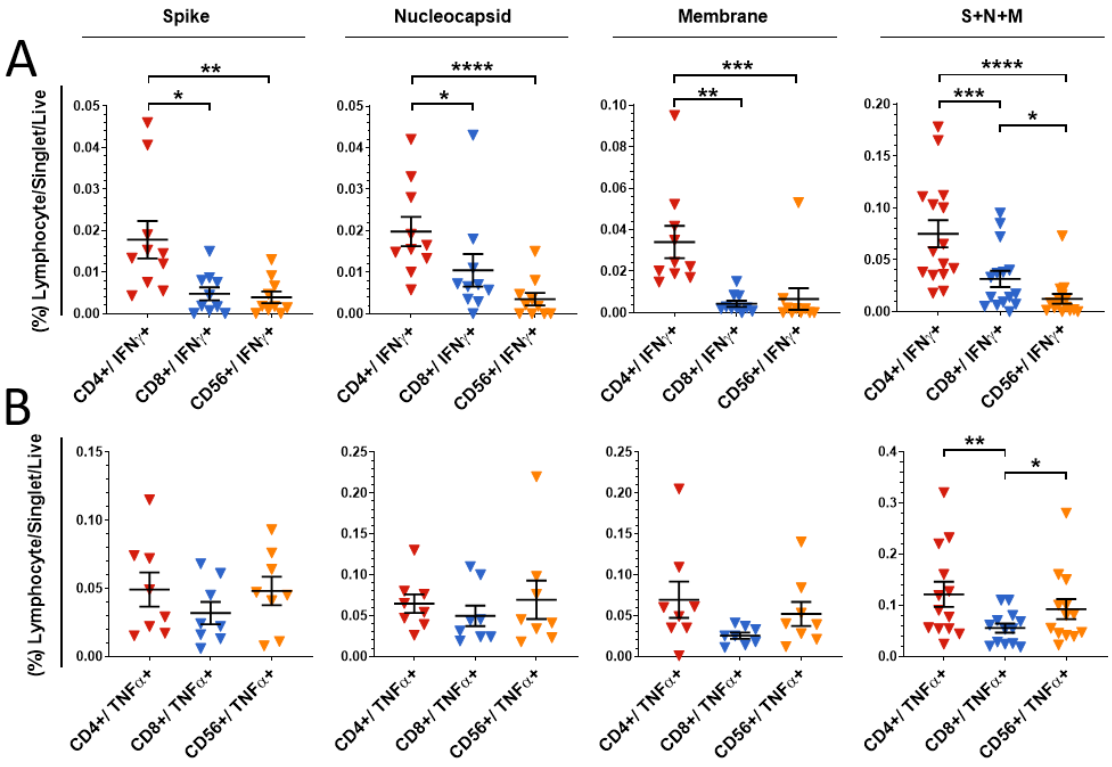

Figure 4.13 - Th, CTL and NK cell responses to SARS-CoV-2 peptides.

Gated lymphocyte subsets within CCD PBMC population were compared for Thelper cells (CD3+/CD4+, red triangles), cytotoxic T cells (CD3+/CD8+, blue triangles) and NK cells (CD56+/CD3-, orange triangles) responsive to SARS-CoV-2 peptide stimulation. Each subset is compared for **(A)** IFN-γ response and **(B)** TNF-α response. Data is represented as mean ± SEM. All significance was determined using RM one-way ANOVA with Geisser-Greenhouse correction where *p≤0.05, **p≤0.01, ***p≤0.001 and **** p≤ 0.0001.

TNF-α+ cell frequencies here are generally higher for all three lymphocyte subsets, which may indicate TNF-α is a more important cytokine for antiviral responses to SARS-CoV-2, and therefore intracellular TNF-α secretion may be able to detect and isolate more SARS-CoV-2 VST. This is discussed further in Chapter 5.

4.3 Isolation of SARS-CoV-2 VST

4.3.1 Isolation of SARS-CoV-2 VST by IFN-γ capture selection

Since peptide-responsive SARS-CoV-2 VST were detectable by intracellular IFN-γ secretion, it was next determined whether SARS-CoV-2 VST could be successfully isolated by IFN-γ capture selection. To this end, PBMC were plated overnight and stimulated the following morning for 5 hours with pooled S+N+M peptides. The IFN-γ CCS assay was performed as according to the manufacturer's protocol, with subsequent non-target and isolated IFN-γ+ target fractions collected and analysed. The total number of VST within the IFN-γ+ target fraction was determined from CD3+

cell counts on MACSQuant10 analyser, with a mean=8.2x10^5 ± 2x10^5 SEM (**Figure 4.14A**). No significant correlation between the total number of CD3+ cells in IFN-γ+ target fraction versus the same donor's pre-screen % CD3+/IFN-γ+ PBMC reactive to SNM peptides was seen, indicating the pre-screen detection assay is not entirely quantitative of CCS VST isolation yield (**Figure 4.14B**).

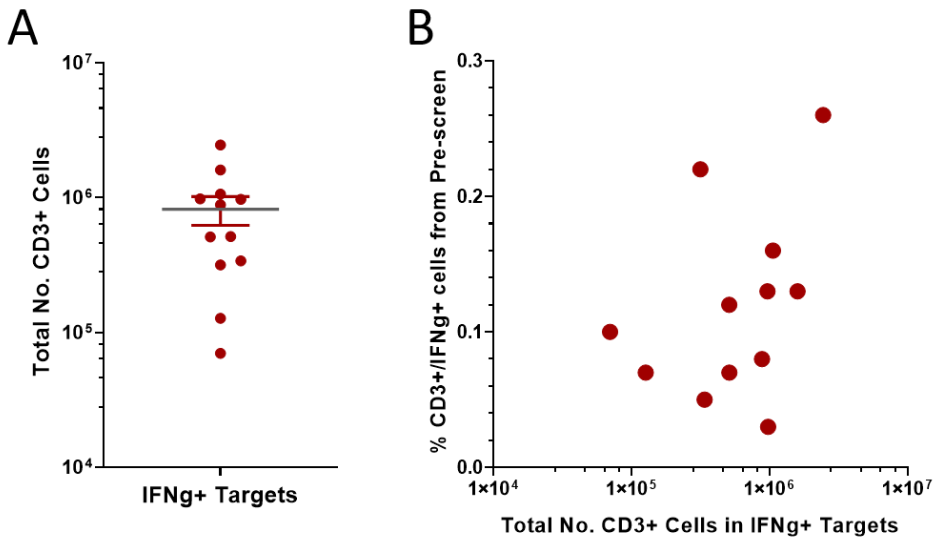

Figure 4.14 - Isolated SARS-CoV-2 VST counts.

SARS-CoV-2 VST reactive to pooled S+N+M peptides were isolated from CCD (n=12) using IFN-γ CCS assay. **(A)** Isolated IFN-γ+ target cells from CCS assay were counted for total number of CD3+ cells using MACSQuant10 analyser. **(B)** No significant correlation was observed between total number of CD3+ cells in the CCS-isolated IFN-γ+ target fraction, versus the % CD3+/IFN-γ+ PBMC from intracellular cytokine screening assay. Data is represented as mean ± SEM. Statistical analysis was performed by generating Pearson correlation coefficients, where $p<0.05$ was considered significant.

4.3.2 Isolated SARS-CoV-2 VST have effector T helper phenotype

Immediate surface phenotyping of a small portion of the positive fraction (IFN-γ+ target cells) following CCS isolation (**Figure 4.15**) revealed this fraction contained an equal ratio of monocytes to T cells (40.45 ± 2.1% and 37.11 ± 3.95% of total cells, respectively). There is also potential for NK cells to be selected on the basis of IFN-γ secretory response, however negligible NK cells (2.25 ± 0.71%) or NKT cells (0.26 ± 0.09%) were isolated in response to the SARS-CoV-2 peptides. CD3+ T cells in the isolated fraction were a mix of CD4+ (53.02 ± 3.94%) and CD8+ (35.73 ± 3.23%) cells; where CD4+ T cells were predominantly effector memory (86.52 ± 3.44%) and CD8+ T cells showing a more differentiated phenotype at 42.1 ± 3.44% effector memory and 41.89 ± 4.2% terminal effector memory RA.

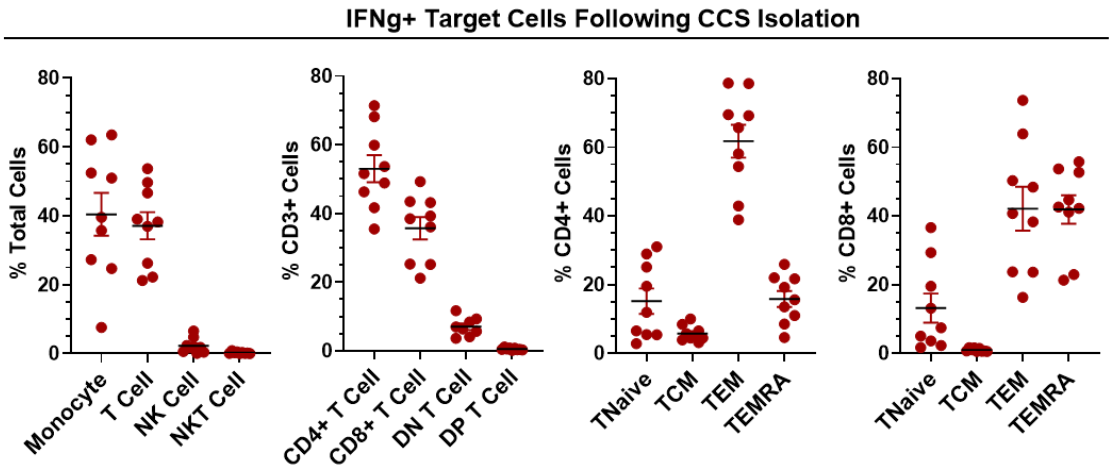

Figure 4.15 - Isolated SARS-CoV-2 VST phenotype.

IFN-γ+ target fractions following CCS isolation were immunophenotyped for frequency of the following populations: monocytes (CD14+);T cells (CD3+/CD56-); NK cells (CD56+/CD3+); NKT cells (CD3+/CD56+); CD4+ T cells (CD3+/CD4+); CD8+ T cells (CD3+/CD8+); DN T cells (CD3+/CD4-/CD8), DP T cells (CD3+/CD4+/CD8+); TNaive (CD62L+/CD45RA+/CD45RO−); TCM central memory (CD62L+/CD45RA−/CD45RO+); TEM effector memory (CD62L−/CD45RA−/CD45RO+); and TEMRA terminal effector memory CD45RA revertant (CD62L−/CD45RA+/CD45RO−). Data is represented as mean ± SEM.

4.4 Expansion of SARS-CoV-2 VST for adoptive cell therapy

Cytokine capture selection was effective in the enrichment of SARS-CoV-2 VST particularly of CD4+ effector memory T cells as demonstrated in section **4.2**. Isolation of VST by CCS for therapeutic use is often a direct autologous or allogeneic CCS isolation with infusion of freshly isolated IFN-γ+ target cells into the patient. This strategy is beneficial in that the process duration is only 1-2 days, and cells are not cryopreserved with the subsequent caveat of cell death/ loss at product thawing. Importantly, since cells are not cultured or manipulated, this cell product would fall under Human Tissue Authority licensure making such a product simpler for clinical regulatory approval. Without cryopreservation however, any product characterisation and safety testing (enumeration, purity, phenotype, sterility, etc) must be performed rapidly to allow minimal hold time prior to patient infusion. A major drawback of this approach is the very low yield of VST from a CCS process, as confirmed in **Figure 4.14**, the mean number of SARS-CoV-2 VST following isolation was $8.2x10^5$ cells (n=12). As a consequence, a single clinical CCS VST process could only be given to one patient, and as such the cost to patient treatment ratio is not economically feasible in most situations. Therefore, following the successful development of a post-isolation culture expansion process for EBV VST (see Chapter

3), it was hypothesised isolated SARS-CoV-2 VST could also be expanded in culture to clinically relevant numbers.

4.4.1 SARS-CoV-2 VST culture requires protein supplementation

Initial attempts to expand SARS-CoV-2 VST in culture followed the protocol validated for EBV VST expansion – whereby CCS non-target cells were irradiated at 40 Gy and co-cultured with the isolated SARS-CoV-2 VST target cells in G-Rex flasks in TexMACS medium supplemented with IL-2 [200 IU/mL]. At day 7 of culture, cells were given a complete medium change and returned to culture. A substantial aggregation of dead cell/debris (which is not seen in EBV VST culture) was visually observed during these medium changes, and flow cytometry analysis confirmed a large accumulation of dead cells/debris by forward and side scatter properties (**Figure 4.16A**). Total cell counts over the culture duration (**Figure 4.16B**) indicated very poor culture expansion, with donors C19BC2 and C19BC4 crashing completely by days 21 and 15 respectively.

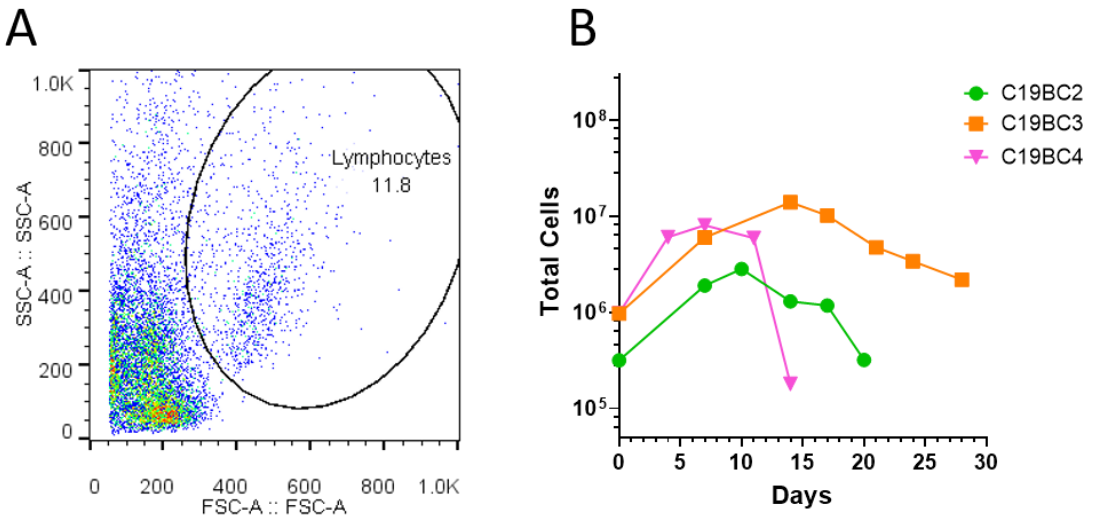

Figure 4.16 - Initial cultures without protein supplementation.

Initial SARS-CoV-2 VST cultures (n=3) were set up in TexMACS medium supplemented with IL-2 only as per protocol for EBV VST expansion. **(A)** Representative flow analysis for C19BC2 at day 7 of culture period demonstrated a poor outgrowth of expanding VST (lymphocytes gate) and accumulation of dead cells/debris along left axis. **(B)** Total cell counts for each culture are shown over the culture period, where donors C19BC2 and C19BC4 died off completely by days 21 and 15 respectively.

Since similar studies of CMV VST report culture with protein supplementation (Rauser et al., 2004), subsequent SARS-CoV-2 VST cultures tested the use of standard culture protein supplement human AB serum (SNBTS) and commercial pathogen-inactivated human platelet lysate n-Liven (Sexton). To compare these supplements,

donor cultures (n=2) were split equally into the three following culture conditions: TexMACS + IL-2 only, TexMACS + IL-2 + ABS and TexMACS + IL-2 + nLiven and monitored over 15 days. Growth curves testing the three conditions are shown for both donors C19BC5 (**Figure 4.17A**) and C19BC6 (**Figure 4.17B**). The fold expansion between day 0 seeding and day 15 culture (**Figure 4.17C**) was dramatically lower in the IL-2 only condition (79 ± 13.3 SEM) compared to medium supplemented with ABS (2090 ± 994 SEM) or nLiven which was the highest overall at (3402 ± 1784 SEM). One-way ANOVA tests could not be applied to compare the groups due to low sample number, however it is clear protein supplementation is needed for a high VST expansion. Flow cytometry analysis demonstrated equivalent phenotype of purified T cells between the protein supplementation conditions (data not shown), indicating ABS or nLiven do not induce preferential outgrowth of a non-T cell population. Since nLiven had the highest overall expansion and is available at GMP-grade, it was used for all subsequent cultures.

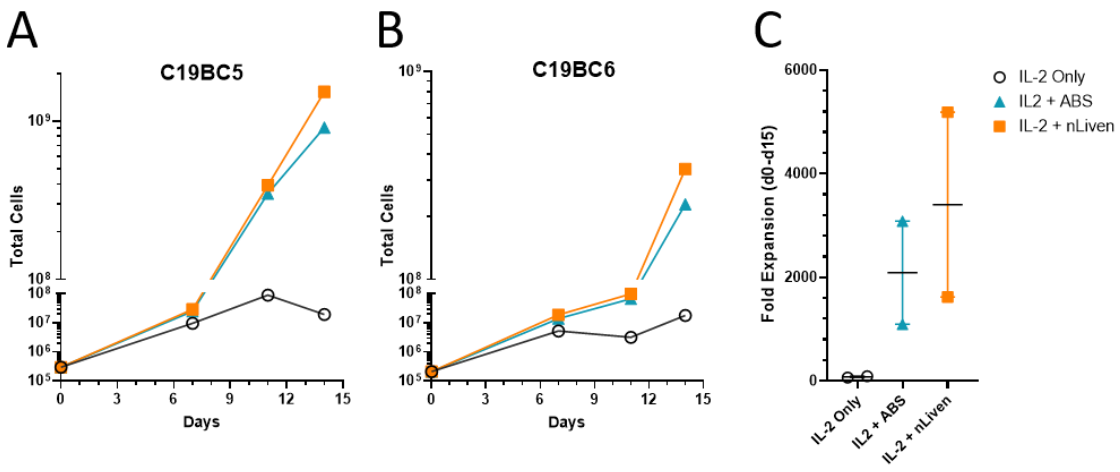

Figure 4.17 - SARS-CoV-2 VST cultures protein supplementation.

SARS-CoV-2 VST cultures (n=2) were divided equally for an intra-donor comparison to test the following medium supplementations: IL-2 only (clear circles), IL-2 + ABS (blue triangles), and IL-2 + nLiven (orange squares). Total CD3+ cell counts taken over 15 days culture are shown for donors **(A)** C19BC5 and **(B)** C19BC6. The calculated mean fold expansion between day 0 culture set up and day 15 **(C)** is shown for the three conditions. Data is represented as mean ± SEM. No statistical analysis was done due to low sample number.

4.4.2 SARS-CoV-2 VST culture optimisation

In addition to protein supplementation, other cytokine supplements have indicated benefits in T cell culture and support growth of particular phenotypes. In particular, addition of IL-7 and IL-15 have been reported to improve T cell expansion with increased retention of central memory T cells in polyclonal T cell culture (Shi et al.,

2013), as well as improved yield and anti-tumour activity in CAR T cell culture (Zhou et al., 2019) and 4T1 mammary carcinoma-specific T cell culture (Cha et al., 2010). While IL-15 was not available for testing at time of this study, addition of IL-7 was tested for benefit in SARS-CoV-2 VST expansion. To investigate this, intra-donor (n=3) comparisons were made by setting up VST in the following supplementation conditions: IL-2 only; IL-2 + nLiven; IL-2 + IL-7; and IL-2 + IL-7 + nLiven. Cultures were counted at day 8 and compared for differences in phenotype. No statistical differences were found in the fold expansion between the different conditions (**Figure 4.18A**), although conditions with nLiven supplementation trended to increased expansion. Phenotypic analysis showed a consistently pure T cell (CD3+/CD56-) phenotype highly enriched for CD4+ TCM, with negligible NKT or NK cells between all conditions (**B-D**). Since IL-7 provided no obvious benefit in expansion or phenotype, it was not included in subsequent cultures.

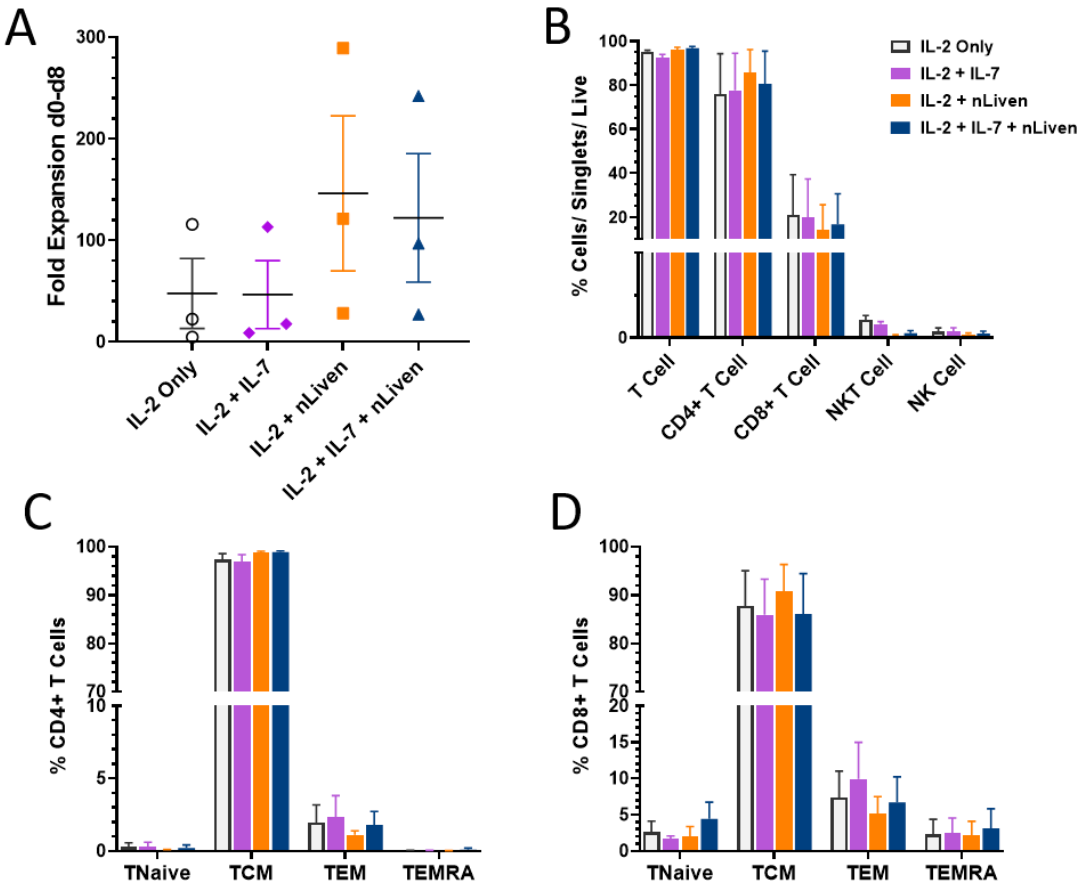

Figure 4.18 - SARS-CoV-2 VST culture IL-7 supplementation.

SARS-CoV-2 VST cultures (n=3) were divided equally for an intra-donor comparison to test the following medium supplementations: IL-2 only (white), IL-2 + IL-7 (purple), IL-2 + nLiven (orange) and IL-2 + IL-7 + nLiven (navy). Comparisons were made for **(A)** fold expansion day 0 to day 8, **(B)** day 8 lymphocyte phenotype, **(C)** day 8 CD4+ memory status, and **(D)** day 8 CD8+ memory status. Data is represented as mean ± SEM. Comparisons between groups were performed using repeated measures one-way ANOVA with Geisser-Greenhouse correction, where $p<0.05$ was considered statistically significant.

4.4.3 Enhancing VST expansion by feeder re-stimulation

Utilising these results for optimised culture medium (TexMACS + IL-2 + nLiven), after 14 days in culture, expansion plateaued (**Figure 4.19A**), and an increased transition from central memory to effector memory phenotype by day 21 was observed (representative plot **Figure 4.19C**). In other studies, expansion of cytokine-selected T cells skewed towards a CD4+ line could be boosted by addition of a feeder re-stimulation step (Chatziandreou et al., 2007, Mazza et al., 2010). To investigate this, irradiated autologous non-target cells (PBMC) not used for culture set up were cryopreserved and stored for use in subsequent feeder re-stimulation. At day 14, VST cultures were divided equally to test addition of thawed irradiated non-targets (feeder re-stimulation, FR) versus standard VST culture control. FR induced a subsequent two log expansion between day 14-21 (**Figure 4.19B**) in all VST cultures tested (n=5). In addition, when cultures were administered a FR at day 14, central memory phenotype was retained at day 21 (**Figure 4.19C**). Cultures were monitored throughout expansion to determine whether FR affected phenotype, but there were no significant differences in lymphocyte subsets (**Figure 4.19D-E**) or T cell memory status (**Figure 4.19F-G**) between cells harvested at day 14 or at day 21.

Since this comparison data indicates equivalent phenotype at day 14 and day 21 FR, final products could be harvested for cryopreservation at either of these time-points. Harvest at day 21 FR would have the obvious benefit of 1-2 fold log expansion of VST, therefore substantially increasing the number of potential patient doses in full-scale manufacture. Conversely, this adds additional protocol steps, longer culture duration, and may be limited by the number of irradiated non-targets available from each donor. Through hypothesized scaling of yield from a full-scale manufacturing run (using leukapheresis starting material), it was estimated the number of cells harvested at day 21 (>200 doses at $1.5x10^8$ VST per dose) would create more patient doses than is possible to freeze down at our facility due to lack of controlled rate freezer (Planer Ltd) and LN_2 tank capacity. Therefore, it was decided to validate the manufacturing process with harvest at day 14 without FR.

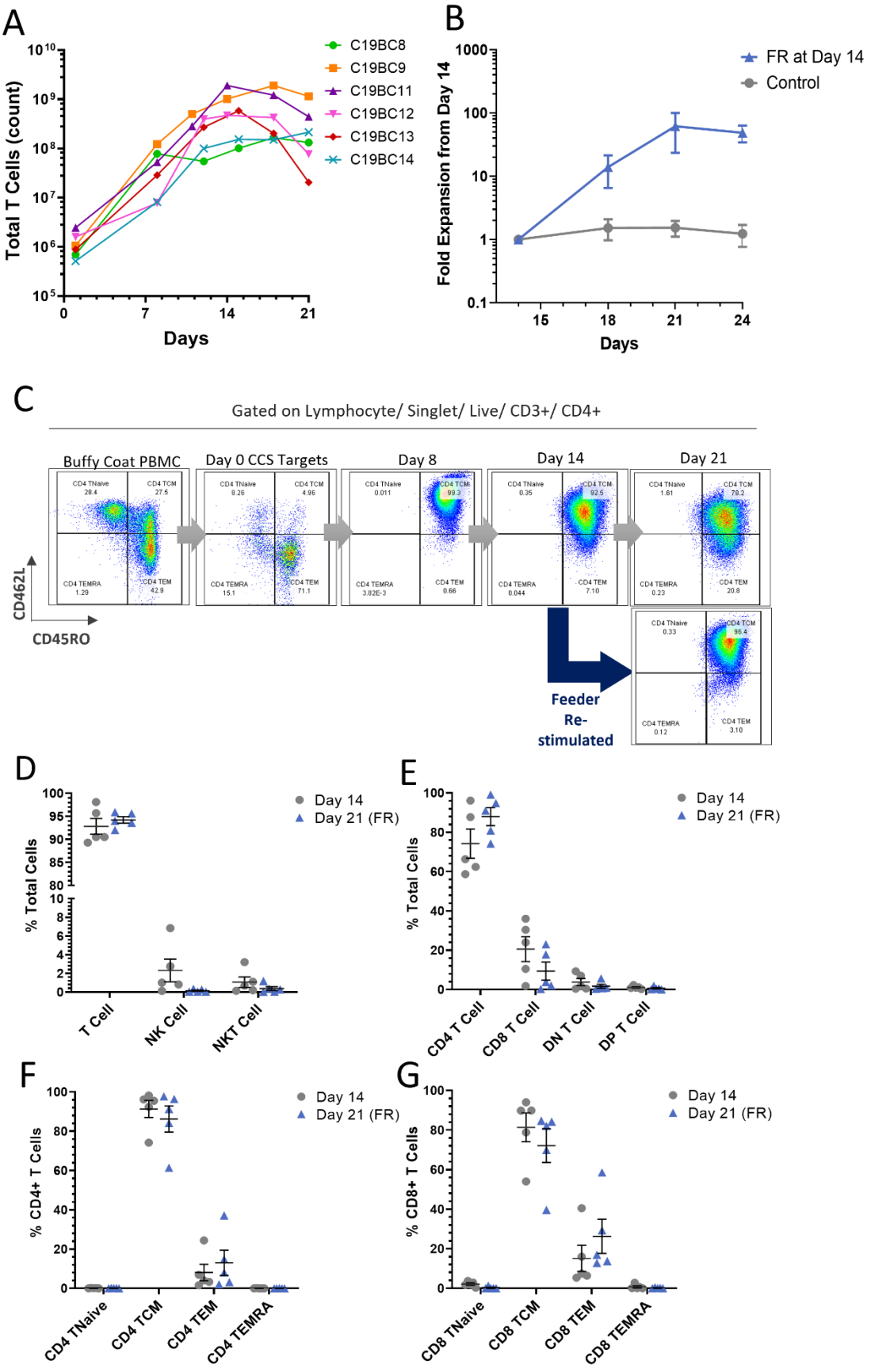

Figure 4.19 - SARS-CoV-2 VST culture feeder re-stimulation.

(A) Isolated SARS-CoV-2 VST from donors C19BC8-14 had a 2-3 log expansion over 21 day culture using an optimized culture expansion protocol. **(B)** VST cultures were split at day 14 to directly compare standard continuation in culture (control, grey circles) and re-stimulation with

autologous irradiated feeders (FR, blue triangles). (**C**) Representative culture C19BC9 by day 21 without re-stimulation indicated some transition of CD4 TCM to CD4 TEM (Day 21 top panel). CD4 CM phenotype was retained when cultures re-stimulated at day 14 with autologous irradiated feeders (Day 21 bottom panel). **(D-G)** Final product phenotype and T cell memory status was compared at both harvest time-points: Day 14 (grey circles) and Day 21 FR (blue triangles). Data is represented as mean ± SEM. No significant differences were observed using paired t-tests with Holm-Šídák correction for multiple comparisons.

4.5 Characterisation of expanded SARS-CoV-2 VST

Using the optimised culture protocol (supplementation with IL-2 + nLiven for 14 days), cells were harvested and characterized for cell identity, phenotype and functional capacity.

4.5.1 SARS-CoV-2 VST culture drives expansion of central memory CD4+ T cells

Cultured cells harvested at day 14 (**Figure 4.20A**), were highly enriched for T cells (87.95 ± 2.99%) with minimal expansion of NK and NKT cells. T cells were predominantly CD4+ (77.86 ± 5.19%) with smaller proportion of CD8+ T cells (18.05 ± 4.4%). Both the CD4+ and CD8+ populations were heavily skewed towards central memory phenotype. Direct intra-donor comparison of populations between IFN-γ+ isolated target cells (as demonstrated in (**Figure 4.15**) and day 14 expansion showed significant differences in monocyte and T cell content, CD4+, CD8+, DN T cells, and memory subpopulations in both the CD4 and CD8 compartment (**Figure 4.20B**). These data demonstrate the developed culture expansion process supports an outgrowth of central memory CD4 cells, and removes contaminating monocytes and naïve T cells from the final product. In particular, naïve T cells are of safety concern for patient infusion due to studies demonstrating naïve T cells but not memory T cells are responsible for inducing GVHD responses in mice (Anderson et al., 2003, Chen et al., 2004, Chen et al., 2007). In addition, expanded VSTs showed negligible co-expression of T cell activation/ exhaustion markers PD-1 and Tim-3 in both the CD4 and CD8 compartment (**Figure 4.20C**) suggesting the culture expansion had not induced an exhausted T cell phenotype.

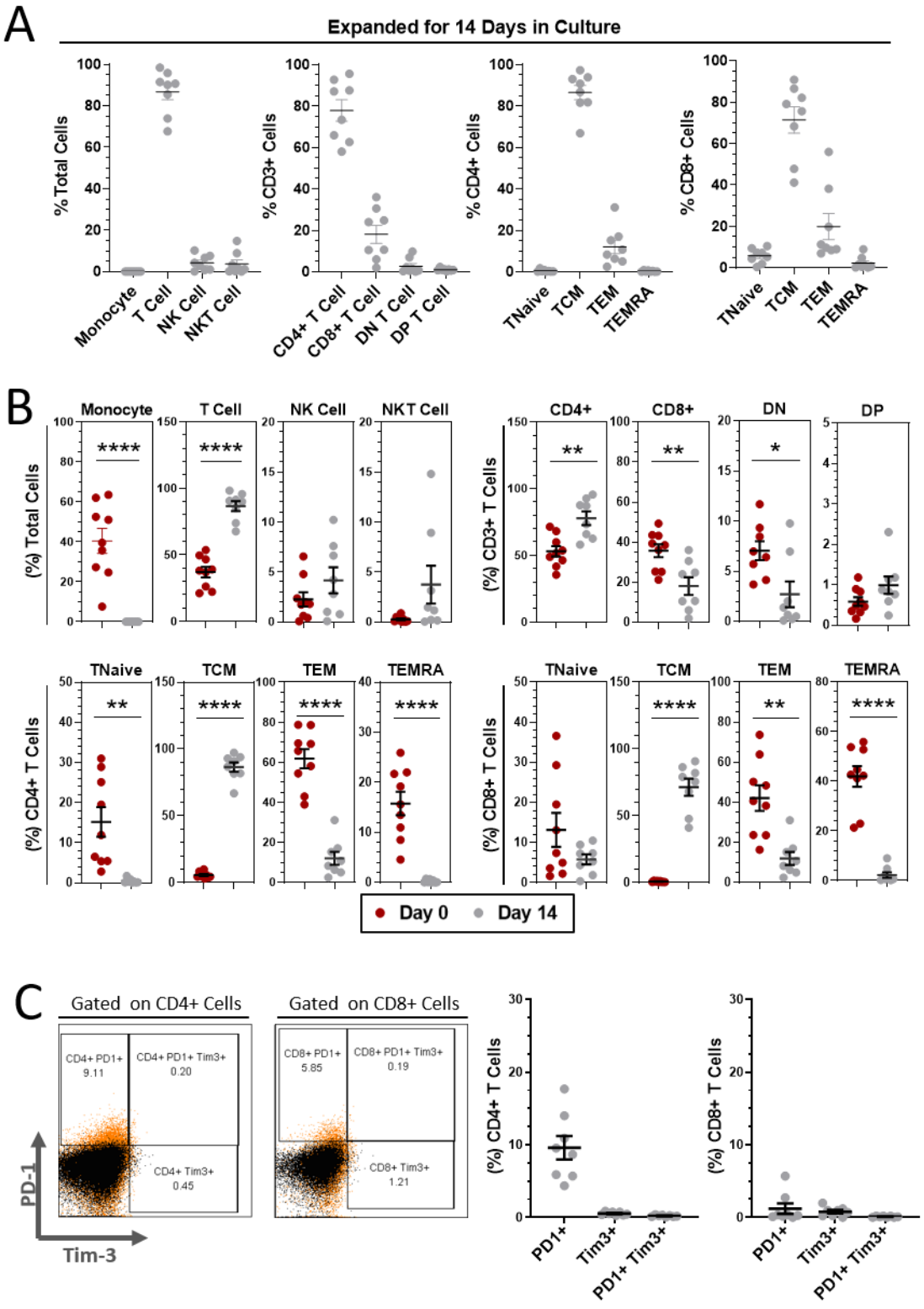

Figure 4.20 - Expanded SARS-CoV-2 VST phenotype.

(A) Expanded SARS-CoV-2 VST at day 14 culture using the optimised expansion protocol were harvested and analysed for frequency of lymphocyte subsets, T cell subpopulation and T cell memory status. **(B)** Direct comparison of T cell subpopulations between day 0 isolated VST and day 14 expanded VST. Significance was calculated using paired t-tests with Holm-Šídák correction for multiple comparisons *p≤0.05, **p≤0.01, p≤0.001 and **** p≤ 0.0001. **(C)** Day 14 expanded VST were also characterised for single and dual expression of exhaustion markers PD-1 and Tim-3 (orange) against isotype controls (black). All data is represented as mean ± SEM.

4.5.2 Development of a DC stimulation assay to assess SARS-CoV-2 VST function

To determine if the T cells expanded in culture were SARS-CoV-2-specific, cells harvested at day 14 of culture were tested for T cell functionality against SARS-CoV-2 stimulus. Since expanded SARS-CoV-2 VST final products were heavily skewed towards CD4+ T cell lines, it was hypothesised effector functionality would primarily be to aid the immune response by production of antiviral cytokines. Although there are numerous reports of cytotoxic CD4+ T cells in chronic viral infections, cancers and autoimmune disorders (Cenerenti et al., 2022, Malyshkina et al., 2023), cytotoxicity of VST could not be tested in the present study due to lack of SARS-CoV-2 infected cells to use as targets. Therefore to measure T cell cytokine production as a surrogate of function, expanded SARS-CoV-2 VST were tested for reactivity to various peptides using the intracellular cytokine assay.

While expanded EBV VST (primarily CD8+ lines) show ability to cross-present peptide pools in the functional ICR assay without addition of APCs via T cell associated HLA Class I (see **section 3.3.6**), it was hypothesised the SARS-CoV-2 VST would require antigen presentation of peptides to activate the CD4+ cells. To test this, harvested SARS-CoV-2 VST were plated in TexMACS medium and stimulated with SARS-CoV-2 peptide pools (individual spike, nucleocapsid, membrane, and pooled S+N+M) as either direct addition of peptides to the VST, or by co-culture of autologous peptide pool-loaded DC with the VST. For this assay, CD14+ monocytes were isolated from the fresh PBMC donation and cultured for 6 days to generate immature DC which were then frozen and stored until use. The day prior to VST harvest, DC were thawed and loaded with peptides for 6 hours, then a maturation cocktail (as detailed in **section 2.7.4**) added overnight. The following morning loaded DC were washed, counted, phenotyped for maturity and co-cultured with the harvested SARS-CoV-2 VST at [10 VST: 1 DC]. All conditions were then stimulated for 5 hours and stained with the intracellular cytokine and activation panel as outlined in **Table 2.8**. Representative flow analysis showing gated T cells (CD3+) IFN-γ response to stimulation with direct peptides and peptide-loaded DC is displayed in (**Figure 4.21A**), negative controls used VST with either no antigen or unloaded DCs respectively. Non-SARS peptides (right panel) were included to measure specificity towards SARS-CoV-2. The mean percentage reactive VST for each SARS-CoV-2 peptide was compared for direct peptide and peptide-loaded DC (**Figure 4.21B),** where VST

reactive to pooled S+N+M was significantly higher using peptide-loaded DC (mean=41.5% ± 9 SEM) than direct peptide(mean=25.8% ± 7 SEM) stimulation (p=0.014). These results indicate addition of DCs for antigen presentation improves the SARS-CoV-2 VST reactivity to peptide stimulation, and therefore should be used to measure maximal functional potency in this assay.

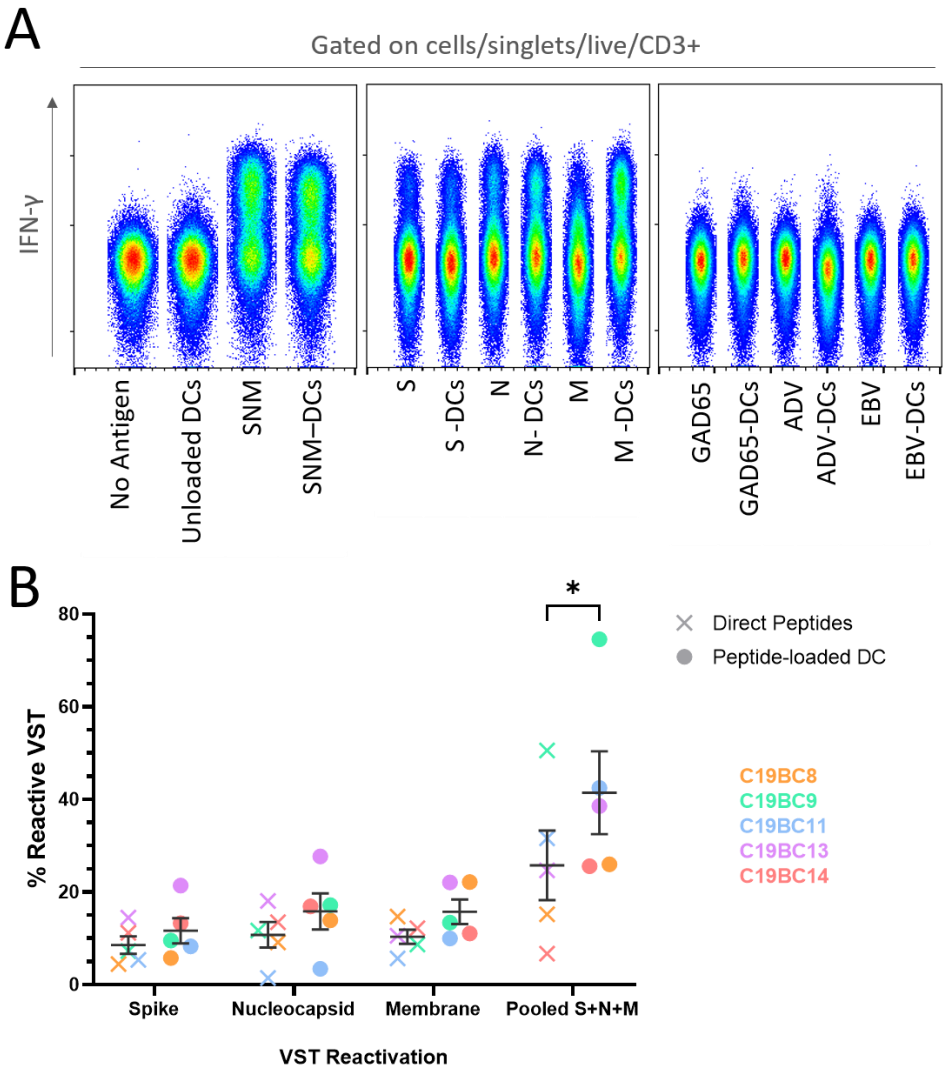

Figure 4.21 - VST reactivity to direct peptide versus peptide-loaded DC.

Expanded SARS-CoV-2 VST were tested for functional reactivity to peptide stimulation by intracellular cytokine secretion assay. VST were stimulated by either by addition of peptides (direct peptides) or co-culture with peptide-loaded DC. **(A)** Flow cytometric representation of gated CD3+ cells IFN-γ response to either direct peptide or peptide-loaded DCs for the following SARS-CoV-2 peptides: spike (S), nucleocapsid (N), membrane (M), pooled S+N+M (SNM). Glutamic acid decarboxylase 65 (GAD65), adenovirus (ADV) and Epstein-Barr virus (EBV) peptides were included as non-SARS peptide controls. Negative controls for VST stimulation with direct peptides and peptide-loaded DC were no antigen and unloaded DC respectively. **(B)** The percentage reactive VST (CD3+/IFN-γ+ cells) corrected to negative controls were compared between direct peptides (crosses) and peptide-loaded DC (circles) for the SARS-CoV-2 peptides, where each different colour represents a paired donor. Data is represented as mean ± SEM, and groups compared using paired t-tests with Holm-Šídák correction for multiple comparisons where *p≤0.05.

4.5.3 SARS-CoV-2 VST are multifunctional

SARS-CoV-2 VST reaction to SNM-DC stimulation was measured using multiple T cell functional markers. Representative flow analysis shows acquisition of the cytokines/ activation markers is differential based on pre-gating CD4+ or CD8+ cells within the overall VST product (**Figure 4.22A**). When gating on overall VST (CD3+), the highest frequency of cells reactive to SNM-DC stimulation was for markers IFN-γ, TNF-α, and CD154; with fewer cells expressing IL-2, CD107a or CD137 (**Figure 4.22B**).

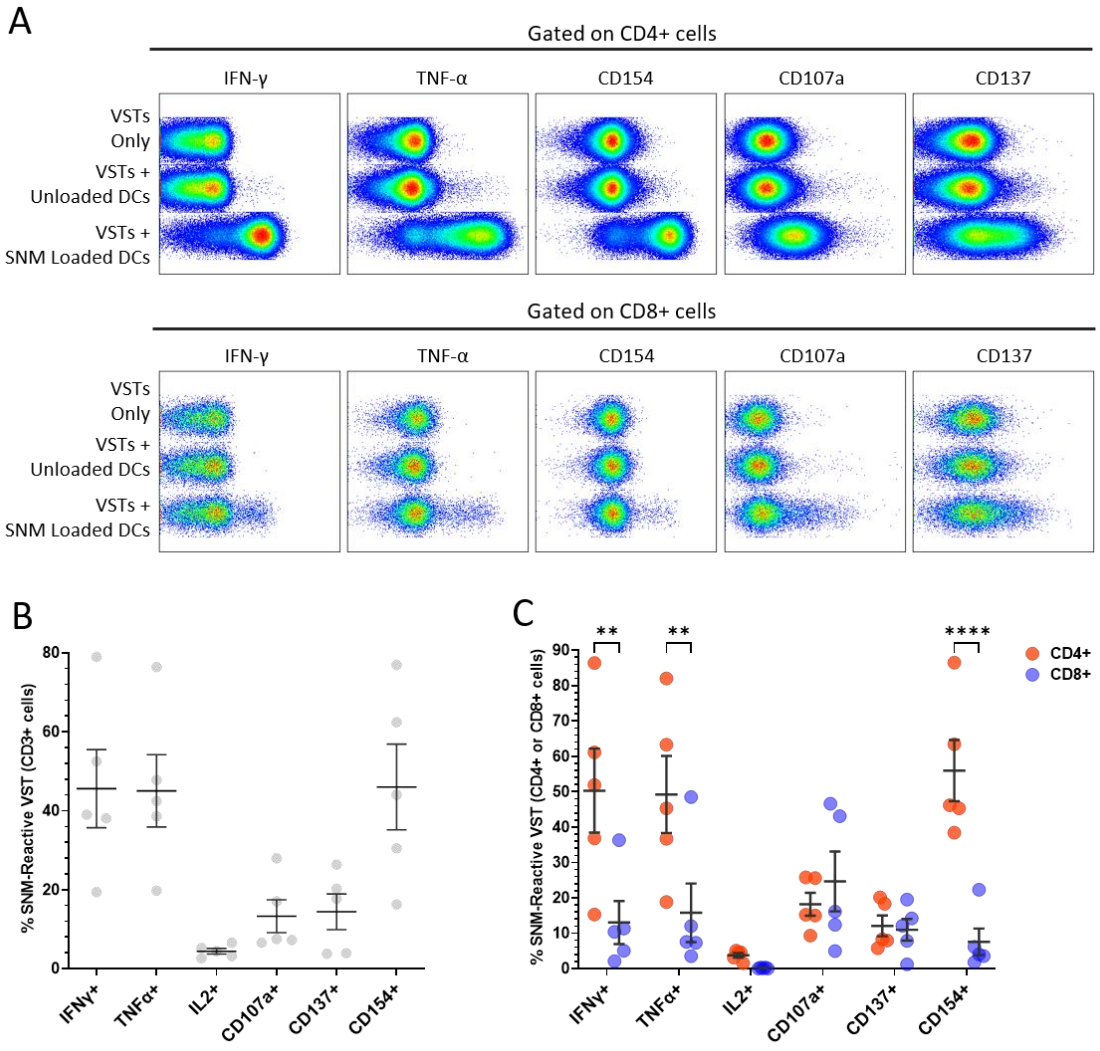

Figure 4.22 - Expanded SARS-CoV-2 VST functional markers.

Expanded SARS-CoV-2 VST reactivity to stimulation with SNM-loaded DCs was confirmed with multiple T cell functional markers: IFN-γ, TNF-α, IL-2, CD107a, CD137 and CD154. **(A)** Flow cytometric analysis on either CD3/CD4+ or CD3/CD8+ cells for IFN-γ, TNF-α, CD154, CD107a and CD137 is shown for negative controls (VSTs Only, and VSTs + Unloaded DCs), and VST + SNM-loaded DCs. **(B)** The percentage of cells expressing functional markers reactive to SNM-DC stimulation is shown for CD3+ gated T cells; and **(C)** compared within the CD4+ versus CD8+ gated compartments. Data is represented as mean ± SEM. Statistical significance was determined using paired t-tests corrected for multiple comparisons using the Holm-Šídák method where **p≤0.01 and **** p≤ 0.0001.

This high frequency of IFN-γ, TNF-α, and CD154 reactive VST was primarily by CD4+ cells, whereas CD8+ cells had significantly lower expression of these markers (**Figure 4.22C**) indicating the CD8+ cells in these lines are less functionally active. This likely reflects the heavy skew of these products to CD4+ T cells, with many of the lines containing negligible CD8+ cells. Interestingly, the mean percentage of CD4+/CD107a+ and CD8+/CD107a+ cells was comparable at ~20% of total cells in the final product. This suggests some CD4+ cells within these lines may have the capacity for degranulation and therefore cytotoxic potential.

As not all CD3+/TNF-α+ cells were reactive to SNM-DC stimulation (range 21-70%), the question remains regarding the other ~60% cells that are unreactive in SNM-DC in this assay? This could be due to multiple reasons: either the T cells are not SARS-CoV-2 specific (and if so are they specific to another antigen?), they are specific to other SARS-CoV-2 proteins not covered by the SNM peptide pools used here, they are SNM-specific but functionally unreactive by way of the tested cytokines in this assay. Another likely possibility is underestimation of SNM reactivity caused by the limitations of this assay. Since time and resources were limited during development of the DC stimulation assay, few parameters could be optimised in these initial studies. This assay was further optimised in later stages as discussed in Chapter 6, which suggests the cytokine responses to peptide-loaded DC here may be underestimated by up to 50% of the reported value for each donor.

4.5.4 SARS-CoV-2 VST functional reactivity to Spike, Nucleocapsid and Membrane

The total T cell IFN-γ and TNF-α response to individual peptide pools spike, nucleocapsid and membrane for each donor VST are shown in **Figure 4.23A** and **Figure 4.23B** respectively. No predominant specificity to a particular antigen was consistent between the donors, as confirmed in the collated IFN-γ response of all donors showing equivalent reactivity to all antigens (**Figure 4.23C**).

Although the total T cell population did not show predominance for any of the SARS-CoV-2 antigen pools, the IFN-γ response was also assessed for the individual antigens gated on CD4+ T cells and CD8+ T cells specifically (**Figure 4.23D**). In CD4+ T cells, there was a similar response to each antigen (**Figure 4.23E**), but in CD8+

compartment, the nucleocapsid peptide pool was clearly immunodominant, inducing the strongest response (**Figure 4.23F**).

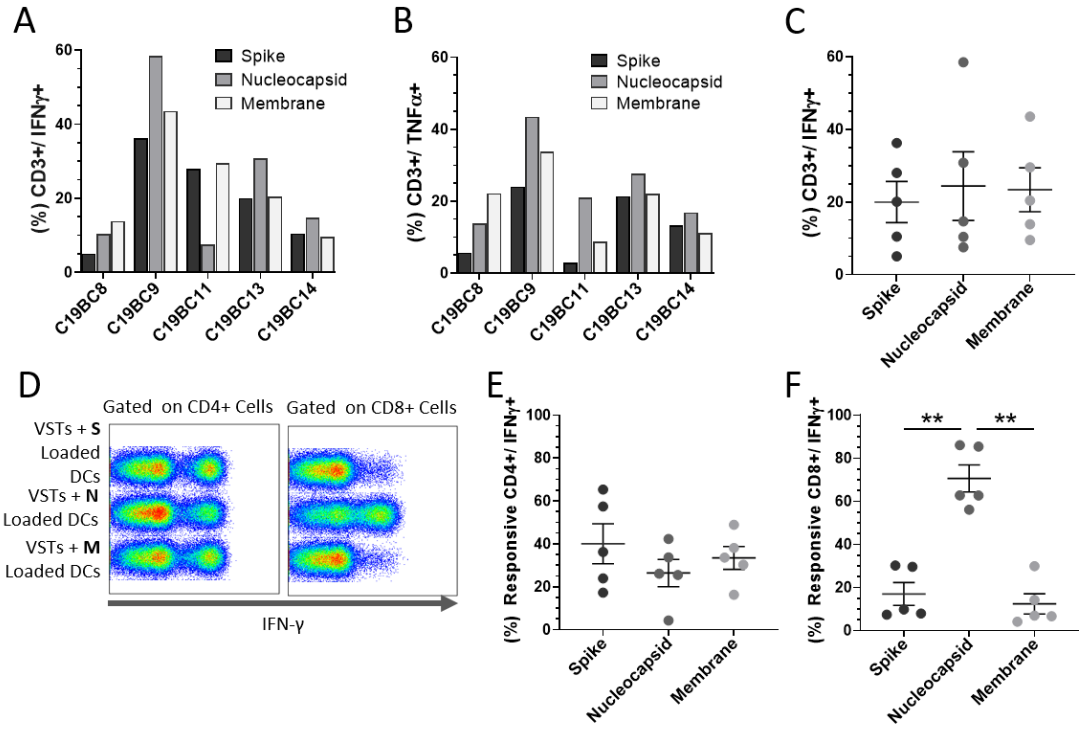

Figure 4.23 - Expanded SARS-CoV-2 VST reactivity to SARS-CoV-2 antigens.

Expanded SARS-CoV-2 VST were assessed for reactivity against DC loaded with individual SARS-CoV-2 peptide pools: Spike, Nucleocapsid and Membrane. Dominance of specificity to the antigens via **(A)** CD3+/IFN-γ+ and **(B)** CD3+/TNF-α+ cells is shown per donor. **(C)** The percentage CD3+/IFN-γ+ cells reactive to each antigen is compared for all donors (n=5, mean ± SEM). **(D)** Individual antigen responses within the CD4+ and CD8+ compartment is shown in representative flow plots for IFN-γ expression. IFN-γ reactivity for all donors (n=5, mean ± SEM) is compared between the individual antigens in both **(E)** CD4+ gated and **(F)** CD8+ gated cells. Significance determined using RM one-way ANOVA with Geisser-Greenhouse correction **p≤0.01).

4.5.5 Negligible reactivity of SARS-CoV-2 VST to non-SARS peptides

Expanded VST were also assessed for specificity by measuring reactivity to DC loaded with peptides of various non-SARS antigens: adenovirus (ADV), EBV and glutamic acid decarboxylase-65 (GAD65). ADV and EBV were included as peptide sequence controls to other common viruses. GAD65 is an autoantigen expressed by pancreatic beta cells involved in type 1 diabetes, therefore was included as a non-viral antigen control. VST reactive by IFN-γ (**Figure 4.24A**) and TNF-α (**Figure 4.24B**) release to stimulation with ADV, EBV and GAD65 were negligible in comparison to SARS-CoV-2 SNM stimulation.

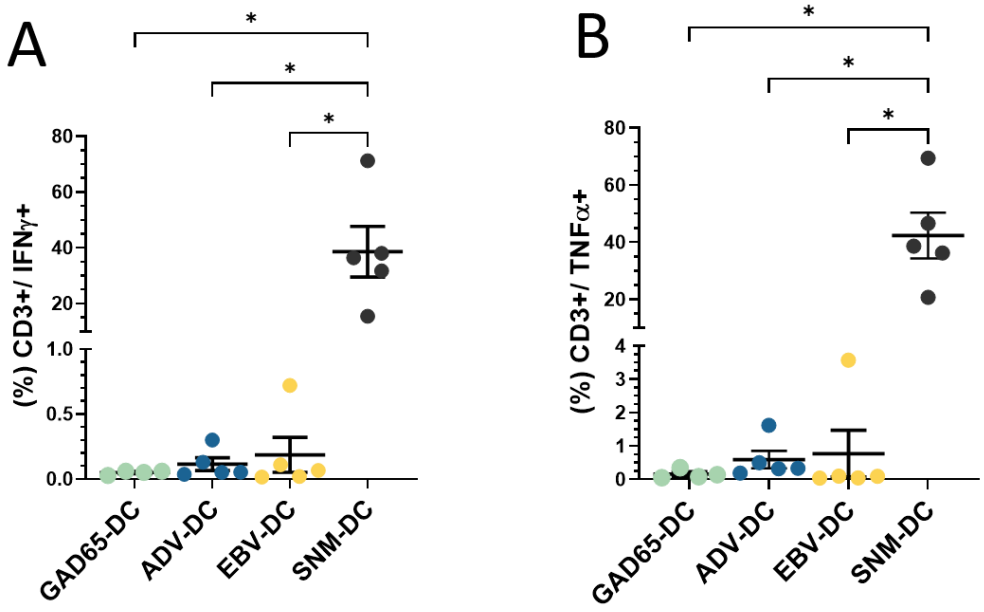

Figure 4.24 - Expanded SARS-CoV-2 VST reactivity to non-SARS peptides.

Expanded SARS-CoV-2 VST were assessed for specificity by measuring reactivity to stimulation with DC loaded with non-SARS peptides. The percentage of **(A)** CD3+/IFN-γ+ cells and **(B)** CD3+/TNF-α+ cells reactive to GAD65-DC, ADV-DC, EBV-DC; and SARS-CoV-2 SNM-DC as comparator. Data is represented as mean ± SEM. Statistical significance was determined using RM one-way ANOVA with Geisser-Greenhouse correction where *p≤0.05.

While only a few non-SARS peptides could be tested due to peptide availability during the study, these results indicate a high degree of specificity of the VST towards SARS-CoV-2 and not just general peptide sequences.

4.6 Discussion

Following the outbreak of SARS-CoV-2, a speedy and collaborative global effort was centred on researching COVID-19 disease pathology, as well as identifying mechanisms of protective immunity. We had a unique opportunity to study SARS-CoV-2 T cell responses in naturally recovered donors recruited through the convalescent plasma programme, were able to rapidly develop a process to isolate the SARS-CoV-2 VST from blood donations and expand in culture to therapeutically relevant numbers, and were one of the first globally to report this approach (Cooper et al, 2021).

Initial reports during the pandemic indicated marked changes in immune compartments within the peripheral blood of patients with progressive/ severe COVID-19. Due to the time taken for individuals with asymptomatic or mild infection

to reach convalescence, we were one of the first groups in the UK to profile immune subsets in the peripheral blood of recovered individuals. To this end, buffy coat samples from fifteen convalescent donors were phenotyped for immune cell subsets and tested for lymphocyte responses to SARS-CoV-2 viral peptides. Though immunophenotyping of PBMC demonstrated broadly similar frequencies of different immune subpopulations compared to uninfected donors, CCD had a significantly reduced CD19+ B cell population. This was further supported by a significant positive correlation in frequency of B cells and SARS-CoV-2 antibody titre within donor peripheral blood. Reduced B cell frequency was observed in a similar study at 3-5 weeks convalescence (Grifoni et al., 2020); and in a much larger cohort (n=95) where B cell lymphopenia was reported in both active COVID-19 infection, and recovered mild patients at two months convalescence (Orologas-Stavrou et al., 2020). Furthermore, a longitudinal immune profiling study demonstrated B cell frequency reduction persisted in convalescent donors at two months to eight months post infection, despite recovery in this timeframe of other immune subsets and overall lymphopenia (Kostopoulos et al., 2021). While anti-SARS-CoV-2 antibodies remained detectable throughout the study, it is suggested the B cell deficiency may indicate either B cell exhaustion or impairment of B cell development due to the hyperinflammatory response in SARS-CoV-2 infection. Other studies however did not observe any difference in B cell frequency between convalescent donors and healthy controls (Bonifacius et al., 2021, Kudryavtsev et al., 2021, Newell et al., 2021), however one group showed around half of their study participants had abnormally low B cell frequency and absolute count over 4-9 months post-infection (Pan et al., 2021) without obvious distinction of clinical or demographic characteristics between the normal and low individuals (e.g. disease severity). Therefore, differences in B cell lymphopenia between studies may reflect unknown differences in patient cohorts from different waves within the pandemic (primary infection versus re-exposure), SARS-CoV-2 strain, or genetic/environmental factors affecting immune response between population demographics, as well as analytical techniques.

Although we did not see any differences in overall T cell frequency or within CD4 and CD8 subpopulations, we did observe a significantly increased frequency of NK cells in convalescent donors compared to uninfected controls. This was also seen in convalescent donors between 1-5months post infection (Bonifacius et al., 2021, Koutsakos et al., 2021, Ryan et al., 2022), however others reported normal NK cell

counts in convalescent individuals (Orologas-Stavrou et al., 2020, Zheng et al., 2020b, Kratzer et al., 2021). More recently, individuals affected with long COVID, a long term post-acute syndrome with physical and neurological symptoms lasting up to months or years after infection resolution, have evidenced high levels of circulating NK cells (Galán et al., 2022). Contrasting results between groups may therefore reflect a bias towards individuals with (at the time of study) undiagnosed long COVID, as well as the aforementioned potential differences between cohorts. Nonetheless, the elevated levels of NK cells could indicate the importance of NK cell immunity in efficient innate clearance of SARS-CoV-2. Reduction of circulating NK cells has correlated with COVID-19 disease severity (Maucourant et al., 2020, Wang et al., 2020b, Wilk et al., 2020, Zheng et al., 2020b). While this may just signify NK cell recruitment to the lungs, an increased frequency of circulating NK cells has also been directly associated with more rapid control of viral load in severe COVID-19 patients (Witkowski et al., 2021) suggesting overall distribution and expansion of peripheral NK cells as a positive prognostic factor. While NK cell frequency generally increases with age (Brauning et al., 2022), we did not observe a correlation between peripheral NK cell frequency and age, likely reflecting the NK cell redistribution following acute infection.

Through optimisation of a T cell stimulation and intracellular activation marker flow cytometry assay, we demonstrated convalescent donors generated a robust T cell response against the spike, nucleocapsid and membrane peptide pools. Use of this assay to detect SARS-CoV-2 responses provides benefits over the widely used IFN-γ enzyme-linked immunospot (ELISPOT) assay including the ability to delineate responses between different immune subpopulations, investigation of numerous effector cytokines or activation markers, and accurate quantification of rare cell populations. Additionally, use of SARS-CoV-2 whole recombinant proteins to stimulate T cells in an intracellular flow cytometry assay induced non-specific responses compared to using SARS-CoV-2 peptide pools which generated highly specific responses (Silva et al., 2021). This suggests that peptide pools are preferable for accurately detecting and quantifying antigen-specific T cell responses, and correspondingly we saw rare antigen-specific T cell populations with high specificity and sensitivity by flow cytometry using SARS-CoV-2 peptide pools.

Response to the individual and combined peptide pools of SARS-CoV-2 antigens were predominantly by CD4+ Th1 cells, with a distinctly smaller population of reactive CD8+ CTL. This may represent a contraction of the CTL clonal population following primary infection, and longitudinal analysis could be done to see if peripheral CD8 SARS-CoV-2 memory T cell pool remains lower over time. Similar studies measuring T cell responses to peptides by way of intracellular IFN-γ and TNF-α expression have also reported a CD4-mediated response, with lower frequency of SARS-CoV-2 reactive CD8+ T cells (Grifoni et al., 2020, Habel et al., 2020, Bonifacius et al., 2021, Law et al., 2021, Simara et al., 2021). Interestingly, we saw a hierarchy of antigen-specific responses of membrane > nucleocapsid > spike, which was consistent across donors. Other studies (Grifoni et al., 2020, Thieme et al., 2020, Kroemer et al., 2022) have also reported highest frequencies of membrane-specific CD4+ T cells out of the three antigens. This may suggest a higher level of transcription of membrane than the other structural proteins in infected cells. Correspondingly, like SARS-CoV-1, membrane has is the most abundantly expressed structural protein of SARS-CoV-2, and is reported to form dimeric complexes with nuclecapsid and envelope that are essential for viral assembly (Zhang et al., 2022). Reactive NK cells producing TNFα in response to SARS-CoV-2 peptide stimulation were observed in some individuals, characteristic of an adaptive NK cell-like population. This observation is investigated further in Chapter 7.

Within our study, the overall frequency of T cells reactive to the pooled SARS-CoV-2 peptides positively correlated to donor SARS-CoV-2 antibody titre. This indicates a link between T cell and humoral immunity within individuals able to naturally resolve the infection without serious illness, which has been replicated in other studies (Grifoni et al., 2020, Peng et al., 2020, Silva et al., 2021). Interestingly, the SARS-CoV-2 VST frequency was also found to decrease over time from resolution of symptoms, which was consistent with other reports of SARS-CoV-2 T cell reduction following primary infection in mild convalescent individuals (Simara et al., 2021, Ma et al., 2021) . In contrast, a group using ELISPOT responses to SARS-CoV-2 peptides indicated a slight increase in S1-specific and pooled SMN-specific T cell responses over time between 1-8 months post symptom onset, whereas antibody responses peaked at 1 month and then significantly declined (Sherina et al., 2021). The contrasting results may reflect differences in techniques to measure SARS-CoV-2 T cell responses, or the longer sampling duration compared to our study may have allowed for donor re-exposure. Extrapolation of our observation here is difficult

because it reflects inter-donor VST frequency over time, whereas longitudinal intra-donor sampling should be done to more accurately indicate T cell memory dynamics following infection resolution.

Asymptomatic infection at this time was estimated in approximately 31% of all SARS-cases (Nishiura et al., 2020), therefore it is not implausible that some individuals within the control cohort could have been asymptomatically infected. However, SARS-CoV-2 peptide-reactive T cells were not detectable in any of the uninfected donors tested, supporting the conclusion that these donors had not been exposed at the time of study. In addition, T cell responses to SARS-CoV-2 peptides have been reported in unexposed individuals (confirmed by SARS-CoV-2 spike S1 seronegativity) indicating cross-reactivity to other coronaviruses. C-terminal peptide pools covering the Spike S2 subunit exhibit high sequence homology to SARS-CoV-1 and other coronavirus strains 229E, NL63, OC43 and HKU1, particularly at MHC-II epitopes. Reactive T cells to S2 but not S1 peptides were observed in unexposed donors (Braun et al., 2020). Another study showed unexposed donor CD4+ T cell responses to spike, membrane, nsp4, nsp6 and nsp14 indicative of cross-reactive responses (Grifoni et al., 2020). Furthermore, patients with previous SARS infection from the 2003 outbreak, but not exposed to SARS-CoV-2, demonstrated T cell responses to SARS-CoV-2 nucleocapsid peptides indicating long-lived cross-reactive memory T cell responses between the two viruses (Le Bert et al., 2020). We did not observe any cross-reactive responses, however, while peptide pools covering the full sequence of nucleocapsid and membrane proteins were used, the spike peptide pool only consisted of select immunodominant regions which may not cover all conserved motifs to other coronaviruses. An assay using peptide pools excluding cross-reactive epitopes has since been validated with 95% accuracy in clinical trial to diagnose SARS-CoV-2 exposure on the basis of T cell response (Titov et al., 2022).

Using a GMP-compliant selection system, we were able to isolate SARS-CoV-2 peptide-reactive VST on the basis of IFN-γ response. Consistent to screening that demonstrated a very low frequency of peripheral SARS-CoV-2 VST, the yield of isolated VST from a full buffy coat starting source material was <1 million cells. While direct selection of antigen-specific T cells and delivery to patients is a beneficial strategy for an autologous cell therapy in terms of only 1-2 day process duration, for use as an allogeneic therapy it would only allow delivery to one patient due to the low

yield. We therefore optimised a post-isolation culture process to expand SARS-CoV-2 VST to allow generation of a therapy able to treat multiple patients. Growth of SARS-CoV-2 VST in culture required supplementation with either human serum or protein supplement alternatives, we proceeded with a GMP-compliant platelet lysate (N-Liven) as a more consistent and translatable reagent for cell therapy manufacture. Expansion of VST with N-Liven and IL-2 supplementation was found to peak at day 14 of culture, however we showed re-stimulation with irradiated non-target cells cryopreserved from the original matched IFN-γ CCS isolation could induce a further 2 log fold expansion by day 21 of culture. Since these 'feeder' cells were non-target PBMC stimulated with the SARS-CoV-2 peptides for CCS, it is likely they provide continued peptide presentation as well as co-stimulatory signalling to drive the subsequent antigen-specific T cell expansion. Through modelling to full-scale manufacture from a leukapheresis starting source material, we estimated an input of 1 billion PBMC to our selection & expansion process would yield ~10 billion SARS-CoV-2 VST by day 14 culture. This was more than sufficient for us to generate many patient doses for initial phase trialling (at $1.5x10^8$ VST per dose) and therefore to keep a shorter manufacturing process with fewer manipulations we decided to make product harvest and formulation at day 14 without re-stimulation. With equivalent product phenotype at day 14 or day 21, feeder re-stimulation could be revisited if required to generate larger VST banks for late-stage clinical trials.

Characterisation of cells harvested at day 14 demonstrated expansion of a highly pure T cell product, enriched for CD4 central memory T cells. This correlates closely with the CD4 predominant expanded populations produced in a similar methodology using spike, nucleocapsid, membrane and envelope peptide pools to pulse PBMC and allow ex vivo VST outgrowth for 10 days in culture (Keller et al., 2020). Comparison of phenotype between day 0 isolated targets and after 14 days expansion shows the culture process supports the outgrowth of memory T cells, whereas monocytes, naïve T cells and terminal effector T cells contract under these culture conditions. While there was small proportion of cells positive for expression of activation marker PD1, co-expression of PD1 and Tim-3 indicative of T cell exhaustion (Baessler and Vignali, 2024) was negligible therefore suggesting products were of high proliferative and functional capacity. This was further supported by development of a functional assay using peptide-pulsed autologous DC to co-culture with day 14 harvested VST, which showed potent product responses upon antigen recall. VST products re-stimulated

with pooled SARS-CoV-2 peptide-pulsed DC had high expression of antiviral cytokines IFN-γ and TNF-α, as well as significant upregulation of co-stimulatory receptor CD154. CD8+ cells within some of the donor products showed expression of degranulation marker CD107a indicating killing potential within these populations. Without access to a SARS-CoV-2 infected cell line, we could not assess direct ability for the generated VST products to elicit specific cell lysis, however this is something addressed in Chapter 6. Expression of multiple effector molecules however demonstrates VST are multifunctional and can induce activation of Th1 associated signaling pathways to initiate antiviral responses. Though antigen reactivity varied between donors, VST had relatively equal frequencies of T cells reactive to spike, nucleocapsid or membrane indicating products that target all three antigens. Interestingly CD8+ cells had consistently higher reactivity towards nucleocapsid compared to spike or membrane, indicating a clear immunodominance of this antigen in the CD8 compartment. This hierarchy of CD8+ predominance towards nucleocapsid was also identified in other studies (Lineburg et al., 2021, Nguyen et al., 2021, Simara et al., 2021, Taus et al., 2022). Induction of CD8+ T cell responses directed towards nucleocapsid epitopes was observed particularly within HLA*B:07 individuals (Lineburg et al., 2021, Nguyen et al., 2021), however we saw predominance towards nucleocapsid in all donors with expanded VST regardless of HLA*B allele expression. With multiple antigen targets to elicit antiviral effector functions, the expanded VST may have improved efficiency to clear SARS-CoV-2 infection. Moreover, this represents a therapy less vulnerable to viral escape mechanisms through mutation of any one antigen. Treatments that are robust against mutational evolution are of importance considering the emergence of SARS-CoV-2 variants of concern.

This study has some limitations, namely the small cohort size of convalescent and uninfected donors tested. As discussed previously, donors were selected on the basis of confirmed SARS-CoV-2 mild or asymptomatic infection and convalescence, whereas other donor demographics such as age, sex, ethnicity, blood group, HLA type were indiscriminate within the cohort. Furthermore our study, like many others of this time period, was intrinsically biased in being only able to recruit health care workers, which may skew towards a healthier cohort with lack of co-morbidities compared to the general population. Additionally, comparison of overall immune subsets between convalescent and uninfected donors was made on the basis of

population frequencies, whereas absolute counts provide valuable diagnostic quantification of immune cell types that can be compared with standard ranges. For detection and isolation of antigen-specific T cells, research-grade peptides to spike, nucleocapsid and membrane were only available at this time. Additional viral antigens may reveal a fuller picture of the immune response to SARS-CoV-2, and therefore if other peptides become available these could be tested in our VST isolation method for a positive additive effect or possibly cross-reactive non-SARS-CoV-2 T cell responses. Testing of the expanded SARS-CoV-2 VST in this study focussed on T cell phenotyping and functional assessment on the basis of antigen recall induced cytokine expression, however a wide range of characterisation and safety assays should be implemented for therapeutic evaluation. This is addressed during clinical manufacture of a SARS-CoV-2 VST bank in Chapter 6, as well as considerations for patient groups that may benefit from an adoptive SARS-CoV-2 T cell therapy.

4.7 Chapter summary

This chapter has characterised the SARS-CoV-2 memory T cell response within the peripheral blood of COVID-19 convalescent donors using viral peptide stimulation and intracellular flow cytometry detection of reactive T cells. SARS-CoV-2-specific T cells within the PBMC population were predominantly CD4 memory Th1 cells demonstrating the importance of this subset in effective disease resolution. Both the CD4 and CD8 memory pools recognised the SARS-CoV-2 spike, nucleocapsid and membrane peptides indicating broad antigen responses to virus. Additionally, SARS-CoV-2 VST were isolated and expanded in culture from nine of the fifteen convalescent donors, yielding a 3-log expansion up to 10^{10} T cells within 14 days. Expanded cells were enriched for desirable central memory CD4 T cells, with negligible contamination of other cell types. The expanded VST had multifunctional production of effector molecules upon antigen recall, with high expression of antiviral Th1 cytokines and minimal evidence of T cell exhaustion. VST products functionally targeted all three SARS-CoV-2 antigens, with minimal reactivity to non-SARS antigens tested, and therefore may provide a highly specific immunotherapy less susceptible to viral mutational escape. Importantly we demonstrate the feasibility of generating many VST patient treatment doses for potential use in clinical trials to support SARS-CoV-2 infections where the endogenous T cell response may be compromised.

Chapter 5

Comparing mechanisms to isolate SARS-CoV-2 VST

Chapter 5 – Comparing mechanisms to isolate SARS-CoV-2 VST

5.1 Introduction and aims

Over a year following the outbreak of SARS-CoV-2, the resultant COVID-19 disease was reported to have been associated with over 3.9 million deaths worldwide (as of June 2021, WHO). The rapid development of safe SARS-CoV-2 vaccines and remarkable successes implementing vaccination programmes offered a glimmer of hope and began cessation of strict public health policies, with data suggesting vaccines protect 75-95% of individuals(dependent on vaccine and age group) against symptomatic COVID-19 disease (Pormohammad et al., 2021). While SARS-CoV-2 transmissibility is not fully prevented by vaccination (Hodgson et al., 2021), it remains fundamental for the transition from this global pandemic to controllable endemic to find effective treatments for those most vulnerable. While numerous drugs that dampen down the hyperinflammatory response seen in severe stages of the disease have shown clinical efficacy (Zizzo et al., 2022), other therapeutics are in trials to regulate viral infection in mild to moderate disease stages to prevent a threatening dysfunctional inflammatory response. One such therapy being investigated by numerous groups to treat high risk/ immunocompromised patients is the adoptive transfer of SARS-CoV-2 VST in order to control disease and prevent aberrant T cell-driven cytokine response to the infection.

The process used in Chapter 4 for isolating the very low frequency of SARS-CoV-2 VST from blood donations from convalescent donors is based on stimulation with SARS-CoV-2 peptide pools (covering the spike, nucleocapsid and membrane proteins) and subsequent magnetic based selection of the responding VST secreting IFN-γ using CCS methodology (Campbell, 2003). Although CCS kits are only available at GMP manufacturing standard for IFN-γ, we and others have reported blunted SARS-CoV-2 VST IFN-γ responses relative to other SARS-CoV-2 T cell effector markers (Bonifacius et al., 2021, Cooper et al., 2020, Peng et al., 2020, Sekine et al., 2020).

All reported studies using a direct selection method to isolate SARS-CoV-2 VST have used IFN-γ CCS, again likely due to the GMP compliant standard of this reagent and automated CE-marked process for CliniMACS Prodigy selection (Bonifacius et al., 2022, Leung et al., 2020, Chu et al., 2023, Cooper et al., 2020). However, there are

numerous alternative T cell effector markers that can be used to isolate antigen-specific T cells depending on the T cell subset and function(s). In the case of classic anti-viral Th1 or cytotoxic T cells, the main cytokines produced in response to viral recognition are IFN-γ and TNF-α. Enrichment of TNF-α-secreting T cells using the same CCS protocol has been demonstrated to isolate a subset of HIV VST with enhanced cytotoxic capacity (Lichterfeld et al., 2004).

Activation-induced marker CD137 (tumor necrosis factor receptor superfamily member 9) can also be used to isolate antigen-specific T cells with a simplified magnetic microbead protocol separated by surface expression of CD137. Clinical-grade CD137 isolation kits are available and have been used to isolate CMV VST (Peggs et al., 2003, Feuchtinger et al., 2010) and adenovirus (ADV) VST (Feuchtinger et al., 2006) for adoptive transfer in allogeneic HSCT patients with CMV or ADV infection/reactivations respectively. In a study developing a multi-virus VST product specific to CMV, EBV, ADV and influenza, it was found upon incubation with peptide pools that IFN-γ production peaked at different times for each individual virus (Zandvliet et al., 2011). IFN-γ production following stimulation was maximal at 4 hours in CMV & EBV VST, at 8-24 hours in ADV VST, and 4-48 hours in influenza VSTs. In contrast, CD137 surface expression peaked at 48 hours and was stable up to 96 hours post-stimulation with the differential viral peptide pools. Isolation of multi-virus VST with these peptide pools had equivalent viral antigen specificity and CD4:CD8 ratio for IFN-γ and CD137 selection, however CD137 selection was more efficient with a higher yield of targets. Therefore in applications requiring sorting of multiple antigen-specific T cell types, the CD137 approach may be optimal where kinetics of cytokine secretion are different between antigenic activations. In addition, CD137 selection has been used to isolate tumour-specific T cells by stimulation with tumour-associated antigens such as Wilms tumour antigen 1 (WT1) for immunotherapy (Wolfl et al., 2007). In the tumour setting, CD137 is predominantly expressed on activated CD8+ antigen-specific T cells (Ugolini and Nuti, 2021). There is conflicting evidence for use of CD137 selection to isolate different virus-specific CD4+ T cells (Watanabe et al., 2008, Wehler et al., 2008, Zandvliet et al., 2011). This likely reflects the viral antigen(s) in question and whether antigen-specific activation induces a CD4+ T cell CD137 upregulation. Our initial screening studies of COVID-19 convalescent donor buffy coats indicated SARS-CoV-2 S+N+M peptide stimulation induced poor CD137 expression on responsive CD4+ T cells (see Chapter 4).

Another activation-induced marker, CD154, has been more commonly used for enrichment of antigen-specific CD4+ T cells. Also referred to as CD40 ligand (CD40L), CD154 is a member of the tumour necrosis factor receptor (TNFR) superfamily that exists as both a transmembrane homotrimeric protein complex, and as a soluble receptor. While the predominant cell type for expression of CD154 is activated CD4+ T cells, CD154 is also expressed on activated B cells, CD8+ T cells (Hermann et al., 1995), platelets, monocytes, DC (Ma and Clark, 2009), eosinophils and natural killer cells. Although not currently available as a clinical or GMP-grade reagent, CD154 enrichment kits have demonstrated efficient isolation of CMV VST (Frentsch et al., 2005, Chattopadhyay et al., 2006), HIV VST (Chattopadhyay et al., 2006), and ADV VST (Bacher et al., 2013). Furthermore, CD154 selection has proven a successful protocol to enrich for rare WT1-specific CD4+ T cells allowing investigation into the lesser-studied tumour specific CD4 T cell responses (Schmied et al., 2015). Since CD154 expression is not biased to a particular CD4 cytokine-producing Th subset, CD154 selection has also been used to isolate bacterial (tetanus) and fungal (*A. fumigatus, C. albicans*) antigen-specific CD4+ T cells (Bacher et al., 2013). This study comparing CD154 enrichment of antigen-specific T cells between tetanus, *A. fumigatus*, *C. albicans*, CMV and ADV antigen stimulations showed expanded lines had recall cytokine reactivity expected of the subset, i.e. tetanus lines produced high levels of IL-4, IL-5 and IL-13 characteristic of Th2 cells, whereas *C. albicans* lines produced high levels of IL-17 and IL-22 typical of Th17 cells. Interestingly, upon antigen recall the enriched and expanded T cell lines for all antigens had highest reactivity by way of TNF-α production and CD154 expression, whereas IFN-γ production characteristic to Th1 responses was limited only to the CMV and ADV lines. This demonstrates the advantages of both CD154 and TNF-α selection methods in applications to enrich for the total population of antigen-specific CD4+ T cells with unbiased Th subsets. Our initial screening of convalescent donor T cell responses to SARS-CoV-2 peptides indicated using CD154 selection gave the highest frequency of antigen-reactive T cells (refer to Chapter 4), suggesting IFN-γ detection and selection may only be selecting a subset of the full population of SARS-CoV-2 VST.

It was therefore the aim of this chapter to investigate different markers of SARS-CoV-2 T cell memory response and compare isolation and expansion of SARS-CoV-2 VST based on these chosen selection markers.

5.2 Comparing markers for detection of SARS-CoV-2 VST

The ability to detect and quantify virus-specific T cells is imperative to understanding mechanisms of cellular response and protection, as well as dysregulation to viral infections. The gold standard methodology for the detection of antigen-specific T cells is through staining with fluorochrome-conjugated peptide-MHC multimers which allow binding of the particular antigenic sequence to their cognate T cell antigen receptor. Since soluble peptide-MHC complexes have fast dissociation rates and low avidity to TCR, it is difficult to detect antigen-specific T cells using soluble peptide-MHC monomers. Multimeric peptide-MHC complexes were therefore developed that can bind more than one cognate TCR and generate higher avidity and slower dissociation rates (Altman et al., 1996). While use of tetramers is more commonly reported, peptide-MHC dimers, pentamers and dextramers also have relevance in detection of antigen-specific T cells dependent on affinity and avidity of the TCR in question (Chang, 2021). Since multimer binding to TCR is independent of T cell activity, this is considered the most accurate method to detect and quantify all, even functionally inactive, antigen-specific T cells. However, HLA allele restriction limits the use of this approach in high-throughput screening of multiple individuals. Also in terms of detection of virus-specific T cells, the delineation into individual viral antigen peptide-MHC complexes adds additional cost and complexity that may obscure the overall responses to the virus. Other assays rely on functional responses to antigenic stimulation, thereby requiring a pre-incubation with peptide antigens, whole proteins or viral-infected cells and interaction with appropriate antigen-presenting cells. Readouts of the T cell response can then be made by assaying cell proliferation, cytokine ELISPOT, intracellular cytokine release (ICR), or activation-induced marker (AIM) expression.

T cell proliferation assays are typically performed by antigen stimulation of peripheral blood cells for 4-7 days; followed by measurement of proliferation by either uptake of radiolabelled-thymidine using radioactivity beta counter (Di Blasi et al., 2020), or dilution of a membrane-bound proliferation dye such as carboxyfluorescein succinimidyl ester (CFSE) or less toxic dye CellTrace using flow cytometry (Ten Brinke et al., 2017). Indeed a T cell proliferation assay using incorporation of H^3-thymidine following a 5 day PBMC stimulation with SARS-CoV-2 peptide pools was validated for detection of SARS-CoV-2 VSTs (Chu et al., 2022). This

study reports assay specificity of 100% and sensitivity of 95.7% when comparing T cell response versus IgG (spike1) antibody titre of vaccinated and unvaccinated health care worker cohorts. To achieve assay specificity of 100%, the T cell proliferation index was set at a threshold based on the control cohort of 88 non-vaccinated patients without evidence of SARS-CoV-2 infection, however this approach does not account for potentially exposed but asymptomatic individuals or individuals with cross-reactive immunity to other coronaviruses. However, there is a clear discrimination between vaccinated versus infected participants using this assay by comparing T cell proliferation to only spike peptide pools; or spike, nucleocapsid and membrane peptide pools respectively. In addition, the data extrapolated from these assays are limited since the assay by nature directly induces proliferation of the responding cells, and therefore the initial frequency or count of antigen-specific T cells in the original sample cannot be quantified (Poloni et al., 2023). These assays are however advantageous for applications requiring higher sensitivity such as for weakly immunogenic antigens due to the ability to amplify the T cell responses over an extended time. In this way, T cell proliferation for 7 days showed responses to S1 and S2 subunits of spike in healthy seronegative individuals likely suggestive of weakly cross-reactive memory responses to seasonal coronaviruses, which was undetectable using an ELISPOT assay (Ogbe et al., 2021).

ELISPOT assays are widely utilised across the field to detect T cell response to antigenic stimulation by production of a cytokine, most commonly IFN-γ. In this method, a monolayer of cells are plated in wells with membrane-bound IFN-γ antibody. Following antigenic stimulation, an enzyme-conjugated detection antibody and chromogenic substrate are added, inducing a precipitation of colour dots around a specifically stimulated cell (Leehan and Koelsch, 2015). Wells can then be analysed manually by light microscope or using an automated ELISPOT reader to quantify the number of spot-forming units (SFU). A study testing the use of commercial ELISPOT assay against Spike S1 and Nucleocapsid peptide pools (*T-SPOT.COVID,* Oxford Immunotec) demonstrated higher sensitivity (98.4%) to detect infected participants compared to SARS-CoV-2 serology testing (82.8%) within 2-8 weeks following NAAT diagnosis (Kruse et al., 2021). ELISPOT assays can also measure dual cytokine secretion, such as the FluoroSpot SARS-CoV-2 assay detecting IFN-γ and IL-2 response as a diagnostic tool with 92-96% sensitivity depending on patient cohorts (Mangsbo et al., 2021). While a limitation of ELISPOT assays using whole blood or

PBMC samples is the inability to delineate responses by particular cell types, pre-depletion or enrichment techniques can be incorporated. Prior CD4 or CD8 depletion of PBMCs with IFN-γ ELISPOT indicated responses to Spike, Non-Structural 8 (NS8), Membrane and Nucleocapsid were dominated by CD8-depleted PBMC to infer responses mediated by CD4 T cells (Cassaniti et al., 2021). While a major advantage of ELISPOT assays are high sensitivity of detection at very low cell numbers (as low as 200,000 PBMC), limitations include the inability to detect more than two cytokines, inability to further distinguish or phenotype different cellular subsets, and subjectivity in SFU threshold detection (Law and Watts, 2023).

Flow cytometry-based stimulation assays with readouts of intracellular cytokine release (ICR) or T cell activation-induced markers (AIM) assays address the limitations associated with ELISPOT. Through multi-parameter panel design additional markers can be incorporated to identify T cell subsets including CD2, CD3, CD4, CD8, TCR-αβ, TCR-γδ and CD56, etc. Our group has also previously reported incorporation of T cell memory markers CCR7, CD45RA and CD45RO as a method to phenotype different memory T cell subpopulations and the cytokine responses to stimulation (Cooper et al., 2021). Combining phenotyping with intracellular cytokine staining means consideration must be given to choosing markers unaffected by cell activation, or fixation and permeabilisation steps of the protocol. Broad profiling of multiple cytokines can allow classification of responses to particular T cell subsets. While antiviral CD4 T cells are typically Th1, flow cytometry panels incorporating cytokines for Th2, Th9, Th17 and Tfh subsets have confirmed that SARS-CoV-2 responses in peripheral blood are generally driven by Th1 effector cytokines IFN-γ, TNF-α and/or IL-2 (Rodda et al., 2021, Rodda et al., 2022). Spike-specific circulating Tfh cells were also reported to correlate with neutralizing antibody titre in individuals post-vaccination, with Tfh cell memory responses stable for up to a year (Rodda et al., 2021). While the majority of ELISPOT assays assess IFN-γ responses only, ICR assays of COVID-19 patients following peptide stimulation indicated IFN-γ as the dominant cytokine produced in CD8 T cells, whereas TNF-α responses were higher in CD4 T cells (Peng et al., 2020). Similarly, the frequency of peptide-responsive CD4 T cells secreting TNF-α or IL-2 was higher than IFN-γ in convalescent individuals, whereas TNF-α and IL-2 responses were both negligible in the CD8 compartment (Sekine et al., 2020). While another study confirmed higher frequency of TNF-α-reactive than IFN-γ-reactive cells in both CD4 and CD8 subsets by ICR,

concentration of IFN-γ [pg/mL] secreted in response to SARS-CoV-2 peptide stimulation was 10x fold higher than TNF-α concentration when measured by Luminex (Bonifacius et al., 2021). This indicates more potent secretion of IFN-γ in peptide-reactive cells despite the lower number of cells producing IFN-γ. Our initial study into convalescent donor responses (summarised in Chapter 4) also confirmed a higher frequency of TNF-α than IFN-γ responses to SARS-CoV-2 peptides in CD4 and CD8 T cells (Cooper et al., 2020). While ICR assays are useful for quantifying frequency or absolute count of cytokine-secreting antigen-specific T cells, kinetics of production are complex and delineation into individual cytokines may underestimate the number of total activated T cells.

Flow cytometric AIM assays can have advantages over ICR by using surface markers to detect antigen-specific T cells without the complexity/ timespan of intracellular staining. Numerous surface markers are upregulated on antigen-specific T cells upon TCR stimulation including CD69, CD107a, CD134, CD137, and CD154. Signalling of TCR particularly on CD8+ cells induces upregulation of CD69, the type II C-lectin receptor, whereby surface expression peaks at 16 hours post-stimulation. However CD69 can also be expressed on subsets of NK cells, B cells or Tregs and therefore for detection of antigen-specific T cells should be used in conjunction with another activation marker (Wu et al., 2019). Conversely, CD134 (also known as OX40) expression is limited to activated CD4+ T cells in humans that is tightly regulated by TCR signalling and CD28/ IL-2 and IL-4 co-stimulatory signalling (Redmond et al., 2009). Expression of CD134 however peaks between 48-72 hours following antigen recognition and can be used to detect multiple Th subsets including Th1, Treg and Tfh cells. As previously discussed, CD137 (also known as 4-1BB) is upregulated on antigen-specific T cells following binding to CD137L on APC during TCR activation. It is a useful AIM since upon antigenic stimulation as it induces survival signals and drives proliferation of activated T cells (Watts, 2005). With similar kinetics to CD69, CD137 expression peaks at 16-24 hours following activation, co-expression of CD69+ CD137+ is commonly used for CD8+ antigen-specific T cell detection assays (Wu et al., 2019). A study investigating SARS-CoV-2 Spike-specific T cell responses observed intracellular staining of CD69+ CD137+ T cells was concordant with Th1 cytokine+ (IFN-γ, TNF-α and/or IL-2) cells (Altosole et al., 2023) indicating this as a surrogate assay for VST detection. Similarly in a study testing numerous AIM markers, the highest frequency of Spike-specific cells was detected using co-expression of CD69 &

CD137, whereas combinations including CD25 or CD134 did not identify the maximal number of reactive cells (Gatti et al., 2023). Spike-reactive T cells were also detected in more convalescent individuals using AIM CD69/CD137 co-expression (14/22 subjects) compared to QuantiFERON IFN-γ ELISA (10/22 subjects) indicating a higher assay sensitivity with AIM. A further TNF superfamily member CD154 as described earlier is primarily expressed on activated CD4+ cells and to some extent on CD8+ cells, with peak surface expression at 6 hours following stimulation. This marker is usually co-expressed on T cells that produce large amounts of effector cytokines and/or have diverse cytokine profiles upon antigen recognition and therefore is useful for detecting different effector T cell subsets (Chattopadhyay et al., 2006). Given different AIM markers are often skewed to expression on either CD4+ or CD8+ cells, it is important to incorporate multiple AIM into analyses to understand the breadth of T cell subset responses. Combination of surface and intracellular staining protocols, with optimised assay durations for peak expression of markers, large flow cytometry panels with numerous AIM and cytokines can comprehensively delineate the multitude of functional, or more interestingly, dysfunctional SARS-CoV-2 T cell responses (Dan et al., 2021, Rydyznski Moderbacher et al., 2020).

5.2.1 Optimal markers for VST responses to SARS-CoV-2 peptides

During the first wave of the pandemic, our initial screening using a combination of antigen-specific T cell markers including IFN-γ, TNF-α, IL-2 and CD154 on n=15 convalescent donors indicated highest detection of SNM-reactive T cells using CD154 expression (see **Figure 4.11**). Following from this initial study, numerous donors recruited through the convalescent plasma programme were screened for T cell responses to select optimal donors for SARS-CoV-2 VST bank manufacture. It was also important to continue testing responses with multiple markers and cytokines to understand the kinetics and different responses of circulating SARS-CoV-2 VST to emerging new variants as well as vaccines. Between August 2020-April 2021 a total of 109 donors were screened, with n=46 demonstrating detectable SNM-specific T cells using the intracellular staining assay as shown in **Figure 5.1**.

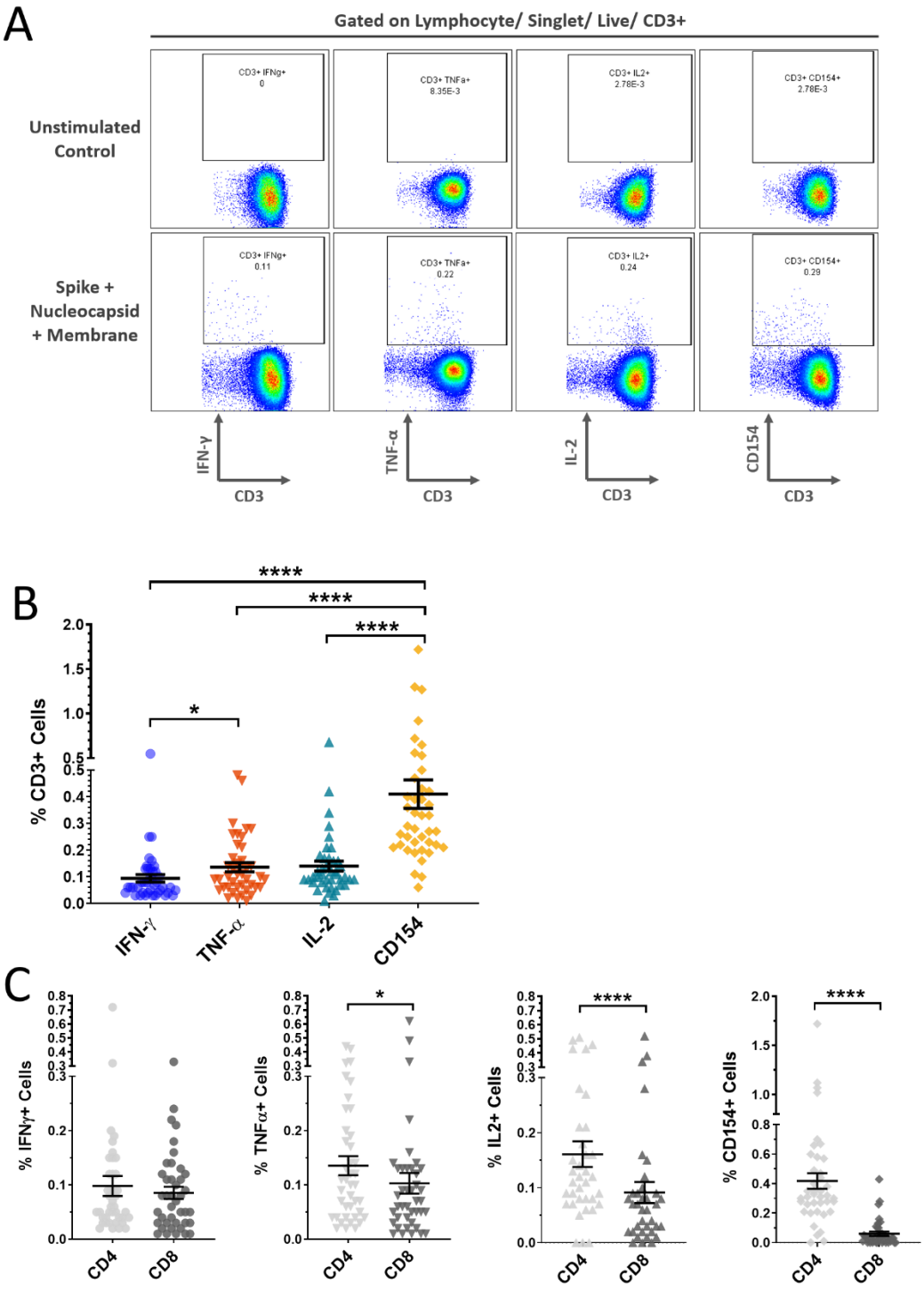

Figure 5.1 - CCD T cell responses to SARS-CoV-2 peptides in peripheral blood.

Buffy coat-derived PBMCs were incubated with SARS-CoV-2 peptides (Spike + Nucleocapsid + Membrane) for 5 hours and corrected against an unstimulated control well for expression of T cell effector markers: IFN-γ, TNF-α, IL-2 and CD154. **(A)** All flow analyses were gated for lymphocytes/ singlets/ live cells/ CD3+ and subsequently gated for IFN-γ, TNF-α, IL-2 or CD154 expression. **(B)** The percentage of CD3+/IFN-γ+, CD3+/TNF-α+, CD3+/IL-2+ and CD3+/CD154+ cells reactive to SARS-CoV-2 peptides was compared for n=46 CCD. Statistical significance between groups used repeated measures one-way ANOVA with the Geisser-Greenhouse correction. **(C)** Further subdivision of SARS-CoV-2 peptide responses into CD4 T cells and CD8 T cells demonstrated TNF-α, IL-2 and CD154 peptide-specific expression was significantly higher in CD4+ cells than CD8+ cells. Data is represented as mean ± SEM. Statistical significance between CD4 and CD8 responses were determined using paired t-tests, where p*<0.05 and p****<0.0001.

To identify SNM-reactive T cells within the PBMC population **(Figure 5.1A),** flow analyses were subject to initial gating of lymphocytes/ singlets/ live cells, followed by gating on CD3+ T cells. Gated T cells were then assessed for either IFN-γ, TNF-α, IL-2 or CD154 expression by quantifying marker acquisition in SNM-treated sample minus the unstimulated (DMSO only) to control for DMSO in the peptide formulation. The calculated frequency of reactive T cells to SNM peptides for each marker (**Figure 5.1B**) indicated the frequency of CD154-reactive T cells was significantly higher compared to all the cytokine-reactive cells ($p<0.0001$ each for IFN-γ, TNF-α and IL-2 comparisons). IFN-γ was the lowest expressed marker on reactive T cells, with the IFN-γ-reactive T cell frequency significantly lower than TNF-α-reactive T cells ($p=0.0249$). To understand differential marker expression within T cell compartments, CD3+ T cells were sub-gated into CD4+ or CD8+ T cells to compare responses (**Figure 5.1C**). While the frequency of IFN-γ-reactive T cells was equivalent between CD4 and CD8 cells; TNF-α ($p=0.0144$), IL-2 ($p<0.0001$) and CD154 ($p<0.0001$) expression was significantly higher on CD4+ compared to CD8+ T cells. This indicates that CD4 SARS-CoV-2-reactive T cells are the principal secretors of TNF-α and IL-2 cytokines and co-express CD154.

The frequency of SARS-CoV-2 T cells in peripheral blood was also tested for correlations with other infection factors/ donor characteristics (**Figure 5.2**). To this end, the frequency of CD3+/IFN-γ+ (blue), CD3+/TNF-α+ (red), CD3+/IL-2+ (teal) and CD3+/CD154+ cells (yellow) cells was assessed for relationship with (**A**) SARS-CoV-2 antibody titre, (**B**) days from symptoms resolution to donation, and (**C**) donor age. Although there was a significant positive correlation between the frequency of CD3+/IFN-γ+ SARS-CoV-2 VSTs and antibody titre was seen in the first wave donor cohort ($n=15$, $p=0.0381$, see **Figure 4.11**), this finding was not replicated in the later larger donor cohort. Furthermore, antibody titre did not correlate with SARS-CoV-2 VST using any of the detection markers tested (**Figure 5.2A**). Similarly the days from resolution of symptoms to donation had a significant negative correlation with CD3+/IFN-γ+ SARS-CoV-2 VSTs in the first wave cohort ($n=15$, $p=0.0021$), however no correlations were observed in the current donor cohort for the detection markers tested (**Figure 5.2B**). Donor age also showed no associations with frequency of CD3+/IFN-γ+, CD3+/TNF-α+, CD3+/IL-2+ or CD3+/CD154+ SARS-CoV-2 VSTs (**Figure 5.2C**).

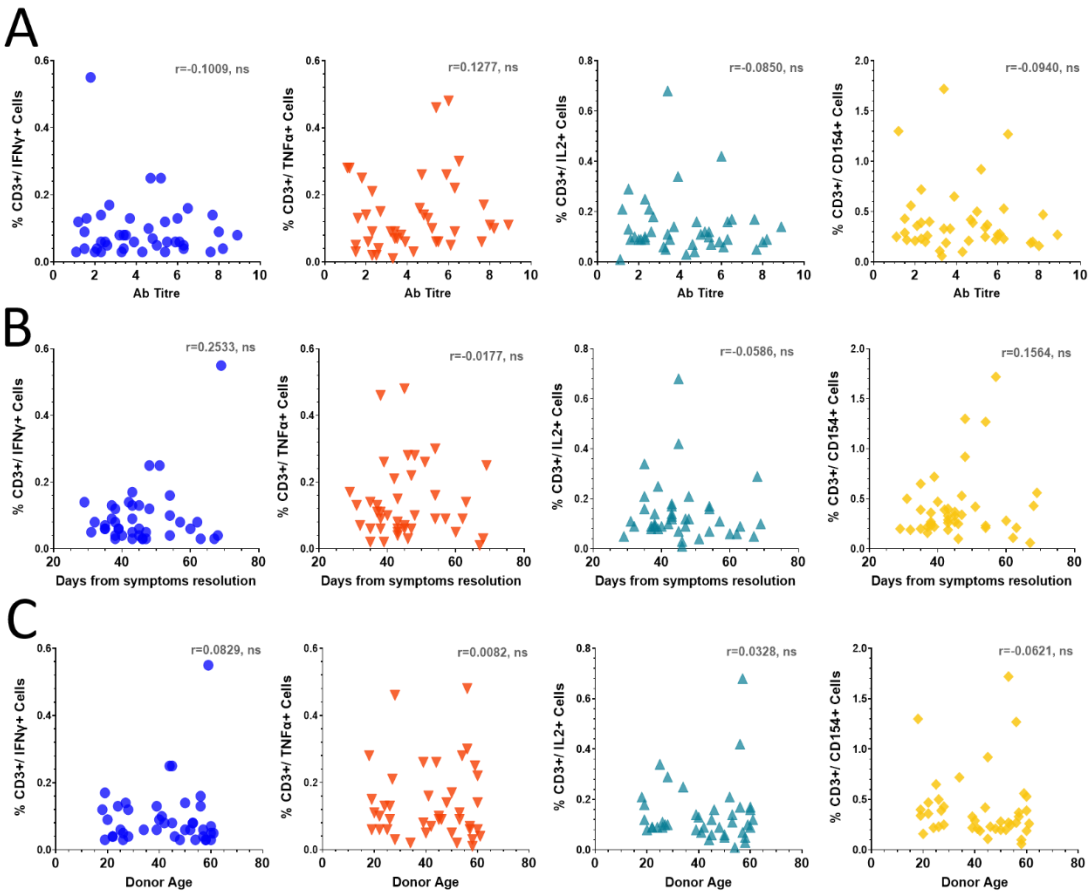

Figure 5.2 - SARS-CoV-2 T cell responses correlations with Ab titre, DFSR and donor age.

Buffy coat-derived T cell responses to SARS-CoV-2 peptides (Spike + Nucleocapsid + Membrane) were assessed for associations with other donor or infection parameters. The frequency of SARS-CoV-2 VSTs was measured for each marker: CD3+/IFN-γ+ (blue circles), CD3+/TNF-α+ (red triangles), CD3+/IL-2+ (teal triangles) and CD3+/CD154+ cells (yellow diamonds). Reactive T cell frequencies were tested for correlations against **(A)** antibody titre at donation measured by EuroImmun, **(B)** number of days from resolution of symptoms to donation, and **(C)** donor age. Calculation was performed using Pearson correlation coefficient. For each correlation test, the r value and p value are reported where p>0.05 was non-significant (ns).

The change in correlations between the two donor cohorts may simply be due the different cohort sizes (n=15 versus n=46), however a number of variables may also be impacting the results. Firstly, in the first wave cohort where donor blood was collected between April to June 2020, it was highly likely these donors had been exposed to SARS-CoV-2 once. However, with the latter cohort collected between August 2020-April 2021, it is impossible to know the number of antigen re-exposures these donors may have had, or if they had an asymptomatic re-exposure close to their time of donation, which may lead to peak or contractions of T cell/ antibody responses. Additionally different variants emerged over 2020-2021 which may have affected the kinetics of T cell responses to the original SARS-CoV-2 peptide pools used in this assay.

5.3 Isolation of SARS-CoV-2 VST using differential marker expression

Initial development of SARS-CoV-2 VST generation for potential therapeutic use was done using IFN-γ CCS and rapid culture expansion (see **section 2.3.5**) since IFN-γ CCS reagents are GMP-compliant and CE-marked for *in vitro* isolation of cells for clinical use. Given the screening data above actually suggests IFN-γ viral-specific T cell response is generally lower than that of TNF-α and CD154, isolation of SARS-CoV-2 VST was also tested using these markers. For direct comparison studies, leukapheresis starting source material was stimulated for 5 hours with pooled SNM peptides, and following stimulation cells were equally divided into three to isolate in parallel by (1) IFN-γ CCS, (2) TNF-α CCS, and (3) CD154 standard magnetic bead enrichment. Note, leukapheresis was used at this stage of development to allow full-scale manufacturing runs using the CliniMACS Prodigy, but since leukaphereses are such large white cell donations, plenty of residual WBC were available for use in research in these small-scale comparison studies. Ethics were in place to utilise this material from the donors. For the remainder of this chapter, groups are colour coded as follows: IFN-γ-isolated (blue), TNF-α-isolated (red) and CD154-isolated (orange).

5.3.1 Optimisation of CD154 sort for SARS-CoV-2 VST

The protocol for cytokine capture selection for IFN-γ and TNF-α is identical except for the use of the respective IFN-γ or TNF-α double-ended antibody catch matrices, and IFN-γ or TNF-α-conjugated microbeads for the labelling steps. Since CD154 is expressed at the cell surface, it can be used to isolate cells using the direct antibody-conjugated microbead magnetic selection. To this end, after the 5 hour stimulation of donor leukapheresis cells with the pooled SNM peptides, a third of cells were taken for CD154 sorting and labelled with CD154-Biotin-conjugated antibody, followed by labelling with anti-Biotin microbeads. Overall, this procedure is similar to the CCS protocol, however does not include the initial 1 hour cytokine secretion and 'catch' step required for the CCS assay.

Since activation-induced expression of CD154 on T cells is transient, with rapid internalisation, degradation or secretion (Yellin et al., 1994, Graf et al., 1995); protocols have suggested use of a CD40 monoclonal blocking antibody to stabilise surface expression of CD154 throughout the stimulation period (Frentsch et al., 2005,

Chattopadhyay et al., 2006). While all CD154 detection results in this and previous chapters have been by intracellular staining, where intracellular CD154 expression is stabilised by Brefeldin A; surface staining with CD154 had not yet been done. Since an adequate surface expression of CD154 is required for isolation of CD154+ cells, addition of the CD40 blocking antibody was tested for improved detection and isolation of CD154+ cells. To this end, PBMCs were divided equally into the following conditions: addition of CD40 blocking antibody (+ CD40) or without addition of CD40 blocking antibody (control). Both conditions were then stimulated with SNM peptides for 5 hours, followed by labelling and isolation as according to the CD154 protocol (see **section 2.3.7**). A pre-sort sample was taken to compare detection of CD154 surface expression. As can be seen by flow cytometric analysis of the pre-sort samples (**Figure 5.3**), CD154 surface expression was distinctly increased by blocking CD40 (2.33% CD154+ T cells) compared to control (0.71% CD154+ T cells).

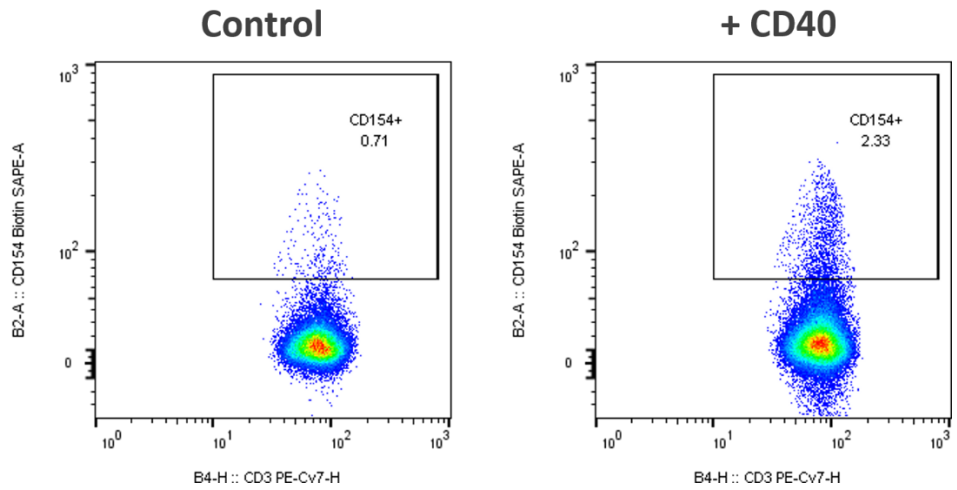

Figure 5.3 - CD154 surface expression comparison.

Donor C19UKD3 PBMCs were stimulated for 5 hours with SARS-CoV-2 SNM peptides in two conditions: with addition of CD40 blocking antibody (+CD40) or with no additions to the culture stimulation (control). Flow cytometric analysis following stimulation and labelling with CD154-Biotin-SAPE shows surface expression of CD154 on CD3+ T cells between the two conditions. Analysis was subject to pre-sequential gating on lymphocytes/ singlets/ live / CD3+ cells.

Following magnetic selection, small samples of the target fractions from each condition were taken for count and phenotypic analysis. Flow cytometric analysis reveals CD154+ targets isolated with the addition of CD40 during stimulation had increased frequency of lymphocytes, CD3+ cells and CD4+ cells as compared to the control (**Figure 5.4**). As well as improved purity, cell concentration quantified by the MACSQuant10 counting function indicated improved CD3+ cell yield as well as frequency in the CD40 blocking antibody treated condition.

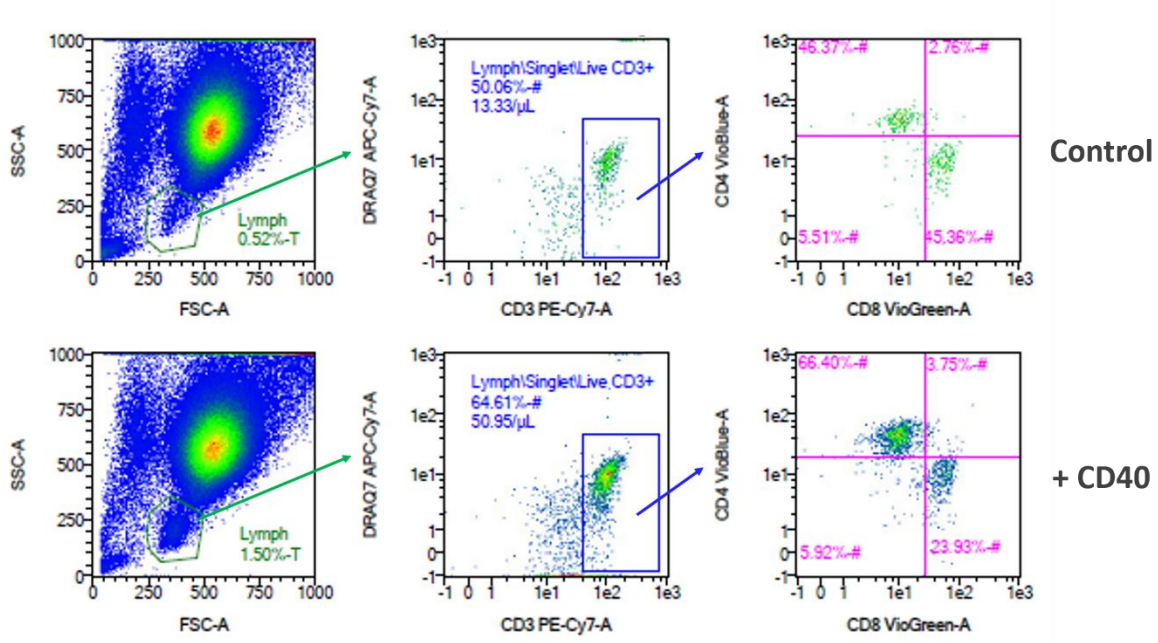

Figure 5.4 - CD154 isolation optimisation targets comparison.

Donor C19UKD3 flow analysis of CD154-isolated target cells. Top panels shows target of CD154 isolation with no additions to the culture stimulation (control); versus bottom panels show targets of CD154 isolation where CD40 blocking antibody was added prior to culture stimulation to prevent downregulation of CD154 during the stimulation period (+ CD40).

Given the improved detection and isolation of surface labelled CD154+ cells, addition of CD40 blocking antibody was used for all subsequent CD154 isolations.

5.3.2 Comparison of IFN-γ-, TNF-α- and CD154-isolated target cells

Intra-donor comparisons were made to test isolation of SARS-CoV-2 VST by the three different markers IFN-γ, TNF-α and CD154. While there was delay in getting reagents for CD154 isolations, the first three donors compared only IFN-γ versus TNF-α CCS. Donors and their sort comparisons for this chapter are listed in **Table 5.1**.

Donor	Sorts Tested
C19USA2	IFN-γ vs TNF-α
C19USA4	IFN-γ vs TNF-α
C19UKD1	IFN-γ vs TNF-α
C19UKD3	IFN-γ vs TNF-α vs CD154
C19UKD6	IFN-γ vs TNF-α vs CD154
C19UKD7	IFN-γ vs TNF-α vs CD154
C19UKD8	IFN-γ vs TNF-α vs CD154
C19UKD9	IFN-γ vs TNF-α vs CD154

Table 5.1 – Intra-donor SARS-CoV-2 VST sort comparisons.

Following the labelling procedures, all conditions were sorted through magnetic columns to separate unbound non-target cells (negative fraction), and magnetically bound target cells (positive fraction), with samples taken for counts and flow cytometry to assess the individual fractions.

Following magnetic separation, samples were taken to compare negative fraction and target cell fraction populations by flow cytometry. Due to very low cell numbers in the target fractions, post-sort cells were phenotyped and characterised using only one flow cytometry panel. Interestingly, based on scatter properties differences in monocyte and lymphocyte populations were observed between the different sorting markers. Using representative analysis from donor C19UKD7 for direct comparison (**Figure 5.5A**), CD154-isolated targets had a massively increased monocyte contamination compared to the IFN-γ-isolated and TNF-α-isolated targets. The frequency of lymphocytes was significantly higher ($p=0.0138$) in IFN-γ-isolated compared to CD154-isolated targets (**Figure 5.5B** – left panel). Conversely, the frequency of monocytes (middle panel) was significantly higher in CD154-isolated targets compared to both IFN-γ-isolated ($p=0.0012$) and TNF-α-isolated ($p=0.0012$) targets. In concordance to this result, the monocyte to lymphocyte ratio as calculated using percentage frequency (right panel) was significantly increased in CD154-isolated targets than both IFN-γ-isolated ($p=0.010$) and TNF-α-isolated ($p=0.00113$) groups. Since the percentage frequency could be skewed by presence of different forward scatter low populations (likely debris/ dead cells/ or red blood cells – see **Figure 5.5A**), direct comparison of the lymphocyte and monocyte populations were also made using absolute counts (**Figure 5.5C**). The absolute count of lymphocytes (left panel) was significantly increased in TNF-α-isolated compared to IFN-γ-isolated ($p=0.017$) and CD154-isolated targets ($p=0.049$). CD154-isolated targets had a significantly higher absolute count of monocytes (middle panel) than both IFN-γ-isolated ($p=0.0078$) and TNF-α-isolated ($p=0.0107$) targets. The monocyte to lymphocyte ratio as calculated using absolute count (right panel) was also significantly increased in CD154-isolated compared to IFN-γ-isolated targets ($p=0.107$) and TNF-α-isolated targets ($p=0.011$). Since the lymphocyte count is similar between the sorting methods, this supports that difference in frequencies and counts between the populations is due to heavy monocyte contamination in CD154 isolations.

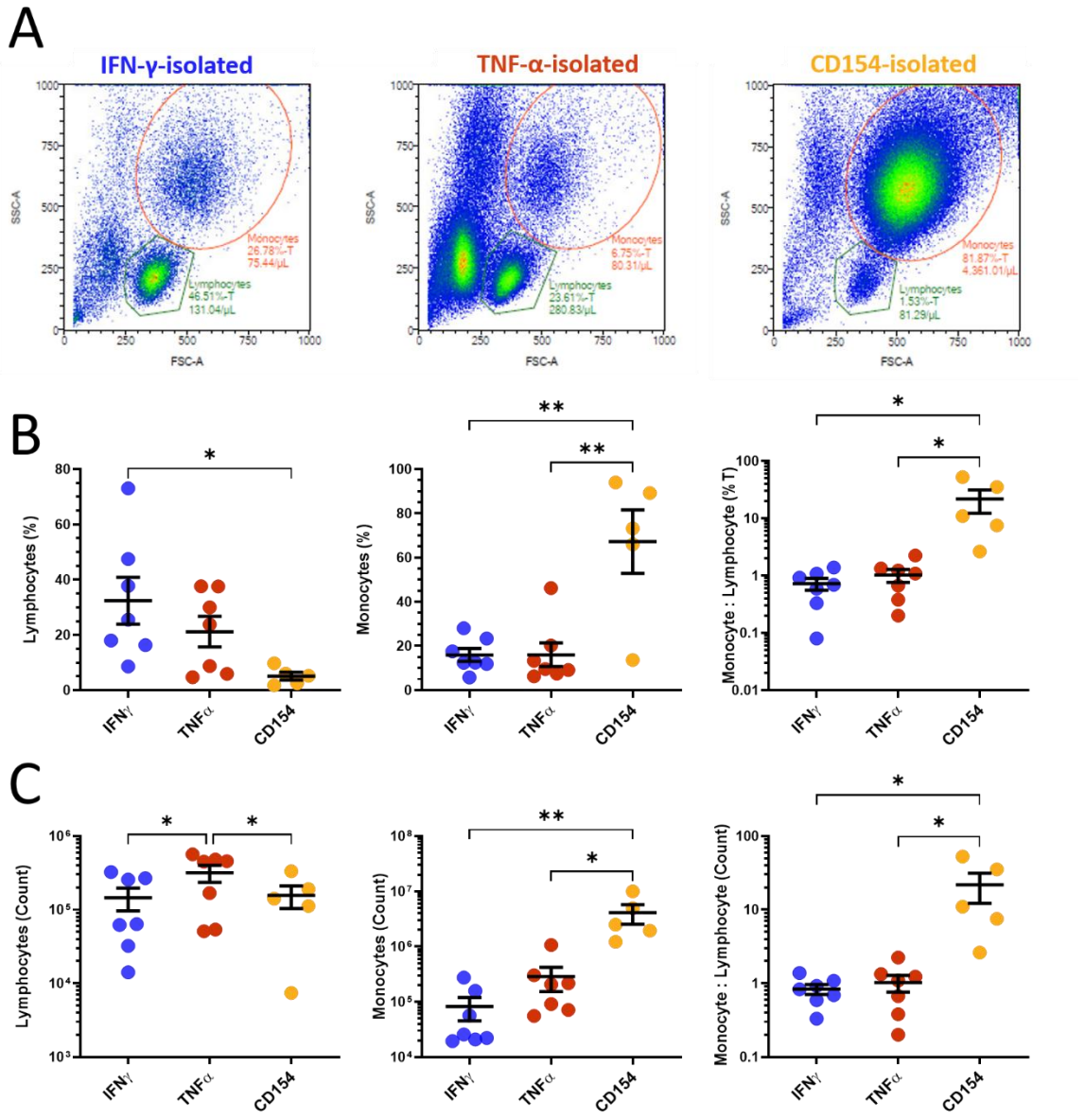

Figure 5.5 - Monocytes contamination in CD154 sorts.

Target positive fractions for each VST isolation were analysed for lymphocyte and monocyte content by flow cytometry. **(A)** Representative flow analysis for donor C19UKD7 shows higher frequency (%T) and count (cells/µL) of gated monocytes in CD154-isolated targets compared to IFN-γ-isolated and TNF-α-isolated targets. Matched donor analysis (n=7) of lymphocytes, monocytes and lymphocyte: monocyte ratio is compared between groups as both percentage frequency **(B)** and absolute count **(C)**. Data is represented as mean ± SEM. Comparisons between the three isolation groups were made using RM one-way ANOVA where *p≤0.05 and **p≤0.005.

Within the gated viable lymphocyte population, analyses of lymphocyte and T cell markers were made using the gating strategy outlined in **Figure 2.4** to identify CD3- CD56+ NK cells, CD3+ CD56+ NKT cells, and CD3+ CD56- T cells. T cells were then subgated for CD4+, CD8+, DP and DN T cells. Finally each CD4+ and CD8+ population was assessed for T cell memory as follows CD62L+ CD45RO- TNaive, CD62L+ CD45RO+ TCM, CD62L- CD45RO+ TEM and CD62L- CD45RO- TEMRA. Comparisons of population frequency between the three groups are shown in **Figure 5.6**.

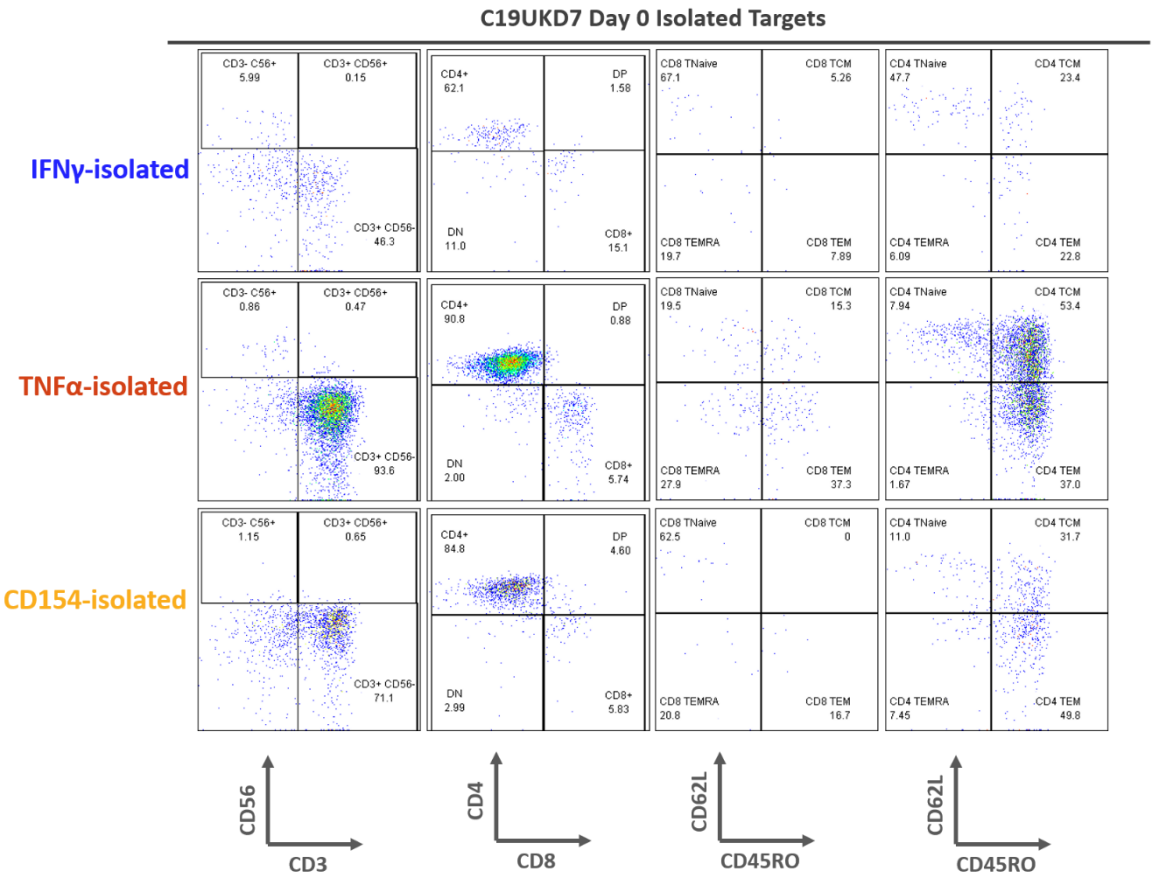

Figure 5.6 - Isolated targets flow representative analysis.

Representative flow gating analysis is shown for donor C19UKD7 of each IFN-γ-isolated, TNF-α-isolated and CD154-isolated target fractions. Analyses were subject to initial gating on lymphocytes/ singlets/ live cells. Lymphocyte populations were then identified as follows: NK cells (CD3+ CD56-), NKT cells (CD3+ CD56+), T cells (CD3+ CD56-), CD4 T cells (CD3+ CD56- CD4+ CD8-), CD8 T cells (CD3+ CD56- CD4- CD8+), DP T cells (CD3+ CD56- CD4+ CD8+) and DN T cells (CD3+ CD56- CD4- CD8-). In addition, each CD4 and CD8 T cell population was analysed for T cell memory subpopulations as follows: TNaive (CD62L+ CD45RO-), TCM (CD62L+ CD45RO+), TEM (CD62L- CD45RO+) and TEMRA (CD62L- CD45RO-).

Using this analysis, the mean population frequencies for all donors tested were compared between the groups in **Figure 5.7**. Of the total gated viable lymphocytes **(A),** overall percentages of CD45+ cells, NKT cells and NK cells were comparable between groups, however TNF-α-isolated targets had a significantly higher percentage (p=0.0167) of T cells compared to the IFN-γ-isolated targets. Of the CD3+ gated T cells **(B)**, TNF-α-isolated targets had a significantly higher frequency of CD4+ T cells (p=0.048) compared to IFN-γ-isolated targets. Correspondingly, the percentage of CD8+ T cells was significantly lower (p=0.0205) in TNF-α-isolated targets than IFN-γ-isolated targets. Within the CD4 compartment **(C),** TNF-α-isolated targets had a significantly higher (p=0.0214) frequency of central memory T cells (TCM) than IFN-γ-isolated targets. All other CD4+, and CD8+ **(D)** memory populations were similar between groups. These data indicate TNF-α isolation enriches for a purer population

of T cells skewed towards CD4+ central memory phenotype. This is not unexpected given the initial buffy coat T cell screening responses in **Figure 4.13** demonstrate a higher frequency of TNF-α+ cells are CD4 cells than CD8 cells, whereas IFN-γ+ cells had a fairly equal CD4:CD8 ratio. While CD154-isolated targets also trend towards CD4 subtype **(B)** which is not unexpected considering the CD154 molecule is predominantly expressed on CD4+ cells compared to CD8+ T cells or other lymphocytes (Banchereau et al., 1994, Cron, 2003), no statistical significance compared to IFN-γ or TNF-α groups was found. This may be due to the smaller sample size of the CD154 group.

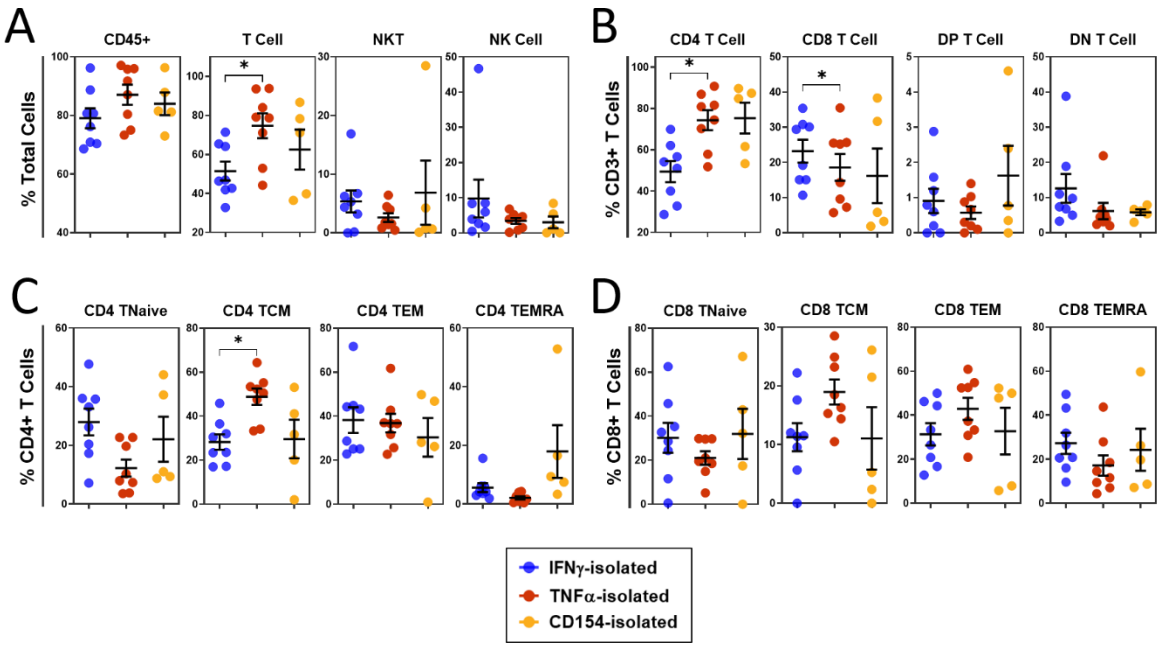

Figure 5.7 - Isolated targets phenotype comparison.

Gated viable lymphocytes of target samples were compared for the frequency of different phenotypic populations between IFN-γ-isolated (n=8), TNF-α-isolated (n=8) and CD154-isolated (n=5) groups. **(A)** Gating on total lymphocytes, groups were compared for CD45+ cells, T cells, NKT cells and NK cell frequency. **(B)** Gated T cells (CD3+) were then assessed for T cell subtypes: CD4, CD8, double positive (DP) and double negative (DN). Each CD4+ **(C)** and CD8+ **(D)** T cell population was further assessed for T cell memory populations: naïve (TNaive), central memory (TCM), effector memory (TEM), and terminally differentiated effector memory RA (TEMRA). Data is represented as mean ± SEM. Statistical significance was determined using RM one-way ANOVA with Geisser-Greenhouse correction where *p≤0.05.

To evaluate sort efficiency between the different isolation methods, counts were performed on all pre-sort and post-sort samples. The total number of viable cells in the target fractions was compared between sorting methods for each individual donor (**Figure 5.8A**), with a trend towards an increased number of target cells by TNF-α isolation. Although TNF-α isolation trended towards higher percentage yield of viable target cells normalised to each sort input (**Figure 5.8B**) no statistically

significant differences were seen between the groups. Concurrent with manual isolations with for each marker, donor leukaphereses were also screened for IFN-γ, TNF-α and CD154 expression in response to SARS-CoV-2 peptide stimulation using the intracellular cytokine screening assay. No significant correlation was observed between the percentage of peptide-responsive cells (by expression of each marker) and the actual yield of cells isolated from each respective marker sorted population (**Figure 5.8C**).

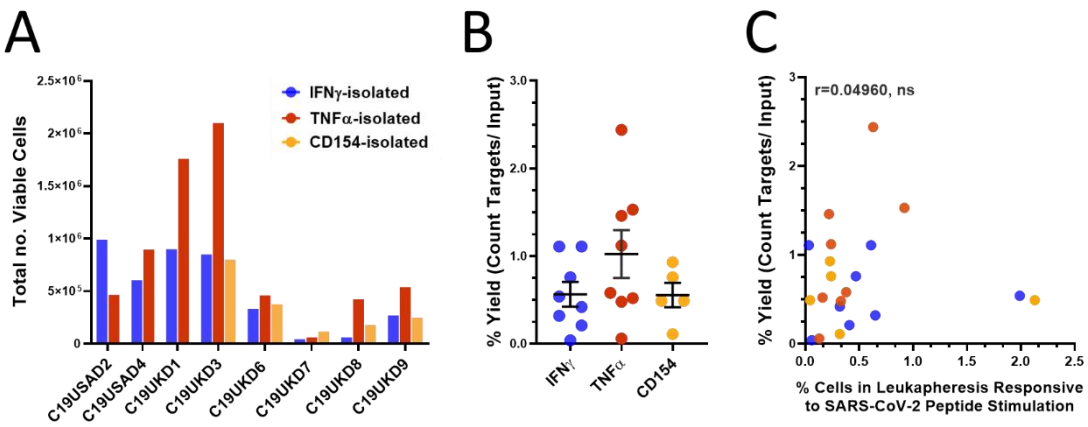

Figure 5.8 - IFN-γ-isolated, TNF-α-isolated and CD154-isolated targets yield comparison.

(A) The total number of viable cells in target fractions from the different isolations (IFN-γ, TNF-α, and CD154) is shown for each individual donor. **(B)** The percentage yield was calculated dividing the total viable cell count in target fractions by the input count for each sort. Data is represented as mean ± SEM and groups compared using RM one-way ANOVA. **(C)** The percentage yield of target cells from all sorts was assessed for correlation with the frequency of SARS-CoV-2 peptide-responsive cells within the leukapheresis starting material as determined using the intracellular cytokine screening assay. Statistical analysis was performed by generating Pearson correlation coefficients, where $p<0.05$ was considered significant.

Finally, the different isolated target populations were compared for purity and enrichment efficiency. Since the antibody microbeads for each method were conjugated to a phycoerythrin (PE) fluorochrome (IFN-γ-PE, TNF-α-PE or CD154-PE), the frequency of PE+ cells was quantified in the pre-sort, post-sort non-target and post-sort target fractions. The percentage of PE+ lymphocytes in the target fraction (**Figure 5.9A**) was highest in IFN-γ isolations at mean=39.53±11.3%. In CD154 isolations, the frequency of PE+ lymphocytes was significantly lower ($p=0.0127$) compared to IFN-γ indicating poorer enrichment using this marker. The absolute count of PE+ lymphocytes (**Figure 5.9B**) was comparable between the groups in both the non-target fraction and target fraction. Of note here, the count of PE+ lymphocytes in the non-target fractions for each sort were similar to the target fractions, showing many PE+ cells were not captured in the sorts. To measure this as

a percentage yield (**Figure 5.9C**), the absolute count of PE+ lymphocytes in the target fraction was divided by this count in both post-sort fractions (target + non-target). The mean percentage yield of PE+ lymphocytes was 49.13±12.8% and 52.37±10.4% for IFN-γ and TNF-α isolations respectively. CD154 isolations however had a significantly lower PE+ lymphocyte yield than both IFN-γ (p=0.025) and TNF-α (p=0.017) groups at a mean=7.5±4.9%. This indicates a much poorer enrichment efficiency in CD154 isolations with high counts of CD154+ cells remaining in the non-target fractions, as well as poorer overall CD154+ cell purity in the target fractions.

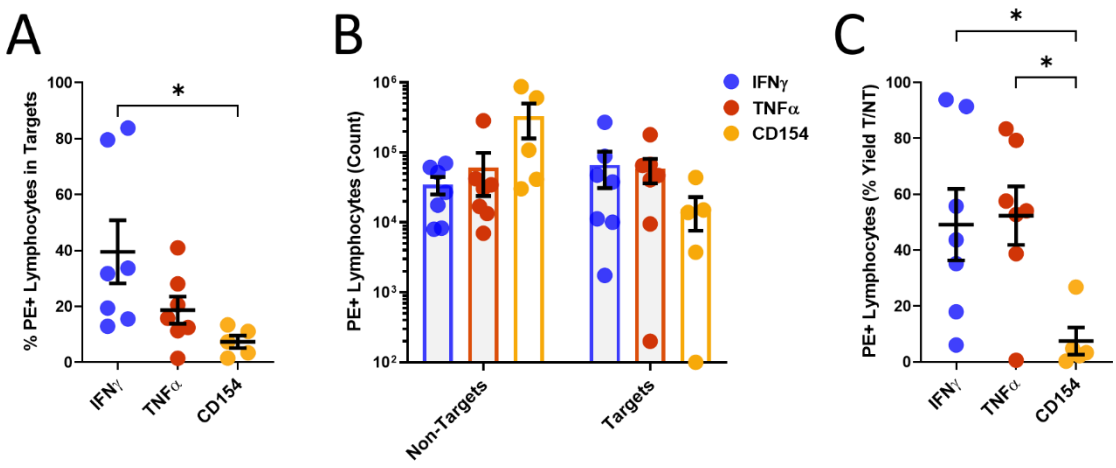

Figure 5.9 - IFN-γ, TNF-α and CD154 sort efficiency comparison.

Magnetic bead isolations were made with each sorting marker (IFN-γ, TNF-α orCD154) antibody conjugated to a PE fluorochrome, therefore samples were analysed for PE+ lymphocyte expression to measure target cell purity. **(A)** Comparison of percentage of PE+ lymphocytes within the post-sort target fraction was made between IFN-γ-isolated (n=8), TNF-α-isolated (n=8) and CD154-isolated (n=5) groups. **(B)** The absolute count of PE+ lymphocytes was compared for all marker groups in both the post-sort target cell fraction, and the post-sort unbound non-target cell fraction. **(C)** The percentage yield PE+ lymphocytes was compared between groups where yield was calculated as PE+ lymphocyte count (targets/ (targets + non-targets)). Data is represented as mean ± SEM. Comparisons between groups were made using RM one-way ANOVA where *p≤0.05.

5.3.3 Expansion of IFN-γ-, TNF-α- and CD154-isolated VST.

As described previously, since the SARS-CoV-2 VSTs are a rare cell population and isolation recovers a very small number of target cells (~10^6 cells), these cells have to be expanded post-sort to generate therapeutically relevant numbers. Therefore, the IFN-γ-isolated, TNF-α-isolated and CD154-isolated target VST were subsequently expanded using the SARS-CoV-2 VST culture expansion protocol described in Chapter 4. Briefly, isolated target cells were co-cultured with irradiated non-target cells from each sort in TexMACS medium supplemented with T-Liven [2%] and IL-2 [200

IU/mL] in G-Rex plates or flasks for 14 days, with feed and passage time-points at day 7 and 11.

Intra-donor direct comparisons of growth kinetics between IFN-γ-isolated, TNF-α-isolated and CD154-isolated VST are shown in (**Figure 5.10**). The individual donor growth curves (**Figure 5.10A**) indicate a similar growth profile between IFN-γ-isolated and TNF-α-isolated VST (n=4), however CD154-isolated VST show slightly improved growth curves (n=3). The fold expansion between day 0 targets and day 14 harvest (**Figure 5.10B**) was similar between groups, though TNF-α-isolated VST trended towards a lower fold expansion. Given the comparable harvest count between IFN-γ-isolated and TNF-α-isolated VST, this lower fold expansion likely reflects an initial higher TNF-α target lymphocyte count as demonstrated previously in **Figure 5.5C**. The fold expansion of all isolated targets was tested for correlation with the starting target cell count (**Figure 5.10C**), however starting number did not significantly relate to expansion scale. Overall no major differences in growth kinetics were seen between the different isolated VST.

Expanded target VST from each isolation were assessed for differences in phenotype and function. Using the flow cytometry surface phenotyping assay; lymphocyte, T cell subtypes and T cell memory populations were quantified as outlined in **Figure 2.4** and **Figure 2.5**. Intra-donor comparisons in population frequency were made, with representative donor C19UKD7 flow analysis at day 14 shown in **Figure 5.11**. All analyses were subject to initial gating on cells (debris excluded on basis of FSC/SSC), for singlets and viable DRAQ7- cells. Of note, IFN-γ-isolated VST contained larger populations of CD8+ T cells, and CD3- CD56+ NK cells, whereas TNF-α-isolated and CD154-isolated were much more enriched for CD4+ T cells.

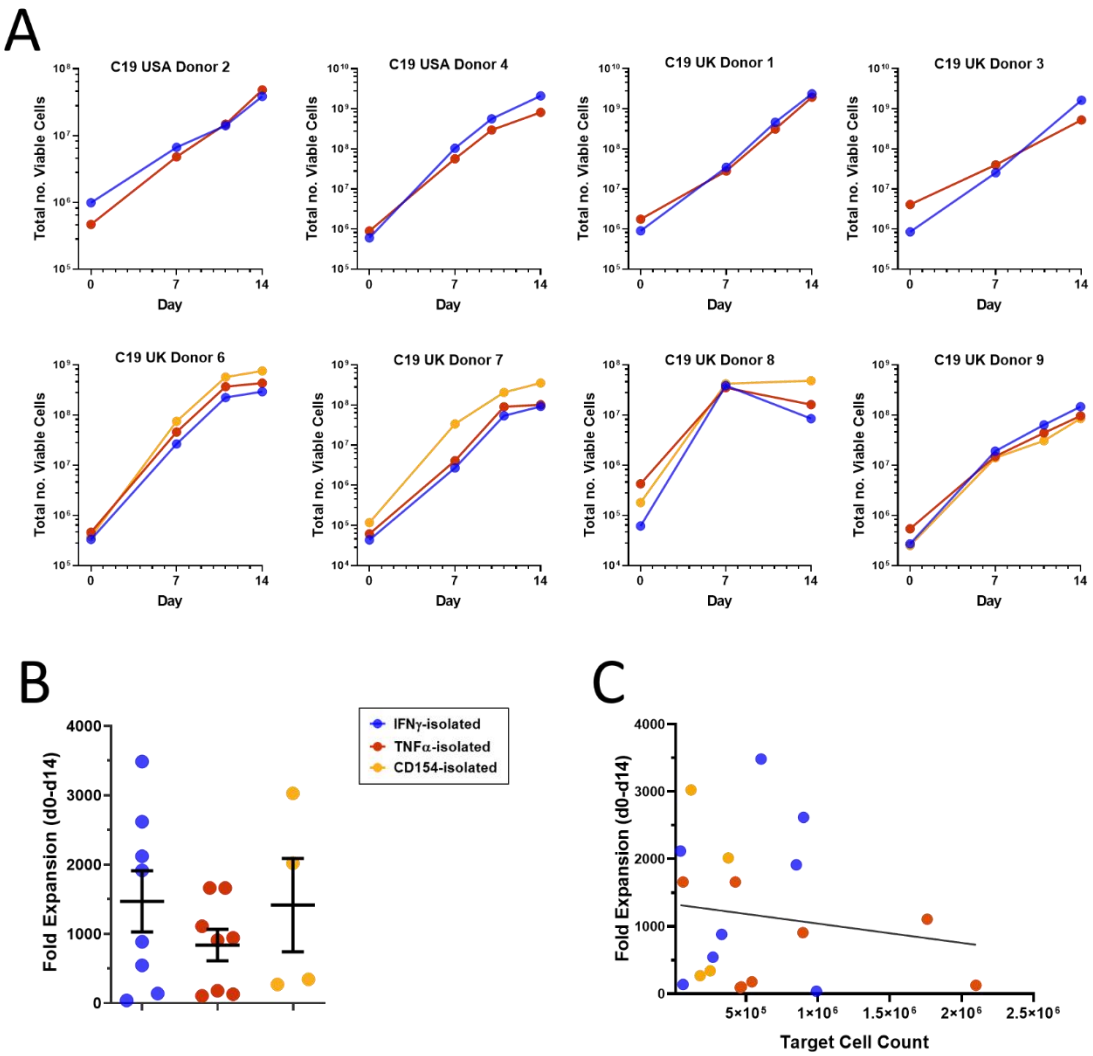

Figure 5.10 - IFN-γ-isolated, TNF-α-isolated and CD154-isolated VST culture growth curves.

SARS-CoV-2 target VST isolated by IFN-γ, TNF-α or CD154 expression were subsequently cultured for 14 days to drive VST expansion. **(A)** Intra-donor growth curves are shown for the different isolation methods of total viable cells from isolated targets at day 0 to day 14 culture harvest. **(B)** The fold expansion between day 0 targets and day 14 harvest was compared between the isolation groups. Data is represented as mean ± SEM and comparisons between groups made using RM one-way ANOVA. **(C)** The fold expansion in culture was tested for correlation with the absolute target cell count from each isolation. Statistical analysis was made by generating Pearson correlation coefficients.

Population frequencies of day 14 expanded VST were compared between the different isolation groups in **Figure 5.12**. Of the total gated viable cells (**Figure 5.12A**), groups were comparable showing high purity for CD45+ cells and T cells (CD3+ CD56-). The frequency of NKT cells (CD3+ CD56+) was also similar between the three isolation groups. Although there was no significant difference in NK cell (CD3- CD56+) frequency, two donors did have increased NK cell contamination in IFN-γ-isolated VST, probably because IFN-γ is an important anti-viral cytokine for NK cells (Sun et al., 2009). Within the gated CD3+ T cells (**Figure 5.12B**), the percentage of CD4+ T cells was significantly lower in IFN-γ-isolated VST compared to both TNF-

α-isolated (p=0.0177) and CD154-isolated groups (p=0.0297). Correspondingly, the frequency of CD8+ T cells was significantly higher in IFN-γ-isolated VST compared to TNF-α-isolated (p=0.0314) and CD154-isolated VST (p=0.02229). The IFN-γ-isolated group also contained a significantly higher population of DP T cells (CD4+ CD8+) compared to TNF-α-isolated VST (p=0.0476). The frequency of DN T cells was comparably low between the groups.

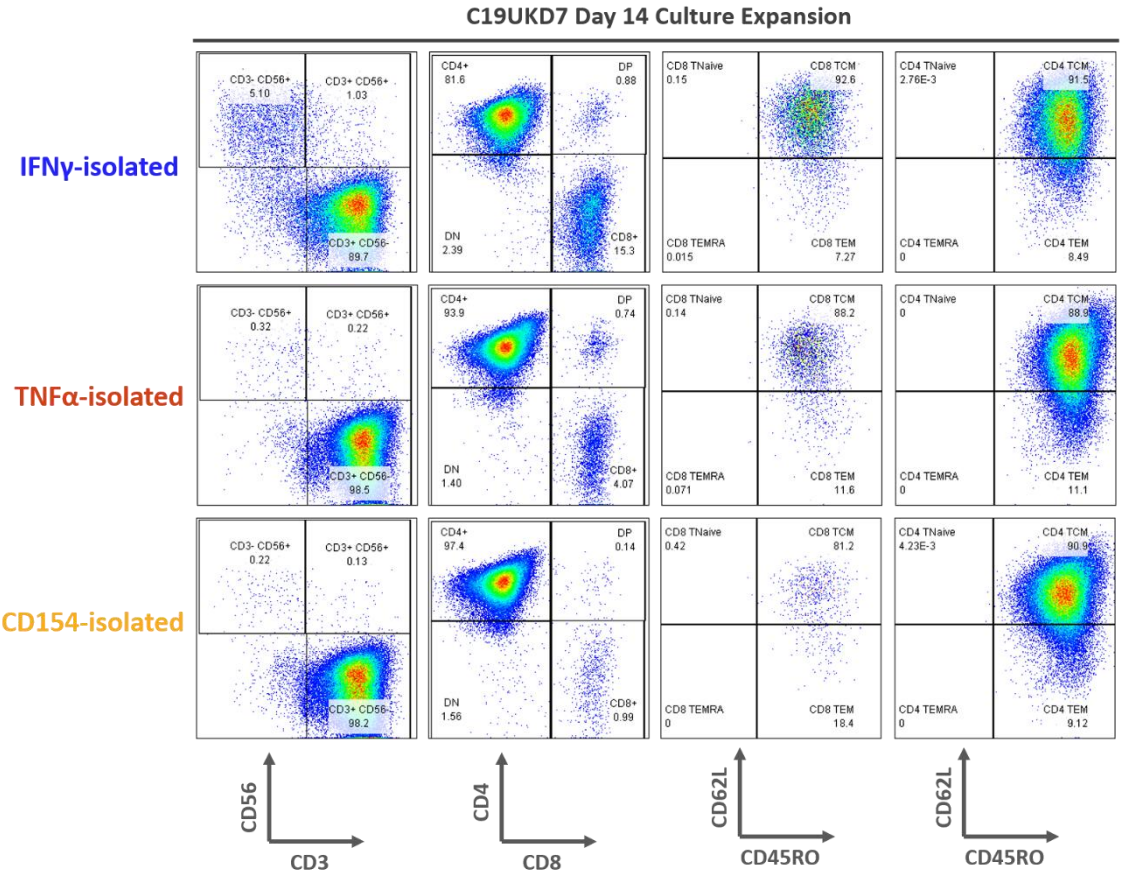

Figure 5.11 - Expanded VST flow cytometry representative analysis.

Representative flow gating analysis is shown for donor C19UKD7 of each IFN-γ-isolated, TNF-α-isolated and CD154-isolated VST expanded for 14 days in culture. Analyses were subject to initial gating on all cells/ singlets/ live cells. Lymphocyte populations were then identified as follows: NK cells (CD3+ CD56-), NKT cells (CD3+ CD56+), T cells (CD3+ CD56-), CD4 T cells (CD3+ CD56- CD4+ CD8-), CD8 T cells (CD3+ CD56- CD4- CD8+), DP T cells (CD3+ CD56- CD4+ CD8+) and DN T cells (CD3+ CD56- CD4- CD8-). In addition, each CD4 and CD8 T cell population was analysed for T cell memory subpopulations as follows: TNaive (CD62L+ CD45RO-), TCM (CD62L+ CD45RO+), TEM (CD62L- CD45RO+) and TEMRA (CD62L- CD45RO-).

Within the CD4+ compartment (**Figure 5.12C**), all groups contained negligible naïve T cells (TNaive) and terminally differentiated effector memory RA T cells (TEMRA). All groups were skewed toward central memory (TCM) phenotype, with a small population of effector memory T cells (TEM). Similarly within the CD8+ gated

population (**Figure 5.12D**) all groups were comparable with an enrichment of TCM and TEM, and negligible TEMRA or naïve T cells in the day 14 expanded VST.

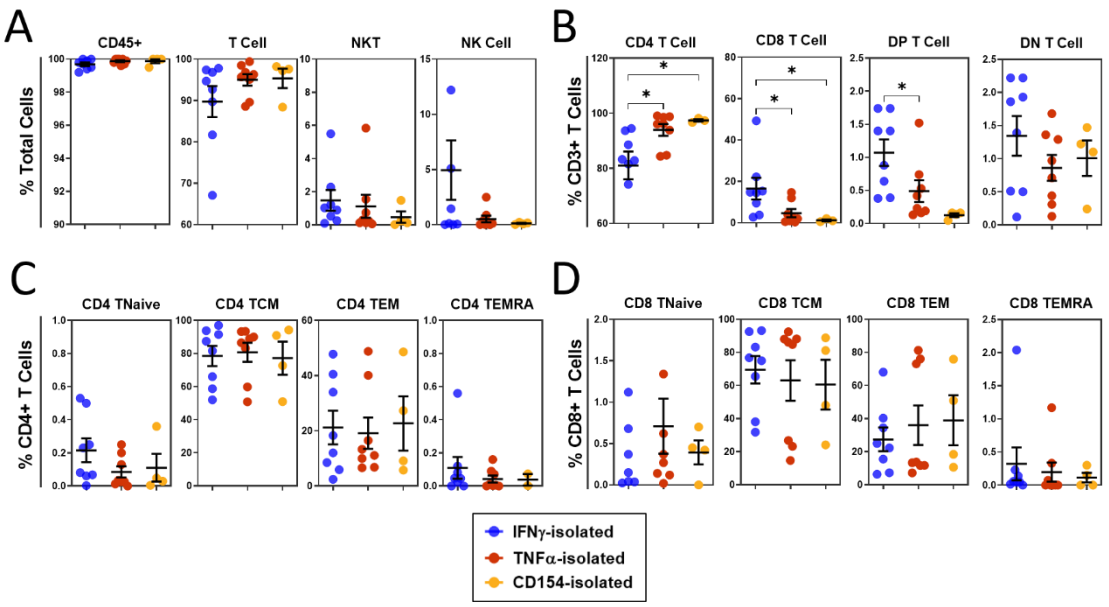

Figure 5.12 - Comparison of expanded VST final products phenotype.

VST expanded for 14 days in culture were compared for the frequency of different phenotypic populations between IFN-γ-isolated (n=8), TNF-α-isolated (n=8) and CD154-isolated (n=4) groups. **(A)** Gating on total lymphocytes, groups were compared for CD45+ cells, T cells, NKT cells and NK cell frequency. **(B)** Gated T cells (CD3+) were then assessed for T cell subtypes: CD4, CD8, double positive (DP) and double negative (DN). Each CD4+ **(C)** and CD8+ **(D)** T cell population was further assessed for T cell memory populations: naïve (TNaive), central memory (TCM), effector memory (TEM), and terminally differentiated effector memory RA (TEMRA). Data is represented as mean ± SEM. Statistical significance was determined using RM one-way ANOVA with Geisser-Greenhouse correction where *p≤0.05.

Day 14 expanded VST were also analysed by flow cytometry for expression of chemokine receptors as outlined in **Figure 2.7** to identify potential migratory mechanisms. The percentage expression of chemokine receptors tested on viable final product cells was compared between the isolation groups (**Figure 5.13**). Note, due to timeframe of these experiments only early donors were tested before addition of CD154 isolations to the study, therefore only IFN-γ-isolated and TNF-α-isolated groups were tested. Analyses were pre-gated on CD4+ **(Figure 5.13A)** and CD8+ **(Figure 5.13B)** cells to account for differences in CD4:CD8 ratio between IFN-γ-isolated and TNF-α-isolated VST as described above. CD4+ and CD8+ from both VST groups showed a consistently high level of expression (>50%) of CCR2, CCR4, CCR5, CXCR3, CXCR4 and CXCR6. Both groups also contained a small population of cells (10-30%) with positive expression of CCR6 and CCR7. There was negligible expression of CCR1, CCR3 and CXCR5 in the VST tested. No significant differences were observed in chemokine receptor expression between the groups. Expression was also comparable

between CD4+ and CD8+ cells except for a slightly higher expression of CCR4 on CD4+ T cells.

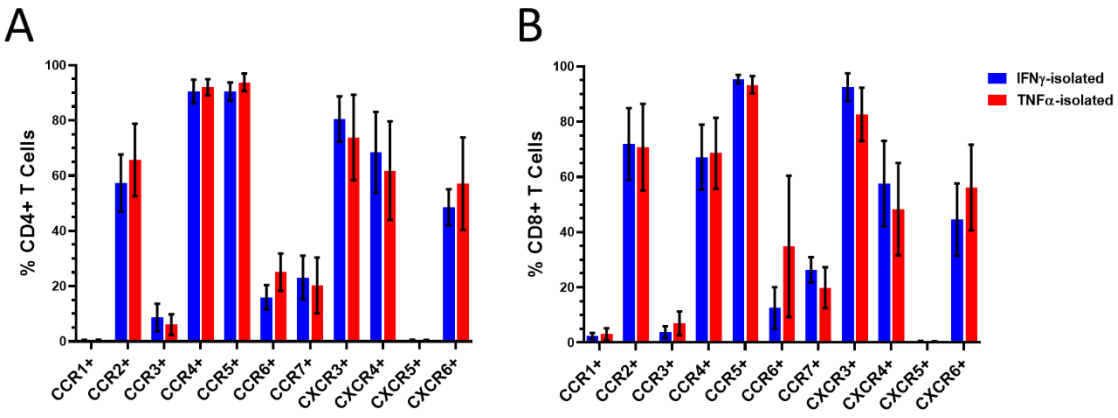

Figure 5.13 - Comparison of expanded VST final products chemokine receptor profile.

SARS-CoV-2 VST expanded for 14 days were compared for chemokine receptor profile between IFN-γ-isolated (n=4) and TNF-α-isolated (n=4) VST groups. Using a flow cytometry surface staining assay, cells were subject to initial gating on cells/singlets/ viable cells. Cells were then gated on **(A)** CD4+ or **(B)** CD8+ T cells and analysed for expression of chemokine receptors: CCR1, CCR2, CCR3, CCR4, CCR5, CCR6, CCR7, CXCR3, CXCR4, CXCR5, and CXCR6. Data is represented as mean ± SEM and groups compared using paired t-tests with Holm-Šídák correction for multiple tests.

Finally, day 14 expanded SARS-CoV-2 VST isolated using each marker were assessed for functionality using the DC stimulation assay described in Chapter 4. Briefly, DCs generated from each donor were loaded with SARS-CoV-2 peptides, and co-cultured with final product VST for 5 hours to stimulate T cell activation/ cytokine production as compared to unloaded DC controls. Cells were then harvested and stained for intracellular acquisition of activation marker CD154 and cytokines IFN-γ, TNF-α and IL-2. Comparisons of functional reactivity to different SARS-CoV-2 peptide stimulation between groups are summarised in **Figure 5.14**. To determine antigen specificity, VST were stimulated with individual SARS-CoV-2 peptides: spike, nucleocapsid or membrane. Functional reactivity was measured as % IFN-γ+ T cells (**Figure 5.14A**) or TNF-α+ T cells (**Figure 5.14B**) as normalised to unloaded DC controls. Both measures of reactive cells demonstrated a higher final product reactivity towards membrane, with lowest response to spike. This is concordant with previous observations of the early development SARS-CoV-2 VST lines generated from buffy coats in Chapter 4. No significant differences in antigen reactivity were observed between the different isolation methods, however CD154-isolated VST showed a trend towards lower reactivity to nucleocapsid and membrane peptides. This may be biased however due to lower sample size of donors tested for individual

antigens since C19UKD8 and C19UKD9 generated a limited number of DC available for the assay stimulations. Overall reactivity to pooled SARS-CoV-2 peptides (spike + nucleocapsid + membrane, SNM) was compared between the three isolation methods (**C-D**). The groups showed comparable expression of T cell effector markers IFN-γ, TNF-α, IL-2 and CD154 in response to SNM-loaded DC stimulation (**Figure 5.14C**). Co-expression of cytokines IFN-γ, TNF-α & IL-2 was also quantified as outlined in **Figure 2.8**, where all groups were skewed towards subpopulations IFN-γ+ TNF-α+ double positive, and IFN-γ+ TNF-α+ IL2+ triple positive (**Figure 5.14D**). These data indicate VST are multi-functional effector subpopulations with specificity slightly skewed towards membrane, and high overall SARS-CoV-2 reactivity.

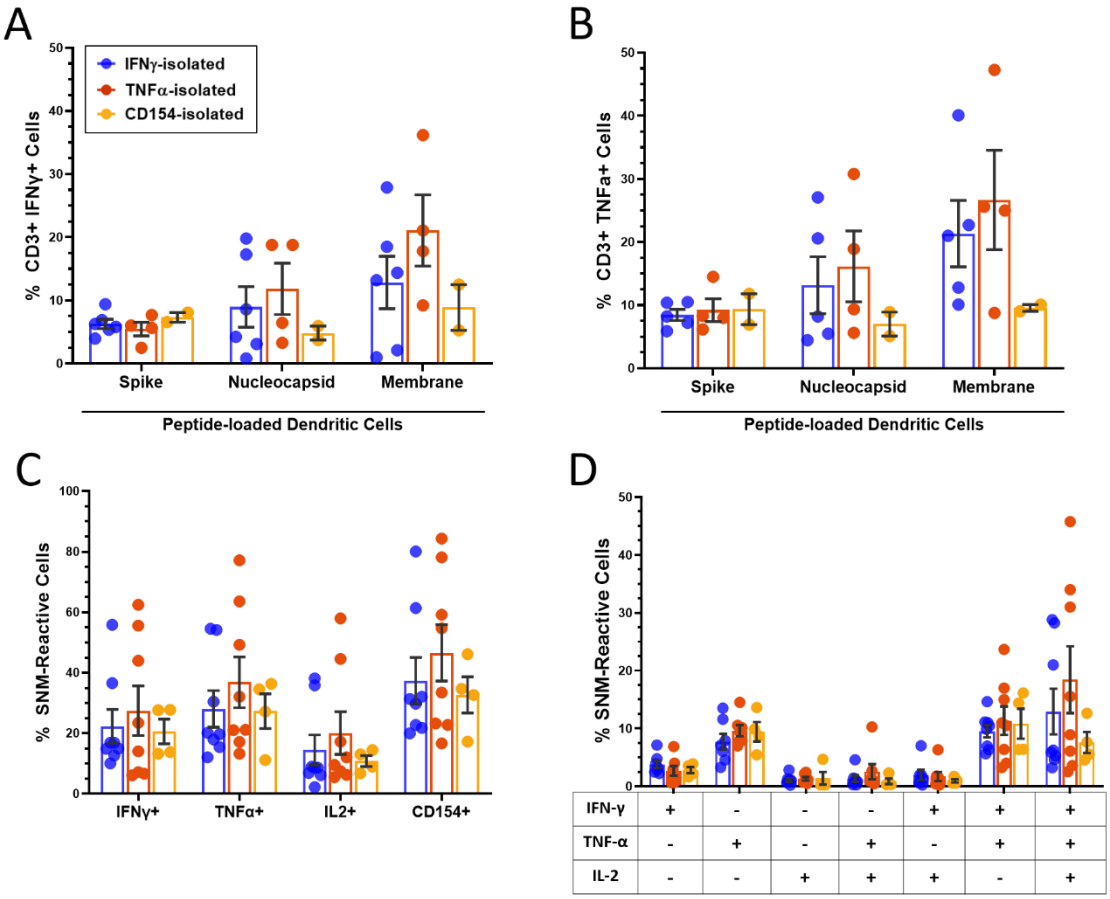

Figure 5.14 - Comparison of expanded VST final product functional reactivity.

SARS-CoV-2 VST expanded for 14 days were compared for functional reactivity to SARS-CoV-2 peptides (loaded to autologous DC for VST stimulations) between IFN-γ-isolated (n=8), TNF-α-isolated (n=8) and CD154-isolated (n=4) groups. VST were tested for functional responses towards individual SARS-CoV-2 peptides: Spike, Nucleocapsid and Membrane, with reactive VST quantified as **(A)** % CD3+ IFN-γ+ cells and **(B)** CD3+ TNF-α+ cells. To measure reactivity to pooled SARS-CoV-2 peptides (SNM), each group was quantified for **(C)** total expression of IFN-γ, TNF-α, IL-2 and CD154; and (**D**) cytokine co-expression populations. All peptide-reactive cells were normalised to unloaded DC controls. Data is represented as mean ± SEM and statistical significance was determined using RM one-way ANOVA with Geisser-Greenhouse correction.

5.4 Clonal repertoire of IFN-γ-, TNF-α- and CD154-isolated VST

Through the cytometric profiling and functional testing outlined above, SARS-CoV-2 VST isolated using the different markers showed similar antigen specificity and functional recall to SARS-CoV-2 pooled peptides, however there were some distinctions in T cell phenotype between the groups.

To better elucidate the potential efficacy of these cells to clear natural infection upon patient infusion, it was the aim of this study to assess the T cell receptor (TCR) repertoire diversity of the differentially isolated SARS-CoV-2 VST. Initial reports have shown increased SARS-CoV-2 TCR clonal diversity in COVID-19 patients with mild disease as opposed to severe disease (Chang et al., 2021, Zhang et al., 2020) which may indicate a protective effect of a broad TCR repertoire. However it remains unknown if peptide-stimulated isolation and culture expansion techniques maintain a polyclonal T cell population or induces a target selection of specific T cell clones. Particularly, isolation using the different markers may be selecting for different clones. To this end, TCR-β chains of expanded SARS-CoV-2 VST were examined using next-generation sequencing and analysed for presence of dominant clones and clonal diversity.

5.4.1 Clonal diversity of IFN-γ-, TNF-α- and CD154-isolated VST.

Numerous studies have investigated TCR clonal diversity in COVID-19 patients, naturally convalescent donors and individuals pre- and post-vaccination. Asymptomatic and mild disease have been associated with more diverse TCR repertoire generation, whereas patients with severe disease have a significantly restricted TCRβ repertoire which is likely a consequence of COVID-induced lymphopenia (Chang et al., 2021, Jian et al., 2023, Kockelbergh et al., 2022, Niu et al., 2020, Sidhom and Baras, 2021). Interestingly, in both asymptomatic/mild and severe disease, the peripheral blood TCR repertoire diversity increases during convalescence (Khoo et al., 2023, Shomuradova et al., 2020, Schultheiß et al., 2020). To assess repertoire diversity of expanded SARS-CoV-2 VST isolated using the different markers, total T cell final products were sequenced for the TCRVβ region and analysed for unique clonotypes as outlined in **section 2.11**. Pan T cells isolated directly from peripheral blood using CD3 microbead enrichment from donors

matched to the SARS-CoV-2 VST were used as high diversity controls. The count of specific clonotypes between CD3+ T cells and SARS-CoV-2 VST generated using IFN-γ, TNF-α or CD154 isolation are compared in **Figure 5.15**.

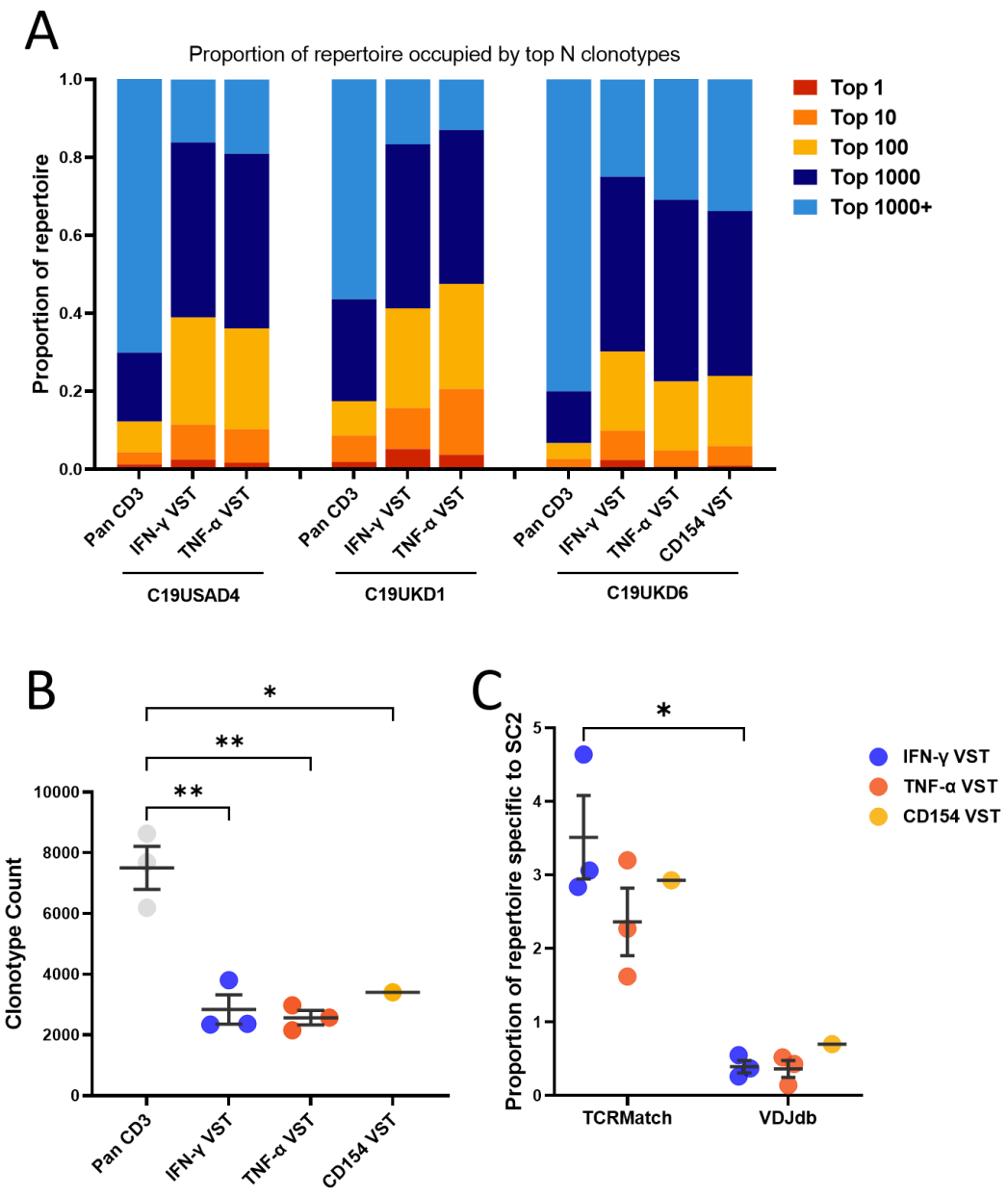

Figure 5.15 - IFN-γ-, TNF-α- and CD154-isolated VST clonotype comparison.

Sequencing of the TCR-Vβ region allowed comparison of clonal diversity between IFN-γ-isolated, TNF-α-isolated and CD154-isolated final product (day 14 expanded VST). Pan CD3 T cells from matched donor starting leukapheresis material was included as a high diversity control. **(A)** Stacked bars represent the proportion of the repertoire occupied by the top N clones in that repertoire. SARS-CoV-2 VST show restricted repertoire diversity compared to pan T cell controls however still retain a highly polyclonal repertoire. **(B)** Clonotype counts corrected for unique molecular identifier (UMI) size matching demonstrate all VST groups had significantly reduced diversity compared to pan T cells. Data is represented as mean ± SEM and statistical significance was determined using RM one-way ANOVA. **(C)** The proportion of each repertoire with an exact CDR3 amino acid sequence match specific to SARS-CoV-2 in databases TCRMatch and VDJdb was limited in both groups tested. Data is represented as mean ± SEM and statistical significance determined using RM two-way ANOVA.

The proportion of TCR repertoire comprised of a top 1, 10, 100, 1000 or >1000 unique clonotypes for each donor is displayed in **Figure 5.15A**. As can be seen, each donor pan CD3+ T cell sample was highly diverse, with 60-80% of the repertoire composed of >1000 small clonotypes, and no single clonotype occupying more than 1% of the repertoire. Each SARS-CoV-2 final product VST line generated by IFN-γ, TNF-α or CD154 isolation shows a restriction in repertoire diversity, however these lines are highly polyclonal with the vast majority of repertoire dominated by the top 100-1000 clones. The clonotype count (**Figure 5.15B**), i.e. the number of unique CDR3 amino acid sequences in the sample was significantly higher in pan CD3+ T cells compared to IFN-γ VST (p=0.0028), TNF-α VST (p=0.0021) and CD154 VST (p=0.028) as expected, as the VST represent a selected subset. Using TCR antigen specificity databases to match CDR3 sequences (**Figure 5.15C**), a small proportion of the repertoire (<4%) matched SARS-CoV-2-specific CDR3 sequences by TCRMatch and negligible matches were found through VDJdb. The IFN-γ-isolated VST lines showed significantly higher database CDR3 sequence matches using TCRMatch than VDJdb.

The similarity of TCR repertoire between samples was also tested to determine if many clones were shared between donors and/ or between sample type (**Figure 5.16**). Clonotype overlap was mapped using pairwise Morista-Horn index to account for CDR3 species abundance, whereby a lower value (blue) indicates no sharing and higher index (yellow) indicates greater similarity. As can be seen, pan CD3+ T cells clustered at the top left show negligible overlap with any other samples, including donor-matched VST lines or the inter-donor CD3+ T cell samples. This likely reflects the highly diverse clonal repertoire of the pan T cells confirming their use as an appropriate diversity control. Thereafter, SARS-CoV-2 lines clustered for similarity within the matched donor treatments. C19USAD4 IFN-γ-isolated VST had high overlap with C19USAD4 TNF-α -isolated VST at 0.6 Morista-Horn index, and similarly C19UKD1 IFN-γ-isolated VST and C19UKD1 TNF-α -isolated VST had high similarity at 0.7 Morista-Horn index. Donor C19UKD6 also shows similarity to the differentially isolated lines but at a lower index than C19USAD4 & C19UKD1. Interestingly, within C19UKD6 lines IFN-γ-isolated and TNF-α -isolated VST showed equivalent similarity to TNF-α -isolated and CD154-isolated VST (~0.5 Morista-Horn index); whereas IFN-γ-isolated and CD154-isolated VST had reduced similarity at 0.4 Morista-Horn index. This suggests IFN-γ and CD154 selection processes are more likely to enrich for different T cell clones.

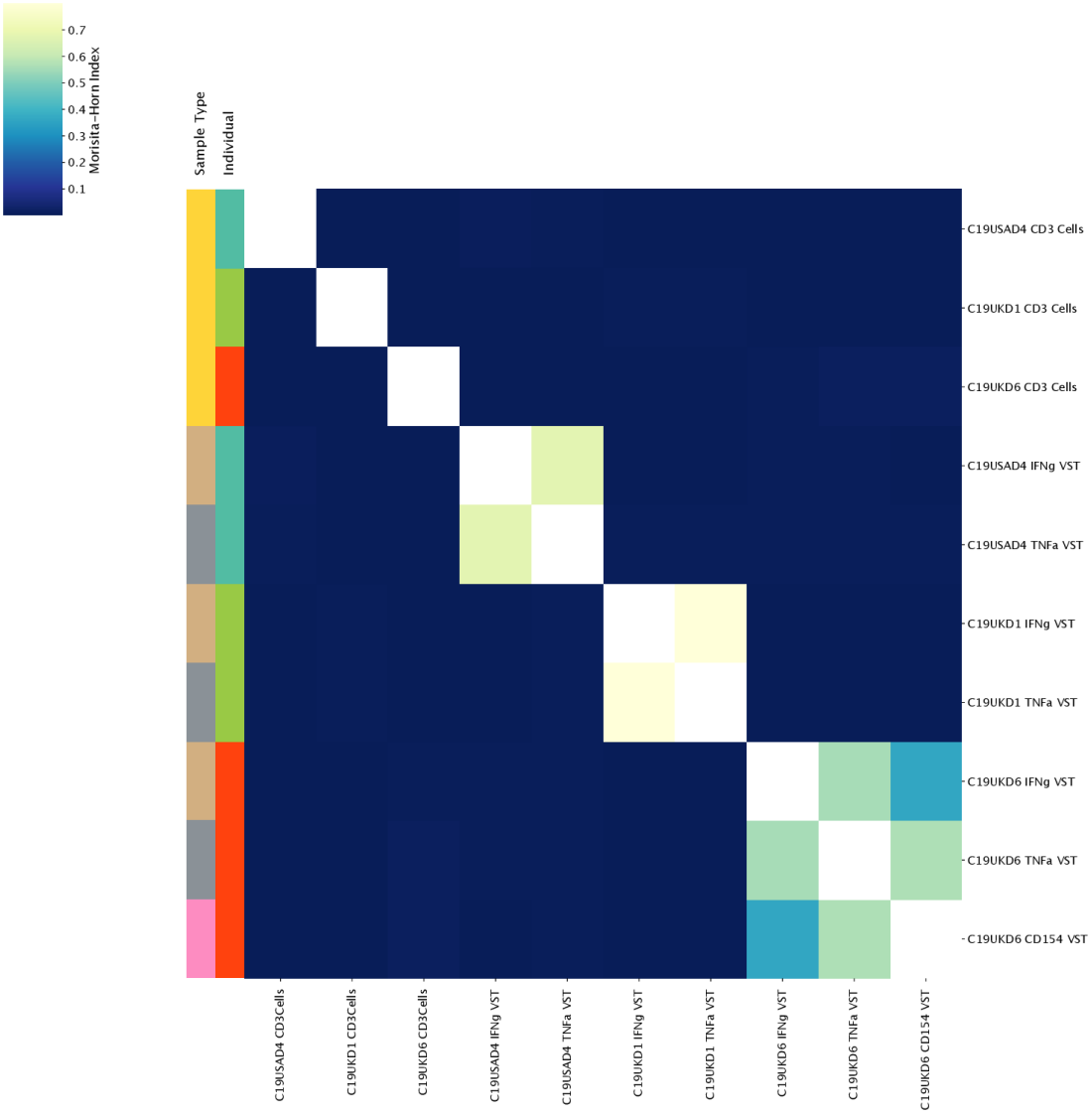

Figure 5.16 - Clonotype overlap similarity between different marker isolations.

Heat map of pairwise Morista-Horn Index size-matched individual repertoires of matched donor pan CD3 T Cells, and either IFN-γ, TNF-α, or CD154-isolated VST final product samples. Reads were downsized to 9542 UMIs to allow comparison between samples. Grouping is coloured on the y-axis either to sample type: CD3 cells (yellow), IFN-γ VST (brown), TNF-α VST (grey) and CD154 VST (pink); or by donor individual: C19USAD4 (aqua), C19UKD1 (green) or C9UKD6 (red).

Another measure of clonal repertoire similarity was made by comparing the TRBV/ TRBJ gene usage overlap between samples (**Figure 5.17**). Again, samples were grouped into pan CD3 T cells at the top left, followed by SARS-CoV-2 VST lines grouped by donor. Using Manhattan distance, a value of 0 (burgundy) indicates identical usage of TRBV/ TRBJ gene combinations, whereas a distance >0 indicates increasing variation in gene combination overlaps.

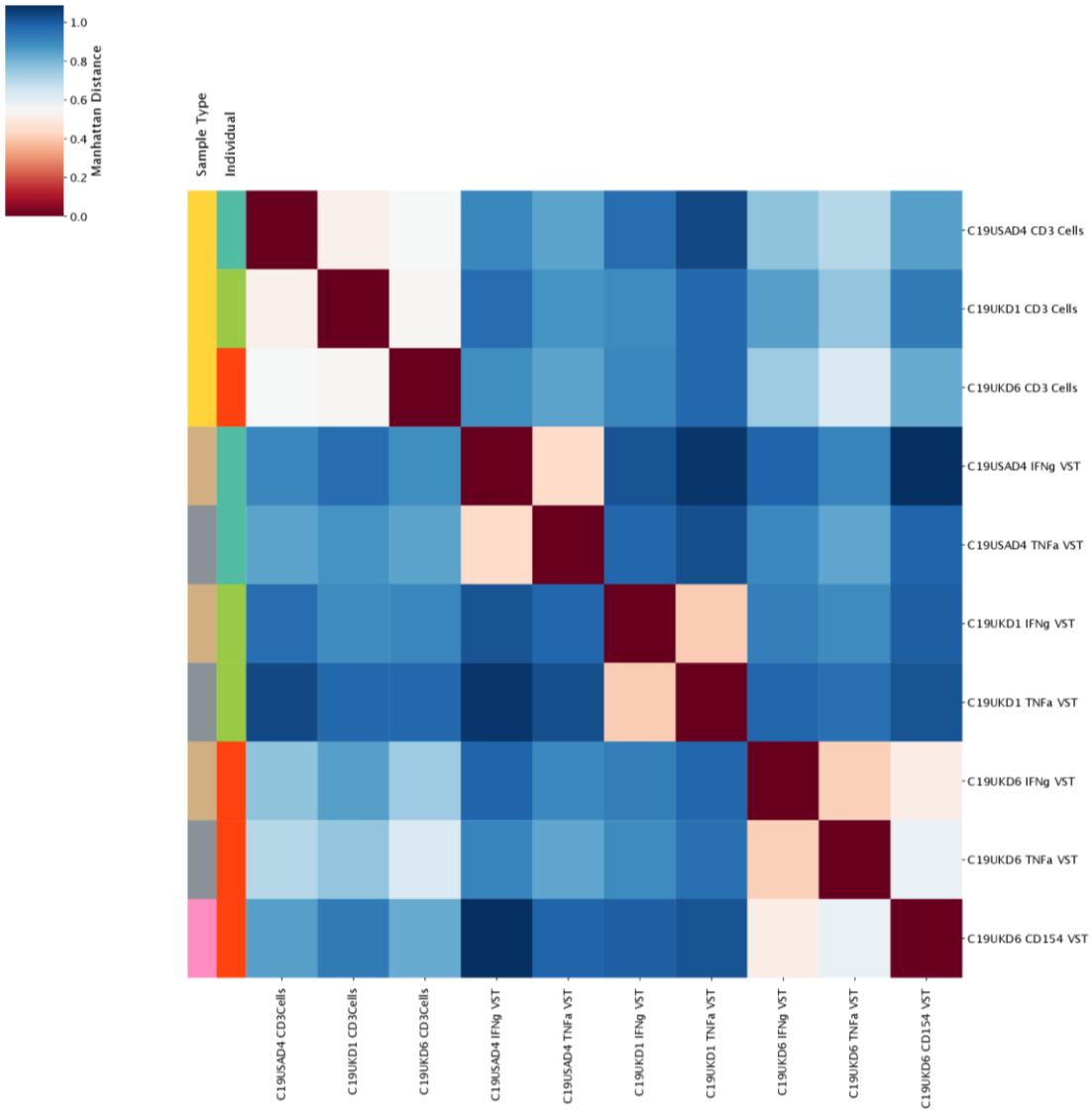

Figure 5.17 - TRBV/TRBJ gene usage overlap between different marker isolations.

Heat map of Manhattan distance matrix of unique TRBV/TRBJ gene combinations. A distance of 0 demonstrates identical usage of TRBV/TRBJ gene combinations, therefore a small distance (burgundy) indicates greater similarity whereas a larger distance (blue) indicates less similarity between samples. Grouping is coloured on the y-axis either to sample type: CD3 cells (yellow), IFN-γ VST (brown), TNF-α VST (grey) and CD154 VST (pink); or by donor individual: C19USAD4 (aqua), C19UKD1 (green) or C19UKD6 (red).

Corresponding to the Morista-horn index, Manhattan distance of SARS-CoV-2 VST lines group in similarity within intra-donor lines rather than by isolation group. Using Manhattan distance, C19UKD6 has least similarity between TNF-α -isolated and CD154-isolated VST which contrasts with the Morista-horn index pair-wise comparisons. Interestingly, pan CD3+ T cells between donors have similar gene usage patterns (Manhattan distance 0.5) which contrasts with the Morista-horn comparison suggesting an entirely dissimilar CDR3 sequence repertoire between CD3+ samples.

5.4.2 Antigen specificity of IFN-γ-, TNF-α- and CD154-isolated VST.

Further examination using TCR antigen specificity databases allowed identification of CDR3 sequences with known antigen specificity. Exact matches of CDR3 sequences to a range of viruses was compared between the differentially isolated SARS-CoV-2 VST (**Figure 5.18**). Using database IEDB TCRMatch (**Figure 5.18A**), the highest matched specificity for the VST lines was expectedly SARS-CoV-2 at 2-5% of the TCR repertoire. Additionally, a small proportion of sequences (0.2-1%) were also specific to Influenza A, whereas matches were negligible to the other viruses investigated.

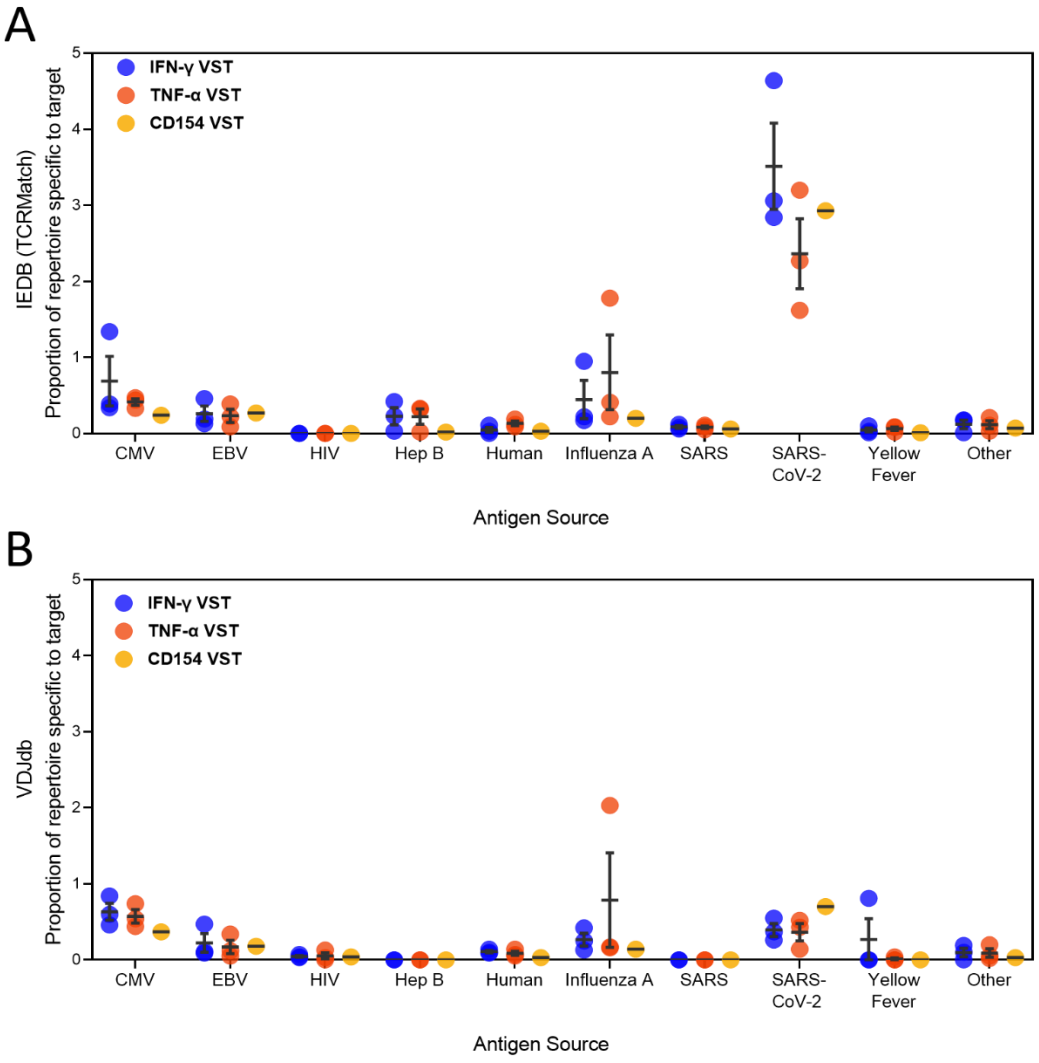

Figure 5.18 – Viral specificities of IFN-γ, TNF-α, and CD154 VST.

Proportion of each repertoire specific to antigens from various viral sources as annotated by exact match to CDR3 amino acid sequences in **(A)** IEDB TCRMatch and **(B)** VDJdb databases. Data is represented as mean ± SEM and comparisons between IFN-γ, TNF-α, and CD154 VST groups made using RM one-way ANOVA.

A considerably smaller proportion of CDR3 sequences had matches using VDJdb (**Figure 5.18B**) with a comparably low proportion 0 .5-1% specific to SARS-CoV-2, CMV and Influenza A. No significant differences in repertoire specificity were observed between the VST isolation groups using either database matching.

These databases were also used to assess VST specificities to individual SARS-CoV-2 antigens (**Figure 5.19**). Matches to CDR3 sequences using the IEDB TCRMatch database (**Figure 5.19A**) were highest for ORF1ab and spike at ~1-4% of the repertoire. Low proportions (0.1-1%) of the repertoire showed specificity to membrane, nucleocapsid, and ORF7b; with negligible matches to the other SARS-CoV-2 antigens investigated.

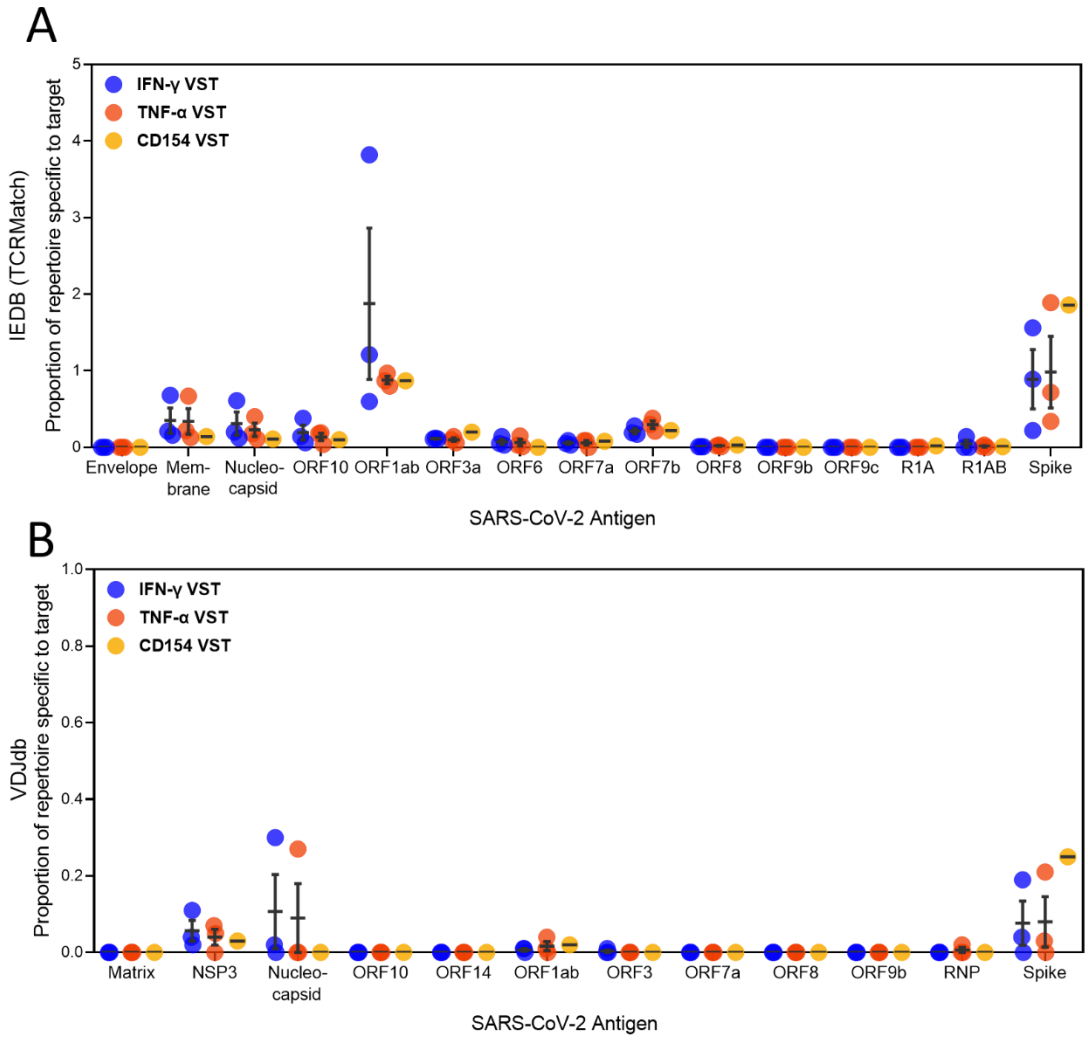

Figure 5.19 – SARS-CoV-2 antigen specificities of IFN-γ, TNF-α, and CD154 VST.

Proportion of each repertoire specific to individual SARS-CoV-2 antigens as annotated by exact match to CDR3 amino acid sequences in **(A)** IEDB TCRMatch and **(B)** VDJdb databases. Data is represented as mean ± SEM and comparisons between IFN-γ, TNF-α, and CD154 VST isolation groups made using RM one-way ANOVA.

As above, analysis using the VDJdb database (**Figure 5.19B**) had extremely low CDR3 sequence matches, with only one donor line showing >0.1% of the repertoire specific to spike and nucleocapsid.

Interestingly, dominance of specificity towards Spike in these lines does not correspond with the aforementioned functional reactivity data. Graphs comparing spike, nucleocapsid and membrane specificity are shown in **Figure 5.20** using either **(A)** TCR repertoire IEDB TCRMatch specificity or **(B)** functional reactivity to peptide-loaded DCs measured by the frequency of cytokine-producing cells. Although the two techniques can't be directly compared, it is interesting to note the trend within each analysis differs such that specificity via repertoire matching is skewed to spike, whereas spike has the lowest frequency of functionally reactive cells compared to membrane and nucleocapsid.

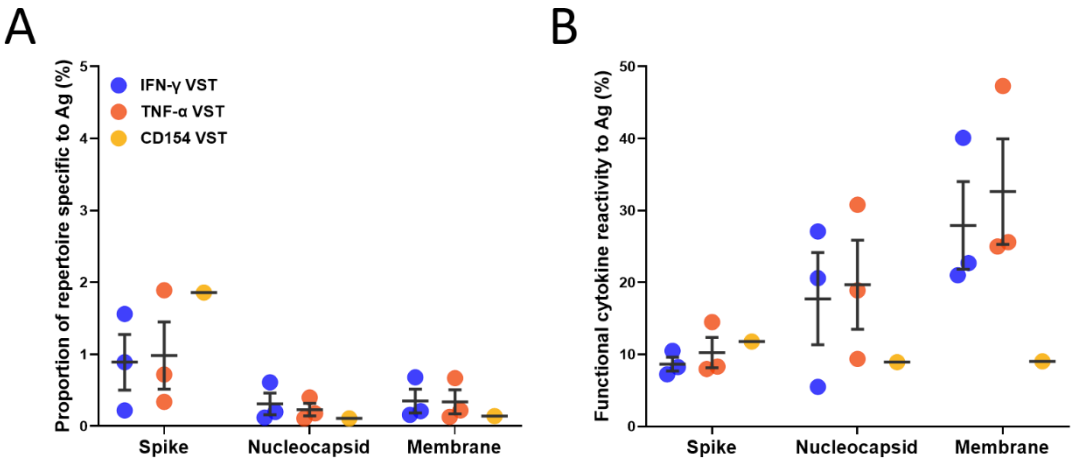

Figure 5.20 - Comparison of SARS-CoV-2 antigen TCR specificity versus functional reactivity.

Comparison of VST lines clonal specificity versus functional reactivity to individual SARS-CoV-2 antigens. **(A)** Repertoire specificity of CDR3 sequence matches using IEDB TCRMatch as shown in **Figure 5.19** condensed to only Spike, Nucleocapsid and Membrane. **(B)** Frequency of functionally reactive cells to Spike, Nucleocapsid and Membrane by cytokine production as shown in **Figure 5.14** condensed to only donors C19USAD4, C19UKD1, and C19UKD6 corresponding to the TCR sequencing data.

5.5 Discussion

Virus-specific T cells can be identified and isolated from mixed blood preparations using different techniques and detection markers. While fluorescently-conjugated MHC-multimers are the gold standard for binding exact MHC-restricted antigen epitopes, the requirement of HLA-specific reagents limits high-throughput

applications for VST detection. Instead, antigen stimulation assays are used to identify functionally reactive antigen-specific T cells via upregulation of a T cell AIM or effector cytokine. Though this may quantify the number of functional T cells in the isolate and act as a measure of potency, it will underestimate the total number of VST present.

T cell activation markers or cytokines vary in expression depending upon T cell subset, antigen, memory recall and signalling pathways involved in effector responses. As discussed in Chapter 3, natural long-term protection to EBV infection is provided by a cytotoxic, degranulating CD8+ central memory EBV VST population, whereby IFN-γ or CD107a are prime markers for detection. Initial results assessing T cell responses to SARS-CoV-2 in convalescent donors presented in Chapter 4 indicated CD4+ central and effector Th1 cells dominated within the circulation following primary infection. To identify and select multiple donors with wide-ranging HLA spread and good SARS-CoV-2 T cell responses for manufacturing a SARS-CoV-2 VST bank, 109 COVID-19 convalescent donors were screened for response to SARS-CoV-2 peptides. The process developed for this manufacture relies upon IFN-γ capture as it is the only GMP-compliant option and therefore basic screening could be done with T cell markers and IFN-γ alone. However it was clearly important to extend this isolation approach using other activation markers to assess whether the cultured isolates would have quantifiable improvements over the standard method. This research would also clarify whether there were changes in effector responses following re-exposure, vaccination or mutated SARS-CoV-2 variants.

To this end, all convalescent donors were screened to detect IFN-γ, TNF-α- IL-2 or CD154-expressing cells reactive to stimulation with SARS-CoV-2 peptide pools. The frequency of CD154+ T cells was significantly higher than that of any of the cytokines tested, indicating a significant proportion of activated CD154+ VST do not secrete Th1 cytokines. This may suggest some CD154+ VST have different effector functions or are more functionally exhausted at least in terms of cytokine production (Saggau et al., 2024). This may also reflect a difference in kinetics of cytokine granule formation and secretion in comparison to CD154 molecule upregulation. The latter hypothesis could be investigated by testing for IFN-γ, TNF-α, IL-2 and CD154 T cell expression over a time-course of 4-24 hours following SARS-CoV-2 peptide stimulation. This was out of scope for the current study whereby duration of stimulation was fixed at 5

hours as optimised for selection using the cytokine capture method. Interestingly, of the cytokines tested using this assay, the frequency of IFN-γ-expressing T cells was lower than TNF-α and IL-2-expressing T cells; indicating IFN-γ as a detection marker underestimates the total responsive VST pool. Further analysis of SARS-CoV-2 peptide-reactive T cell populations, showed IFN-γ-reactive T cells had an equal CD4:CD8 ratio, whereas peptide-reactive TNF-α+ cells and IL-2+ cells were skewed to CD4 T cells, and CD154+ cells had the highest CD4:CD8 ratio. Interestingly, the frequency of peptide-reactive CD8 cells was comparable between all markers at approximately 0.1% of the total T cell population. This suggests the hierarchical frequencies of SARS-CoV-2 T cell responses as IFN-γ < TNF-α < IL-2 < CD154 is due to increased peptide-reactive CD4 cells detected by these markers.

To investigate the viral-specific T cells by different marker reactivities further, intra-donor comparison studies were done to isolate SARS-CoV-2 reactive VST within each donor by IFN-γ CCS, TNF-α CCS, and CD154 surface magnetic bead enrichment. Sorts were carried out in parallel to ensure the same conditions for source material and peptide stimulation.

The T cell screening studies using an intracellular cytokine assay incorporated protein transport inhibitor Brefeldin A to allow accumulation of proteins intracellularly for detection. Surface expression of CD154 was also optimised for sorting purposes. Addition of the CD40 blocking antibody prior to 5 hour stimulation with SARS-CoV-2 peptide pools was found to significantly increase surface CD154 expression, and correspondingly to enrich for a higher frequency and total number of CD3+ lymphocytes in the CD154-isolated target cell population. This correlates with a study showing surface CD154 expression peaked at 6 hours and was rapidly degraded by 8 hours post-stimulation with *Staphylococcus aureus* enterotoxin B (SEB) alone, however stimulation with SEB + CD40 both increased the frequency of CD154-expressing cells and stabilised expression from 6-12 hours post-stimulation (Frentsch et al., 2005).

Comparison of the target cells immediately following isolation demonstrated a consistent higher monocyte to lymphocyte ratio in CD154-isolated targets compared to both IFN-γ-isolated and TNF-α-isolated targets. This was found to be due to a higher count (10^7) of monocytes contaminating the CD154 targets compared to IFN-

γ-isolated and TNF-α-isolated which contained 10^5-10^6 monocytes in target fractions. Conversely lymphocyte count was relatively comparable at 10^5-10^6 lymphocytes between different sorted target fractions. In this analysis cells have been crudely classified as monocytes based on size and scatter gating. However, CD154 expression has been detected on blood-derived myeloid DC (Pinchuk et al., 1996) or plasmacytoid DC (pDC) (Kuwajima et al., 2006) following CD40 stimulation. This may indicate circulating blood-derived DC or pDC are specifically isolated in the CD154 sorts by activation-induced CD40-CD154 interactions, or potentially monocytes are non-specifically bound to beads possibly through phagocytic mechanisms during the column isolation (Gu et al., 2014). To investigate this further, future studies should use a flow cytometric panel of monocyte or DC markers to characterise this population. Interestingly while present at a significantly lower frequency, a similar monocyte-sized population was also caught in the IFN-γ-isolated and TNF-α-isolated targets. This has also been reported by a group characterising IFN-γ-isolated SARS-CoV-2 VST after CCS, whereby target fractions contained ~5% monocytes (CD11c+ CD14+ HLADR+) and 10-15% DCs (CD11c+ CD14– CD123low CD183+ HLADR+) (Chu et al., 2023). Therefore, it is unconfirmed whether this population is undergoing a peptide-specific response and is specifically isolated, or caught up as contamination in the magnetic sort process, and whether this reflects different mechanisms/ populations between the target groups.

Phenotyping with lymphocyte markers demonstrated TNF-α sortied targets with highest CD3+ CD56- T cell purity compared to IFN-γ sorting. In addition, TNF-α targets had a significantly higher CD4 to CD8 cell ratio compared to IFN-γ targets. CD154 targets similarly had a comparable high CD4 to CD8 ratio, however lack of significant difference in statistical comparison test to IFN-γ targets is likely due to the smaller sample number of CD154 sorts. Within the CD4 compartment, frequency of central memory cells was also significantly increased in TNF-α targets compared to IFN-γ targets. Together these data indicate direct selection using TNF-α or CD154 enrich for a CD4-skewed population, whereas IFN-γ CCS isolates a more equal distribution of CD4+ and CD8+ antigen-reactive cells which may be an important consideration when choosing sorting method dependent on the desired product phenotype. Despite a higher frequency of CD154 expression detected using the intracellular screening assay, yield of target cells was comparable between the different sorting markers. This suggests the CD154 sort using surface expression

optimised in this protocol is inefficient at isolating all the CD154-expressing SARS-CoV-2 VST even with the addition of CD40. In every donor-matched sort except C19USAD3, TNF-α selection isolated the highest number of viable target cells, and although not statistically significant had the greatest target cell yield from initial input of marker-expressing cells. Purity of PE-labelled lymphocytes however was highest in IFN-γ targets compared to TNF-α and CD154 targets. This suggests although absolute yield is lower, purity is enhanced in IFN-γ CCS; illustrating the fine balance between purity and efficiency in rare cell enrichment.

It is the strategy of numerous centres to do a direct selection of SARS-CoV-2 VST using IFN-γ CCS and deliver the immediate Prodigy-isolated target cells immediately as the patient therapy (Bonifacius et al., 2022, Leung et al., 2020, Chu et al., 2023). Given this process is limited by target cell yield, ranging between 1-3x10^6 VST per full scale manufacture, we developed a subsequent expansion protocol to allow generation of sufficient cells for multiple patient doses. In addition to inducing a 1000x fold expansion of SARS-CoV-2 VST, the culture protocol supported T cell outgrowth and consequently resulted in a highly purified and specific VST final product in comparison to the IFN-γ CCS target cells at the start (refer to Chapter 4). Therefore, it was important to determine whether TNF-α and CD154-isolated targets had different growth capacity in standard culture, and whether the conditions preferentially selected for any particular T cell subpopulations. Growth kinetics were comparable between the different isolation groups, with a mean 1000-2000x fold expansion over the culture period. Interestingly, fold expansion did not correlate with the initial number of isolated targets which may reflect robustness of the culture system no matter how small the target fraction. However, this may also be indicative of unknown donor-specific variables as to why certain lines have relatively poor culture expansions even with good target isolation. This is investigated further in Chapter 6.

Expanded SARS-CoV-2 VST final products were highly purified for T cells (>90%) between the different sorting groups. While not statistically significant, some donors final product VST from IFN-γ isolations had a small NK cell contamination (2-12%) that were not present in the matched donor TNF-α and CD154-isolated VST expansions. Since IFN-γ is an important antiviral cytokine produced by NK cells, NK cell co-isolation during IFN-γ CCS and survival in culture is a potential limitation of

this technique. IFN-γ-isolated products also had a considerable population of CD8+ T cells at ~10-20% of expanded VST. In contrast both TNF-α and CD154-isolated VST were highly purified for CD4+ T cells (95-100%) with negligible CD8+ T cells following culture expansion. All isolation approaches successfully expanded CD4+ and CD8+ VST highly skewed to central memory with some residual effector memory cells with negligible TEMRA or naïve T cells. The CD4 to CD8 ratio would likely be extremely important in the context of therapeutic strategy, whereby patients much earlier in infection may benefit from infusion with cytotoxic CD8+ SARS-CoV-2 VST to clear virally infected lung epithelial cells. However administration of enriched CD8+ VST in later progressive COVID-19 disease states may contribute to dysregulated inflammatory damage within the lungs and therefore be potentially harmful to these patients. Therefore the therapy approach, patient group targeted and therapeutic window should be carefully considered when choosing the SARS-CoV-2 VST selection method. While several human trials are underway infusing allogeneic CD4-skewed SARS-CoV-2 VST lines (Vasileiou et al., 2023, Martits-Chalangari et al., 2022, Leung et al., 2020, Chu et al., 2023) to at risk early stage COVID-19 patients with the hypothesis that helper Th1 mediation may re-set the balance in favour of conventional adaptive responses, the mechanism by which these cells may act is not yet known. Conversely other groups have developed SARS-CoV-2 VST products more equal in CD4:CD8 (Papayanni et al., 2021, Papadopoulou et al., 2023, Bonifacius et al., 2022, Basar et al., 2021); or CD8-skewed (Keller et al., 2020, Durkee-Shock et al., 2022, Cochran and Li, 2021). This emphasises the need for appropriate models of SARS-CoV-2 infection with characteristic lung inflammation to critically test the benefit and risk balance of CD4/CD8 composition in SARS-CoV-2 VST lines.

SARS-CoV-2 VST final products showed a consistent pattern of chemokine receptor expression regardless of isolation approach. Each showed high expression of inflammatory chemokine receptors CCR2, CCR4, CCR5, CXCR3, CXCR4 and CXCR6 (discussed in more detail in Chapter 6). While CD154-isolated VST lines were not analysed in this assay, IFN-γ and TNF-α-isolated VST lines were equivalent in their protein level chemokine receptor expression indicating the isolation method does not alter the potential T cell migratory or trafficking mechanisms and the culture method may encourage outgrowth of antigen-specific T cells with a particular chemokine receptor pattern. Similarly, functional recall testing to pooled SARS-CoV-2 antigens indicated equivalent cytokine production between the differentially isolated VST

lines. Individual antigen specificity testing showed no significant differences between the isolation groups, however the CD154-isolated VST had an incomplete dataset and may skew observed trends due to low sample size within this group. The lower reactivity to nucleocapsid and membrane antigens was also seen in the matched donor IFN-γ and TNF-α-isolated VST lines. To further elucidate any differences in effector functions between the isolation groups, more CD154-isolated VST should be tested for individual antigen reactivity. In addition, different Th subset cytokines of VST supernatants following SARS-CoV-2 peptide recall could be assessed using multiplex ELISA and would further elucidate potential effector functions. Since CD154 can capture a broader range of antigen-specific CD4+ T cells, it would be interesting to test for IL-6 and IL-21 secretion since spike-reactive follicular helper (Tfh) cells have been reported in peripheral blood (Rodda et al., 2021). Also given the difference in CD8+ T cell content between the groups, it would be prudent to directly compare VST lines in degranulation and/or cytotoxicity assays against infected or antigen-pulsed target cell lines. It is likely given the presence of CD8+ T cells in IFN-γ-isolated VST this group would exhibit increased cytolytic activity. However, it is not inconceivable that TNF-α or CD154-isolated VST may also have some cytolytic capacity even in absence of CD8+ T cells through potential cytotoxic CD4+ T cells. The ability to test these research VST lines in the cytotoxicity assay described in Chapter 6 was out of scope of the present study.

TCRVβ sequencing revealed equivalent clonal repertoire diversity between the groups, with all isolated and expanded SARS-CoV-2 VST composed of a highly polyclonal repertoire dominated by a top 100-1000 clonotypes. Due to the timeframe of this sequencing experiment, comparisons were limited by a lower sample number of donor-matched isolated VST. In particular only n=1 sample of CD154-isolated VST was available at the time of sequencing, and therefore consideration should be taken in the interpretation of this data. Previous studies have described a more diverse TCR repertoire of peripheral CD4+ T cells than CD8+ T cells (Qi et al., 2014, Li et al., 2016), therefore higher CD8+ content in IFN-γ-isolated VST could confer a slightly more restricted repertoire in T cells isolated using this method compared to TNF-α or CD154 isolation. Interestingly in the single donor-matched comparison of all 3 isolations, IFN-γ-isolated VST and CD154-isolated VST showed the least overlap of clonotype sequences indicating a greater repertoire dissimilarity between these isolated T cells.

Matching of clonal sequences to IEDB TCRMatch indicated highest repertoire specificity to SARS-CoV-2 as compared to other common viruses, and individual SARS-CoV-2 antigen specificity to ORF1ab and Spike. Using the TCRMatch matches to SARS-CoV-2 antigens, CDR3 sequences present were highest for spike, whereas very low proportions of the repertoire (<1%) showed specificity for nucleocapsid or Membrane. This does not correspond with the functional reactivity of the same VST lines to DCs loaded with individual SARS-CoV-2 peptides, whereby 20-50% final product VST expressed cytokine in response to nucleocapsid or membrane stimulation, with fewer cells responsive to spike (~10%). The divergence in antigen specificity between the two techniques may reflect TCR database bias towards SARS-CoV-2 spike sequences given the unparalleled investigation into Spike-specific T cell responses throughout and following vaccine development. As of October 2023, the IEDB database has listed 3006 spike, 789 nucleocapsid and 270 membrane human T cell epitope sequences. In addition, distinct variations in read matches were seen between the IEDB and VDJdb databases, which likely reflects different CDR3 sequences between HLA alleles. Furthermore, these databases are largely biased towards peptides recognised by MHC-I restricted molecules. At the time of analysis (05/06/2023) IEDB had 170,396 MHC-I restricted and 5161 MHC-II restricted TCR sequences. Similarly in the VDJdb, 37,627 TCRβ sequences were MHC-I restricted, whereas only 1,725 were MHC-II restricted. Therefore it is likely since SARS-CoV-2 VST lines are composed mainly of CD4+ T cells, matching to MHC-II restricted sequences will be limited on generalised databases. This suggests specificity may be underestimated using TCR sequencing matches, and the functional reactivity data may give a more accurate measure of T cell antigen specificity.

5.6 Chapter summary

This chapter has investigated using different markers to isolate activated virus-specific T cells with evaluation of processes and products for an allogeneic cell therapy. To this end, intra-donor comparisons were made between IFN-γ, TNF-α and CD154 magnetic enrichment protocols to isolate peptide-reactive SARS-CoV-2 VSTs with subsequent rapid culture expansion. While the frequency of reactive SARS-CoV-2 VST in PBMC was highest with CD154 expression, the overall VST yield from magnetic isolations and consequent fold expansion following culture were equivalent between the different marker isolations. Although final product clonal composition, phenotype

and functional recall to SARS-CoV-2 antigens were largely comparable between the groups, the major difference observed was a higher frequency of CD8+ T cells in IFN-γ-isolated VST, whereas TNF-α and even more so CD154-isolated VST were highly purified for CD4+ T cells. In terms of cell therapy manufacture, CD154 enrichment is a simpler surface marker bead isolation that can be carried out on a standard automated CliniMACS Plus processor compared to the cytokine capture selection which requires a CliniMACS Prodigy processor with added cost and duration to the process. However with differences in VST populations isolated and expanded between the sorting markers, choice of sorting process should be determined by the therapeutic strategy and patient group targeted. Where a desired mechanism of action includes targeted cytotoxic functionality, IFN-γ CCS would be the optimal process for isolating SARS-CoV-2 VST. Or conversely if targeting COVID-19 patients with more progressive disease where CD8+ mediated cytotoxicity may be detrimental to disease resolution, TNF-α or CD154 isolation processes would be ideal for generating purified Th cells. Since CD154 is also expressed on multiple Th subsets, generation of a multi effector CD4+ SARS-CoV-2 VST product may be optimal by CD154 isolation, however this needs to be investigated further to fully characterise CD154-isolated SARS-CoV-2 VST subsets. In summary, TNF-α and CD154 enrichment processes are useful alternative sorting methods to the widely used IFN-γ capture selection to isolate and expand SARS-CoV-2 VST purified for helper T cell subset, and may therefore be advantageous with better understanding of disease progression.

Chapter 6

Manufacture of a GMP-compliant allogeneic SARS-CoV-2 VST bank

Chapter 6 – Manufacture of a GMP-compliant allogeneic SARS-CoV-2 VST bank

6.1 Introduction and aims

As time goes on since the outbreak of SARS-CoV-2, evolution of the virus, changes between primary infection versus re-infection responses, as well as ongoing vaccination programs, means we are still gaining valuable insights into aspects of SARS-CoV-2 immune protection and dysfunction. In addition to drugs targeting viral mechanisms of infection or progressive disease pathophysiology, numerous therapies conferring SARS-CoV-2-specific immunity to individuals at high risk of severe COVID-19 have been investigated as preventative or intervention strategies.

A major initial approach to COVID-19 therapy, particularly prior to availability of vaccines, was adoptive transfer of convalescent plasma (CP) containing SARS-CoV-2-specific antibodies from naturally recovered donors. CP has now been trialled in numerous countries however results over whether CP actually confers any clinical efficacy in hospitalised COVID-19 patients is inconclusive (Klassen et al., 2021). While T cell dysfunction is still a consistent feature of COVID-19 immune dysregulation, inconsistent results of CP and vaccines to fully prevent infection suggest antibody responses alone are not sufficient to control the clinical course of moderate to severe disease in COVID-19. Interestingly, SARS-CoV-2-specific T cell responses have been observed in convalescent donors with confirmed PCR positive test, without detectable S1 IgG antibodies, indicating a disconnect between T cell and humoral immunity (Schwarzkopf et al, 2021). Importance of host SARS-CoV-2-specific T cell responses in providing protection suggests there may still be a role for T cell therapies to treat vulnerable patient groups. While adoptive transfer of SARS-CoV-2-specific T cells could potentially exacerbate the aggressive inflammatory response of severe patients presenting with cytokine storm syndrome, it is the strategy of numerous groups to target adoptive transfer of allogeneic VST to high-risk hospitalised patients to clear infection in the early-moderate stages and prevent progression to severe systemic complications (Hanley et al., 2020).

Methods to manufacture adoptive T cell therapies with anti-SARS-CoV-2 immunity so far fall into 3 main categories: peptide-pulsed APC stimulation and VST outgrowth (Basar et al., 2021, Durkee-Shock et al., 2022, Keller et al., 2020, Kim et al., 2021,

Martits-Chalangari et al., 2022, Papadopoulou et al., 2023, Papayanni et al., 2021, Vasileiou et al., 2023), CD45RA+ naïve T cell depletion (Ferreras et al., 2021), or direct selection of VST by CCS (Bonifacius et al., 2022, Chu et al., 2023, Cooper et al., 2020, Leung et al., 2020).

Depletion of CD45RA+ T cells has the advantage of providing immunity to numerous pathogens whilst removing alloreactive naïve T cells and is therefore highly beneficial as a prophylaxis for HSCT or cancer patients to prevent acute infection of numerous viruses. However, in the overall antigen-specific T cell population produced there is only a very small number of memory VST specific to any particular virus, and therefore this approach may be limited as a therapy against an active viral infection.

Peptide-pulsed APC stimulation and VST outgrowth without a selection step is effective for maintaining a good VST yield, as well as ensuring process simplicity/ cost, however the lack of selection will impact on product specificity due to dilution by bystander leukocytes. Functional recall of *ex vivo* expanded SARS-CoV-2 VST (n=16 donor lines) demonstrated SARS-CoV-2 peptide specificity of 10-16% within CD4+ cells and 4-6% within CD8+ cells (Vasileiou et al., 2023). Keller and colleagues report 0-3% expanded VST expressing IFN-γ in response to individual antigen stimulation to SARS-CoV-2 membrane, nucleocapsid and spike peptides (Keller et al., 2020); and a further 5-25% responsive to pooled SARS-CoV-2 peptides measured as both IFN-γ+/TNFα+ cells and CD107a+ cells (Durkee-Shock et al., 2022). A group using a similar protocol (SARS-CoV-2 peptide-pulsed APC *ex vivo* expansion for 3-4 weeks) reported a mean of 10% CD3+/ IFN-γ+ cells responsive to individual spike, nucleocapsid and membrane peptivator stimulation (Kim et al., 2021). A similar finding was observed in expanded SARS-CoV-2 VST both with and without glucocorticoid deletion, as potential strategy to provide corticosteroid resistance, with ~ 20% IFN-γ+ cells upon recall with SARS-CoV-2 pepmixes (Basar et al., 2021).

Direct selection conversely allows isolation of highly purified antigen-specific T cells, however this is weighted against a low frequency of the desired antigen-specific T cells within the whole PBMC population. As corresponding to our findings other groups have confirmed similar yields of approximately 1-2x10^6 IFN-γ+ target cells responding to SARS-CoV-2 peptide pools from Prodigy CCS isolation (Bonifacius et al., 2022, Chu et al., 2023, García-Ríos et al., 2022, Leung et al., 2020). As discussed in

Chapter 4, we developed a post-selection culture protocol which induced a mean 1000x fold expansion in CCS IFN-γ+ target cells within 14 days, with expanded cells retaining functional potency and specificity. As of October 2023, there appears only one other reported study that combines CCS isolation with an expansion protocol to generate a SARS-CoV-2 VST product with clinically relevant numbers (Gil-Bescós et al., 2023). This approach however uses an initial 14 day culture period with SARS-CoV-2 peptivator Select to expand peptide-reactive VST within the PBMC population, followed by an IFN-γ CCS at day 14 – essentially the reverse of our approach. While the absolute numbers of final product were not reported, the frequency of SARS-CoV-2 reactive VST in PBMC population increased from 0.02 ± 0.01% at day 0, to 3.9 ± 2.4% at day 14 expansion (n=9 donors). This allowed a very efficient IFN-γ CCS enrichment at day 14 with isolated products at 75.5 ± 11.0% IFN-γ+ target cells. This process would be particularly useful for generating SARS-CoV-2 VST from individuals with very low frequency SARS-CoV-2 responsive T cells at initial blood donation.

Since our developed process induced sufficient yield for multiple patient doses, our centre proceeded to GMP manufacture a SARS-CoV-2 VST bank for clinical use. To this end, full scale development runs with commercial USA donor leukapheresis (n=4 donors) as starting material were used to translate and validate the process within the clean room environment. COVID-19 convalescent UK donors screened with sufficient SARS-CoV-2 peptide T cell responses were then invited to donate leukapheresis for full GMP clean room manufacture (n=9 donors). Therefore, it was the aim of this chapter to summarise my work to assess process translation from research phase to GMP manufacture, with evaluation of product yield, phenotype and effector functionality. Also with high yields of VST, cells were available for more additional functional characterisation and safety testing. All data gathered from my investigations were used for an Investigational Medicinal Product Dossier to administer partially HLA-matched SARS-CoV-2 VST in a first in human phase I safety trial (DEFINE trial NCT04473053) for hospitalised COVID-19 patients.

6.2 Research process translation to full-scale GMP manufacture

Initial development of the process to generate SARS-CoV-2 VST was done on a reduced scale research protocol, using donor buffy coat as starting source material, and open process CCS isolation and culture methods to allow testing of multiple

conditions (as described in Chapter 4). Prior to clean room production of the SARS-CoV-2 VST bank, full-scale development was done using leukapheresis starting source material to understand VST yield and product comparability when using automated CCS isolation and closed-process culture expansion. Since it was unethical to use a full leukapheresis donation for development purposes within the UK, commercial leukapheresis material with ethical consent for research use including genetic testing was acquired from USA donors with confirmed previous COVID-19 infection by PCR. Four USA donors were used for development runs. While USA donors could not be pre-screened for T cell responses to SARS-CoV-2 peptivator S+N+M peptide pools prior to apheresis, upon arrival the raw leukapheresis was screened using the SARS-CoV-2 screen assay in tandem with the Prodigy CCS isolation. From the screening assay, donor C19USAD1 had insufficient CD3+/IFN-γ+ frequency as per our 0.08% of T cells threshold criterion for manufacture, therefore due to significant costs of Prodigy consumables this donor sample was not run on Prodigy isolation. Details of subsequent USA donor material used in translation are outlined in **Table 6.1**.

Donor	Sex	Blood Group
C19USAD2	M	AB+
C19USAD3	M	A+
C19USAD4	M	O+

Table 6.1 – SARS-CoV-2 VST translation donor details.

6.2.1 SARS-CoV-2 VST isolation using an automated closed-system cell processor

Since leukapheresis is highly enriched for leukocytes, full-scale manufacturing was made from raw leukapheresis material, unlike the buffy coats which required an initial PBMC isolation step. Therefore, upon shipment from the USA (approximately 48-72 hours), the leukapheresis start material was volume adjusted with acid citrate dextrose (ACD-A), and immediately set up to run an IFN-γ CCS isolation on automated CliniMACS Prodigy cell processor. Following the standard Prodigy CCS programme, target cells were collected and a small sample taken for count and phenotyping. The total number of Prodigy target cells for each donor is shown in **Figure 6.1A**, where all donors had consistent input leukapheresis WBC count. No significant correlation was seen between the number of CD3+ Prodigy CCS targets isolated versus the frequency of CD3+/IFN-γ+ cells in the leukapheresis screen assay (**Figure 6.1B**). The mean CCS

percentage yield of target cells from input WBC was comparable between Prodigy USA donors and previous manual CCS buffy coat isolations (**Figure 6.1C**).

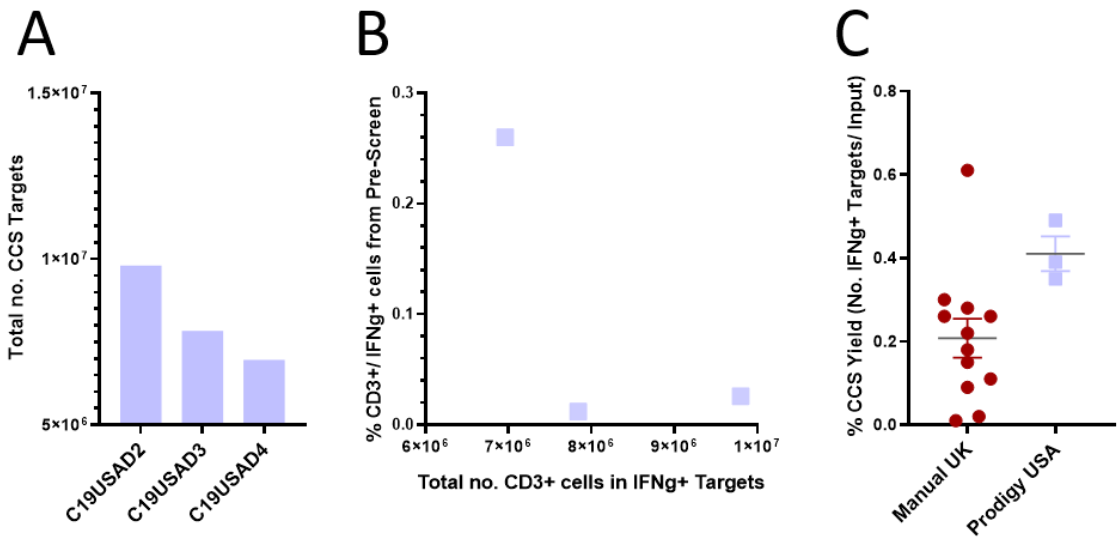

Figure 6.1 - Manual versus Prodigy IFN-γ isolated targets yield comparison.

SARS-CoV-2 VST reactive to pooled S+N+M peptides were isolated from full-scale leukapheresis of COVID-19 convalescent USA donors (lilac squares, n=3) using automated Prodigy IFN-γ CCS assay. **(A)** Isolated IFN-γ+ target cells from CCS assay were counted for total number of CD3+ cells using MACSQuant10 analyser for each USA donor. **(B)** No significant correlation was observed between total number of CD3+ cells in the CCS-isolated IFN-γ+ target fraction, versus the % CD3+/IFN-γ+ PBMC from intracellular cytokine screening assay. Statistical analysis was performed by generating Pearson correlation coefficients, where $p<0.05$ was considered significant. **(C)** The CCS yield (no. of CD3+ CCS target cells/ no. of WBC input) was compared between Prodigy isolated USA donors (n=3) and manual isolated UK donors (from Chapter 4, burgundy circles, n=12). Data is represented as mean ± SEM. No significant differences were observed using unpaired t-tests.

A small sample of positive fraction target cells from the prodigy CCS isolation were also phenotyped using the T cell surface phenotype panel as per **Table 2.5**. The target cell phenotype of Prodigy CCS isolations from leukapheresis was again compared to manual column CCS isolated targets from buffy coats (data from initial research phase in Chapter 4). As can be seen, the percentage of monocytes, CD3+ T cells, CD3+/CD56- NK cells and CD3+/CD56+ NKT cells was equivalent between Prodigy CCS targets and manual CCS targets (**Figure 6.2A**). Of the gated CD3+ T cells (**Figure 6.2B**), there was a similar frequency of CD8+ and DP T cells, however a significantly ($p=0.005$) lower percentage of CD4+ T cells in Prodigy CCS targets compared to manual CCS targets. This likely reflects the significantly higher ($p<0.0001$) percentage of DN (CD4-/CD8-) T cells in Prodigy CCS targets than manual CCS targets. This observation may be due to the more intense stimulation and cell processing involved in automated Prodigy CCS. One feature of the automated prodigy CCS programme is leukapheresis cells are run through the magnetic column twice to optimize purity,

however this was not done for manual column isolations. Debris in particular was notably high in Prodigy CCS isolation (discussed in **section 6.4.1**) which is thought to be due to the automated closed processing and double column enrichment. Since T cells can downregulate CD4 and CD8 receptors upon significant or chronic activation (Xiao et al., 2007, Grishkan et al., 2013), the higher frequency of DN T cells may reflect the intense stimulation and processing through the magnetic column in this closed system. Within the CD4+ T cell population (**Figure 6.2C**), the frequency of memory subtypes were comparable between the two groups, however differences were seen within the CD8+ T cell population (**Figure 6.2D**). The frequency of central memory cells (CD8 TCM) was significantly higher (p=0.035) in Prodigy CCS targets than manual CCS targets, however with low effect size. The mean percentage of effector memory (CD8 TEM) was also significantly increased (p=0.0227) in Prodigy CCS targets than manual CCS targets, and consequently a reduced frequency (p=0.0145) of terminal effector cells (CD8 TEMRA) in Prodigy CCS targets than manual CCS targets. Again this suggests there are discrete phenotypic differences in targets isolated using the Prodigy CCS versus manual CCS protocol, however it should be noted there is unequal variance in the two groups due to a low sample size in the prodigy (n=3) versus manual (n=9) groups that may bias the statistical observations.

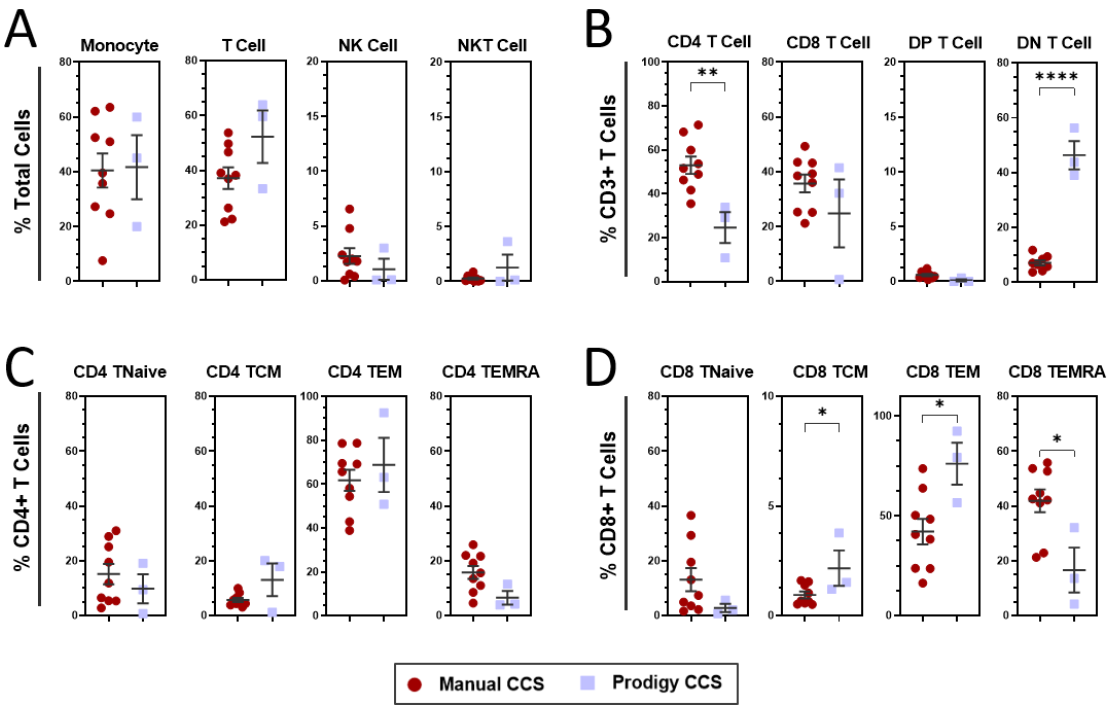

Figure 6.2 - Manual versus Prodigy IFN-γ isolated targets phenotype comparison.

Gated viable lymphocytes of target samples were compared for the frequency of different phenotypic populations between manual column CCS (n=9, burgundy circles) or automated Prodigy CCS (n=3, lilac squares) VST isolations. **(A)** Gating on total lymphocytes, groups were compared for monocytes, T cells, NKT cells and NK cell frequency. **(B)** Gated T cells (CD3+) were

then assessed for T cell subtypes: CD4, CD8, double positive (DP) and double negative (DN). Each CD4+ **(C)** and CD8+ **(D)** T cell population was further assessed for T cell memory populations: naïve (TNaive), central memory (TCM), effector memory (TEM), and terminally differentiated effector memory RA (TEMRA). Data is represented as mean ± SEM. Statistical significance was determined using unpaired t-tests where *p≤0.05 and *p≤0.0001.

6.2.2 Culture expansion process translation: small-scale to large-scale

As in Chapter 4, Prodigy isolated targets were set up in co-culture with irradiated non-target cells and expanded in culture. Using the optimised culture protocol as per **section 2.3.10**, day 14 was chosen as the optimal day of product harvest to allow maximised expansion without need of a feeder re-stimulation step. The growth curves of USA donor full-scale development runs are shown in **Figure 6.3A**. The fold expansion between day 0 isolated CCS targets and day 14 cultures was not significantly different between Prodigy USA donors and previous manual CCS buffy coat isolations (**Figure 6.3B**), however there was considerable variation between USA donor cultures – in particular C19USAD4 demonstrated a 3000x expansion.

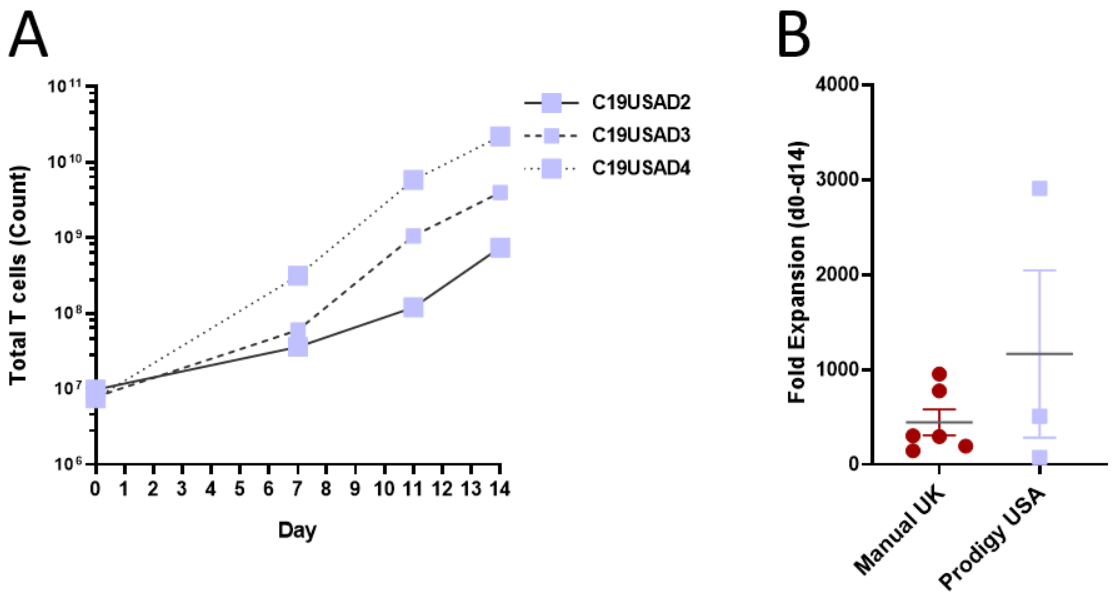

Figure 6.3 - Full-scale development runs growth curves.

(**A**) Full-scale development cultures demonstrated a 2-3 log expansion over 14 days using the validated SARS-CoV-2 VST culture protocol. **(B)** Fold expansion from day 0 targets to day 14 harvested VST using the optimised protocol was compared between Prodigy-isolated USA donors (lilac squares) and manual-isolated UK donors (burgundy circles – C198BC8-14). Data is represented as mean ± SEM. No significant differences were observed using unpaired t-tests.

6.2.3 Comparison of SARS-CoV-2 VST from manual versus Prodigy isolations

As shown above, there were some discrete differences in CCS targets between Prodigy versus manual isolations (see **section 6.2.1**). Day 14 expanded VST were therefore also compared for phenotype between Prodigy-isolated and manual-isolated groups to see if these differences were maintained in the culture expansion process. No significant differences were seen in the frequency of monocytes, T cells, NK cells or NKT cells in the final products between Prodigy isolations than manual isolations (**Figure 6.4A**). Although there was a high frequency of DN T cells in the prodigy CCS target cells (**Figure 6.2B**), the frequency of CD4, CD8, DP and DN T cells was equivalent between the two groups in the final product expanded cells (**Figure 6.4B**). This suggests either the DN T cells in Prodigy CCS targets did not expand in culture and were outcompeted by CD4+ and CD8+ T cell expansion; or that there was a transient downregulation of CD4 and CD8 receptors during the Prodigy CCS isolation, but receptor expression recovered during the culture process. Both CD4 (**Figure 6.4C**) and CD8 compartments (**Figure 6.4D**) had comparable memory subpopulations between the two groups. Altogether these data suggest that the phenotypic differences of target cells between Prodigy and manual CCS is lost over the culture period demonstrating robustness in the protocol to favour central memory CD4 and CD8 T cell expansion.

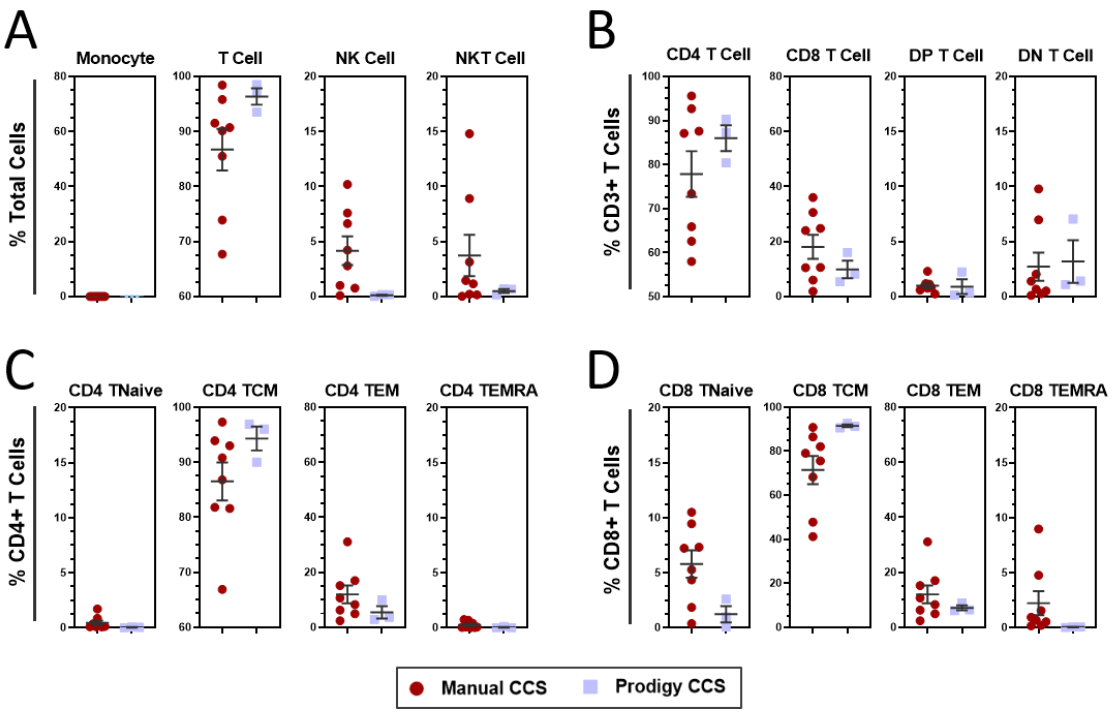

Figure 6.4 - Manual versus Prodigy VST final product phenotype comparison.

VST expanded for 14 days in culture were compared for the frequency of different phenotypic populations between manual column CCS (burgundy circles) or automated Prodigy CCS (lilac squares) isolations. **(A)** Gating on total lymphocytes, groups were compared for CD45+ cells, T cells, NKT cells and NK cell frequency. **(B)** Gated T cells (CD3+) were then assessed for T cell subtypes: CD4, CD8, double positive (DP) and double negative (DN). Each CD4+ **(C)** and CD8+ **(D)** T cell population was further assessed for T cell memory populations: naïve (TNaive), central memory (TCM), effector memory (TEM), and terminally differentiated effector memory RA (TEMRA). Data is represented as mean ± SEM. Statistical significance was determined using unpaired t-tests corrected for multiple comparisons with Holm-Šídák method test where *p≤0.05.

Expanded SARS-CoV-2 VST were also compared for functional reactivity between Prodigy isolations versus manual isolations using the DC co-culture ICR assay outlined in section. Briefly, autologous DC were loaded with pooled SNM peptides and co-cultured with the day 14 expanded VST at [1 DC: 10 VST] for a 5 hour stimulation. Antigen recall was then assessed by flow cytometry intracellular expression of T cell effector cytokines IFN-γ, TNF-α, IL-2; and Th cell activation marker CD154 normalised to unloaded DC controls. No significant differences were observed in the percentage of peptide-reactive IFN-γ+, TNF-α+, IL-2+ or CD154+ T cells between the two groups (**Figure 6.5**), indicating comparable effector functionality between Prodigy-isolated and manual-isolated VST.

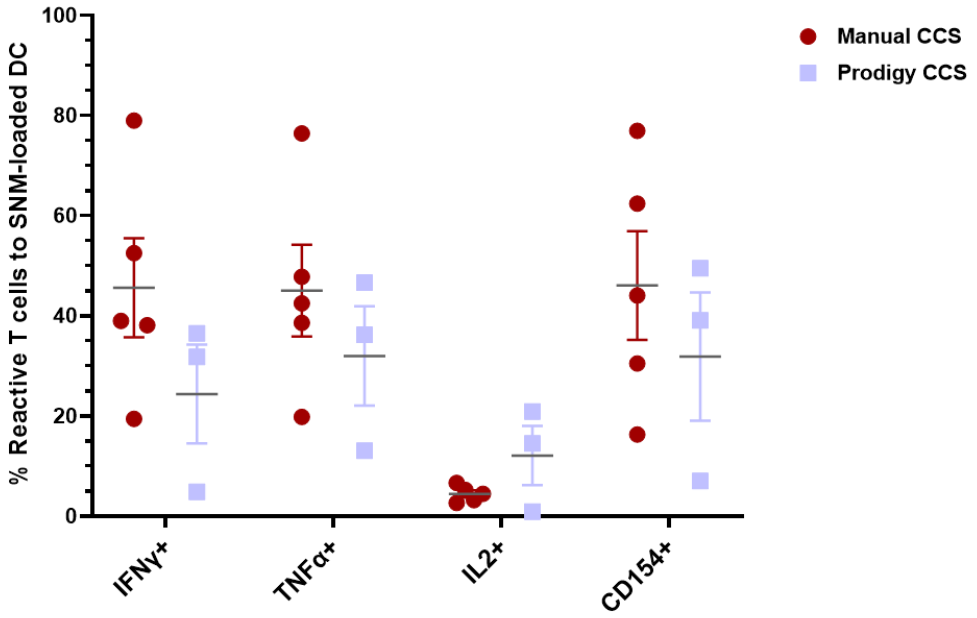

Figure 6.5 - Manual versus Prodigy VST functional reactivity comparison.

SARS-CoV-2 VST expanded for 14 days from either manual CCS isolations (n=4, burgundy circles) versus Prodigy CCS isolations (n=3, lilac squares) were compared for functional reactivity to SARS-CoV-2 peptides. For this, autologous DC (generated by Dr Paul Burgoyne) were loaded with pooled SARS-CoV-2 Spike + Nucleocapsid + Membrane (SNM) peptides. SNM-loaded or unloaded DC controls were co-cultured with VST at [1 DC: 10 VST] for 5 hours and co-cultures subsequently stained for intracellular cytokines & activation markers. To measure VST reactivity to pooled SNM peptides, gated CD3+ T cells were quantified for expression of IFN-γ, TNF-α, IL-2 and CD154. All peptide-reactive cells were normalised to unloaded DC controls. Data is represented as mean ± SEM and tested for statistical significance using unpaired t-tests.

Altogether these data indicate there is no significant difference in fold expansion, final product phenotype and final product functional response between manual versus Prodigy-isolated VST. Therefore, these data demonstrate that the closed system automated isolation and culture approach scales equivalently to the established manual process and is suitable for full-scale VST production.

6.3 Donor selection for SARS-CoV-2 VST bank manufacture

As learnt from previous development and manufacture of the EBV VST bank using peptides and CCS, manufacture failure rate was greatly reduced by implementing a peripheral blood pre-screen assay to test T cell peptide responses. While all donors for this work were EBV-seropositive, not all had detectable EBV peptide T cell responses at donation, which was linked to poor yield at prodigy CCS isolation and subsequent failure to expand (Cooper et al., 2024). Therefore for this bank, a minimum threshold of 0.08% CD3+ IFN-γ+ cells reactive to EBV peptides in buffy coat pre-screen was considered sufficient for a successful EBV VST product manufacture.

Given this experience, and combined with the observations in Chapter 4 that the frequency of SARS-CoV-2 VST in buffy coat PBMC showed a trend to decline over time from infection, it was deemed crucial to set a similar pre-screen threshold for a donor to be eligible for SARS-CoV-2 VST bank manufacture.

6.3.1 Banked donors buffy coat SARS-CoV-2 T cell responses

While SARS-CoV-2 T cell responses for the full cohort of screened buffy coat donors is discussed in Chapter 5, the frequency of CD3+ IFN-γ+ cells reactive to pooled SNM stimulation for the final SARS-CoV-2 VST banked donors is shown in **Figure 6.6**. All buffy coats were screened between August 2020 to April 2021, with a minimum criterion of >0.08% CD3+ IFN-γ+ cells to be detected prior to being contacted for donor consent for bank manufacture. As can be seen, while most donors have a frequency of 0.1-0.2% SNM-reactive T cells, two donors had >0.5% reactive SNM-reactive T cells at time of buffy coat screening.

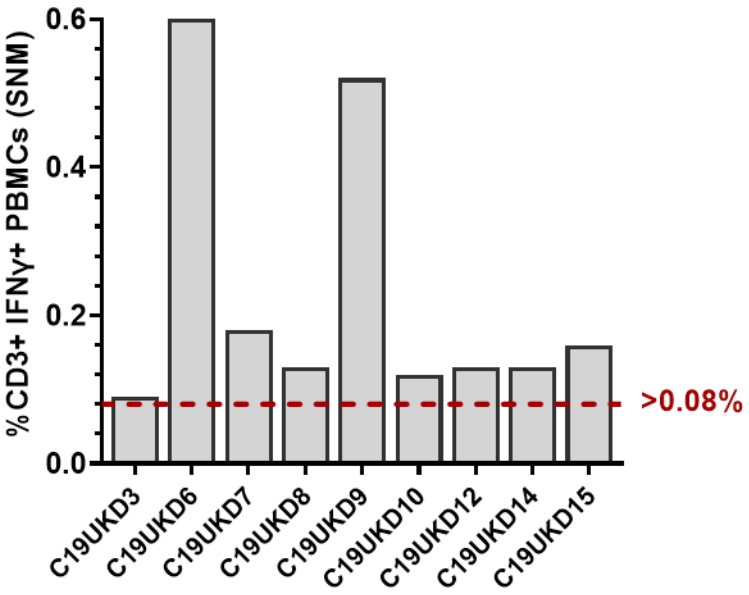

Figure 6.6 - Buffy coat donors IFN-γ responses to SARS-CoV-2 SNM peptides.

Buffy coat PBMC peptide screening of T cell responses to SARS-CoV-2 pooled SNM peptides stimulation. A threshold of >0.08% CD3+ IFN-γ+ lymphocytes was set for a donor to be eligible for VST bank manufacture. The frequency of SNM-reactive T cells is shown for the final banked SARS-CoV-2 VST donors.

With the rapid development and delivery of the SARS-CoV-2 vaccine program in the UK, by the time most bank donors were scheduled to donate leukapheresis they had received Spike-directed vaccines. Therefore, screening responses were compared between their initial buffy coat screen and later leukapheresis pre-screen in attempt to elucidate differences in natural virus versus vaccine T cell responses (**Figure 6.7**). For donor 1 the response to pooled SARS-CoV-2 peptides markedly increased from 0.12% to 0.78% CD3+ IFN-γ+ cells between initial screen (29 days after virus infection natural resolution) and leukapheresis pre-screen (61 days after first dose of Pfizer vaccine). Interestingly, individual peptide responses showed Spike-reactive VST levels were slightly lower than that of Nucleocapsid and Membrane demonstrating the T cell response is not particularly oriented towards Spike antigen recognition despite a dose of Spike-targeted vaccine. Instead, the increase in response seen between time-points is more indicative of a recent community reinfection. Donor 2 however showed a decreased response to pooled peptides (0.52% to 0.29% CD3+ IFN-γ+ cells respectively) between initial screen (65 days after infection resolution) and leukapheresis pre-screen (99 days after second dose Pfizer vaccine). Donor 2 showed negligible T cell IFN-γ reactivity to Nucleocapsid at the latter screen, with more T cells reactive to Spike and Membrane which may indicate a re-distribution of the peripheral SARS-CoV-2 memory T cell compartment after vaccine.

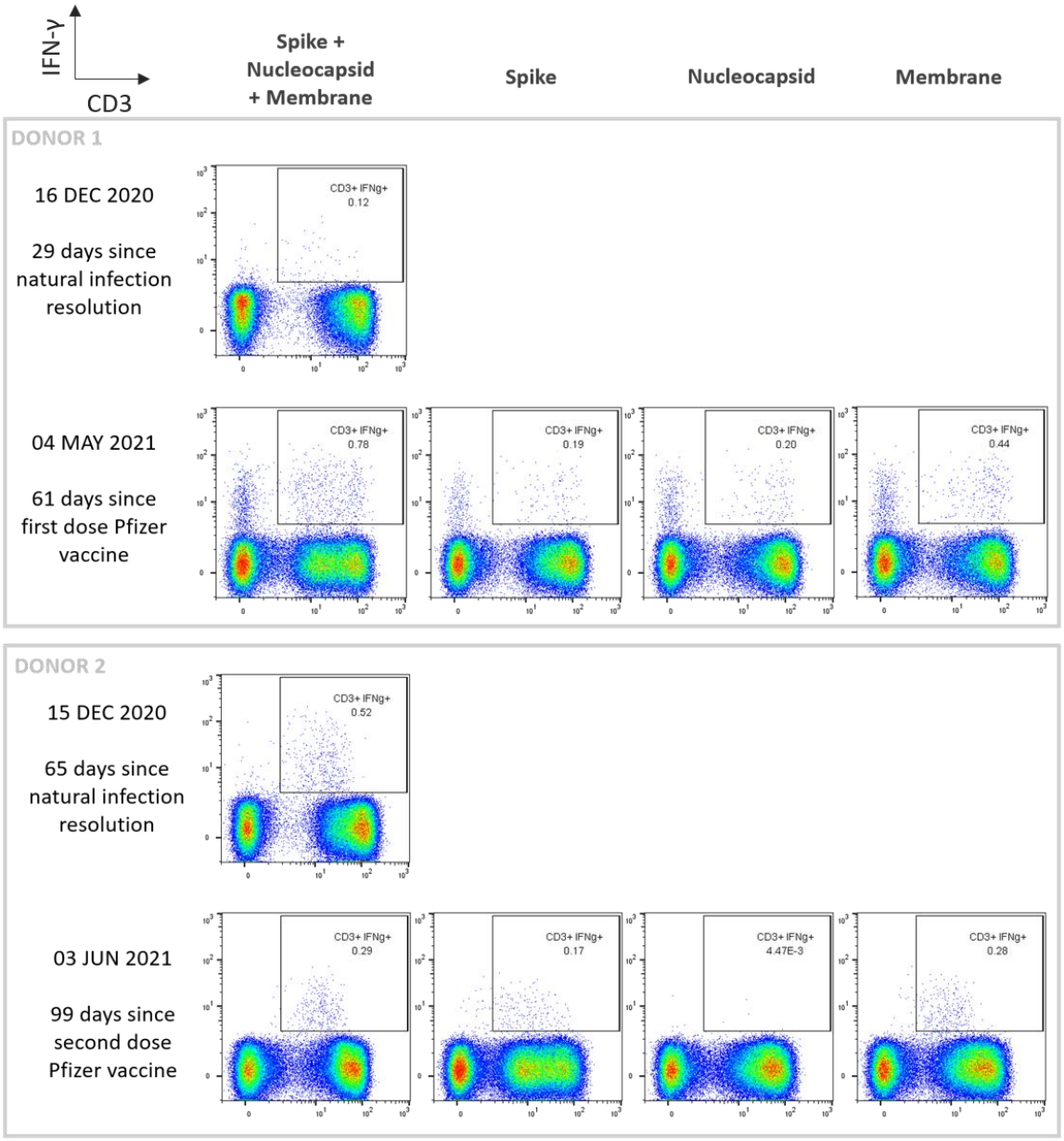

Figure 6.7 - Case studies of T cell virus versus vaccine responses.

The frequency of SNM-reactive VST (CD3+ IFN-γ+ cells) in peripheral blood PBMC is compared between two time-points: initial buffy coat screen after natural virus infection resolution (top panel for each donor) and at leukapheresis pre-screen at indicated time after receiving spike-targeted vaccines (bottom panels for each donor).

6.3.2 Donors selected for SARS-CoV-2 VST bank manufacture

An initial 15 COVID-19 convalescent donors were consented to donate leukapheresis for SARS-CoV-2 VST bank manufacture. Donors C19UKD1 and C19UKD2 successfully generated SARS-CoV-2 VST using the clean room validated process, however these initial runs took place between December 2020 and January 2021 using S+N+M premium-grade peptide pools as used all throughout the development. In February 2021, GMP-grade SARS-CoV-2 (SC-2) Select peptide pools were released by Miltenyi Biotec and therefore these were tested for use in the SARS-CoV-2 VST manufacturing

process. Donor C19UKD3 had a parallel clean room process to directly compare isolation with premium-grade S+N+M versus GMP-grade peptide pools. Since this intra-donor comparison demonstrated equivalent expansion, final product phenotype and functionality (data not shown), GMP SC-2 Select peptides were taken forward for the bank manufacture to ensure the process was fully GMP-compliant. C19UKD3 and all following donor VST banked were generated against GMP SC-2 Select peptides. Four donors (C19UKD4, C19UKD5, C19UKD11, C19UKD13) failed the clinical apheresis unit screening tests and therefore did not proceed to leukapheresis donation. The remaining nine donors were run in GMP clean room manufacture as per **Table 6.2**, in which they are colour coded according to final product yield (green =good yield, yellow = poor yield, orange=not sufficient product for inclusion in the bank).

Donor	Age	Time of Infection	~Days Infection to Donation	Most Prevalent Variant	Vaccine Status	~Days Last Vaccine to Donation
C19UKD3	30	Apr-20	299	Wild type	Not vaccinated	N/A
C19UKD6	50	Oct-20	185	Wild type	Single vaccinated (Pfizer)	66
C19UKD7	59	Oct-20	213	Wild type	Double vaccinated (Pfizer)	97
C19UKD8	56	Oct-20	255	Wild type	Double vaccinated (AstraZeneca)	37
C19UKD9	49	Oct-20	290	Wild type	Double vaccinated (AstraZeneca)	29
C19UKD10	58	Jul-20	431	Wild type	Double vaccinated	203
C19UKD12	41	Jul-21	122	Delta	Double vaccinated	91
C19UKD14	25	Jun-21	178	Delta	Double vaccinated	117
C19UKD15	45	Jan-21	331	Alpha	Triple vaccinated (Pfizer + Moderna)	85

Table 6.2 - SARS-CoV-2 VST banked donor infection and vaccination details.

6.3.3 Leukapheresis screen of SARS-CoV-2 VST banked donors

Donors selected on the basis of T cell peptide responses in initial 2020 buffy coat screening were consented for leukapheresis donation for potential inclusion in VST bank manufacture. Since the duration between initial buffy coat screen and leukapheresis donation was between 2-12 months, donors had a small volume of

peripheral blood taken one to two weeks prior to their scheduled leukapheresis, to re-test for peptides responses to ensure VST numbers hadn't declined to undetectable levels. All donors had sufficient peptide-reactive T cells (>0.08%) at peripheral blood testing. Donors that passed standard clinical apheresis screening on health, behaviour and blood counts then went ahead for 5L Optia leukapheresis collection. While $2x10^9$ WBC from leukapheresis was taken straight for Prodigy CCS isolation, residual cells were again screened for SARS-CoV-2 peptide responses to understand differences between peripheral blood PBMC and raw leukapheresis WBC responses. It was important to ensure peptide-reactive T cells were still detectable at sufficient level in unprocessed leukapheresis, or if these were insufficient, a PBMC isolation step may be required for the manufacturing process. As can be seen in **Figure 6.8A**, responses to Spike, Nucleocapsid or Membrane were highly variable between donors, with no consistent skewing towards any individual peptide (**Figure 6.8B)**. Donor leukapheresis was also tested for responses to pooled SNM research-grade peptides used in initial development, versus GMP-grade SC-2 Select used for manufacture (**Figure 6.8C**). Although there trended towards higher responses to pooled SNM compared to GMP SC2 Select, this was not statistically significant (**Figure 6.8D**).

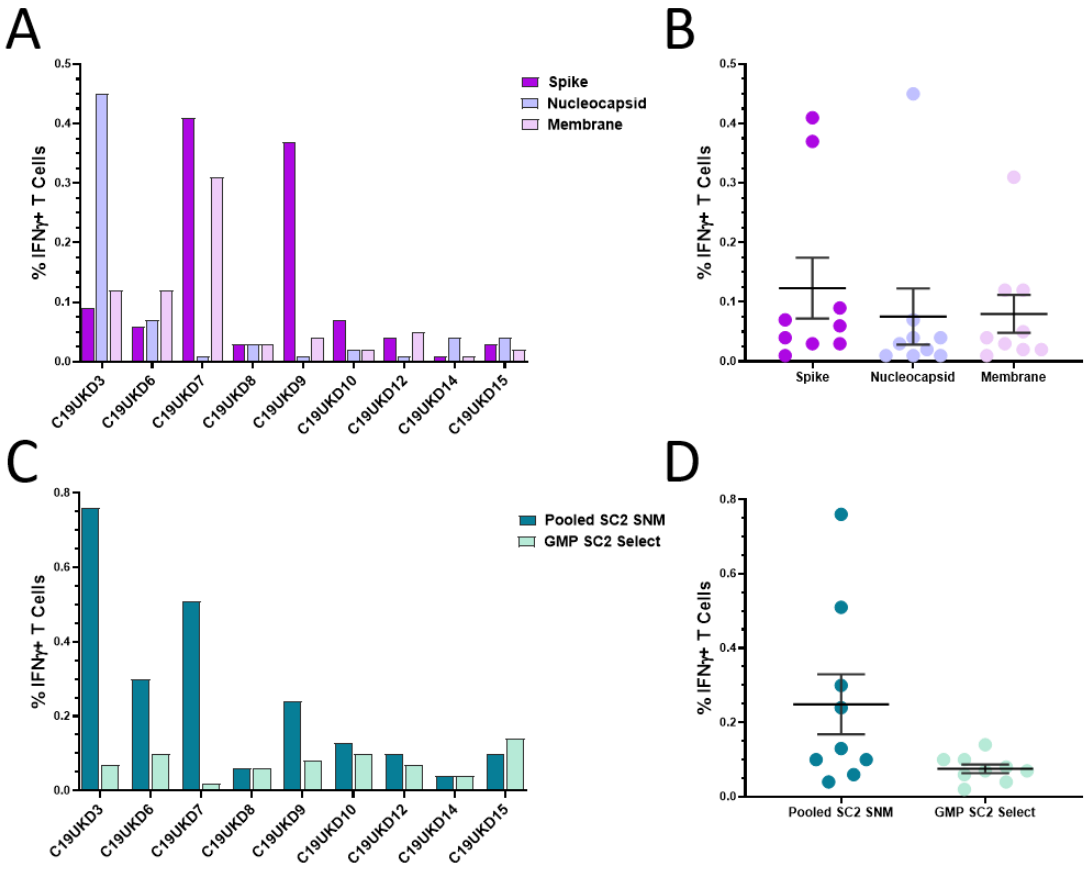

Figure 6.8 - Leukapheresis screen response to different SARS-CoV-2 peptides.

Leukapheresis material from COVID-19 convalescent donors selected for SARS-CoV-2 VST bank manufacture was tested for responses to different SARS-CoV-2 peptides. The frequency of CD3+/ IFN-γ+ cells within the lymphocyte population for individual protein SARS-CoV-2 peptides: Spike, Nucleocapsid and Membrane is shown per donor **(A)** and as **(B)** mean ± SEM (n=9). Comparisons between groups were made using RM one-way ANOVA where *p≤0.05 was considered statistically significant. The frequency of CD3+/ IFN-γ+ cells within the lymphocyte population for mixed SARS-CoV-2 peptides: pooled SNM (research-grade) and SARS-CoV-2 Peptivator Select (GMP-grade) for each donor **(C)** and as **(D)** mean ± SEM (n=9). Comparisons between groups were made using paired two-tailed T tests where *p≤0.05 was considered statistically significant.

Comparison of T cell responses to the GMP SARS-CoV-2 peptides was made between the peripheral blood isolated PBMC (taken 1-2 weeks prior to leukapheresis donation) and unprocessed raw leukapheresis (**Figure 6.9**). All donors except for C19UKD8 and C19UKD15 demonstrated a reduction in peptide-reactive T cells in the raw leukapheresis compared to peripheral blood isolated PBMC (**Figure 6.9A**), which was a significant difference as mean of all donors (**Figure 6.9B**). Although there was a 1-2 week gap between sampling points that may indicate a contraction in the VST population in this time, it is more likely the variation reflects the different processing and ultimately different population compositions of the blood samples.

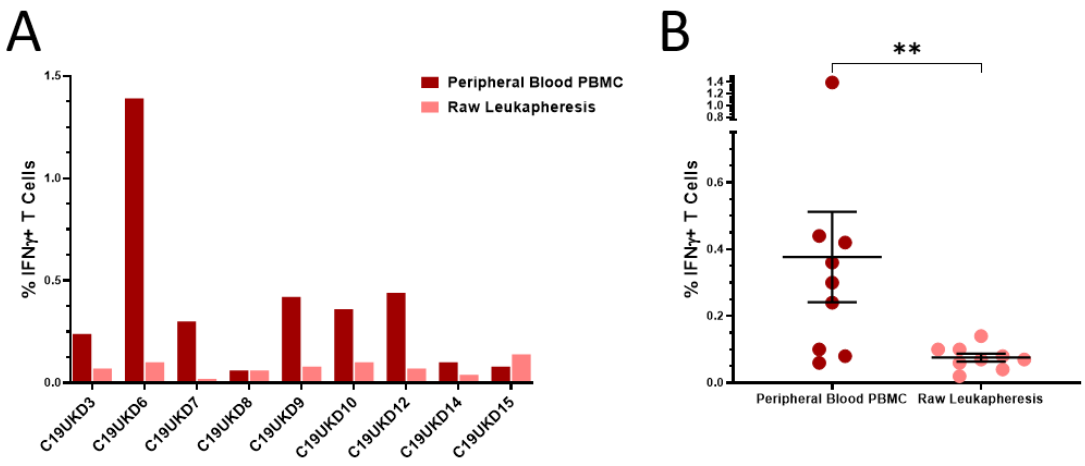

Figure 6.9 - Comparison of peripheral blood pre-screen and leukapheresis T cell responses.

T cell responses to SARS-CoV-2 Peptivator Select were compared between peripheral blood isolated PBMC (two weeks prior to leukapheresis donation) and raw leukapheresis material. The frequency of CD3+/ IFN-γ+ cells within the lymphocyte population for the two samples are shown per donor **(A)** and as **(B)** mean ± SEM (n=9). Comparisons between groups were made using paired two-tailed T tests where **p≤0.01.

6.4 SARS-CoV-2 VST bank manufacture

Within 24 hours of collection, leukapheresis donations were set up for CliniMACS Prodigy CCS isolation with GMP SARS-CoV-2 Peptivator Select. The following morning, samples were taken from both IFN-γ+ targets and non-target fractions for counts using TruCount enumeration. Non-target cells were irradiated and co-cultures

set up at [100 Non-targets: 1 Target] in G-Rex100M-CS flasks for a 14 day culture expansion, with feeds and passage at days 7 and 11. Samples from IFN-γ+ targets at day 0 and day 14 expanded final product cells were phenotyped. Exemplar flow cytometry analysis of targets and final product samples between a 'good' expansion donor and a 'bad' expansion donor is shown in **Figure 6.10**.

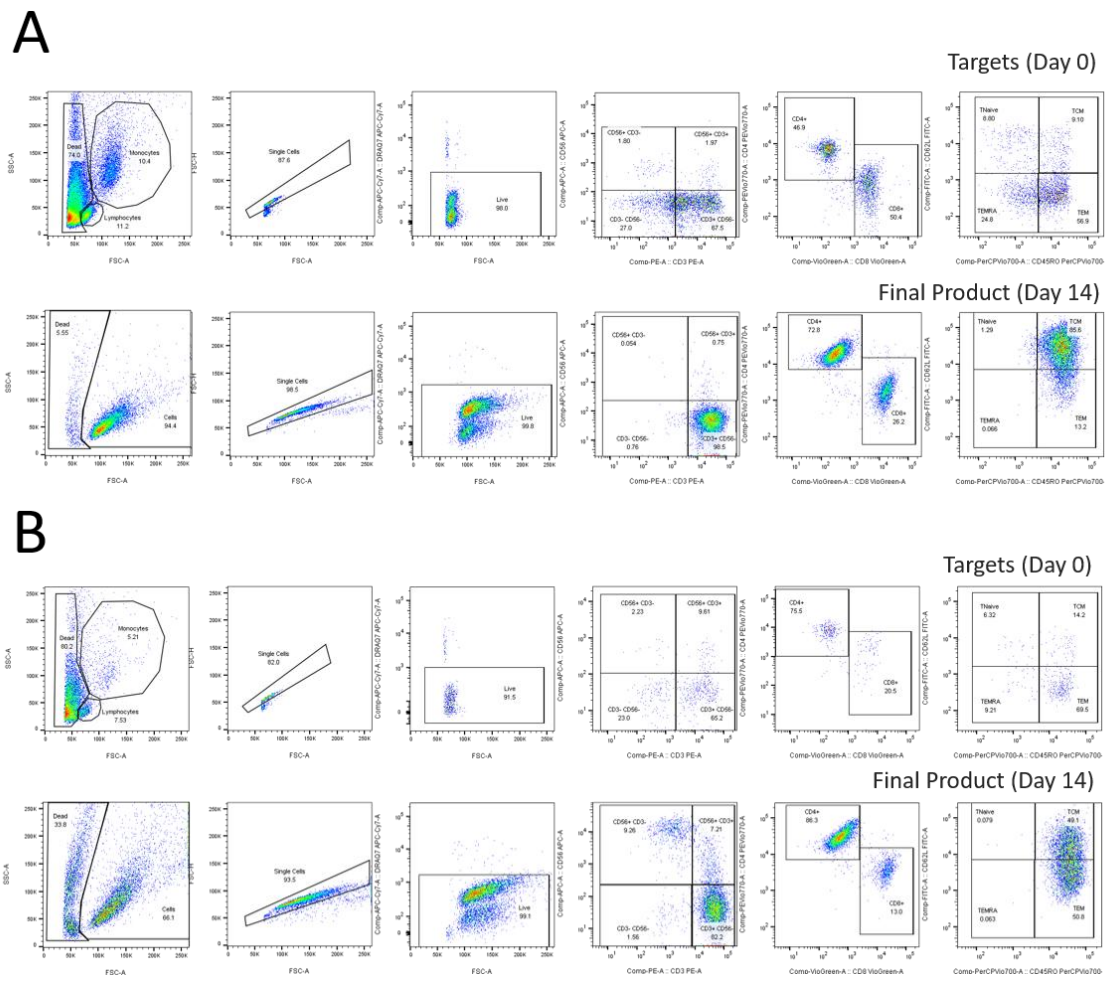

Figure 6.10 - Flow cytometry representative phenotype analysis of targets and final product.
QC analysis of VST surface phenotype at day 0 isolated targets versus day 14 final product is shown for exemplar **(A)** 'good' expansion donor C19UKD7, as compared to **(B)** 'poor' expansion donor C19UKD9.

6.4.1 SARS-CoV-2 VST banked donors Prodigy isolations

Prodigy CCS isolations were analysed for successful selection of target VST on the basis of yield and enrichment purity. Enumeration of CCS IFN-γ+ target cells was made using Trucount assay counting the total number of viable cells (CD45+/ DRAQ7-). Total counts for each donor isolation are shown in (**Figure 6.11A**). No significant correlations were seen by the number of isolated target cells and the duration between first infection and leukapheresis donation (**Figure 6.11B**). In

addition, no correlations were observed between the number of isolated targets versus the frequency of peptide-reactive VST and peripheral blood pre-screen (**Figure 6.11C**) or leukapheresis screen (**Figure 6.11D**).

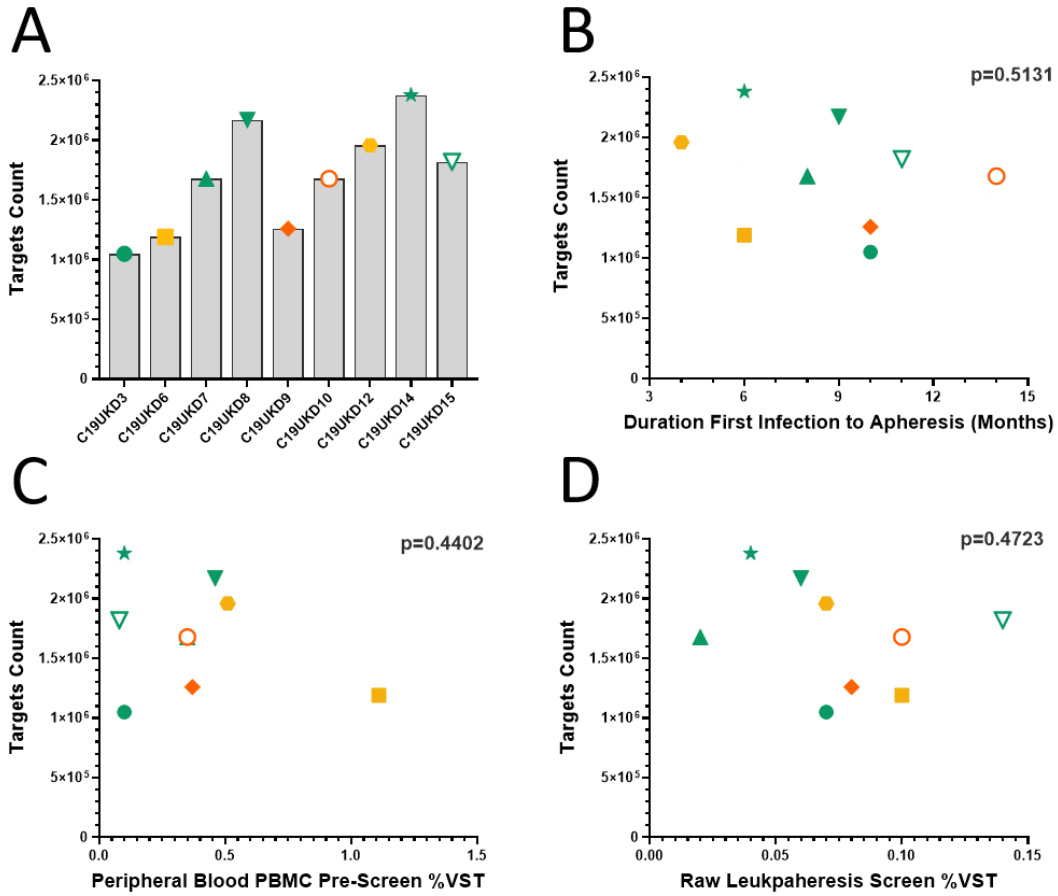

Figure 6.11 - Banked VST Prodigy targets yield correlations.

Samples of prodigy-isolated IFN-γ+ targets were taken for cell enumeration using TruCount assay. **(A)** The total number of CD45+/ DRAQ7- (viable WBC) is shown per donor. Correlations between target viable count were made between **(B)** the duration from first infection to leukapheresis donation, **(C)** the frequency of peptide-reactive VST at peripheral blood PBMC pre-screen and **(D)** the frequency of peptide-reactive VST in the leukapheresis screen. Calculation was performed using Pearson correlation coefficient. For each correlation test, the p value was reported where p>0.05 was non-significant.

The phenotype of CCS isolated targets was analysed as outlined in **Figure 6.10**. Initial characterisation based on scatter properties demonstrated target cell composition was 10-20% lymphocytes (**Figure 6.12A**), 5-10% monocytes (**Figure 6.12B**), and 65-80% dead cells/ debris (**Figure 6.12D**), demonstrating the relatively harsh effects of closed-system CCS isolation. The ratio of lymphocytes to monocytes and thereby overall targets lymphocyte purity discounting dead cells was variable between donors (**Figure 6.12C**). Within the viable lymphocyte population, target samples had variable frequencies of NK cells (**Figure 6.12E**) and NKT cells (**Figure 6.12F**)

between 0-15% between donors, but were largely enriched for T cells (**Figure 6.12G**) at 60-80% CD3+/ CD56- cells. Within the T cell population, most donor target cells were skewed toward CD4+ cells, however some donors had a more equal CD4:CD8 T cell ratio (**Figure 6.12H**). In terms of T cell memory (**Figure 6.12I**), targets were consistently enriched for effector memory (TEM), with small populations of terminal effector (TEMRA) and central memory (TCM), and negligible naïve T cells (TNaive).

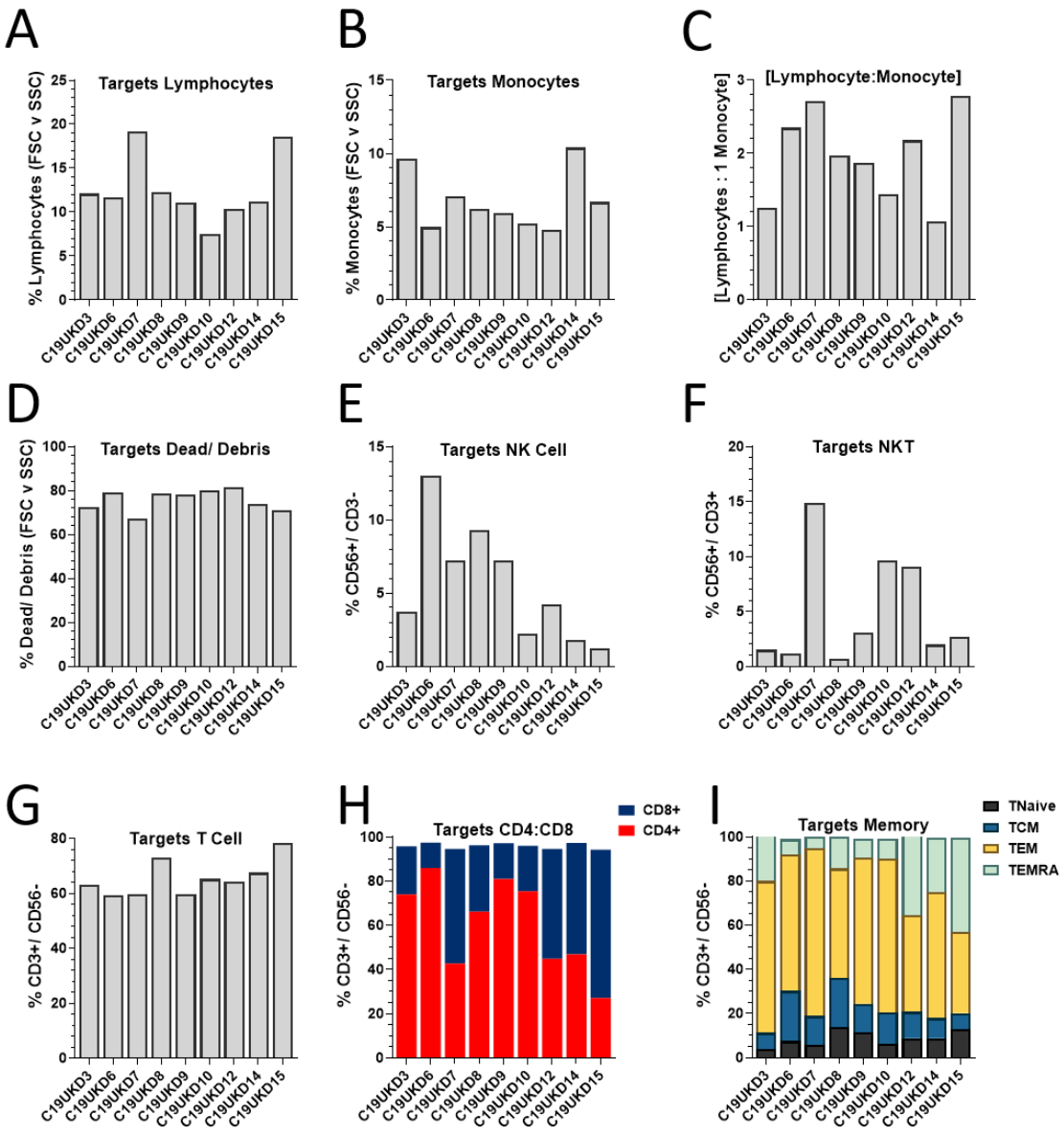

Figure 6.12 - Banked VST Prodigy IFN-γ targets phenotype.

Samples of prodigy-isolated IFN-γ+ targets of banked VST manufacturing runs were taken for flow cytometry phenotyping. From ungated total events, **(A)** % lymphocytes, **(B)** % monocytes, **(C)** lymphocyte: monocyte ratio and **(D)** % dead cells/ debris is shown per donor. Within the viable lymphocyte population (gated lymphocytes/ singlets/ live), each donor was quantified for **(E)** % NK cells, **(F)** % NKT cells, and **(G)** T cells. Gated T cells were further assessed for **(H)** CD4: CD8 ratio and **(I)** T cell memory populations: naïve (TNaive), central memory (TCM), effector memory (TEM), and terminally differentiated effector memory RA (TEMRA).

6.4.2 SARS-CoV-2 banked donors culture expansion

Following clean room culture expansion, final product cells were harvested and formulated into bagged patient doses (1.5x10^8 VST/dose) and cryopreserved for LN_2 VST bank storage. Most donors demonstrated a 3x log fold expansion over the 14 day culture, however donors C19UKD9 & C19UKD10 only achieved a 2x log fold expansion by final product (**Figure 6.13A**). The number of final product patient doses cryopreserved for clinical use was highly variable between donors (**Figure 6.13B**). Since a minimum of 4 bags was required for various final product testing procedures, donors C19UKD9 and C19UKD10 had insufficient doses to be included in the final VST bank. While donors C19UKD14 and C19UKD15 generated a significantly large number of product doses, Planer controlled rate freezer and liquid nitrogen tank capacity limited number cryopreserved for clinical use to 80 bags highlighting the physical practicalities of even large-scale manufacturing centres such as SNBTS.

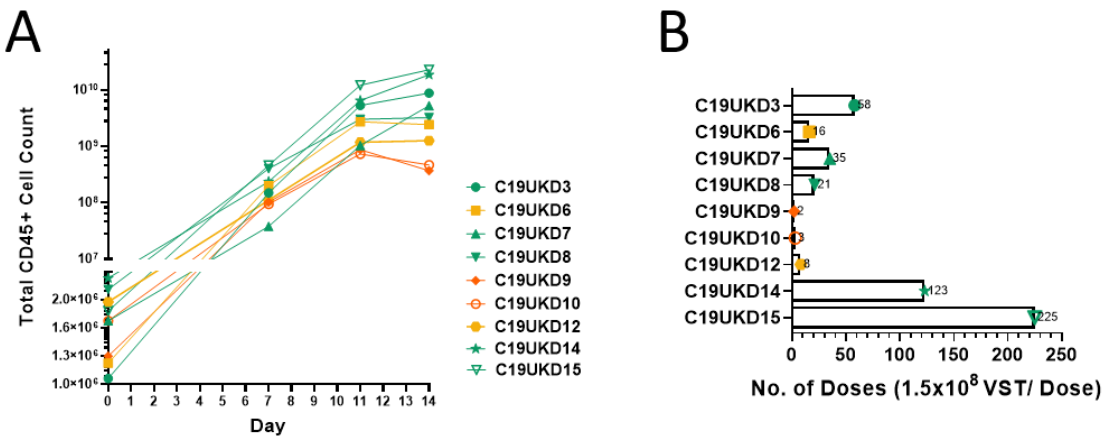

Figure 6.13 - Banked VST growth curves and final product yield.

Growth kinetics of banked donors VST culture expansions. **(A)** Growth curves between day 0 isolated targets and day 14 of culture expansion are shown for all donors. **(B)** The number of final product patient doses cryopreserved for clinical use (formulated at 1.5x10^8 VST per dose) was highly variable between donors.

The total number of harvested final product VST was tested for manufacturing correlations (**Figure 6.14**). Day 14 VST count did not correlate with the duration between initial infection to leukapheresis donation (**Figure 6.14A**) or the number of target cells isolated by prodigy CCS (**Figure 6.14B**). Similarly, no relationships were observed with final product yield and frequency of peptide-reactive VST at the peripheral blood PBMC pre-screen (**Figure 6.14C**) or leukapheresis screen (**Figure 6.14D**).

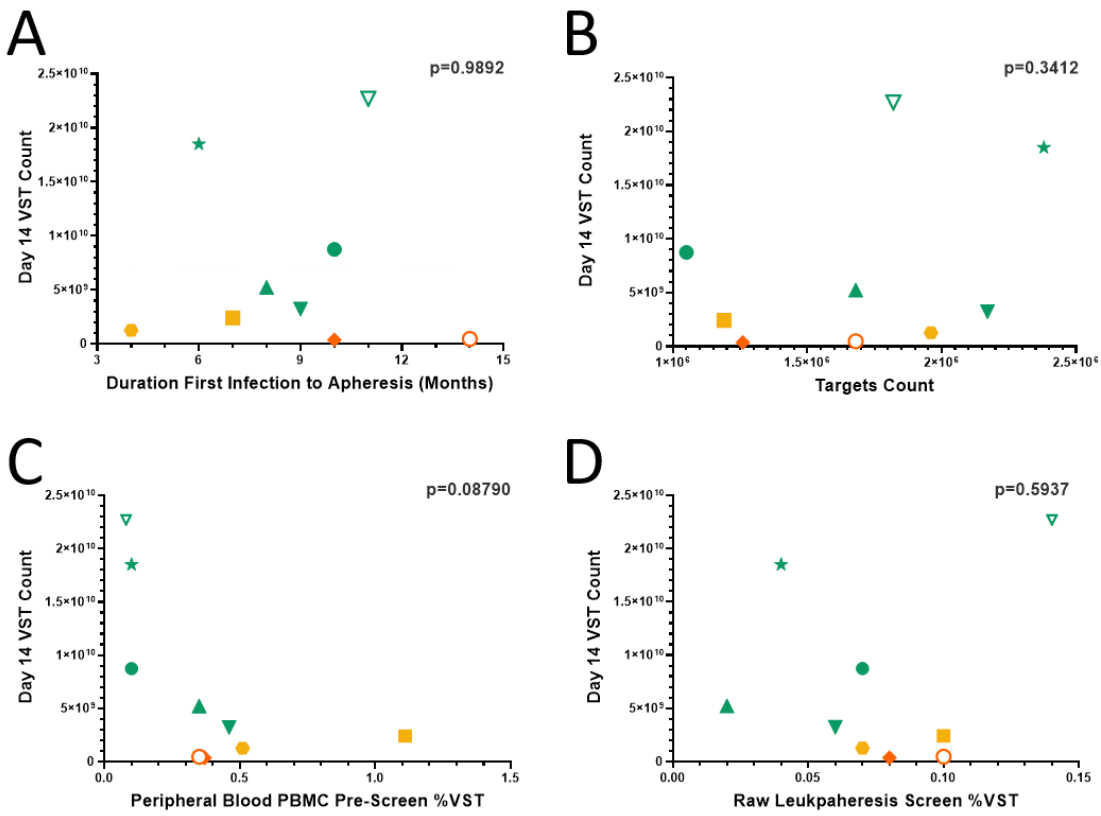

Figure 6.14 - Banked VST final product yield manufacturing correlations.

Final product cells harvested following 14 days expansion were enumerated for CD45+/DRAQ7- viable cells using TruCount assay. Day 14 VST count was tested for correlations between **(A)** duration between first infection and leukapheresis donation, **(B)** Prodigy targets count, **(C)** frequency peptide-reactive VST at peripheral blood pre-screen, and **(D)** frequency of peptide-reactive VST at leukapheresis screen. Calculation was performed using Pearson correlation coefficient. For each correlation test, the p value are reported where p>0.05 was non-significant.

The final product yield was also assessed for correlation with prodigy target phenotype to understand if certain populations positively or negative impacted culture expansion (**Figure 6.15**). No significant correlations were observed with final product count and the frequency of lymphocytes, monocytes or dead cells/ debris in Prodigy target fractions (**A-D**). Similarly, no relationships were seen between final product yield and frequency of NK cells, NKT cells or T cells in the target population (**E-G**). A negative correlation was observed with day 14 VST count and frequency of CD4+ T cells in target fractions (**H**). Correspondingly there was a positive association between frequency of CD8+ T cells in the target fraction and final product yield (**I**). Finally, no correlations were observed with final product count and target fraction frequency of central memory, effector memory, or terminal effector memory (**J-L**). These data indicate VST yield is dependent on CD4 to CD8 content of the targets, whereby CD8+ T cells have greater capacity for expansion in our culture process.

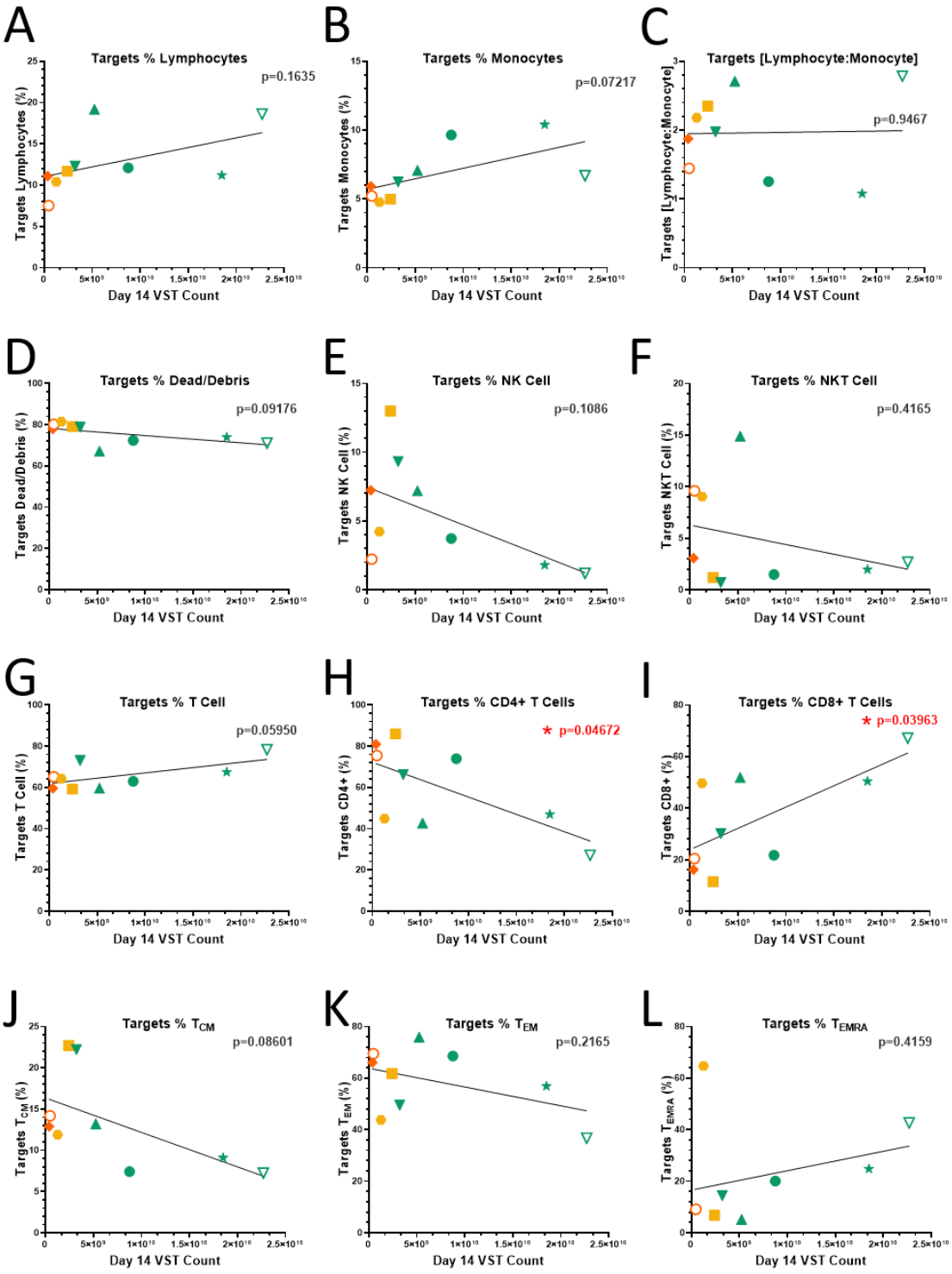

Figure 6.15 - Prodigy IFN-γ targets phenotype to final product yield correlations.

Final product yield was assessed for relationship with Prodigy IFN-γ targets phenotype. Day 14 VST count was tested for correlation with target samples **(A)** % lymphocytes, **(B)** % monocytes, **(C)** lymphocyte to monocyte ratio, **(D)** % dead cells/ debris, **(E)** % NK cells, **(F)** % NKT cells, **(G)** % T cells, **(H)** % CD4+ T cells, **(I)** % CD8+ T cells, **(J)** % TCM, **(K)** % TEM and **(L)** % TEMRA. Calculation was performed using Pearson correlation coefficient. For each correlation test, the p value was reported where $p<0.05$ was considered statistically significant.

6.4.3 Elevated peptide-reactive NK cells in low expansion donors

The frequency of NK cells within the target population isolated by CCS, though not statistically significant, trended towards an association with lower VST final product yield (**Figure 6.15E**). To further investigate this, the flow cytometry leukapheresis screen of SARS-CoV-2 peptide responses was retrospectively analysed to focus on NK cell responses. Flow analysis of all banked VST donors leukapheresis stimulated with SARS-CoV-2 peptivator select is shown in **Figure 6.16A** where analyses were gated on lymphocytes/singlets/live/IFN-γ+ cells. The whole IFN-γ-reactive population was then assessed for frequency of NK cells (CD56+/CD3-) versus T cells (CD3+/CD56-). As can be seen, in the donors which elicited a high expansion of SARS-CoV-2 VST in our manufacturing process coded in green (top panel) the IFN-γ-reactive population consisted primarily of T cells (ranging 56-6-87.1%) with negligible reactive NK cells (ranging 2.3-10.5%). Donors C19UKD6, C19UKD8 and C19UKD10 however had a considerable population of NK cells within the IFN-γ+ population (50.8-56.6%) which exceeded the frequency of peptide-reactive T cells (29.4-36.6%). Although the frequency of peptide-reactive NK cells within IFN-γ+ population did not significantly correlate with day 14 count of SARS-CoV-2 VST (**Figure 6.16B**), there is a clear observation that a large frequency of peptide-reactive NK cells was only present in the lower expansion donors. This observation may suggest an increased population of NK cells secreting IFN-γ within the leukapheresis material upon SARS-CoV-2 peptide stimulation may hinder T cell IFN-γ catch matrix staining or interfere with the microbead column selection in the CCS assay. Lack of statistical significance is likely due to donor C19UKD12 that had low expansion but also fewer IFN-γ+ NK cells, however it is not implausible for a different unrelated mechanism attributing a poor expansion in this donor. Ultimately more donors should be assessed to increase the dataset size to understand if this is a truly correlative phenomenon.

To explore this further, retrospective analysis was done to compare the intra-donor NK cell response between their initial buffy coat screen to determine eligibility in terms of a minimum criteria of SARS-CoV-2 peptide-reactive T cells (done between September to December 2020) and their subsequent leukapheresis screen during VST manufacture (done between February to October 2021).

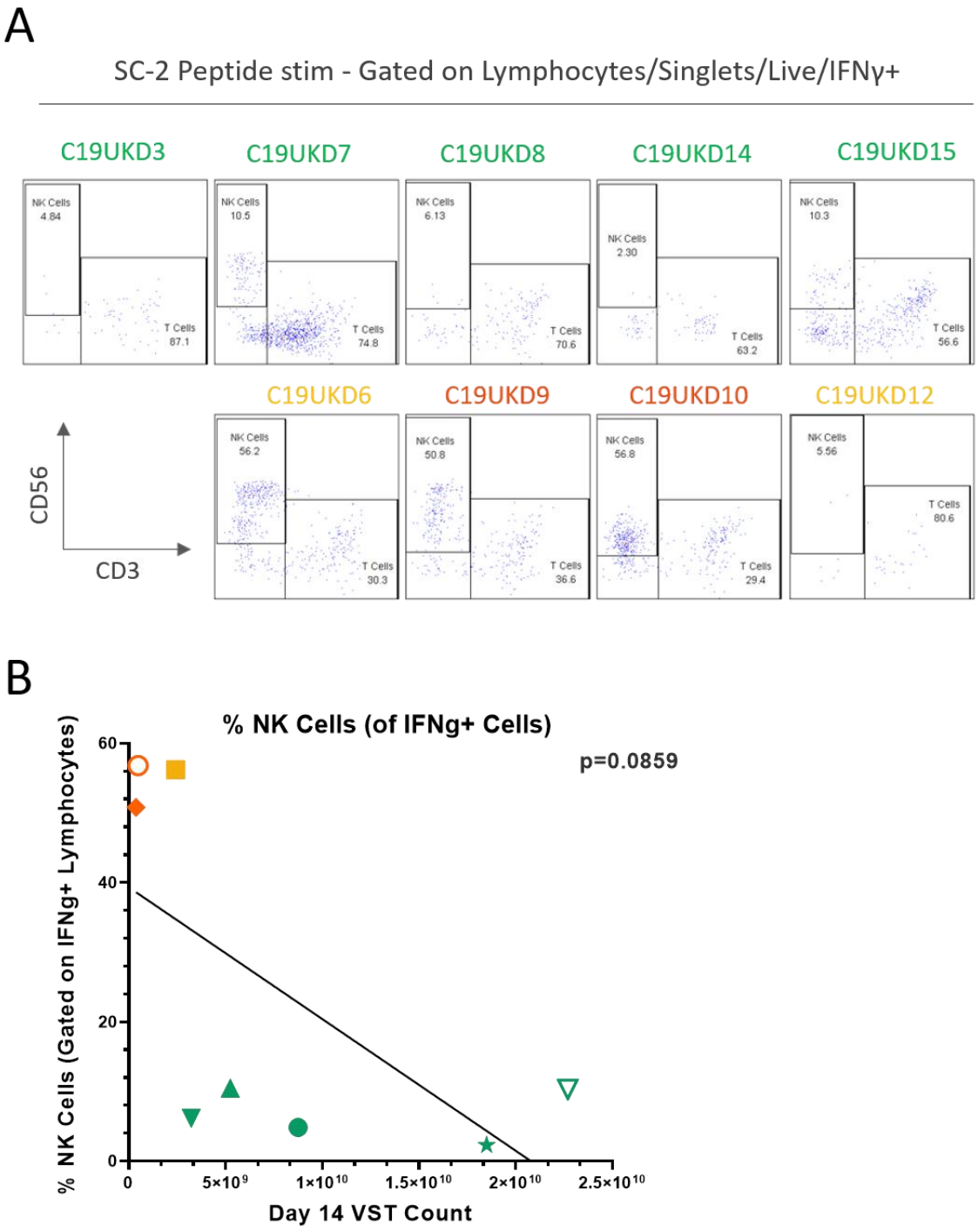

Figure 6.16 - SARS-CoV-2 peptide-reactive NK cells in low expansion donors.

Donor leukapheresis screening revealed a large NK cell population expressing IFN-γ in response to SARS-CoV-2 peptides stimulation in donors that had low expansion in the SARS-CoV-2 VST manufacture. **(A)** Flow cytometry analysis of all bank manufacture donors leukapheresis screen. Analyses were gated on lymphocytes/ singlets/ live cells/ IFN-γ+ cells, and then total IFN-γ population reactive to SARS-CoV-2 peptide stimulation assessed for frequency of NK cells (CD56+/ CD3-) and T cells (CD3+/ CD56-). In all 'good' expansion donors coded in green (top panel) the frequency of peptide-reactive IFN-γ+ cells was made up by a majority of T cells, whereas 'poor' expansion donors coded in orange and red (bottom panel) had a considerable frequency of peptide-reactive IFN-γ+ NK cells. **(B)** The frequency of peptide-reactive IFN-γ+ NK cells (corrected to unstimulated negative controls) in the donor leukapheresis screen was tested for association with day 14 VST count. Calculation was performed using Pearson correlation coefficient, where $p<0.05$ was considered statistically significant.

Interestingly, the overall NK cell population (gated CD56+/CD3-) showed a marked downregulation of CD56 upon SNM peptide stimulation compared to the no antigen control in the buffy coat PBMC screen, whereas SARS-CoV-2 peptide stimulation did not affect NK cell frequency in the leukapheresis screen (**Figure 6.17**).

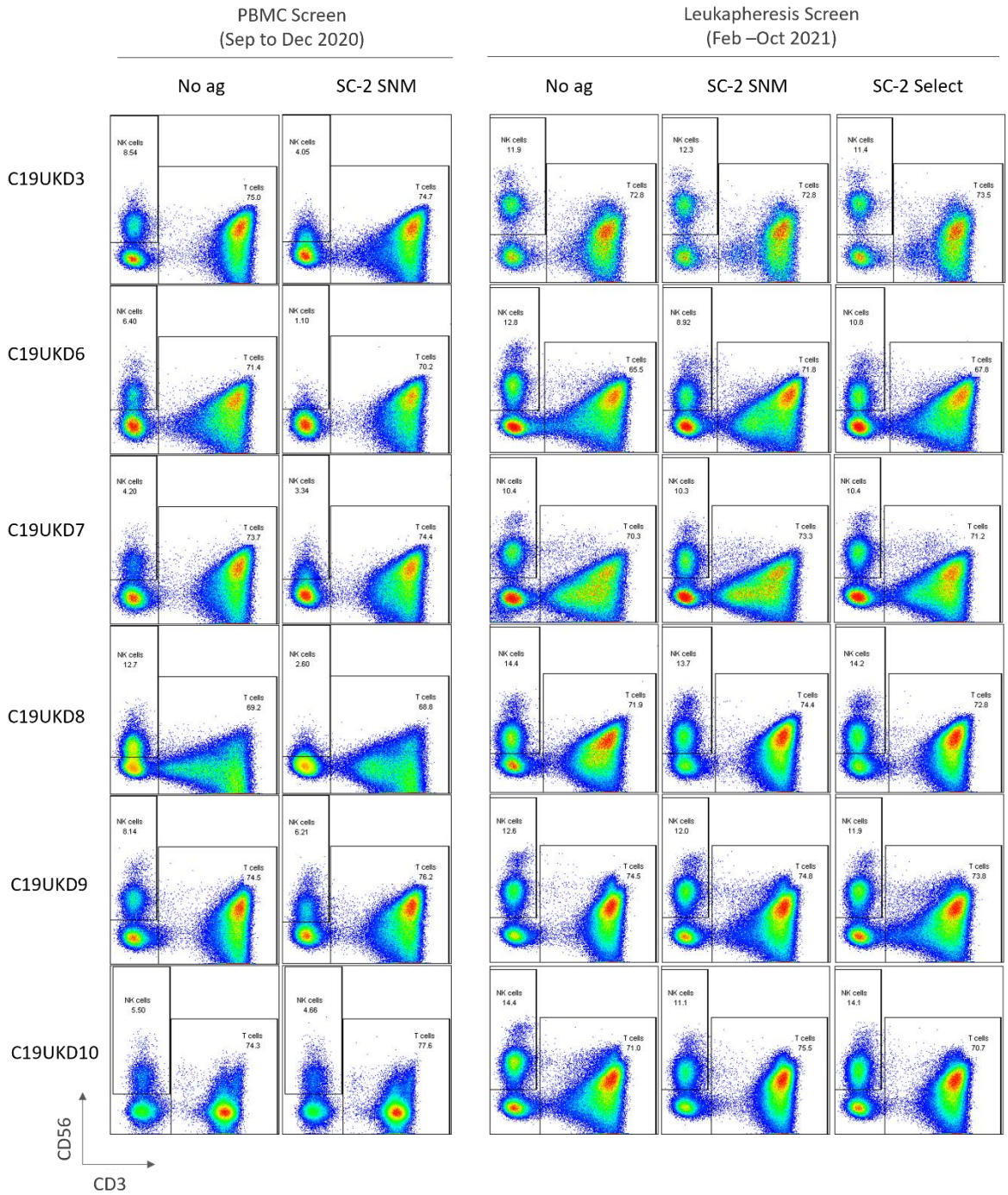

Figure 6.17 - SARS-CoV-2 peptide stimulation CD56 downregulation.

Flow cytometric analysis of SARS-CoV-2 (SC-2) peptide screens of initial buffy coat (done between September to December 2020) versus the same donor's leukapheresis screen (February to October 2021). Analyses were pre-gated on lymphocytes/singlets/live. Above flow plots show CD3 on x-axis versus CD56 on y-axis to gate on overall T cell population (CD3+) versus overall NK cell population (CD56+/CD3-). Buffy coat screen only included negative control (no antigen) and pooled SNM, whereas the leukapheresis screen included the additional SARS-CoV-2 Select peptides which were released in 2021 and used for manufacture. Donors C19UKD12-15 were not added to the analysis since buffy coat screens were not done for these donors.

Further interrogation of the NK cell population revealed the elevated frequency of IFN-γ-reactive NK cells present in the leukapheresis screen of poor expansion donors C19UKD6, C19UKD9 and C19UKD10 in response to SARS-CoV-2 peptide stimulation was not as prominent in the initial buffy coat screen (**Figure 6.18**).

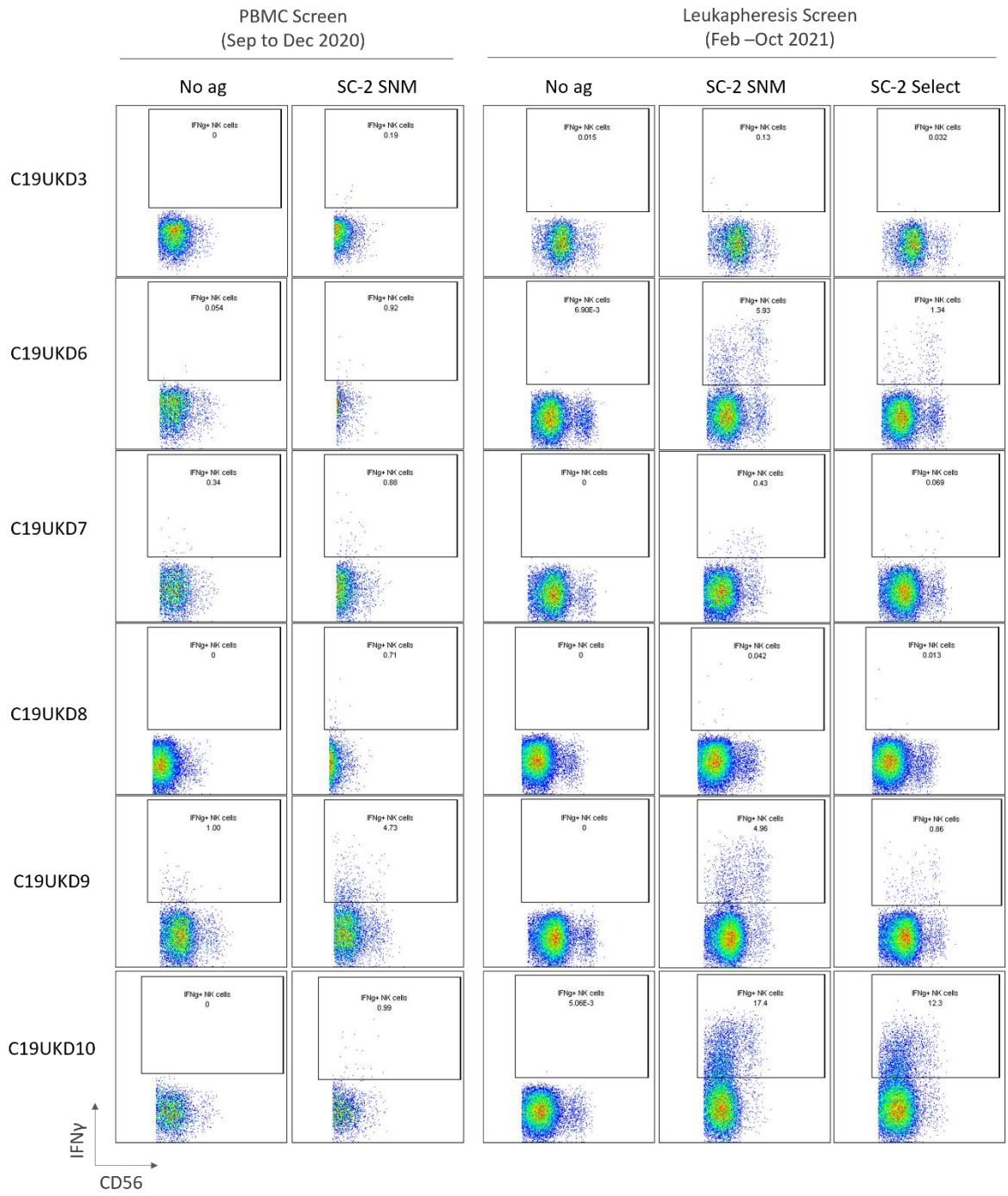

Figure 6.18 - SARS-CoV-2 peptide stimulation IFN-γ-reactive NK cells.

Flow cytometric analysis of SARS-CoV-2 peptide screens of initial buffy coat (done between September to December 2020) versus the same donor's leukapheresis screen (February to October 2021). Flow plots show CD56 on x-axis versus IFN-γ on y-axis to gate on IFN-γ-reactive NK cells (pre-gated on lymphocytes/singlets/live/NK cells). Buffy coat screen only included negative control (no antigen) and pooled SNM, whereas the leukapheresis screen included these two conditions plus the additional SARS-CoV-2 Select peptides which were released in 2021 and used for manufacture. Donors C19UKD12-15 were not added to the analysis since buffy coat screens were not done for these donors.

To quantify this, the frequency of IFN-γ-reactive NK cells was compared for the buffy coat PBMC screen of SNM peptides, the leukapheresis screen of SNM peptides and the leukapheresis screen of SARS-CoV-2 select peptides (**Figure 6.19A**). Note since SARS-CoV-2 select peptides were not yet available during the PBMC screen, SNM response was used to compare responses between these time periods. IFN-γ-reactive NK cells to each individual SARS-CoV-2 peptide (**Figure 6.19B**) indicates slightly higher NK cell responses to Spike and Membrane as compared to Nucleocapsid.

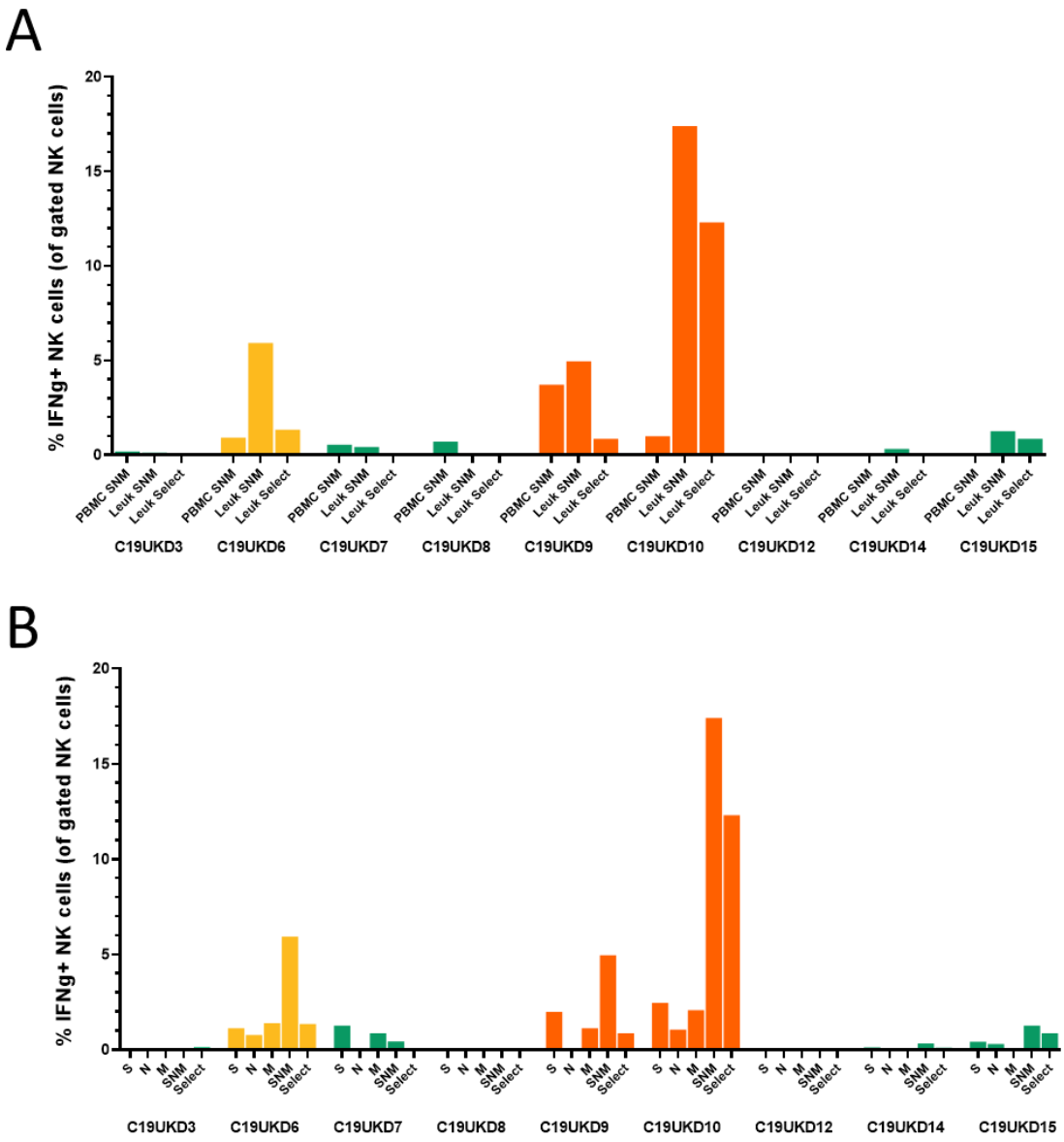

Figure 6.19 - IFN-γ-reactive NK cells response to SARS-CoV-2 peptides.

Frequency of IFN-γ-reactive cells in responses to SARS-CoV-2 peptide stimulation. **(A)** Each donor frequency of IFN-γ+ NK cells within gated NK cell population is shown for buffy coat PBMC SNM, leukapheresis SNM and leukapheresis SARS-CoV-2 Select. **(B)** Each donor frequency of IFN-γ+ NK cells within gated NK cell population is shown for leukapheresis response to peptides: Spike (S), Nucleocapsid (N), Membrane (M), pooled SNM and SARS-CoV-2 Select. All peptide response frequencies are corrected to no antigen negative controls.

6.5 Characterisation of banked SARS-CoV-2 VST

Final product SARS-CoV-2 VST banked for clinical use were subject to an extensive range of testing assessing product phenotype, functionality, clonal repertoire and safety to gather as much information as possible prior to potential use in a Phase I clinical trial.

6.5.1 Banked SARS-CoV-2 VST phenotypic analysis

To assess identity of final product populations, harvested cells were analysed for phenotype as outlined in **Figure 6.10.** Release criteria for inclusion in the bank were ≥70% viability, ≥90% T cells and ≤10% NK cells. Frequency of final product populations for each donor is shown in **Figure 6.20**. To make distinctions between good and poor expansion donors, final product dead cells/ debris is shown here as the opposite of percentage viability. As can be seen in **Figure 6.20A**, poor expansion donor C19UKD9 & C19UKD10 are the only products exceeding 20% dead cells/ debris which maintained a characteristic smear across the left of the FSC/SSC axis compared to good expansion product. All donors passed the NK cell **(Figure 6.20B**) and T cell (**Figure 6.20D**) release criteria, however some donors had a small population of double positive CD3+/CD56+ NKT cells (0-20%) in the final product (**Figure 6.20C**). Most donor VST products were CD4-skewed (**Figure 6.20E**), however n=3 donors had CD8-skewed final products. All products were primarily composed of central memory T cells with a small population of effector memory T cells (**Figure 6.20F**). Naïve T cells and terminal effector T cells were negligible at final product harvest.

To understand population expansions and contractions caused by the culture process, day 0 targets and final product phenotype were compared for each donor. All donors showed a reduction in the frequency of NK cells (**Figure 6.21A**) except poor expansion donor C19UKD9 (orange diamonds), indicating the culture process supported an outgrowth of NK cells in this donor which may have contributed to VST expansion failure. Contrastingly, NKT cell growth was relatively variable between donors (**Figure 6.21B**). The CD4+ cell compartment generally remained level or contracted, whereas correspondingly CD8+ cells expanded to some extent in all donors except C19UKD9 (**Figure 6.21C-D**). Central memory T cells (TCM) showed a consistent substantial expansion over the culture period (**Figure 6.21E**). Frequency

of effector memory T cells was reduced in the final product, and while this may be a population contraction it more likely reflects the significant outgrowth of central memory T cells (**Figure 6.21F**). Interestingly, C19UKD9 had the smallest TCM expansion of all donors which may indicate a poor central memory SARS-CoV-2 VST response in this donor which allowed space for NK cell expansion during culture.

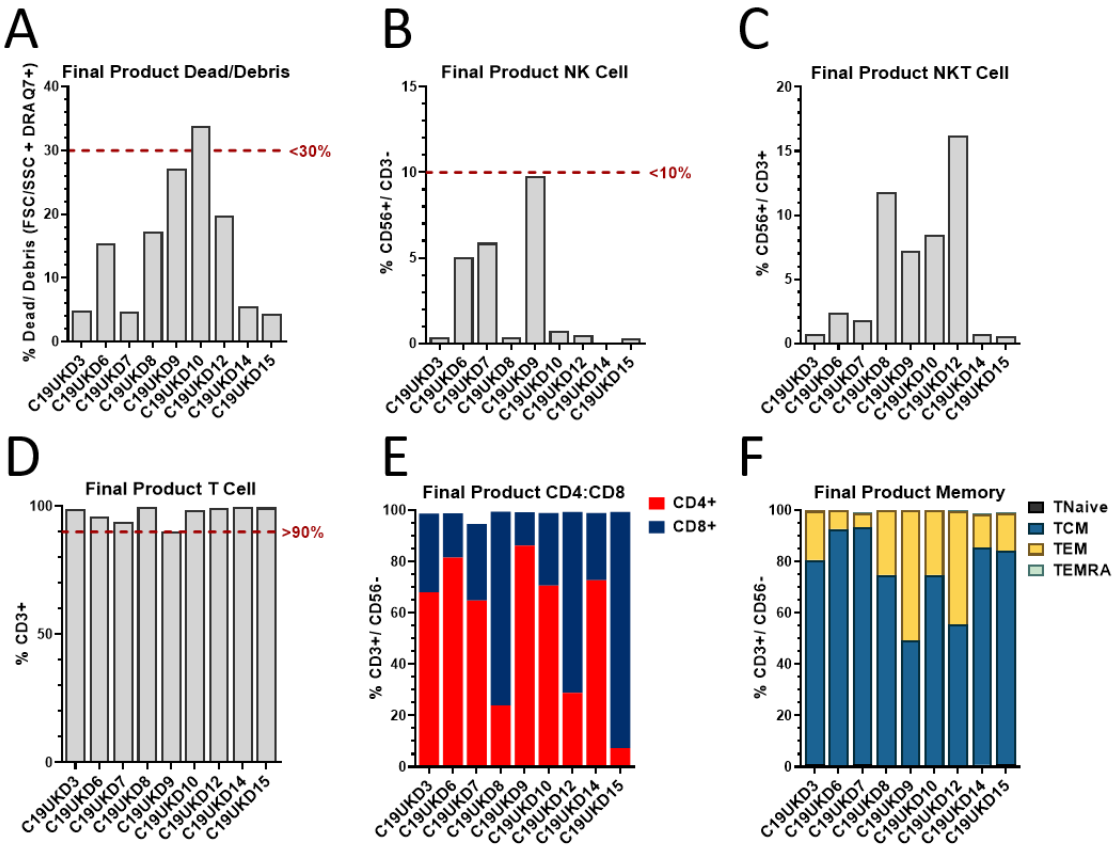

Figure 6.20 - Banked SARS-CoV-2 VST final product T cell phenotype.

Final product samples of banked SARS-CoV-2 VST manufacturing runs were taken for flow cytometry phenotyping. From ungated total events, **(A)** % dead cells/ debris is shown per donor. Within the viable total cells population (gated lymphocytes/ singlets/ live), each donor was quantified for **(B)** % NK cells, **(C)** % NKT cells, and **(D)** % T cells. Gated T cells were further assessed for **(E)** CD4: CD8 ratio and **(F)** T cell memory populations: naïve (TNaive), central memory (TCM), effector memory (TEM), and terminally differentiated effector memory RA (TEMRA). Release criteria for final products were viability >70%, CD56+/CD3- NK cells <10% and CD3+ T cells >90%.

6.5.2 Inhibitory marker expression correlates with poor expansion

SARS-CoV-2 VST samples taken on day of harvest were also assessed for expression of markers associated with activation and exhaustion (PD-1, Tim-3 and LAG-3) to evaluate potential T cell exhaustion in the expanded product. The percentage of CD3+ gated T cells with positive expression of PD-1 is shown per donor (**Figure 6.22A**)

which demonstrated a significant negative correlation with final product day 14 VST yield (**Figure 6.22B**).

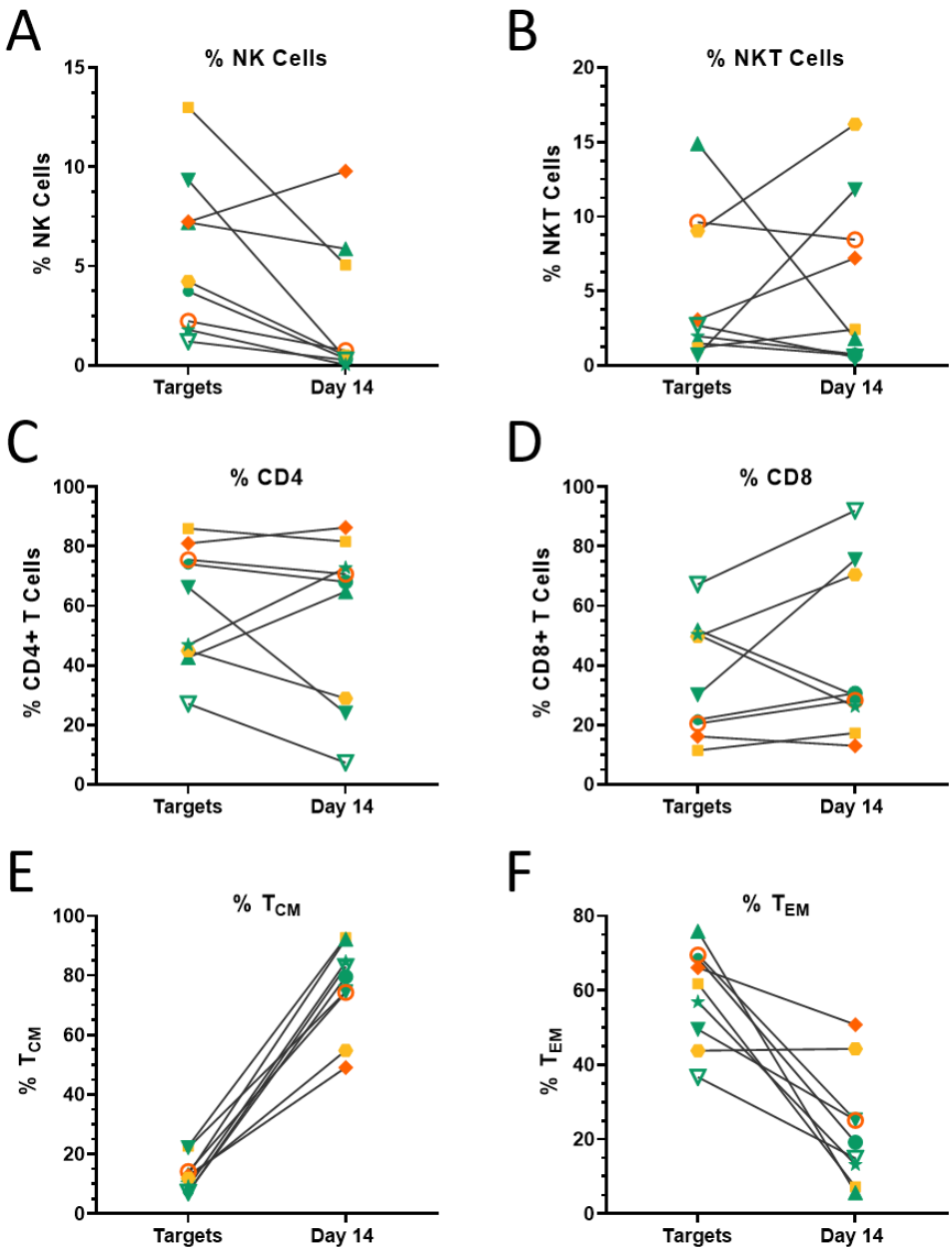

Figure 6.21 - Population expansions from Prodigy targets to final product.

Population expansion and contractions over culture are shown for each donor. Day 0 prodigy targets and day 14 final product were compared for frequency **(A)** NK cells, **(B)** NKT cells, **(C)** CD4+ T cells, **(D)** CD8+ T cells, **(E)** central memory T cells (TCM) and **(F)** effector memory T cells (TEM).

Where possible samples were also analysed for co-expression of multiple inhibitory markers (PD-1, LAG-3 and TIM-3) as a more indicative measure of true T cell exhaustion (Baessler and Vignali, 2024). The percentage of cells in final product material with dual expression (LAG3+/PD1+, LAG3+/TIM3+, or PD1+/TIM3+) and

triple expression (LAG3+/PD1+/TIM3+) are shown per donor in **Figure 6.23**. Of the total T cell population (**Figure 6.23A**), poor expansion donor C19UKD10 had a high accumulation of total dual and triple positive inhibitory marker populations at >60% of all cells compared to 10-30% seen in other donors.

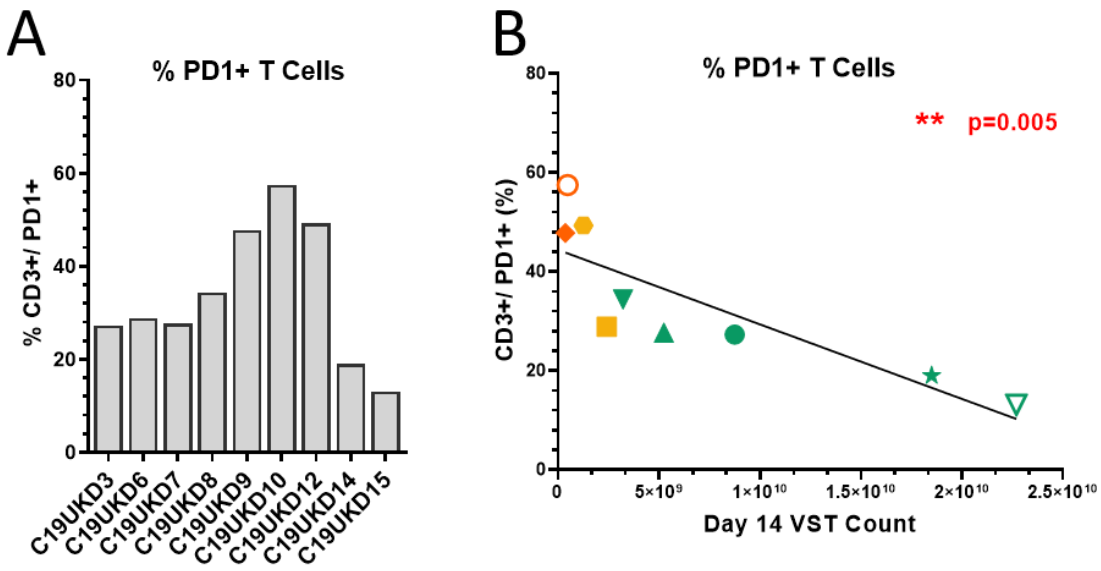

Figure 6.22 - Banked VST final products PD1 expression.

Final product samples of banked SARS-CoV-2 VST manufacturing runs were taken for flow cytometry phenotyping. **(A)** The frequency of PD1+ T cells the within final product (cells/singlets/live/CD3+/PD1+) is shown for all banked donors. **(B)** The percentage of PD1+ T cells significantly correlated with final product day 14 yield. Calculation was performed using Pearson correlation coefficient, where $p<0.05$ was considered statistically significant.

Sub-gating within the CD4 and CD8 compartments, it can be seen CD4+ cells (**Figure 6.23B**) have a greater frequency of exhaustion marker positive cells, whereas CD8+ cells (**Figure 6.23C**) have a much lower level of total dual and triple positive inhibitory marker populations. Interestingly within the CD8 compartments, there is a higher frequency of LAG3+/TIM3+ dual positive cells, whereas LAG3+/PD1+ cells, PD1+/TIM3+ and LAG3+/PD1+/TIM3+ populations are negligible. This may indicate LAG-3 is more likely to be upregulated upon CD8+ cell exhaustion whereas exhausted CD4+ cells preferentially upregulate PD-1. Due to low cell numbers of the other poor expansion donor C19UKD9, these VST were not further analysed for expression of the three inhibitory markers. Without a full dataset, all correlations between final product yield and the different dual and triple expressing exhaustion marker populations were not statistically significant, however this may reflect the lack of data from both poor expansion batches C19UKD9 and C19UKD10 in the analysis.

Together these data suggest a relationship between VST exhaustion and poor culture expansion, particularly for PD-1 expression. While CD4+ T cells demonstrate an earlier exhausted phenotype than CD8+ T cells, this supports the previous observation that expansion capacity between donors is in part determined by CD4 and CD8 composition, whereby CD8-skewed VST lines are more likely to have a large fold expansion.

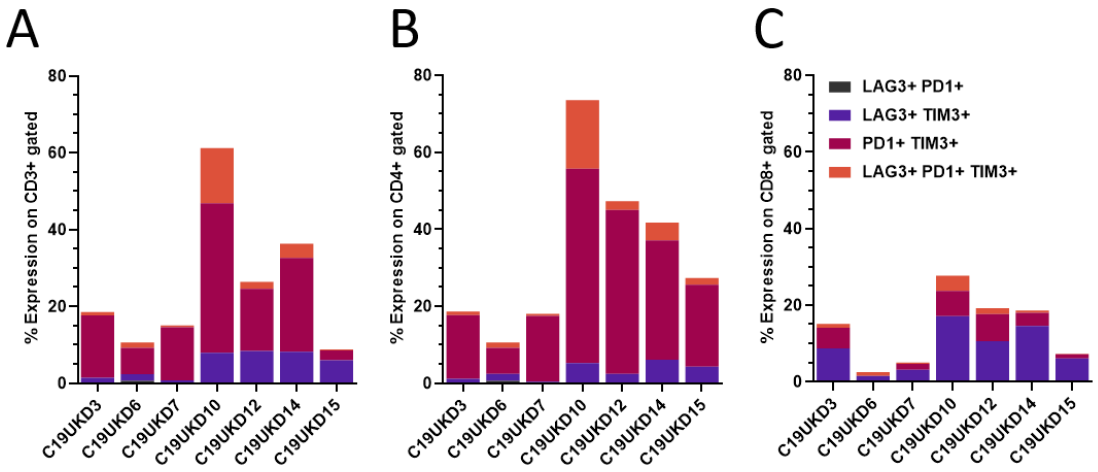

Figure 6.23 - Banked VST inhibitory markers co-expression.

Final product samples of banked SARS-CoV-2 VST manufacturing runs were taken for flow cytometry analysis of inhibitory markers to analyse T cell exhaustion. **(A)** Total CD3+ T cells, **(B)** CD4+ T cells and **(C)** CD8+ T cells were analysed for the percentage of dual or triple expression of inhibitory markers LAG-3, PD-1 and TIM-3. Populations were defined as follows: LAG3+/PD1+ (black), LAG3+/TIM3+ (purple), PD1+/TIM3+ (pink) and LAG3+/PD1+/TIM3+ (orange).

6.5.3 Banked SARS-CoV-2 VST chemokine receptor profile

The expanded SARS-CoV-2 VST were also analysed for chemokine receptor expression as described in **section 2.6**. For this, harvested VST cultures were washed and stained at rest for CD4, CD8 and for the following chemokine receptors: CCR1, CCR2, CCR3, CCR4, CCR5, CCR6, CCR7, CXCR3, CXCR4, CXCR5 and CXCR6. For analysis, cells were initially gated on viable singlet cells, and then into CD4+ or CD8+ T cells for expression of each chemokine receptor within each compartment. Due to insufficient cell numbers for the chemokine receptor assay from poor expansion batches C19UKD9 and C19UKD10, only the final banked VST lines were included in analysis (**Figure 6.24**). The banked SARS-CoV-2 VST demonstrated high expression (mean > 60% of cells) of CCR2, CCR4, CCR5, CXCR3 and CXCR4 suggesting a wide capacity of these cells to migrate to inflamed sites or lung-associated lymph nodes to target exert anti-SARS-CoV-2 effector functions. A minor proportion of VST (mean 10-30% of

cells) expressed CCR6, CCR7 and CXCR6; whereas there was negligible expression of CCR1, CCR3 and CXCR5. No significant differences were observed between CD4 and CD8 populations for expression of any of the chemokine receptors tested.

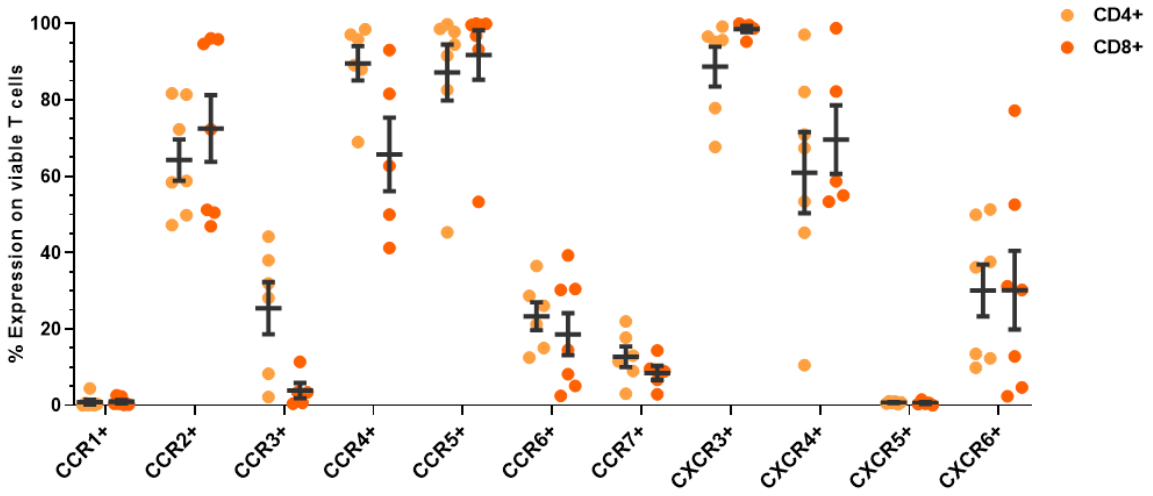

Figure 6.24 - Banked VST final products chemokine receptor profile.

Final product banked SARS-CoV-2 VST (n=7) were analysed for chemokine receptor profile. Using a flow cytometry surface staining assay, cells were subject to initial gating on cells/singlets/ viable cells. Viable cells were then gated on CD4+ or CD8+ T cells and analysed for expression of chemokine receptors corrected to FMO controls: CCR1, CCR2, CCR3, CCR4, CCR5, CCR6, CCR7, CXCR3, CXCR4, CXCR5, and CXCR6. Data is represented as mean ± SEM and comparisons of chemokine receptor expression between CD4+ and CD8+ gated T cells made using paired t-tests with Holm-Šídák correction for multiple tests.

6.5.4 Banked SARS-CoV-2 VST functionality analysis

All clean room manufactured SARS-CoV-2 VST products were tested for functionality. As described in Chapter 4, since SARS-CoV-2 VST were mainly CD4-skewed T cells, antigen recall was used as the principal functional assay to assess production of antiviral cytokines. The developed assay (**section 2.7.5**) co-cultured peptide-loaded DCs with VST at [1:5] at day 14 for 5 hours followed by intracellular staining to measure expression of cytokines IFN-γ, TNF-α, IL-2 and T cell activation marker CD154. Overall responses to SARS-CoV-2 select peptides (covering Spike, Nucleocapsid, Membrane and Envelope proteins) are shown in **Figure 6.25**. The total CD3+ T cell population reactive to SARS-CoV-2 peptide stimulation (**Figure 6.25A**) had highest expression of functionality markers CD154 and TNF-α, with slightly reduced expression of IFN-γ. Expression of IL-2 was significantly lower than all other molecules tested. Comparison of CD4+ and CD8+ T cells (**Figure 6.25B**) demonstrated CD4+ T cells had significantly higher expression of all functional

markers. This indicates The CD4 population of VST products has higher capacity to generate cytokines in response the SARS-CoV-2 peptides tested in this assay.

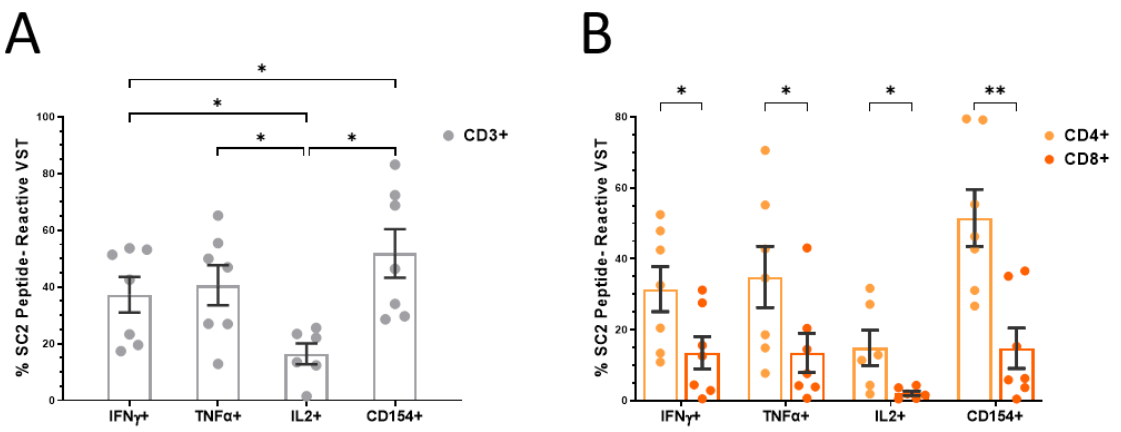

Figure 6.25 - Banked SARS-CoV-2 VST individual functional marker expression.

Final product banked SARS-CoV-2 VST (n=7) were co-cultured with peptide-loaded DC to analyse antigen recall response to SARS-CoV-2 Peptivator Select compared to unloaded DC controls. Following antigen stimulation, cells were assessed for intracellular expression of IFN-γ, TNF-α, IL-2 and CD154. **(A)** Total CD3+ gated SC-2 peptide-reactive VST were compared for expression of the individual functional markers. Comparisons between groups were made using RM one-way ANOVA where *p≤0.05 was considered statistically significant. **(B)** Expression of individual markers was compared between CD4+ gated and CD8+ gated populations. Comparisons between groups were made using paired two-tailed T tests where * p≤0.05 and **p≤0.01.
Autologous monocyte-derived DC used for this assay were generated and characterised by Dr Paul Burgoyne (SNBTS TCAT).

To assess co-expression of multiple effector molecules, populations were gated based on multiple or singular expression of markers IFN-γ, TNF-α, IL-2 and CD154. As demonstrated for final product VST C19UKD3, stochastic neighbour embedding (t-SNE) analysis was used to cluster populations based on functional marker expression (**Figure 6.26A**). Using the mean of all banked SARS-CoV-2 VST lines (**Figure 6.26B**), the majority of reactive cells triple positive (orange) for functional marker expression were CD154+/IFN-γ+/TNF-α+ at mean=30.6 ±2.7% of all cells. A small population of cells were single positive (purple) for CD154+ expression (mean=12.6 ±3.1%) whilst all other single positive populations were negligible (<5%). This indicates CD154 expression is prolonged in this assay compared to cytokines which may have more transient expression. The mean percentage of overall populations with quadruple, triple, dual, singular or null expression (none) is shown in **Figure 6.26C**. As can be seen, the majority of SARS-CoV-2 peptide-reactive cells are multifunctional with quadruple (8.7%), triple (32.3%) or dual (10.9%) expression of functional markers. A significant proportion of cells (32 ± 5.6%) were negative for expression of all four

functional markers tested, indicating these cells were either not Th1 phenotype, functionally exhausted, or unreactive in this assay.

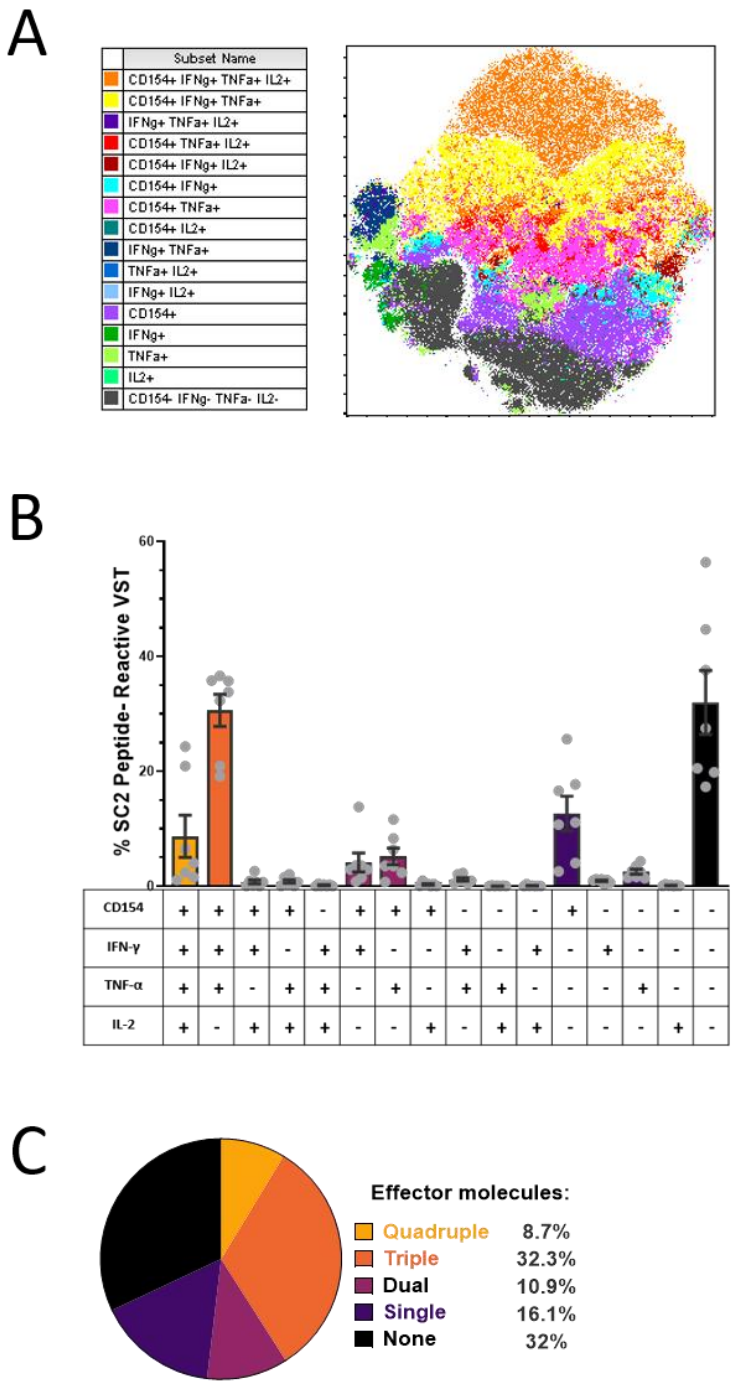

Figure 6.26 - Banked SARS-CoV-2 VST are multi-functional.

Final product banked SARS-CoV-2 VST (n=7) were co-cultured with peptide-loaded DC to analyse antigen recall response to SARS-CoV-2 Peptivator Select compared to unloaded DC controls. Following antigen stimulation, cells were assessed for intracellular expression of IFN-γ, TNF-α, IL-2 and CD154. **(A)** Stochastic neighbour embedding analysis (t-SNE) was used to cluster populations based on co-expression or singular expression of functional markers as displayed for donor C19UKD3. **(B)** The percentage expression of each functional marker population is shown for mean ± SEM for all banked SARS-CoV-2 VST lines (n=7). **(C)** The percentage of reactive VST expression quadruple, triple, dual, single or null expression (none) of functional markers is shown as the mean of all banked SARS-CoV-2 VST lines (n=7).

Autologous monocyte-derived DC used for this assay were generated and characterised by Dr Paul Burgoyne (SNBTS TCAT).

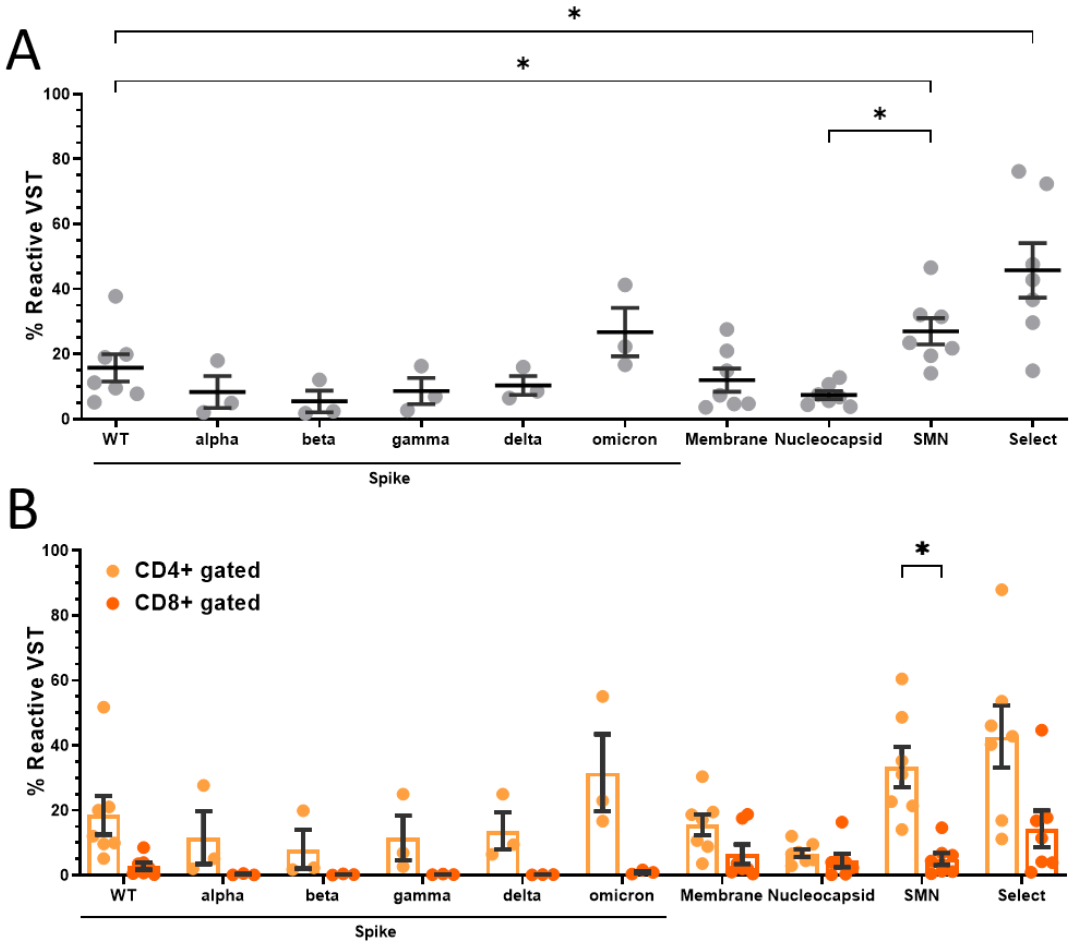

Figure 6.27 - Banked SARS-CoV-2 VST antigen functional reactivity.

Final product banked SARS-CoV-2 VST (n=7) were co-cultured with peptide-loaded DC to analyse antigen recall T cell functional reactivity through intracellular expression of CD154 to the following SARS-CoV-2 Peptivators: Spike WT, Spike alpha, Spike beta, Spike gamma, Spike delta, Spike omicron, Membrane, Nucleocapsid SNM mix, and SARS-CoV-2 Select. Peptivator conditions were normalised to unloaded DC controls. **(A)** Total CD3+ gated peptide-reactive VST were compared for the different SARS-CoV-2 antigens. Comparisons between groups were made using RM one-way ANOVA where *p≤0.05 was considered statistically significant. **(B)** The frequency of peptide-reactive VST to each SARS-CoV-2 antigen was compared between CD4+ gated and CD8+ gated populations. Comparisons between groups were made using paired two-tailed T tests where * p≤0.05.

Autologous monocyte-derived DC used for this assay were generated and characterised by Dr Paul Burgoyne (SNBTS TCAT).

Using this assay, final product VST were also tested for reactivity to individual SARS-CoV-2 antigens to assess T cell targeting. As above, VST were co-cultured with autologous DC loaded with the following peptides: Spike wild type (WT), Spike alpha, Spike beta, Spike gamma, Spike delta, Spike omicron, Membrane, Nucleocapsid. Mixed Spike + Nucleocapsid + Membrane (SMN), and SARS-CoV-2 Select. Since CD154 had the highest expression in both CD4 and CD8 compartments compared to the other effector molecules (**Figure 6.26**), this was used as the output measure to compare reactivity to the individual SARS-CoV-2 antigens. The escaped mutant Spike

peptivators were only available later during the pandemic after initial donors C19UKD3-C19UKD10 had already been manufactured. Therefore, VST responses to these peptivators could only be tested in later time-point donors: C19UKD12, C19UKD14 & C19UKD15. Predictably, data from these three donors had the highest mean percentage T cell reactivity of all the individual antigens to Spike omicron (**Figure 6.27A**) which was the most the abundant variant at the time of manufacture for these donors. However, there were no statistically significant differences in responses to the escaped Spike mutants likely due to small sample number (n=3 donors). The frequency of T cells to Spike WT, Membrane and Nucleocapsid were similar with a hierarchical targeting S>M>N (respective means: Spike WT = 15.8 ± 4.2%, Membrane = 12 ± 3.5%, Nucleocapsid = 7.4 ± 1.2%, n=7). The pooled SNM mixed stimulation had significantly higher reactivity than individual Nucleocapsid (p=0.040) and Spike WT (p=0.035). Similarly, the SARS-CoV-2 Peptivator Select, covering sequences for 88 MHC-restricted peptides (Class I & II) across the SARS-CoV-2 genome, had a significantly higher T cell reactivity than individual Spike WT (p=0.38). T cell reactivity to individual and mixed peptide conditions were further analysed to compare responses between the CD4 and CD8 compartments (**Figure 6.27B**). The percentage of cells reactive to SMN stimulation was significantly higher in CD4+ T cells compared to CD8+ T cells (p=0.033). While all other peptide conditions tested also trended higher reactivity in the CD4+ cells compared to negligible CD8+ T cell responses, this was not statistically different. Reactivity was also analysed for IFN-γ+, TNF-α+, and IL-2+ expression to limit bias in the effector molecule production between CD4 and CD8 subtypes, however these results verified negligible peptide reactivity in the CD8+ T cells (data not shown). Altogether this data highlights the VST generated using SARS-CoV-2 Select Peptivator were composed of T cell populations mainly targeted towards Spike and Membrane, with lesser Nucleocapsid-specific T cells being selected and/or expanded in the process. Since there is a slightly higher response between Select and SNM peptides, this suggests VST were reactive to other structural and non-structural SARS-CoV-2 proteins (such as envelope) that are included in the Select peptide pools (see **Table 2.3**).

6.5.5 Banked SARS-CoV-2 VST cytotoxicity analysis

Gold standard assays for measuring potency of virus-specific T cell therapies are usually to assess the ability of T cell induced cytotoxicity to target cells expressing

viral antigens. Though we could not access SARS-CoV-2 infected target cell lines to use in a cytotoxicity assay at this time, we established a collaboration with Oxford university through the lab of Professor Tao Dong, an international expert on virus-specific T cell responses. We sent COVID-19 convalescent donor leukapheresis samples to Professor Tao Dong's lab at the University of Oxford with the aim of establishing donor-specific B cell lines (BCL) transduced with the ACE-2 receptor to allow SARS-CoV-2 entry and natural antigen processing by these B cell lines. Transduction of the BCL lines with ACE-2 was however not successful (data not shown) and instead cytotoxicity was tested against BCL pulsed with SARS-CoV-2 peptides as the target cells. Co-cultures between effector SARS-CoV-2 VST and autologous pulsed target cells were set up at multiple ratios to measure dose-dependent killing. To this end, B cell lines were made for each banked VST donor by standard EBV transformation using EBV supernatant culture of PBMC for 6 to 8 weeks. Prior to co-culture set up, B cell lines were harvested and washed, and pulsed with or without SARS-CoV-2 Peptivator Select [1μM] for 1 hour. SARS-CoV-2 VST (effector) and autologous peptide pulsed B cells (targets) were then co-cultured at E:T ratios of 1:1, 2:1, 4:1 and 0:1 (B cell only controls) for 6 hours. All treatments were then harvested and stained with CD19 to identify B cells and dead cell marker 7-AAD. Gating was performed whereby events were initially gated with a broad all cells gate (to exclude debris only), followed by gating on CD19+ B cell targets, and subsequently CD19+/7AAD+ to measure the percentage dead of the B cell population. The baseline death of B cell target only controls (**Figure 6.28A** top plots) is shown for both SARS-CoV-2 peptide pulsed B cells versus the B cells not pulsed with peptides. Each E:T ratio also contained VST co-cultured with SARS-CoV-2 peptide pulsed targets versus no peptide target controls as shown for C19UKD7 at [1:1] in **Figure 6.28A** bottom plots.

Analyses were made with the percentage dead in each E:T ratio of VST against SARS-CoV-2 peptide-pulsed targets corrected to either the targets only control (**Figure 6.28 B-C**) or corrected to the respective E:T ratio against unpulsed no peptide control targets (**Figure 6.28D-E**). Spike-specific bulk CD8+ T cells generated by the lab for use as assay positive controls were used to compare killing potential.

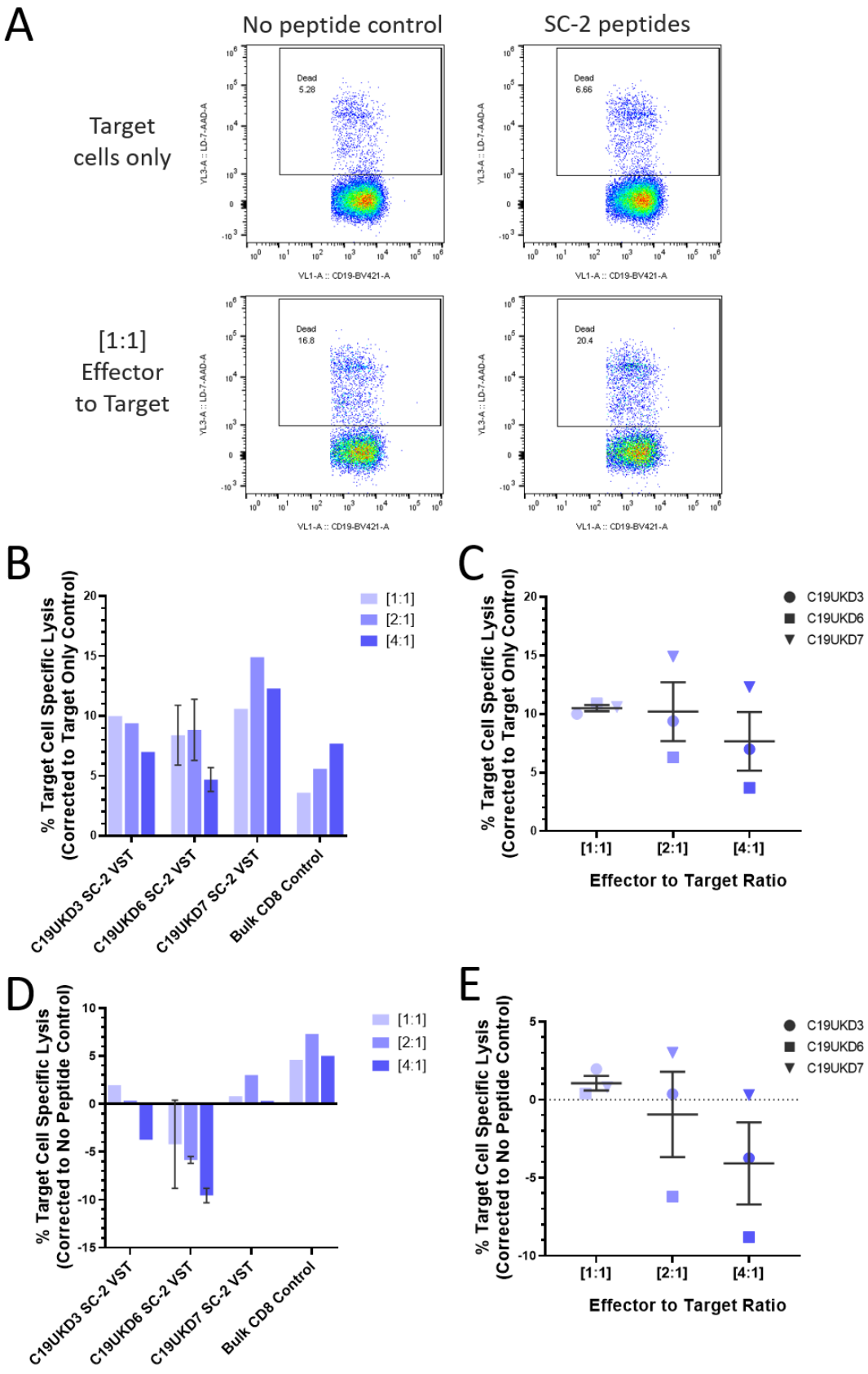

Figure 6.28 - Banked SARS-CoV-2 VST cytotoxicity potential.

SARS-CoV-2 VST final products were tested in a cytotoxicity assay against autologous transformed B cell lines (BCL) pulsed with SARS-CoV-2 peptides [1μM] versus no peptide controls. Co-cultures were set up at numerous effector (VST) to target (BCL) ratios of [1:1], [2:1], [4:1], and BCL only [0:1] controls. Spike-specific CD8+ bulk cell effector lines isolated by the lab were used as positive killing controls. Co-cultures were incubated for 6 hours and subsequently stained with CD19 and dead cell marker 7-AAD. To measure target cell lysis, analyses were gated on all cells

followed by CD19+ to identify target cells. **(A)** CD19+ cells were subsequently gated for positive expression of 7-AAD to measure target cell death in target only controls (top plots) versus each effector to target ratio (shown as 1:1 in bottom plots). Duplicates were also set up to compare killing of target cells pre-loaded with SARS-CoV-2 peptides (left plots) versus unloaded peptide controls (right plots). Specific lysis of each E:T ratio measured corrected to the target only controls is shown for **(B)** each donor SARS-CoV-2 VST and bulk CD8+ T cell lines and **(C)** the mean ± SEM of SARS-CoV-2 VST donors (n=3). Specific lysis of each E:T ratio measured corrected to the no peptides controls is shown for **(D)** each donor SARS-CoV-2 VST and bulk CD8+ T cell lines and **(E)** the mean ± SEM of SARS-CoV-2 VST donors (n=3). Replicate wells could only be set up for donor CD19UKD6 (n=2), the other lines had insufficient cells for technical replicates. All assay procedure and acquisition of flow cytometry samples was performed by Dr Yanchun Peng at MRC Human Immunology Unit, University of Oxford, and subsequent data analysis performed myself.

As can be seen, when corrected to the targets only control (**Figure 6.28B**) each SARS-CoV-2 donor VST line induced between 5-15% specific lysis of targets, however no line induced a dose-dependent killing effect except for the bulk CD8 control line which elicited increased killing with increased effector CD8+ cells. The mean of SARS-CoV-2 VST donor lines tested (n=3) demonstrated comparable specific lysis of targets across all E:T ratios when corrected to target only controls (**Figure 6.28C**). Analyses subject to correction against the no peptide B cell co-culture controls showed very variable cytotoxicity (**Figure 6.28D**) where numerous conditions had higher percentage of dead targets in the SARS-CoV-2 peptide pulsed targets compared to no peptides targets resulting in a negative specific lysis. The mean specific lysis compared to no peptide target controls showed a trend to lower killing with higher effector to target ratios (**Figure 6.28E**). The variability in specific target cell lysis between analyses corrected to different controls is difficult to extrapolate, and may reflect that the assay was not fully optimised. If using the no peptide pulsed target controls to quantify SARS-CoV-2-specific killing, the data suggest negligible cytotoxicity by the SARS-CoV-2 VST lines compared to CD8+ spike-specific T cell line. Target specific lysis by SARS-CoV-2 VST lines when corrected to the target cell only control wells ranged 5-15% indicating cytotoxic potential, however may also suggest SARS-CoV-2 VST killing the unpulsed B cell targets in a non-specific antigenic manner. Altogether the conflicting quantification dependent on controls used for analysis suggest inconclusive results which may reflect a lack of killing potential by these largely CD4-skewed SARS-CoV-2 VST lines. However true estimation of cytotoxicity is limited by using peptide-pulsed B cell targets instead of natural SARS-CoV-2 infected cells, and low sample/ replicate number.

6.5.6 Banked SARS-CoV-2 VST have polyclonal TCR repertoire

As discussed in Chapter 5, SARS-CoV-2 VST products generated by different manual isolation methods were assessed for T cell receptor (TCR) clonal diversity and specificity using next generation sequencing. Bank manufactured SARS-CoV-2 VST were also analysed for clonal repertoire to investigate if the Prodigy automated CCS selection and subsequent closed culture expansion impacts the clones selected for.

The clonal repertoire composition of Prodigy-isolated VST at day 14 harvest is shown in **Figure 6.29A**, with matched donor CD3+ pan T cells included as controls. As can be seen, the majority of the TCR repertoire for pan T cells is composed of >1000 clones demonstrating high diversity in the sequences obtained. Prodigy-isolated VST day 14 products showed a restriction in TCR diversity, however all donors generated diverse polyclonal products with the majority of the repertoire dominated by a top 100 to 1000 clones. Restriction in clonotype count (**Figure 6.29B**) was significant ($p<0.0001$) between pan T cell starting material (mean = 7556 ± 295 clones) and prodigy-isolated VST final products (mean = 2068 ± 281 clones). Furthermore, TCR antigen specificity databases TCRMatch and VDBJ were used to match SARS-CoV-2-specific CDR3 sequences (**Figure 6.29C**). While final product VST showed 3-12% of the repertoire had SARS-CoV-2-specific sequences in TCRMatch database, there were negligible (<1%) SARS-CoV-2-specific sequence matches using VDBJ database. Comparison of Prodigy VST final products with matched donor VST expanded from manual isolations (manual IFN-γ, manual TNF-α, manual CD154; refer to Chapter 5) demonstrated similar clonotype count (**Figure 6.30A**) and the proportion of SARS-CoV-2-specific sequence matches using TCRMatch (**Figure 6.30B**). These data suggest Prodigy automated isolation and closed system expansion has comparable clonal selection to the manually isolated and expanded VST.

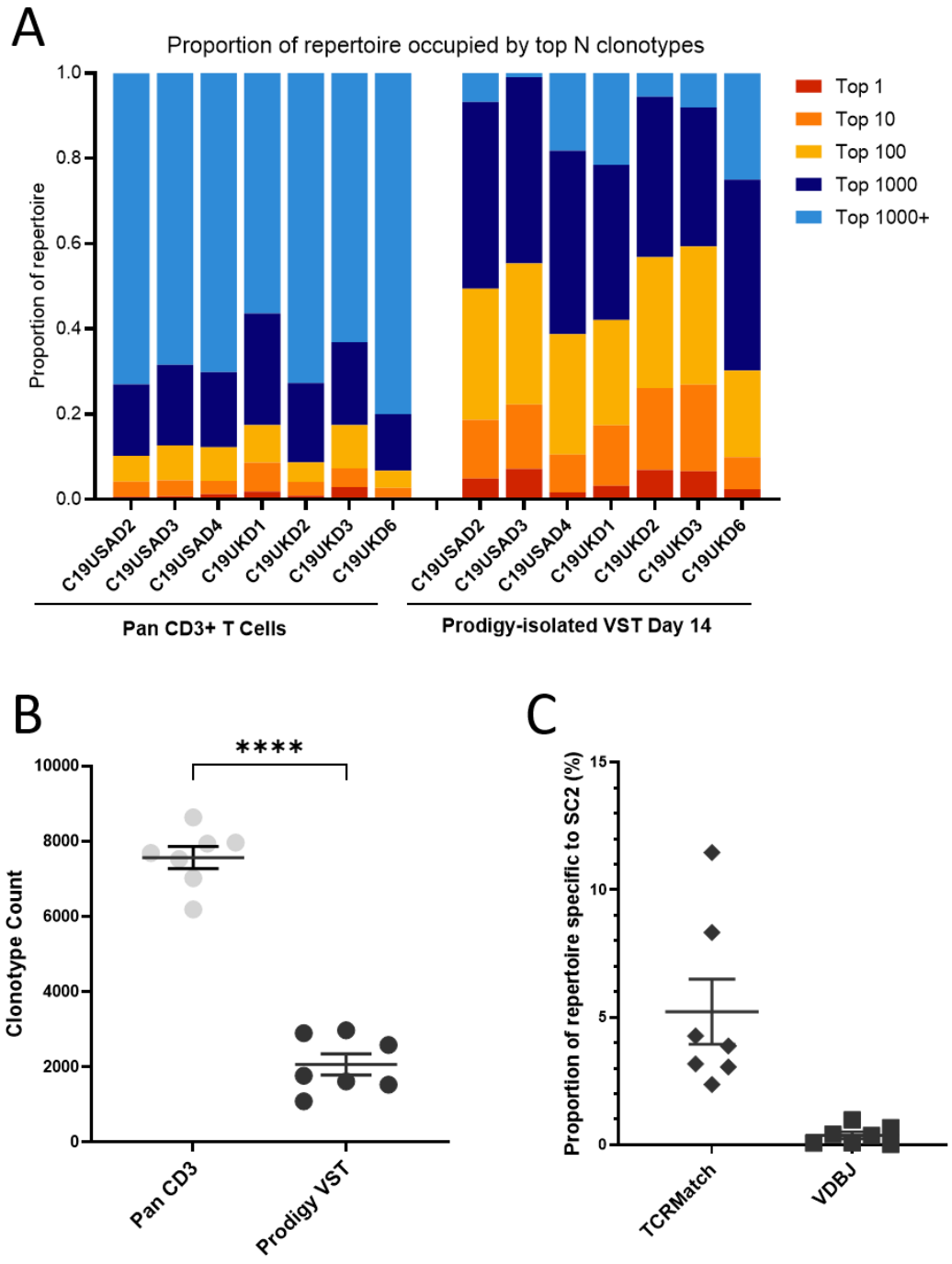

Figure 6.29 - Banked SARS-CoV-2 VST clonotype composition.
Sequencing of the TCR-Vβ region allowed comparison of Prodigy Day 14 VST and pan CD3 T cells from matched donor starting leukapheresis material. **(A)** Stacked bars represent the proportion of the repertoire occupied by the top n clones in that repertoire. SARS-CoV-2 VST show restricted repertoire diversity compared to pan T cell controls however still retain a highly polyclonal repertoire. **(B)** Clonotype counts corrected for UMI size matching demonstrate Prodigy VST had significantly reduced diversity compared to pan T cells. Data is represented as mean ± SEM and statistical significance was determined using paired t-tests. **(C)** The proportion of each repertoire with an exact CDR3 amino acid sequence match specific to SARS-CoV-2 in databases TCRMatch and VDJdb was limited in both groups tested. Data is represented as mean ± SEM and statistical significance was determined using paired t-tests.

Bioinformatical analysis of sequencing results and TCR matching was performed by Dr Catherine Sutherland, Institute of Immunology & Infection Research, University of Edinburgh.

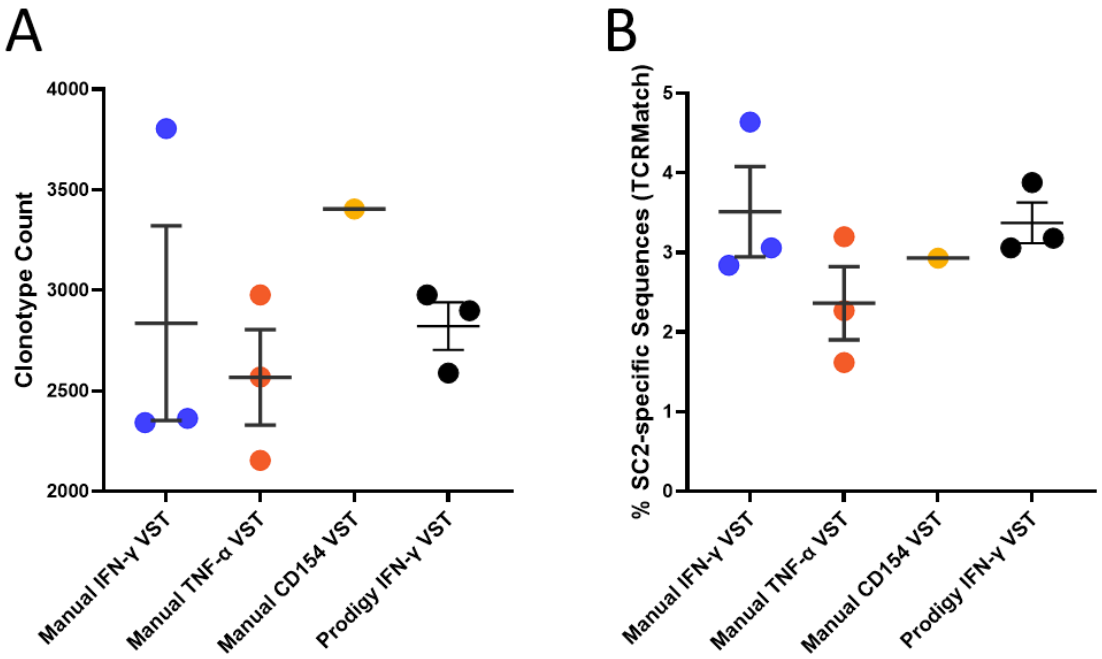

Figure 6.30 - Manual versus Prodigy isolated VST clonotype comparison.

Matched donors C19USA4, C19UKD1 & C19UKD6 were compared for final product VST clonal repertoire between between manual IFN-γ, manual TNF-α, manual CD154 and Prodigy IFN-γ isolations. **(A)** Clonotype counts corrected for UMI size matching is compared between groups. **(B)** The proportion of each repertoire with an exact CDR3 amino acid sequence match specific to SARS-CoV-2 using TCRMatch database was compared between groups. All data is represented as mean ± SEM and tested for statistical significance using paired t-tests.

Bioinformatical analysis of sequencing results and TCR matching was performed by Dr Catherine Sutherland, Institute of Immunology & Infection Research, University of Edinburgh.

TCR antigen databases were further utilised to assess CDR3 sequence matches to a range of other viruses. Comparisons were made between pan CD3+ T cell starting material and the Prodigy-isolated SARS-CoV-2 VST final products to investigate selection of particular viral clones during the VST isolation and expansion process. Using the TCRMatch database (**Figure 6.31A**) sequences matches are highest for SARS-CoV-2 (range 2-12%), and negligible (<2%) to all viruses examined. Interestingly, SARS-CoV-2-specific sequences are similar between pan CD3 T cells (mean = 4.15 ± 0.1%) and prodigy VST (mean = 5.22 ± 1.3%) suggestive of limited SARS-CoV-2 clone enrichment between starting material and final product. Analysis using the VDBJ database (**Figure 6.31B**) has negligible sequences (<2%) matches for all viruses including SARS-CoV-2. There is however a marginal increased percentage of CMV-specific and EBV-specific sequences in pan CD3 T cells compared to the other viruses which is to be expected of these prevalent viruses within the human population. Although non-significant, the percentage of CMV-specific and EBV-specific

clones decreases in the prodigy VST which indirectly suggests a level of purification of SARS-CoV-2 specific clones during the manufacturing process.

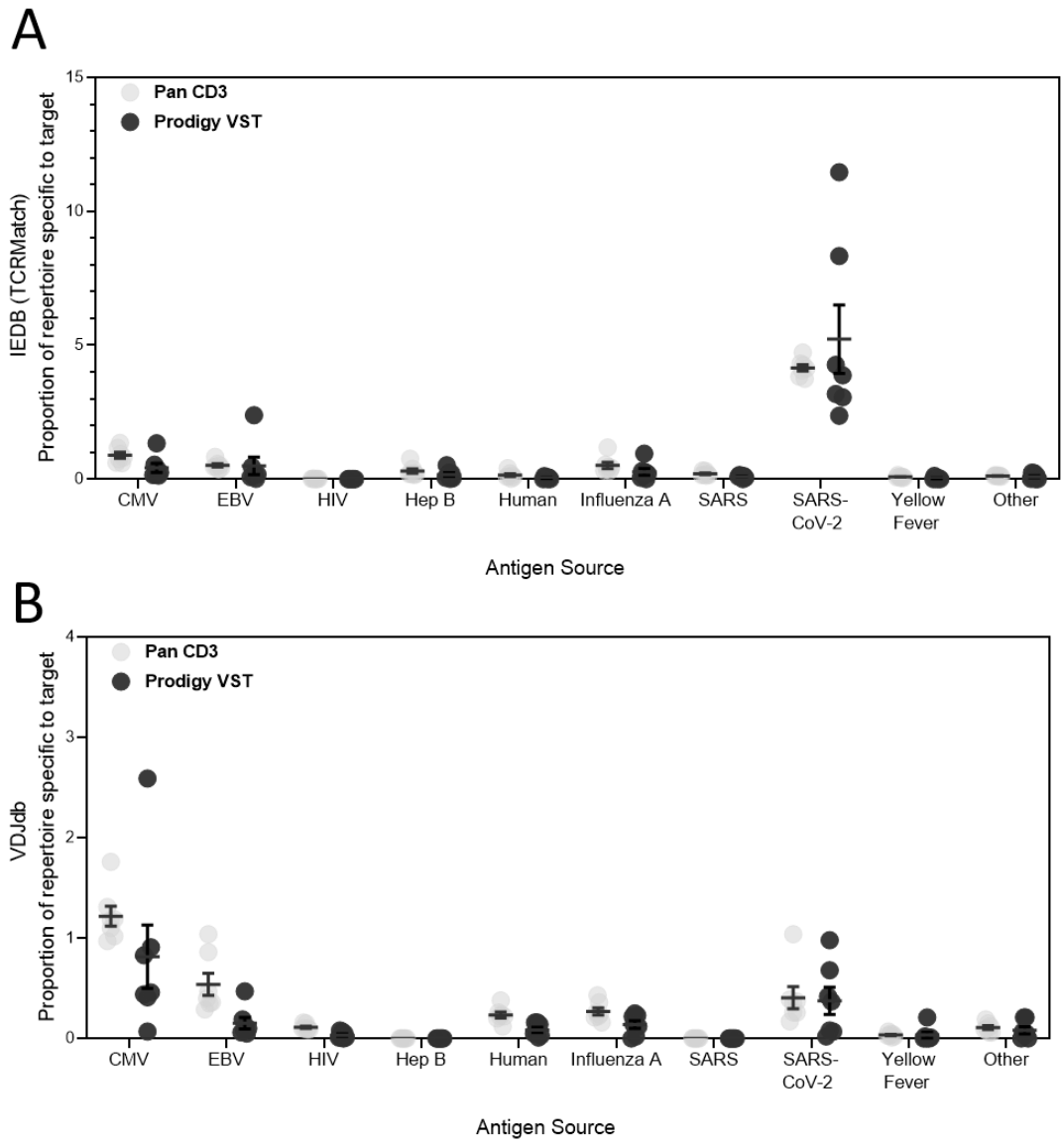

Figure 6.31 - Banked SARS-CoV-2 VST viral specificity.

Proportion of each repertoire specific to antigens from various viral sources as annotated by exact match to CDR3 amino acid sequences in **(A)** IEDB TCRMatch and **(B)** VDJdb databases. Data is represented as mean ± SEM and comparisons between matched donor pan CD3 T cell starting material and Prodigy-isolated VST final products using paired t-tests.

Bioinformatical analysis of sequencing results and TCR matching was performed by Dr Catherine Sutherland, Institute of Immunology & Infection Research, University of Edinburgh.

Samples were also assessed for sequence matches specific to different SARS-CoV-2 viral antigens (**Figure 6.32**). Again, the TCRMatch database showed a greater number of matches, with the highest proportion of final product VST matching ORF1 (3.2 ± 1.2%) and Spike (1.9 ± 0.9%) specific sequences (**Figure 6.32A**). The frequency of SARS-CoV-2 antigen-specific sequence matches using the VDBJ database were all

<0.2% of the repertoire and as such not detectable using this database (**Figure 6.32B**).

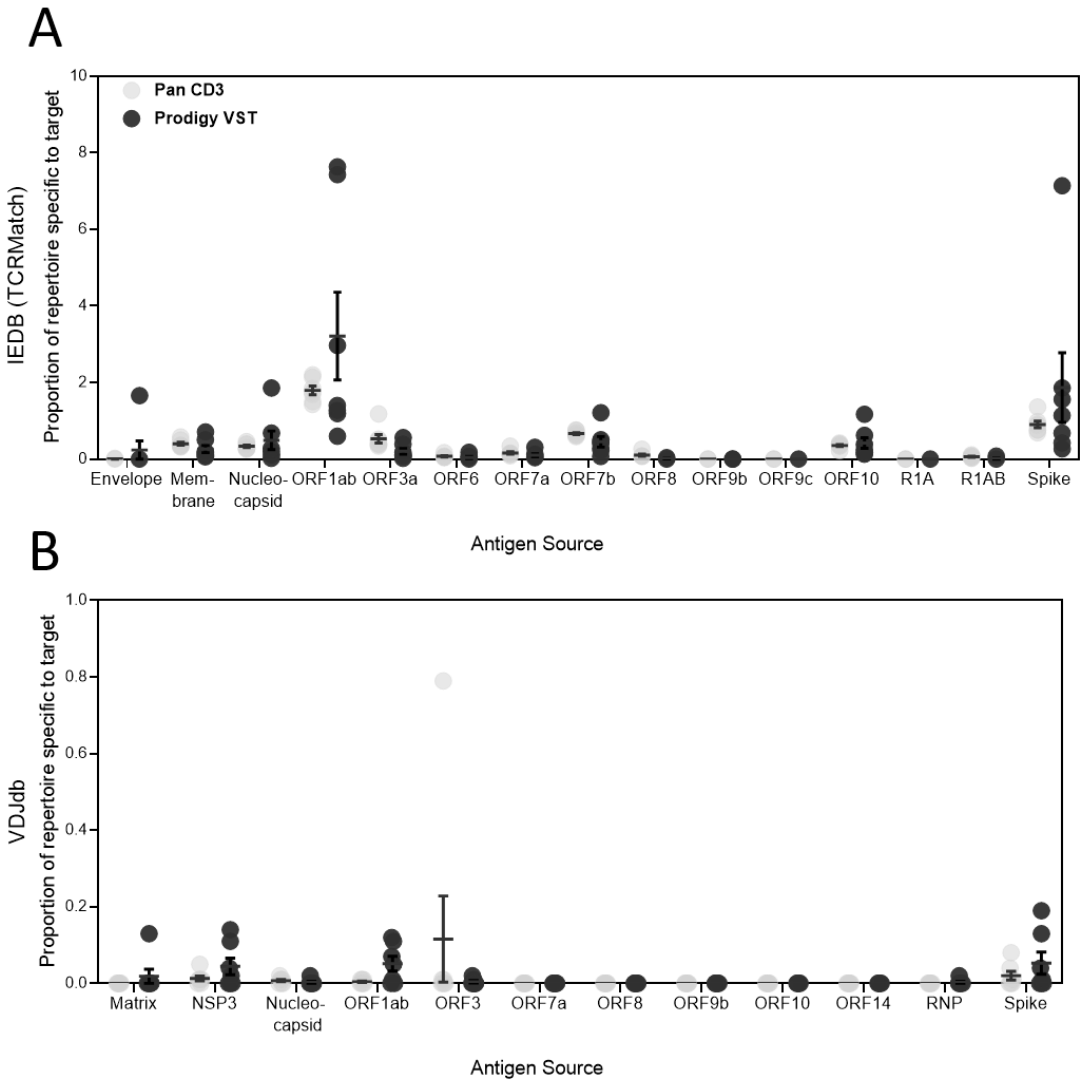

Figure 6.32 - Banked SARS-CoV-2 VST antigen specificity.

Proportion of each repertoire specific to various SARS-CoV-2 antigens as annotated by exact match to CDR3 amino acid sequences in **(A)** IEDB TCRMatch and **(B)** VDJdb databases. Data is represented as mean ± SEM and comparisons between matched donor pan CD3 T cell starting material and Prodigy-isolated VST final products using paired t-tests.

Bioinformatical analysis of sequencing results and TCR matching was performed by Dr Catherine Sutherland, Institute of Immunology & Infection Research, University of Edinburgh.

6.5.7 SARS-CoV-2 VST safety testing

In addition to standard cell product safety testing such as viral, BactALERT, endotoxin and mycoplasma; manufactured SARS-CoV-2 were also tested in additional safety assays for immunogenic and tumourigenic potential.

To assess immunogenicity, samples were sent for mixed lymphocyte reaction (MLR) testing in a commercial Skimune® assay by Alcyomics®. In this assay, MLR co-cultures were set up between SARS-CoV-2 VST with healthy volunteer (HV) PBMCs for 7 days. Each SARS-CoV-2 donor was tested for MLR against n=3 HV with minimal or no HLA matches (**see Table 6.3**). At day 7, samples were taken for assessment of T cell proliferation, cytokine production, and MLR cells further co-cultured with HV skin biopsies for GVHD responses.

											No. of Matches	
Donors	Ax	Ay	Bx	By	Cx	Cy	DRB1x	DRB1y	DQB1x	DQB1y	Class I	Class II
C19USA3	02:01	68:01	15:18	39:01	07:04	12:03	01:01	01:01	05:01	05:01		
HV2	02:01	68:01	13:02	51:01	06:02	15:02	01:91	15:01	05:01	06:02	2	2
HV3	03:01	25:01	07:02	55:01	03:03	07:02	14:54	15:01	05:03	06:02	1	1
C19USA4	02:01	32:01	27:05	35:03	02:02	04:01	01:01	16:01	05:01	05:02		
HV5	02:01	68:01	13:02	51:01	06:02	15:02	01:91	15:01	05:01	06:02	1	2
HV6	03:01	25:01	07:02	55:01	03:03	07:02	14:54	15:01	05:03	06:02	0	1
C19UKD1	01:01	24:02	38:01	57:01	06:02	12:03	01:01	14:01	05:01	05:03		
HV7	01:01	02:01	08:01	44:03	04:01	07:01	04:01	07:01	02:02	03:02	1	0
HV8	02:01	11:01	15:01	44:02	03:04	15:01	04:01	04:01	03:02	01:03	0	0
HV9	03:01	11:01	44:02	55:01	03:03	07:04	14:54	15:01	05:03	06:02	0	2
C19UKD3	01:01	31:01	18:01	35:01	04:01	07:01	07:01	11:04	02:01	03:03		
HV10	01:01	02:01	08:01	44:03	04:01	07:01	04:01	07:01	02:02	03:02	3	3
HV11	02:01	11:01	15:01	44:02	03:04	15:01	04:01	04:01	03:02	01:03	0	1
HV12	03:01	11:01	44:02	55:01	03:03	07:04	14:54	15:01	05:03	06:02	1	0
C19UKD7	02:xx	11:xx	18:xx	55:xx	03:xx	01:xx	01:xx	03:xx	02:xx	05:xx		
HV13	02:05	29:02	44:03	50:01	06:02	16:01	07:01	07:01	02:02	02:02	1	2
HV14	01:01	02:01	08:01	44:02	05:01	07:01	03:01	13:02	02:01	06:04	1	2
HV15	02:01	02:01	44:02	51:01	05:01	15:02	04:01	15:01	03:01	06:02	2	0
C19UKD14	01:01	24:02	08:01	15:01	03:03	03:01	03:01	04:01	02:01	03:02		
HV16	02:05	29:02	44:03	50:01	06:02	16:01	07:01	07:01	02:02	02:02	0	2
HV17	01:01	02:01	08:01	44:02	05:01	07:01	03:01	13:02	02:01	06:04	2	2
HV18	02:01	02:01	44:02	51:01	05:01	15:02	04:01	15:01	03:01	06:02	0	2

Table 6.3 - Mixed lymphocyte reaction co-cultures donor HLA matches.

Each SARS-CoV-2 VST donor HLA type is shown shaded in grey. HLA matches with corresponding healthy volunteer (HV) donors used for mixed lymphocyte reaction co-cultures is shaded as light orange for low resolution match and dark orange as high resolution match. The total number of class I and class II HLA matches are quantified in the right-hand columns.

T cell proliferation following the 7 day MLR co-culture was measured using a thymidine uptake assay. The counts per minute (cpm) is shown for SARS-CoV-2 donor co-cultures with n=3 healthy volunteers in **Figure 6.33**. Each co-culture had triplicate wells, therefore each co-culture is grouped per HV donor (purple, navy or

light blue). HV autologous PBMC were included as a negative control to assess baseline T cell proliferation in autologous co-cultures. As can be seen, SARS-CoV-2 donor PBMC had highest T cell proliferation of all tests, indicating the starting material contains alloreactive T cells causing T cell proliferation when mixed with HV donor PBMC.

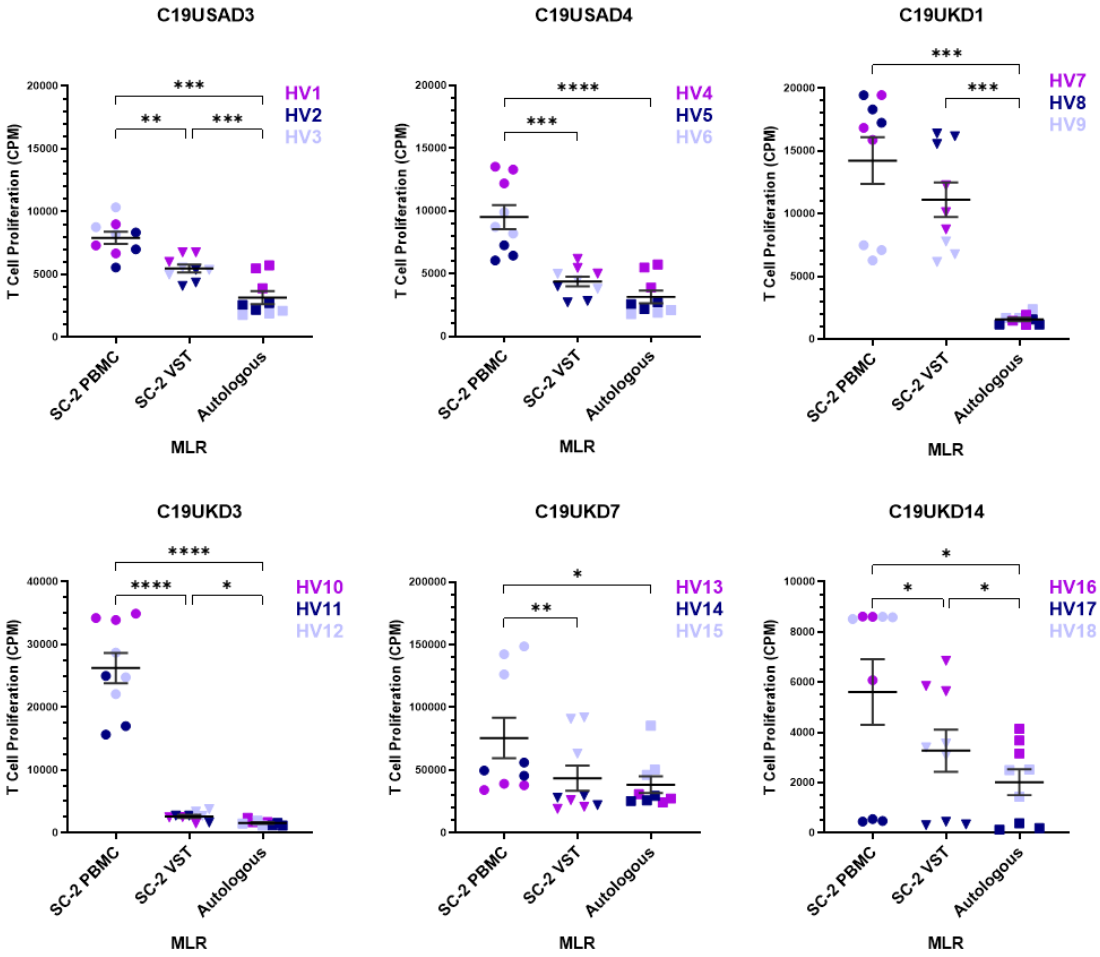

Figure 6.33 - Mixed lymphocyte reaction T cell proliferation.

Starting source material (PBMC) and final product SARS-CoV-2 VST were thawed and tested in mixed lymphocyte reactions (MLR) with healthy volunteer (HV) PBMC for 7 day co-cultures. T cell proliferation in response to MLR co-culture was compared between each SC-2 donor PBMC, donor VST and autologous HV PBMC. Data is represented as mean ± SEM of three HV donor MLR tests, each with triplicate wells (n=9), where triplicates are grouped for each HV donor by colour (purple, navy or light blue). Comparisons between groups were made using RM one-way ANOVA with Geisser-Greenhouse correction where *p≤0.05, **p≤0.01, ***p≤0.001 and **** p≤ 0.0001.

MLR set up and T cell proliferation assay was performed by Dr Shaheda Ahmed, Alcyomics®.

All SARS-CoV-2 donor VST (except C19UKD1) induced a significantly lower T cell proliferation than the matched SARS-CoV-2 donor PBMC suggesting considerable antigen specificity of the VST products. Donors C19USAD4, C19UKD3 and C19UKD7 VST had induced T cell proliferation comparable with the autologous co-culture

controls, indicating these lines have minimal alloreactivity potential. Interestingly, some MLR co-cultures have segmented T cell proliferation dependent on HV used in test. For example with the C19UKD14 MLRs, T cell proliferation was negligible with HV17 co-cultures compared to the other two HV donor tests. This likely reflects the higher number of both class I- and class II-restricted HLA matches between C19UKD14 & HV17, as compared to C19UKD14 with HV16 or HV18 (**Table 6.3**).

Supernatants from the MLR co-cultures were also taken after 7 days to measure production of inflammatory cytokines using a multiplex cytokine assay. The concentration of cytokines produced is shown in pg/mL (**Figure 6.34**) for each HV co-culture with either SARS-CoV-2 donor PBMC (circles), SARS-CoV-2 VST final products (triangles) or autologous HV PBMC controls (squares). Each data point is coloured for the HV donor, where each point represents the mean of concentration of triplicate wells. Groups were quantified as the mean ± SEM of n=3 HV tests, and comparisons between SC-2 PBMC, SC-2 VST and autologous PBMC groups made by ANOVA. As can be seen, production of IL-10, IL-12p70, IL-13, IL-1b, IL-2, IL-4 and TNF-α was negligible in all MLR co-cultures. SARS-CoV-2 PBMC induced production of IFN-γ (~1000pg/mL) in most donor co-cultures tested, however limited IFN-γ accumulated in the SARS-CoV-2 VST or autologous PBMC co-cultures. Production of IL-6 was relatively high in most co-cultures tested ranging between 5,000-50,000 [pg/mL], however the IL-6 concentration was comparable between SC-2 PBMC, SC-2 VST and autologous PBMC groups indicating a nonspecific production of IL-6 independent of HLA mismatches. In exception to this general finding, IL-6 secretion was not detected in C19UKD14 MLR co-cultures with any of the HV co-cultures tested which may suggest a technical failure for this multiplex assay.

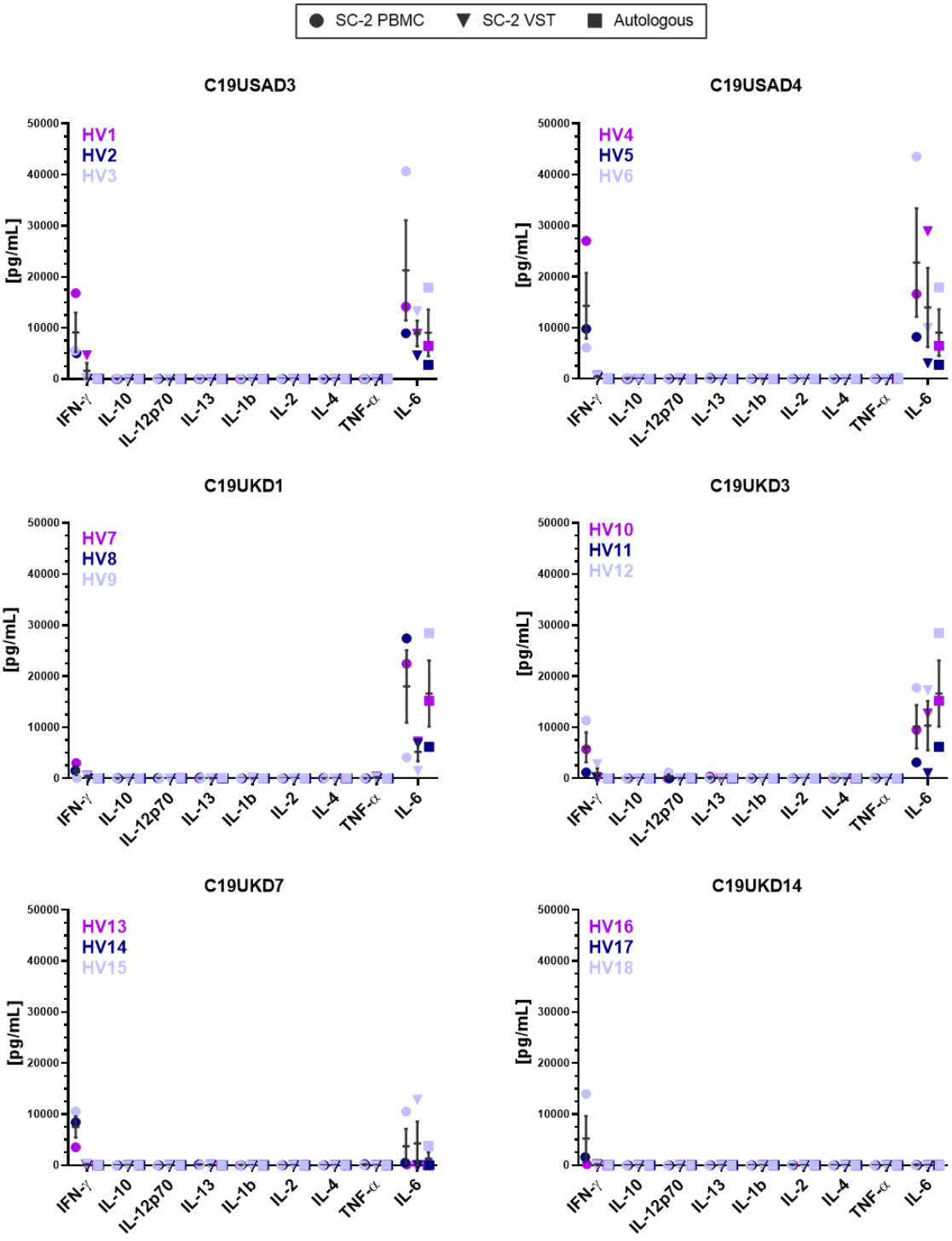

Figure 6.34 - Mixed lymphocyte reaction cytokine multiplex.

Mixed lymphocyte reaction co-cultures were set up for 7 days to test HV volunteer PBMC mixed with: SARS-CoV-2 donor PBMC (circles), SARS-CoV-2 donor VST (triangles) and autologous HV PBMC controls (squares). Supernatants from each MLR co-culture were analysed for cytokine concentration by luminex of pro-inflammatory cytokines IFN-γ, IL-10, IL-12p70, IL-13, IL-1b, IL-4, TNF-α and IL-6. Data is represented as mean ± SEM of three HV donor MLR tests (purple, navy or light blue; where each data point is the mean of n=3 triplicate wells). Comparisons between groups were made using RM one-way ANOVA with Geisser-Greenhouse correction.

MLR set up and cytokine multiplex assay was performed by Dr Shaheda Ahmed, Alcyomics®.

Following the initial 7 day co-culture, MLR cells were harvested and further co-cultured for 3 days with HV skin explants. Again, HV skin was co-cultured with both SARS-CoV-2 starting material PBMC and SARS-CoV-2 donor final product VST, as well as HV autologous PBMC and medium only for negative controls. Co-cultures were then formalin fixed, paraffin embedded, sectioned and H&E stained, with GVHD graded by histology as outlined in **Figure 6.35**. Grade I was considered a negative GVHD response, and Grades II-IV were positive responses with increasing severity.

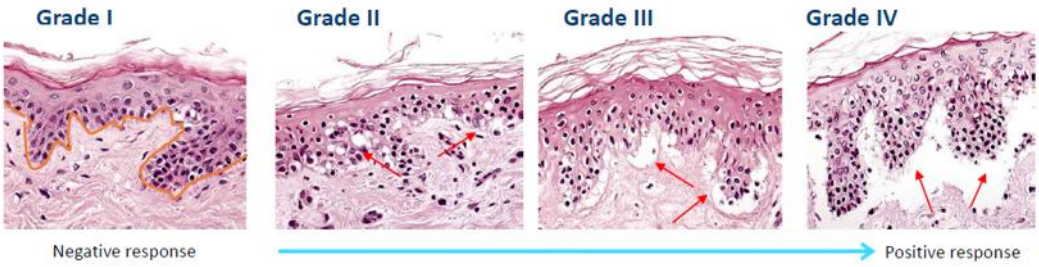

Figure 6.35 – Mixed lymphocyte reaction Skimune assay GVHD grading by histology.

Exemplar histology readout to determine GVHD responses for negative skin response (Grade I) versus positive responses (Grade II, Grade II and Grade IV) according to the severity of the skin tissue damage observed. Grade I is considered negative, with intact upper keratinocyte layer. Grade II refers to vacuolisation of the epidermis. Grade III shows severe damage of the epidermis layer, with initial separation of the epidermis and dermis layers. Grade IV refers to severe damage, with complete separation of the epidermis and dermis layer.

MLR, Skimune® assay, histology and analysis was performed by Dr Shaheda Ahmed, Alcyomics®.

GVHD grading of skin explants for each SARS-CoV-2 donor is shown in **Table 6.4**. Since each SARS-CoV-2 donor was set up with MLRs with three HV donors, each with duplicate wells, the number of GVHD positive tests (grade II or higher) was quantified out of the total (n=6) wells. Where there were issues with insufficient cells fewer wells were plated, in which case results are listed as not done (ND). The percentage of GVHD positive wells was then calculated to allow comparison between donors and treatment groups.

C19USAD3 - Full Scale Development (SNM Peptides)							
	Class I Matches	Class II Matches	Test	C19USA3 PBMC	C19USA3 VST	Medium	Autologous (HV) PBMC
HV1	Not HLA typed		well 1	III	II	I	II
			well 2	III	I	I	ND
HV2	2	1	well 1	III	I	I	I
			well 2	II	I	ND	ND
HV3	1	1	well 1	I	I	I	I
			well 2	I	I	I	ND
Total positive responses/ No. of tests				4/6 (66.7%)	1/6 (16.7%)	0/5 (0%)	1/3 (33.3%)
C19USAD4 - Full Scale Development (SNM Peptides)							
	Class I Matches	Class II Matches	Test	C19USA4 PBMC	C19USA4 VST	Medium	Autologous (HV) PBMC
HV4	Not HLA typed		well 1	III	I	I	II
			well 2	III	I	I	ND
HV5	1	2	well 1	II	I	I	I
			well 2	II	I	ND	ND
HV6	0	1	well 1	I	I	I	I
			well 2	ND	I	I	ND
Total positive responses/ No. of tests				4/5 (80%)	0/6 (0%)	0/5 (0%)	1/3 (33.3%)
C19UKD1 - Full Scale Development (SNM Peptides)							
	Class I Matches	Class II Matches	Test	C19UKD1 PBMC	C19UKD1 VST	Medium	Autologous (HV) PBMC
HV7	1	0	well 1	III	III	I	I
			well 2	III	III	I	ND
HV8	0	0	well 1	II	I	I	I
			well 2	II	I	I	I
HV9	0	2	well 1	III	II	I	II
			well 2	III	III	ND	I
Total positive responses/ No. of tests				6/6 (100%)	4/6 (66.7%)	0/6 (0%)	1/5 (20%)
C19UKD3 - Banked (SARS-CoV-2 Select Peptides)							
	Class I Matches	Class II Matches	Test	C19UKD3 PBMC	C19UKD3 VST	Medium	Autologous (HV) PBMC
HV10	3	3	well 1	II	I	I	I
			well 2	II	I	I	ND
HV11	0	1	well 1	II	I	I	I
			well 2	III	I	I	I
HV12	1	0	well 1	III	II	I	II
			well 2	III	II	ND	I
Total positive responses/ No. of tests				4/5 (80%)	0/6 (0%)	0/5 (0%)	1/5 (20%)
C19UKD7 - Banked (SARS-CoV-2 Select Peptides)							
	Class I Matches	Class II Matches	Test	C19UKD7 PBMC	C19UKD7 VST	Medium	Autologous (HV) PBMC
HV13	1	2	well 1	III	I	I	I
			well 2	III	I	I	II
HV14	1	2	well 1	II	II	I	II
			well 2	III	ND	I	ND
HV15	2	0	well 1	II	I	I	II
			well 2	II	ND	ND	II
Total positive responses/ No. of tests				6/6 (100%)	¼ (25%)	0/5 (0%)	3/5 (60%)
C19UKD14 - Banked (SARS-CoV-2 Select Peptides)							
	Class I Matches	Class II Matches	Test	C19UKD14 PBMC	C19UKD14 VST	Medium	Autologous (HV) PBMC
HV16	0	2	well 1	I	I	I	I
			well 2	I	I	ND	ND
HV17	2	2	well 1	I	I	I	I
			well 2	I	I	ND	ND
HV18	0	2	well 1	I	I	I	I
			well 2	II	I	ND	ND
Total positive responses/ No. of tests (%)				1/6 (16.7%)	0/6 (0%)	0/3 (0%)	0/3 (0%)

Table 6.4 - Mixed lymphocyte reaction skin explant GVHD testing results.

Representative images of skin sections following treatment with cells from MLRs of C19USAD3 PBMC, C19USAD3 VST, autologous HV PBMC or medium only are shown in **Figure 6.36A**. The mean percentage of GVHD positive responses was compared for the different treatment groups (**Figure 6.36B**) where each data point represents an individual SARS-CoV-2 donor with the percentage GVHD positive wells of n=6 wells as above. SARS-CoV-2 donor PBMC MLRs had a significantly higher percentage of GVHD positive responses than SARS-CoV-2 VST (p=0.0137) and the autologous PBMC (p=0.0133) and medium controls (p=0.008).

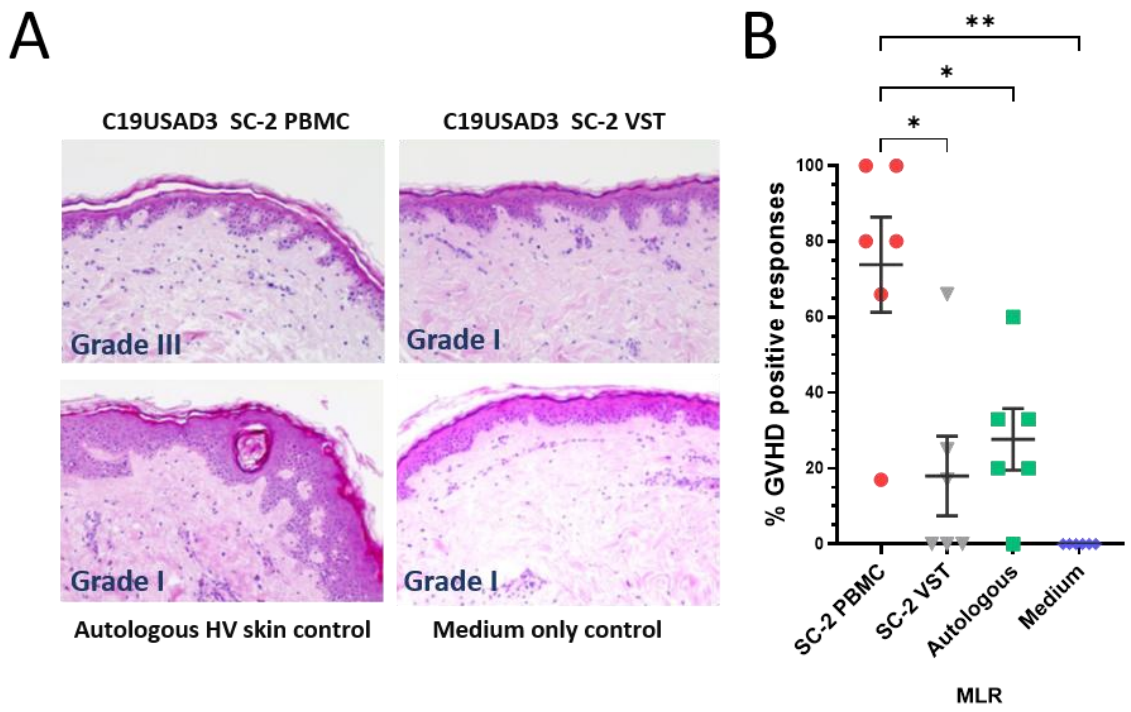

Figure 6.36 – Mixed lymphocyte reaction Skimune assay GVHD positive responses.

Each SARS-CoV-2 donor was set up in an MLR with HV skin biopsies for Skimune assay GVHD histology analysis. Skin explant MLR co-cultures tested HV cells with SARS-CoV-2 donor VST and SARS-CoV-2 donor PBMCs were as a positive immunogenic control. Further skin explant MLR co-cultures tested autologous HV PBMC & medium only as negative controls. **(A)** Representative analysis of skin histology following Skimune assay for SARS-CoV-2 donor C19USAD3 with HV2. **(B)** The mean percentage positive GVHD response (Grade II or above) to all HV tests was compared between groups where each data point represents a single SARS-CoV-2 donor tested against n=3 HV each with duplicate wells. Data is represented as mean ± SEM of n=6 SARS-CoV-2 donors and comparisons between groups made using RM one-way ANOVA with Geisser-Greenhouse correction where *p≤0.05 and **p≤0.01.

MLR, Skimune® assay, histology and analysis was performed by Dr Shaheda Ahmed, Alcyomics®.

Since GVHD positive responses were consistently low between SARS-CoV-2 VST (mean = 18 ± 10.5%) and autologous control (mean = 27.7 ± 8.1%) MLR co-cultures, this indicates a very limited immunogenic potential of VST even for these assays where allogeneic co-cultures were set up with minimal or no HLA matches.

Interestingly, even autologous controls exerted GVHD responses in some cases, implying autologous PBMC have potential to cause low level skin damage perhaps driven by a difference in residential response between PBMC and skin cells.

As well as immunogenicity, progression in the cell therapy field requires more comprehensive tumourogenicity testing, particularly for processes that involve culture expansion whereby cell culture has the potential to transform cells. To assess tumourogeneicity, we sent genomic (g) DNA samples to an accredited NHS molecular haematology oncology laboratory to test for 50 cancer associated genes in a short nucleotide polymorphism (SNP) array. Both starting material leukapheresis gDNA and final product SARS-CoV-2 VST gDNA were tested for each donor to determine if the VST isolation and culture expansion process was likely to induce upregulation of oncogenes. Due to ethical regulations, we could only perform genetic testing on the commercial USA donor material generated during the full-scale manufacturing translation phase. Results of SNP variants detected for C19USA donors (n=3) for the fifty cancer associated genes is outlined in **Table 6.5**.

	Leukapheresis Starting Material		SARS-CoV-2 VST Final Product	
Donor	**Variant**	**Frequency**	**Variant**	**Frequency**
C19USAD2	No variants detected		No variants detected	
C19USAD3	FBXW7: c.1727C>T p.(Thr576Met)	48%	FBXW7: c.1727C>T p.(Thr576Met)	52%
	ATM: c.998C>T p.(Ser333Phe)	47%	ATM: c.998C>T p.(Ser333Phe)	52%
	AKT1:c.138C>A p.(Asp46Glu)	52%	AKT1:c.138C>A p.(Asp46Glu)	49%
	JAK3:c.2164G>A p.(Val722Ile)	51%	JAK3:c.2164G>A p.(Val722Ile)	51%
C19USAD4	No variants detected		No variants detected	

Table 6.5 - Single nucleotide polymorphisms in oncogenes of SARS-CoV-2 VST.

Sequence single nucleotide polymorphism (SNP) variants for 50 oncogenes: ABL1, AKT1, ALK, APC, ATM, BRAF, CDH1, CDKN2A, CSF1R, CTNNB1, EGFR, ERBB2, ERBB4, EZH2, FBXW7, FGFR1, FGFR2, FGFR3, FLT3, GNA11, GNAS, GNAQ, HNF1A, HRAS, IDH1, IDH2, JAK2, JAK3, KDR, KIT, KRAS, MET, MLH1, MPL, NOTCH1, NPM1, NRAS, PDGFRA, PIK3CA, PTEN, PTPN11, RB1, RET, SMAD4, SMARCB1, SMO, SRC, STK11, TP53, VHL.

SNP array and analysis was performed Oxford Molecular Haematology laboratory at John Radcliffe Hospital, University of Oxford.

As can be seen, no oncogene variants were detected in either the leukapheresis starting material or SARS-CoV-2 VST final product for donors C19USAD2 and C19USAD4. Coding mutations were present in four oncogenes tested for C19USAD3: FBXW7 (F-box/WD repeat-containing 7), ATM (ataxia telangiectasia mutated), AKT1 (alpha serine threonine kinase 1) and JAK3 (janus kinase 3). However since these

variants were present at approximately 50% frequency this is indicative of heterozygous constitutional variants specific to the donor. In addition, since the same gene variants were detected at similar frequency in both the starting material leukapheresis and final product VST this suggests no change in variant expression during the isolation and culture expansion protocol. Therefore, data from these representative C19USA donors indicates the SARS-CoV-2 VST manufacturing process does not induce upregulation of the tested cancer associated genes and therefore risk of tumourogenicity is negligible using this assay.

6.6 SARS-CoV-2 VST first in human trial to treat hospitalised patients with COVID-19

All GMP manufactured SARS-CoV-2 VST banked for clinical use follow a stability program to ensure long term product stability and functionality.

6.6.1 Phase I safety trial design

Banked SARS-CoV-2 VST have been approved for use in a first in human phase I clinical trial (NCT04473053) to treat hospitalised patients with active COVID-19 infection run by principal investigator Professor Kev Dhaliwal, University of Edinburgh. While the overall strategy of this therapeutic is to treat at risk immunosuppressed or compromised patients, to run through the phase I trial participants were required to be immunocompetent to assess safety of infused allogeneic SARS-CoV-2 VST. Full inclusion and exclusion criteria for participants to be included in the trial are outlined in **Table 6.6**. Briefly, participants had to be over the age of 16, not pregnant or breastfeeding, and with no current or history of severe cardiac, liver, or renal diseases. In addition, participants were excluded on the basis of haemoglobinopathies, severe diabetes mellitus or individuals on immune suppressive drugs or otherwise immunocompromised. To be included patients must have been COVID-19 positive within the last 14 days by PCR test, maintain oxygen saturations >92% prior to infusion, and must not have received any vaccination up to 3 weeks prior to infusion. While the trial became active in August 2022, the first two patients were infused in January and March 2023, and recruitment significantly dropped following this. This was mainly due to the cessation of mandatory COVID-19 testing within hospitals, combined with supplemental oxygenation rapidly becoming the first

line standard of care for COVID-19 patients, meaning any potential infected participants would be excluded on the basis of oxygen saturation levels.

INCLUSION CRITERIA ▪ Provision of informed consent. ▪ Aged at least 16 years. ▪ COVID-19 positive PCR test result within last 14 days**.** ▪ Maintaining oxygen saturations of ≥92% at time of screening and for 24 hours prior to commencement of infusion. ▪ If the patient is of child bearing potential, or is a male with a female partner with child bearing potential, the patient, and their partner(s), agree to use a highly effective method of contraception for 4 weeks following the date of the infusion. Methods considered highly effective are those that achieve a failure rate of less than 1% per year when used consistently.
EXCLUSION CRITERIA ▪ Current or recent history, as determined by the Investigator, of severe, progressive, and/or uncontrolled cardiac disease (NYHA class IV), uncontrolled renal disease (eGFR <30 mL/min/1.73 m^2), severe liver dysfunction (ALT >5x ULN) or anaemia (Hb <80 g/L). ▪ Women who are pregnant or breastfeeding. ▪ Participation in another clinical trial of an Investigational Medicinal Product (CTIMP). ▪ Known hypersensitivity to advanced therapy medical products (ATMP) or excipients. ▪ Patients (or their partners) planning on donating sperm/eggs during the trial period. ▪ Ongoing dialysis. ▪ History of serious liver disease (Child Pugh score > 10). ▪ Severe uncontrolled diabetes mellitus. ▪ Concomitant use of treatments for COVID-19 that are not recognised as locally approved standard care. ▪ In the Investigator's opinion, patient is unwilling or unable to comply with trial intervention (e.g. IMP/ATMP administration plan), laboratory tests or other study procedures. ▪ O_2 saturations <92% on air at time of screening or during the 24 hours prior to infusion. ▪ Individuals who are immunocompromised and/or immunosuppressed. ▪ Individuals with haemoglobinopathies. ▪ Patients who have received any vaccine (including COVID-19 vaccine) within the preceding 3 weeks, or are due any vaccine within the 6 week trial follow up period following the infusion (it may be problematic to discriminate a reaction to a vaccine from signs/symptoms of the ongoing infection or a reaction to the SARS-CoV-2 VST).

Table 6.6 – DEFINE First in human trial for SARS-CoV-2 VST participant criteria.

Abbreviations: NYHA, New York heart association; eGFR, estimated glomerular filtration rate; ALT, alanine transaminase; ULN, upper limit normal; Hb, haemoglobin.

Patients successfully recruited and consented to the trial were split into cohorts to test dose escalation as show in **Figure 6.37**. The proposed dosing regime for the study was a single dose of low dose (group 1 – $1.5x10^6$ cells total), mid dose (group 2 – $1.5x10^7$ cells total), or full dose (group 3 – $1.5x10^8$ cells total). Dose group 1 entailed treatment of n=3 participants with 3 weeks between each participant. Dose group 2 entailed treatment of n=3 participants with a minimum of 3 days between patients.

Full dose group 3 required treatment of 5 participants with a minimum of 3 days between infusions. Data monitoring committee review and agreement to proceed to the next cohort was required between each dose group.

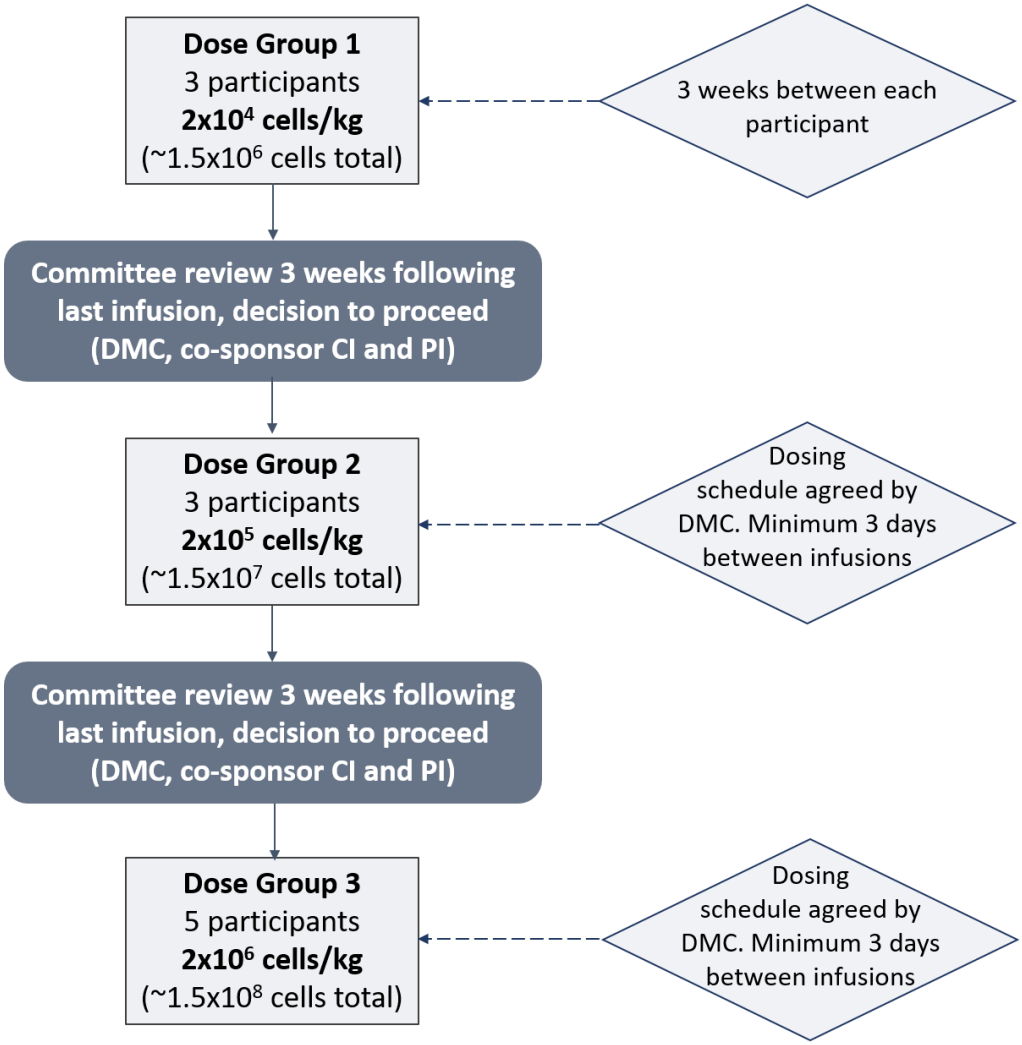

Figure 6.37 - DEFINE First in human trial for SARS-CoV-2 VST dosing regime patient cohorts.

The initial phase I DEFINE clinical trial to assess safety of SARS-CoV-2 VST was designed to incorporate numerous patient cohorts for dose escalation testing. Dose group 1 requires three participants at lowest dose ($2x10^4$ cells/kg) with three weeks between each participant. The data monitoring committee (DMC) will then review and decide to proceed to dose group 2 which requires three participants at middle dose ($2x10^5$ cells/kg) with a minimum of three days between patient infusions. Following DMC agreement to move to final cohort dose group 3, five participants will receive the full dose ($2x10^6$ cells/kg) again with a minimum of three days between infusions.

6.6.2 SARS-CoV-2 VST product selection

Upon enrolment into the trial, participants were HLA typed at the SNBTS Histocompatability & Immunogenetics laboratory within the Royal Infirmary Edinburgh. A SARS-CoV-2 VST product will be selected from the bank on the basis of best HLA matches – with class II matches preferentially selected due to the CD4+

composition of most banked VST lines. If there is a case where a patient did not have any matches with any of the banked SARS-CoV-2 VST lines, the patient would be withdrawn from the trial. Additionally, it must be ensured that there is at least one HLA mismatch between patient and VST product to avoid the risk of transfusion-associated GVHD (Rühl et al., 2009). The HLA type, blood group and age of all donors with SARS-CoV-2 VST products banked for clinical use is outlined in **Table 6.7**.

VST Donor	Age	Blood Group	HLA									
			A*	A*	B*	B*	C*	C*	DRB1 *	DRB1 *	DQB1 *	DQB1 *
C19UKD3	30	O pos	1:01	31:01	18:01	35:01	4:01	07:01	7:01	11:04	02:01	03:03
C19UKD6	50	O pos	11:01	29:02	40:02	51:01	01:02	02:02	01:01	15:01	05:01	06:02
C19UKD7	59	O neg	02:01	11:01	18:01	55:01	03:01	05:01	01:01	03:01	02:01	05:01
C19UKD8	56	O neg	1:01	24:02	8:01	15:01	3:03	7:01	3:01	4:01	02:01	03:02
C19UKD12	41	O pos	2:01	26:01	15:01	27:05	2:02	3:04	4:08	11:01	03:01	03:01
C19UKD14	25	O neg	1:01	32:01	7:02		3:03	7:02	15:01		6:02	
C19UKD15	45	O pos	1:01	11:01	8:01	35:01	4:01	7:01	4:01	7:01	02:02	03:01

Table 6.7 - SARS-CoV-2 VST banked donor HLA types.
HLA typing was performed by Dr Richard Battle, Histocompatibility & Immunogenetics, SNBTS.

6.6.3 SARS-CoV-2 VST product administration

Following selection of the most suitable SARS-CoV-2 VST product from the bank, VST were sent to Royal Infirmary of Edinburgh in a liquid nitrogen shipper. At the bedside, bags were thawed in a water bath and administered to the patient intravenously with a saline flush to ensure maximal recovery of cells from the tubing. Patients were monitored in hospital according to standard transfusion procedures for at least 48 hours post-administration with the expectation that any adverse transfusion related reaction may occur in that time period. Full patient monitoring will run for 6 weeks post-infusion, with daily recording of oxygen saturation levels for the first 21 days. Full details of patient monitoring assessments and testing time-points are outlined in **Table 6.8**. Research samples taken to assess disease resolution and therapy efficacy include standard SARS-CoV-2 swab and viral load PCR and blood SARS-CoV-2 antibody testing, and blood plasma marker testing for inflammatory molecules and markers for disease resolution by diagnostic flow cytometry.

Activities	Screening & Enrolment	Day 0 Baseline	Day 1	Day 2	Day 7 (+/- 1 day)	Day 14 (+/- 1 day)	Day 21 (+/- 1 day)	6 weeks (+/- 1 week)
Clinical study procedures and assessments								
NEWS2 Score and WHO ordinal scale		✓	✓	✓[1]				
Vital signs (SpO2, FiO2, RR, PR, temperature, blood pressure)	✓	✓	✓	✓[1]				
Physical assessment (baseline medical examination, height, weight)	✓							
Directed cardio-respiratory physical examination		✓	✓	✓[1]				
Cough symptom score		✓	✓	✓[1]			✓*	
Child Pugh score	✓							
Oxygen saturation via pulse oximeter[1]	✓	✓	✓	✓	✓	✓	✓	
Safety assessments								
Laboratory Safety Assessments[2]	✓	✓[3]	✓	✓[1]	✓		✓	
AE/SAE recording and assessment	✓	✓	✓	✓[1]	✓	✓	✓	✓
Graft Versus Host Disease check[4]								✓
Research assessments								
SARS-CoV-2 viral load (saliva)	✓*			✓* (+/- 1 day)	✓*		✓*	
SARS-CoV-2 nasal swab test	✓*			✓* Day 2 & 4	✓*		✓*	
SARS-CoV-2 blood sample	✓*			✓* Day 2 & 4	✓*		✓*	
SARS-CoV-2 VST tracking ICR assay[5]	✓*			✓* Day 2 & 4	✓*		✓*	
Plasma marker testing[6]	✓*			✓* Day 2 & 4	✓*		✓*	

Table 6.8 - SARS-CoV-2 VST therapy administration and patient monitoring time-points.

1. Daily until day 21.
2. **Biochemistry** – Urea, sodium, potassium, chloride, magnesium, bicarbonate, creatinine, C-reactive protein, ferritin, troponin; creatine kinase and estimated glomerular filtration rate; **LFTs** - Total bilirubin, alanine aminotransferase and aspartate aminotransferase; **Haematology** – full blood count (haemoglobin, haematocrit, red cell count, white cell count and differential white cell count (excluding eosinophils) and platelets);

   Coagulation - activated partial thromboplastin time, prothrombin time, fibrinogen.
3. Samples to be taken pre-infusion and again 2-3 hours post infusion. For pre-infusion sample results should be reported prior to commencement of infusion.
4. Via phone call, participant asked whether they have any new symptoms such as skin rashes. It can take up to 20-40 days post infusion for symptoms of TA-GvHD to become apparent.
5. Only to be carried out on samples from participants receiving a target of $2x10^5$ cells/kg ($15x10^6$ cells dose) and $2x10^6$ cells/kg ($150x10^6$ cells dose).
6. Plasma marker testing will include, for example, markers of inflammation and disease resolution.

* This assessment will be desirable. If the participant declines, the sample will not be taken and will not be considered a deviation.

6.6.4 Clinical trial patient results

Patient enrolment for the SARS-CoV-2 therapy arm of DEFINE –evaluating therapies for COVID-19 phase I safety trial opened in January 2023. As of July 2025, two patients have been infused with SARS-CoV-2 VST at the lowest dose ($1.5x10^6$ cells) as detailed in **Table 6.9**. The SARS-CoV-2 VST infused for each patient was chosen based on best HLA match determined by SNBTS H&I team, selecting the VST batch with highest number of restricted HLA matches. In cases of multiple VST batches with equal number of restricted HLA matches, preference was given to either HLA class I or class II allele matches dependent on CD4/CD8 ratio of that VST product.

	Patient				Donor VST Infused				
	No.	Infusion Date	Gender	Age	Donor Code	No. HLA Matches	HLA Restricted Matches	% CD4+	% CD8+
Low Dose $1.5x10^6$	1	12 JAN 2023	Male	66	C19UKD8	5 restricted (7 total)	A*01:01; A*24:02; B*08:01; C*07:01; DRB1*03:01	19.17	78.69
	2	22 MAR 2023	Female	78	C19UKD14	3 restricted (5 total)	B*07:02, C*07:02, DRB1*15:01	72.13	26.84
	3	Not Done							
Mid Dose $1.5x10^7$	4	Not Done							
	5	Not Done							
	6	Not Done							
Top Dose $1.5x10^8$	7	Not Done							
	8	Not Done							
	9	Not Done							
	10	Not Done							
	11	Not Done							

Table 6.9 - DEFINE First in human trial for SARS-CoV-2 VST patient infusions.

6.7 Discussion

Numerous T cell therapies have now been developed and initiated testing in trials for a potential prophylaxis or treatment for COVID-19. All COVID-19 T cell therapies in clinical trials as of January 2025, are collated and detailed in **Table 6.10** colour coded into three categories: SARS-CoV-2 VST manufactured using peptide-pulsed APC stimulation and VST outgrowth (blue), SARS-CoV-2 VST manufactured using selection methods (orange), and other types of T cell associated therapy (green). Trials now terminated are shaded in dark grey. Of the SARS-CoV-2 VST therapies manufactured using peptide-pulsed APC stimulation and outgrowth, QC characterisation demonstrates high T cell purity, with ranging specificity between products. Interestingly three of these trials (NCT04742595, NCT04401410 and NCT05447013) are testing CD4-skewed T cell therapies with negligible cytotoxic functionality, whereas the other two trials (NCT05141058 and NCT04765449) are testing CD8 T

cell products. Of the SARS-CoV-2 VST therapies manufactured using CCS, ours (highlighted in dark orange) is the only process that includes a post-selection culture expansion. While the lack of culture expansion after CCS has obvious advantages of being a very rapid manufacturing process (<48 hours) and being a minimally manipulated therapeutic product, our strategy to combine selection and culture expansion uniquely allows us provide much higher dose treatments and multiple doses for patients. Of course, at present it is currently unknown what would be an optimal T cell dose for COVID-19 therapy and is likely to be different between patient cohorts, however given these patients are not iatrogenically immune suppressed a higher dose may be required to permeate the host T cell compartment and provide sufficient numbers for therapeutic functionality. As shown by comparing the phenotypic characterisation of our Prodigy CCS target cells and final product, purity and specificity is not optimal without subsequent expansion. Enrichment of a rare T cell population is limited to 100-400x the initial frequency within the unselected blood starting source material. Therefore, our optimised culture process also has benefits in inducing further T cell enrichment, and drives expansion of desirable central and effector memory populations with high functional specificity and potency. This is further discussed throughout this section.

Trial/Location	Company/ PI	Dose	Patients	Process	Phenotype	Function	Status
NCT04406064 Cincinnati, USA	Adam Nelson	?	Symptomatic COVID-19 requiring oxygen or ventilation			Withdrawn due to steroid use for COVID prevents VST use in these patients, 0 patients enrolled	
NCT04742595 Houston, USA	Katy Rezvani	?	COVID-19 cancer patients with pneumonia	Pepmix-pulsed PBMC (S, M, N, E, Aps, NSPs, ORFs) 14 days expansion 100-1000 FE	CD4+ 60-75% CD8+ 20-40% TCM 10-20%	S<N=M Specificity ~20%	Recruiting, last update August 2023
NCT04401410 Houston, USA (ALVR109)	AlloVir Premal Lulla	$4x10^7$ total	Hospitalised patients with COVID-19 at high risk of ventilation	Pepmix-pulsed PBMC (S,M,N,E, AP7, SNP4) 10-16 days expansion 15x banked lines	CD3+ 94-99.9% CD4+ 73.6-97.1% CD8+ 2-23.2% NK <1% TCM 20-70%	S<N<M<NSP4=AP7 Specificity 10-16% Cytotoxicity 10-20% Alloreactivity <1%	Terminated December 2022 due to poor recruitment, 4 patients enrolled
NCT05447013 Thessaloniki, Greece	Anastasia Papadopoulou	$2x10^7$/ m2	Hospitalised patients with pneumonia & leukopenia	Pepmix-pulsed PBMC (S,M,N,E) 9-11 days expansion 30x banked lines $5-10x10^8$	CD3+ >90% CD4+ 60-90% CD8+ 0-40% TCM 27%	S<M<N Cytotoxicity <10%	Recruiting, last update November 2022
NCT05141058 Washington, Baltimore, USA	Michael Keller Catherine Bollard	$4x10^7$/ m2	Immunocompromised HSCT (prophylaxis)	Peptide-pulsed PBMC (S,M,N,E) 10 days expansion	CD3+ >90% CD4+ 25-27% CD8+ 20-70% B cell 0-10% NK cell 0-5%	M<S<N=Actin Specificity 22-75% Alloreactivity 0%	Recruiting, last update September 2022
NCT04765449 Philadelphia, USA (TVGN-489)	Tevogen Bio	$3x10^6$/ kg	Elderly and high risk COVID-19 patients	"primed and selected using APCS" peptides from COVID-19 gene/ORF	CD3+ CD8+ >95% Tetramer+ >60%	Cytotoxicity >60% HLA-A*01:01 >50% ORF1ab	Completed, 30 patients enrolled

NCT04457726 Singapore	Wing Hang Leung	<1x10^6 total	Severe COVID-19	CliniMACS IFN-γ CCS (SC-2 Select Peptivator) No expansion 6x banked lines ~1 million cells	CD3+ 33-71% CD4+ 62-77% CD8+ 25-38% B cell 25-64% NK cell 2-4% TCM 12-35%	Purity 20-74% Specificity ~15%	Unknown, last update on recruitment July 2020
NCT04762186 Cologne, Germany	Miltenyi Phillip Kohler	5x10^3 /kg	Moderate COVID-19	CliniMACS IFN-γ CCS (SC-2 Select Peptivator) No expansion 4x banked lines ~1 million cells	CD3+ 30-40% CD4+ 30-40% CD8+ 50-60% NK <0.5% TCM <5%	Mean purity 33.3% Cytotoxicity ~40%	Terminated September 2022 due to poor recruitment
NCT04896606 New York, Wisconsin, USA		<2x10^6 total	Hospitalised mild to moderate COVID-19	CliniMACS IFN-γ CCS (S,M,N Peptivators) No expansion Mean yield 1.7x10^6	CD3+ ~50% CD4+ 27.78% CD8+ 5.34% B cell 7-20% NK cell 0-2%	Specificity 30-40%	Recruiting, last update March 2023
NCT04473053 Edinburgh, UK	SNBTS Kev Dhaliwal	1.5x10^8 total	Hospitalised COVID-19 patients	CliniMACS IFN-γ CCS (SC-2 Select Peptivator) 14 days expansion 7x banked lines Mean yield 9x10^9	CD3+ >98% CD4+ 66% CD8+ 34% NK cell 0-4% TCM 55-90%	Specificity 40-83% Cytotoxicity <10% Alloreactivity <1%	Recruiting, last update November 2023
NCT04389385 Kayseri, Turkey	Mustafa Cetin		COVID-19 patients with early stage NCV pneumonia	Aerosol Inhalation of the Allogenic SARS-CoV-2 VST-derived exosomes (not HLA-matched)		Unknown status, last update May 2020.	
NCT04834128 Newcastle, UK TCB008	TC Biopharm		Hospitalised high risk patients	Allogeneic gamma delta T cells			Terminated due to current COVID-19 status in UK and trial involved parenterally administer IMP/ inpatient care. 0 patients enrolled.
NCT04737161 Stanford, USA	Joe Hsu		High risk COVID-19 DNR ARDs patients	Allogeneic Treg			Withdrawn as funding not secured, 0 patients enrolled.
NCT05027815 Chapel Hill, USA	Jeffrey Bluestone NIAID		COVID-19 ARDS patients	Allogeneic Treg			Terminated due to decrease in COVID-19 cases, 7 patients enrolled.

Table 6.10 - Clinical trials of T cell therapies for COVID-19.

Initial process translation from the research small scale isolation and expansion of SARS-CoV-2 VST using buffy coats in Chapter 4 was tested using leukapheresis as the starting material, automated Prodigy CCS for isolation, and closed-system large flasks for culture expansion. Commercial leukapheresis from USA COVID-19 convalescent donors was used for this development phase, however donors could not be tested for SARS-CoV-2 T cell responses ahead of collection and shipment to our centre for processing. Instead, the SARS-CoV-2 peptide T cell screening assay was run in tandem to the Prodigy CCS isolation in attempt to assess the efficiency of IFN-γ CCS enrichment on the prodigy. The yield of IFN-γ+ target cells from the CCS assay using Prodigy automated selection appeared markedly increased as compared to yield using the manual selection, although not statistically significant likely due to small sample size in the Prodigy group. While there was no apparent association between

the number of IFN-γ+ target cells from Prodigy CCS and the percentage of SARS-CoV-2 peptide-reactive IFN-γ+ in the leukapheresis screen assay, it is likely the improved CCS yield in Prodigy selections reflects the overall higher input of leukapheresis WBC into the CCS assay which is needed for isolating such rare cell populations. Interestingly, phenotyping the isolated target cells revealed a significantly increased population of DN CD3+ T cells in the Prodigy CCS compared to manual CCS. Downregulation of CD4 or CD8 on the target T cells is likely due to a more intense stimulation and processing through the closed automated system column selection. A significantly reduced frequency of CD4+ T cells in the Prodigy targets further suggests the DN T cells are highly activated CD4 T cells transiently downregulate the CD4 receptor. Target cells were then expanded for 14 days using the culture process optimised in Chapter 4, and with an initial higher number of target cells accordingly grown in larger closed-system G-Rex100M-CS flasks. The full-scale USA donor cultures elicited a 2-3 log expansion over 14 days, comparable to the fold expansion seen in research phase manual isolation cultures. Phenotyping the expanded cells following 14 days culture demonstrated final products were highly purified for T cells, with negligible NK cells or NKT cells. The CD4 population had increased to 80-90%, with a small population of accompanying CD8 T cells and negligible DP or DN T cells, further supporting that the target cells were primarily CD4 T cells with a transient downregulation of CD4 receptor due to intense stimulation in the Prodigy CCS assay. Within both CD4 and CD8 subsets, cells were highly skewed to central memory phenotype demonstrating a consistent final product memory status between the research and full-scale process translation. Antigen recall testing using SARS-CoV-2 SNM pooled peptide-loaded DC indicated a comparable functional Th1 response of the Prodigy-isolated final product cells.

Since process translation demonstrated the Prodigy closed system isolation and expansion was suitable for full-scale manufacture, we rapidly initiated clean room manufacture of a SARS-CoV-2 VST bank. To select donors with the best SARS-CoV-2 T cell responses, buffy coats from n=109 COVID-19 convalescent donors were screened (data in Chapter 5), with n=46 donors showing detectable T cell responses to the SNM-pooled peptides. Donors with the highest frequency of CD3+/IFN-γ+ cells in the screen assay were approached for consent to donate leukapheresis for production of SARS-CoV-2 VST lines to be used in a clinical trial. Since donor buffy coat screening went on over numerous months (August 2020 to April 2021), and that we observed a

general decline in SARS-CoV-2 VST frequency over time since infection (see Chapter 4), we implemented a secondary peripheral blood T cell screen between one to two weeks before the consented donor was scheduled to for leukapheresis collection. A minimum criterion of >0.08% CD3+/IFN-γ+ cells, as well as the standard apheresis screening tests was required for the donor to be eligible to donate leukapheresis for VST manufacture. Interestingly, comparison of donor T cell responses between their initial buffy coat screen in 2020 versus later screen prior to manufacture in 2021 indicated responses to all three antigens were maintained, and not particularly directed toward spike even after one or multiple spike-targeted vaccines. Due to relaxation of public health policies beginning in summer 2021 in the UK, and unsurprisingly the emergence of new viral strain variants, it is not improbable that donors sustained SARS-CoV-2 T cell responses could have been due to community re-exposure.

The initial two donors were manufactured in clean room (C19UKD1 & C19UKD2) using SARS-CoV-2 SNM pooled peptides (premium-grade) as per all preceding process development runs, until new GMP-grade SARS-CoV-2 peptides (Peptivator SARS-CoV-2 Select) were released in February 2021. Differences between the peptide pools are detailed in **Table 2.3**; where the premium-grade peptides were individual pools with full coverage of the nucleocapsid and membrane protein, and immunodominant regions of the spike protein, and the GMP Peptivator Select pool was HLA-restricted for selected immunodominant regions of the whole SARS-CoV-2 proteome (spike, nucleocapsid, membrane and envelope). Since differences between the premium-grade SNM versus GMP-grade select were considerable in terms of sequence, leukapheresis from the next donor for manufacture (C19UKD3) was split to undertake a parallel clean room process to directly compare isolation using the different peptide pools. Since the intra-donor comparison demonstrated equivalent expansion and final product characterisation/ functional potency, we converted all subsequent manufacture to use the GMP Select peptides to ensure full regulatory compliance for manufacture of an ATMP. Nine donor manufacturing process were completed using the GMP peptides (C19UKD3, C19UKD6, C19UKD7, C19UKD8, C19UKD9, C19UKD10, C19UKD12, C19UKD14 & C19UKD15). Four donors (C19UKD4, C19UKD5, C19UKD11, C19UKD13) were consented however failed the clinical apheresis unit screening tests and so could not donate leukapheresis for the manufacturing process. Manufacturing of the bank took several months between

February 2021 to March 2022, and therefore as well as variables in donor age, sex, and time since natural SARS-CoV-2 infection, there was also high variation in vaccination status and the most prevalent SARS-CoV-2 variant at time of donation. Although donor characteristics and their SARS-CoV-2 T cell immunity are potentially quite variable due to timing of manufacture, ultimately due to the month long procedure (donor peripheral blood checks, VST 14 day expansion, freeze down and time-point 0 thaw stability testing) and that it is was not recommended in the SNBTS clean rooms to overlap manufacturing processes, the bank could not have been made any faster. This presents an interesting consideration for potential platform translation to future emerging viruses: even with extensive staff resourcing there will always be considerable lag period in manufacture of clinical-use virus-specific T cells to allow time for donor recruitment, supply of viral peptides of an appropriate standard, testing of peptide-induced T cell responses and optimisation/validation of all manufacturing and characterisation processes.

Of the nine donor manufacturing products, two donors (C19UKD9 & C19UKD10) generated insufficient final product SARS-CoV-2 VST to be included in the clinical use bank (<3 patient bagged doses at $1.5x10^8$ VST per dose). Since final product bags must be taken for additional safety testing such as BactAlert, endotoxin and post-thaw stability, a minimum of four bags was required to have a dose available for patient use in clinical trial. Final product yield was variable between donors ranging from 2-225 doses, with some of the higher expansions generating too many cells for us to actually cryopreserve or store as doses for clinical use. An in-depth investigation of all donations, processing and characterisation data was undertaken to understand why some donors had relatively poor VST expansions in order to identify exclusion criteria to prevent future 'manufacturing failures'. In addition to preventing financial waste through significant manufacturing costs and staff time, it is of primary importance to us as a public health body that donors do not undergo unnecessary procedures that are not entirely risk-free such as apheresis collection.

While there were no obvious correlations between VST expansion and donor demographics, duration between infection and donation, or pre-screen VST frequency, a significantly elevated population of SARS-CoV-2 peptide IFN-γ-reactive NK cells was observed in three of the four low expansion donors. Comparison of the intra-donor reactivity to SARS-CoV-2 peptides between their initial buffy coat screen

in autumn-winter 2020, and their later leukapheresis screen in 2021 revealed an interesting NK cell response. The overall NK cell population (CD56+/CD3- cells) significantly decreased upon stimulation with SARS-CoV-2 SNM peptides compared to the no antigen control at the buffy coat screen, which did not occur in the later leukapheresis screen where NK cell population remained stable upon SARS-CoV-2 peptides stimulation. These results may have captured a transient effect on the NK cell compartment of natural primary SARS-CoV-2 infection, whereby antigen re-exposure even in these convalescent donors with a mild primary infection induced a substantial downregulation of CD56 on NK cells. By the time of the leukapheresis screening, it is likely these individuals may have had multiple re-exposures to SARS-CoV-2 virus, and almost all had also been vaccinated, which appears to have re-stabilised NK cell SARS-CoV-2 immunity (Lucas et al., 2021). Differences in the peptide-induced downregulation of CD56 may also be due to differences in blood subsets and processing between the buffy coat PBMC and leukapheresis samples, however it seems unlikely that such a large effect would be down to subset composition. Initial screening of the donor leukapheresis prior to manufacture demonstrated a substantial SARS-CoV-2 peptide-induced expression of IFN-γ in the low expansion donors. The frequency of NK cells positive for IFN-γ in these donors was higher in response to stimulation with pooled SNM peptides compared to the SARS-CoV-2 Select peptides indicating an increased NK cell reactivity to regions not covered in the SARS-CoV-2 Select peptide sequences. Further breakdown looking at individual antigen peptides in the leukapheresis screen showed a slightly higher frequency of IFN-γ-reactive NK cells in these donors to Spike and/ or membrane whereas there was a trend towards a lower response to Nucleocapsid, although there was degree of variability between donors. While the membrane-specific NK cells demonstrates immunity the natural virus, it would be interesting to see if continued exposure to spike-directed vaccines affects this altered NK cell immune response over time.

Although NK cells usually elicit innate immune response in a transient antigen-independent manner, CMV infection has been reported to induce expansion of NK cells with long-lived persistence and antigen response upon viral re-challenge mimicking an adaptive memory-like response (Gumá et al., 2006a, Sun et al., 2009). This memory NK cell population was observed up to a year following infection in CMV seropositive individuals and was characterised with positive expression of NKG2C,

lymphocyte maturation marker CD57, antibody-dependent cellular cytotoxicity marker CD16, IFN-γ secretion upon viral re-challenge and absence of inhibitory receptor NKG2A (Foley et al., 2012b). Interestingly, the presence of expansive NKG2C+ NK cells in healthy donor PBMC was specific to CMV seropositive donors, whereas this association was not observed for herpes simplex virus (HSV) or EBV serology status (Gumá et al., 2004, Hendricks et al., 2014), and is supported by a larger cohort study demonstrating no CMV seronegative donors (n=69) had expression of NKG2C+ NK cells. Furthermore a study investigating memory NK cells in the setting of HSCT transplantation showed the frequency and absolute counts of NKG2C+ NK cells significantly expanded up to a year following transplant only in cases where both the donor and recipient were CMV seropositive, or post-transplant CMV reactivation had occurred (Foley et al., 2012a). In cases where the donor was CMV seronegative, NKG2C+ NK cell frequency and absolute count remained undetectable throughout the time-course. This expansion in NKG2C+ NK cells in donor seropositive/ recipient seropositive cases but in the absence of detectable CMV viremia indicated low level subclinical latent CMV antigen stimulation was required to maintain persistence of this memory NK cell population. CMV seronegative recipients who received a HSCT graft from CMV seropositive donors had an increased expansion of NKG2C+ cells with higher IFN-γ functional responses at one year post-transplant compared to grafts from CMV seronegative donors indicating a transfer of memory NK cell immunity. Epigenetic analysis revealed distinct methylation patterns of memory-like NK cells in CMV seropositive donors that mirrored effector cytotoxic T cells, and responses to CMV re-challenge in FcεRγ- adaptive NK cells (Schlums et al., 2015).

Expansion of NKG2C+ memory-like NK cells has also been reported following hantavirus (Björkström et al., 2011), chikungunya virus (Petitdemange et al., 2011), dengue virus (Petitdemange et al., 2016), and human immunodeficiency virus (HIV) (Gumá et al., 2006b, Zhou et al., 2015, Ma et al., 2017, Peppa et al., 2018) infection. In all these studies, NKG2C+ memory NK cells were only observed in CMV seropositive individuals. Although CMV seroprevalence is estimated at 78-88% of the general population globally (Zuhair et al., 2019), a large cohort study observed presence of NKG2C+ memory NK cells in around 30% of all CMV seropositive individuals (Schlums et al., 2015). This was found to be largely dependent upon CMV strain, with differential clonal expansion capacity of NKG2C+ NK cells in response to distinct UL40

peptide sequences (Hammer et al., 2018). Therefore current evidence suggests strain-specific chronic CMV infection is essential for development of the NKG2C+ NK cell population capable of adaptive responses, and this population can further expand and elicit antiviral functionality in response to coinfection with a range of other viruses (Barnes et al., 2020).

Interestingly, a few other groups have also observed adaptive NK cell responses following SARS-CoV-2 infection (Maucourant et al., 2020, Bergantini et al., 2021, Herrera et al., 2022). Maucourant and colleagues reported a significantly increased NKG2C+/CD57+ CD56dim NK cell population in severe COVID-19 patients during active infection compared to patients with moderate disease and healthy controls (Maucourant et al., 2020). Expansion of the NKG2C+ NK cell population in these COVID-19 patients (moderate and severe) was confined to CMV seropositive individuals, with no association with CMV viral load or CMV IgG titre, further supporting the theory that these memory NK cells originated following CMV infection however expanded in response to SARS-CoV-2 infection and not a CMV reactivation. Another study also observed a significantly higher frequency of NKG2C+/CD57+ adaptive NK cells in patients with severe COVID-19 compared to patients with mild or moderate symptoms during active infection (Bergantini et al., 2021).

Herrera and colleagues also observed our findings of NK cells secreting IFN-γ in response to SARS-CoV-2 peptide stimulation in COVID-19 convalescent donors (Herrera et al., 2022). Responses to SARS-CoV-2 peptides were also variable between six donors investigated whereby two donors had a higher frequency of IFN-γ-reactive NK cells to spike peptides, and a further donor had IFN-γ-reactive NK cells only responsive to membrane peptides. Interestingly, one donor with a 5-20% IFN-γ-reactive NK cells to the three SARS-CoV-2 peptides at 4 months post-infection, dropped to <3% for all three SARS-CoV-2 peptides at 9 months post-infection demonstrating a significant reduction in this donors' SARS-CoV-2 NK cell immunity over convalescence. Further characterisation of the IFN-γ-reactive NK cells revealed a higher population of NKG2C+/CD57+ cells as compared to donors without SARS-CoV-2-specific NK cell responses. The authors proposed the host pro-inflammatory environment during infection may induce a sustained NK cell activation via upregulation of HLA-E, which could lead to memory NK cells capable of recognising soluble-specific peptides through the NKCG2C receptor.

A recent study of responses to SARS-CoV-2 vaccines reported a substantial expansion of NKG2C+/CD16+/CD56dim NK cells up to 9 months following a second vaccination and one 1 month following a third 'booster' dose of the original Pfizer Comirnaty vaccine (Gentili et al., 2023). This population showed high CD107a and IFN-γ responses when stimulated with SARS-CoV-2 spike peptide-loaded APC, indicating an expansion of the memory NK cell population with anti-SARS-CoV-2 activity following vaccination. Importantly, they demonstrated these adaptive NK cells respond to the original Wuhan Spike peptide, as well as variants alpha, delta and omicron; indicating vaccination with mRNA sequence to the original Wuhan spike still confers memory NK cell recognition to the mutated variants.

With our donors, variation in the number of vaccines received, time since last vaccine, and vaccine provider/formulation, it is difficult to distinguish responses to the natural virus versus the different vaccines. Certainly, some donors demonstrated adaptive IFN-γ-reactive NK cells in their initial buffy coat screen prior to vaccinations indicating an expansion of this subset in response to SARS-CoV-2 infection, and responses to peptides other than spike in their leukapheresis screen further indicates memory to the virus itself rather than just vaccine induced expansions. Furthermore, all the donors that exhibited SARS-CoV-2 peptide NK cell responses were CMV seropositive, whereas the two donors in our bank who were CMV seronegative did not have IFN-γ-reactive NK cells, supporting the theory that these cells originated after CMV infection rather than developing in SARS-CoV-2 infection, however a larger cohort size with more CMV seronegative individuals would be needed to confirm this hypothesis. Interestingly we don't see this adaptive NK cell IFN-γ response to EBV peptides in screening or CCS isolation (see Chapter 3) indicating a potential role for the crossover of immunity between CMV and SARS-CoV-2. In terms of choosing donors to manufacture SARS-CoV-2 VST, it would be simple to incorporate more NK cell markers such as NKG2C/ CD57/ CD16 into the peptide screening assay to define the presence of this adaptive NK population in donors, and further screen out donors where this population has IFN-γ response to SARS-CoV-2 peptides to prevent hindrance during the CCS assay.

Additionally, phenotyping of the target cells isolated by Prodigy CCS revealed a significant correlation of increased final product yield with increasing frequency of target CD8+ cells. This suggests CD8 cells isolated from this process have higher

proliferative capacity than the SARS-CoV-2-specific CD4+ cells. This data could be utilised in the future for more sophisticated screening of donors prior to manufacture to minimise expansion failures by selecting donors with greater CD8+ T cell-specific responses to peptides. However biasing the selection of donors in this way would need to be weighted against understanding the desirable phenotype of T cells for therapy of the particular disease, which should ideally be investigated in preclinical models. Furthermore, phenotyping of the final product VST demonstrated a negative correlation between VST expansion and PD-1 expression on the day 14 expanded T cells. While expression of PD-1 alone is considered to be a marker of activation rather than exhaustion (Baessler and Vignali, 2024), this result suggests a link between lines with lower expansive capacity having a highly activated T cell phenotype. While co-expression of multiple inhibitory receptors (PD-1, LAG-3, and TIM-3) did not correlate with VST expansion, expression of these dual or triple-positive populations were considerably higher in final product CD4+ cells than CD8+ cells. This may reflect either two (not necessarily unrelated) phenomena, CD4+ SARS-CoV-2 VST are more rapidly exhausted following antigenic stimulation, or CD8+ SARS-CoV-2 VST are highly proliferative and consequently less likely to be affected by antigenic stimulatory exhaustion. Earlier exhaustion and lack of effector functionality of virus-specific CD4+ T cells compared to CD8+ T cells has been reported during HIV infection (Kaufmann et al., 2007).

While these three factors were associated with relatively low VST expansion, it is difficult to elucidate if these are linked or there may reflect independent mechanisms by which the SARS-CoV-2 VST failed to expand in our culture process. Unless another root cause can be determined for the differences in CD4/CD8 ratio in the CCS isolated targets, or the higher PD1 expression in some VST final products, only the presence of peptide-reactive NK cells at pre-screen could be incorporated as a criterion to screen out donors to prevent failed manufactures despite the lack of a clear mechanism underpinning this finding.

Banked SARS-CoV-2 VST were also subject to numerous additional testing procedures to comprehensively characterise different parameters of T cell function and factors involved in allogeneic cell therapy infusion. Flow cytometric profiling of chemokine receptor expression demonstrated SARS-CoV-2 VST products had consistently high expression of CCR2, CCR4, CCR5, CXCR3 and CXCR4. SARS-CoV-2 infection induces

expression of CCL2, CCL5, CXCL1, CXCL9 and CXCL10 in airway vasculature and alveolar capillaries of the lung parenchyma (Alon et al., 2021). This is thought to be crucial for effector CD4+ and CD8+ T cells to successfully migrate through these vessels and enter the lamina propria via expression of CCR2, CCR4, CXCR3 and/or CCR5 for natural host immune resolution, thereby indicating intravenously infused therapeutic SARS-CoV-2 VST would be able to home to the lungs accordingly. CCR4 expression has also been shown to be important in influenza-specific T cell responses, whereby infection induces lung DC imprinting of T cells to home to lung through high expression of CCR4. Adoptive transfer experiments in infected mice demonstrated lung DC activated CCR4 knockout T cells were unable to migrate to the lungs and mice continued to harbour high influenza viral load with corresponding decreased survival rates, whereas transfer of lung DC activated CCR4+ T cells efficiently resolved infection within 10 days (Mikhak et al., 2013). Both CCR4 and CCR5 have been found to be significantly upregulated on CD4+ and CD8+ T cells within the peripheral blood of COVID-19 patients with severe pulmonary complications compared to mild disease (Spoerl et al., 2021) indicating the importance of these receptors to mount a stronger T cell response directed to the lungs. Furthermore, positron emission tomography (PET) tracing of CD8+ cells in patients in response to early stage SARS-CoV-2 infection revealed trafficking to the upper respiratory tract and both PLO and SLO was mediated by high expression of CXCR3 and CCR4 (Koenen et al., 2024). This suggests CXCR3+ and CCR4+ SARS-CoV-2 VST would have increased capacity to migrate from the circulation to the site of inflammation and into the peripheral tissues. While chemokine receptor profiling gives an indication of the migratory potential of T cell therapies, *in vivo* models should be tested to elucidate where cells actually traffic to following adoptive transfer in an inflamed disease host.

To test the ability of SARS-CoV-2 VST to elicit effector functions upon antigen recognition, VST were co-cultured with autologous DC loaded with SARS-CoV-2 peptides and analysed for expression of cytokines and activation markers. Final product VST had a high frequency of multifunctional effector T cells with 20-40% triple positive for CD154/ IFN-γ/ TNF-α, and 2-25% quadruple positive for CD154/ IFN-γ/ TNF-α/ IL-2 indicating a high specificity of these products to SARS-CoV-2 re-challenge. Furthermore, VST had broad reactivity to membrane, nucleocapsid and the different spike variant peptides which indicates the therapy would be less susceptible to immune escape by viral mutational evolution. Cytotoxicity against autologous

SARS-CoV-2 peptide-loaded B cell targets indicated negligible (<5%) target cell specific lysis when compared to co-cultured VST + unloaded B cell controls. This slightly increased to 5-15% specific lysis if analysis was changed to use unloaded B cells only (no VST co-cultured) as the control which may suggest the VST elicit a low level killing of the B cell targets regardless of SARS-CoV-2 peptide loading, however the assays were not completely optimised in terms of small sample number, cell counts and thawing protocols. Also due to the timeframe of these assays with a collaborating lab, only the first three manufactured VST lines were sent for cytotoxicity analysis, all of which were highly skewed CD4+ T cell lines. Therefore killing assays should be repeated on the other banked VST lines, particularly donors C19UKD8, C19UKD12 and C19UKD15 which produced mainly CD8+ VST and hence should have a greater potential for direct cytolytic activity.

Sequencing the TCR-Vβ region of generated SARS-CoV-2 VST products demonstrated a consistently polyclonal TCR repertoire between donors occupied by a top 100-1000 T cell clones. Matched donor comparison of the fresh leukapheresis CD3+ FACS-isolated pan T cells as expected had highly diverse repertoires of >10,000 clones, and therefore demonstrates our manufacturing process does indeed induce a selection of the TCR repertoire (albeit still very polyclonal in SARS-CoV-2 VST as compared to our manufactured EBV VST in Chapter 3 – this is discussed in more detail in Chapter 7). It was of interest to test if the TCR repertoire restriction already existed in target IFN-γ+ cells and were therefore selected for at CCS isolation, or whether the two week culture expansion selects for particular clones. This question was investigated by testing the CCS target cells in comparison to day 14 final product, however since the CCS assay isolates so few target cells to take samples from, these samples failed to generate sufficient amplified TCR-β PCR products for gel extraction. With the total number of target cells ranging 1-2.5x10^6 cells from a full-scale leukapheresis Prodigy CCS isolation, likely all these target cells would be required for TCR-β amplification to ensure PCR products are of adequate quality for next generation sequencing, however this would leave no target cells available for the subsequent culture expansion. Theoretically two full-scale prodigy isolations per donor could be set up in tandem with one to manufacture and culture expand the clinical VST product, and the other to take target cells solely for clonotypic analysis however the cost implications to run duplicate Prodigy CCS isolations for multiple donors would be colossal. Use of TCR antigen databases to assess CDR3 sequence matching offers a supplementary

approach to assessing the clonal responsiveness of the final products. Tests indicated that a higher proportion of the VST repertoire was specific to SARS-CoV-2 epitope sequences compared to other common viruses tested, and a moderately higher specificity to ORF1a and Spike sequences compared to other SARS-CoV-2 antigens. This skewed specificity does not correspond to the aforementioned functional responses to antigen re-challenge which indicated higher reactivity to nucleocapsid or membrane peptides. As discussed in depth in Chapter 5, it is difficult to compare specificity between TCR epitope matching and functional reactivity to antigenic peptides, and as such data from both techniques should be taken into consideration for meaningful inference. However current analysis using TCR databases may be underestimating sequence matching due to biases towards more uploaded sequences for Spike, MHC-I restricted TCR, and sequences for particular HLA alleles. Equally functional reactivity in the peptide-loaded DC assay is limited by the range of SARS-CoV-2 peptides tested, efficiency of DC to process and present these peptides in the assay timeframe, and does not identify T cells which may be SARS-CoV-2-specific but fail to demonstrate a functional response captured in this assay. Indeed this assay was entirely biased to detect only Th1 or CTL degranulation responses, and therefore other Th effector functionality cannot be ruled out. Expression of some cytokines that classify the different Th subsets are difficult to detect by flow cytometry, but could be assessed using transcriptional factor analysis. Cytokine secretion following antigen re-challenge could be measured by ELISA to detect potential differing antigen-specific Th responses, however this technique would not enable quantification of Th subpopulations within the T cell product. Also, with the requirement of APC to present peptides to VST it would be difficult to delineate cytokine secretions between cell types within the co-cultures using ELISA assays. Overall it is unlikely the isolated and expanded SARS-CoV-2 VST lines include T cells other than classic Th1 or CTL, however given the presence of follicular helper T cells has been reported to expand following COVID-19 infection, this should be investigated in future research.

Potential immunogenicity of this allogeneic T cell product was measured using a mixed lymphocyte reaction whereby SARS-CoV-2 VST were co-cultured with allogeneic HLA-unmatched PBMC for seven days, and analysed for output parameters of T cell proliferation, inflammatory cytokine secretion and skin explant GVHD response by histology. All VST lines were tested against three healthy volunteers with limited HLA matching. In most of our banked SARS-CoV-2 donors, VST lines induced

comparable levels of T cell proliferation as the autologous healthy volunteer PBMC co-culture controls, indicating negligible alloreactivity in the VST products. While two donors had increased T cell proliferation compared to the autologous control, all donor VST lines induced significantly lower T cell proliferation than PBMC starting material demonstrating alloreactive lymphocytes are removed in our manufacturing process. Cytokine secretion in response to MLR was negligible for all cytokines tested in an inflammatory luminex array, except for a relatively high concentration of IL-6 [5,000-50,000 pg/mL]. However IL-6 concentration was equivalent between allogeneic PBMC, allogeneic VST and autologous PBMC conditions indicating a non-specific secretion of IL-6 in these co-cultures independent of HLA matching. Histological grading of skin explants in response to MLR co-cultures further supported the T cell proliferation results, where SARS-CoV-2 VST had low GVHD responses in comparison with the autologous PBMC controls, and this was significantly reduced compared to the same SARS-CoV-2 donor PBMC starting material. Interestingly in this assay, autologous PBMC MLR that were used as the negative controls did elicit a degree of GVHD response in ~20% of co-culture tests as compared to skin explants with medium-only controls. This may suggest the simple washing and processing of skin biopsies to set up the co-cultures is sufficient to incur cell damage or exposure to antigens or neoantigens which can then stimulate the PBMC to recognise their autologous skin cells as foreign. These results may also reflect the fact although the volunteers recruited to donate skin biospies were deemed 'healthy' in donor screening testing/ questionnaires, some may have had unknown underlying autoimmune conditions stimulating their PBMC to have an autoimmune response against self. Altogether these data indicate our isolated and expanded virus-specific T cell lines exert negligible immunogenic responses in this assay. The potential for allogeneic cell therapies with a high proportion of unspecific T cells to induce a potentially fatal patient GVHD response is a major concern that understandably deters willingness for their clinical use (Jiang et al., 2021, Moradi et al., 2023). Due to this, advances in technology to manufacture or process cell therapies, particularly in the case of HSCT and CART therapies have been made to limit the alloreactivity potential, such as pre-depletion of naïve T cells from the source material or various gene modifying or non-gene modifying techniques to remove αβ TCR T cells whilst maintaining desired therapeutic function (Lv et al., 2023). Although a retrospective study of allogeneic EBV and multi-virus VST given to 153 HSCT transplant patients demonstrated impressive safety profiles of VST with no

incidences of de novo acute GVHD even in cases where *in vitro* allo-HLA reactivity was present in VST lines (Melenhorst et al., 2010), the potential for alloreactivity will be dependent on manufacturing and cell product specific variables. As such there is a fundamental requirement for assays to test potential immunogenicity across different allogeneic cells therapies prior to patient delivery which is largely sorely lacking in the field. The Skimune® MLR assay delivered by Alcyomics® has previously demonstrated that testing for positive GVHD responses between PBMC from allogeneic HSCT grafts and recipient patient skin biopsies is predictive of GVHD outcomes following transplantation (Dickinson et al., 1998). This assay has been beneficial in showing the manufactured SARS-CoV-2 VST exert limited potential for skin GVHD pathologies even against unmatched recipients, whereas VST will only be delivered to patients with a minimum of one HLA match, with preference of matches based on the VST line CD4:CD8 ratio and restriction of the SARS-CoV-2 peptides used for manufacture. While the percentage of positive GVHD responses was low in all banked SARS-CoV-2 VST lines tested (mean=8.3%, n=3), comparisons between different SARS-CoV-2 donor products is limited by the disparity in both number of HLA matches between donors and healthy volunteers and immunodominance of particular HLA alleles/ alloreactive peptide sequences (Archbold et al., 2008).

Additional safety testing for cell therapies other than contamination and immunogenic potential includes measure of oncogenicity. While the potential to form tumours is mainly a risk for stem cell based therapies, T cells are capable of a massive clonal expansion and therefore in the current landscape of cellular therapies should also be tested for tumourogenicity (Sato et al., 2019) though there is evidence that T cells are capable of enormous expansion without accumulation of genetic errors leading to mutagenesis (Soerens et al., 2023). Assessment through oncogene array demonstrated the SARS-CoV-2 VST lines analysed did not present SNP variants in any of the oncogenes tested indicating a limited oncogenic potential. Since ethical restrictions prevented this level of genetic testing to be done on our healthy donor-derived material, we could only test representative VST lines manufactured from commercially acquired leukapheresis material which had ethical approval for genetic testing associated with each unit purchased. This reveals a major limitation in the field whereby so many cell therapies rely on healthy donor sources, and therefore ethically this safety test currently cannot be performed on each clinical product.

At the time of this study, there were no widely available animal models for SARS-CoV-2 infection that accurately represented the natural disease pathogenesis of severe COVID-19, however numerous transgenic mouse models, ferret, hamster and non-human primate are being developed and analysed for comparative human respiratory disease mechanisms (Dillard et al., 2023, Chen et al., 2024). Since the extensive profiling of banked SARS-CoV-2 VST lines have indicated a purified T cell product with desired memory status, SARS-CoV-2 specificity and favourable safety results from the suite of *in vitro* assays; supported by our clinical data of EBV VST in patients, this therapy was approved by the Medicines Health Regulatory Agency (MHRA) as a Clinical Trial Investigational Medicinal Product (CTIMP) in August 2022. To date, two high risk hospitalised patients have been infused with the lowest dose of SARS-CoV-2 VST for this phase I safety trial, with no reported adverse events. Due to changes in mandatory testing for COVID-19, as well as more treatment and vaccination options available, recruitment to the trial has significantly slowed down. However, between August 2023 to January 2024, a total of 484 patients were screened but not eligible for participation in the trial due to: requirement of supplemental oxygen (n=221), unable to self-consent (n=137), had renal dysfunction (n=31), had cardiac dysfunction (n=18), or were immunocompromised (n=17). Of the eligible screened patients, participation in the trial did not go ahead due to: patient discharge within 48 hours of screening (n=38), patient refused (n=15), or patient on end-of-life care (n=7). This shows that despite the significant decrease in number and severity of COVID-19 cases, there are still large numbers of infected patients in hospitals, however the vast majority of patients are not being recruited for cell therapy intervention due to being given supplemental oxygen. Given that supplemental oxygen has become a first line standard of care for COVID-19 patients with a saturated pulse oxygen <95% on room air at sea level, this rules out the majority of hospitalised infected patients. Therefore, a clinical trial amendment has been submitted as of May 2024 to change eligibility to include patients maintaining saturations at >92% on a minimum of 28% supplemental oxygen therapy which may increase trial recruitment. While the initial strategy was to validate SARS-CoV-2 VST safety in a generally healthy patient group, this raises an important issue in trial design for treatments of emerging viruses. The time taken to develop and manufacture the products and then gain approval to undertake a phase I clinical trial for a new infection will likely lag behind the general population reaching herd immunity. In the case of this particular product, the development and manufacturing

time was remarkably quick but the timing was such that the SARS-CoV-2 virus was already becoming attenuated in the population, retaining high infection rates but with fewer cases of severe or lethal disease. Therefore for potential future pandemic or endemic viral emergencies it may be prudent to target clinical trials to the likely final patient group intended, i.e. immunocompromised individuals, though this is understandably a more difficult route due to the inherent risks of immunotherapy for these individuals.

6.8 Chapter summary

This chapter has discussed the translation, clinical manufacture and first in human trial investigation of allogeneic SARS-CoV-2 VST for the treatment of COVID-19 patients. From application of research protocols for the detection, isolation and expansion of SARS-CoV-2 VST from naturally COVID-19 convalescent donors developed in previous chapters, to collective efforts within a licensed institute for cell therapy manufacture allowing rapid translation of the process and clean room production of nine SARS-CoV-2 VST lines. While seven SARS-CoV-2 VST lines were banked for clinical use, two donors failed to expand sufficient T cells for banking by this process. Investigation revealed a memory NK cell population reactive to SARS-CoV-2 peptides which investigation indicated had hindered the IFN-γ cell isolations in these donors. Furthermore, extensive characterisation and profiling of the banked SARS-CoV-2 VST lines utilised numerous collaborative investigations. Manufacture of SARS-CoV-2 VST produced mainly CD4 T cell lines with Th1 functional status determined by expression of multiple antiviral cytokines and CD4 activation markers. Some of the banked VST lines were CD8-skewed with similar functional cytokine response, however the cytotoxic potential of these lines has not yet been determined. Sequencing of the TCR-Vβ revealed a polyclonal TCR repertoire, and VST lines had broad functional reactivity to different SARS-CoV-2 antigens which may ensure efficacy against antigenic mutational escape. Finally, safety testing indicated negligible potential of immunogenic reactions or tumourogenic potential by VST product infusion. All this data was instrumental to support approval for a first in human trial for this therapy, which has been infused in two COVID-19 patients thus far. Continuation of this dose-escalation phase I trial to patient cohorts receiving higher doses will be required to demonstrate product safety, and patient monitoring

assays of infection course, inflammatory and immune responses may elucidate aspects of potential therapeutic functional mechanisms.

Chapter 7

General Discussion

Chapter 7 – General Discussion

7.1 Introduction

Development of cell therapies has frequently been associated with the 'valley of death', an analogy which highlights the fact that complex products for rare diseases seldom make it through late-stage trials successfully. However, in recent years we are finally seeing a surge in cell therapies being authorised and licenced for clinical use. While this is largely due to increased investment to appropriately fund development through to clinical trials, increased success also reflects advances in manufacturing technology, regulatory infrastructure, product testing and pre-clinical models, standards of compliance for materials and processes, as well as improved application of complex cellular and genetic techniques. Within the immunotherapy field, CAR T cells and TCR-engineered T cells currently dominate focus due to the ability to make personalised products against natural or more intricately designed targets. However, with use of genetic modification and increasingly complex techniques comes increased risk of adverse events or manufacturing issues, therefore there is always need to simplify processes as much as possible. VST represent one of the more straight-forward cell therapies in this regard and due to early clinical successes have already built up a substantial safety and efficacy profile for the treatment of life-threatening viral infections.

It was the overall aim of this thesis to investigate an array of assays to comprehensively characterise VST therapies. This suite of quantitative analytic assays supported the development and refinement of protocols to generate virus-specific T cells, as well as constructing the preclinical profile of two novel SNBTS cell therapies that are now under clinical testing. Chapter 3 compared two methodologies for the clinical manufacture of EBV-specific VST; a long-established protocol using repeated autologous EBV+ LCL stimulations, and our newly developed EBV peptide-mediated isolation and expansion platform. Evaluation of processes and products was compared in the context of adoptive therapy of post-transplant EBV+ latency III lymphoproliferative disorders. Rapidly following outbreak of the emergent coronavirus pandemic, in Chapter 4 the peptide-based platform was used to detect and isolate T cells reactive to different SARS-CoV-2 proteins from COVID-19 convalescent donors, and to develop a culture protocol for optimal VST expansion.

Chapter 5 compared alternative approaches to the IFN-γ mediated VST isolation process and assessed whether TNF-α or CD154 could be used as activation-induced markers for the isolation of SARS-CoV-2 VST. The final products generated by these different processes were compared to determine differences in phenotype, effector functions and population expansion. Finally, Chapter 6 amalgamated the research and developmental work of previous chapters to validate protocols for the clean room manufacture and QC characterisation of SARS-CoV-2 VST. Clinical products were cryopreserved and are currently under testing in a phase I clinical trial for high-risk hospitalised COVID-19 patients. This chapter will discuss the findings from these chapters in order to predict potential mechanisms EBV VST and SARS-CoV-2 VST function in their respective patient groups, as well as evaluate manufacturing methods and characterisation assays for use in cell therapy development.

7.2 EBV VST for therapy of EBV lymphoma

Given that allogeneic EBV VST have been utilised clinically by numerous centres for well over 20 years, we have built up a good clinical picture of responses within different patient groups. This therapy has proven safety and efficacy particularly in EBV+ PTLD patients and robust trials of larger cohorts have demonstrated a range of between 51-80% overall response rates (see Table 1.5). PTLD represents a particularly diverse patient group, with widely varied factors that impact upon disease severity and rate of progression including: age, sex, prior EBV immunity, transplant type, level of HLA matching to the transplant donor, transplant immunosuppressive regime, site(s) of lymphoproliferation, tumour antigen expression, tumour morphology and presence of other infections. Therefore, the lack of response to EBV VST adoptive transfer seen in some patients is likely largely due to huge demographic and disease heterogeneity. Nonetheless the early clinical successes with this therapy have driven development of new techniques/technology to improve EBV VST product manufacture. We compared the established LCL stimulation method, a technique still used to manufacture the vast majority of current EBV VST therapies globally (see **Table 1.5**), with pooled EBV peptide-mediated isolation which is becoming a popular alternative approach to generate GMP-compliant EBV VST in the field.

7.2.1 Peptide- EBV VST have improved phenotype, functionality and viral specificity.

Both the LCL and peptide methods generated expanded products that were highly enriched for T cells (>96% in all donor cultures generated), with negligible 'contaminating' cell types. It is hugely important in cell therapy manufacture to have a high purity product to eliminate risk of other cells inducing off-target and/or unknown effects. Due to this, many ATMP are set a release criteria of >90% purity for the particular cell type which ensures any products not meeting this specification are not allowed for clinical use. However, it is worthwhile to initially focus on development of a culture process that consistently and reproducibly generates the desired cell type in order to reduce the risk of manufacturing failures in later stages of translation. As such, we have optimised the key reagents and conditions in our EBV VST protocols to robustly drive expansion of highly-enriched T cells. Both processes similarly generate predominantly CD8+ T cell products which is desirable for PTLD therapy to induce both anti-tumour and anti-viral functions. While final products from both processes generally contained a low percentage of CD4+ T cells, LCL-derived EBV VST had a wider range of CD4 content, though this may reflect the bigger sample size of products analysed from LCL-derived compared to peptide-derived groups. Although statistically similar in this analysis, EBV VST from the peptide-derived bank will be carefully monitored for response upon clinical use, given that previous reports have indicated that a higher CD4+ content is associated with improved efficacy (Peggs et al., 2003, Haque et al., 2007, Prockop et al., 2020). Ideally to investigate this, patient blood samples could be taken longitudinally pre- and post-infusion of EBV VST and tracked for CD4+ expansions of both host and the transferred T cells through a mismatched HLA allele. Currently however, due to regulations of the Specials license under which we issue EBV VST for relapsed/refractory PTLD, we are unable to carry out patient monitoring assessments that could delineate these *in vivo* mechanisms.

Notably, both CD4+ and CD8+ T cells within peptide-derived EBV VST were highly skewed towards a central memory phenotype compared to the effector phenotype demonstrated by the LCL-derived VST. As such, the smaller CD4+ percentage within peptide-derived T cell products may have negligible consequences on persistence if these cells have increased expansion capacity after adoptive transfer to the patient. Importantly, peptide-derived EBV VST also contain a sizeable population of effector T

cells which should drive immediate effector functions, though again it would be useful to be able to monitor patients to compare with the predominantly effector-biased LCL-derived products for any lag in clinical response. Certainly, cytotoxicity against allogeneic HLA-matched LCL using a 6 hour *in vitro* assay was comparable between VST generated by both processes, which indicates the peptide-derived products are not disadvantaged for rapid target-specific killing despite having a smaller effector population. It is of course difficult to compare the different LCL to VST ratios used in cytotoxicity assays to what might be in the clinical situation dependent on PTLD tumour(s) size and the level of patient lymphopenia. Nonetheless, peptide-derived VST demonstrated enhanced degranulation and production of effector Th1 cytokines upon EBV recall compared to the LCL-derived VST, suggesting increased functional capacity. This may be linked to a more exhausted phenotype of LCL-derived VST particularly within the CD4 compartment, which may limit cytokine secretion and helper cell signalling.

Interestingly, peptide-derived VST exhibited CD4+ T cells with degranulation phenotype and cytotoxic capabilities in response to EBV peptide stimulation and demonstrated target-specific lysis of LCL when CD4+ T cells were sorted and used in cytotoxicity assay. These data suggest CD4+ T cells grown using the peptide process are able to directly lyse EBV+ target cells, though more lines should be tested in this assay to determine if this is a consistent feature between donors. Furthermore, *in vivo* experiments would be required to confirm if CD4+ cells with cytotoxic capacity actually perform this function to directly lyse EBV+ tumours upon adoptive transfer, or whether they act predominantly through Th1 effector functions. One mechanism to test this would be to look at blocking of IFN-γ, TNF-α, granzyme B or FasL with neutralising antibodies in the cytotoxicity assay to determine the role of each in CD4 lysis of target cells. Given the aforementioned association of improved and maintained PTLD tumour remission with higher frequency of CD4+ T cells in the VST product (Haque et al., 2007), it would imply the transferred CD4+ T cells are providing a supplementary therapeutic role to classic CD8-mediated cytotoxicity. It may be the case however that cytotoxic CD4+ T cells are important for natural host responses to control EBV+ tumourigenesis via MHC class II-dependent cytotoxic pathways (Malyshkina et al., 2023). A recent study reported accumulation of cytotoxic CD4+ T cells in the spleen of transgenic mice following transfer of LMP1+ B cells, which were found to be primed by LMP1-induced expression of co-stimulatory

molecule CD70 (Choi et al., 2018). Adoptive transfer of purified splenic cytotoxic CD4+ T cells showed superior regression of LMP1+ lymphomas than CD8+ T cells which may implicate an essential role for cytotoxic CD4+ T cells in natural immunity to LMP1+ tumours.

Finally, EBV VST derived from both processes contained an oligoclonal repertoire of T cells, with donor lines frequently dominated by 1-10 clones. By matching generated CDR3 sequences to that of TCR databases, clones were mainly directed to immediate-early lytic proteins BMLF1, BRLF1 and BZLF1 and latent proteins EBNA3A, EBNA3C and LMP2. This was corroborated by functional reactivity of CD8+ T cells mainly to BRLF1, BZLF1, EBNA3A, EBNA3C and LMP2 and though not seen in the CDR3 matching analysis, CD8+ functional response was very high to EBNALP in the vast majority of donor lines. Exact profiles of clonal repertoires are currently limited to previously identified public EBV-specific clones uploaded to TCR databases (Huisman et al., 2022), which should improve as more CDR3 sequences from different HLA types are added to public databases. Overall CD8+ functional reactivity to dominant antigen EBNA3A was markedly higher in peptide-derived VST, which suggests more clones are able to direct immediate lysis to EBNA3C+ PTLD tumours. Furthermore, CD4+ T cells within peptide-derived EBV VST also had enhanced functional reactivity to EBNA3A, as well as EBNA1 and EBNA2. With a higher frequency of clones able to mount effector responses to multiple dominant and subdominant EBV antigens, peptide-derived VST may enhance remission of tumour cells with differential antigen expression and prevent tumour evasion mechanisms.

Overall, characterisation and functional profiling indicated peptide-derived EBV VST had a more desirable phenotype and enhanced effector capacity for a PTLD therapy when compared to LCL-derived EBV VST. Moreover, with a significantly shorter and simpler culture protocol, fewer manipulations and lack of use of an infectious agent; the peptide process presents numerous safety advantages for the product, facility and staff (see process comparison in **Table 3.5**). Of huge importance to cell therapy manufacture, the peptide process also generated a significantly greater yield of EBV VST than the LCL process which allows us to generate more treatments for the bank (used at $1.5x10^8$ cells/dose x 4 doses per patient) than in other PTLD trials (O'Reilly et al., 2023). This has obvious advantages in making the therapy more cost-effective

and deliverable to many more patients from a single donor manufacturing process and also allows effective dosing that may prolong patient remissions.

7.2.2 Suitability of EBV VST to target different EBV disorders.

SNBTS holds an MHRA-approved Specials license to issue EBV VST (both LCL and peptide-derived) to relapsed/refractory PTLD patients. A major aim of this thesis was to compare antigenic targets between EBV VST to evaluate the suitability to treat PTLD. Building on the development and analysis of these clinical products is the question of whether the produced EBV VST could also target other EBV+ disorders.

On the whole, EBV antigen specificity of the CD8+ T cells was similar between LCL-derived and peptide-derived VST. Expanded VST lines were typically restricted to targeting BRLF1, BZLF1, EBNALP, EBNA3A, and EBNA3C. Interestingly, peptide-derived lines contained significantly more EBNA3A-specific T cells than LCL-derived lines, which was unexpected considering EBNA3A is an immunodominant target for T cell responses (Murray et al., 1992). Though there was variability between donors which likely reflects different HLA alleles restricting presentation of particular epitope sequences, LCL-derived VST had a lower overall frequency of T cells specific to the EBV antigens tested. This may suggest specificity to other EBV lytic antigens not tested in this assay, though reports suggest LCL do not express high levels of lytic antigens. More likely this may reflect that LCL transformation can also induce the expression of cellular tumour-associated antigens, and therefore T cells generated against LCL may expand clones targeted to particular cellular antigen epitopes (Ozgyin et al., 2019). A third option could be the process expanded T cell clones not specific to EBV or LCL antigens, however this is not likely given the culture process comprises 7-12 rounds of LCL stimulation. The cytotoxicity data also does not support this theory since EBV VST expanded after several stimulations have strong cytotoxic specificity to LCL compared to control cell lines in this assay. Furthermore, since our assay to assess antigenic specificity is by way of cytokine or CD107a expression upon antigen recall, this may be underestimating the total specificity to the antigens tested based upon the cells' functional capacity. A good way to overcome this limitation would be to directly measure antigen-specific epitopes by multimer staining, however this method was deemed impractical to resource all individual EBV antigen-specific multimers covering the wide range of HLA types in the present dataset, other approaches may include TCR sequencing.

It would be interesting to compare the two EBV VST products in terms of LCL cellular antigen-specific clones. Since the peptides used for the generation of EBV VST were purely against HLA-restricted EBV antigens, the expanded T cells are highly unlikely to target cellular antigens. On one hand, it may be useful to have anti-LCL clones in EBV VST therapies, since cellular antigens are rapidly upregulated within the five days of LCL immortalisation (Long et al., 2009), found to be induced in transformed cells by LMP1 (Choi et al., 2018). One interesting study generated polyclonal EBV VST against LCL in cultures containing acyclovir to prevent lytic antigen presentation, with some of the expanded T cell lines confirmed to lack specificity to latent EBV antigens, but still highly reactive to LCL (Linnerbauer et al., 2014). Transfer of these non-virion antigen-specific T cells to a PTLD-like tumour model (SCID mice injected with human LCL with subsequent xenograft lymphomas) had uncompromised anti-tumour efficacy, indicating T cells targeted towards cellular antigens still provided therapeutic responses. In a clinical study of other EBV+ lymphomas, adoptive transfer of LCL-derived EBV VST was associated with increased peripheral blood T cell responses to MAGE, survivin and PRAME only in responding patients, suggesting responses against these tumour associated antigens (TAA) were important for therapeutic efficacy (Bollard et al., 2014). Although these studies indicate TAA on LCL can be specifically targeted by LCL-derived T cells, it is unclear to what extent such antigens induced by laboratory strain B95-8 are also expressed on patient PTLD tumours. Moreover, expression of TAA or patient-specific neoantigens may be highly variable between PTLD tumours dependent on tumour site, morphology and/or disease stage and therefore more difficult to standardise as targets for allogeneic cell therapy.

Taking into account the overall antigen specificity, cytotoxicity and clonal repertoire data, the *in vitro* characterisation indicates suitability of both LCL-derived and peptide-derived EBV VST to target PTLD tumours. This is of course corroborated by substantial clinical evidence of complete responses maintained in many of our patients treated with LCL-derived EBV VST (Vickers et al., 2014, Chiou et al., 2018, Kazi et al., 2019). The peptide-derived EBV VST have been issued clinically since 2023 to 19 patients to date, and although we don't have long term data there are early indications of good clinical responses.

In addition, while results have shown adoptive transfer of EBV-specific T cells have been effective for PTLD patients, attempts to treat other EBV-related malignancies with EBV VST have so far been less efficacious. It was a supplementary aim of this study to consider whether the EBV VST lines generated could potentially target other latency EBV cancers. The mean CD8+ T cell specificity to restricted latency I or II antigens was low between both groups, however some donor lines had small populations (5-20%) of EBNA1, LMP1 or LMP2 reactive T cells. Furthermore, peptide-derived VST expanded significantly higher proportions of CD4+ cells specific particularly to EBNA1 and LMP1 than LCL-derived VST. Therefore, individual donor lines could have therapeutic potential against latency I or II tumours, and could even be sorted again by CCS or multimer selection to purify for only EBNA1, LMP1 and LMP2-specific VST.

The majority of T cell therapy trials for latency II NPC patients have tested autologous LCL-derived EBV VST with modest clinical results (Li et al., 2022). Similar to our results, the LCL-derived EBV VST were found to contain dominant clones recognising lytic or latency III antigens, which may explain the limited anti-tumour response in NPC patients (Wang et al., 2021). A novel approach to generate EBV VST restricted to latency II antigens has been recently developed using an adenovirus-based vector to deliver EBNA1, LMP1 and LMP2 antigen expression (Smith et al., 2017, Huang et al., 2017, Pender et al., 2018). The EBV VST products generated however have shown relatively low specificity to the latency II antigens, which is reflected in their limited clinical responses. Translation of our peptide-mediated CCS method with EBNA1 and LMP peptides may present a better approach to generate latency I or II EBV VST. In preliminary experiments I've investigated since my PhD studies, we have successfully isolated EBNA1/LMP-specific VST from healthy donors using this method, with very high specificity (40-80%) to these antigens, likely due to the isolation step (data not shown). This further shows the potential for translation of this method to generate T cells for other antigenic targets, and next steps plan to investigate development of VST targeted to subdominant EBV antigens to treat other EBV+ malignancies.

7.3 SARS-CoV-2 VST for therapy of COVID-19

Chapters 4-6 focussed on the generation of SARS-CoV-2 VST, from primary research and development to clean room manufacture and clinical trial. Such rapid translation

of a therapy from bench to bedside in just 2 years is the result of momentous effort and co-ordination of numerous teams across various disciplines in SNBTS. For this, COVID-19 convalescent donors were identified through the SNBTS convalescent plasma programme, with recruitment and buffy coat collection at multiple sites co-ordinated through the donor services clinical team and blood processing teams. Donor buffy coats were HLA-typed by SNBTS Histocompatibility & Immunogenetics services and screened for mandatory pathogens and SARS-CoV-2 viral and antibody titres by SNBTS National Microbiology Reference Unit. Buffy coats were then assessed for SARS-CoV-2 T cell responses, and protocols developed for the isolation, expansion and characterisation of SARS-CoV-2 VST by myself and others within the development (TCAT DEV) team. The processes were rapidly translated to clean room manufacture and QC testing by TCAT GMP and Quality teams. All work was ensured for compliance within the ATMP regulatory framework, and Investigative Medicines Product Dossier (IMPD) and Investigators Brochure (IB) were compiled by the Regulatory team from data supplied by TCAT DEV. Finally, the clinical trial is being co-ordinated and managed by numerous hospital and clinical teams at the Royal Infirmary Edinburgh and University of Edinburgh. With limited clinical history for inference, much of the development was to optimise methods to isolate and expand SARS-CoV-2 VST, and utilise a plethora of characterisation testing to predict how SARS-CoV-2 VST might act after adoptive transfer to COVID-19 patients.

7.3.1 Comparison of IFN-γ, TNF-α and CD154 for VST isolation.

The rapid development of protocols to isolate and expand SARS-CoV-2 VST was made possible by the ability to translate the peptide-mediated EBV VST process to any suitable peptide antigens. Initial research studied T cell responses to peptide pools covering the whole sequences of SARS-CoV-2 Spike, Nucleocapsid, and Membrane proteins; with later development using a GMP-grade consensus HLA-restricted peptide pool covering immunodominant sequences of the whole viral proteome. Memory SARS-CoV-2 VST and correlated SARS-CoV-2 antibody titres in peripheral blood were observed in all convalescent donors as compared to those considered unexposed in the early months of the pandemic. We were one of the first groups in the UK to report the decline in peripheral blood SARS-CoV-2 VST frequency over time from the resolution of infection (Cooper et al., 2020), which is now a well-known feature of T cell immunity to SARS-CoV-2.

By looking at numerous T cell activation-induced markers (AIM), we saw the AIM with greatest expression upon stimulation with SARS-CoV-2 peptides was CD154, followed by TNF-α and IFN-γ. Currently the only clinically approved GMP-compliant isolation kit for use on the CliniMACS Prodigy is for IFN-γ, so we developed and translated the protocol for SARS-CoV-2 VST generation based on an initial IFN-γ isolation. The IFN-γ-isolated SARS-CoV-2 VST were expanded in an optimised 14-day culture protocol, with products eliciting functional responses upon antigen recall. However, since the frequency of SARS-CoV-2 VST in PBMC was significantly higher when using TNF-α or CD154 expression, it became a primary objective to investigate isolation and expansion of SARS-CoV-2 VST using these markers.

To understand the effect of AIM choice on the isolated antigen-specific T cell profile, intra-donor experiments were performed to directly compare isolation by IFN-γ, TNF-α or CD154 magnetic bead selection. Analysis of the target cells immediately after isolation demonstrated both TNF-α-isolated and CD154-isolated were skewed towards CD4 phenotype with mixed memory populations, whereas IFN-γ-isolated had a different CD4 to CD8 ratio. The overall purity of CD3+/CD56- T cells was lower in IFN-γ isolates, likely because there was a slightly higher frequency of NKT cells and NK cells present using IFN-γ isolation. Interestingly, CD154 sorts were heavily contaminated with a population of large granular cells, identified through their side scatter profile. Since certain DC populations have been reported to upregulate CD154 following CD40 stimulation (Pinchuk et al., 1996, Kuwajima et al., 2006), the contaminating cells may be DC caught up during the activation-induced CD40-CD154 interactions in these sorts. This population was also present in target cells of the respective intra-donor IFN-γ or TNF-α isolations, though at a much lower frequency. Another group reporting IFN-γ Prodigy isolations of SARS-CoV-2 VST also had contaminating granular cells in their target fractions, with phenotypic characterisation indicating 5% monocytes and 10-15% DC (Chu et al., 2023). We would need to perform additional phenotyping of the target cells to corroborate this finding, however extensive characterisation of CCS target fractions is limited by the extremely low cell numbers yielded from the isolations. Such limitations should hopefully improve in the new wave of spectral cytometry able to characterise many parameters in the same multicolour panel, however sufficient cell numbers would still be required to label suitable controls.

All of the SARS-CoV-2 VST expanded for 14 days were highly enriched for T cells, including that of the CD154-isolates, demonstrating monocytes were not supported in the culture system. Expansion further enhanced the already high frequency of CD4+ T cells from TNF-α and CD154 isolations, with negligible CD8+ T cells in these products. While CD4+ T cells were also enriched over expansion from IFN-γ isolations to approximately 80% in final products, these cultures also contained a small population of CD8+ T cells as well as highly activated DP T cells. All expanded SARS-CoV-2 VST from the differential isolations were skewed towards central memory phenotype with a small population of effector memory T cells, demonstrating a robust culture protocol for supporting highly proliferative antigen-specific clones. Furthermore, SARS-CoV-2 from all experiment groups elicited multifunctional effector responses upon antigen recall through Th1 cytokine production. Due to a smaller sample size of CD154 isolated VST lines, only IFN-γ and TNF-α-isolated VST were compared for expression of chemokine receptors and TCR repertoire analysis. The chemokine receptor profile was equivalent between the two isolation approaches, with expanded SARS-CoV-2 VST demonstrating high expression of inflammatory chemokine receptors CCR2, CCR4, CCR5, CXCR3, CXCR4 and CXCR6. Clonal diversity and TCR matching to SARS-CoV-2-specific sequences in public databases was also comparable between the groups, with repertoire selection from the bulk T cell starting material, however maintaining a highly polyclonal repertoire in the expanded SARS-CoV-2 VST lines. While other studies have used IFN-γ CCS to isolate SARS-CoV-2 VST, it was the strategy of these trials to directly infuse the CCS targets into COVID-19 patients (Bonifacius et al., 2022, Leung et al., 2020, Chu et al., 2023), therefore at present there are no CCS-isolated, *ex vivo* expanded SARS-CoV-2 VST products reported with which to compare our data.

Overall, the main effect of using these differential markers for isolation of SARS-CoV-2 VST was the varied CD4 to CD8 ratio of T cell products that was maintained throughout the culture. The presence of CD8+ T cells in IFN-γ-isolated VST likely indicates these products will have cytotoxic functionality, whereas enriched CD4+ T cells in TNF-α and CD154 isolated lines may act only through Th cytokine production. All groups would need to be tested in a relevant cytotoxicity assay to confirm targeted cytolytic capacity against SARS-CoV-2 infected lung epithelial cells. CD8 content may have important indications on the therapeutic strategy for adoptive transfer, whereby patients with early infection may be more likely to benefit from infusion of VST able

to elicit direct cytotoxic clearance of infected cells in the lung. However, administration of cytotoxic T cells that contribute to inflammatory damage may be potentially harmful to patients with late-stage cytokine storm. Conversely, having some cytotoxic T cells may be required to fully clear infection and induce a therapeutic response, in which case isolation with TNF-α or CD154 would not generate appropriate VST lines. A number of human trials utilising SARS-CoV-2 VST for COVID-19 patient groups have been initiated and dependent on manufacturing approach VST products greatly differ in CD4 to CD8 ratio (Keller et al., 2020, Leung et al., 2020, Basar et al., 2021, Papayanni et al., 2021, Bonifacius et al., 2022, Durkee-Shock et al., 2022, Martits-Chalangari et al., 2022, Chu et al., 2023, Papadopoulou et al., 2023, Vasileiou et al., 2023). Results from these trials should be carefully interpreted, especially in regard to patient disease context, to understand the therapeutic mechanisms (if any) of different T cell effector functions. Finally, although this direct comparison study was performed using SARS-CoV-2 peptides to stimulate activation markers for T cell isolation, the results may be translatable to development of other antigen-specific T cell therapies. Since it is clear TNF-α and CD154 are more likely to enrich CD4+ T cells, it may be a strategy where a product requires more CD4 content, to potentially combine isolation markers to generate a mixed CD4/CD8 product. Isolation of EBV VST is coincidentally a good example, with some donors generating expanded products almost entirely of CD8+ T cells, though previous clinical data suggests having a CD4+ population in the transferred T cell therapies increases longevity of the anti-tumour remissions. In this way, the approach to manufacture should be considered for ultimately deriving the most desired cell type to treat a particular disease/ patient group. By incorporating specific cell markers into an isolation process can optimally bias selection to a given population or subset capable of the preferred therapeutic functionality.

Leaders in the field often advocate to start with the end in mind, where it is important to implement a strategy that prioritises the appropriate GMP-compliant methods and techniques right at the start of research and development. This hopefully ensures that the translation process is seamless and does not require re-validation of materials or processes. This approach substantially reduces the time taken to develop new cell therapies and helps in the context of delivering the most beneficial and practical therapy to the target patient group.

7.3.2 Predicting SARS-CoV-2 VST function in COVID-19 patients.

Design of therapies for SARS-CoV-2 infection has focused on different approaches appropriate to the stage of disease. As shown in **Table 4.1**, SARS-CoV-2 infection is divided into four stages defined by clinical observations and increasing severity, each requiring distinct strategies for intervention (Toussi et al., 2023).

Stage 0, prior to SARS-CoV-2 exposure, is the opportune window for prophylaxis in terms of vaccine administration as discussed in Chapter 4. Strategies in the initial years of the pandemic were to vaccinate the majority of the population to induce widespread immune protection in the majority of the population. This approach was adopted in order to protect the vulnerable members of the community (sometimes described as herd immunity). As time has progressed, it has been reported that SARS-CoV-2 is now endemic globally, reducing the need to continue vaccination campaigns except for vulnerable groups. However as with influenza, the mutational rate of SARS-CoV-2 has been high leading to emergence of mutated strains that initial vaccines may not protect against. As with the seasonal 'flu jab' the current strategy is to provide a yearly SARS-CoV-2 vaccine targeting the most common circulating strains at the given time, which can be offered to the elderly, immune-compromised individuals, and healthcare staff.

For high-risk patients this may also be an ideal time-point for intervention with other prophylactic agents such as neutralising antibodies or antivirals balanced accordingly to the safety profile of the therapy. This is already a practiced strategy to prevent HSCT recipients from developing a fatal infection to common viruses by prophylactic administration of memory VST. A simple approach to conferring adoptive memory VST immunity has been transfer of healthy donor CD45RA-depleted leukapheresis products. This strategy was investigated following numerous longitudinal studies observing associations between higher naïve T cell content in HSCT allografts and risk of GVHD (Yakoub-Agha et al., 2006, Chang et al., 2009). This was supported by direct comparison studies using either sorting (Chen et al., 2007, Chérel et al., 2014) or transduction (Fernández et al., 2017) that demonstrated CD45RA- T cells had no alloreactivity compared to CD45RA+ cells in various *in vitro* and *in vivo* GVHD models. A comparison of two clinical studies comparing haematological malignancy patients who received CD3-depleted versus CD45RA-depleted allografts indicated occurrence of viraemia and associated disease of CMV and ADV, as well as incidence of acute

GVHD grade III-IV, was significantly reduced in CD45RA-depleted grafts (Triplett et al., 2018). To this end, Ferreras and colleagues developed a biobank of CD45RA-depleted cells from numerous convalescent donors with good SARS-CoV-2 T cell responses using a CliniMACS Plus closed-system depletion and subsequent cryopreservation into multiple doses (Ferreras et al., 2021). Results from a Phase I safety clinical trial using this therapy as a single dose of either $1x10^5$ cells/kg or $1x10^6$ cells/kg for COVID19+ patients with pneumonia or lymphopenia (n=9) reported no adverse events (Pérez-Martínez et al., 2021). A phase II randomised controlled trial is underway to compare CD45RA-depleted cell treatments against standard therapies to evaluate safety and efficacy in severe COVID19+ patients with pneumonia (García-García et al., 2021). While this initial trial is being tested for patients with greater disease severity for safety and ethical reasons, this approach has been flagged as of interest by clinicians for use in high-risk haematological malignancy patients due to the prospect of protection from multiple pathogens. As an additional benefit, because the manufacturing process involves minimal manipulation, this therapy can be licensed under a Human Tissue Authority licensed tissues and cells product instead of under ATMP regulations, making this approach require a less complex regulatory process (Al-Akioui Sanz et al., 2023).

As an alternate approach, this study and those from other groups have developed targeted SARS-CoV-2 VST therapies for allogeneic transfer to either high-risk or severe disease state COVID-19 patients. Current SARS-CoV-2 VST therapies in clinical trials have been manufactured either using peptide-pulsed APC stimulation and outgrowth, or direct selection of VST by CCS. As shown in **Table 6.10**, the final product characteristics vary widely with differences in T cell purity, CD4 to CD8 ratio, contaminating cell types, overall SARS-CoV-2 specificity, individual SARS-CoV-2 antigenic targets, and effector functionality (cytokine secretion and/or cytotoxicity). These trials are also targeting different patient cohorts with clinical doses ranging from $1x10^6$ to $3x10^8$ cells per adult dose. Therefore, it may be difficult to infer correlative factors beneficial to patient responses between the therapies, which is further hindered by the poor recruitment status and/or early termination of some of these trials.

Nonetheless, it has been important to build a preclinical profile of our developed SARS-CoV-2 VST therapy to predict how we think it may function in patients. We

manufactured a cryopreserved bank of seven donor SARS-CoV-2 VST lines in the clean room, which were subsequently released for clinical use in a Phase I trial for high-risk hospitalised patients with SARS-CoV-2 infection. The SARS-CoV-2 VST products were predominantly skewed to high CD4 frequency, though this varied between donors and is likely reflective of the HLA-restricted peptides (rather than peptide pools) used for manufacture, as well as potential viral re-exposure selecting out particular clones in these immune competent individuals. Without an appropriate assay to estimate killing of virus-infected cells, infusion of VST products with different CD4 to CD8 content should be carefully monitored to understand which T cell effector functions are beneficial or potentially harmful to patients. Importantly, all banked VST lines exhibited central memory phenotype and limited exhaustion profile, indicating the cells may have prolonged responses and ability to clonally expand in patients, though previous reports of adoptive VST persistence is usually in the context of immunosuppressed patients (Haque et al., 2007, Heslop et al., 2010). Though the level of leukopenia may vary between COVID-19 patients, our target cohort are not under iatrogenic immunosuppression and therefore it is unclear without establishment of a lymphopenic niche whether the infused T cells would engraft long-term in patients. However, given our manufacturing process was able to yield high numbers of functional SARS-CoV-2 VST and therefore we were able to formulate larger doses than many of the other trialled products, infusion of these cells should have better ability to infiltrate the host T cell compartment and overturn potential inappropriate host immune mechanisms. Our manufactured bank of SARS-CoV-2 VST had consistently high expression of CCR2, CCR4, CCR5, CXCR3, and CXCR4 which have been shown to be important for *in vivo* T cell trafficking mechanisms to lung parenchyma and lymphoid organs in SARS-CoV-2 infection (Alon et al., 2021, Koenen et al., 2024). Banked SARS-CoV-2 VST also had multifunctional effector cytokine and activation responses upon antigen recall, indicating the therapy should be able to migrate to appropriate disease sites and elicit targeted helper antiviral functions. Furthermore, broad VST responses across SARS-CoV-2 antigenic variants and the polyclonal TCR repertoire should render this therapy less susceptible to viral immune escape mechanisms. As the VST recognition included robust responses to conserved membrane, envelope and nucleocapsid antigens it ensures that the therapy does not become ineffective as new Spike mutants evolve. This means that there will be less necessity to re-manufacture the therapy with new peptide sequences. Finally, the negligible alloreactive responses in MLR GVHD assays likely reflect the product purity

for memory T cells and high specificity to SARS-CoV-2 antigens. This indicates the product has low potential for GVHD reactions even between donor and recipients with limited HLA matching. Along with demonstrable lack of oncogenic changes associated with the manufacture process confirmed using SNP testing, this confirms the therapeutic safety of this product in terms of limited immunogenic effects or potential to form tumours. As of April 2025, two patients have been infused with SARS-CoV-2 VST with no adverse events, though more patient testing with full doses are required to confirm product safety.

While the concept of VST adoptive transfer to kill viral-induced tumours is relatively simple, the biggest unknown in use of such a therapy for COVID-19 is the result of adding highly functional effector T cells into the inflammatory disease context. Since one of the major safety concerns for T cell therapies in general is the risk of inducing cytokine release syndrome (CRS), the risk may be higher in patients with late-stage COVID-19 disease. Initial studies reported some severe COVID-19 patients presenting with a biphasic disease profile, whereby clinical deterioration began around 10 days following symptom onset despite a decreasing viral load within the upper respiratory tract. This led to the hypothesis that pathology in patients who progress to severe disease is driven by a hyperinflammatory response rather than direct viral damage, however whether COVID-19 represents a true cytokine storm syndrome is still debated (Mehta and Fajgenbaum, 2021). While many inflammatory cytokines are significantly elevated in severe COVID-19 patients, the actual circulating cytokine concentrations are approximately 100x-fold lower than other cytokine storm syndromes (Leisman et al., 2020). Even trials which have targeted critically ill COVID-19 patients with immunomodulatory mesenchymal stem cell therapy (Lu et al., 2024), or cytokine removal with CytoSorb® absorbent devices (Becker et al., 2023) have modest responses compared to control cohorts, indicating that dampening the immune response alone is not sufficient to resolve disease in these patients. Furthermore, other cytokine storm disorders do not classically present with reduced T cell numbers or exhausted T cell functionality, which is a hallmark of severe COVID-19. Therefore, while some opinions in the field hypothesise that adoptive T cell therapy with SARS-CoV-2 VST might be detrimental for COVID-19 patients with critical disease, there may still be a place for this therapy to protect high risk patients, or in the immunocompromised patient setting.

7.4 Evaluation of peptide-mediated selection & expansion method

Development of a new process to generate EBV VST aimed to improve the product and utilise modern techniques, however the primary intention was to avoid the use of live virus and shorten and refine the cell therapy manufacturing process. Though various methodologies for making VST have been developed, we chose to utilise viral peptide-induced cytokine secretion and selection of antigen-specific T cells first described by Campbell (2003) as the optimal technique for production. We also optimised a closed-culture expansion protocol to allow generation of therapeutically relevant numbers for dosing. In theory, this platform could be applied to make T cell therapies directed to any antigenic target so long as there are appropriate peptides available. This was rapidly evidenced by translating this process to generate SARS-CoV-2 VST in Chapters 4-6. Following official global pandemic outbreak in March 2020, we had access to SARS-CoV-2 peptide pools appropriate for APC processing and T cell recognition by April 2020, and the exemplar SARS-CoV-2 VST development products from fifteen COVID-19 convalescent donors were made by July 2020. As such, the development of two VST therapies against different viral targets allowed detailed evaluation of the peptide process and the subsequent VST products.

7.4.1 Comparison of VST from novel primary infection versus latent infection.

As discussed previously, we utilised a comprehensive suite of T cell characterisation approaches for both the EBV VST and SARS-CoV-2 VST produced using the peptide-mediated selection and expansion protocol. Given the population of antigen-specific T cells following IFN-γ capture can be variable between peptide pools used, and between donors; this highlights that our developed culture protocol is robust in supporting expansion of particular T cell phenotypes. To fully understand the influence of process, peptide-derived EBV VST and SARS-CoV-2 VST final products were compared for differences in all parameters whereby identical characterisation assays were performed.

Phenotypic analysis of lymphocyte, T cell subtypes and memory status is shown in **Figure 7.1**. Both EBV and SARS-CoV-2 VST products were highly purified for T cells, with negligible contaminating cells (**Figure 7.1A**). Three SARS-CoV-2 VST products

contained a small population (5-10%) of NK cells which appears higher than EBV VST, however this was not statistically different. This may reflect that SARS-CoV-2 is able to prime a peptide-specific response from adaptive NK cells (Barnes et al., 2020) as discussed in **section 6.4.3** and therefore these cells can be caught up in the SARS-CoV-2 peptide selection process and further expanded in culture. Within the T cell population (**Figure 7.1B**), EBV VST products were primarily CD8+ T cells, whereas SARS-CoV-2 VST were skewed towards CD4+ T cells. The CD4:CD8 content is likely dictated by the frequency of these antigen-specific cell types within the peripheral blood which can be variable with differential viral immune responses, as well as time-course within the infection. In the case of SARS-CoV-2, initial reports indicated a balanced frequency of CD4 and CD8 SARS-CoV-2 specific T cells following primary infection and convalescence, however this ratio may change as individuals are repeatedly exposed over time to new viral variants and vaccines.

Within both the CD4 (**Figure 7.1C**) and CD8 (**Figure 7.1D**) compartments, memory status was largely comparable except for a small increase in naïve T cells in SARS-CoV-2 compared to EBV VST. While the frequency is low (<1% naïve T cells), infusion of SARS-CoV-2 VST should be carefully monitored for potential alloreactive responses. Other T cell products that were depleted to <1% alloreactive T cells still were sufficient to elicit a GVHD reaction (Qasim et al., 2017). Both VST products were heavily skewed to central memory phenotype, suggesting our developed culture process supports the expansion of this early proliferative memory population.

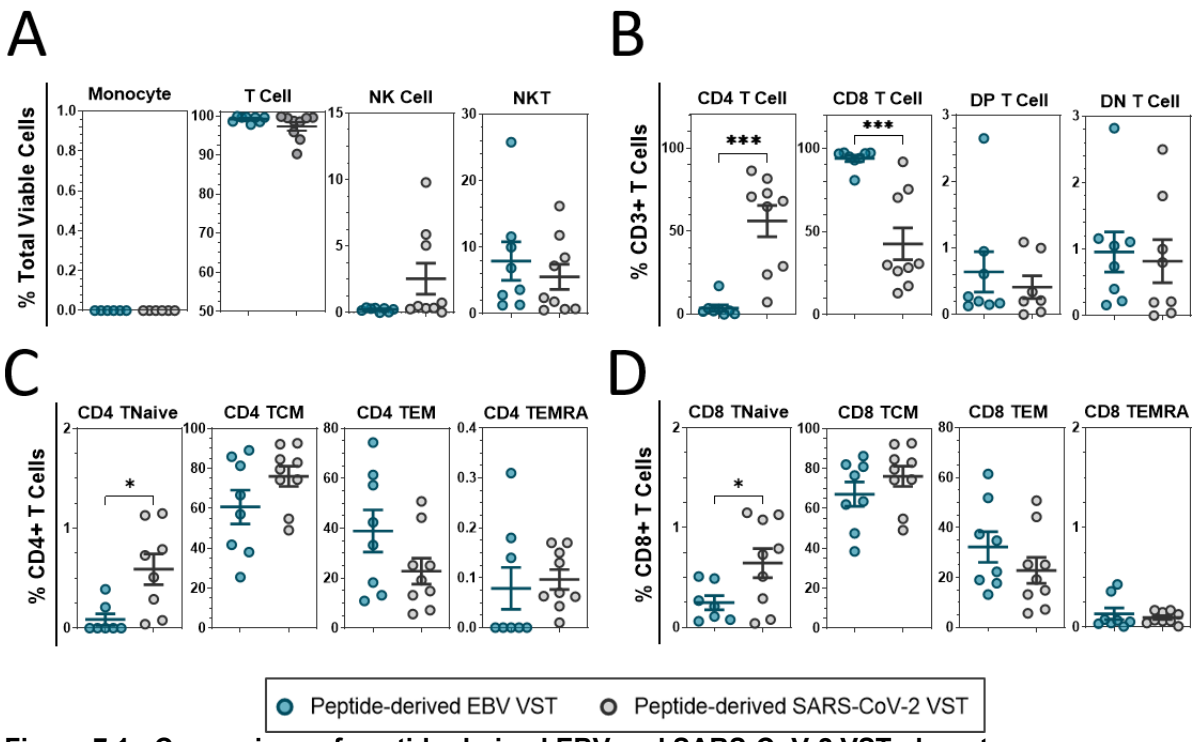

Figure 7.1 - Comparison of peptide-derived EBV and SARS-CoV-2 VST phenotype.

Phenotyping products compared lymphocyte populations between EBV VST (n=8) and SARS-CoV-2 VST (n=9) both derived using peptide-mediated selection and expansion process. **(A)** Gated on the total viable cells, analyses were quantified for T cells (CD3+), NKT cells (CD3+/CD56+), NK cells (CD3-/CD56+) and B cells (CD19+). **(B)** Gated CD3+ T cells were then sequentially gated for T cell subtypes: CD8 T cells (CD8+/CD4-), CD4 T cells (CD4+/CD8-), DP T cells (CD4+/CD8+) and DN T cells (CD4-/CD8-). Within the **(C)** CD8 or **(D)** CD4 compartments, T cells were assessed for differentiation status as follows: naïve T cells (CD62L+/CD45RA+/CD45RO-), TCM (CD62L+/CD45RA-/CD45RO+), TEM (CD62L-/CD45RA-/CD45RO+) and TEMRA (CD62L-/CD45RA+/CD45RO-). All data is represented as mean ± SEM. Statistical analysis was done using unpaired t-tests where *p≤0.05 and ***p≤0.001.

TCR repertoire analysis was also carried out within the same sequencing run allowing comparison between the peptide-derived VST products. Across all donor lines tested, SARS-CoV-2 VST consistently contained a more diverse TCR repertoire than EBV VST as shown in **Figure 7.2**. SARS-CoV-2 VST lines were highly polyclonal with the repertoire taken up by >1000 unique clones, whereas the majority of EBV VST repertoires were dominated by a top 10 expanded clones (**Figure 7.2A**). Clonotype count was higher (**Figure 7.2B**) in SARS-CoV-2 VST lines than EBV VST lines ranging between 1092-3596 and 122-633 respectively. The highly diverse repertoire of SARS-CoV-2 VST here may reflect the fact that this T cell response is to a primary SARS-CoV-2 infection given the donors in this group were recruited in the first years of outbreak. The immune response is therefore highly heterogeneous and clearly results in a very diverse T cell response. It is likely that continued re-exposure to the virus and/or vaccine would select out and expand the best clones for response, with the repertoire honing throughout the individual's lifespan similar to that of influenza A T

cell immunity (Gil et al., 2015). This hypothesis could be tested by taking longitudinal samples to expand SARS-CoV-2 VST from a donor with repeated infections to assess changes in repertoire composition. The hypothesis is also demonstrated by the T cell repertoire seen in our EBV VST products. In this case EBV infection usually occurs early in life and remains dormant. Occasional reactivation of the virus drives a progressive refinement of the T cell response, resulting in an oligoclonal population of highly-specific and effective T cell clones seen in the final products. Preliminary studies have shown persistence of SARS-CoV-2-specific clones up to 15 months following primary infection (Gittelman et al., 2022) and after vaccinations (Ford et al., 2024), but TCR diversity over time was highly variable between donors. Further studies investigating the SARS-CoV-2 TCR repertoire of long COVID-19 patients would be particularly interesting to identify potential T cell responses associated with the ongoing disease symptoms in these individuals.

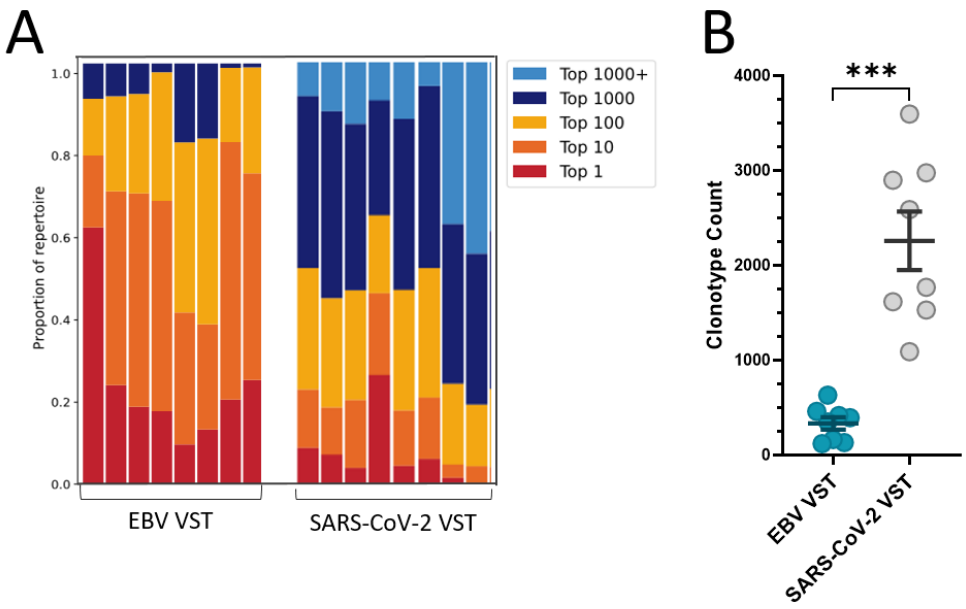

Figure 7.2 - Comparison of peptide-derived EBV and SARS-CoV-2 VST clonal repertoire.

TCR-β sequencing was used to assess T cell repertoire diversity between EBV VST (n=8) and SARS-CoV-2 VST (n=9) both therapies derived using peptide-mediated IFN-γ selection and expansion process. **(A)** Stacked bars represent the proportion of the TCR repertoire occupied by the top n clones in that repertoire, where each bar represents a different donor. **(B)** Clonotype counts for UMI size matched repertoires (9542 UMIs) were compared between the groups. Statistical analysis was done using unpaired t-tests where ***p≤0.001.

Similarly, it would be interesting to compare EBV VST clonal repertoire at primary infection, compared to the donor lines shown above which were mainly from middle aged donors with latent infection, to understand the clonal diversity of the initial EBV T cell response. The frequency of clones specific for EBV BMLF1 were found to be

incredibly stable intra-donor over time up to 15 years after initial testing, though initial testing was still in adults (Couturaud et al., 2023). It is clearly much more challenging to identify donors during EBV primary infection due to the mild/ asymptomatic presentation in the majority of individuals. Understanding differences in clonal response between standard primary EBV infection as compared to IM primary infection would be particularly useful given IM diagnosis is usually associated with heightened risk for development of further EBV pathologies. Overall, TCR sequencing of these two VST products together has allowed the perfect control for analysis to compare repertoire diversity and antigen specificity of T cells isolated and expanded by the same methodology but targeting different viruses.

7.4.2 Robustness and ease of process translation to new viruses.

While initially SARS-CoV-2 VST isolated by IFN-γ capture struggled to proliferate in the culture process developed for EBV VST expansion, the protocol was quickly optimised to support SARS-CoV-2 VST growth. Numerous variables were tested to optimise the culture protocol including different protein supplements, cytokine supplements in addition to IL-2 as per the original protocol, different seeding densities, and re-stimulating plateauing cultures with peptide-loaded feeder cells. From these comparison experiments, the only alteration from the EBV culture protocol implemented was the addition of platelet lysate (T-Liven PR™) into the culture medium (TexMACS medium with IL-2). Supplementation with T-Liven PR™ induced such a substantial increase in fold expansion that we found that day 14 was optimal for harvest to gain sufficient SARS-CoV-2 VST numbers for clinical use as cryopreserved patient doses. In the developed EBV VST protocol, expansion in TexMACS supplemented with IL-2 only generated optimal numbers for cryopreservation by day 18-19. Following manufacture of the SARS-CoV-2 VST bank we ran intra-donor comparison experiments to test the addition of T-Liven PR™ into the EBV VST process which did induce a higher fold expansion within the culture period (data not shown). In theory this could be applied to improve the EBV VST manufacturing process, however as discussed previously EBV VST generally grow to higher numbers than our facility is able to cryopreserve on a single harvest day due to controlled rate freezer limits even with IL-2 supplementation only. As for manufacture of all medicinal products, any simplification or removal of unnecessary materials is always beneficial to minimise any safety risks. T-Liven PR™ is a GMP-

compliant platelet lysate, manufactured by pooling platelet units from approximately 100 human donors. Though it undergoes a pathogen reduction step by electron beam irradiation reducing potential contaminating viruses to undetectable levels, CMV has the potential to propagate in human T cells and therefore could be amplified during our T cell expansion process. Since pathogen reduction reduces CMV to ≤0.85 genome equivalents (ge)/mL this is considered far too low a titre to infect cells *in vitro* (Ljungman, 2004). However since T-Liven PR™ was required for SARS-CoV-2 VST expansion we further mitigated any risk by incorporating a CMV PCR test on the final products. This exemplifies the importance of tailoring relevant characterisation and safety testing around risks associated with the manufacturing process as discussed in section **7.5.1**.

Although we required very few modifications between processes for generating EBV and SARS-CoV-2 VST, it is likely growth kinetics of other antigen-specific T cells may be dependent upon the antigenic target, frequency/input of the T cells into culture, and stability of the population under stimulation and expansion. Therefore, for the platform to be effectively translated, culture conditions should be optimised to support the antigen-specific T cells of interest. The combination of flow cytometric analyses developed in this thesis to characterise the VST during expansion should make that process consistent and quantifiable.

While IL-2 is the most commonly used growth factor in T cell culture as the minimal requirement to promote T cell proliferation, the concentration widely varies between protocols. A comparative study testing different IL-2 concentrations reported T cells grown in high dose IL-2 [600 IU/mL] had high proliferation and maximal secretion of IFN-γ, but had very low direct cytotoxic capacity (Besser et al., 2009). Conversely, in manufacture of autologous TIL therapies isolated from the patient's own tumour, culture IL-2 concentrations of 3000-6000 IU/mL have been optimised to support TIL expansion (Jin et al., 2012, Shah et al., 2022). This highlights the importance of fine-tuning the IL-2 concentration depending on the application or desired T cell phenotype. Since over-proliferation of T cells may detrimentally impact effector functionality, consideration should be taken in protocols involving additive factors promoting T cell expansion.

Other commonly used cytokines in T cell culture include IL-4, IL-7, IL-15, and IL-21. Various combinations and concentrations of these cytokines have been shown to induce diverse effects on T cell viability, proliferative capacity, differentiation, and selection of particular T cell subsets dependent on the T cell culture system (Sudarsanam et al., 2022). One study investigating the optimal combinations reported the best condition for CD4+ T cell expansion was high IL-2 and high IL-7, with no IL-15 supplementation, likely due to the critical role of IL-7 in promoting CD4+ T cell survival (Coppola et al., 2020). Supplementation with IL-15 has been shown to improve cultured T cell anti-tumour cytotoxicity and IFN-γ production, indicating this cytokine helps support T cell activation and effector functionality (Shi et al., 2013, Alizadeh et al., 2019, Zhou et al., 2019). Furthermore, addition of IL-21 to activated T cell cultures has been shown to retain memory stem T cells (TSCM) characterised as CCR7+/CD27+/CD45RA+/CD45RO-/CD95+ through activation of the STAT3 pathway (Alvarez-Fernández et al., 2016). Since sustained activation of STAT3 prevents the cleavage of CD27, CD45RA, CD62L and the IL-7Rα, IL-2 signalling continues the self-renewal of this undifferentiated TSCM phenotype (Gattinoni et al., 2012). In this way, tailored culture supplements may also be able to drive expansion of a particular subtype of T cell optimised for the therapeutic target.

Appropriate feeder cells may also be considered to provide support and co-stimulatory signalling to T cells during culture. Typically, PBMC irradiated to prevent outgrowth are used as feeders due to the diverse co-stimulatory mechanisms enabled by the mixed blood cell populations present. We used the non-target PBMC following CCS stimulation since the monocytes, DC and B cells which act as APC within this fraction are still loaded with antigenic peptides and can provide continued presentation in culture during the early phase of expansion. However mixed blood feeder cells may increase the variability of effect to T cell culture phenotype. Interestingly, one study testing direct comparison of T cell cultures found presence of contaminating RBC significantly reduced T cell culture expansion, compared to cultures without contaminating RBC (Nelson et al., 2020b). Furthermore, addition of RBC was found to drive more T cells to differentiate into effector memory T cells, whereas more T cells in RBC absent cultures maintained a central memory phenotype. Some studies have also reported use of engineered or artificial feeder cells to support T cell culture (Dave et al., 2017, Xiao et al., 2018, Choi et al., 2021), though this approach imposes heightened regulatory scrutiny through use of

modified cells in a clinical cell therapy manufacture protocol in order to ensure that they are not carried over into the final drug substance / drug product.

Should the process be translated to other antigens or viruses, other potential culture conditions to optimise include the basal medium, vessels or bioreactors, seeding densities, or further supplements that provide benefits to therapeutic T cell culture. There are now several GMP-compliant specialist T cell culture media available including TexMACS™, Immunocult™, CelThera™, CellGenix™ and Excellerate™, each of which may suitable for manufacture of T cell products.

While we chose to use a selection process to isolate virus-specific T cells from seropositive individuals, there may be applications where adoptive transfer from seropositive donors would not be a safe strategy for therapy. Human immunodeficiency virus (HIV) for example is a category 3 pathogen that propagates in human CD4+ T cells and monocytes, and therefore isolation and expansion of HIV-specific T cells from HIV seropositive individuals would be a safety risk both to the operator during the manufacturing process and also the final product. To this end, selection and culture techniques would not be suitable to make an HIV-targeting VST therapy, however protocols have been developed to use DC pulsed with HIV gag, pol and nef peptides to expand HIV VST from HIV-naïve donors (Patel et al., 2018). Powell and colleagues similarly expanded HIV VST from HIV-naïve donors through APC presentation of peptides, and further engineered the cells to secrete a broadly neutralising antibody against the HIV envelope to induce antibody dependent cellular cytotoxicity thereby combining innate and adaptive immune mechanisms for therapy (Powell et al., 2020). Further cell therapy approaches to treat HIV have been to generate CAR-T cells targeted against CD4 and HIV envelope (Mu et al., 2020, Namdari et al., 2020). While first generation HIV CAR T cell therapies demonstrated limited efficacy in clinical trials, advances in later generation CAR constructs in the adoptive T cells aim to address challenges seen in these early trials, such as viral escape and CAR T exhaustion (Jiang et al., 2021). One major challenge for HIV T cell therapies is that HIV can infect the infused T cell product (Cruz and Bollard, 2017, Campos-Gonzalez et al., 2023). To prevent this, gene editing techniques to disrupt or knock out the HIV co-entry receptor CCR5 have been used to develop HIV-resistant CAR T cells (Rothemejer et al., 2023).

7.5 Evaluation of characterisation assays for VST therapies

The aim of this thesis was to comprehensively characterise the different T cell therapies using a suite of primarily flow-based assays qualified at the time of study, with a generous budget/ resource allocation compared to most labs. It could be postulated that not every assay utilised in this project is essential for profiling the T cell therapies, therefore this section will focus on evaluating the characterisation assays in the context of adoptive cell therapy manufacture.

7.5.1 Determination of assays appropriate to product.

If there was no restriction on resources, would it be beneficial to test manufactured T cell final products in assays for all cell types within a lineage? For example, a product made from blood as starting material would be functionally tested for all haematopoietic lineages to determine whether there is a potential for off-target effects. In an ideal world this would be good early data to ease certain safety concerns, however even with the impracticalities and high cost to perform so many supplemental assays, such tests may also fail to detect cell-specific functions induced by the disease context. Also, such high cell numbers are required to test each clinical batch for sterility, characterisation, potency, stability, and genetic abnormalities that this often limits the number of patient doses that can be manufactured. Therefore, it is important to consider the key relevant assays that will identify any safety risks of the cells tailored around the manufacturing process. For ATMP manufacture, current regulations state any product must be characterised in terms of identity, purity and potency. While the British Pharmacopoeia has published a guidance manual of ATMP T cell and NK cell characterisation assays suggested for product approval by the MHRA, this guide provides a wide range of assays to cover multiple T cell and NK cell therapies. Therefore many characterisation assays, such as transduction efficiency for CAR T cells, or phenotyping of NK cells is not applicable to the current VST therapies. As such, the strategy of broad spectrum characterisation is useful in initial development stages, however during product development/clinical translation, the range of assays should be refined to test the essential criteria specific for the therapy manufactured.

For instance, in the LCL method to make EBV VST, the major impurity of concern was the LCL themselves used in the co-culture stimulations. The manufacturing process was developed to prevent infusion of viable LCL with oncogenic potential by irradiation prior to T cell stimulation, rendering the cells unable to proliferate. While there may still be a residual danger in infusing large numbers of limited lifespan EBV+ LCL to immunosuppressed patients, a maximum limit of 2% CD19+ B cells was set as a release criterion for the LCL manufacture of EBV VST. Conversely, since the peptide process contained an isolation step, this already greatly reduced the potential for impurities within the product, and this was confirmed by the fact that the mean T cell content in both EBV- and SARS-VST was over 95%. One key consideration for this manufacturing method instead was what cells may be inadvertently carried along during a positive enrichment which could continue to expand during the culture period. As the antibody-conjugated beads used in the selection can potentially pick up any CD45+ leukocyte able to produce IFN-γ, cells other than VST could be co-isolated. Since NK cells mediate effector functions through secretion of IFN-γ and could therefore be caught up in the EBV peptide selection, we incorporated NK markers in the analysis panel to quantify NK cell contamination. Accordingly for the peptide manufacture for EBV VST, a maximum limit of 10% CD56+/CD3- NK cells was set as a criterion for product release, though all banked products tested were much lower than this. Interestingly, some COVID-19 convalescent donors were found to expand a population of adaptive memory-like NK cells reactive to SARS-CoV-2 peptide stimulation. As such the use of 10% maximal limit of NK cells was justified to ensure release only of SARS-CoV-2 VST products highly enriched for T cells.

The main phenotypic difference between EBV and SARS-CoV-2 was the CD4 to CD8 ratio of expanded VST. Since EBV VST are generated from a primarily antiviral CD8 T cell response, the final manufactured products contained predominantly CD8+ T cells and it is important to design functional assays that are appropriate to assess degranulation and cytotoxic effector functions of these cells to quantify the potency of the product. Two independent assays were used including expression of degranulation markers CD107a, perforins and granzymes in response to EBV peptide stimulation and specific lysis against HLA-matched virus antigen-expressing LCL. Stimulation *in vitro* with EBV peptides demonstrated that responses can be generated against processed viral-specific antigen sequences, whereas cytotoxicity against LCL verifies the T cells can recognise and kill viral-infected tumour cells. Combination of

these alternative targets could also be useful in investigating whether expanded T cells recognise cellular as opposed to viral antigens as discussed previously. Conversely, SARS-CoV-2 VST predominantly contained CD4+ T cells. To ascertain helper subtypes, T cells could be characterised for expression of effector cytokines and/or transcription factors. While ELISA-based assays are commonly used to quantify production of different cytokines by T cells stimulated with antigen, these methods are limited by inability to delineate which cell in the culture produced the cytokine(s). As such, intracellular cytokine staining is a superior approach to identify the potential multitude of different helper T cell subtypes within a population. Furthermore, since Th1 and CD8+ effector cells can both produce IFN-γ, TNF-α, and IL-2; intracellular cytokine staining can determine functional reactivity between CD4+ and CD8+ T cells in mixed CD4/CD8 lines. Combined profiling of T cell inhibitory markers and effector cytokine production is also vital for demonstrating that the T cell therapies generated have therapeutic potential and this can be confirmed by correlation with cytotoxic assays. We determined that combined IFN-γ and TNF-a expression correlated significantly with cytotoxicity and therefore cytokine profiling could be used as a surrogate for cytotoxicity in circumstances where conventional cytotoxicity assays are not available due to the lack of a suitable target cell. Quantification of cell therapy potency is a regulatory requirement and mechanism of action is rapidly becoming an essential criterion for cell therapies so that it can be demonstrated that a patient is not undergoing unnecessary risk by infusing an inert cell therapy. Moreover, intracellular staining assays allow the identification of CD4+ T cells expressing degranulation markers, and could therefore be the first step in indicating which T cell lines contain potential CD4+ cytotoxic T cells. Though we are keen to test the cytotoxic potential of SARS-CoV-2 VST in the research setting, the lack of relevant SARS-CoV-2 infected target cells signified the use of cytokine production in response to SARS-CoV-2 peptide-loaded DC as the more appropriate functional assay for this cell therapy.

Phenotypic profiling also allowed us to characterise the memory status of VST products. While both expanded VST products contained negligible percentages of naïve T cells, it was useful to test SARS-CoV-2 VST as the novel cell therapy for alloreactive responses in a relevant immunogenicity assay (Dickinson et al., 1998). This model tested the allogeneic cell therapy with donor PBMC in an MLR with a quantitative assessment of GVHD using histological analysis of skin explants, along

with T cell proliferation and inflammatory cytokine production data. With the three different outputs for measuring the potential for adverse immunological reactions, this provided a comprehensive assessment of the potential for cells to drive alloreactive responses. While the PBMC donors were retrospectively HLA typed to calculate HLA matches in MLR cultures, this assay could be optimised by choosing donors beforehand based on particular HLA alleles. We tested our allogeneic cell therapy in this model based on minimal or no HLA matches to understand the worst-case scenario, however the model could also be utilised in the choice of donor lines for any given patient as a predictive measure of any potential harmful effects, though this would slow down the administration of VST therapy. While our selection and expansion process clearly highly enriches for antigen-specific T cells, use of memory profiling and GVHD testing should be a fundamental requirement for characterisation during the development of allogeneic T cell therapies to ensure manufacturing processes generate low-risk cells for clinical use.

7.5.2 Establishment of a profile to assess VST therapies.

Assays currently required to provide an overall profile of cellular therapies fall into the following categories: identity, quality, functionality and safety. This study has identified and evaluated the main assays beneficial for characterising T cell therapies as shown in **Table 7.1**. Suitable parameters and techniques for quantitative or qualitative assessment should be chosen to most effectively answer each question or concern related to testing of cell therapies for clinical use. As a rapidly developing field, standards of quality testing are becoming more defined with guidelines being written for individual cell types (Capelli et al., 2023). As can be seen, this table only includes assays pertinent to testing non-modified T cell therapies, whereas CAR T cells or engineered TCR T cell therapies would require substantial additional testing to ensure safety following genetic modification. It will be fundamental to clarify which assays should be performed at different stages of development, versus which assays are essential to release every batch manufactured for clinical use as more cellular therapies are translated to the bedside.

Question	Parameters(s)	Assay(s)
		Identity
What is the T cell purity?	CD2, CD3	Flow cytometry
What type of T cells are present?	CD4, CD8, TCR-αβ, TCR-γδ	Flow cytometry
What contaminating cells are present?	CD14, CD19, CD45, CD56, CD235a	Flow cytometry
		Quality
Are the cells healthy?	Viability stains	Imaging
	Dead cell dyes	Flow cytometry
	Telomere length	PCR
What is the memory state?	CCR7, CD45RA, CD45RO, CD62L	Flow cytometry
Are the cells exhausted?	CTLA-4, LAG-3, PD-1, TIGIT, TIM-3	Flow cytometry PCR
		Functional
What are the antigen-specific effector functions?	Cytotoxicity against targets	Flow cytometry ^{51}Chromium release
	Degranulation: CD107a, Granzymes, Perforin	Intracellular flow cytometry
	Activation: CD28, CD137, CD154	Intracellular flow cytometry
	Cytokines: IFNs, TNFs, ILs	Intracellular flow cytometry ELISA/ ELISPOT
Will cells migrate to disease site?	Chemokines and receptors: CCs, CCRs, CXCRs	Flow cytometry PCR
	Chemotaxis assay	Imaging
What is the antigen specificity?	Cytokines: IFNs, TNFs, ILs	Intracellular flow cytometry
	TCRβ epitope matching	Next generation sequencing
	HLA-specific multimer analysis	Flow cytometry
		Safety
Are naïve T cells present?	CCR7, CD45RA, CD45RO, CD62L	Flow cytometry
What is the immunogenic potential?	T cell proliferation GVHD histology Inflammatory cytokines	Flow cytometry Imaging ELISA
What is the oncogenic potential?	Cancer genes screen	SNP array
Are products contaminated?	Endotoxin	Endo-LISA
	Mycoplasma	PCR
	Bacteria	Bac-T/ALERT
	Viruses	PCR

Table 7.1 - T cell therapy characterisation assays.

7.6 Challenges & future directions in allogeneic VST therapies

Substantial progress has been made to establish numerous approved VST cellular products for clinical use as equivalent or superior therapies to standardised pharmacological treatments. While in some diseases it has been easier to demonstrate adoptive VST efficacy, other disease contexts, particularly that of viral malignancies in relatively immunocompetent individuals, require more advanced approaches to therapy design. This section will discuss the major challenges currently in the field, and some of the innovative strategies in development to improve allogeneic VST therapy for poor prognostic indications.

7.6.1 Alloreactivity and reducing immunogenic potential.

The greatest benefit of allogeneic virus-specific T cells in adoptively transferring healthy donor immunity is also the biggest limitation of this therapeutic approach. Given that HLA molecules can be highly immunogenic, insufficient HLA matching can risk both infused T cell attack of the host (GVHD), as well as host attack of the grafted T cells causing rejection. The combination of TCR sequence specificity, functional antigen reactivity and skin explant GVHD testing within this study indicates a very low potential for alloreactivity of our VST therapies produced. The outcomes from this *in vitro* testing correlate well with the results from our long-term clinical use of LCL-derived EBV VST which have demonstrated lack of alloreactivity or adverse events associated with GVHD (Haque et al., 2007, Haque et al., 2010, Vickers et al., 2014, Chiou et al., 2018, Kazi et al., 2019). Indeed, this reflects experience with EBV and other VST therapies from numerous centres, which have corroborated the safety of allogeneic VST in clinical trials (Leen et al., 2013, Withers et al., 2017, Nelson et al., 2020, Prockop et al., 2020, Olson et al., 2021, Rubinstein et al., 2021).

Nonetheless novel approaches are being investigated to prevent GVHD potential from allogeneic T cell products, including knockout of the αβ-TCR by CRISPR/Cas9 editing to generate CAR+ TCR- cells (Georgiadis et al., 2018, Stenger et al., 2020). Since transduction techniques generally don't result in complete knock out efficiency, gene editing should be followed by subsequent selection or depletion strategies to ensure no residual αβ-TCR with GVHD potential are transferred to patients. In one case study, despite αβ-TCR depletion resulting in <1% αβ+ CAR T cells, transfusion into an

infant with relapsed refractory B cell acute lymphoblastic leukaemia resulted in a grade 2 skin GVHD after 9 weeks which was found to be due to expansion of CD3+ αβ+ CAR T cells (Qasim et al., 2017). This demonstrates the potential of even very low doses of alloreactive T cells to induce off-target effects and highlights the requirement for advances in cellular therapy alloreactivity testing.

Conversely, the ability to eliminate all host alloreactive lymphocytes to prevent host rejection of the infused T cell therapy is unfeasible. Instead, advances have been made to knockout HLA molecules on the allogeneic T cell therapy, thereby preventing recognition by host alloreactive T cells. Such studies have generated gene-edited T cells lacking HLA class I, class II and/or TCR by knockout of β-2 microglobulin, class II transactivator (CIITA) and TCR alpha constant (TRAC) genes respectively (Ren et al., 2017, Kagoya et al., 2020, Lee et al., 2020). As well as the regulatory complexities to manufacture genetically modified effector cells 'invisible' to the immune system, this approach may also be limited in clinical use due to the potential of HLA class I-negative cells becoming targets for host NK cell lysis, unless T cell therapies could be modified to force expression of non-classical HLA class I molecules such as HLA-E (Gornalusse et al., 2017, Quach et al., 2023). An elegant alternative approach has been to make T cell therapies engineered to express a chimeric HLA accessory receptor that is able to kill host alloreactive T cells that engage with class I alloantigens (Quach et al., 2019, Ramos et al., 2020, Mo et al., 2021). This approach has been applied to generating EBV VST modified to express a CD30-targeted CAR, which allows the allogeneic EBV VST to kill alloreactive CD30+ T cells as well as CD30+ tumour cells (Quach et al., 2024). Such 'rejection-resistant' CD30 CAR EBV VST were protected from elimination in alloreactivity *in vitro* assays, and are being tested for safety in phase I trials for CD30+ HL patients.

7.6.2 HLA restriction and improving donor to patient matching.

Alongside having the potential to cause harmful immunogenic responses, insufficient HLA matching also limits the therapeutic potential of infused allogeneic VST therapies. It is very unlikely a donor VST product and the recipient match all 12 major surface HLA class I and II alleles, and therefore TCR within VST products will only be able to recognise viral peptides presented by shared HLA alleles. For this reason, VST banks should be manufactured from donors with diverse HLA types to allow greater chance of finding a VST line with both class I and class II matches to any given patient.

Our centre has shown in two clinical studies, patient complete responses to allogeneic EBV VST therapy significantly increases with higher number of HLA matches between the donor VST line and patient (Haque et al., 2007, Kazi et al., 2019). Simulation modelling indicated a panel of 25 well-chosen donors covered 85% of the UK patient population (Vickers et al., 2014). However, with the remaining population presenting rarer HLA types, increasing the donor panel did not increase the HLA coverage any further. While we manufactured the LCL-derived EBV VST bank from 25 donors, within the last 15 years of issuing there are still a few donor lines that have rarely been administered due to other lines having better matches for the patient. Furthermore, while the number of matches is important, there is a hierarchy in HLA presentation and therefore some HLA haplotypes are more important for matching than others, making the choice of the best donor cell therapy incredibly complex (Mangum and Caywood, 2022). HLA matching algorithms are usually made on the basis of impact on the outcome of HSCT which obviously infuses a mix of leukocyte populations. As T cell therapies are used more routinely, it may become pertinent to choose best HLA matches between donor and patient based on the product given, particularly in terms of CD4 to CD8 content of T cell lines. Where patients have been biopsied for tumour antigen expression, it could also become a more personalised approach to choosing T cell lines HLA matched to particular peptide targets.

7.6.3 Overcoming tumour evasion and enhancing persistence.

In addition to HLA recognition limiting the therapeutic potential of allogeneic T cell therapies, the disease context, immunosuppression regimen and/or tumour microenvironment can all render infused T cells ineffective. Numerous cases have reported administration of VST therapies with initial reduction in viral load and improved symptoms, however the limited persistence or functional inhibition of the infused T cells results in disease relapse (Brestrich et al., 2009).

When severe viral infections arise following transplant, VST therapies are often given concurrently with immunosuppressive agents, and for many patients this management is required long-term to prevent organ rejection or allow efficient stem cell reconstitution (Barrett and Bollard, 2015). In particular, treatment with steroids such as glucocorticoids can induce T cell apoptosis (Herold et al., 2006), and treatment with calcineurin inhibitors such as cyclosporine A and tacrolimus inhibit T cell activation and pro-inflammatory cytokine production (Tsuda et al., 2012).

Numerous studies have demonstrated generation of allogeneic VST therapies gene edited to be resistant to various immunosuppressive drugs including glucocorticoids (Menger et al., 2015, Kaeuferle et al., 2020, Basar et al., 2020, Basar et al., 2021) and tacrolimus (De Angelis et al., 2009, Ricciardelli et al., 2013, Amini et al., 2021, Peter et al., 2022). Moreover, VST therapies with resistance to multiple immunosuppressive agents are under development to allow treatment of patients under combined immunosuppression regimens (Brewin et al., 2009, Chen et al., 2023, Lin et al., 2023). Many of these novel therapies are being tested in clinical trials to validate if the engineered T cells maintain functionality and resistance to immunosuppressive mechanisms long-term in diseased patients. These approaches mean that it is possible to consider using VST as a front-line treatment for viral-driven malignant diseases, rather than a second-line or rescue therapy in cases of refractory or relapsed disease, where control of the disease becomes more challenging.

In addition to iatrogenic immune suppression limiting T cell responses, tumours also develop mechanisms to supress or inhibit the immune system. Tumour evasion mechanisms include inefficient presentation of tumour antigens to immune cells, selection of tumour cells that have mutated to lose expression of tumour antigens targeted by T cells and creation of a profoundly immunosuppressive tumour microenvironment via recruitment of immunomodulatory cells which inhibit pro-immune cells. Strategies to overcome the tumour microenvironment have included genetic modification to generate VST therapies resistant to immunosuppressive molecules secreted by tumours such as TGF-β (Bollard et al., 2002). By development of a dominant-negative TGF-β receptor modified to delete the cytoplasmic signalling domain, generated LMP-specific T cells were resistant to TGF-β inhibition (Foster et al., 2008). A phase I study demonstrated such TGF-β receptor-modified LMP-specific T cells persisted for more than 4 years in HL patients with maintained clinical responses, with one patient showing complete remission 7 years after transduced LMP VST therapy who had previously only shown a partial response to the unmodified LMP-specific VST therapy (Bollard et al., 2018). Another approach to develop VST resistant to the inhibitory TME has been modification of TCR to induce production of IL-12 upon antigen recognition (Wagner et al., 2004). This inducible delivery of IL-12 improved pro-inflammatory Th1 and cytotoxic EBV VST responses, and improved monocyte and NK cell recruitment using *in vitro* assays (Dragon et al., 2020). Similar attempts to modify T cells to improve signalling of other pro-

inflammatory interleukins have been made for CAR T cells (Hurton et al., 2016, Shum et al., 2017, Shi et al., 2023, Nguyen et al., 2024, Steffin et al., 2025), that may be applicable to enhance function of VST therapies in particularly inhibitory TME contexts. While there is great promise of gene editing to enhance VST therapies, techniques should be developed that allow vector-free non-integrative modifications to facilitate the wider clinical application of these approaches.

7.6.4 Combinatorial therapy and sensitization of tumours.

Further to modifying the T cells themselves, other strategies have explored combination with pharmacological modulation to improve the efficacy of VST therapies. Histone deacetylase inhibitors (HDI) have been previously used to induce reactivation of HIV in order to diminish latent reservoirs, and are similarly being investigated for the potential to reactivate lytic EBV to make silent latency I or II tumours more therapeutically targetable. While various HDI compounds target different signalling pathways, the overall mechanism is to reduce chromatin suppression which usually binds the EBV episome to host chromosomes thereby maintaining viral latency. Sensitization of EBV+ BL tumours with numerous HDI has demonstrated effective induction of EBV lytic phase with upregulation of lytic antigens which then responded to ganciclovir antiviral treatment (Ghosh et al., 2012, Liao et al., 2025). Early trials testing HDI compounds indicated considerable toxicity or poor efficiency of viral reactivation, and therefore recent research has focussed on identifying non-toxic small molecules with high selectivity of EBV reactivation (Tikhmyanova et al., 2019).

A particularly selective HDI demonstrated upregulation of immunogenic latency antigens EBNA2, EBNA3A, EBNA3C and LMP1 in BL tumours *in vitro* without significant lytic induction, (Dalton et al., 2020). The upregulation of latency III antigens persisted at least 7 days following removal of HDI, which rendered the BL tumours more susceptible to adoptively transferred EBV VST homing and killing in a mouse model, as compared to negligible T cell tumour killing in mice without prior HDI sensitization. Another *in vivo* model showed regression of EBV+ NPC tumours was improved with HDI-induced EBV reactivation, though clearance by T cells couldn't be tested in the nude mice and was instead found to be mediated by tumour infiltrating macrophages (Novalić et al., 2017). Further preclinical studies will be needed to comprehensively test molecules to ensure they induce lytic or latency III

reactivation in all tumour cells, such as to prevent advantageous selection of latency I or II clones able to evade immune detection (Heslop, 2020).

Other approaches to tumour sensitization have used checkpoint inhibitors to block tumour over-expression of inhibitory ligands. Treatment with PD-L1 blocking antibodies to sensitize EBV+ HL tumours has also been shown to alleviate T cell exhaustion and augment host anti-tumour responses (Younes et al., 2016), with promising clinical responses in a phase II trial (Armand et al., 2018). Similar results were seen using PD-L1 blocking antibodies to sensitize EBV+ DLBCL tumours prior to R-CHOP therapy with improved survival rates in a phase II clinical trial (Manos et al., 2023). In this way, treatment with immune checkpoint inhibitors may alleviate the immunosuppressive tumour microenvironment to prevent induced exhaustion of infiltrating T cells, and may therefore be useful as a combinatorial therapy to potentiate the functional efficacy of adoptively transferred VST.

7.7 Chapter Summary

This chapter has reviewed how my project evaluated the development, testing and clinical manufacture of peptide-derived VST for both EBV and subsequently SARS-CoV-2. This was an expansion of the originally-planned project whose scope was to compare the differences in final EBV-VST product from two different manufacturing approaches. The COVID-19 pandemic, while a huge block to many scientists, provided an unparalleled opportunity to utilise the developmental research from my project to generate a new VST product for SARS-CoV-2. Both VST products developed during my PhD studies have now been manufactured and released for clinical use. Rapid development of these allogeneic T cell therapies has reflected the expertise of SNBTS as a blood and tissues supplier, with unique understanding of the all the components required to manufacture and deliver ATMP for human trials. In addition to the considerations for cell manufacture, I developed a well-characterised and qualified suite of assays which were used to comprehensively analyse T cell phenotype and function and build a developmental profile of their therapeutic function. These assays were then refined and validated into QC assays required for QP release of final manufactured products. This platform can be applied generally to manufacture other antigen-specific T cell for therapy of viral or malignant disorders. Furthermore, the techniques and assays developed could be utilised to design more advanced

approaches to T cell therapy manufacture or broaden applicability to target harder to treat diseases.

List of References

ABBAS, A. K., TROTTA, E., D, R. S., MARSON, A. & BLUESTONE, J. A. 2018. Revisiting IL-2: Biology and therapeutic prospects. *Sci Immunol,* 3.

ABBOTT, R. J., PACHNIO, A., PEDROZA-PACHECO, I., LEESE, A. M., BEGUM, J., LONG, H. M., CROOM-CARTER, D., STACEY, A., MOSS, P. A. H., HISLOP, A. D., BORROW, P., RICKINSON, A. B. & BELL, A. I. 2017. Asymptomatic Primary Infection with Epstein-Barr Virus: Observations on Young Adult Cases. *J Virol,* 91.

ABBOTT, R. J., QUINN, L. L., LEESE, A. M., SCHOLES, H. M., PACHNIO, A. & RICKINSON, A. B. 2013. CD8+ T cell responses to lytic EBV infection: late antigen specificities as subdominant components of the total response. *J Immunol,* 191**,** 5398–409.

ABLASSER, A., BAUERNFEIND, F., HARTMANN, G., LATZ, E., FITZGERALD, K. A. & HORNUNG, V. 2009. RIG-I-dependent sensing of poly(dA:dT) through the induction of an RNA polymerase III-transcribed RNA intermediate. *Nat Immunol,* 10**,** 1065–72.

ABUSALAH, M. A. H., GAN, S. H., AL-HATAMLEH, M. A. I., IREKEOLA, A. A., SHUEB, R. H. & YEAN YEAN, C. 2020. Recent Advances in Diagnostic Approaches for Epstein-Barr Virus. *Pathogens,* 9.

AGATA, Y., KAWASAKI, A., NISHIMURA, H., ISHIDA, Y., TSUBATA, T., YAGITA, H. & HONJO, T. 1996. Expression of the PD-1 antigen on the surface of stimulated mouse T and B lymphocytes. *Int Immunol,* 8**,** 765–72.

AGGARWAL, V., WORKMAN, C. J. & VIGNALI, D. A. A. 2023. LAG-3 as the third checkpoint inhibitor. *Nat Immunol,* 24**,** 1415–1422.

AKTAS, E., KUCUKSEZER, U. C., BILGIC, S., ERTEN, G. & DENIZ, G. 2009. Relationship between CD107a expression and cytotoxic activity. *Cell Immunol,* 254**,** 149–54.

AL-AKIOUI SANZ, K., ECHECOPAR PARENTE, C., FERRERAS, C., MENÉNDEZ RIBES, M., NAVARRO, A., MESTRE, C., CLARES, L., VICARIO, J. L., BALAS, A., DE PAZ, R., LÓPEZ GRANADOS, E., SÁNCHEZ ZAPARDIEL, E., JIMÉNEZ, C., LÓPEZ-OLIVA, M., RAMOS, E., HERNÁNDEZ-OLIVEROS, F. & PÉREZ-MARTÍNEZ, A. 2023. Familial CD45RA(-) T cells to treat severe refractory infections in immunocompromised patients. *Front Med (Lausanne),* 10**,** 1083215.

AL-MANSOUR, Z., NELSON, B. P. & EVENS, A. M. 2013. Post-transplant lymphoproliferative disease (PTLD): risk factors, diagnosis, and current treatment strategies. *Curr Hematol Malig Rep,* 8**,** 173–83.

AL-SAMKARI, H., KARP LEAF, R. S., DZIK, W. H., CARLSON, J. C. T., FOGERTY, A. E., WAHEED, A., GOODARZI, K., BENDAPUDI, P. K., BORNIKOVA, L., GUPTA, S., LEAF, D. E., KUTER, D. J. & ROSOVSKY, R. P. 2020. COVID-19 and coagulation: bleeding and thrombotic manifestations of SARS-CoV-2 infection. *Blood,* 136**,** 489–500.

AL HAMED, R., BAZARBACHI, A. H. & MOHTY, M. 2020. Epstein-Barr virus-related post-transplant lymphoproliferative disease (EBV-PTLD) in the setting of allogeneic stem cell transplantation: a comprehensive review from pathogenesis to forthcoming treatment modalities. *Bone Marrow Transplant,* 55**,** 25–39.

ALAGGIO, R., AMADOR, C., ANAGNOSTOPOULOS, I., ATTYGALLE, A. D., ARAUJO, I. B. O., BERTI, E., BHAGAT, G., BORGES, A. M., BOYER, D., CALAMINICI, M., CHADBURN, A., CHAN, J. K. C., CHEUK, W., CHNG, W. J., CHOI, J. K., CHUANG, S. S., COUPLAND, S. E., CZADER, M., DAVE, S. S., DE JONG, D.,

DU, M. Q., ELENITOBA-JOHNSON, K. S., FERRY, J., GEYER, J., GRATZINGER, D., GUITART, J., GUJRAL, S., HARRIS, M., HARRISON, C. J., HARTMANN, S., HOCHHAUS, A., JANSEN, P. M., KARUBE, K., KEMPF, W., KHOURY, J., KIMURA, H., KLAPPER, W., KOVACH, A. E., KUMAR, S., LAZAR, A. J., LAZZI, S., LEONCINI, L., LEUNG, N., LEVENTAKI, V., LI, X. Q., LIM, M. S., LIU, W. P., LOUISSAINT, A., JR., MARCOGLIESE, A., MEDEIROS, L. J., MICHAL, M., MIRANDA, R. N., MITTELDORF, C., MONTES-MORENO, S., MORICE, W., NARDI, V., NARESH, K. N., NATKUNAM, Y., NG, S. B., OSCHLIES, I., OTT, G., PARRENS, M., PULITZER, M., RAJKUMAR, S. V., RAWSTRON, A. C., RECH, K., ROSENWALD, A., SAID, J., SARKOZY, C., SAYED, S., SAYGIN, C., SCHUH, A., SEWELL, W., SIEBERT, R., SOHANI, A. R., TOOZE, R., TRAVERSE-GLEHEN, A., VEGA, F., VERGIER, B., WECHALEKAR, A. D., WOOD, B., XERRI, L. & XIAO, W. 2022. The 5th edition of the World Health Organization Classification of Haematolymphoid Tumours: Lymphoid Neoplasms. *Leukemia,* 36**,** 1720–1748.

ALBANESE, M., TAGAWA, T., BOUVET, M., MALIQI, L., LUTTER, D., HOSER, J., HASTREITER, M., HAYES, M., SUGDEN, B., MARTIN, L., MOOSMANN, A. & HAMMERSCHMIDT, W. 2016. Epstein-Barr virus microRNAs reduce immune surveillance by virus-specific CD8+ T cells. *Proc Natl Acad Sci U S A,* 113**,** E6467–e6475.

ALBON, S. J., MANCAO, C., GILMOUR, K., WHITE, G., RICCIARDELLI, I., BREWIN, J., LUGTHART, G., WALLACE, R. & AMROLIA, P. J. 2013. Optimization of methodology for production of CD25/CD71 allodepleted donor T cells for clinical use. *Cytotherapy,* 15**,** 109–21.

ALIZADEH, D., WONG, R. A., YANG, X., WANG, D., PECORARO, J. R., KUO, C. F., AGUILAR, B., QI, Y., ANN, D. K., STARR, R., URAK, R., WANG, X., FORMAN, S. J. & BROWN, C. E. 2019. IL15 Enhances CAR-T Cell Antitumor Activity by Reducing mTORC1 Activity and Preserving Their Stem Cell Memory Phenotype. *Cancer Immunol Res,* 7**,** 759–772.

ALLDAY, M. J., BAZOT, Q. & WHITE, R. E. 2015. The EBNA3 Family: Two Oncoproteins and a Tumour Suppressor that Are Central to the Biology of EBV in B Cells. *Curr Top Microbiol Immunol,* 391**,** 61–117.

ALLEN, U. D. & PREIKSAITIS, J. K. 2019. Post-transplant lymphoproliferative disorders, Epstein-Barr virus infection, and disease in solid organ transplantation: Guidelines from the American Society of Transplantation Infectious Diseases Community of Practice. *Clin Transplant,* 33**,** e13652.

ALON, R., SPORTIELLO, M., KOZLOVSKI, S., KUMAR, A., REILLY, E. C., ZARBOCK, A., GARBI, N. & TOPHAM, D. J. 2021. Leukocyte trafficking to the lungs and beyond: lessons from influenza for COVID-19. *Nat Rev Immunol,* 21**,** 49–64.

ALTMAN, J. D., MOSS, P. A., GOULDER, P. J., BAROUCH, D. H., MCHEYZER-WILLIAMS, M. G., BELL, J. I., MCMICHAEL, A. J. & DAVIS, M. M. 1996. Phenotypic analysis of antigen-specific T lymphocytes. *Science,* 274**,** 94–6.

ALTOSOLE, T., ROTTA, G., URAS, C. R. M., BORNHEIMER, S. J. & FENOGLIO, D. 2023. An optimized flow cytometry protocol for simultaneous detection of T cell activation induced markers and intracellular cytokines: Application to SARS-CoV-2 immune individuals. *J Immunol Methods,* 515**,** 113443.

ALWINE, J. C., CASADEVALL, A., ENQUIST, L. W., GOODRUM, F. D. & IMPERIALE, M. J. 2023. A Critical Analysis of the Evidence for the SARS-CoV-2 Origin Hypotheses. *J Virol,* 97**,** e0036523.

AMINI, L., WAGNER, D. L., RÖSSLER, U., ZARRINRAD, G., WAGNER, L. F., VOLLMER, T., WENDERING, D. J., KORNAK, U., VOLK, H. D., REINKE, P. &

SCHMUECK-HENNERESSE, M. 2021. CRISPR-Cas9-Edited Tacrolimus-Resistant Antiviral T Cells for Advanced Adoptive Immunotherapy in Transplant Recipients. *Mol Ther,* 29**,** 32–46.

AMROLIA, P. J., MUCCIOLI-CASADEI, G., HULS, H., ADAMS, S., DURETT, A., GEE, A., YVON, E., WEISS, H., COBBOLD, M., GASPAR, H. B., ROONEY, C., KUEHNLE, I., GHETIE, V., SCHINDLER, J., KRANCE, R., HESLOP, H. E., VEYS, P., VITETTA, E. & BRENNER, M. K. 2006. Adoptive immunotherapy with allodepleted donor T-cells improves immune reconstitution after haploidentical stem cell transplantation. *Blood,* 108**,** 1797–808.

AMROLIA, P. J., MUCCIOLI-CASADEI, G., YVON, E., HULS, H., SILI, U., WIEDER, E. D., BOLLARD, C., MICHALEK, J., GHETIE, V., HESLOP, H. E., MOLLDREM, J. J., ROONEY, C. M., SCHLINDER, J., VITETTA, E. & BRENNER, M. K. 2003. Selective depletion of donor alloreactive T cells without loss of antiviral or antileukemic responses. *Blood,* 102**,** 2292–9.

AMYES, E., HATTON, C., MONTAMAT-SICOTTE, D., GUDGEON, N., RICKINSON, A. B., MCMICHAEL, A. J. & CALLAN, M. F. 2003. Characterization of the CD4+ T cell response to Epstein-Barr virus during primary and persistent infection. *J Exp Med,* 198**,** 903–11.

ANDERSEN, K. G., RAMBAUT, A., LIPKIN, W. I., HOLMES, E. C. & GARRY, R. F. 2020. The proximal origin of SARS-CoV-2. *Nat Med,* 26**,** 450–452.

ANDERSON, A. C., ANDERSON, D. E., BREGOLI, L., HASTINGS, W. D., KASSAM, N., LEI, C., CHANDWASKAR, R., KARMAN, J., SU, E. W., HIRASHIMA, M., BRUCE, J. N., KANE, L. P., KUCHROO, V. K. & HAFLER, D. A. 2007. Promotion of tissue inflammation by the immune receptor Tim-3 expressed on innate immune cells. *Science,* 318**,** 1141–3.

ANDERSON, B. E., MCNIFF, J., YAN, J., DOYLE, H., MAMULA, M., SHLOMCHIK, M. J. & SHLOMCHIK, W. D. 2003. Memory CD4+ T cells do not induce graft-versus-host disease. *J Clin Invest,* 112**,** 101–8.

ANDREI, G., TROMPET, E. & SNOECK, R. 2019. Novel Therapeutics for Epstein–Barr Virus. *Molecules,* 24.

ANGELINI, M. M., AKHLAGHPOUR, M., NEUMAN, B. W. & BUCHMEIER, M. J. 2013. Severe acute respiratory syndrome coronavirus nonstructural proteins 3, 4, and 6 induce double-membrane vesicles. *mBio,* 4.

ANSARI, M. A., SINGH, V. V., DUTTA, S., VEETTIL, M. V., DUTTA, D., CHIKOTI, L., LU, J., EVERLY, D. & CHANDRAN, B. 2013. Constitutive interferon-inducible protein 16-inflammasome activation during Epstein-Barr virus latency I, II, and III in B and epithelial cells. *J Virol,* 87**,** 8606–23.

APCHER, S., DASKALOGIANNI, C., MANOURY, B. & FÅHRAEUS, R. 2010. Epstein Barr virus-encoded EBNA1 interference with MHC class I antigen presentation reveals a close correlation between mRNA translation initiation and antigen presentation. *PLoS Pathog,* 6**,** e1001151.

ARCHBOLD, J. K., ELY, L. K., KJER-NIELSEN, L., BURROWS, S. R., ROSSJOHN, J., MCCLUSKEY, J. & MACDONALD, W. A. 2008. T cell allorecognition and MHC restriction--A case of Jekyll and Hyde? *Mol Immunol,* 45**,** 583–98.

ARMAND, P., ENGERT, A., YOUNES, A., FANALE, M., SANTORO, A., ZINZANI, P. L., TIMMERMAN, J. M., COLLINS, G. P., RAMCHANDREN, R., COHEN, J. B., DE BOER, J. P., KURUVILLA, J., SAVAGE, K. J., TRNENY, M., SHIPP, M. A., KATO, K., SUMBUL, A., FARSACI, B. & ANSELL, S. M. 2018. Nivolumab for Relapsed/Refractory Classic Hodgkin Lymphoma After Failure of Autologous Hematopoietic Cell Transplantation: Extended Follow-Up of the Multicohort Single-Arm Phase II CheckMate 205 Trial. *J Clin Oncol,* 36**,** 1428–1439.

ARVEY, A., TEMPERA, I., TSAI, K., CHEN, H. S., TIKHMYANOVA, N., KLICHINSKY, M., LESLIE, C. & LIEBERMAN, P. M. 2012. An atlas of the Epstein-Barr virus transcriptome and epigenome reveals host-virus regulatory interactions. *Cell Host Microbe,* 12**,** 233–45.

ARYA, R., KUMARI, S., PANDEY, B., MISTRY, H., BIHANI, S. C., DAS, A., PRASHAR, V., GUPTA, G. D., PANICKER, L. & KUMAR, M. 2021. Structural insights into SARS-CoV-2 proteins. *J Mol Biol,* 433**,** 166725.

ASHBY, K. M. & HOGQUIST, K. A. 2024. A guide to thymic selection of T cells. *Nat Rev Immunol,* 24**,** 103–117.

ASLEH, R., CLAVELL, A. L., PEREIRA, N. L., SMITH, B., BRIASOULIS, A., ALNSASRA, H., KREMERS, W. K., HABERMANN, T. M., OTLEY, C. C., LI, X., EDWARDS, B. S., STULAK, J. M., DALY, R. C. & KUSHWAHA, S. S. 2019. Incidence of Malignancies in Patients Treated With Sirolimus Following Heart Transplantation. *J Am Coll Cardiol,* 73**,** 2676–2688.

ATALLAH-YUNES, S. A., SALMAN, O. & ROBERTSON, M. J. 2023. Post-transplant lymphoproliferative disorder: Update on treatment and novel therapies. *Br J Haematol,* 201**,** 383–395.

AZZI, T., LÜNEMANN, A., MURER, A., UEDA, S., BÉZIAT, V., MALMBERG, K. J., STAUBLI, G., GYSIN, C., BERGER, C., MÜNZ, C., CHIJIOKE, O. & NADAL, D. 2014. Role for early-differentiated natural killer cells in infectious mononucleosis. *Blood,* 124**,** 2533–43.

BACHER, P., SCHINK, C., TEUTSCHBEIN, J., KNIEMEYER, O., ASSENMACHER, M., BRAKHAGE, A. A. & SCHEFFOLD, A. 2013. Antigen-reactive T cell enrichment for direct, high-resolution analysis of the human naive and memory Th cell repertoire. *J Immunol,* 190**,** 3967–76.

BACHMANN, M. F., GALLIMORE, A., JONES, E., ECABERT, B., ACHA-ORBEA, H. & KOPF, M. 2001. Normal pathogen-specific immune responses mounted by CTLA-4-deficient T cells: a paradigm reconsidered. *Eur J Immunol,* 31**,** 450–8.

BAER, R., BANKIER, A. T., BIGGIN, M. D., DEININGER, P. L., FARRELL, P. J., GIBSON, T. J., HATFULL, G., HUDSON, G. S., SATCHWELL, S. C., SÉGUIN, C. & ET AL. 1984. DNA sequence and expression of the B95-8 Epstein-Barr virus genome. *Nature,* 310**,** 207–11.

BAESSLER, A. & VIGNALI, D. A. A. 2024. T Cell Exhaustion. *Annu Rev Immunol,* 42**,** 179–206.

BAGAEV, D. V., VROOMANS, R. M. A., SAMIR, J., STERVBO, U., RIUS, C., DOLTON, G., GREENSHIELDS-WATSON, A., ATTAF, M., EGOROV, E. S., ZVYAGIN, I. V., BABEL, N., COLE, D. K., GODKIN, A. J., SEWELL, A. K., KESMIR, C., CHUDAKOV, D. M., LUCIANI, F. & SHUGAY, M. 2020. VDJdb in 2019: database extension, new analysis infrastructure and a T-cell receptor motif compendium. *Nucleic Acids Res,* 48**,** D1057–d1062.

BAGDONAITE, I. & WANDALL, H. H. 2018. Global aspects of viral glycosylation. *Glycobiology,* 28**,** 443–467.

BAI, C., ZHONG, Q. & GAO, G. F. 2022. Overview of SARS-CoV-2 genome-encoded proteins. *Sci China Life Sci,* 65**,** 280–294.

BALFOUR, H. H., JR., ODUMADE, O. A., SCHMELING, D. O., MULLAN, B. D., ED, J. A., KNIGHT, J. A., VEZINA, H. E., THOMAS, W. & HOGQUIST, K. A. 2013. Behavioral, virologic, and immunologic factors associated with acquisition and severity of primary Epstein-Barr virus infection in university students. *J Infect Dis,* 207**,** 80–8.

BANCHEREAU, J., BAZAN, F., BLANCHARD, D., BRIÈRE, F., GALIZZI, J. P., VAN KOOTEN, C., LIU, Y. J., ROUSSET, F. & SAELAND, S. 1994. The CD40 antigen and its ligand. *Annu Rev Immunol,* 12**,** 881–922.

BANKIER, A. T., DEININGER, P. L., SATCHWELL, S. C., BAER, R., FARRELL, P. J. & BARRELL, B. G. 1983. DNA sequence analysis of the EcoRI Dhet fragment of B95-8 Epstein-Barr virus containing the terminal repeat sequences. *Mol Biol Med,* 1**,** 425–45.

BANTA, K. L., XU, X., CHITRE, A. S., AU-YEUNG, A., TAKAHASHI, C., O'GORMAN, W. E., WU, T. D., MITTMAN, S., CUBAS, R., COMPS-AGRAR, L., FULZELE, A., BENNETT, E. J., GROGAN, J. L., HUI, E., CHIANG, E. Y. & MELLMAN, I. 2022. Mechanistic convergence of the TIGIT and PD-1 inhibitory pathways necessitates co-blockade to optimize anti-tumor CD8(+) T cell responses. *Immunity,* 55**,** 512–526.e9.

BANU, N., PANIKAR, S. S., LEAL, L. R. & LEAL, A. R. 2020. Protective role of ACE2 and its downregulation in SARS-CoV-2 infection leading to Macrophage Activation Syndrome: Therapeutic implications. *Life Sci,* 256**,** 117905.

BARDHAN, K., ANAGNOSTOU, T. & BOUSSIOTIS, V. A. 2016. The PD1:PD-L1/2 Pathway from Discovery to Clinical Implementation. *Front Immunol,* 7**,** 550.

BARKER, J. N., DOUBROVINA, E., SAUTER, C., JAROSCAK, J. J., PERALES, M. A., DOUBROVIN, M., PROCKOP, S. E., KOEHNE, G. & O'REILLY, R. J. 2010. Successful treatment of EBV-associated posttransplantation lymphoma after cord blood transplantation using third-party EBV-specific cytotoxic T lymphocytes. *Blood,* 116**,** 5045–9.

BARNES, S., SCHILIZZI, O., AUDSLEY, K. M., NEWNES, H. V. & FOLEY, B. 2020. Deciphering the Immunological Phenomenon of Adaptive Natural Killer (NK) Cells and Cytomegalovirus (CMV). *Int J Mol Sci,* 21.

BARRETT, A. J. & BOLLARD, C. M. 2015. The coming of age of adoptive T-cell therapy for viral infection after stem cell transplantation. *Ann Transl Med,* 3**,** 62.

BARROS, M. H., VERA-LOZADA, G., SOARES, F. A., NIEDOBITEK, G. & HASSAN, R. 2012. Tumor microenvironment composition in pediatric classical Hodgkin lymphoma is modulated by age and Epstein-Barr virus infection. *Int J Cancer,* 131**,** 1142–52.

BASAR, R., DAHER, M., UPRETY, N., GOKDEMIR, E., ALSULIMAN, A., ENSLEY, E., OZCAN, G., MENDT, M., HERNANDEZ SANABRIA, M., KERBAUY, L. N., NUNEZ CORTES, A. K., LI, L., BANERJEE, P. P., MUNIZ-FELICIANO, L., ACHARYA, S., FOWLKES, N. W., LU, J., LI, S., MIELKE, S., KAPLAN, M., NANDIVADA, V., BDAIWI, M., KONTOYIANNIS, A. D., LI, Y., LIU, E., ANG, S., MARIN, D., BRUNETTI, L., GUNDRY, M. C., TURK, R., SCHUBERT, M. S., RETTIG, G. R., MCNEILL, M. S., KURGAN, G., BEHLKE, M. A., CHAMPLIN, R., SHPALL, E. J. & REZVANI, K. 2020. Large-scale GMP-compliant CRISPR-Cas9-mediated deletion of the glucocorticoid receptor in multivirus-specific T cells. *Blood Adv,* 4**,** 3357–3367.

BASAR, R., UPRETY, N., ENSLEY, E., DAHER, M., KLEIN, K., MARTINEZ, F., AUNG, F., SHANLEY, M., HU, B., GOKDEMIR, E., NUNEZ CORTES, A. K., MENDT, M., REYES SILVA, F., ACHARYA, S., LASKOWSKI, T., MUNIZ-FELICIANO, L., BANERJEE, P. P., LI, Y., LI, S., MELO GARCIA, L., LIN, P., SHAIM, H., YATES, S. G., MARIN, D., KAUR, I., RAO, S., MAK, D., LIN, A., MIAO, Q., DOU, J., CHEN, K., CHAMPLIN, R. E., SHPALL, E. J. & REZVANI, K. 2021. Generation of glucocorticoid-resistant SARS-CoV-2 T cells for adoptive cell therapy. *Cell Rep,* 36**,** 109432.

BASTIAN, M., HEYMANN, S. & JACOMY, M. 2009. Gephi: An Open Source Software for Exploring and Manipulating Networks. *Proceedings of the International AAAI Conference on Web and Social Media,* 3**,** 361–362.

BASTIEN, J. P., KROSL, G., THERIEN, C., RASHKOVAN, M., SCOTTO, C., COHEN, S., ALLAN, D. S., HOGGE, D., EGELER, R. M., PERREAULT, C. & ROY, D. C. 2010. Photodepletion differentially affects CD4+ Tregs versus CD4+ effector T cells from patients with chronic graft-versus-host disease. *Blood,* 116**,** 4859–69.

BECK, A., PÄZOLT, D., GRABENBAUER, G. G., NICHOLLS, J. M., HERBST, H., YOUNG, L. S. & NIEDOBITEK, G. 2001. Expression of cytokine and chemokine genes in Epstein-Barr virus-associated nasopharyngeal carcinoma: comparison with Hodgkin's disease. *J Pathol,* 194**,** 145–51.

BECKER, S., LANG, H., VOLLMER BARBOSA, C., TIAN, Z., MELK, A. & SCHMIDT, B. M. W. 2023. Efficacy of CytoSorb®: a systematic review and meta-analysis. *Crit Care,* 27**,** 215.

BERGANTINI, L., D'ALESSANDRO, M., CAMELI, P., CAVALLARO, D., GANGI, S., CEKORJA, B., SESTINI, P. & BARGAGLI, E. 2021. NK and T Cell Immunological Signatures in Hospitalized Patients with COVID-19. *Cells,* 10.

BERGER, C., JENSEN, M. C., LANSDORP, P. M., GOUGH, M., ELLIOTT, C. & RIDDELL, S. R. 2008. Adoptive transfer of effector CD8+ T cells derived from central memory cells establishes persistent T cell memory in primates. *J Clin Invest,* 118**,** 294–305.

BERGHUIS, D., DE HOOGE, A. S., SANTOS, S. J., HORST, D., WIERTZ, E. J., VAN EGGERMOND, M. C., VAN DEN ELSEN, P. J., TAMINIAU, A. H., OTTAVIANO, L., SCHAEFER, K. L., DIRKSEN, U., HOOIJBERG, E., MULDER, A., MELIEF, C. J., EGELER, R. M., SCHILHAM, M. W., JORDANOVA, E. S., HOGENDOORN, P. C. & LANKESTER, A. C. 2009. Reduced human leukocyte antigen expression in advanced-stage Ewing sarcoma: implications for immune recognition. *J Pathol,* 218**,** 222–31.

BETTS, M. R., BRENCHLEY, J. M., PRICE, D. A., DE ROSA, S. C., DOUEK, D. C., ROEDERER, M. & KOUP, R. A. 2003. Sensitive and viable identification of antigen-specific CD8+ T cells by a flow cytometric assay for degranulation. *J Immunol Methods,* 281**,** 65–78.

BIRKENBACH, M., TONG, X., BRADBURY, L. E., TEDDER, T. F. & KIEFF, E. 1992. Characterization of an Epstein-Barr virus receptor on human epithelial cells. *J Exp Med,* 176**,** 1405–14.

BISHNOI, S., KOTASEK, D., AGHMESHEH, M., YAU, T., COSMAN, R., PRAWIRA, A., MOORE, M., CHAN, S. L., MANT, A., EEK, R., ZIELINSKI, R., SU, R., PAN, Z., MA, Y., LI, F., LI, P. & TSE, A. N. 2024. Dual CTLA-4 and PD-1 checkpoint blockade using CS1002 and CS1003 (nofazinlimab) in patients with advanced solid tumors: A first-in-human, dose-escalation, and dose-expansion study. *Cancer,* 130**,** 1991–2002.

BJÖRKSTRÖM, N. K., LINDGREN, T., STOLTZ, M., FAURIAT, C., BRAUN, M., EVANDER, M., MICHAËLSSON, J., MALMBERG, K. J., KLINGSTRÖM, J., AHLM, C. & LJUNGGREN, H. G. 2011. Rapid expansion and long-term persistence of elevated NK cell numbers in humans infected with hantavirus. *J Exp Med,* 208**,** 13–21.

BLANK, C. U., HAINING, W. N., HELD, W., HOGAN, P. G., KALLIES, A., LUGLI, E., LYNN, R. C., PHILIP, M., RAO, A., RESTIFO, N. P., SCHIETINGER, A., SCHUMACHER, T. N., SCHWARTZBERG, P. L., SHARPE, A. H., SPEISER, D. E., WHERRY, E. J., YOUNGBLOOD, B. A. & ZEHN, D. 2019. Defining 'T cell exhaustion'. *Nat Rev Immunol,* 19**,** 665–674.

BLOSS, T. A. & SUGDEN, B. 1994. Optimal lengths for DNAs encapsidated by Epstein-Barr virus. *J Virol,* 68**,** 8217–22.

BOD, L., KYE, Y. C., SHI, J., TORLAI TRIGLIA, E., SCHNELL, A., FESSLER, J., OSTROWSKI, S. M., VON-FRANQUE, M. Y., KUCHROO, J. R., BARILLA, R. M., ZAGHOUANI, S., CHRISTIAN, E., DELOREY, T. M., MOHIB, K., XIAO, S., SLINGERLAND, N., GIULIANO, C. J., ASHENBERG, O., LI, Z., ROTHSTEIN, D. M., FISHER, D. E., ROZENBLATT-ROSEN, O., SHARPE, A. H., QUINTANA, F. J., APETOH, L., REGEV, A. & KUCHROO, V. K. 2023. B-cell-specific checkpoint molecules that regulate anti-tumour immunity. *Nature,* 619**,** 348–356.

BOECKH, M., ERARD, V., ZERR, D. & ENGLUND, J. 2005. Emerging viral infections after hematopoietic cell transplantation. *Pediatr Transplant,* 9 Suppl 7**,** 48–54.

BOGUNIA-KUBIK, K., JASKULA, E. & LANGE, A. 2007. The presence of functional CCR5 and EBV reactivation after allogeneic haematopoietic stem cell transplantation. *Bone Marrow Transplant,* 40**,** 145–50.

BOISE, L. H., MINN, A. J., NOEL, P. J., JUNE, C. H., ACCAVITTI, M. A., LINDSTEN, T. & THOMPSON, C. B. 1995. CD28 costimulation can promote T cell survival by enhancing the expression of Bcl-XL. *Immunity,* 3**,** 87–98.

BOLLARD, C. M., AGUILAR, L., STRAATHOF, K. C., GAHN, B., HULS, M. H., ROUSSEAU, A., SIXBEY, J., GRESIK, M. V., CARRUM, G., HUDSON, M., DILLOO, D., GEE, A., BRENNER, M. K., ROONEY, C. M. & HESLOP, H. E. 2004. Cytotoxic T lymphocyte therapy for Epstein-Barr virus+ Hodgkin's disease. *J Exp Med,* 200**,** 1623–33.

BOLLARD, C. M., GOTTSCHALK, S., TORRANO, V., DIOUF, O., KU, S., HAZRAT, Y., CARRUM, G., RAMOS, C., FAYAD, L., SHPALL, E. J., PRO, B., LIU, H., WU, M. F., LEE, D., SHEEHAN, A. M., ZU, Y., GEE, A. P., BRENNER, M. K., HESLOP, H. E. & ROONEY, C. M. 2014. Sustained complete responses in patients with lymphoma receiving autologous cytotoxic T lymphocytes targeting Epstein-Barr virus latent membrane proteins. *J Clin Oncol,* 32**,** 798–808.

BOLLARD, C. M. & HESLOP, H. E. 2016. T cells for viral infections after allogeneic hematopoietic stem cell transplant. *Blood,* 127**,** 3331–40.

BOLLARD, C. M., ROONEY, C. M. & HESLOP, H. E. 2012. T-cell therapy in the treatment of post-transplant lymphoproliferative disease. *Nat Rev Clin Oncol,* 9**,** 510–9.

BOLLARD, C. M., RÖSSIG, C., CALONGE, M. J., HULS, M. H., WAGNER, H. J., MASSAGUE, J., BRENNER, M. K., HESLOP, H. E. & ROONEY, C. M. 2002. Adapting a transforming growth factor beta-related tumor protection strategy to enhance antitumor immunity. *Blood,* 99**,** 3179–87.

BOLLARD, C. M., TRIPIC, T., CRUZ, C. R., DOTTI, G., GOTTSCHALK, S., TORRANO, V., DAKHOVA, O., CARRUM, G., RAMOS, C. A., LIU, H., WU, M. F., MARCOGLIESE, A. N., BARESE, C., ZU, Y., LEE, D. Y., O'CONNOR, O., GEE, A. P., BRENNER, M. K., HESLOP, H. E. & ROONEY, C. M. 2018. Tumor-Specific T-Cells Engineered to Overcome Tumor Immune Evasion Induce Clinical Responses in Patients With Relapsed Hodgkin Lymphoma. *J Clin Oncol,* 36**,** 1128–1139.

BONECCHI, R. & GRAHAM, G. J. 2016. Atypical Chemokine Receptors and Their Roles in the Resolution of the Inflammatory Response. *Front Immunol,* 7**,** 224.

BONIFACIUS, A., LAMOTTKE, B., TISCHER-ZIMMERMANN, S., SCHULTZE-FLOREY, R., GOUDEVA, L., HEUFT, H. G., ARSENIEV, L., BEIER, R., BEUTEL, G., CARIO, G., FRÖHLICH, B., GREIL, J., HANSMANN, L., HASENKAMP, J., HÖFS, M., HUNDSDOERFER, P., JOST, E., KAFA, K., KRIEGE, O., KRÖGER, N., MATHAS, S., MEISEL, R., NATHRATH, M., PUTKONEN, M., RAVENS, S.,

REINHARDT, H. C., SALA, E., SAUER, M. G., SCHMITT, C., SCHROERS, R., STECKEL, N. K., TRAPPE, R. U., VERBEEK, M., WOLFF, D., BLASCZYK, R., EIZ-VESPER, B. & MAECKER-KOLHOFF, B. 2023. Patient-tailored adoptive immunotherapy with EBV-specific T cells from related and unrelated donors. *J Clin Invest,* 133.

BONIFACIUS, A., TISCHER-ZIMMERMANN, S., DRAGON, A. C., GUSSAROW, D., VOGEL, A., KRETTEK, U., GÖDECKE, N., YILMAZ, M., KRAFT, A. R. M., HOEPER, M. M., PINK, I., SCHMIDT, J. J., LI, Y., WELTE, T., MAECKER-KOLHOFF, B., MARTENS, J., BERGER, M. M., LOBENWEIN, C., STANKOV, M. V., CORNBERG, M., DAVID, S., BEHRENS, G. M. N., WITZKE, O., BLASCZYK, R. & EIZ-VESPER, B. 2021. COVID-19 immune signatures reveal stable antiviral T cell function despite declining humoral responses. *Immunity,* 54**,** 340–354.e6.

BONIFACIUS, A., TISCHER-ZIMMERMANN, S., SANTAMORENA, M. M., MAUSBERG, P., SCHENK, J., KOCH, S., BARNSTORF-BRANDES, J., GÖDECKE, N., MARTENS, J., GOUDEVA, L., VERBOOM, M., WITTIG, J., MAECKER-KOLHOFF, B., BAURMANN, H., CLARK, C., BRAUNS, O., SIMON, M., LANG, P., CORNELY, O. A., HALLEK, M., BLASCZYK, R., SEIFERLING, D., KÖHLER, P. & EIZ-VESPER, B. 2022. Rapid Manufacturing of Highly Cytotoxic Clinical-Grade SARS-CoV-2-specific T Cell Products Covering SARS-CoV-2 and Its Variants for Adoptive T Cell Therapy. *Front Bioeng Biotechnol,* 10**,** 867042.

BORDIGNON, C., CARLO-STELLA, C., COLOMBO, M. P., DE VINCENTIIS, A., LANATA, L., LEMOLI, R. M., LOCATELLI, F., OLIVIERI, A., RONDELLI, D., ZANON, P. & TURA, S. 1999. Cell therapy: achievements and perspectives. *Haematologica,* 84**,** 1110–49.

BORZA, C. M. & HUTT-FLETCHER, L. M. 2002. Alternate replication in B cells and epithelial cells switches tropism of Epstein-Barr virus. *Nat Med,* 8**,** 594–9.

BOURBON, E., MAUCORT-BOULCH, D., FONTAINE, J., MAUDUIT, C., SESQUES, P., SAFAR, V., FERRANT, E., GOLFIER, C., GHERGUS, D., KARLIN, L., LAZARETH, A., BOUAFIA, F., PICA, G. M., ORSINI-PIOCELLE, F., ROCHER, C., GROS, F. X., PARRENS, M., DONY, A., ROSSI, C., GHESQUIÈRES, H., BACHY, E., TRAVERSE-GLEHEN, A. & SARKOZY, C. 2021. Clinicopathological features and survival in EBV-positive diffuse large B-cell lymphoma not otherwise specified. *Blood Adv,* 5**,** 3227–3239.

BOUSSIOTIS, V. A. 2016. Molecular and Biochemical Aspects of the PD-1 Checkpoint Pathway. *N Engl J Med,* 375**,** 1767–1778.

BRAUN, J., LOYAL, L., FRENTSCH, M., WENDISCH, D., GEORG, P., KURTH, F., HIPPENSTIEL, S., DINGELDEY, M., KRUSE, B., FAUCHERE, F., BAYSAL, E., MANGOLD, M., HENZE, L., LAUSTER, R., MALL, M. A., BEYER, K., RÖHMEL, J., VOIGT, S., SCHMITZ, J., MILTENYI, S., DEMUTH, I., MÜLLER, M. A., HOCKE, A., WITZENRATH, M., SUTTORP, N., KERN, F., REIMER, U., WENSCHUH, H., DROSTEN, C., CORMAN, V. M., GIESECKE-THIEL, C., SANDER, L. E. & THIEL, A. 2020. SARS-CoV-2-reactive T cells in healthy donors and patients with COVID-19. *Nature,* 587**,** 270–274.

BRAUNECK, F., FISCHER, B., WITT, M., MUSCHHAMMER, J., OELRICH, J., DA COSTA AVELAR, P. H., TSOKA, S., BULLINGER, L., SEUBERT, E., SMIT, D. J., BOKEMEYER, C., ACKERMANN, C., WELLBROCK, J., HAAG, F. & FIEDLER, W. 2022. TIGIT blockade repolarizes AML-associated TIGIT(+) M2 macrophages to an M1 phenotype and increases CD47-mediated phagocytosis. *J Immunother Cancer,* 10.

BRAUNING, A., RAE, M., ZHU, G., FULTON, E., ADMASU, T. D., STOLZING, A. & SHARMA, A. 2022. Aging of the Immune System: Focus on Natural Killer Cells Phenotype and Functions. *Cells,* 11.

BRESTRICH, G., ZWINGER, S., FISCHER, A., SCHMÜCK, M., RÖHMHILD, A., HAMMER, M. H., KURTZ, A., UHAREK, L., KNOSALLA, C., LEHMKUHL, H., VOLK, H. D. & REINKE, P. 2009. Adoptive T-cell therapy of a lung transplanted patient with severe CMV disease and resistance to antiviral therapy. *Am J Transplant,* 9**,** 1679–84.

BREWIN, J., MANCAO, C., STRAATHOF, K., KARLSSON, H., SAMARASINGHE, S., AMROLIA, P. J. & PULE, M. 2009. Generation of EBV-specific cytotoxic T cells that are resistant to calcineurin inhibitors for the treatment of posttransplantation lymphoproliferative disease. *Blood,* 114**,** 4792–803.

BRISTOL, J. A., NELSON, S. E., OHASHI, M., CASCO, A., HAYES, M., RANHEIM, E. A., PAWELSKI, A. S., SINGH, D. R., HODSON, D. J., JOHANNSEN, E. C. & KENNEY, S. C. 2024. Latent Epstein-Barr virus infection collaborates with Myc over-expression in normal human B cells to induce Burkitt-like Lymphomas in mice. *PLoS Pathog,* 20**,** e1012132.

BRITANOVA, O. V., SHUGAY, M., MERZLYAK, E. M., STAROVEROV, D. B., PUTINTSEVA, E. V., TURCHANINOVA, M. A., MAMEDOV, I. Z., POGORELYY, M. V., BOLOTIN, D. A., IZRAELSON, M., DAVYDOV, A. N., EGOROV, E. S., KASATSKAYA, S. A., REBRIKOV, D. V., LUKYANOV, S. & CHUDAKOV, D. M. 2016. Dynamics of Individual T Cell Repertoires: From Cord Blood to Centenarians. *J Immunol,* 196**,** 5005–13.

BRODIN, P. 2021. Immune determinants of COVID-19 disease presentation and severity. *Nat Med,* 27**,** 28–33.

BROMBERG, J. E. C., ISSA, S., BAKUNINA, K., MINNEMA, M. C., SEUTE, T., DURIAN, M., CULL, G., SCHOUTEN, H. C., STEVENS, W. B. C., ZIJLSTRA, J. M., BAARS, J. W., NIJLAND, M., MASON, K. D., BEEKER, A., VAN DEN BENT, M. J., BEIJERT, M., GONZALES, M., DE JONG, D. & DOORDUIJN, J. K. 2019. Rituximab in patients with primary CNS lymphoma (HOVON 105/ALLG NHL 24): a randomised, open-label, phase 3 intergroup study. *Lancet Oncol,* 20**,** 216–228.

BRUNET, J. F., DENIZOT, F., LUCIANI, M. F., ROUX-DOSSETO, M., SUZAN, M., MATTEI, M. G. & GOLSTEIN, P. 1987. A new member of the immunoglobulin superfamily--CTLA-4. *Nature,* 328**,** 267–70.

BRYANT, H. & FARRELL, P. J. 2002. Signal Transduction and Transcription Factor Modification during Reactivation of Epstein-Barr Virus from Latency. *J Virol,* 76**,** 10290–8.

BU, W., JOYCE, M. G., NGUYEN, H., BANH, D. V., AGUILAR, F., TARIQ, Z., YAP, M. L., TSUJIMURA, Y., GILLESPIE, R. A., TSYBOVSKY, Y., ANDREWS, S. F., NARPALA, S. R., MCDERMOTT, A. B., ROSSMANN, M. G., YASUTOMI, Y., NABEL, G. J., KANEKIYO, M. & COHEN, J. I. 2019. Immunization with Components of the Viral Fusion Apparatus Elicits Antibodies That Neutralize Epstein-Barr Virus in B Cells and Epithelial Cells. *Immunity,* 50**,** 1305–1316.e6.

BUTTE, M. J., KEIR, M. E., PHAMDUY, T. B., SHARPE, A. H. & FREEMAN, G. J. 2007. Programmed death-1 ligand 1 interacts specifically with the B7-1 costimulatory molecule to inhibit T cell responses. *Immunity,* 27**,** 111–22.

CADUFF, N., MCHUGH, D., MURER, A., RÄMER, P., RAYKOVA, A., LANDTWING, V., RIEBLE, L., KELLER, C. W., PRUMMER, M., HOFFMANN, L., LAM, J. K. P., CHIANG, A. K. S., RAULF, F., AZZI, T., BERGER, C., RUBIC-SCHNEIDER, T., TRAGGIAI, E., LÜNEMANN, J. D., KAMMÜLLER, M. & MÜNZ, C. 2020. Immunosuppressive FK506 treatment leads to more frequent EBV-

associated lymphoproliferative disease in humanized mice. *PLoS Pathog,* 16**,** e1008477.

CAMPBELL, G. R., TO, R. K., HANNA, J. & SPECTOR, S. A. 2021. SARS-CoV-2, SARS-CoV-1, and HIV-1 derived ssRNA sequences activate the NLRP3 inflammasome in human macrophages through a non-classical pathway. *iScience,* 24**,** 102295.

CAMPBELL, J. D. 2003. Detection and enrichment of antigen-specific CD4+ and CD8+ T cells based on cytokine secretion. *Methods,* 31**,** 150–9.

CAMPBELL, J. D., FOERSTER, A., LASMANOWICZ, V., NIEMÖLLER, M., SCHEFFOLD, A., FAHRENDORFF, M., RAUSER, G., ASSENMACHER, M. & RICHTER, A. 2011. Rapid detection, enrichment and propagation of specific T cell subsets based on cytokine secretion. *Clin Exp Immunol,* 163**,** 1–10.

CAMPO, E., JAFFE, E. S., COOK, J. R., QUINTANILLA-MARTINEZ, L., SWERDLOW, S. H., ANDERSON, K. C., BROUSSET, P., CERRONI, L., DE LEVAL, L., DIRNHOFER, S., DOGAN, A., FELDMAN, A. L., FEND, F., FRIEDBERG, J. W., GAULARD, P., GHIA, P., HORWITZ, S. M., KING, R. L., SALLES, G., SAN-MIGUEL, J., SEYMOUR, J. F., TREON, S. P., VOSE, J. M., ZUCCA, E., ADVANI, R., ANSELL, S., AU, W. Y., BARRIONUEVO, C., BERGSAGEL, L., CHAN, W. C., COHEN, J. I., D'AMORE, F., DAVIES, A., FALINI, B., GHOBRIAL, I. M., GOODLAD, J. R., GRIBBEN, J. G., HSI, E. D., KAHL, B. S., KIM, W. S., KUMAR, S., LACASCE, A. S., LAURENT, C., LENZ, G., LEONARD, J. P., LINK, M. P., LOPEZ-GUILLERMO, A., MATEOS, M. V., MACINTYRE, E., MELNICK, A. M., MORSCHHAUSER, F., NAKAMURA, S., NARBAITZ, M., PAVLOVSKY, A., PILERI, S. A., PIRIS, M., PRO, B., RAJKUMAR, V., ROSEN, S. T., SANDER, B., SEHN, L., SHIPP, M. A., SMITH, S. M., STAUDT, L. M., THIEBLEMONT, C., TOUSSEYN, T., WILSON, W. H., YOSHINO, T., ZINZANI, P. L., DREYLING, M., SCOTT, D. W., WINTER, J. N. & ZELENETZ, A. D. 2022. The International Consensus Classification of Mature Lymphoid Neoplasms: a report from the Clinical Advisory Committee. *Blood,* 140**,** 1229–1253.

CAO, X. 2020. COVID-19: immunopathology and its implications for therapy. *Nat Rev Immunol,* 20**,** 269–270.

CAPELLI, C., CUOFANO, C., PAVONI, C., FRIGERIO, S., LISINI, D., NAVA, S., QUARONI, M., COLOMBO, V., GALLI, F., BEZUKLADOVA, S., PANINA-BORDIGNON, P., GAIPA, G., COMOLI, P., COSSU, G., MARTINO, G., BIONDI, A., INTRONA, M. & GOLAY, J. 2023. Potency assays and biomarkers for cell-based advanced therapy medicinal products. *Front Immunol,* 14**,** 1186224.

CÁRDENAS SIERRA, D., VÉLEZ COLMENARES, G., ORFAO DE MATOS, A., FIORENTINO GÓMEZ, S. & QUIJANO GÓMEZ, S. M. 2014. Age-associated Epstein-Barr virus-specific T cell responses in seropositive healthy adults. *Clin Exp Immunol,* 177**,** 320–32.

CARSANA, L., SONZOGNI, A., NASR, A., ROSSI, R. S., PELLEGRINELLI, A., ZERBI, P., RECH, R., COLOMBO, R., ANTINORI, S., CORBELLINO, M., GALLI, M., CATENA, E., TOSONI, A., GIANATTI, A. & NEBULONI, M. 2020. Pulmonary post-mortem findings in a series of COVID-19 cases from northern Italy: a two-centre descriptive study. *Lancet Infect Dis,* 20**,** 1135–1140.

CASCELLA, M., RAJNIK, M., ALEEM, A., DULEBOHN, S. C. & DI NAPOLI, R. 2024. Features, Evaluation, and Treatment of Coronavirus (COVID-19). *StatPearls.* Treasure Island (FL) ineligible companies. Disclosure: Michael Rajnik declares no relevant financial relationships with ineligible companies. Disclosure: Abdul Aleem declares no relevant financial relationships with ineligible companies. Disclosure: Scott Dulebohn

declares no relevant financial relationships with ineligible companies. Disclosure: Raffaela Di Napoli declares no relevant financial relationships with ineligible companies.: StatPearls Publishing

CASSANITI, I., PERCIVALLE, E., BERGAMI, F., PIRALLA, A., COMOLLI, G., BRUNO, R., VECCHIA, M., SAMBO, M., COLANERI, M., ZUCCARO, V., BENAZZO, M., ROBOTTI, C., CALASTRI, A., MAIORANO, E., FERRARI, A., CAMBIÈ, G. & BALDANTI, F. 2021. SARS-CoV-2 specific T-cell immunity in COVID-19 convalescent patients and unexposed controls measured by ex vivo ELISpot assay. *Clin Microbiol Infect,* 27**,** 1029–1034.

CATALINA, M. D., SULLIVAN, J. L., BAK, K. R. & LUZURIAGA, K. 2001. Differential evolution and stability of epitope-specific CD8(+) T cell responses in EBV infection. *J Immunol,* 167**,** 4450–7.

CENERENTI, M., SAILLARD, M., ROMERO, P. & JANDUS, C. 2022. The Era of Cytotoxic CD4 T Cells. *Front Immunol,* 13**,** 867189.

CHA, E., GRAHAM, L., MANJILI, M. H. & BEAR, H. D. 2010. IL-7 + IL-15 are superior to IL-2 for the ex vivo expansion of 4T1 mammary carcinoma-specific T cells with greater efficacy against tumors in vivo. *Breast Cancer Res Treat,* 122**,** 359–69.

CHANG, C. M., FENG, P. H., WU, T. H., ALACHKAR, H., LEE, K. Y. & CHANG, W. C. 2021. Profiling of T Cell Repertoire in SARS-CoV-2-Infected COVID-19 Patients Between Mild Disease and Pneumonia. *J Clin Immunol,* 41**,** 1131–1145.

CHANG, J. 2021. MHC multimer: A Molecular Toolbox for Immunologists. *Mol Cells,* 44**,** 328–334.

CHANG, Y. J., ZHAO, X. Y., HUO, M. R. & HUANG, X. J. 2009. Expression of CD62L on donor CD4(+) T cells in allografts: correlation with graft-versus-host disease after unmanipulated allogeneic blood and marrow transplantation. *J Clin Immunol,* 29**,** 696–704.

CHANNAPPANAVAR, R., FEHR, A. R., VIJAY, R., MACK, M., ZHAO, J., MEYERHOLZ, D. K. & PERLMAN, S. 2016. Dysregulated Type I Interferon and Inflammatory Monocyte-Macrophage Responses Cause Lethal Pneumonia in SARS-CoV-Infected Mice. *Cell Host Microbe,* 19**,** 181–93.

CHAPMAN, A. L., RICKINSON, A. B., THOMAS, W. A., JARRETT, R. F., CROCKER, J. & LEE, S. P. 2001. Epstein-Barr virus-specific cytotoxic T lymphocyte responses in the blood and tumor site of Hodgkin's disease patients: implications for a T-cell-based therapy. *Cancer Res,* 61**,** 6219–26.

CHAPUIS, A. G., DESMARAIS, C., EMERSON, R., SCHMITT, T. M., SHIBUYA, K., LAI, I., WAGENER, F., CHOU, J., ROBERTS, I. M., COFFEY, D. G., WARREN, E., ROBBINS, H., GREENBERG, P. D. & YEE, C. 2017. Tracking the Fate and Origin of Clinically Relevant Adoptively Transferred CD8(+) T Cells In Vivo. *Sci Immunol,* 2.

CHATTOPADHYAY, P. K., YU, J. & ROEDERER, M. 2006. Live-cell assay to detect antigen-specific CD4+ T-cell responses by CD154 expression. *Nat Protoc,* 1**,** 1–6.

CHATZIANDREOU, I., GILMOUR, K. C., MCNICOL, A. M., COSTABILE, M., SINCLAIR, J., CUBITT, D., CAMPBELL, J. D., KINNON, C., QASIM, W. & GASPAR, H. B. 2007. Capture and generation of adenovirus specific T cells for adoptive immunotherapy. *Br J Haematol,* 136**,** 117–26.

CHEMNITZ, J. M., PARRY, R. V., NICHOLS, K. E., JUNE, C. H. & RILEY, J. L. 2004. SHP-1 and SHP-2 associate with immunoreceptor tyrosine-based switch motif of programmed death 1 upon primary human T cell stimulation, but only receptor ligation prevents T cell activation. *J Immunol,* 173**,** 945–54.

CHEN, B. J., CUI, X., LIU, C. & CHAO, N. J. 2002. Prevention of graft-versus-host disease while preserving graft-versus-leukemia effect after selective depletion of host-reactive T cells by photodynamic cell purging process. *Blood,* 99**,** 3083–8.

CHEN, B. J., CUI, X., SEMPOWSKI, G. D., LIU, C. & CHAO, N. J. 2004. Transfer of allogeneic CD62L- memory T cells without graft-versus-host disease. *Blood,* 103**,** 1534–41.

CHEN, B. J., DEOLIVEIRA, D., CUI, X., LE, N. T., SON, J., WHITESIDES, J. F. & CHAO, N. J. 2007. Inability of memory T cells to induce graft-versus-host disease is a result of an abortive alloresponse. *Blood,* 109**,** 3115–23.

CHEN, G., WU, D., GUO, W., CAO, Y., HUANG, D., WANG, H., WANG, T., ZHANG, X., CHEN, H., YU, H., ZHANG, X., ZHANG, M., WU, S., SONG, J., CHEN, T., HAN, M., LI, S., LUO, X., ZHAO, J. & NING, Q. 2020. Clinical and immunological features of severe and moderate coronavirus disease 2019. *J Clin Invest,* 130**,** 2620–2629.

CHEN, L. & FLIES, D. B. 2013. Molecular mechanisms of T cell co-stimulation and co-inhibition. *Nat Rev Immunol,* 13**,** 227–42.

CHEN, Q., CHIA, A., HANG, S. K., LIM, A., KOH, W. K., PENG, Y., GAO, F., CHEN, J., HO, Z., WAI, L. E., KUNASEGARAN, K., TAN, A. T., LE BERT, N., LOH, C. Y., GOH, Y. S., RENIA, L., DONG, T., VATHSALA, A. & BERTOLETTI, A. 2023. Engineering immunosuppressive drug-resistant armored (IDRA) SARS-CoV-2 T cells for cell therapy. *Cell Mol Immunol,* 20**,** 1300–1312.

CHEN, Z., YUAN, Y., HU, Q., ZHU, A., CHEN, F., LI, S., GUAN, X., LV, C., TANG, T., HE, Y., CHENG, J., ZHENG, J., HU, X., ZHAO, J., ZHAO, J. & SUN, J. 2024. SARS-CoV-2 immunity in animal models. *Cell Mol Immunol,* 21**,** 119–133.

CHÉREL, M., CHOUFI, B., TRAUET, J., CRACCO, P., DESSAINT, J. P., YAKOUB-AGHA, I. & LABALETTE, M. 2014. Naïve subset develops the most important alloreactive response among human CD4+ T lymphocytes in human leukocyte antigen-identical related setting. *Eur J Haematol,* 92**,** 491–6.

CHESNOKOVA, L. S., NISHIMURA, S. L. & HUTT-FLETCHER, L. M. 2009. Fusion of epithelial cells by Epstein-Barr virus proteins is triggered by binding of viral glycoproteins gHgL to integrins alphavbeta6 or alphavbeta8. *Proc Natl Acad Sci U S A,* 106**,** 20464–9.

CHETAILLE, B., BERTUCCI, F., FINETTI, P., ESTERNI, B., STAMATOULLAS, A., PICQUENOT, J. M., COPIN, M. C., MORSCHHAUSER, F., CASASNOVAS, O., PETRELLA, T., MOLINA, T., VEKHOFF, A., FEUGIER, P., BOUABDALLAH, R., BIRNBAUM, D., OLIVE, D. & XERRI, L. 2009. Molecular profiling of classical Hodgkin lymphoma tissues uncovers variations in the tumor microenvironment and correlations with EBV infection and outcome. *Blood,* 113**,** 2765–3775.

CHEUNG, S. T., LEUNG, S. F., LO, K. W., CHIU, K. W., TAM, J. S., FOK, T. F., JOHNSON, P. J., LEE, J. C. & HUANG, D. P. 1998. Specific latent membrane protein 1 gene sequences in type 1 and type 2 Epstein-Barr virus from nasopharyngeal carcinoma in Hong Kong. *Int J Cancer,* 76**,** 399–406.

CHIA, T. Y., BILLINGHAM, L. K., BOLAND, L., KATZ, J. L., ARRIETA, V. A., SHIREMAN, J., ROSAS, A. L., DELAY, S. L., ZILLINGER, K., GENG, Y., KRUGER, J., SILVERS, C., WANG, H., VAZQUEZ CERVANTES, G. I., HOU, D., WANG, S., WAN, H., SONABEND, A., ZHANG, P., LEE-CHANG, C. & MISKA, J. 2023. The CXCL16-CXCR6 axis in glioblastoma modulates T-cell activity in a spatiotemporal context. *Front Immunol,* 14**,** 1331287.

CHIFFELLE, J., GENOLET, R., PEREZ, M. A., COUKOS, G., ZOETE, V. & HARARI, A. 2020. T-cell repertoire analysis and metrics of diversity and clonality. *Curr Opin Biotechnol,* 65**,** 284–295.

CHIKUMA, S. & BLUESTONE, J. A. 2007. Expression of CTLA-4 and FOXP3 in cis protects from lethal lymphoproliferative disease. *Eur J Immunol,* 37**,** 1285–9.

CHIOU, F. K., BEATH, S. V., WILKIE, G. M., VICKERS, M. A., MORLAND, B. & GUPTE, G. L. 2018. Cytotoxic T-lymphocyte therapy for post-transplant lymphoproliferative disorder after solid organ transplantation in children. *Pediatr Transplant,* 22.

CHIU, S. H., WU, M. C., WU, C. C., CHEN, Y. C., LIN, S. F., HSU, J. T., YANG, C. S., TSAI, C. H., TAKADA, K., CHEN, M. R. & CHEN, J. Y. 2014. Epstein-Barr virus BALF3 has nuclease activity and mediates mature virion production during the lytic cycle. *J Virol,* 88**,** 4962–75.

CHIU, Y. F., SUGDEN, A. U. & SUGDEN, B. 2013. Epstein-Barr viral productive amplification reprograms nuclear architecture, DNA replication, and histone deposition. *Cell Host Microbe,* 14**,** 607–18.

CHOI, H., LEE, Y., HUR, G., LEE, S. E., CHO, H. I., SOHN, H. J., CHO, B. S., KIM, H. J. & KIM, T. G. 2021. γδ T cells cultured with artificial antigen-presenting cells and IL-2 show long-term proliferation and enhanced effector functions compared with γδ T cells cultured with only IL-2 after stimulation with zoledronic acid. *Cytotherapy,* 23**,** 908–917.

CHOI, I. K., WANG, Z., KE, Q., HONG, M., QIAN, Y., ZHAO, X., LIU, Y., KIM, H. J., RITZ, J., CANTOR, H., RAJEWSKY, K., WUCHERPFENNIG, K. W. & ZHANG, B. 2018. Signaling by the Epstein-Barr virus LMP1 protein induces potent cytotoxic CD4(+) and CD8(+) T cell responses. *Proc Natl Acad Sci U S A,* 115**,** E686–e695.

CHRONISTER, W. D., CRINKLAW, A., MAHAJAN, S., VITA, R., KOŞALOĞLU-YALÇıN, Z., YAN, Z., GREENBAUM, J. A., JESSEN, L. E., NIELSEN, M., CHRISTLEY, S., COWELL, L. G., SETTE, A. & PETERS, B. 2021. TCRMatch: Predicting T-Cell Receptor Specificity Based on Sequence Similarity to Previously Characterized Receptors. *Front Immunol,* 12**,** 640725.

CHU, C., SCHÖNBRUNN, A., ELITOK, S., KERN, F., SCHNATBAUM, K., WENSCHUH, H., KLEMM, K., VON BAEHR, V., KRÄMER, B. K. & HOCHER, B. 2022. T-cell proliferation assay for the detection of SARS-CoV-2-specific T-cells. *Clin Chim Acta,* 532**,** 130–136.

CHU, Y., MILNER, J., LAMB, M., MARYAMCHIK, E., RIGOT, O., AYELLO, J., HARRISON, L., SHAW, R., BEHBEHANI, G. K., MARDIS, E. R., MILLER, K., PRAKRUTHI RAO VENKATA, L., CHANG, H., LEE, D., ROSENTHAL, E., KADAUKE, S., BUNIN, N., TALANO, J. A., JOHNSON, B., WANG, Y. & CAIRO, M. S. 2023. Manufacture and Characterization of Good Manufacturing Practice-Compliant SARS-COV-2 Cytotoxic T Lymphocytes. *J Infect Dis,* 227**,** 788–799.

CHUNG, B. K., TSAI, K., ALLAN, L. L., ZHENG, D. J., NIE, J. C., BIGGS, C. M., HASAN, M. R., KOZAK, F. K., VAN DEN ELZEN, P., PRIATEL, J. J. & TAN, R. 2013. Innate immune control of EBV-infected B cells by invariant natural killer T cells. *Blood,* 122**,** 2600–8.

CLAYTON, K. L., HAALAND, M. S., DOUGLAS-VAIL, M. B., MUJIB, S., CHEW, G. M., NDHLOVU, L. C. & OSTROWSKI, M. A. 2014. T cell Ig and mucin domain-containing protein 3 is recruited to the immune synapse, disrupts stable synapse formation, and associates with receptor phosphatases. *J Immunol,* 192**,** 782–91.

CLERICO, M., DOGLIOTTI, I., AROLDI, A., CONSOLI, C., GIACCONE, L., BRUNO, B. & CAVALLO, F. 2022. Post-Transplant Lymphoproliferative Disease (PTLD) after Allogeneic Hematopoietic Stem Cell Transplantation: Biology and Treatment Options. *J Clin Med,* 11.

COCHRAN, T. & LI, W. 2021. Frequent internuclear bridging in a Fanconi anemia patient with FANCG mutation. *Blood,* 138**,** 738.

COCKFIELD, S. M. 2001. Identifying the patient at risk for post-transplant lymphoproliferative disorder. *Transpl Infect Dis,* 3**,** 70–8.

COLLINS, A. V., BRODIE, D. W., GILBERT, R. J., IABONI, A., MANSO-SANCHO, R., WALSE, B., STUART, D. I., VAN DER MERWE, P. A. & DAVIS, S. J. 2002. The interaction properties of costimulatory molecules revisited. *Immunity,* 17**,** 201–10.

CONACHER, M., CALLARD, R., MCAULAY, K., CHAPEL, H., WEBSTER, D., KUMARARATNE, D., CHANDRA, A., SPICKETT, G., HOPWOOD, P. A. & CRAWFORD, D. H. 2005. Epstein-Barr virus can establish infection in the absence of a classical memory B-cell population. *J Virol,* 79**,** 11128–34.

COOPER, M. D., PETERSON, R. D. & GOOD, R. A. 1965. DELINEATION OF THE THYMIC AND BURSAL LYMPHOID SYSTEMS IN THE CHICKEN. *Nature,* 205**,** 143–6.

COOPER, M. D., RAYMOND, D. A., PETERSON, R. D., SOUTH, M. A. & GOOD, R. A. 1966. The functions of the thymus system and the bursa system in the chicken. *J Exp Med,* 123**,** 75–102.

COOPER, R. S., FRASER, A. R., SMITH, L., BURGOYNE, P., IMLACH, S. N., JARVIS, L. M., TURNER, D. M., ZAHRA, S., TURNER, M. L. & CAMPBELL, J. D. M. 2020. Rapid GMP-Compliant Expansion of SARS-CoV-2-Specific T Cells From Convalescent Donors for Use as an Allogeneic Cell Therapy for COVID-19. *Front Immunol,* 11**,** 598402.

COOPER, R. S., KOWALCZUK, A., WILKIE, G., VICKERS, M. A., TURNER, M. L., CAMPBELL, J. D. M. & FRASER, A. R. 2021. Cytometric analysis of T cell phenotype using cytokine profiling for improved manufacturing of an EBV-specific T cell therapy. *Clin Exp Immunol,* 206**,** 68–81.

COOPER, R. S., SUTHERLAND, C., SMITH, L. M., COWAN, G., BARNETT, M., MITCHELL, D., MCLEAN, C., IMLACH, S., HAYES, A., ZAHRA, S., MANCHANAYAKE, C., VICKERS, M. A., GRAHAM, G., MCGOWAN, N. W. A., TURNER, M. L., CAMPBELL, J. D. M. & FRASER, A. R. 2024. EBV T-cell immunotherapy generated by peptide selection has enhanced effector functionality compared to LCL stimulation. *Front Immunol,* 15**,** 1412211.

CORNBERG, M., CLUTE, S. C., WATKIN, L. B., SACCOCCIO, F. M., KIM, S. K., NAUMOV, Y. N., BREHM, M. A., ASLAN, N., WELSH, R. M. & SELIN, L. K. 2010. CD8 T cell cross-reactivity networks mediate heterologous immunity in human EBV and murine vaccinia virus infections. *J Immunol,* 184**,** 2825–38.

CORREIA, S., BRIDGES, R., WEGNER, F., VENTURINI, C., PALSER, A., MIDDELDORP, J. M., COHEN, J. I., LORENZETTI, M. A., BASSANO, I., WHITE, R. E., KELLAM, P., BREUER, J. & FARRELL, P. J. 2018. Sequence Variation of Epstein-Barr Virus: Viral Types, Geography, Codon Usage, and Diseases. *J Virol,* 92.

CORTESE, M., LEE, J. Y., CERIKAN, B., NEUFELDT, C. J., OORSCHOT, V. M. J., KÖHRER, S., HENNIES, J., SCHIEBER, N. L., RONCHI, P., MIZZON, G., ROMERO-BREY, I., SANTARELLA-MELLWIG, R., SCHORB, M., BOERMEL, M., MOCAER, K., BECKWITH, M. S., TEMPLIN, R. M., GROSS, V., PAPE, C., TISCHER, C., FRANKISH, J., HORVAT, N. K., LAKETA, V., STANIFER, M., BOULANT, S., RUGGIERI, A., CHATEL-CHAIX, L., SCHWAB, Y. &

BARTENSCHLAGER, R. 2020. Integrative Imaging Reveals SARS-CoV-2-Induced Reshaping of Subcellular Morphologies. *Cell Host Microbe,* 28**,** 853–866.e5.

COSCHI, C. H. & JUERGENS, R. A. 2023. Overcoming Resistance Mechanisms to Immune Checkpoint Inhibitors: Leveraging the Anti-Tumor Immune Response. *Curr Oncol,* 31**,** 1–23.

COUTURAUD, B., DOIX, B., CARRETERO-IGLESIA, L., ALLARD, M., PRADERVAND, S., HEBEISEN, M. & RUFER, N. 2023. Overall avidity declines in TCR repertoires during latent CMV but not EBV infection. *Front Immunol,* 14**,** 1293090.

CRAWFORD, D. H. & ANDO, I. 1986. EB virus induction is associated with B-cell maturation. *Immunology,* 59**,** 405–9.

CRAWFORD, D. H., MACSWEEN, K. F., HIGGINS, C. D., THOMAS, R., MCAULAY, K., WILLIAMS, H., HARRISON, N., REID, S., CONACHER, M., DOUGLAS, J. & SWERDLOW, A. J. 2006. A cohort study among university students: identification of risk factors for Epstein-Barr virus seroconversion and infectious mononucleosis. *Clin Infect Dis,* 43**,** 276–82.

CRON, R. Q. 2003. CD154 transcriptional regulation in primary human CD4 T cells. *Immunol Res,* 27**,** 185–202.

CUI, S., CHEN, S., LI, X., LIU, S. & WANG, F. 2020. Prevalence of venous thromboembolism in patients with severe novel coronavirus pneumonia. *J Thromb Haemost,* 18**,** 1421–1424.

CURIGLIANO, G., GELDERBLOM, H., MACH, N., DOI, T., TAI, D., FORDE, P. M., SARANTOPOULOS, J., BEDARD, P. L., LIN, C. C., HODI, F. S., WILGENHOF, S., SANTORO, A., SABATOS-PEYTON, C. A., LONGMIRE, T. A., XYRAFAS, A., SUN, H., GUTZWILLER, S., MANENTI, L. & NAING, A. 2021. Phase I/Ib Clinical Trial of Sabatolimab, an Anti-TIM-3 Antibody, Alone and in Combination with Spartalizumab, an Anti-PD-1 Antibody, in Advanced Solid Tumors. *Clin Cancer Res,* 27**,** 3620–3629.

DADWAL, S. S., BANSAL, R., SCHUSTER, M. W., YARED, J. A., MYERS, G. D., MATZKO, M., ADNAN, S., MCNEEL, D., MA, J., GILMORE, S. A., VASILEIOU, S., LEEN, A. M., HILL, J. A. & YOUNG, J. H. 2024. Final outcomes from a phase 2 trial of posoleucel in allogeneic hematopoietic cell transplant recipients. *Blood Adv,* 8**,** 4740–4750.

DALTON, T., DOUBROVINA, E., PANKOV, D., REYNOLDS, R., SCHOLZE, H., SELVAKUMAR, A., VIZCONDE, T., SAVALIA, B., DYOMIN, V., WEIGEL, C., OAKES, C. C., ALONSO, A., ELEMENTO, O., PAN, H., PHILLIP, J. M., O'REILLY, R. J., GEWURZ, B. E., CESARMAN, E. & GIULINO-ROTH, L. 2020. Epigenetic reprogramming sensitizes immunologically silent EBV+ lymphomas to virus-directed immunotherapy. *Blood,* 135**,** 1870–1881.

DAMANIA, B., KENNEY, S. C. & RAAB-TRAUB, N. 2022. Epstein-Barr virus: Biology and clinical disease. *Cell,* 185**,** 3652–3670.

DAMANIA, B. & PIPAS, J. M. 2009. *DNA tumor viruses,* New York, Springer Science + Business Media.

DAMBAUGH, T., HENNESSY, K., CHAMNANKIT, L. & KIEFF, E. 1984. U2 region of Epstein-Barr virus DNA may encode Epstein-Barr nuclear antigen 2. *Proc Natl Acad Sci U S A,* 81**,** 7632–6.

DAN, J. M., MATEUS, J., KATO, Y., HASTIE, K. M., YU, E. D., FALITI, C. E., GRIFONI, A., RAMIREZ, S. I., HAUPT, S., FRAZIER, A., NAKAO, C., RAYAPROLU, V., RAWLINGS, S. A., PETERS, B., KRAMMER, F., SIMON, V., SAPHIRE, E. O., SMITH, D. M., WEISKOPF, D., SETTE, A. & CROTTY, S. 2021. Immunological memory to SARS-CoV-2 assessed for up to 8 months after infection. *Science,* 371.

DAVE, H., LUO, M., BLANEY, J. W., PATEL, S., BARESE, C., CRUZ, C. R., SHPALL, E. J., BOLLARD, C. M. & HANLEY, P. J. 2017. Toward a Rapid Production of Multivirus-Specific T Cells Targeting BKV, Adenovirus, CMV, and EBV from Umbilical Cord Blood. *Mol Ther Methods Clin Dev,* 5**,** 13–21.

DE ANGELIS, B., DOTTI, G., QUINTARELLI, C., HUYE, L. E., ZHANG, L., ZHANG, M., PANE, F., HESLOP, H. E., BRENNER, M. K., ROONEY, C. M. & SAVOLDO, B. 2009. Generation of Epstein-Barr virus-specific cytotoxic T lymphocytes resistant to the immunosuppressive drug tacrolimus (FK506). *Blood,* 114**,** 4784–91.

DE JESUS, O., SMITH, P. R., SPENDER, L. C., ELGUETA KARSTEGL, C., NILLER, H. H., HUANG, D. & FARRELL, P. J. 2003. Updated Epstein-Barr virus (EBV) DNA sequence and analysis of a promoter for the BART (CST, BARF0) RNAs of EBV. *J Gen Virol,* 84**,** 1443–1450.

DE LUCA, M. & COSSU, G. 2023. Cost and availability of novel cell and gene therapies: Can we avoid a catastrophic second valley of death?: Can we avoid a catastrophic second valley of death? *EMBO Rep,* 24**,** e56661.

DHARNIDHARKA, V. R., LAMB, K. E., GREGG, J. A. & MEIER-KRIESCHE, H. U. 2012. Associations between EBV serostatus and organ transplant type in PTLD risk: an analysis of the SRTR National Registry Data in the United States. *Am J Transplant,* 12**,** 976–83.

DI BLASI, D., CLAESSEN, I., TURKSMA, A. W., VAN BEEK, J. & TEN BRINKE, A. 2020. Guidelines for analysis of low-frequency antigen-specific T cell results: Dye-based proliferation assay vs (3)H-thymidine incorporation. *J Immunol Methods,* 487**,** 112907.

DI STASI, A., DE ANGELIS, B., ROONEY, C. M., ZHANG, L., MAHENDRAVADA, A., FOSTER, A. E., HESLOP, H. E., BRENNER, M. K., DOTTI, G. & SAVOLDO, B. 2009. T lymphocytes coexpressing CCR4 and a chimeric antigen receptor targeting CD30 have improved homing and antitumor activity in a Hodgkin tumor model. *Blood,* 113**,** 6392–402.

DIAO, B., WANG, C., TAN, Y., CHEN, X., LIU, Y., NING, L., CHEN, L., LI, M., LIU, Y., WANG, G., YUAN, Z., FENG, Z., ZHANG, Y., WU, Y. & CHEN, Y. 2020. Reduction and Functional Exhaustion of T Cells in Patients With Coronavirus Disease 2019 (COVID-19). *Front Immunol,* 11**,** 827.

DICKINSON, A. M., SVILAND, L., WANG, X. N., JACKSON, G., TAYLOR, P. R., DUNN, A. & PROCTOR, S. J. 1998. Predicting graft-versus-host disease in HLA-identical bone marrow transplant: a comparison of T-cell frequency analysis and a human skin explant model. *Transplantation,* 66**,** 857–63.

DIERICKX, D. & HABERMANN, T. M. 2018. Post-Transplantation Lymphoproliferative Disorders in Adults. *N Engl J Med,* 378**,** 549–562.

DILLARD, J. A., MARTINEZ, S. A., DEARING, J. J., MONTGOMERY, S. A. & BAXTER, V. K. 2023. Animal Models for the Study of SARS-CoV-2-Induced Respiratory Disease and Pathology. *Comp Med,* 73**,** 72–90.

DIRMEIER, U., NEUHIERL, B., KILGER, E., REISBACH, G., SANDBERG, M. L. & HAMMERSCHMIDT, W. 2003. Latent membrane protein 1 is critical for efficient growth transformation of human B cells by epstein-barr virus. *Cancer Res,* 63**,** 2982–9.

DISPINSERI, S., SECCHI, M., PIRILLO, M. F., TOLAZZI, M., BORGHI, M., BRIGATTI, C., DE ANGELIS, M. L., BARATELLA, M., BAZZIGALUPPI, E., VENTURI, G., SIRONI, F., CANITANO, A., MARZINOTTO, I., TRESOLDI, C., CICERI, F., PIEMONTI, L., NEGRI, D., CARA, A., LAMPASONA, V. & SCARLATTI, G. 2021. Neutralizing antibody responses to SARS-CoV-2 in symptomatic COVID-19 is persistent and critical for survival. *Nat Commun,* 12**,** 2670.

DJAOUD, Z., GUETHLEIN, L. A., HOROWITZ, A., AZZI, T., NEMAT-GORGANI, N., OLIVE, D., NADAL, D., NORMAN, P. J., MÜNZ, C. & PARHAM, P. 2017. Two alternate strategies for innate immunity to Epstein-Barr virus: One using NK cells and the other NK cells and γδ T cells. *J Exp Med,* 214**,** 1827–1841.

DOLAN, A., ADDISON, C., GATHERER, D., DAVISON, A. J. & MCGEOCH, D. J. 2006. The genome of Epstein-Barr virus type 2 strain AG876. *Virology,* 350**,** 164–70.

DOUBROVINA, E., OFLAZ-SOZMEN, B., PROCKOP, S. E., KERNAN, N. A., ABRAMSON, S., TERUYA-FELDSTEIN, J., HEDVAT, C., CHOU, J. F., HELLER, G., BARKER, J. N., BOULAD, F., CASTRO-MALASPINA, H., GEORGE, D., JAKUBOWSKI, A., KOEHNE, G., PAPADOPOULOS, E. B., SCARADAVOU, A., SMALL, T. N., KHALAF, R., YOUNG, J. W. & O'REILLY, R. J. 2012. Adoptive immunotherapy with unselected or EBV-specific T cells for biopsy-proven EBV+ lymphomas after allogeneic hematopoietic cell transplantation. *Blood,* 119**,** 2644–56.

DRAGON, A. C., ZIMMERMANN, K., NERRETER, T., SANDFORT, D., LAHRBERG, J., KLÖß, S., KLOTH, C., MANGARE, C., BONIFACIUS, A., TISCHER-ZIMMERMANN, S., BLASCZYK, R., MAECKER-KOLHOFF, B., UCHANSKA-ZIEGLER, B., ABKEN, H., SCHAMBACH, A., HUDECEK, M. & EIZ-VESPER, B. 2020. CAR-T cells and TRUCKs that recognize an EBNA-3C-derived epitope presented on HLA-B*35 control Epstein-Barr virus-associated lymphoproliferation. *J Immunother Cancer,* 8.

DUAN, Y., LI, Z., CHENG, S., CHEN, Y., ZHANG, L., HE, J., LIAO, Q., YANG, L., GONG, Z. & SUN, L. Q. 2015. Nasopharyngeal carcinoma progression is mediated by EBER-triggered inflammation via the RIG-I pathway. *Cancer Lett,* 361**,** 67–74.

DUNMIRE, S. K., GRIMM, J. M., SCHMELING, D. O., BALFOUR, H. H., JR. & HOGQUIST, K. A. 2015. The Incubation Period of Primary Epstein-Barr Virus Infection: Viral Dynamics and Immunologic Events. *PLoS Pathog,* 11**,** e1005286.

DURKEE-SHOCK, J., LAZARSKI, C. A., JENSEN-WACHSPRESS, M. A., ZHANG, A., SON, A., KANKATE, V. V., FIELD, N. E., WEBBER, K., LANG, H., CONWAY, S. R., HANLEY, P. J., BOLLARD, C. M., KELLER, M. D. & SCHWARTZ, D. M. 2022. Transcriptomic analysis reveals optimal cytokine combinations for SARS-CoV-2-specific T cell therapy products. *Mol Ther Methods Clin Dev,* 25**,** 439–447.

DUSTIN, M. L. 2008. T-cell activation through immunological synapses and kinapses. *Immunol Rev,* 221**,** 77–89.

EHLERS, B., SPIESS, K., LEENDERTZ, F., PEETERS, M., BOESCH, C., GATHERER, D. & MCGEOCH, D. J. 2010. Lymphocryptovirus phylogeny and the origins of Epstein-Barr virus. *J Gen Virol,* 91**,** 630–42.

EL-MALLAWANY, N. K. & ROUCE, R. H. 2024. EBV and post-transplant lymphoproliferative disorder: a complex relationship. *Hematology Am Soc Hematol Educ Program,* 2024**,** 728–735.

ESLAMI, N., AGHBASH, P. S., SHAMEKH, A., ENTEZARI-MALEKI, T., NAHAND, J. S., SALES, A. J. & BAGHI, H. B. 2022. SARS-CoV-2: Receptor and Co-receptor Tropism Probability. *Curr Microbiol,* 79**,** 133.

ESSALMANI, R., JAIN, J., SUSAN-RESIGA, D., ANDRÉO, U., EVAGELIDIS, A., DERBALI, R. M., HUYNH, D. N., DALLAIRE, F., LAPORTE, M., DELPAL, A., SUTTO-ORTIZ, P., COUTARD, B., MAPA, C., WILCOXEN, K., DECROLY, E., NQ PHAM, T., COHEN É, A. & SEIDAH, N. G. 2022. Distinctive Roles of Furin and TMPRSS2 in SARS-CoV-2 Infectivity. *J Virol,* 96**,** e0012822.

FARNAULT, L., GERTNER-DARDENNE, J., GONDOIS-REY, F., MICHEL, G., CHAMBOST, H., HIRSCH, I. & OLIVE, D. 2013. Clinical evidence implicating gamma-delta T cells in EBV control following cord blood transplantation. *Bone Marrow Transplant,* 48**,** 1478–9.

FAULKNER, G. C., BURROWS, S. R., KHANNA, R., MOSS, D. J., BIRD, A. G. & CRAWFORD, D. H. 1999. X-Linked agammaglobulinemia patients are not infected with Epstein-Barr virus: implications for the biology of the virus. *J Virol,* 73**,** 1555–64.

FEHSE, B., GOLDMANN, M., FRERK, O., BULDUK, M. & ZANDER, A. R. 2000. Depletion of alloreactive donor T cells using immunomagnetic cell selection. *Bone Marrow Transplant,* 25 Suppl 2**,** S39–42.

FERNÁNDEZ, L., METAIS, J. Y., ESCUDERO, A., VELA, M., VALENTÍN, J., VALLCORBA, I., LEIVAS, A., TORRES, J., VALERI, A., PATIÑO-GARCÍA, A., MARTÍNEZ, J., LEUNG, W. & PÉREZ-MARTÍNEZ, A. 2017. Memory T Cells Expressing an NKG2D-CAR Efficiently Target Osteosarcoma Cells. *Clin Cancer Res,* 23**,** 5824–5835.

FERRERAS, C., PASCUAL-MIGUEL, B., MESTRE-DURÁN, C., NAVARRO-ZAPATA, A., CLARES-VILLA, L., MARTÍN-CORTÁZAR, C., DE PAZ, R., MARCOS, A., VICARIO, J. L., BALAS, A., GARCÍA-SÁNCHEZ, F., EGUIZABAL, C., SOLANO, C., MORA-RILLO, M., SORIA, B. & PÉREZ-MARTÍNEZ, A. 2021. SARS-CoV-2-Specific Memory T Lymphocytes From COVID-19 Convalescent Donors: Identification, Biobanking, and Large-Scale Production for Adoptive Cell Therapy. *Front Cell Dev Biol,* 9**,** 620730.

FEUCHTINGER, T., MATTHES-MARTIN, S., RICHARD, C., LION, T., FUHRER, M., HAMPRECHT, K., HANDGRETINGER, R., PETERS, C., SCHUSTER, F. R., BECK, R., SCHUMM, M., LOTFI, R., JAHN, G. & LANG, P. 2006. Safe adoptive transfer of virus-specific T-cell immunity for the treatment of systemic adenovirus infection after allogeneic stem cell transplantation. *Br J Haematol,* 134**,** 64–76.

FEUCHTINGER, T., OPHERK, K., BETHGE, W. A., TOPP, M. S., SCHUSTER, F. R., WEISSINGER, E. M., MOHTY, M., OR, R., MASCHAN, M., SCHUMM, M., HAMPRECHT, K., HANDGRETINGER, R., LANG, P. & EINSELE, H. 2010. Adoptive transfer of pp65-specific T cells for the treatment of chemorefractory cytomegalovirus disease or reactivation after haploidentical and matched unrelated stem cell transplantation. *Blood,* 116**,** 4360–7.

FIOLA, S., GOSSELIN, D., TAKADA, K. & GOSSELIN, J. 2010. TLR9 contributes to the recognition of EBV by primary monocytes and plasmacytoid dendritic cells. *J Immunol,* 185**,** 3620–31.

FLERI, W., PAUL, S., DHANDA, S. K., MAHAJAN, S., XU, X., PETERS, B. & SETTE, A. 2017. The Immune Epitope Database and Analysis Resource in Epitope Discovery and Synthetic Vaccine Design. *Front Immunol,* 8**,** 278.

FOK, V., FRIEND, K. & STEITZ, J. A. 2006. Epstein-Barr virus noncoding RNAs are confined to the nucleus, whereas their partner, the human La protein, undergoes nucleocytoplasmic shuttling. *J Cell Biol,* 173**,** 319–25.

FOLEY, B., COOLEY, S., VERNERIS, M. R., CURTSINGER, J., LUO, X., WALLER, E. K., ANASETTI, C., WEISDORF, D. & MILLER, J. S. 2012a. Human cytomegalovirus (CMV)-induced memory-like NKG2C(+) NK cells are transplantable and expand in vivo in response to recipient CMV antigen. *J Immunol,* 189**,** 5082–8.

FOLEY, B., COOLEY, S., VERNERIS, M. R., PITT, M., CURTSINGER, J., LUO, X., LOPEZ-VERGÈS, S., LANIER, L. L., WEISDORF, D. & MILLER, J. S. 2012b. Cytomegalovirus reactivation after allogeneic transplantation promotes a

lasting increase in educated NKG2C+ natural killer cells with potent function. *Blood,* 119**,** 2665–74.

FOLLIS, K. E., YORK, J. & NUNBERG, J. H. 2006. Furin cleavage of the SARS coronavirus spike glycoprotein enhances cell-cell fusion but does not affect virion entry. *Virology,* 350**,** 358–69.

FORD, E. S., MAYER-BLACKWELL, K., JING, L., LAING, K. J., SHOLUKH, A. M., ST GERMAIN, R., BOSSARD, E. L., XIE, H., PULLIAM, T. H., JANI, S., SELKE, S., BURROW, C. J., MCCLURKAN, C. L., WALD, A., GRENINGER, A. L., HOLBROOK, M. R., EATON, B., EUDY, E., MURPHY, M., POSTNIKOVA, E., ROBINS, H. S., ELYANOW, R., GITTELMAN, R. M., ECSEDI, M., WILCOX, E., CHAPUIS, A. G., FIORE-GARTLAND, A. & KOELLE, D. M. 2024. Repeated mRNA vaccination sequentially boosts SARS-CoV-2-specific CD8(+) T cells in persons with previous COVID-19. *Nat Immunol,* 25**,** 166–177.

FORGET, M. A., HAYMAKER, C., DENNISON, J. B., TOTH, C., MAITI, S., FULBRIGHT, O. J., COOPER, L. J., HWU, P., RADVANYI, L. G. & BERNATCHEZ, C. 2016. The beneficial effects of a gas-permeable flask for expansion of Tumor-Infiltrating lymphocytes as reflected in their mitochondrial function and respiration capacity. *Oncoimmunology,* 5**,** e1057386.

FOSTER, A. E., DOTTI, G., LU, A., KHALIL, M., BRENNER, M. K., HESLOP, H. E., ROONEY, C. M. & BOLLARD, C. M. 2008. Antitumor activity of EBV-specific T lymphocytes transduced with a dominant negative TGF-beta receptor. *J Immunother,* 31**,** 500–5.

FOSTER, A. E., FORRESTER, K., GOTTLIEB, D. J., BARTON, G. W., ROMAGNOLI, J. A. & BRADSTOCK, K. F. 2004. Large-scale expansion of cytomegalovirus-specific cytotoxic T cells in suspension culture. *Biotechnol Bioeng,* 85**,** 138–46.

FRASER, A. R., CURBISHLEY, S. M., ROEMHILD, A. & TSANG, K. 2024. Editorial: Bringing function to the forefront of cell therapy: how do we demonstrate potency? *Front Immunol,* 15**,** 1472727.

FRENTSCH, M., ARBACH, O., KIRCHHOFF, D., MOEWES, B., WORM, M., ROTHE, M., SCHEFFOLD, A. & THIEL, A. 2005. Direct access to CD4+ T cells specific for defined antigens according to CD154 expression. *Nat Med,* 11**,** 1118–24.

FRIEDLINE, R. H., BROWN, D. S., NGUYEN, H., KORNFELD, H., LEE, J., ZHANG, Y., APPLEBY, M., DER, S. D., KANG, J. & CHAMBERS, C. A. 2009. CD4+ regulatory T cells require CTLA-4 for the maintenance of systemic tolerance. *J Exp Med,* 206**,** 421–34.

FUJIMOTO, A., HIRAMOTO, N., YAMASAKI, S., INAMOTO, Y., UCHIDA, N., MAEDA, T., MORI, T., KANDA, Y., KONDO, T., SHIRATORI, S., MIYAKOSHI, S., ISHIYAMA, K., IKEGAME, K., MATSUHASHI, Y., TANAKA, J., ICHINOHE, T., ATSUTA, Y., OGATA, M. & SUZUKI, R. 2019. Risk Factors and Predictive Scoring System For Post-Transplant Lymphoproliferative Disorder after Hematopoietic Stem Cell Transplantation. *Biol Blood Marrow Transplant,* 25**,** 1441–1449.

FUJISHIMA, N., HIROKAWA, M., FUJISHIMA, M., YAMASHITA, J., SAITOH, H., ICHIKAWA, Y., HORIUCHI, T., KAWABATA, Y. & SAWADA, K. I. 2007. Skewed T cell receptor repertoire of Vdelta1(+) gammadelta T lymphocytes after human allogeneic haematopoietic stem cell transplantation and the potential role for Epstein-Barr virus-infected B cells in clonal restriction. *Clin Exp Immunol,* 149**,** 70–9.

GAGLIARDI, C., KHALIL, M. & FOSTER, A. E. 2019. Streamlined production of genetically modified T cells with activation, transduction and expansion in closed-system G-Rex bioreactors. *Cytotherapy,* 21**,** 1246–1257.

GALÁN, M., VIGÓN, L., FUERTES, D., MURCIANO-ANTÓN, M. A., CASADO-FERNÁNDEZ, G., DOMÍNGUEZ-MATEOS, S., MATEOS, E., RAMOS-MARTÍN, F., PLANELLES, V., TORRES, M., RODRÍGUEZ-MORA, S., LÓPEZ-HUERTAS, M. R. & COIRAS, M. 2022. Persistent Overactive Cytotoxic Immune Response in a Spanish Cohort of Individuals With Long-COVID: Identification of Diagnostic Biomarkers. *Front Immunol,* 13**,** 848886.

GALLOT, G., VOLLANT, S., SAÏAGH, S., CLÉMENCEAU, B., VIVIEN, R., CERATO, E., BIGNON, J. D., FERRAND, C., JACCARD, A., VIGOUROUX, S., CHOQUET, S., DALLE, J. H., FRACHON, I., BRUNO, B., MOTHY, M., MECHINAUD, F., LEBLOND, V., MILPIED, N. & VIÉ, H. 2014. T-cell therapy using a bank of EBV-specific cytotoxic T cells: lessons from a phase I/II feasibility and safety study. *J Immunother,* 37**,** 170–9.

GANDHI, M. K., WILKIE, G. M., DUA, U., MOLLEE, P. N., GRIMMETT, K., WILLIAMS, T., WHITAKER, N., GILL, D. & CRAWFORD, D. H. 2007. Immunity, homing and efficacy of allogeneic adoptive immunotherapy for posttransplant lymphoproliferative disorders. *Am J Transplant,* 7**,** 1293–9.

GANEEVA, I., ZMIEVSKAYA, E., VALIULLINA, A., KUDRIAEVA, A., MIFTAKHOVA, R., RYBALOV, A. & BULATOV, E. 2022. Recent Advances in the Development of Bioreactors for Manufacturing of Adoptive Cell Immunotherapies. *Bioengineering (Basel),* 9.

GAO, X., ZHU, Y., LI, G., HUANG, H., ZHANG, G., WANG, F., SUN, J., YANG, Q., ZHANG, X. & LU, B. 2012. TIM-3 expression characterizes regulatory T cells in tumor tissues and is associated with lung cancer progression. *PLoS One,* 7**,** e30676.

GARCÍA-GARCÍA, I., GUERRA-GARCÍA, P., FERRERAS, C., BOROBIA, A. M., CARCAS, A. J., QUEIRUGA-PARADA, J., VICARIO, J. L., MIRONES, I., SOLANO, C., EGUIZABAL, C., SORIA, B. & PÉREZ-MARTÍNEZ, A. 2021. A phase I/II dose-escalation multi-center study to evaluate the safety of infusion of natural killer cells or memory T cells as adoptive therapy in coronavirus pneumonia and/or lymphopenia: RELEASE study protocol. *Trials,* 22**,** 674.

GARCÍA-RÍOS, E., LEIVAS, A., MANCEBO, F. J., SÁNCHEZ-VEGA, L., LANZAROT, D., AGUADO, J. M., MARTÍNEZ-LÓPEZ, J., PACIELLO, M. L. & PÉREZ-ROMERO, P. 2022. Isolation of Functional SARS-CoV-2 Antigen-Specific T-Cells with Specific Viral Cytotoxic Activity for Adoptive Therapy of COVID-19. *Biomedicines,* 10.

GARCÍA, L. F. 2020. Immune Response, Inflammation, and the Clinical Spectrum of COVID-19. *Front Immunol,* 11**,** 1441.

GATTI, A., ZIZZO, G., DE PASCHALE, M., TAMBURELLO, A., CASTELNOVO, L., FAGGIOLI, P. M., CLERICI, P., BRANDO, B. & MAZZONE, A. 2023. Assessing SARS-CoV-2-specific T-cell reactivity in late convalescents and vaccinees: Comparison and combination of QuantiFERON and activation-induced marker assays, and relation with antibody status. *PLoS One,* 18**,** e0285728.

GATTINONI, L., KLEBANOFF, C. A., PALMER, D. C., WRZESINSKI, C., KERSTANN, K., YU, Z., FINKELSTEIN, S. E., THEORET, M. R., ROSENBERG, S. A. & RESTIFO, N. P. 2005. Acquisition of full effector function in vitro paradoxically impairs the in vivo antitumor efficacy of adoptively transferred CD8+ T cells. *J Clin Invest,* 115**,** 1616–26.

GAUDREAULT, E., FIOLA, S., OLIVIER, M. & GOSSELIN, J. 2007. Epstein-Barr virus induces MCP-1 secretion by human monocytes via TLR2. *J Virol,* 81**,** 8016–24.

GENTILI, V., BORTOLOTTI, D., MORANDI, L., RIZZO, S., SCHIUMA, G., BELTRAMI, S., CASCIANO, F., PAPI, A., CONTOLI, M., ZAULI, G. & RIZZO, R. 2023. Natural Killer Cells in SARS-CoV-2-Vaccinated Subjects with Increased Effector Cytotoxic CD56(dim) Cells and Memory-Like CD57(+)NKG2C(+)CD56(dim) Cells. *Front Biosci (Landmark Ed),* 28**,** 156.

GEORGIADIS, C., PREECE, R., NICKOLAY, L., ETUK, A., PETROVA, A., LADON, D., DANYI, A., HUMPHRYES-KIRILOV, N., AJETUNMOBI, A., KIM, D., KIM, J. S. & QASIM, W. 2018. Long Terminal Repeat CRISPR-CAR-Coupled "Universal" T Cells Mediate Potent Anti-leukemic Effects. *Mol Ther,* 26**,** 1215–1227.

GÉRARD, A., COPE, A. P., KEMPER, C., ALON, R. & KÖCHL, R. 2021. LFA-1 in T cell priming, differentiation, and effector functions. *Trends Immunol,* 42**,** 706–722.

GERDEMANN, U., KATARI, U. L., PAPADOPOULOU, A., KEIRNAN, J. M., CRADDOCK, J. A., LIU, H., MARTINEZ, C. A., KENNEDY-NASSER, A., LEUNG, K. S., GOTTSCHALK, S. M., KRANCE, R. A., BRENNER, M. K., ROONEY, C. M., HESLOP, H. E. & LEEN, A. M. 2013. Safety and clinical efficacy of rapidly-generated trivirus-directed T cells as treatment for adenovirus, EBV, and CMV infections after allogeneic hematopoietic stem cell transplant. *Mol Ther,* 21**,** 2113–21.

GHOSH, S., DELLIBOVI-RAGHEB, T. A., KERVIEL, A., PAK, E., QIU, Q., FISHER, M., TAKVORIAN, P. M., BLECK, C., HSU, V. W., FEHR, A. R., PERLMAN, S., ACHAR, S. R., STRAUS, M. R., WHITTAKER, G. R., DE HAAN, C. A. M., KEHRL, J., ALTAN-BONNET, G. & ALTAN-BONNET, N. 2020. ß-Coronaviruses Use Lysosomes for Egress Instead of the Biosynthetic Secretory Pathway. *Cell,* 183**,** 1520–1535.e14.

GHOSH, S. K., PERRINE, S. P., WILLIAMS, R. M. & FALLER, D. V. 2012. Histone deacetylase inhibitors are potent inducers of gene expression in latent EBV and sensitize lymphoma cells to nucleoside antiviral agents. *Blood,* 119**,** 1008–17.

GIL-BESCÓS, R., OSTIZ, A., ZALBA, S., TAMAYO, I., BANDRÉS, E., ROJAS-DE-MIGUEL, E., REDONDO, M., ZABALZA, A. & RAMÍREZ, N. 2023. Potency assessment of IFNγ-producing SARS-CoV-2-specific T cells from COVID-19 convalescent subjects. *Life Sci Alliance,* 6.

GIL, A., YASSAI, M. B., NAUMOV, Y. N. & SELIN, L. K. 2015. Narrowing of human influenza A virus-specific T cell receptor α and ß repertoires with increasing age. *J Virol,* 89**,** 4102–16.

GILES, J. R., GLOBIG, A. M., KAECH, S. M. & WHERRY, E. J. 2023. CD8(+) T cells in the cancer-immunity cycle. *Immunity,* 56**,** 2231–2253.

GITTELMAN, R. M., LAVEZZO, E., SNYDER, T. M., ZAHID, H. J., CARTY, C. L., ELYANOW, R., DALAI, S., KIRSCH, I., BALDO, L., MANUTO, L., FRANCHIN, E., DEL VECCHIO, C., PACENTI, M., BOLDRIN, C., CATTAI, M., SALUZZO, F., PADOAN, A., PLEBANI, M., SIMEONI, F., BORDINI, J., LORÈ, N. I., LAZAREVIĆ, D., CIRILLO, D. M., GHIA, P., TOPPO, S., CARLSON, J. M., ROBINS, H. S., CRISANTI, A. & TONON, G. 2022. Longitudinal analysis of T cell receptor repertoires reveals shared patterns of antigen-specific response to SARS-CoV-2 infection. *JCI Insight,* 7.

GODOY-RAMIREZ, K., FRANCK, K., MAHDAVIFAR, S., ANDERSSON, L. & GAINES, H. 2004. Optimum culture conditions for specific and nonspecific activation of whole blood and PBMC for intracellular cytokine assessment by flow cytometry. *J Immunol Methods,* 292**,** 1–15.

GONZÁLEZ-BARCA, E., CAPOTE, F. J., GÓMEZ-CODINA, J., PANIZO, C., SALAR, A., SANCHO, J. M., LÓPEZ, A., BRIONES, J., MUÑOZ, A., ENCUENTRA, M., MERCADAL, S., DOMINGO-DOMENECH, E. & DE SEVILLA, A. F. 2021. Long-term follow-up of a prospective phase 2 clinical trial of extended treatment with rituximab in patients with B cell post-transplant lymphoproliferative disease and validation in real world patients. *Ann Hematol,* 100**,** 1023–1029.

GOPALLAWA, I. & UHAL, B. D. 2014. Molecular and cellular mechanisms of the inhibitory effects of ACE-2/ANG1-7/Mas axis on lung injury. *Curr Top Pharmacol,* 18**,** 71–80.

GORDON, J., WALKER, L., GUY, G., BROWN, G., ROWE, M. & RICKINSON, A. 1986. Control of human B-lymphocyte replication. II. Transforming Epstein-Barr virus exploits three distinct viral signals to undermine three separate control points in B-cell growth. *Immunology,* 58**,** 591–5.

GORNALUSSE, G. G., HIRATA, R. K., FUNK, S. E., RIOLOBOS, L., LOPES, V. S., MANSKE, G., PRUNKARD, D., COLUNGA, A. G., HANAFI, L. A., CLEGG, D. O., TURTLE, C. & RUSSELL, D. W. 2017. HLA-E-expressing pluripotent stem cells escape allogeneic responses and lysis by NK cells. *Nat Biotechnol,* 35**,** 765–772.

GOTTI, E., TETTAMANTI, S., ZANINELLI, S., CUOFANO, C., CATTANEO, I., ROTIROTI, M. C., CRIBIOLI, S., ALZANI, R., RAMBALDI, A., INTRONA, M. & GOLAY, J. 2022. Optimization of therapeutic T cell expansion in G-Rex device and applicability to large-scale production for clinical use. *Cytotherapy,* 24**,** 334–343.

GRAF, D., MÜLLER, S., KORTHÄUER, U., VAN KOOTEN, C., WEISE, C. & KROCZEK, R. A. 1995. A soluble form of TRAP (CD40 ligand) is rapidly released after T cell activation. *Eur J Immunol,* 25**,** 1749–54.

GRASSELLI, G., TONETTI, T., PROTTI, A., LANGER, T., GIRARDIS, M., BELLANI, G., LAFFEY, J., CARRAFIELLO, G., CARSANA, L., RIZZUTO, C., ZANELLA, A., SCARAVILLI, V., PIZZILLI, G., GRIECO, D. L., DI MEGLIO, L., DE PASCALE, G., LANZA, E., MONTEDURO, F., ZOMPATORI, M., FILIPPINI, C., LOCATELLI, F., CECCONI, M., FUMAGALLI, R., NAVA, S., VINCENT, J. L., ANTONELLI, M., SLUTSKY, A. S., PESENTI, A. & RANIERI, V. M. 2020. Pathophysiology of COVID-19-associated acute respiratory distress syndrome: a multicentre prospective observational study. *Lancet Respir Med,* 8**,** 1201–1208.

GRATAMA, J. W., OOSTERVEER, M. A., LEPOUTRE, J. M., VAN ROOD, J. J., ZWAAN, F. E., VOSSEN, J. M., KAPSENBERG, J. G., RICHEL, D., KLEIN, G. & ERNBERG, I. 1990. Serological and molecular studies of Epstein-Barr virus infection in allogeneic marrow graft recipients. *Transplantation,* 49**,** 725–30.

GREGOROVIC, G., BOULDEN, E. A., BOSSHARD, R., ELGUETA KARSTEGL, C., SKALSKY, R., CULLEN, B. R., GUJER, C., RÄMER, P., MÜNZ, C. & FARRELL, P. J. 2015. Epstein-Barr Viruses (EBVs) Deficient in EBV-Encoded RNAs Have Higher Levels of Latent Membrane Protein 2 RNA Expression in Lymphoblastoid Cell Lines and Efficiently Establish Persistent Infections in Humanized Mice. *J Virol,* 89**,** 11711–4.

GRIFONI, A., WEISKOPF, D., RAMIREZ, S. I., MATEUS, J., DAN, J. M., MODERBACHER, C. R., RAWLINGS, S. A., SUTHERLAND, A., PREMKUMAR, L., JADI, R. S., MARRAMA, D., DE SILVA, A. M., FRAZIER, A., CARLIN, A. F., GREENBAUM, J. A., PETERS, B., KRAMMER, F., SMITH, D. M., CROTTY, S. & SETTE, A. 2020. Targets of T Cell Responses to SARS-CoV-2 Coronavirus in

Humans with COVID-19 Disease and Unexposed Individuals. *Cell,* 181**,** 1489–1501.e15.
GRISHKAN, I. V., NTRANOS, A., CALABRESI, P. A. & GOCKE, A. R. 2013. Helper T cells down-regulate CD4 expression upon chronic stimulation giving rise to double-negative T cells. *Cell Immunol,* 284**,** 68–74.
GU, B. J., SUN, C., FULLER, S., SKARRATT, K. K., PETROU, S. & WILEY, J. S. 2014. A quantitative method for measuring innate phagocytosis by human monocytes using real-time flow cytometry. *Cytometry A,* 85**,** 313–21.
GUERRERO-RAMOS, A., PATEL, M., KADAKIA, K. & HAQUE, T. 2014. Performance of the architect EBV antibody panel for determination of Epstein-Barr virus infection stage in immunocompetent adolescents and young adults with clinical suspicion of infectious mononucleosis. *Clin Vaccine Immunol,* 21**,** 817–23.
GUIMOND, M., BALASSY, A., BARRETTE, M., BROCHU, S., PERREAULT, C. & ROY, D. C. 2002. P-glycoprotein targeting: a unique strategy to selectively eliminate immunoreactive T cells. *Blood,* 100**,** 375–82.
GUMÁ, M., ANGULO, A., VILCHES, C., GÓMEZ-LOZANO, N., MALATS, N. & LÓPEZ-BOTET, M. 2004. Imprint of human cytomegalovirus infection on the NK cell receptor repertoire. *Blood,* 104**,** 3664–71.
GUMÁ, M., BUDT, M., SÁEZ, A., BRCKALO, T., HENGEL, H., ANGULO, A. & LÓPEZ-BOTET, M. 2006a. Expansion of CD94/NKG2C+ NK cells in response to human cytomegalovirus-infected fibroblasts. *Blood,* 107**,** 3624–31.
GUMÁ, M., CABRERA, C., ERKIZIA, I., BOFILL, M., CLOTET, B., RUIZ, L. & LÓPEZ-BOTET, M. 2006b. Human cytomegalovirus infection is associated with increased proportions of NK cells that express the CD94/NKG2C receptor in aviremic HIV-1-positive patients. *J Infect Dis,* 194**,** 38–41.
GUPTA, R. K., ABDUL-JAWAD, S., MCCOY, L. E., MOK, H. P., PEPPA, D., SALGADO, M., MARTINEZ-PICADO, J., NIJHUIS, M., WENSING, A. M. J., LEE, H., GRANT, P., NASTOULI, E., LAMBERT, J., PACE, M., SALASC, F., MONIT, C., INNES, A. J., MUIR, L., WATERS, L., FRATER, J., LEVER, A. M. L., EDWARDS, S. G., GABRIEL, I. H. & OLAVARRIA, E. 2019. HIV-1 remission following CCR5Δ32/Δ32 haematopoietic stem-cell transplantation. *Nature,* 568**,** 244–248.
GUSTAFSSON, A., LEVITSKY, V., ZOU, J. Z., FRISAN, T., DALIANIS, T., LJUNGMAN, P., RINGDEN, O., WINIARSKI, J., ERNBERG, I. & MASUCCI, M. G. 2000. Epstein-Barr virus (EBV) load in bone marrow transplant recipients at risk to develop posttransplant lymphoproliferative disease: prophylactic infusion of EBV-specific cytotoxic T cells. *Blood,* 95**,** 807–14.
GUY, C., MITREA, D. M., CHOU, P. C., TEMIROV, J., VIGNALI, K. M., LIU, X., ZHANG, H., KRIWACKI, R., BRUCHEZ, M. P., WATKINS, S. C., WORKMAN, C. J. & VIGNALI, D. A. A. 2022. LAG3 associates with TCR-CD3 complexes and suppresses signaling by driving co-receptor-Lck dissociation. *Nat Immunol,* 23**,** 757–767.
HAAGMANS, B. L., KUIKEN, T., MARTINA, B. E., FOUCHIER, R. A., RIMMELZWAAN, G. F., VAN AMERONGEN, G., VAN RIEL, D., DE JONG, T., ITAMURA, S., CHAN, K. H., TASHIRO, M. & OSTERHAUS, A. D. 2004. Pegylated interferon-alpha protects type 1 pneumocytes against SARS coronavirus infection in macaques. *Nat Med,* 10**,** 290–3.
HABEL, J. R., NGUYEN, T. H. O., VAN DE SANDT, C. E., JUNO, J. A., CHAURASIA, P., WRAGG, K., KOUTSAKOS, M., HENSEN, L., JIA, X., CHUA, B., ZHANG, W., TAN, H. X., FLANAGAN, K. L., DOOLAN, D. L., TORRESI, J., CHEN, W., WAKIM, L. M., CHENG, A. C., DOHERTY, P. C., PETERSEN, J., ROSSJOHN, J., WHEATLEY, A. K., KENT, S. J., ROWNTREE, L. C. & KEDZIERSKA, K.

2020. Suboptimal SARS-CoV-2-specific CD8(+) T cell response associated with the prominent HLA-A*02:01 phenotype. *Proc Natl Acad Sci U S A,* 117**,** 24384–24391.

HACKBART, M., DENG, X. & BAKER, S. C. 2020. Coronavirus endoribonuclease targets viral polyuridine sequences to evade activating host sensors. *Proc Natl Acad Sci U S A,* 117**,** 8094–8103.

HADJADJ, J., YATIM, N., BARNABEI, L., CORNEAU, A., BOUSSIER, J., SMITH, N., PÉRÉ, H., CHARBIT, B., BONDET, V., CHENEVIER-GOBEAUX, C., BREILLAT, P., CARLIER, N., GAUZIT, R., MORBIEU, C., PÈNE, F., MARIN, N., ROCHE, N., SZWEBEL, T. A., MERKLING, S. H., TRELUYER, J. M., VEYER, D., MOUTHON, L., BLANC, C., THARAUX, P. L., ROZENBERG, F., FISCHER, A., DUFFY, D., RIEUX-LAUCAT, F., KERNÉIS, S. & TERRIER, B. 2020. Impaired type I interferon activity and inflammatory responses in severe COVID-19 patients. *Science,* 369**,** 718–724.

HAIGH, T. A., LIN, X., JIA, H., HUI, E. P., CHAN, A. T., RICKINSON, A. B. & TAYLOR, G. S. 2008. EBV latent membrane proteins (LMPs) 1 and 2 as immunotherapeutic targets: LMP-specific CD4+ cytotoxic T cell recognition of EBV-transformed B cell lines. *J Immunol,* 180**,** 1643–54.

HALE, B. G. 2021. Avoiding culture shock with the SARS-CoV-2 spike protein. *Elife,* 10.

HAMMER, M. H., BRESTRICH, G., MITTENZWEIG, A., ROEMHILD, A., ZWINGER, S., SUBKLEWE, M., BEIER, C., KURTZ, A., BABEL, N., VOLK, H. D. & REINKE, P. 2007. Generation of EBV-specific T cells for adoptive immunotherapy: a novel protocol using formalin-fixed stimulator cells to increase biosafety. *J Immunother,* 30**,** 817–24.

HAMMER, M. H., MEYER, S., BRESTRICH, G., MOOSMANN, A., KERN, F., TESFA, L., BABEL, N., MITTENZWEIG, A., ROONEY, C. M., HAMMERSCHMIDT, W., VOLK, H. D. & REINKE, P. 2005. HLA type-independent generation of antigen-specific T cells for adoptive immunotherapy. *Eur J Immunol,* 35**,** 2250–8.

HAMMER, Q., RÜCKERT, T., BORST, E. M., DUNST, J., HAUBNER, A., DUREK, P., HEINRICH, F., GASPARONI, G., BABIC, M., TOMIC, A., PIETRA, G., NIENEN, M., BLAU, I. W., HOFMANN, J., NA, I. K., PRINZ, I., KOENECKE, C., HEMMATI, P., BABEL, N., ARNOLD, R., WALTER, J., THURLEY, K., MASHREGHI, M. F., MESSERLE, M. & ROMAGNANI, C. 2018. Peptide-specific recognition of human cytomegalovirus strains controls adaptive natural killer cells. *Nat Immunol,* 19**,** 453–463.

HAMMERSCHMIDT, W. & SUGDEN, B. 1988. Identification and characterization of oriLyt, a lytic origin of DNA replication of Epstein-Barr virus. *Cell,* 55**,** 427–33.

HAN, J., ZHANG, B., ZHENG, S., JIANG, Y., ZHANG, X. & MAO, K. 2024. The Progress and Prospects of Immune Cell Therapy for the Treatment of Cancer. *Cell Transplant,* 33**,** 9636897241231892.

HAQUE, T., AMLOT, P. L., HELLING, N., THOMAS, J. A., SWENY, P., ROLLES, K., BURROUGHS, A. K., PRENTICE, H. G. & CRAWFORD, D. H. 1998. Reconstitution of EBV-specific T cell immunity in solid organ transplant recipients. *J Immunol,* 160**,** 6204–9.

HAQUE, T., CHAGGAR, T., SCHAFERS, J., ATKINSON, C., MCAULAY, K. A. & CRAWFORD, D. H. 2011. Soluble CD30: a serum marker for Epstein-Barr virus-associated lymphoproliferative diseases. *J Med Virol,* 83**,** 311–6.

HAQUE, T., MCAULAY, K. A., KELLY, D. & CRAWFORD, D. H. 2010. Allogeneic T-cell therapy for Epstein-Barr virus-positive posttransplant

lymphoproliferative disease: long-term follow-up. *Transplantation,* 90**,** 93–4.

HAQUE, T., TAYLOR, C., WILKIE, G. M., MURAD, P., AMLOT, P. L., BEATH, S., MCKIERNAN, P. J. & CRAWFORD, D. H. 2001. Complete regression of posttransplant lymphoproliferative disease using partially HLA-matched Epstein Barr virus-specific cytotoxic T cells. *Transplantation,* 72**,** 1399–402.

HAQUE, T., WILKIE, G. M., JONES, M. M., HIGGINS, C. D., URQUHART, G., WINGATE, P., BURNS, D., MCAULAY, K., TURNER, M., BELLAMY, C., AMLOT, P. L., KELLY, D., MACGILCHRIST, A., GANDHI, M. K., SWERDLOW, A. J. & CRAWFORD, D. H. 2007. Allogeneic cytotoxic T-cell therapy for EBV-positive posttransplantation lymphoproliferative disease: results of a phase 2 multicenter clinical trial. *Blood,* 110**,** 1123–31.

HAQUE, T., WILKIE, G. M., TAYLOR, C., AMLOT, P. L., MURAD, P., ILEY, A., DOMBAGODA, D., BRITTON, K. M., SWERDLOW, A. J. & CRAWFORD, D. H. 2002. Treatment of Epstein-Barr-virus-positive post-transplantation lymphoproliferative disease with partly HLA-matched allogeneic cytotoxic T cells. *Lancet,* 360**,** 436–42.

HARTENIAN, E., NANDAKUMAR, D., LARI, A., LY, M., TUCKER, J. M. & GLAUNSINGER, B. A. 2020. The molecular virology of coronaviruses. *J Biol Chem,* 295**,** 12910–12934.

HARTWIG, U. F., NONN, M., KHAN, S., MEYER, R. G., HUBER, C. & HERR, W. 2006. Depletion of alloreactive T cells via CD69: implications on antiviral, antileukemic and immunoregulatory T lymphocytes. *Bone Marrow Transplant,* 37**,** 297–305.

HASSAN, J., FEIGHERY, C., BRESNIHAN, B. & WHELAN, A. 1991. Elevated T cell receptor gamma delta + T cells in patients with infectious mononucleosis. *Br J Haematol,* 77**,** 255–6.

HE, X., LAU, E. H. Y., WU, P., DENG, X., WANG, J., HAO, X., LAU, Y. C., WONG, J. Y., GUAN, Y., TAN, X., MO, X., CHEN, Y., LIAO, B., CHEN, W., HU, F., ZHANG, Q., ZHONG, M., WU, Y., ZHAO, L., ZHANG, F., COWLING, B. J., LI, F. & LEUNG, G. M. 2020. Temporal dynamics in viral shedding and transmissibility of COVID-19. *Nat Med,* 26**,** 672–675.

HENDRICKS, D. W., BALFOUR, H. H., JR., DUNMIRE, S. K., SCHMELING, D. O., HOGQUIST, K. A. & LANIER, L. L. 2014. Cutting edge: NKG2C(hi)CD57+ NK cells respond specifically to acute infection with cytomegalovirus and not Epstein-Barr virus. *J Immunol,* 192**,** 4492–6.

HERMANN, P., VAN-KOOTEN, C., GAILLARD, C., BANCHEREAU, J. & BLANCHARD, D. 1995. CD40 ligand-positive CD8+ T cell clones allow B cell growth and differentiation. *Eur J Immunol,* 25**,** 2972–7.

HEROLD, M. J., MCPHERSON, K. G. & REICHARDT, H. M. 2006. Glucocorticoids in T cell apoptosis and function. *Cell Mol Life Sci,* 63**,** 60–72.

HERRERA, L., MARTIN-INARAJA, M., SANTOS, S., INGLÉS-FERRÁNDIZ, M., AZKARATE, A., PEREZ-VAQUERO, M. A., VESGA, M. A., VICARIO, J. L., SORIA, B., SOLANO, C., DE PAZ, R., MARCOS, A., FERRERAS, C., PEREZ-MARTINEZ, A. & EGUIZABAL, C. 2022. Identifying SARS-CoV-2 'memory' NK cells from COVID-19 convalescent donors for adoptive cell therapy. *Immunology,* 165**,** 234–249.

HESLOP, H. E. 2020. Sensitizing Burkitt lymphoma to EBV-CTLs. *Blood,* 135**,** 1822–1823.

HESLOP, H. E., BRENNER, M. K. & ROONEY, C. M. 1994. Donor T cells to treat EBV-associated lymphoma. *N Engl J Med,* 331**,** 679–80.

HESLOP, H. E., NG, C. Y., LI, C., SMITH, C. A., LOFTIN, S. K., KRANCE, R. A., BRENNER, M. K. & ROONEY, C. M. 1996. Long-term restoration of immunity against Epstein-Barr virus infection by adoptive transfer of gene-modified virus-specific T lymphocytes. *Nat Med,* 2**,** 551–5.

HESLOP, H. E., SLOBOD, K. S., PULE, M. A., HALE, G. A., ROUSSEAU, A., SMITH, C. A., BOLLARD, C. M., LIU, H., WU, M. F., ROCHESTER, R. J., AMROLIA, P. J., HURWITZ, J. L., BRENNER, M. K. & ROONEY, C. M. 2010. Long-term outcome of EBV-specific T-cell infusions to prevent or treat EBV-related lymphoproliferative disease in transplant recipients. *Blood,* 115**,** 925–35.

HIKMET, F., MÉAR, L., EDVINSSON, Å., MICKE, P., UHLÉN, M. & LINDSKOG, C. 2020. The protein expression profile of ACE2 in human tissues. *Mol Syst Biol,* 16**,** e9610.

HINDERER, W., LANG, D., ROTHE, M., VORNHAGEN, R., SONNEBORN, H. H. & WOLF, H. 1999. Serodiagnosis of Epstein-Barr virus infection by using recombinant viral capsid antigen fragments and autologous gene fusion. *J Clin Microbiol,* 37**,** 3239–44.

HINRICHS, C., WENDLAND, S., ZIMMERMANN, H., EURICH, D., NEUHAUS, R., SCHLATTMANN, P., BABEL, N., RIESS, H., GÄRTNER, B., ANAGNOSTOPOULOS, I., REINKE, P. & TRAPPE, R. U. 2011. IL-6 and IL-10 in post-transplant lymphoproliferative disorders development and maintenance: a longitudinal study of cytokine plasma levels and T-cell subsets in 38 patients undergoing treatment. *Transpl Int,* 24**,** 892–903.

HISLOP, A. D., ANNELS, N. E., GUDGEON, N. H., LEESE, A. M. & RICKINSON, A. B. 2002. Epitope-specific evolution of human CD8(+) T cell responses from primary to persistent phases of Epstein-Barr virus infection. *J Exp Med,* 195**,** 893–905.

HISLOP, A. D., TAYLOR, G. S., SAUCE, D. & RICKINSON, A. B. 2007. Cellular responses to viral infection in humans: lessons from Epstein-Barr virus. *Annu Rev Immunol,* 25**,** 587–617.

HODGSON, S. H., MANSATTA, K., MALLETT, G., HARRIS, V., EMARY, K. R. W. & POLLARD, A. J. 2021. What defines an efficacious COVID-19 vaccine? A review of the challenges assessing the clinical efficacy of vaccines against SARS-CoV-2. *Lancet Infect Dis,* 21**,** e26–e35.

HOEGH-PETERSEN, M., GOODYEAR, D., GEDDES, M. N., LIU, S., UGARTE-TORRES, A., LIU, Y., WALKER, J. T., FONSECA, K., DALY, A., DUGGAN, P., STEWART, D., RUSSELL, J. A. & STOREK, J. 2011. High incidence of post transplant lymphoproliferative disorder after antithymocyte globulin-based conditioning and ineffective prediction by day 28 EBV-specific T lymphocyte counts. *Bone Marrow Transplantation,* 46**,** 1104–1112.

HOFFMANN, M., KLEINE-WEBER, H. & PÖHLMANN, S. 2020a. A Multibasic Cleavage Site in the Spike Protein of SARS-CoV-2 Is Essential for Infection of Human Lung Cells. *Mol Cell,* 78**,** 779–784.e5.

HOFFMANN, M., KLEINE-WEBER, H., SCHROEDER, S., KRÜGER, N., HERRLER, T., ERICHSEN, S., SCHIERGENS, T. S., HERRLER, G., WU, N. H., NITSCHE, A., MÜLLER, M. A., DROSTEN, C. & PÖHLMANN, S. 2020b. SARS-CoV-2 Cell Entry Depends on ACE2 and TMPRSS2 and Is Blocked by a Clinically Proven Protease Inhibitor. *Cell,* 181**,** 271–280.e8.

HOLLYMAN, D., STEFANSKI, J., PRZYBYLOWSKI, M., BARTIDO, S., BORQUEZ-OJEDA, O., TAYLOR, C., YEH, R., CAPACIO, V., OLSZEWSKA, M., HOSEY, J., SADELAIN, M., BRENTJENS, R. J. & RIVIÈRE, I. 2009. Manufacturing validation of biologically functional T cells targeted to CD19 antigen for autologous adoptive cell therapy. *J Immunother,* 32**,** 169–80.

HOMANN, D., DUMMER, W., WOLFE, T., RODRIGO, E., THEOFILOPOULOS, A. N., OLDSTONE, M. B. & VON HERRATH, M. G. 2006. Lack of intrinsic CTLA-4 expression has minimal effect on regulation of antiviral T-cell immunity. *J Virol,* 80**,** 270–80.

HOSOKAWA, H. & ROTHENBERG, E. V. 2021. How transcription factors drive choice of the T cell fate. *Nat Rev Immunol,* 21**,** 162–176.

HOU, Y. J., OKUDA, K., EDWARDS, C. E., MARTINEZ, D. R., ASAKURA, T., DINNON, K. H., 3RD, KATO, T., LEE, R. E., YOUNT, B. L., MASCENIK, T. M., CHEN, G., OLIVIER, K. N., GHIO, A., TSE, L. V., LEIST, S. R., GRALINSKI, L. E., SCHÄFER, A., DANG, H., GILMORE, R., NAKANO, S., SUN, L., FULCHER, M. L., LIVRAGHI-BUTRICO, A., NICELY, N. I., CAMERON, M., CAMERON, C., KELVIN, D. J., DE SILVA, A., MARGOLIS, D. M., MARKMANN, A., BARTELT, L., ZUMWALT, R., MARTINEZ, F. J., SALVATORE, S. P., BORCZUK, A., TATA, P. R., SONTAKE, V., KIMPLE, A., JASPERS, I., O'NEAL, W. K., RANDELL, S. H., BOUCHER, R. C. & BARIC, R. S. 2020. SARS-CoV-2 Reverse Genetics Reveals a Variable Infection Gradient in the Respiratory Tract. *Cell,* 182**,** 429–446.e14.

HOULDCROFT, C. J., PETROVA, V., LIU, J. Z., FRAMPTON, D., ANDERSON, C. A., GALL, A. & KELLAM, P. 2014. Host genetic variants and gene expression patterns associated with Epstein-Barr virus copy number in lymphoblastoid cell lines. *PLoS One,* 9**,** e108384.

HOWLEY, P. M. 2022. *Fields virology: DNA viruses,* Philadelphia, Wolters Kluwer.

HROMAS, R., CORNETTA, K., SROUR, E., BLANKE, C. & BROUN, E. R. 1994. Donor leukocyte infusion as therapy of life-threatening adenoviral infections after T-cell-depleted bone marrow transplantation. *Blood,* 84**,** 1689–90.

HUANG, C., WANG, Y., LI, X., REN, L., ZHAO, J., HU, Y., ZHANG, L., FAN, G., XU, J., GU, X., CHENG, Z., YU, T., XIA, J., WEI, Y., WU, W., XIE, X., YIN, W., LI, H., LIU, M., XIAO, Y., GAO, H., GUO, L., XIE, J., WANG, G., JIANG, R., GAO, Z., JIN, Q., WANG, J. & CAO, B. 2020a. Clinical features of patients infected with 2019 novel coronavirus in Wuhan, China. *Lancet,* 395**,** 497–506.

HUANG, H., WANG, C., RUBELT, F., SCRIBA, T. J. & DAVIS, M. M. 2020b. Analyzing the Mycobacterium tuberculosis immune response by T-cell receptor clustering with GLIPH2 and genome-wide antigen screening. *Nat Biotechnol,* 38**,** 1194–1202.

HUANG, J., FOGG, M., WIRTH, L. J., DALEY, H., RITZ, J., POSNER, M. R., WANG, F. C. & LORCH, J. H. 2017. Epstein-Barr virus-specific adoptive immunotherapy for recurrent, metastatic nasopharyngeal carcinoma. *Cancer,* 123**,** 2642–2650.

HUANG, W., BAI, L. & TANG, H. 2023. Epstein-Barr virus infection: the micro and macro worlds. *Virol J,* 20**,** 220.

HUGHES, C. E. & NIBBS, R. J. B. 2018. A guide to chemokines and their receptors. *Febs j,* 285**,** 2944–2971.

HUISMAN, W., HAGEMAN, L., LEBOUX, D. A. T., KHMELEVSKAYA, A., EFIMOV, G. A., ROEX, M. C. J., AMSEN, D., FALKENBURG, J. H. F. & JEDEMA, I. 2022. Public T-Cell Receptors (TCRs) Revisited by Analysis of the Magnitude of Identical and Highly-Similar TCRs in Virus-Specific T-Cell Repertoires of Healthy Individuals. *Front Immunol,* 13**,** 851868.

HUMME, S., REISBACH, G., FEEDERLE, R., DELECLUSE, H. J., BOUSSET, K., HAMMERSCHMIDT, W. & SCHEPERS, A. 2003. The EBV nuclear antigen 1 (EBNA1) enhances B cell immortalization several thousandfold. *Proc Natl Acad Sci U S A,* 100**,** 10989–94.

HURTON, L. V., SINGH, H., NAJJAR, A. M., SWITZER, K. C., MI, T., MAITI, S., OLIVARES, S., RABINOVICH, B., HULS, H., FORGET, M. A., DATAR, V., KEBRIAEI, P., LEE, D. A., CHAMPLIN, R. E. & COOPER, L. J. 2016. Tethered IL-15 augments antitumor activity and promotes a stem-cell memory subset in tumor-specific T cells. *Proc Natl Acad Sci U S A,* 113**,** E7788–e7797.

HUTT-FLETCHER, L. M. 2015. EBV glycoproteins: where are we now? *Future Virol,* 10**,** 1155–1162.

ICHEVA, V., KAYSER, S., WOLFF, D., TUVE, S., KYZIRAKOS, C., BETHGE, W., GREIL, J., ALBERT, M. H., SCHWINGER, W., NATHRATH, M., SCHUMM, M., STEVANOVIC, S., HANDGRETINGER, R., LANG, P. & FEUCHTINGER, T. 2013. Adoptive transfer of epstein-barr virus (EBV) nuclear antigen 1-specific t cells as treatment for EBV reactivation and lymphoproliferative disorders after allogeneic stem-cell transplantation. *J Clin Oncol,* 31**,** 39–48.

ISHIDA, Y., AGATA, Y., SHIBAHARA, K. & HONJO, T. 1992. Induced expression of PD-1, a novel member of the immunoglobulin gene superfamily, upon programmed cell death. *Embo j,* 11**,** 3887–95.

IWAKIRI, D., ZHOU, L., SAMANTA, M., MATSUMOTO, M., EBIHARA, T., SEYA, T., IMAI, S., FUJIEDA, M., KAWA, K. & TAKADA, K. 2009. Epstein-Barr virus (EBV)-encoded small RNA is released from EBV-infected cells and activates signaling from Toll-like receptor 3. *J Exp Med,* 206**,** 2091–9.

JACKSON, C. B., FARZAN, M., CHEN, B. & CHOE, H. 2022. Mechanisms of SARS-CoV-2 entry into cells. *Nat Rev Mol Cell Biol,* 23**,** 3–20.

JAIN, N., NGUYEN, H., CHAMBERS, C. & KANG, J. 2010. Dual function of CTLA-4 in regulatory T cells and conventional T cells to prevent multiorgan autoimmunity. *Proc Natl Acad Sci U S A,* 107**,** 1524–8.

JANGRA, S., DE VRIEZE, J., CHOI, A., RATHNASINGHE, R., LAGHLALI, G., UVYN, A., VAN HERCK, S., NUHN, L., DESWARTE, K., ZHONG, Z., SANDERS, N. N., LIENENKLAUS, S., DAVID, S. A., STROHMEIER, S., AMANAT, F., KRAMMER, F., HAMMAD, H., LAMBRECHT, B. N., COUGHLAN, L., GARCÍA-SASTRE, A., DE GEEST, B. G. & SCHOTSAERT, M. 2021. Sterilizing Immunity against SARS-CoV-2 Infection in Mice by a Single-Shot and Lipid Amphiphile Imidazoquinoline TLR7/8 Agonist-Adjuvanted Recombinant Spike Protein Vaccine*. *Angew Chem Int Ed Engl,* 60**,** 9467–9473.

JANTZ-NAEEM, N., BÖTTCHER-LOSCHINSKI, R., BORUCKI, K., MITCHELL-FLACK, M., BÖTTCHER, M., SCHRAVEN, B., MOUGIAKAKOS, D. & KAHLFUSS, S. 2023. TIGIT signaling and its influence on T cell metabolism and immune cell function in the tumor microenvironment. *Front Oncol,* 13**,** 1060112.

JAYASOORIYA, S., DE SILVA, T. I., NJIE-JOBE, J., SANYANG, C., LEESE, A. M., BELL, A. I., MCAULAY, K. A., YANCHUN, P., LONG, H. M., DONG, T., WHITTLE, H. C., RICKINSON, A. B., ROWLAND-JONES, S. L., HISLOP, A. D. & FLANAGAN, K. L. 2015. Early virological and immunological events in asymptomatic Epstein-Barr virus infection in African children. *PLoS Pathog,* 11**,** e1004746.

JHA, H. C., MEHTA, D., LU, J., EL-NACCACHE, D., SHUKLA, S. K., KOVACSICS, C., KOLSON, D. & ROBERTSON, E. S. 2015. Gammaherpesvirus Infection of Human Neuronal Cells. *mBio,* 6**,** e01844–15.

JIAN, X., ZHANG, Y., ZHAO, J., ZHAO, Z., LU, M. & XIE, L. 2023. CoV2-TCR: A web server for screening TCR CDR3 from TCR immune repertoire of COVID-19 patients and their recognized SARS-CoV-2 epitopes. *Comput Struct Biotechnol J,* 21**,** 1362–1371.

JIANG, H., FU, D., BIDGOLI, A. & PACZESNY, S. 2021. T Cell Subsets in Graft Versus Host Disease and Graft Versus Tumor. *Front Immunol,* 12**,** 761448.

JIANG, R., SCOTT, R. S. & HUTT-FLETCHER, L. M. 2006. Epstein-Barr virus shed in saliva is high in B-cell-tropic glycoprotein gp42. *J Virol,* 80**,** 7281–3.

JIANG, S., HILLYER, C. & DU, L. 2020. Neutralizing Antibodies against SARS-CoV-2 and Other Human Coronaviruses. *Trends Immunol,* 41**,** 355–359.

JIANG, W., CLANCY, L. E., AVDIC, S., SUTRAVE, G., STREET, J., SIMMS, R., MCGUIRE, H. M., PATRICK, E., CHAN, A. S., MCCAUGHAN, G., MYERS, N., MICKLETHWAITE, K. P., ANTONENAS, V., SELIM, A. G., RITCHIE, D., BATEMAN, C. M., SHAW, P. J., BLYTH, E. & GOTTLIEB, D. J. 2022. Third-party CMV- and EBV-specific T-cells for first viral reactivation after allogeneic stem cell transplant. *Blood Adv,* 6**,** 4949–4966.

JIN, J., SABATINO, M., SOMERVILLE, R., WILSON, J. R., DUDLEY, M. E., STRONCEK, D. F. & ROSENBERG, S. A. 2012. Simplified method of the growth of human tumor infiltrating lymphocytes in gas-permeable flasks to numbers needed for patient treatment. *J Immunother,* 35**,** 283–92.

JOHNSON, B. A., XIE, X., BAILEY, A. L., KALVERAM, B., LOKUGAMAGE, K. G., MURUATO, A., ZOU, J., ZHANG, X., JUELICH, T., SMITH, J. K., ZHANG, L., BOPP, N., SCHINDEWOLF, C., VU, M., VANDERHEIDEN, A., WINKLER, E. S., SWETNAM, D., PLANTE, J. A., AGUILAR, P., PLANTE, K. S., POPOV, V., LEE, B., WEAVER, S. C., SUTHAR, M. S., ROUTH, A. L., REN, P., KU, Z., AN, Z., DEBBINK, K., DIAMOND, M. S., SHI, P. Y., FREIBERG, A. N. & MENACHERY, V. D. 2021. Loss of furin cleavage site attenuates SARS-CoV-2 pathogenesis. *Nature,* 591**,** 293–299.

JOHNSTON, R. J., COMPS-AGRAR, L., HACKNEY, J., YU, X., HUSENI, M., YANG, Y., PARK, S., JAVINAL, V., CHIU, H., IRVING, B., EATON, D. L. & GROGAN, J. L. 2014. The immunoreceptor TIGIT regulates antitumor and antiviral CD8(+) T cell effector function. *Cancer Cell,* 26**,** 923–937.

JOSHI, K., MILIGHETTI, M. & CHAIN, B. M. 2022. Application of T cell receptor (TCR) repertoire analysis for the advancement of cancer immunotherapy. *Curr Opin Immunol,* 74**,** 1–8.

JU, B., ZHANG, Q., GE, J., WANG, R., SUN, J., GE, X., YU, J., SHAN, S., ZHOU, B., SONG, S., TANG, X., YU, J., LAN, J., YUAN, J., WANG, H., ZHAO, J., ZHANG, S., WANG, Y., SHI, X., LIU, L., ZHAO, J., WANG, X., ZHANG, Z. & ZHANG, L. 2020. Human neutralizing antibodies elicited by SARS-CoV-2 infection. *Nature,* 584**,** 115–119.

JUNE, C. H., LEDBETTER, J. A., GILLESPIE, M. M., LINDSTEN, T. & THOMPSON, C. B. 1987. T-cell proliferation involving the CD28 pathway is associated with cyclosporine-resistant interleukin 2 gene expression. *Mol Cell Biol,* 7**,** 4472–81.

KAEUFERLE, T., DEISENBERGER, L., JABLONOWSKI, L., STIEF, T. A., BLAESCHKE, F., WILLIER, S. & FEUCHTINGER, T. 2020. CRISPR-Cas9-Mediated Glucocorticoid Resistance in Virus-Specific T Cells for Adoptive T Cell Therapy Posttransplantation. *Mol Ther,* 28**,** 1965–1973.

KAGOYA, Y., GUO, T., YEUNG, B., SASO, K., ANCZUROWSKI, M., WANG, C. H., MURATA, K., SUGATA, K., SAIJO, H., MATSUNAGA, Y., OHASHI, Y., BUTLER, M. O. & HIRANO, N. 2020. Genetic Ablation of HLA Class I, Class II, and the T-cell Receptor Enables Allogeneic T Cells to Be Used for Adoptive T-cell Therapy. *Cancer Immunol Res,* 8**,** 926–936.

KÁLLAY, K., KASSA, C., RÉTI, M., KARÁSZI, É., SINKÓ, J., GODA, V., STRÉHN, A., CSORDÁS, K., HORVÁTH, O., SZEDERJESI, A., TASNÁDY, S., HARDI, A. & KRIVÁN, G. 2018. Early Experience With CliniMACS Prodigy CCS (IFN-gamma) System in Selection of Virus-specific T Cells From Third-party Donors for Pediatric Patients With Severe Viral Infections After Hematopoietic Stem Cell Transplantation. *J Immunother,* 41**,** 158–163.

KANAMORI, M., WATANABE, S., HONMA, R., KURODA, M., IMAI, S., TAKADA, K., YAMAMOTO, N., NISHIYAMA, Y. & KAWAGUCHI, Y. 2004. Epstein-Barr virus nuclear antigen leader protein induces expression of thymus- and activation-regulated chemokine in B cells. *J Virol,* 78**,** 3984–93.

KANDA, T., FURUSE, Y., OSHITANI, H. & KIYONO, T. 2016. Highly Efficient CRISPR/Cas9-Mediated Cloning and Functional Characterization of Gastric Cancer-Derived Epstein-Barr Virus Strains. *J Virol,* 90**,** 4383–93.

KANDA, T., HORIKOSHI, N., MURATA, T., KAWASHIMA, D., SUGIMOTO, A., NARITA, Y., KURUMIZAKA, H. & TSURUMI, T. 2013. Interaction between basic residues of Epstein-Barr virus EBNA1 protein and cellular chromatin mediates viral plasmid maintenance. *J Biol Chem,* 288**,** 24189–99.

KANG, S., TANAKA, T., INOUE, H., ONO, C., HASHIMOTO, S., KIOI, Y., MATSUMOTO, H., MATSUURA, H., MATSUBARA, T., SHIMIZU, K., OGURA, H., MATSUURA, Y. & KISHIMOTO, T. 2020. IL-6 trans-signaling induces plasminogen activator inhibitor-1 from vascular endothelial cells in cytokine release syndrome. *Proc Natl Acad Sci U S A,* 117**,** 22351–22356.

KAUFMANN, D. E., KAVANAGH, D. G., PEREYRA, F., ZAUNDERS, J. J., MACKEY, E. W., MIURA, T., PALMER, S., BROCKMAN, M., RATHOD, A., PIECHOCKA-TROCHA, A., BAKER, B., ZHU, B., LE GALL, S., WARING, M. T., AHERN, R., MOSS, K., KELLEHER, A. D., COFFIN, J. M., FREEMAN, G. J., ROSENBERG, E. S. & WALKER, B. D. 2007. Upregulation of CTLA-4 by HIV-specific CD4+ T cells correlates with disease progression and defines a reversible immune dysfunction. *Nat Immunol,* 8**,** 1246–54.

KAYMAZ, Y., ODUOR, C. I., AYDEMIR, O., LUFTIG, M. A., OTIENO, J. A., ONG'ECHA, J. M., BAILEY, J. A. & MOORMANN, A. M. 2020. Epstein-Barr Virus Genomes Reveal Population Structure and Type 1 Association with Endemic Burkitt Lymphoma. *J Virol,* 94.

KAZI, S., MATHUR, A., WILKIE, G., CHEAL, K., BATTLE, R., MCGOWAN, N., FRASER, N., HARGREAVES, E., TURNER, D., CAMPBELL, J. D. M., TURNER, M. & VICKERS, M. A. 2019. Long-term follow up after third-party viral-specific cytotoxic lymphocytes for immunosuppression- and Epstein-Barr virus-associated lymphoproliferative disease. *Haematologica,* 104**,** e356–e359.

KELLER, M. D., DARKO, S., LANG, H., RANSIER, A., LAZARSKI, C. A., WANG, Y., HANLEY, P. J., DAVILA, B. J., HEIMALL, J. R., AMBINDER, R. F., BARRETT, A. J., ROONEY, C. M., HESLOP, H. E., DOUEK, D. C. & BOLLARD, C. M. 2019. T-cell receptor sequencing demonstrates persistence of virus-specific T cells after antiviral immunotherapy. *Br J Haematol,* 187**,** 206–218.

KELLER, M. D., HARRIS, K. M., JENSEN-WACHSPRESS, M. A., KANKATE, V. V., LANG, H., LAZARSKI, C. A., DURKEE-SHOCK, J., LEE, P. H., CHAUDHRY, K., WEBBER, K., DATAR, A., TERPILOWSKI, M., REYNOLDS, E. K., STEVENSON, E. M., VAL, S., SHANCER, Z., ZHANG, N., ULREY, R., EKANEM, U., STANOJEVIC, M., GEIGER, A., LIANG, H., HOQ, F., ABRAHAM, A. A., HANLEY, P. J., CRUZ, C. R., FERRER, K., DROPULIC, L., GANGLER, K., BURBELO, P. D., JONES, R. B., COHEN, J. I. & BOLLARD, C. M. 2020. SARS-CoV-2-specific T cells are rapidly expanded for therapeutic use and target conserved regions of the membrane protein. *Blood,* 136**,** 2905–2917.

KELLY, G. L., LONG, H. M., STYLIANOU, J., THOMAS, W. A., LEESE, A., BELL, A. I., BORNKAMM, G. W., MAUTNER, J., RICKINSON, A. B. & ROWE, M. 2009. An Epstein-Barr virus anti-apoptotic protein constitutively expressed in transformed cells and implicated in burkitt lymphomagenesis: the Wp/BHRF1 link. *PLoS Pathog,* 5**,** e1000341.

KENNEY, S. C. & MERTZ, J. E. 2014. Regulation of the latent-lytic switch in Epstein-Barr virus. *Semin Cancer Biol,* 26, 60–8.

KHAN, N., HISLOP, A., GUDGEON, N., COBBOLD, M., KHANNA, R., NAYAK, L., RICKINSON, A. B. & MOSS, P. A. 2004. Herpesvirus-specific CD8 T cell immunity in old age: cytomegalovirus impairs the response to a coresident EBV infection. *J Immunol,* 173, 7481–9.

KHAN, N., SHARIFF, N., COBBOLD, M., BRUTON, R., AINSWORTH, J. A., SINCLAIR, A. J., NAYAK, L. & MOSS, P. A. 2002. Cytomegalovirus seropositivity drives the CD8 T cell repertoire toward greater clonality in healthy elderly individuals. *J Immunol,* 169, 1984–92.

KHANNA, R., BELL, S., SHERRITT, M., GALBRAITH, A., BURROWS, S. R., RAFTER, L., CLARKE, B., SLAUGHTER, R., FALK, M. C., DOUGLASS, J., WILLIAMS, T., ELLIOTT, S. L. & MOSS, D. J. 1999. Activation and adoptive transfer of Epstein-Barr virus-specific cytotoxic T cells in solid organ transplant patients with posttransplant lymphoproliferative disease. *Proc Natl Acad Sci U S A,* 96, 10391–6.

KHOO, W. H., JACKSON, K., PHETSOUPHANH, C., ZAUNDERS, J. J., ALQUICIRA-HERNANDEZ, J., YAZAR, S., RUIZ-DIAZ, S., SINGH, M., DHENNI, R., KYAW, W., TEA, F., MERHEB, V., LEE, F. X. Z., BURRELL, R., HOWARD-JONES, A., KOIRALA, A., ZHOU, L., YUKSEL, A., CATCHPOOLE, D. R., LAI, C. L., VITAGLIANO, T. L., ROUET, R., CHRIST, D., TANG, B., WEST, N. P., GEORGE, S., GERRARD, J., CROUCHER, P. I., KELLEHER, A. D., GOODNOW, C. G., SPRENT, J. D., POWELL, J. E., BRILOT, F., NANAN, R., HSU, P. S., DEENICK, E. K., BRITTON, P. N. & PHAN, T. G. 2023. Tracking the clonal dynamics of SARS-CoV-2-specific T cells in children and adults with mild/asymptomatic COVID-19. *Clin Immunol,* 246, 109209.

KIEFF, E. Epstein-Barr virus and its replication. 1996.

KIESER, A. & STERZ, K. R. 2015. The Latent Membrane Protein 1 (LMP1). *Curr Top Microbiol Immunol,* 391, 119–49.

KIM, D., LEE, J. Y., YANG, J. S., KIM, J. W., KIM, V. N. & CHANG, H. 2020a. The Architecture of SARS-CoV-2 Transcriptome. *Cell,* 181, 914–921.e10.

KIM, J. M., CHUNG, Y. S., JO, H. J., LEE, N. J., KIM, M. S., WOO, S. H., PARK, S., KIM, J. W., KIM, H. M. & HAN, M. G. 2020b. Identification of Coronavirus Isolated from a Patient in Korea with COVID-19. *Osong Public Health Res Perspect,* 11, 3–7.

KIM, N., LEE, J. M., OH, E. J., JEKARL, D. W., LEE, D. G., IM, K. I. & CHO, S. G. 2021. Off-the-Shelf Partial HLA Matching SARS-CoV-2 Antigen Specific T Cell Therapy: A New Possibility for COVID-19 Treatment. *Front Immunol,* 12, 751869.

KIM, N., NAM, Y. S., IM, K. I., LIM, J. Y., JEON, Y. W., SONG, Y., LEE, J. W. & CHO, S. G. 2018. Robust Production of Cytomegalovirus pp65-Specific T Cells Using a Fully Automated IFN-γ Cytokine Capture System. *Transfus Med Hemother,* 45, 13–22.

KINCH, A., SUNDSTRÖM, C., TUFVESON, G. & GLIMELIUS, I. 2016. Association between HLA-A1 and -A2 types and Epstein-Barr virus status of post-transplant lymphoproliferative disorder. *Leuk Lymphoma,* 57, 2351–8.

KINZEL, M., DOWHAN, M., KALRA, A., WILLIAMSON, T. S., DABAS, R., JAMANI, K., CHAUDHRY, A., SHAFEY, M., JIMENEZ-ZEPEDA, V., DUGGAN, P., DALY, A., DHARMANI-KHAN, P., KHAN, F. & STOREK, J. 2022. Risk Factors for the Incidence of and the Mortality due to Post-Transplant Lymphoproliferative Disorder after Hematopoietic Cell Transplantation. *Transplant Cell Ther,* 28, 53.e1–53.e10.

KIRTIPAL, N., BHARADWAJ, S. & KANG, S. G. 2020. From SARS to SARS-CoV-2, insights on structure, pathogenicity and immunity aspects of pandemic human coronaviruses. *Infect Genet Evol,* 85**,** 104502.

KLASSEN, S. A., SENEFELD, J. W., SENESE, K. A., JOHNSON, P. W., WIGGINS, C. C., BAKER, S. E., VAN HELMOND, N., BRUNO, K. A., PIROFSKI, L. A., SHOHAM, S., GROSSMAN, B. J., HENDERSON, J. P., WRIGHT, R. S., FAIRWEATHER, D., PANETH, N. S., CARTER, R. E., CASADEVALL, A. & JOYNER, M. J. 2021. Convalescent Plasma Therapy for COVID-19: A Graphical Mosaic of the Worldwide Evidence. *Front Med (Lausanne),* 8**,** 684151.

KLEBANOFF, C. A., GATTINONI, L., TORABI-PARIZI, P., KERSTANN, K., CARDONES, A. R., FINKELSTEIN, S. E., PALMER, D. C., ANTONY, P. A., HWANG, S. T., ROSENBERG, S. A., WALDMANN, T. A. & RESTIFO, N. P. 2005. Central memory self/tumor-reactive CD8+ T cells confer superior antitumor immunity compared with effector memory T cells. *Proc Natl Acad Sci U S A,* 102**,** 9571–6.

KLEIN, G. 1994. Epstein-Barr virus strategy in normal and neoplastic B cells. *Cell,* 77**,** 791–3.

KLEIN, S., CORTESE, M., WINTER, S. L., WACHSMUTH-MELM, M., NEUFELDT, C. J., CERIKAN, B., STANIFER, M. L., BOULANT, S., BARTENSCHLAGER, R. & CHLANDA, P. 2020. SARS-CoV-2 structure and replication characterized by in situ cryo-electron tomography. *Nat Commun,* 11**,** 5885.

KLOK, F. A., KRUIP, M., VAN DER MEER, N. J. M., ARBOUS, M. S., GOMMERS, D., KANT, K. M., KAPTEIN, F. H. J., VAN PAASSEN, J., STALS, M. A. M., HUISMAN, M. V. & ENDEMAN, H. 2020. Confirmation of the high cumulative incidence of thrombotic complications in critically ill ICU patients with COVID-19: An updated analysis. *Thromb Res,* 191**,** 148–150.

KOCKELBERGH, H., EVANS, S., DENG, T., CLYNE, E., KYRIAKIDOU, A., ECONOMOU, A., LUU HOANG, K. N., WOODMANSEY, S., FOERS, A., FOWLER, A. & SOILLEUX, E. J. 2022. Utility of Bulk T-Cell Receptor Repertoire Sequencing Analysis in Understanding Immune Responses to COVID-19. *Diagnostics (Basel),* 12.

KOENEN, H., KOUIJZER, I. J. E., DE GROOT, M., PETERS, S., LOBEEK, D., VAN GENUGTEN, E. A. J., DIAVATOPOULOS, D. A., VAN OOSTEN, N., GIANOTTEN, S., PROKOP, M. M., NETEA, M. G., VAN DE VEERDONK, F. L. & AARNTZEN, E. 2024. Preliminary evidence of localizing CD8+ T-cell responses in COVID-19 patients with PET imaging. *Front Med (Lausanne),* 11**,** 1414415.

KOSTOPOULOS, I. V., OROLOGAS-STAVROU, N., ROUSAKIS, P., PANTELI, C., NTANASIS-STATHOPOULOS, I., CHARITAKI, I., KOROMPOKI, E., GAVRIATOPOULOU, M., KASTRITIS, E., TROUGAKOS, I. P., DIMOPOULOS, M. A., TSITSILONIS, O. E. & TERPOS, E. 2021. Recovery of Innate Immune Cells and Persisting Alterations in Adaptive Immunity in the Peripheral Blood of Convalescent Plasma Donors at Eight Months Post SARS-CoV-2 Infection. *Microorganisms,* 9.

KOUO, T., HUANG, L., PUCSEK, A. B., CAO, M., SOLT, S., ARMSTRONG, T. & JAFFEE, E. 2015. Galectin-3 Shapes Antitumor Immune Responses by Suppressing CD8+ T Cells via LAG-3 and Inhibiting Expansion of Plasmacytoid Dendritic Cells. *Cancer Immunol Res,* 3**,** 412–23.

KOUTSAKOS, M., ROWNTREE, L. C., HENSEN, L., CHUA, B. Y., VAN DE SANDT, C. E., HABEL, J. R., ZHANG, W., JIA, X., KEDZIERSKI, L., ASHHURST, T. M., PUTRI, G. H., MARSH-WAKEFIELD, F., READ, M. N., EDWARDS, D. N., CLEMENS, E. B., WONG, C. Y., MORDANT, F. L., JUNO, J. A., AMANAT, F.,

AUDSLEY, J., HOLMES, N. E., GORDON, C. L., SMIBERT, O. C., TRUBIANO, J. A., HUGHES, C. M., CATTON, M., DENHOLM, J. T., TONG, S. Y. C., DOOLAN, D. L., KOTSIMBOS, T. C., JACKSON, D. C., KRAMMER, F., GODFREY, D. I., CHUNG, A. W., KING, N. J. C., LEWIN, S. R., WHEATLEY, A. K., KENT, S. J., SUBBARAO, K., MCMAHON, J., THEVARAJAN, I., NGUYEN, T. H. O., CHENG, A. C. & KEDZIERSKA, K. 2021. Integrated immune dynamics define correlates of COVID-19 severity and antibody responses. *Cell Rep Med,* 2**,** 100208.

KRATZER, B., TRAPIN, D., ETTEL, P., KÖRMÖCZI, U., ROTTAL, A., TUPPY, F., FEICHTER, M., GATTINGER, P., BOROCHOVA, K., DOROFEEVA, Y., TULAEVA, I., WEBER, M., GRABMEIER-PFISTERSHAMMER, K., TAUBER, P. A., GERDOV, M., MÜHL, B., PERKMANN, T., FAE, I., WENDA, S., FÜHRER, H., HENNING, R., VALENTA, R. & PICKL, W. F. 2021. Immunological imprint of COVID-19 on human peripheral blood leukocyte populations. *Allergy,* 76**,** 751–765.

KROEMER, M., BOULLEROT, L., RAMSEYER, M., SPEHNER, L., BARISIEN, C., GRAVELIN, E., RENAUDIN, A., COGNASSE, F., GALLIAN, P., HERMINE, O., LACOMBE, K., TIBERGHIEN, P. & ADOTÉVI, O. 2022. The Quality of Anti-SARS-CoV-2 T Cell Responses Predicts the Neutralizing Antibody Titer in Convalescent Plasma Donors. *Front Public Health,* 10**,** 816848.

KRUMMEL, M. F. & ALLISON, J. P. 1995. CD28 and CTLA-4 have opposing effects on the response of T cells to stimulation. *J Exp Med,* 182**,** 459–65.

KRUSE, M., DARK, C., ASPDEN, M., COCHRANE, D., COMPETIELLO, R., PELTZ, M., TORRES, L., WRIGHTON-SMITH, P. & DUDEK, M. 2021. Performance of the T-SPOT(®).COVID test for detecting SARS-CoV-2-responsive T cells. *Int J Infect Dis,* 113**,** 155–161.

KUBA, K., IMAI, Y., RAO, S., GAO, H., GUO, F., GUAN, B., HUAN, Y., YANG, P., ZHANG, Y., DENG, W., BAO, L., ZHANG, B., LIU, G., WANG, Z., CHAPPELL, M., LIU, Y., ZHENG, D., LEIBBRANDT, A., WADA, T., SLUTSKY, A. S., LIU, D., QIN, C., JIANG, C. & PENNINGER, J. M. 2005. A crucial role of angiotensin converting enzyme 2 (ACE2) in SARS coronavirus-induced lung injury. *Nat Med,* 11**,** 875–9.

KUDRYAVTSEV, I. V., ARSENTIEVA, N. A., BATSUNOV, O. K., KOROBOVA, Z. R., KHAMITOVA, I. V., ISAKOV, D. V., KUZNETSOVA, R. N., RUBINSTEIN, A. A., STANEVICH, O. V., LEBEDEVA, A. A., VOROBYOV, E. A., VOROBYOVA, S. V., KULIKOV, A. N., SHARAPOVA, M. A., PEVTCOV, D. E. & TOTOLIAN, A. A. 2021. Alterations in B Cell and Follicular T-Helper Cell Subsets in Patients with Acute COVID-19 and COVID-19 Convalescents. *Curr Issues Mol Biol,* 44**,** 194–205.

KUEBERUWA, G., GORNALL, H., ALCANTAR-OROZCO, E. M., BOUVIER, D., KAPACEE, Z. A., HAWKINS, R. E. & GILHAM, D. E. 2017. CCR7(+) selected gene-modified T cells maintain a central memory phenotype and display enhanced persistence in peripheral blood in vivo. *J Immunother Cancer,* 5**,** 14.

KULWICHIT, W., EDWARDS, R. H., DAVENPORT, E. M., BASKAR, J. F., GODFREY, V. & RAAB-TRAUB, N. 1998. Expression of the Epstein-Barr virus latent membrane protein 1 induces B cell lymphoma in transgenic mice. *Proc Natl Acad Sci U S A,* 95**,** 11963–8.

KUMAKI, Y., ENNIS, J., RAHBAR, R., TURNER, J. D., WANDERSEE, M. K., SMITH, A. J., BAILEY, K. W., VEST, Z. G., MADSEN, J. R., LI, J. K. & BARNARD, D. L. 2011. Single-dose intranasal administration with mDEF201 (adenovirus

vectored mouse interferon-alpha) confers protection from mortality in a lethal SARS-CoV BALB/c mouse model. *Antiviral Res,* 89**,** 75–82.
KUMAR, B. V., CONNORS, T. J. & FARBER, D. L. 2018. Human T Cell Development, Localization, and Function throughout Life. *Immunity,* 48**,** 202–213.
KURTH, J., SPIEKER, T., WUSTROW, J., STRICKLER, G. J., HANSMANN, L. M., RAJEWSKY, K. & KÜPPERS, R. 2000. EBV-infected B cells in infectious mononucleosis: viral strategies for spreading in the B cell compartment and establishing latency. *Immunity,* 13**,** 485–95.
KUWAJIMA, S., SATO, T., ISHIDA, K., TADA, H., TEZUKA, H. & OHTEKI, T. 2006. Interleukin 15-dependent crosstalk between conventional and plasmacytoid dendritic cells is essential for CpG-induced immune activation. *Nat Immunol,* 7**,** 740–6.
KWOK, H., TONG, A. H., LIN, C. H., LOK, S., FARRELL, P. J., KWONG, D. L. & CHIANG, A. K. 2012. Genomic sequencing and comparative analysis of Epstein-Barr virus genome isolated from primary nasopharyngeal carcinoma biopsy. *PLoS One,* 7**,** e36939.
KWOK, H., WU, C. W., PALSER, A. L., KELLAM, P., SHAM, P. C., KWONG, D. L. & CHIANG, A. K. 2014. Genomic diversity of Epstein-Barr virus genomes isolated from primary nasopharyngeal carcinoma biopsy samples. *J Virol,* 88**,** 10662–72.
L'HUILLIER, A. G., DIPCHAND, A. I., NG, V. L., HEBERT, D., AVITZUR, Y., SOLOMON, M., NGAN, B. Y., STEPHENS, D., PUNNETT, A. S., BARTON, M. & ALLEN, U. D. 2019. Posttransplant lymphoproliferative disorder in pediatric patients: Survival rates according to primary sites of occurrence and a proposed clinical categorization. *Am J Transplant,* 19**,** 2764–2774.
LAICHALK, L. L. & THORLEY-LAWSON, D. A. 2005. Terminal differentiation into plasma cells initiates the replicative cycle of Epstein-Barr virus in vivo. *J Virol,* 79**,** 1296–307.
LAM, T. T., JIA, N., ZHANG, Y. W., SHUM, M. H., JIANG, J. F., ZHU, H. C., TONG, Y. G., SHI, Y. X., NI, X. B., LIAO, Y. S., LI, W. J., JIANG, B. G., WEI, W., YUAN, T. T., ZHENG, K., CUI, X. M., LI, J., PEI, G. Q., QIANG, X., CHEUNG, W. Y., LI, L. F., SUN, F. F., QIN, S., HUANG, J. C., LEUNG, G. M., HOLMES, E. C., HU, Y. L., GUAN, Y. & CAO, W. C. 2020. Identifying SARS-CoV-2-related coronaviruses in Malayan pangolins. *Nature,* 583**,** 282–285.
LAMERS, M. M. & HAAGMANS, B. L. 2022. SARS-CoV-2 pathogenesis. *Nat Rev Microbiol,* 20**,** 270–284.
LAMERS, M. M., MYKYTYN, A. Z., BREUGEM, T. I., WANG, Y., WU, D. C., RIESEBOSCH, S., VAN DEN DOEL, P. B., SCHIPPER, D., BESTEBROER, T., WU, N. C. & HAAGMANS, B. L. 2021. Human airway cells prevent SARS-CoV-2 multibasic cleavage site cell culture adaptation. *Elife,* 10.
LANDAIS, E., SAULQUIN, X., SCOTET, E., TRAUTMANN, L., PEYRAT, M. A., YATES, J. L., KWOK, W. W., BONNEVILLE, M. & HOUSSAINT, E. 2004. Direct killing of Epstein-Barr virus (EBV)-infected B cells by CD4 T cells directed against the EBV lytic protein BHRF1. *Blood,* 103**,** 1408–16.
LANDGREN, O., GILBERT, E. S., RIZZO, J. D., SOCIÉ, G., BANKS, P. M., SOBOCINSKI, K. A., HOROWITZ, M. M., JAFFE, E. S., KINGMA, D. W., TRAVIS, L. B., FLOWERS, M. E., MARTIN, P. J., DEEG, H. J. & CURTIS, R. E. 2009. Risk factors for lymphoproliferative disorders after allogeneic hematopoietic cell transplantation. *Blood,* 113**,** 4992–5001.
LANFERMEIJER, J., DE GREEF, P. C., HENDRIKS, M., VOS, M., VAN BEEK, J., BORGHANS, J. A. M. & VAN BAARLE, D. 2021. Age and CMV-Infection

Jointly Affect the EBV-Specific CD8(+) T-Cell Repertoire. *Front Aging,* 2**,** 665637.

LAU, S. Y., WANG, P., MOK, B. W., ZHANG, A. J., CHU, H., LEE, A. C., DENG, S., CHEN, P., CHAN, K. H., SONG, W., CHEN, Z., TO, K. K., CHAN, J. F., YUEN, K. Y. & CHEN, H. 2020. Attenuated SARS-CoV-2 variants with deletions at the S1/S2 junction. *Emerg Microbes Infect,* 9**,** 837–842.

LAUER, S. A., GRANTZ, K. H., BI, Q., JONES, F. K., ZHENG, Q., MEREDITH, H. R., AZMAN, A. S., REICH, N. G. & LESSLER, J. 2020. The Incubation Period of Coronavirus Disease 2019 (COVID-19) From Publicly Reported Confirmed Cases: Estimation and Application. *Ann Intern Med,* 172**,** 577–582.

LAW, J. C., KOH, W. H., BUDYLOWSKI, P., LIN, J., YUE, F., ABE, K. T., RATHOD, B., GIRARD, M., LI, Z., RINI, J. M., MUBAREKA, S., MCGEER, A., CHAN, A. K., GINGRAS, A. C., WATTS, T. H. & OSTROWSKI, M. A. 2021. Systematic Examination of Antigen-Specific Recall T Cell Responses to SARS-CoV-2 versus Influenza Virus Reveals a Distinct Inflammatory Profile. *J Immunol*, 206**,** 37–50.

LAW, J. C. & WATTS, T. H. 2023. Considerations for Choosing T Cell Assays during a Pandemic. *J Immunol,* 211**,** 169–174.

LE BERT, N., TAN, A. T., KUNASEGARAN, K., THAM, C. Y. L., HAFEZI, M., CHIA, A., CHNG, M. H. Y., LIN, M., TAN, N., LINSTER, M., CHIA, W. N., CHEN, M. I., WANG, L. F., OOI, E. E., KALIMUDDIN, S., TAMBYAH, P. A., LOW, J. G., TAN, Y. J. & BERTOLETTI, A. 2020. SARS-CoV-2-specific T cell immunity in cases of COVID-19 and SARS, and uninfected controls. *Nature,* 584**,** 457–462.

LE, K., KANNAPPAN, S., KIM, T., LEE, J. H., LEE, H. R. & KIM, K. K. 2023. Structural understanding of SARS-CoV-2 virus entry to host cells. *Front Mol Biosci,* 10**,** 1288686.

LEBEDEV, A. A., KRAUSE, M. H., ISIDRO, A. L., VAGIN, A. A., ORLOVA, E. V., TURNER, J., DODSON, E. J., TAVARES, P. & ANTSON, A. A. 2007. Structural framework for DNA translocation via the viral portal protein. *Embo j,* 26**,** 1984–94.

LEE, C. C., HSU, T. C., KUO, C. C., LIU, M. A., ABDELFATTAH, A. M., CHANG, C. N., YAO, M., LI, C. C., WU, K. H., CHEN, T. C., GAU, J. P., WANG, P. N., LIU, Y. C., CHIOU, L. W., LEE, M. Y., LI, S. S., CHAO, T. Y., JOU, S. T. & CHANG, H. H. 2021. Validation of a Post-Transplant Lymphoproliferative Disorder Risk Prediction Score and Derivation of a New Prediction Score Using a National Bone Marrow Transplant Registry Database. *Oncologist,* 26**,** e2034–e2041.

LEE, J., SHEEN, J. H., LIM, O., LEE, Y., RYU, J., SHIN, D., KIM, Y. Y. & KIM, M. 2020. Abrogation of HLA surface expression using CRISPR/Cas9 genome editing: a step toward universal T cell therapy. *Sci Rep,* 10**,** 17753.

LEE, J., SU, E. W., ZHU, C., HAINLINE, S., PHUAH, J., MOROCO, J. A., SMITHGALL, T. E., KUCHROO, V. K. & KANE, L. P. 2011. Phosphotyrosine-dependent coupling of Tim-3 to T-cell receptor signaling pathways. *Mol Cell Biol,* 31**,** 3963–74.

LEE, N., MOSS, W. N., YARIO, T. A. & STEITZ, J. A. 2015. EBV noncoding RNA binds nascent RNA to drive host PAX5 to viral DNA. *Cell,* 160**,** 607–618.

LEEHAN, K. M. & KOELSCH, K. A. 2015. T Cell ELISPOT: For the Identification of Specific Cytokine-Secreting T Cells. *Methods Mol Biol,* 1312**,** 427–34.

LEEN, A., MEIJ, P., REDCHENKO, I., MIDDELDORP, J., BLOEMENA, E., RICKINSON, A. & BLAKE, N. 2001. Differential immunogenicity of Epstein-Barr virus latent-cycle proteins for human CD4(+) T-helper 1 responses. *J Virol,* 75**,** 8649–59.

LEEN, A. M., BOLLARD, C. M., MENDIZABAL, A. M., SHPALL, E. J., SZABOLCS, P., ANTIN, J. H., KAPOOR, N., PAI, S. Y., ROWLEY, S. D., KEBRIAEI, P., DEY, B. R., GRILLEY, B. J., GEE, A. P., BRENNER, M. K., ROONEY, C. M. & HESLOP, H. E. 2013. Multicenter study of banked third-party virus-specific T cells to treat severe viral infections after hematopoietic stem cell transplantation. *Blood,* 121, 5113–23.

LEEN, A. M., HESLOP, H. E. & BRENNER, M. K. 2014. Antiviral T-cell therapy. *Immunol Rev,* 258, 12–29.

LEI, H., LI, T., HUNG, G. C., LI, B., TSAI, S. & LO, S. C. 2013. Identification and characterization of EBV genomes in spontaneously immortalized human peripheral blood B lymphocytes by NGS technology. *BMC Genomics,* 14, 804.

LEISMAN, D. E., RONNER, L., PINOTTI, R., TAYLOR, M. D., SINHA, P., CALFEE, C. S., HIRAYAMA, A. V., MASTROIANI, F., TURTLE, C. J., HARHAY, M. O., LEGRAND, M. & DEUTSCHMAN, C. S. 2020. Cytokine elevation in severe and critical COVID-19: a rapid systematic review, meta-analysis, and comparison with other inflammatory syndromes. *Lancet Respir Med,* 8, 1233–1244.

LERNER, E. C., WORONIECKA, K. I., D'ANNIBALLE, V. M., WILKINSON, D. S., MOHAN, A. A., LORREY, S. J., WAIBL-POLANIA, J., WACHSMUTH, L. P., MIGGELBRINK, A. M., JACKSON, J. D., CUI, X., RAJ, J. A., TOMASZEWSKI, W. H., COOK, S. L., SAMPSON, J. H., PATEL, A. P., KHASRAW, M., GUNN, M. D. & FECCI, P. E. 2023. CD8(+) T cells maintain killing of MHC-I-negative tumor cells through the NKG2D-NKG2DL axis. *Nat Cancer,* 4, 1258–1272.

LERNER, K. G., KAO, G. F., STORB, R., BUCKNER, C. D., CLIFT, R. A. & THOMAS, E. D. 1974. Histopathology of graft-vs.-host reaction (GvHR) in human recipients of marrow from HL-A-matched sibling donors. *Transplant Proc,* 6, 367–71.

LERNER, M. R., ANDREWS, N. C., MILLER, G. & STEITZ, J. A. 1981. Two small RNAs encoded by Epstein-Barr virus and complexed with protein are precipitated by antibodies from patients with systemic lupus erythematosus. *Proc Natl Acad Sci U S A,* 78, 805–9.

LEUNG, A. K. C., LAM, J. M. & BARANKIN, B. 2024. Infectious Mononucleosis: An Updated Review. *Curr Pediatr Rev,* 20, 305–322.

LEUNG, C. S., MAURER, M. A., MEIXLSPERGER, S., LIPPMANN, A., CHEONG, C., ZUO, J., HAIGH, T. A., TAYLOR, G. S. & MÜNZ, C. 2013. Robust T-cell stimulation by Epstein-Barr virus-transformed B cells after antigen targeting to DEC-205. *Blood,* 121, 1584–94.

LEUNG, W., SOH, T. G., LINN, Y. C., LOW, J. G., LOH, J., CHAN, M., CHNG, W. J., KOH, L. P., POON, M. L., NG, K. P., KUICK, C. H., TAN, T. T., TAN, L. K. & SENG, M. S. 2020. Rapid production of clinical-grade SARS-CoV-2 specific T cells. *Adv Cell Gene Ther,* 3, e101.

LI, D., EDWARDS, R. J., MANNE, K., MARTINEZ, D. R., SCHÄFER, A., ALAM, S. M., WIEHE, K., LU, X., PARKS, R., SUTHERLAND, L. L., OGUIN, T. H., 3RD, MCDANAL, C., PEREZ, L. G., MANSOURI, K., GOBEIL, S. M. C., JANOWSKA, K., STALLS, V., KOPP, M., CAI, F., LEE, E., FOULGER, A., HERNANDEZ, G. E., SANZONE, A., TILAHUN, K., JIANG, C., TSE, L. V., BOCK, K. W., MINAI, M., NAGATA, B. M., CRONIN, K., GEE-LAI, V., DEYTON, M., BARR, M., VON HOLLE, T., MACINTYRE, A. N., STOVER, E., FELDMAN, J., HAUSER, B. M., CARADONNA, T. M., SCOBEY, T. D., ROUNTREE, W., WANG, Y., MOODY, M. A., CAIN, D. W., DEMARCO, C. T., DENNY, T. N., WOODS, C. W., PETZOLD, E. W., SCHMIDT, A. G., TENG, I. T., ZHOU, T., KWONG, P. D., MASCOLA,

J. R., GRAHAM, B. S., MOORE, I. N., SEDER, R., ANDERSEN, H., LEWIS, M. G., MONTEFIORI, D. C., SEMPOWSKI, G. D., BARIC, R. S., ACHARYA, P., HAYNES, B. F. & SAUNDERS, K. O. 2021. In vitro and in vivo functions of SARS-CoV-2 infection-enhancing and neutralizing antibodies. *Cell,* 184**,** 4203–4219.e32.

LI, H. M., HIROI, T., ZHANG, Y., SHI, A., CHEN, G., DE, S., METTER, E. J., WOOD, W. H., 3RD, SHAROV, A., MILNER, J. D., BECKER, K. G., ZHAN, M. & WENG, N. P. 2016. TCRß repertoire of CD4+ and CD8+ T cells is distinct in richness, distribution, and CDR3 amino acid composition. *J Leukoc Biol,* 99**,** 505–13.

LI, N., JILISIHAN, B., WANG, W., TANG, Y. & KEYOUMU, S. 2018. Soluble LAG3 acts as a potential prognostic marker of gastric cancer and its positive correlation with CD8+T cell frequency and secretion of IL-12 and INF-γ in peripheral blood. *Cancer Biomark,* 23**,** 341–351.

LI, Q., GUAN, X., WU, P., WANG, X., ZHOU, L., TONG, Y., REN, R., LEUNG, K. S. M., LAU, E. H. Y., WONG, J. Y., XING, X., XIANG, N., WU, Y., LI, C., CHEN, Q., LI, D., LIU, T., ZHAO, J., LIU, M., TU, W., CHEN, C., JIN, L., YANG, R., WANG, Q., ZHOU, S., WANG, R., LIU, H., LUO, Y., LIU, Y., SHAO, G., LI, H., TAO, Z., YANG, Y., DENG, Z., LIU, B., MA, Z., ZHANG, Y., SHI, G., LAM, T. T. Y., WU, J. T., GAO, G. F., COWLING, B. J., YANG, B., LEUNG, G. M. & FENG, Z. 2020. Early Transmission Dynamics in Wuhan, China, of Novel Coronavirus-Infected Pneumonia. *N Engl J Med,* 382**,** 1199–1207.

LI, W., DUAN, X., CHEN, X., ZHAN, M., PENG, H., MENG, Y., LI, X., LI, X. Y., PANG, G. & DOU, X. 2022. Immunotherapeutic approaches in EBV-associated nasopharyngeal carcinoma. *Front Immunol,* 13**,** 1079515.

LI, X., MOLINA-MOLINA, M., ABDUL-HAFEZ, A., UHAL, V., XAUBET, A. & UHAL, B. D. 2008. Angiotensin converting enzyme-2 is protective but downregulated in human and experimental lung fibrosis. *Am J Physiol Lung Cell Mol Physiol,* 295**,** L178–85.

LIANG, H., LUO, D., LIAO, H. & LI, S. 2022. Coronavirus Usurps the Autophagy-Lysosome Pathway and Induces Membranes Rearrangement for Infection and Pathogenesis. *Front Microbiol,* 13**,** 846543.

LIAO, Y., YAN, J., KONG, I., LI, Z., DING, W., CLARK, S., GIULINO-ROTH, L. & GEWURZ, B. E. 2025. The Histone Demethylase LSD1/ZNF217/CoREST Complex is a Major Restriction Factor of Epstein-Barr Virus Lytic Reactivation. *Res Sq*.

LICHTERFELD, M., YU, X. G., WARING, M. T., MUI, S. K., JOHNSTON, M. N., COHEN, D., ADDO, M. M., ZAUNDERS, J., ALTER, G., PAE, E., STRICK, D., ALLEN, T. M., ROSENBERG, E. S., WALKER, B. D. & ALTFELD, M. 2004. HIV-1-specific cytotoxicity is preferentially mediated by a subset of CD8(+) T cells producing both interferon-gamma and tumor necrosis factor-alpha. *Blood,* 104**,** 487–94.

LIN, M., BHAKDI, S. C., TAN, D., LEE, J. J. X., TAI, D. W. M., PAVESI, A., WAI, L. E., WANG, T., BERTOLETTI, A. & TAN, A. T. 2023. Lytic efficiency of immunosuppressive drug-resistant armoured T cells against circulating HBV-related HCC in whole blood. *Immunother Adv,* 3**,** ltad015.

LIN, W., YIP, Y. L., JIA, L., DENG, W., ZHENG, H., DAI, W., KO, J. M. Y., LO, K. W., CHUNG, G. T. Y., YIP, K. Y., LEE, S. D., KWAN, J. S., ZHANG, J., LIU, T., CHAN, J. Y., KWONG, D. L., LEE, V. H., NICHOLLS, J. M., BUSSON, P., LIU, X., CHIANG, A. K. S., HUI, K. F., KWOK, H., CHEUNG, S. T., CHEUNG, Y. C., CHAN, C. K., LI, B., CHEUNG, A. L., HAU, P. M., ZHOU, Y., TSANG, C. M., MIDDELDORP, J., CHEN, H., LUNG, M. L. & TSAO, S. W. 2018.

Establishment and characterization of new tumor xenografts and cancer cell lines from EBV-positive nasopharyngeal carcinoma. *Nat Commun,* 9**,** 4663.

LIN, X., TSAI, M. H., SHUMILOV, A., POIREY, R., BANNERT, H., MIDDELDORP, J. M., FEEDERLE, R. & DELECLUSE, H. J. 2015. The Epstein-Barr Virus BART miRNA Cluster of the M81 Strain Modulates Multiple Functions in Primary B Cells. *PLoS Pathog,* 11**,** e1005344.

LIN, Z., WANG, X., STRONG, M. J., CONCHA, M., BADDOO, M., XU, G., BARIBAULT, C., FEWELL, C., HULME, W., HEDGES, D., TAYLOR, C. M. & FLEMINGTON, E. K. 2013. Whole-genome sequencing of the Akata and Mutu Epstein-Barr virus strains. *J Virol,* 87**,** 1172–82.

LINDSAY, J., KERRIDGE, I., WILCOX, L., TRAN, S., O'BRIEN, T. A., GREENWOOD, M., CHEN, S. C., KONG, D. C. M., PERGAM, S. A., LIU, C. & SLAVIN, M. A. 2021. Infection-Related Mortality in Adults and Children Undergoing Allogeneic Hematopoietic Cell Transplantation: An Australian Registry Report. *Transplant Cell Ther,* 27**,** 798.e1–798.e10.

LINDSTEN, T., LEE, K. P., HARRIS, E. S., PETRYNIAK, B., CRAIGHEAD, N., REYNOLDS, P. J., LOMBARD, D. B., FREEMAN, G. J., NADLER, L. M., GRAY, G. S. & ET AL. 1993. Characterization of CTLA-4 structure and expression on human T cells. *J Immunol,* 151**,** 3489–99.

LINEBURG, K. E., GRANT, E. J., SWAMINATHAN, S., CHATZILEONTIADOU, D. S. M., SZETO, C., SLOANE, H., PANIKKAR, A., RAJU, J., CROOKS, P., REHAN, S., NGUYEN, A. T., LEKIEFFRE, L., NELLER, M. A., TONG, Z. W. M., JAYASINGHE, D., CHEW, K. Y., LOBOS, C. A., HALIM, H., BURROWS, J. M., RIBOLDI-TUNNICLIFFE, A., CHEN, W., D'ORSOGNA, L., KHANNA, R., SHORT, K. R., SMITH, C. & GRAS, S. 2021. CD8(+) T cells specific for an immunodominant SARS-CoV-2 nucleocapsid epitope cross-react with selective seasonal coronaviruses. *Immunity,* 54**,** 1055–1065.e5.

LINNERBAUER, S., BEHRENDS, U., ADHIKARY, D., WITTER, K., BORNKAMM, G. W. & MAUTNER, J. 2014. Virus and autoantigen-specific CD4+ T cells are key effectors in a SCID mouse model of EBV-associated post-transplant lymphoproliferative disorders. *PLoS Pathog,* 10**,** e1004068.

LIPPI, G., PLEBANI, M. & HENRY, B. M. 2020. Thrombocytopenia is associated with severe coronavirus disease 2019 (COVID-19) infections: A meta-analysis. *Clin Chim Acta,* 506**,** 145–148.

LIU, P., FANG, X., FENG, Z., GUO, Y. M., PENG, R. J., LIU, T., HUANG, Z., FENG, Y., SUN, X., XIONG, Z., GUO, X., PANG, S. S., WANG, B., LV, X., FENG, F. T., LI, D. J., CHEN, L. Z., FENG, Q. S., HUANG, W. L., ZENG, M. S., BEI, J. X., ZHANG, Y. & ZENG, Y. X. 2011. Direct sequencing and characterization of a clinical isolate of Epstein-Barr virus from nasopharyngeal carcinoma tissue by using next-generation sequencing technology. *J Virol,* 85**,** 11291–9.

LIU, W., CUI, Y., WANG, C., LI, Z., GONG, D., DAI, X., BI, G. Q., SUN, R. & ZHOU, Z. H. 2020. Structures of capsid and capsid-associated tegument complex inside the Epstein-Barr virus. *Nat Microbiol,* 5**,** 1285–1298.

LIU, Y., LIAO, W., WAN, L., XIANG, T. & ZHANG, W. 2021a. Correlation Between Relative Nasopharyngeal Virus RNA Load and Lymphocyte Count Disease Severity in Patients with COVID-19. *Viral Immunol,* 34**,** 330–335.

LIU, Y., SOH, W. T., KISHIKAWA, J. I., HIROSE, M., NAKAYAMA, E. E., LI, S., SASAI, M., SUZUKI, T., TADA, A., ARAKAWA, A., MATSUOKA, S., AKAMATSU, K., MATSUDA, M., ONO, C., TORII, S., KISHIDA, K., JIN, H., NAKAI, W., ARASE, N., NAKAGAWA, A., MATSUMOTO, M., NAKAZAKI, Y., SHINDO, Y., KOHYAMA, M., TOMII, K., OHMURA, K., OHSHIMA, S.,

OKAMOTO, T., YAMAMOTO, M., NAKAGAMI, H., MATSUURA, Y., NAKAGAWA, A., KATO, T., OKADA, M., STANDLEY, D. M., SHIODA, T. & ARASE, H. 2021b. An infectivity-enhancing site on the SARS-CoV-2 spike protein targeted by antibodies. *Cell,* 184**,** 3452–3466.e18.

LIVAK, K. J. & SCHMITTGEN, T. D. 2001. Analysis of relative gene expression data using real-time quantitative PCR and the 2(-Delta Delta C(T)) Method. *Methods,* 25**,** 402–8.

LODIGIANI, C., IAPICHINO, G., CARENZO, L., CECCONI, M., FERRAZZI, P., SEBASTIAN, T., KUCHER, N., STUDT, J. D., SACCO, C., BERTUZZI, A., SANDRI, M. T. & BARCO, S. 2020. Venous and arterial thromboembolic complications in COVID-19 patients admitted to an academic hospital in Milan, Italy. *Thromb Res,* 191**,** 9–14.

LONG, H. M., HAIGH, T. A., GUDGEON, N. H., LEEN, A. M., TSANG, C. W., BROOKS, J., LANDAIS, E., HOUSSAINT, E., LEE, S. P., RICKINSON, A. B. & TAYLOR, G. S. 2005. CD4+ T-cell responses to Epstein-Barr virus (EBV) latent-cycle antigens and the recognition of EBV-transformed lymphoblastoid cell lines. *J Virol,* 79**,** 4896–907.

LONG, H. M., LEESE, A. M., CHAGOURY, O. L., CONNERTY, S. R., QUARCOOPOME, J., QUINN, L. L., SHANNON-LOWE, C. & RICKINSON, A. B. 2011. Cytotoxic CD4+ T cell responses to EBV contrast with CD8 responses in breadth of lytic cycle antigen choice and in lytic cycle recognition. *J Immunol,* 187**,** 92–101.

LONG, H. M., ZUO, J., LEESE, A. M., GUDGEON, N. H., JIA, H., TAYLOR, G. S. & RICKINSON, A. B. 2009. CD4+ T-cell clones recognizing human lymphoma-associated antigens: generation by in vitro stimulation with autologous Epstein-Barr virus-transformed B cells. *Blood,* 114**,** 807–15.

LÓPEZ-CANTILLO, G., URUEÑA, C., CAMACHO, B. A. & RAMÍREZ-SEGURA, C. 2022. CAR-T Cell Performance: How to Improve Their Persistence? *Front Immunol,* 13**,** 878209.

LOPEZ-CASTANEDA, S., GARCÍA-LARRAGOITI, N., CANO-MENDEZ, A., BLANCAS-AYALA, K., DAMIAN-VÁZQUEZ, G., PEREZ-MEDINA, A. I., CHORA-HERNÁNDEZ, L. D., AREAN-MARTÍNEZ, C. & VIVEROS-SANDOVAL, M. E. 2021. Inflammatory and Prothrombotic Biomarkers Associated With the Severity of COVID-19 Infection. *Clin Appl Thromb Hemost,* 27**,** 1076029621999099.

LOUGARIS, V., TABELLINI, G., BARONIO, M., PATRIZI, O., GAZZURELLI, L., MITSUIKI, N., POZZI, M. R., GRIMBACHER, B., PAROLINI, S. & PLEBANI, A. 2018. CTLA-4 regulates human Natural Killer cell effector functions. *Clin Immunol,* 194**,** 43–45.

LOW, Y. H., LOH, C. J. L., PEH, D. Y. Y., CHU, A. J. M., HAN, S. & TOH, H. C. 2023. Pathogenesis and therapeutic implications of EBV-associated epithelial cancers. *Front Oncol,* 13**,** 1202117.

LU, W., YAN, L., TANG, X., WANG, X., DU, J., ZOU, Z., LI, L., YE, J. & ZHOU, L. 2024. Efficacy and safety of mesenchymal stem cells therapy in COVID-19 patients: a systematic review and meta-analysis of randomized controlled trials. *J Transl Med,* 22**,** 550.

LU, Y., ZHU, Q., FOX, D. M., GAO, C., STANLEY, S. A. & LUO, K. 2022. SARS-CoV-2 down-regulates ACE2 through lysosomal degradation. *Mol Biol Cell,* 33**,** ar147.

LUCAS, C., VOGELS, C. B. F., YILDIRIM, I., ROTHMAN, J. E., LU, P., MONTEIRO, V., GEHLHAUSEN, J. R., CAMPBELL, M., SILVA, J., TABACHNIKOVA, A., PEÑA-HERNANDEZ, M. A., MUENKER, M. C., BREBAN, M. I., FAUVER, J. R., MOHANTY, S., HUANG, J., SHAW, A. C., KO, A. I., OMER, S. B.,

GRUBAUGH, N. D. & IWASAKI, A. 2021. Impact of circulating SARS-CoV-2 variants on mRNA vaccine-induced immunity. *Nature,* 600**,** 523–529.
LUCAS, C., WONG, P., KLEIN, J., CASTRO, T. B. R., SILVA, J., SUNDARAM, M., ELLINGSON, M. K., MAO, T., OH, J. E., ISRAELOW, B., TAKAHASHI, T., TOKUYAMA, M., LU, P., VENKATARAMAN, A., PARK, A., MOHANTY, S., WANG, H., WYLLIE, A. L., VOGELS, C. B. F., EARNEST, R., LAPIDUS, S., OTT, I. M., MOORE, A. J., MUENKER, M. C., FOURNIER, J. B., CAMPBELL, M., ODIO, C. D., CASANOVAS-MASSANA, A., HERBST, R., SHAW, A. C., MEDZHITOV, R., SCHULZ, W. L., GRUBAUGH, N. D., DELA CRUZ, C., FARHADIAN, S., KO, A. I., OMER, S. B. & IWASAKI, A. 2020. Longitudinal analyses reveal immunological misfiring in severe COVID-19. *Nature,* 584**,** 463–469.
LUNG, M. L., LI, S. B. & CHANG, R. S. 1991. Study of Epstein-Barr virus (EBV) transmission by EBV genotyping. *J Infect Dis,* 164**,** 213–4.
LV, Z., LUO, F. & CHU, Y. 2023. Strategies for overcoming bottlenecks in allogeneic CAR-T cell therapy. *Front Immunol,* 14**,** 1199145.
LYNCH, D. T., ZIMMERMAN, J. S. & ROWE, D. T. 2002. Epstein-Barr virus latent membrane protein 2B (LMP2B) co-localizes with LMP2A in perinuclear regions in transiently transfected cells. *J Gen Virol,* 83**,** 1025–1035.
LYONS, G. E., ROSZKOWSKI, J. J., MAN, S., YEE, C., KAST, W. M. & NISHIMURA, M. I. 2006. T-cell receptor tetramer binding or the lack there of does not necessitate antigen reactivity in T-cell receptor transduced T cells. *Cancer Immunol Immunother,* 55**,** 1142–50.
MA, D. Y. & CLARK, E. A. 2009. The role of CD40 and CD154/CD40L in dendritic cells. *Semin Immunol,* 21**,** 265–72.
MA, M., WANG, Z., CHEN, X., TAO, A., HE, L., FU, S., ZHANG, Z., FU, Y., GUO, C., LIU, J., HAN, X., XU, J., CHU, Z., DING, H., SHANG, H. & JIANG, Y. 2017. NKG2C(+)NKG2A(-) Natural Killer Cells are Associated with a Lower Viral Set Point and may Predict Disease Progression in Individuals with Primary HIV Infection. *Front Immunol,* 8**,** 1176.
MA, T., RYU, H., MCGREGOR, M., BABCOCK, B., NEIDLEMAN, J., XIE, G., GEORGE, A. F., FROUARD, J., MURRAY, V., GILL, G., GHOSN, E., NEWELL, E. W., LEE, S. A. & ROAN, N. R. 2021. Protracted yet Coordinated Differentiation of Long-Lived SARS-CoV-2-Specific CD8(+) T Cells during Convalescence. *J Immunol,* 207**,** 1344–1356.
MABILANGAN, C., BURTON, C., O'BRIEN, S., PLITT, S., EURICH, D. & PREIKSAITIS, J. 2020. Using blood donors and solid organ transplant donors and recipients to estimate the seroprevalence of cytomegalovirus and Epstein-Barr virus in Canada: A cross-sectional study. *J Assoc Med Microbiol Infect Dis Can,* 5**,** 158–176.
MACKEY, M. F., BARTH, R. J., JR. & NOELLE, R. J. 1998. The role of CD40/CD154 interactions in the priming, differentiation, and effector function of helper and cytotoxic T cells. *J Leukoc Biol,* 63**,** 418–28.
MACKINNON, S., PAPADOPOULOS, E. B., CARABASI, M. H., REICH, L., COLLINS, N. H. & O'REILLY, R. J. 1995. Adoptive immunotherapy using donor leukocytes following bone marrow transplantation for chronic myeloid leukemia: is T cell dose important in determining biological response? *Bone Marrow Transplant,* 15**,** 591–4.
MADARIAGA, A., GARG, S., TCHRAKIAN, N., DHANI, N. C., JIMENEZ, W., WELCH, S., MACKAY, H., ETHIER, J. L., GILBERT, L., LI, X., RODRIGUEZ, A., CHAN, L., BOWERING, V., CLARKE, B., ZHANG, T., KING, I., DOWNS, G., STOCKLEY, T., WANG, L., UDAGANI, S., OZA, A. M. & LHEUREUX, S. 2023. Clinical outcome and biomarker assessments of a multi-centre phase II

trial assessing niraparib with or without dostarlimab in recurrent endometrial carcinoma. *Nat Commun,* 14**,** 1452.
MAEDA, T. K., SUGIURA, D., OKAZAKI, I. M., MARUHASHI, T. & OKAZAKI, T. 2019. Atypical motifs in the cytoplasmic region of the inhibitory immune co-receptor LAG-3 inhibit T cell activation. *J Biol Chem,* 294**,** 6017–6026.
MAGG, T., SCHOBER, T., WALZ, C., LEY-ZAPOROZHAN, J., FACCHETTI, F., KLEIN, C. & HAUCK, F. 2018. Epstein-Barr Virus(+) Smooth Muscle Tumors as Manifestation of Primary Immunodeficiency Disorders. *Front Immunol,* 9**,** 368.
MAGGIO, E. M., VAN DEN BERG, A., VISSER, L., DIEPSTRA, A., KLUIVER, J., EMMENS, R. & POPPEMA, S. 2002. Common and differential chemokine expression patterns in rs cells of NLP, EBV positive and negative classical Hodgkin lymphomas. *Int J Cancer,* 99**,** 665–72.
MAHADEO, K. M., BAIOCCHI, R., BEITINJANEH, A., CHAGANTI, S., CHOQUET, S., DIERICKX, D., DINAVAHI, R., DUAN, X., GAMELIN, L., GHOBADI, A., GUZMAN-BECERRA, N., JOSHI, M., MEHTA, A., NAVARRO, W. H., NIKIFOROW, S., O'REILLY, R. J., RESHEF, R., RUIZ, F., SPINDLER, T. & PROCKOP, S. 2024. Tabelecleucel for allogeneic haematopoietic stem-cell or solid organ transplant recipients with Epstein-Barr virus-positive post-transplant lymphoproliferative disease after failure of rituximab or rituximab and chemotherapy (ALLELE): a phase 3, multicentre, open-label trial. *Lancet Oncol,* 25**,** 376–387.
MALINGA, N. Z., SIWELE, S. C., STEEL, H. C., KWOFIE, L. L. I., MEYER, P. W. A., SMIT, T., ANDERSON, R., RAPOPORT, B. L. & KGOKOLO, M. C. M. 2022. Systemic levels of the soluble co-inhibitory immune checkpoints, CTLA-4, LAG-3, PD-1/PD-L1 and TIM-3 are markedly increased in basal cell carcinoma. *Transl Oncol,* 19**,** 101384.
MALONE, B., URAKOVA, N., SNIJDER, E. J. & CAMPBELL, E. A. 2022. Structures and functions of coronavirus replication-transcription complexes and their relevance for SARS-CoV-2 drug design. *Nat Rev Mol Cell Biol,* 23**,** 21–39.
MALYSHKINA, A., BRÜGGEMANN, A., PASCHEN, A. & DITTMER, U. 2023. Cytotoxic CD4(+) T cells in chronic viral infections and cancer. *Front Immunol,* 14**,** 1271236.
MAMEDOV, I. Z., BRITANOVA, O. V., ZVYAGIN, I. V., TURCHANINOVA, M. A., BOLOTIN, D. A., PUTINTSEVA, E. V., LEBEDEV, Y. B. & CHUDAKOV, D. M. 2013. Preparing unbiased T-cell receptor and antibody cDNA libraries for the deep next generation sequencing profiling. *Front Immunol,* 4**,** 456.
MANCAO, C. & HAMMERSCHMIDT, W. 2007. Epstein-Barr virus latent membrane protein 2A is a B-cell receptor mimic and essential for B-cell survival. *Blood,* 110**,** 3715–21.
MANGSBO, S. M., HAVERVALL, S., LAURÉN, I., LINDSAY, R., JERNBOM FALK, A., MARKING, U., LORD, M., BUGGERT, M., DÖNNES, P., CHRISTOFFERSSON, G., NILSSON, P., HOBER, S., PHILLIPSON, M., KLINGSTRÖM, J. & THÅLIN, C. 2021. An evaluation of a FluoroSpot assay as a diagnostic tool to determine SARS-CoV-2 specific T cell responses. *PLoS One,* 16**,** e0258041.
MANGUM, D. S. & CAYWOOD, E. 2022. A clinician's guide to HLA matching in allogeneic hematopoietic stem cell transplant. *Hum Immunol,* 83**,** 687–694.
MANJILI, R. H., ZAREI, M., HABIBI, M. & MANJILI, M. H. 2020. COVID-19 as an Acute Inflammatory Disease. *J Immunol,* 205**,** 12–19.
MANOS, K., CHONG, G., KEANE, C., LEE, S. T., SMITH, C., CHURILOV, L., MCKENDRICK, J., RENWICK, W., BLOMBERY, P., BURGESS, M., NELSON, N.

E., FANCOURT, T., HAWKING, J., LIN, W., SCOTT, A. M., BARRACLOUGH, A., WIGHT, J., GRIGG, A., FONG, C. Y. & HAWKES, E. A. 2023. Immune priming with avelumab and rituximab prior to R-CHOP in diffuse large B-cell lymphoma: the phase II AvR-CHOP study. *Leukemia,* 37**,** 1092–1102.

MARK, C., MARTIN, G., BAADJES, B., GEERLINKS, A. V., PUNNETT, A. & LAFAY-COUSIN, L. 2024. Treatment of Monomorphic Posttransplant Lymphoproliferative Disorder in Pediatric Solid Organ Transplant: A Multicenter Review. *J Pediatr Hematol Oncol,* 46**,** e127–e130.

MARSHALL, N. A., CHRISTIE, L. E., MUNRO, L. R., CULLIGAN, D. J., JOHNSTON, P. W., BARKER, R. N. & VICKERS, M. A. 2004. Immunosuppressive regulatory T cells are abundant in the reactive lymphocytes of Hodgkin lymphoma. *Blood,* 103**,** 1755–62.

MARTITS-CHALANGARI, K., SPAK, C. W., ASKAR, M., KILLIAN, A., FISHER, T. L., ATILLASOY, E., MARSHALL, W. L., MCNEEL, D., MILLER, M. D., MATHAI, S. K. & GOTTLIEB, R. L. 2022. ALVR109, an off-the-shelf partially HLA matched SARS-CoV-2-specific T cell therapy, to treat refractory severe COVID-19 pneumonia in a heart transplant patient: Case report. *Am J Transplant,* 22**,** 1261–1265.

MARUO, S., ZHAO, B., JOHANNSEN, E., KIEFF, E., ZOU, J. & TAKADA, K. 2011. Epstein-Barr virus nuclear antigens 3C and 3A maintain lymphoblastoid cell growth by repressing p16INK4A and p14ARF expression. *Proc Natl Acad Sci U S A,* 108**,** 1919–24.

MASSINI, G., SIEMER, D. & HOHAUS, S. 2009. EBV in Hodgkin Lymphoma. *Mediterr J Hematol Infect Dis,* 1**,** e2009013.

MATEUS, J., GRIFONI, A., TARKE, A., SIDNEY, J., RAMIREZ, S. I., DAN, J. M., BURGER, Z. C., RAWLINGS, S. A., SMITH, D. M., PHILLIPS, E., MALLAL, S., LAMMERS, M., RUBIRO, P., QUIAMBAO, L., SUTHERLAND, A., YU, E. D., DA SILVA ANTUNES, R., GREENBAUM, J., FRAZIER, A., MARKMANN, A. J., PREMKUMAR, L., DE SILVA, A., PETERS, B., CROTTY, S., SETTE, A. & WEISKOPF, D. 2020. Selective and cross-reactive SARS-CoV-2 T cell epitopes in unexposed humans. *Science,* 370**,** 89–94.

MAUCOURANT, C., FILIPOVIC, I., PONZETTA, A., ALEMAN, S., CORNILLET, M., HERTWIG, L., STRUNZ, B., LENTINI, A., REINIUS, B., BROWNLIE, D., CUAPIO, A., ASK, E. H., HULL, R. M., HAROUN-IZQUIERDO, A., SCHAFFER, M., KLINGSTRÖM, J., FOLKESSON, E., BUGGERT, M., SANDBERG, J. K., ERIKSSON, L. I., ROOYACKERS, O., LJUNGGREN, H. G., MALMBERG, K. J., MICHAËLSSON, J., MARQUARDT, N., HAMMER, Q., STRÅLIN, K. & BJÖRKSTRÖM, N. K. 2020. Natural killer cell immunotypes related to COVID-19 disease severity. *Sci Immunol,* 5.

MAVROUDIS, D. A., JIANG, Y. Z., HENSEL, N., LEWALLE, P., COURIEL, D., KREITMAN, R. J., PASTAN, I. & BARRETT, A. J. 1996. Specific depletion of alloreactivity against haplotype mismatched related individuals by a recombinant immunotoxin: a new approach to graft-versus-host disease prophylaxis in haploidentical bone marrow transplantation. *Bone Marrow Transplant,* 17**,** 793–9.

MAZZA, G., SABATOS-PEYTON, C. A., PROTHEROE, R. E., HERMAN, A., CAMPBELL, J. D. & WRAITH, D. C. 2010. Isolation and characterization of human interleukin-10-secreting T cells from peripheral blood. *Hum Immunol,* 71**,** 225–34.

MCGEOCH, D. J. 2001. Molecular evolution of the gamma-Herpesvirinae. *Philos Trans R Soc Lond B Biol Sci,* 356**,** 421–35.

MCNAUGHTON, A. L., PATON, R. S., EDMANS, M., YOUNGS, J., WELLENS, J., PHALORA, P., FYFE, A., BELIJ-RAMMERSTORFER, S., BOLTON, J. S., BALL,

J., CARNELL, G. W., DEJNIRATTISAI, W., DOLD, C., EYRE, D. W., HOPKINS, P., HOWARTH, A., KOOBLALL, K., KLIM, H., LEAVER, S., LEE, L. N., LÓPEZ-CAMACHO, C., LUMLEY, S. F., MACALLAN, D. C., MENTZER, A. J., PROVINE, N. M., RATCLIFF, J., SLON-COMPOS, J., SKELLY, D., STOLLE, L., SUPASA, P., TEMPERTON, N., WALKER, C., WANG, B., WYNCOLL, D., SIMMONDS, P., LAMBE, T., BAILLIE, J. K., SEMPLE, M. G., OPENSHAW, P. J., OBOLSKI, U., TURNER, M., CARROLL, M., MONGKOLSAPAYA, J., SCREATON, G., KENNEDY, S. H., JARVIS, L., BARNES, E., DUNACHIE, S., LOURENÇO, J., MATTHEWS, P. C., BICANIC, T., KLENERMAN, P., GUPTA, S. & THOMPSON, C. P. 2022. Fatal COVID-19 outcomes are associated with an antibody response targeting epitopes shared with endemic coronaviruses. *JCI Insight,* 7.

MEHTA, P. & FAJGENBAUM, D. C. 2021. Is severe COVID-19 a cytokine storm syndrome: a hyperinflammatory debate. *Curr Opin Rheumatol,* 33**,** 419–430.

MEIJ, P., VERVOORT, M. B., AARBIOU, J., VAN DISSEL, P., BRINK, A., BLOEMENA, E., MEIJER, C. J. & MIDDELDORP, J. M. 1999. Restricted low-level human antibody responses against Epstein-Barr virus (EBV)-encoded latent membrane protein 1 in a subgroup of patients with EBV-associated diseases. *J Infect Dis,* 179**,** 1108–15.

MELENHORST, J. J., LEEN, A. M., BOLLARD, C. M., QUIGLEY, M. F., PRICE, D. A., ROONEY, C. M., BRENNER, M. K., BARRETT, A. J. & HESLOP, H. E. 2010. Allogeneic virus-specific T cells with HLA alloreactivity do not produce GVHD in human subjects. *Blood,* 116**,** 4700–2.

MELENHORST, J. J., SCHEINBERG, P., CHATTOPADHYAY, P. K., LISSINA, A., GOSTICK, E., COLE, D. K., WOOLDRIDGE, L., VAN DEN BERG, H. A., BORNSTEIN, E., HENSEL, N. F., DOUEK, D. C., ROEDERER, M., SEWELL, A. K., BARRETT, A. J. & PRICE, D. A. 2008. Detection of low avidity CD8(+) T cell populations with coreceptor-enhanced peptide-major histocompatibility complex class I tetramers. *J Immunol Methods,* 338**,** 31–9.

MENACHERY, V. D., DINNON, K. H., 3RD, YOUNT, B. L., JR., MCANARNEY, E. T., GRALINSKI, L. E., HALE, A., GRAHAM, R. L., SCOBEY, T., ANTHONY, S. J., WANG, L., GRAHAM, B., RANDELL, S. H., LIPKIN, W. I. & BARIC, R. S. 2020. Trypsin Treatment Unlocks Barrier for Zoonotic Bat Coronavirus Infection. *J Virol,* 94.

MENGER, L., GOUBLE, A., MARZOLINI, M. A., PACHNIO, A., BERGERHOFF, K., HENRY, J. Y., SMITH, J., PULE, M., MOSS, P., RIDDELL, S. R., QUEZADA, S. A. & PEGGS, K. S. 2015. TALEN-mediated genetic inactivation of the glucocorticoid receptor in cytomegalovirus-specific T cells. *Blood,* 126**,** 2781–9.

MENTER, T., HASLBAUER, J. D., NIENHOLD, R., SAVIC, S., HOPFER, H., DEIGENDESCH, N., FRANK, S., TUREK, D., WILLI, N., PARGGER, H., BASSETTI, S., LEUPPI, J. D., CATHOMAS, G., TOLNAY, M., MERTZ, K. D. & TZANKOV, A. 2020. Postmortem examination of COVID-19 patients reveals diffuse alveolar damage with severe capillary congestion and variegated findings in lungs and other organs suggesting vascular dysfunction. *Histopathology,* 77**,** 198–209.

MIDGLEY, R. S., BLAKE, N. W., YAO, Q. Y., CROOM-CARTER, D., CHEUNG, S. T., LEUNG, S. F., CHAN, A. T., JOHNSON, P. J., HUANG, D., RICKINSON, A. B. & LEE, S. P. 2000. Novel intertypic recombinants of epstein-barr virus in the chinese population. *J Virol,* 74**,** 1544–8.

MIELKE, S., MCIVER, Z. A., SHENOY, A., FELLOWES, V., KHUU, H., STRONCEK, D. F., LEITMAN, S. F., CHILDS, R., BATTIWALLA, M., KOKLANARIS, E., HAGGERTY, J., SAVANI, B. N., REZVANI, K. & BARRETT, A. J. 2011. Selectively T cell-depleted allografts from HLA-matched sibling donors followed by low-dose posttransplantation immunosuppression to improve transplantation outcome in patients with hematologic malignancies. *Biol Blood Marrow Transplant,* 17**,** 1855–61.

MIELKE, S., NUNES, R., REZVANI, K., FELLOWES, V. S., VENNE, A., SOLOMON, S. R., FAN, Y., GOSTICK, E., PRICE, D. A., SCOTTO, C., READ, E. J. & BARRETT, A. J. 2008. A clinical-scale selective allodepletion approach for the treatment of HLA-mismatched and matched donor-recipient pairs using expanded T lymphocytes as antigen-presenting cells and a TH9402-based photodepletion technique. *Blood,* 111**,** 4392–402.

MIKA, T., STRATE, K., LADIGAN, S., AIGNER, C., SCHLEGEL, U., TISCHOFF, I., TISCHER-ZIMMERMANN, S., EIZ-VESPER, B., MAECKER-KOLHOFF, B. & SCHROERS, R. 2019. Refractory Epstein-Barr Virus (EBV)-Related Post-transplant Lymphoproliferative Disease: Cure by Combined Brentuximab Vedotin and Allogeneic EBV-Specific T-Lymphocytes. *Front Med (Lausanne),* 6**,** 295.

MIKHAK, Z., STRASSNER, J. P. & LUSTER, A. D. 2013. Lung dendritic cells imprint T cell lung homing and promote lung immunity through the chemokine receptor CCR4. *J Exp Med,* 210**,** 1855–69.

MILLER, J. F. 1959. Role of the thymus in murine leukaemia. *Nature,* 183**,** 1069.

MILLER, J. F. 1961. Immunological function of the thymus. *Lancet,* 2**,** 748–9.

MILLER, J. F. & MITCHELL, G. F. 1968. Cell to cell interaction in the immune response. I. Hemolysin-forming cells in neonatally thymectomized mice reconstituted with thymus or thoracic duct lymphocytes. *J Exp Med,* 128**,** 801–20.

MILLER, N. & HUTT-FLETCHER, L. M. 1992. Epstein-Barr virus enters B cells and epithelial cells by different routes. *J Virol,* 66**,** 3409–14.

MIYAUCHI, K., URANO, E., YOSHIYAMA, H. & KOMANO, J. 2011. Cytokine signatures of transformed B cells with distinct Epstein-Barr virus latencies as a potential diagnostic tool for B cell lymphoma. *Cancer Sci,* 102**,** 1236–41.

MO, F., WATANABE, N., MCKENNA, M. K., HICKS, M. J., SRINIVASAN, M., GOMES-SILVA, D., ATILLA, E., SMITH, T., ATACA ATILLA, P., MA, R., QUACH, D., HESLOP, H. E., BRENNER, M. K. & MAMONKIN, M. 2021. Engineered off-the-shelf therapeutic T cells resist host immune rejection. *Nat Biotechnol,* 39**,** 56–63.

MÖLLER-HACKBARTH, K., DEWITZ, C., SCHWEIGERT, O., TRAD, A., GARBERS, C., ROSE-JOHN, S. & SCHELLER, J. 2013. A disintegrin and metalloprotease (ADAM) 10 and ADAM17 are major sheddases of T cell immunoglobulin and mucin domain 3 (Tim-3). *J Biol Chem,* 288**,** 34529–44.

MONNEY, L., SABATOS, C. A., GAGLIA, J. L., RYU, A., WALDNER, H., CHERNOVA, T., MANNING, S., GREENFIELD, E. A., COYLE, A. J., SOBEL, R. A., FREEMAN, G. J. & KUCHROO, V. K. 2002. Th1-specific cell surface protein Tim-3 regulates macrophage activation and severity of an autoimmune disease. *Nature,* 415**,** 536–41.

MOOSMANN, A., BIGALKE, I., TISCHER, J., SCHIRRMANN, L., KASTEN, J., TIPPMER, S., LEEPING, M., PREVALSEK, D., JAEGER, G., LEDDEROSE, G., MAUTNER, J., HAMMERSCHMIDT, W., SCHENDEL, D. J. & KOLB, H. J. 2010. Effective and long-term control of EBV PTLD after transfer of peptide-selected T cells. *Blood,* 115**,** 2960–70.

MORADI, V., OMIDKHODA, A. & AHMADBEIGI, N. 2023. The paths and challenges of "off-the-shelf" CAR-T cell therapy: An overview of clinical trials. *Biomed Pharmacother,* 169**,** 115888.

MORALES, O., MRIZAK, D., FRANÇOIS, V., MUSTAPHA, R., MIROUX, C., DEPIL, S., DECOUVELAERE, A. V., LIONNE-HUYGHE, P., AURIAULT, C., DE LAUNOIT, Y., PANCRÉ, V. & DELHEM, N. 2014. Epstein-Barr virus infection induces an increase of T regulatory type 1 cells in Hodgkin lymphoma patients. *Br J Haematol,* 166**,** 875–90.

MROZEK-GORSKA, P., BUSCHLE, A., PICH, D., SCHWARZMAYR, T., FECHTNER, R., SCIALDONE, A. & HAMMERSCHMIDT, W. 2019. Epstein-Barr virus reprograms human B lymphocytes immediately in the prelatent phase of infection. *Proc Natl Acad Sci U S A,* 116**,** 16046–16055.

MUKHERJEE, R., BHATTACHARYA, A., BOJKOVA, D., MEHDIPOUR, A. R., SHIN, D., KHAN, K. S., HEI-YIN CHEUNG, H., WONG, K. B., NG, W. L., CINATL, J., GEURINK, P. P., VAN DER HEDEN VAN NOORT, G. J., RAJALINGAM, K., CIESEK, S., HUMMER, G. & DIKIC, I. 2021. Famotidine inhibits toll-like receptor 3-mediated inflammatory signaling in SARS-CoV-2 infection. *J Biol Chem,* 297**,** 100925.

MÜLLER-DUROVIC, B., JÄGER, J., BANTUG, G. R. & HESS, C. 2024. Epstein-Barr virus hijacks B cell metabolism to establish persistent infection and drive pathogenesis. *Trends Immunol*.

MÜNZ, C. 2023. Modulation of Epstein-Barr-Virus (EBV)-Associated Cancers by Co-Infections. *Cancers (Basel),* 15.

MURATA, T. 2018. Encyclopedia of EBV-Encoded Lytic Genes: An Update. *Adv Exp Med Biol*, 1045**,** 395–412.

MURATA, T., SUGIMOTO, A., INAGAKI, T., YANAGI, Y., WATANABE, T., SATO, Y. & KIMURA, H. 2021. Molecular Basis of Epstein-Barr Virus Latency Establishment and Lytic Reactivation. *Viruses,* 13.

MURPHY, P. M., BAGGIOLINI, M., CHARO, I. F., HÉBERT, C. A., HORUK, R., MATSUSHIMA, K., MILLER, L. H., OPPENHEIM, J. J. & POWER, C. A. 2000. International union of pharmacology. XXII. Nomenclature for chemokine receptors. *Pharmacol Rev,* 52**,** 145–76.

MURRAY, R. J., KURILLA, M. G., BROOKS, J. M., THOMAS, W. A., ROWE, M., KIEFF, E. & RICKINSON, A. B. 1992. Identification of target antigens for the human cytotoxic T cell response to Epstein-Barr virus (EBV): implications for the immune control of EBV-positive malignancies. *J Exp Med*, 176**,** 157–68.

NAGARAJU, T., SUGDEN, A. U. & SUGDEN, B. 2019. Four-dimensional analyses show that replication compartments are clonal factories in which Epstein-Barr viral DNA amplification is coordinated. *Proc Natl Acad Sci U S A,* 116**,** 24630–24638.

NAIK, S., NICHOLAS, S. K., MARTINEZ, C. A., LEEN, A. M., HANLEY, P. J., GOTTSCHALK, S. M., ROONEY, C. M., HANSON, I. C., KRANCE, R. A., SHPALL, E. J., CRUZ, C. R., AMROLIA, P., LUCCHINI, G., BUNIN, N., HEIMALL, J., KLEIN, O. R., GENNERY, A. R., SLATTER, M. A., VICKERS, M. A., ORANGE, J. S., HESLOP, H. E., BOLLARD, C. M. & KELLER, M. D. 2016. Adoptive immunotherapy for primary immunodeficiency disorders with virus-specific T lymphocytes. *J Allergy Clin Immunol*, 137**,** 1498–1505.e1.

NAKAYAMA, E. E. & SHIODA, T. 2023. SARS-CoV-2 Related Antibody-Dependent Enhancement Phenomena In Vitro and In Vivo. *Microorganisms,* 11.

NAO, N., YAMAGISHI, J., MIYAMOTO, H., IGARASHI, M., MANZOOR, R., OHNUMA, A., TSUDA, Y., FURUYAMA, W., SHIGENO, A., KAJIHARA, M., KISHIDA, N., YOSHIDA, R. & TAKADA, A. 2017. Genetic Predisposition To Acquire a

Polybasic Cleavage Site for Highly Pathogenic Avian Influenza Virus Hemagglutinin. *mBio,* 8.

NDHLOVU, L. C., LOPEZ-VERGÈS, S., BARBOUR, J. D., JONES, R. B., JHA, A. R., LONG, B. R., SCHOEFFLER, E. C., FUJITA, T., NIXON, D. F. & LANIER, L. L. 2012. Tim-3 marks human natural killer cell maturation and suppresses cell-mediated cytotoxicity. *Blood,* 119**,** 3734–43.

NEILL, L. & PEGGS, K. 2021. Cell therapy for cytomegalovirus infection. *Expert Opin Biol Ther,* 21**,** 649–659.

NELSON, A. S., HEYENBRUCH, D., RUBINSTEIN, J. D., SABULSKI, A., JODELE, S., THOMAS, S., LUTZKO, C., ZHU, X., LEEMHUIS, T., CANCELAS, J. A., KELLER, M., BOLLARD, C. M., HANLEY, P. J., DAVIES, S. M. & GRIMLEY, M. S. 2020. Virus-specific T-cell therapy to treat BK polyomavirus infection in bone marrow and solid organ transplant recipients. *Blood Adv,* 4**,** 5745–5754.

NEWELL, K. L., CLEMMER, D. C., COX, J. B., KAYODE, Y. I., ZOCCOLI-RODRIGUEZ, V., TAYLOR, H. E., ENDY, T. P., WILMORE, J. R. & WINSLOW, G. M. 2021. Switched and unswitched memory B cells detected during SARS-CoV-2 convalescence correlate with limited symptom duration. *PLoS One,* 16**,** e0244855.

NGO, M. C., ANDO, J., LEEN, A. M., ENNAMURI, S., LAPTEVA, N., VERA, J. F., MIN-VENDITTI, A., MIMS, M. P., HESLOP, H. E., BOLLARD, C. M., GOTTSCHALK, S. & ROONEY, C. M. 2014. Complementation of antigen-presenting cells to generate T lymphocytes with broad target specificity. *J Immunother,* 37**,** 193–203.

NGUYEN, R., DOUBROVINA, E., MOUSSET, C. M., JIN, B. Y., OKADA, R., ZHANG, X., CLAVEL, A., REYES-GONZALEZ, J. M., DYOMIN, V., DIAZ, L., ZHANG, L., ABBAS, S., SUN, M., HSIEH, C. M., HO, M., SHERN, J. F., GULLEY, J. L. & HINRICHS, C. S. 2024. Cooperative Armoring of CAR and TCR T Cells by T Cell-Restricted IL15 and IL21 Universally Enhances Solid Tumor Efficacy. *Clin Cancer Res,* 30**,** 1555–1566.

NGUYEN, T. H. O., ROWNTREE, L. C., PETERSEN, J., CHUA, B. Y., HENSEN, L., KEDZIERSKI, L., VAN DE SANDT, C. E., CHAURASIA, P., TAN, H. X., HABEL, J. R., ZHANG, W., ALLEN, L. F., EARNEST, L., MAK, K. Y., JUNO, J. A., WRAGG, K., MORDANT, F. L., AMANAT, F., KRAMMER, F., MIFSUD, N. A., DOOLAN, D. L., FLANAGAN, K. L., SONDA, S., KAUR, J., WAKIM, L. M., WESTALL, G. P., JAMES, F., MOUHTOURIS, E., GORDON, C. L., HOLMES, N. E., SMIBERT, O. C., TRUBIANO, J. A., CHENG, A. C., HARCOURT, P., CLIFTON, P., CRAWFORD, J. C., THOMAS, P. G., WHEATLEY, A. K., KENT, S. J., ROSSJOHN, J., TORRESI, J. & KEDZIERSKA, K. 2021. CD8(+) T cells specific for an immunodominant SARS-CoV-2 nucleocapsid epitope display high naive precursor frequency and TCR promiscuity. *Immunity,* 54**,** 1066–1082.e5.

NIEDOBITEK, G., HERBST, H., YOUNG, L. S., BROOKS, L., MASUCCI, M. G., CROCKER, J., RICKINSON, A. B. & STEIN, H. 1992. Patterns of Epstein-Barr virus infection in non-neoplastic lymphoid tissue. *Blood,* 79**,** 2520–6.

NIH. Accessed March 2024. *COVID-19 Treatment Guidelines Panel. Coronavirus Disease 2019 (COVID-19) Treatment Guidelines. National Institutes of Health.* [Online]. Available: https://www.covid19treatmentguidelines.nih.gov/. [Accessed March 2024].

NING, R. J., XU, X. Q., CHAN, K. H. & CHIANG, A. K. 2011. Long-term carriers generate Epstein-Barr virus (EBV)-specific CD4(+) and CD8(+)

polyfunctional T-cell responses which show immunodominance hierarchies of EBV proteins. *Immunology,* 134**,** 161–71.

NISHIMURA, H., AGATA, Y., KAWASAKI, A., SATO, M., IMAMURA, S., MINATO, N., YAGITA, H., NAKANO, T. & HONJO, T. 1996. Developmentally regulated expression of the PD-1 protein on the surface of double-negative (CD4-CD8-) thymocytes. *Int Immunol,* 8**,** 773–80.

NISHIURA, H., KOBAYASHI, T., MIYAMA, T., SUZUKI, A., JUNG, S. M., HAYASHI, K., KINOSHITA, R., YANG, Y., YUAN, B., AKHMETZHANOV, A. R. & LINTON, N. M. 2020. Estimation of the asymptomatic ratio of novel coronavirus infections (COVID-19). *Int J Infect Dis,* 94**,** 154–155.

NIU, X., LI, S., LI, P., PAN, W., WANG, Q., FENG, Y., MO, X., YAN, Q., YE, X., LUO, J., QU, L., WEBER, D., BYRNE-STEELE, M. L., WANG, Z., YU, F., LI, F., MYERS, R. M., LOTZE, M. T., ZHONG, N., HAN, J. & CHEN, L. 2020. Longitudinal Analysis of T and B Cell Receptor Repertoire Transcripts Reveal Dynamic Immune Response in COVID-19 Patients. *Front Immunol,* 11**,** 582010.

NONN, M., HERR, W., KHAN, S., TODOROVA, M., LINK, I., THIES, J., DISTLER, E., KALTWASSER, M., HOFFMANN, J., HUBER, C. & HARTWIG, U. F. 2008. Selective depletion of alloreactive T lymphocytes using patient-derived nonhematopoietic stimulator cells in allograft engineering. *Transplantation,* 86**,** 1427–35.

NOVALIĆ, Z., VERKUIJLEN, S., VERLAAN, M., EERSELS, J. L. H., DE GREEUW, I., MOLTHOFF, C. F. M., MIDDELDORP, J. M. & GREIJER, A. E. 2017. Cytolytic virus activation therapy and treatment monitoring for Epstein-Barr virus associated nasopharyngeal carcinoma in a mouse tumor model. *J Med Virol,* 89**,** 2207–2216.

NOVY, P., QUIGLEY, M., HUANG, X. & YANG, Y. 2007. CD4 T cells are required for CD8 T cell survival during both primary and memory recall responses. *J Immunol,* 179**,** 8243–51.

O'REILLY, R. J., PROCKOP, S. & OVED, J. H. 2023. Virus-specific T-cells from third party or transplant donors for treatment of EBV lymphoproliferative diseases arising post hematopoietic cell or solid organ transplantation. *Front Immunol,* 14**,** 1290059.

OGBE, A., KRONSTEINER, B., SKELLY, D. T., PACE, M., BROWN, A., ADLAND, E., ADAIR, K., AKHTER, H. D., ALI, M., ALI, S. E., ANGYAL, A., ANSARI, M. A., ARANCIBIA-CÁRCAMO, C. V., BROWN, H., CHINNAKANNAN, S., CONLON, C., DE LARA, C., DE SILVA, T., DOLD, C., DONG, T., DONNISON, T., EYRE, D., FLAXMAN, A., FLETCHER, H., GARDNER, J., GRIST, J. T., HACKSTEIN, C. P., JARUTHAMSOPHON, K., JEFFERY, K., LAMBE, T., LEE, L., LI, W., LIM, N., MATTHEWS, P. C., MENTZER, A. J., MOORE, S. C., NAISBITT, D. J., OGESE, M., OGG, G., OPENSHAW, P., PIRMOHAMED, M., POLLARD, A. J., RAMAMURTHY, N., RONGKARD, P., ROWLAND-JONES, S., SAMPSON, O., SCREATON, G., SETTE, A., STAFFORD, L., THOMPSON, C., THOMSON, P. J., THWAITES, R., VIEIRA, V., WEISKOPF, D., ZACHAROPOULOU, P., TURTLE, L., KLENERMAN, P., GOULDER, P., FRATER, J., BARNES, E. & DUNACHIE, S. 2021. T cell assays differentiate clinical and subclinical SARS-CoV-2 infections from cross-reactive antiviral responses. *Nat Commun,* 12**,** 2055.

OGEMBO, J. G., KANNAN, L., GHIRAN, I., NICHOLSON-WELLER, A., FINBERG, R. W., TSOKOS, G. C. & FINGEROTH, J. D. 2013. Human complement receptor type 1/CD35 is an Epstein-Barr Virus receptor. *Cell Rep,* 3**,** 371–85.

OH, D. Y. & FONG, L. 2021. Cytotoxic CD4(+) T cells in cancer: Expanding the immune effector toolbox. *Immunity,* 54**,** 2701–2711.

OKAZAKI, T., MAEDA, A., NISHIMURA, H., KUROSAKI, T. & HONJO, T. 2001. PD-1 immunoreceptor inhibits B cell receptor-mediated signaling by recruiting src homology 2-domain-containing tyrosine phosphatase 2 to phosphotyrosine. *Proc Natl Acad Sci U S A,* 98**,** 13866–71.

OLSON, A., LIN, R., MARIN, D., RAFEI, H., BDAIWI, M. H., THALL, P. F., BASAR, R., ABUDAYYEH, A., BANERJEE, P., AUNG, F. M., KAUR, I., ABUEG, G., RAO, S., CHEMALY, R., MULANOVICH, V., AL-ATRASH, G., ALOUSI, A. M., ANDERSSON, B. S., ANDERLINI, P., BASHIR, Q., CASTRO, K. M., DAHER, M., GALVAN, I. M., HOSING, C., IM, J. S., JONES, R. B., KEBRIAEI, P., KHOURI, I., MEHTA, R., MOLLDREM, J., NIETO, Y., ORAN, B., POPAT, U., QAZILBASH, M., RONDON, G., SAINI, N., SPENCER, B., SROUR, S., WASHINGTON, D., BARNETT, M., CHAMPLIN, R. E., SHPALL, E. J. & REZVANI, K. 2021. Third-Party BK Virus-Specific Cytotoxic T Lymphocyte Therapy for Hemorrhagic Cystitis Following Allotransplantation. *J Clin Oncol,* 39**,** 2710–2719.

ORANGE, J. S. 2013. Natural killer cell deficiency. *J Allergy Clin Immunol,* 132**,** 515–525.

ORJUELA, M. A., ALOBEID, B., LIU, X., SIEBERT, A. L., KOTT, E. R., ADDONIZIO, L. J., MORRIS, E., GARVIN, J. H., LOBRITTO, S. J. & CAIRO, M. S. 2011. CD20 expression predicts survival in paediatric post-transplant lymphoproliferative disease (PTLD) following solid organ transplantation. *Br J Haematol,* 152**,** 733–42.

ORLANDI, E., IORIO, G. C., BARTONCINI, S., GALLIO, E., CAVALLO, F., SANTORO, F., RICARDI, U. & LEVIS, M. 2021. Role of Radiotherapy in Post-transplant Lymphoproliferative Disorders: Three Case Reports and Review of the Literature. *Clin Lymphoma Myeloma Leuk,* 21**,** e309–e316.

OROLOGAS-STAVROU, N., POLITOU, M., ROUSAKIS, P., KOSTOPOULOS, I. V., NTANASIS-STATHOPOULOS, I., JAHAJ, E., TSILIGKERIDOU, E., GAVRIATOPOULOU, M., KASTRITIS, E., KOTANIDOU, A., DIMOPOULOS, M. A., TSITSILONIS, O. E. & TERPOS, E. 2020. Peripheral Blood Immune Profiling of Convalescent Plasma Donors Reveals Alterations in Specific Immune Subpopulations Even at 2 Months Post SARS-CoV-2 Infection. *Viruses,* 13.

OUYANG, Q., WAGNER, W. M., WALTER, S., MÜLLER, C. A., WIKBY, A., AUBERT, G., KLATT, T., STEVANOVIC, S., DODI, T. & PAWELEC, G. 2003. An age-related increase in the number of CD8+ T cells carrying receptors for an immunodominant Epstein-Barr virus (EBV) epitope is counteracted by a decreased frequency of their antigen-specific responsiveness. *Mech Ageing Dev,* 124**,** 477–85.

OWEN, D. L., SJAASTAD, L. E. & FARRAR, M. A. 2019. Regulatory T Cell Development in the Thymus. *J Immunol,* 203**,** 2031–2041.

OZGYIN, L., HORVATH, A., HEVESSY, Z. & BALINT, B. L. 2019. Extensive epigenetic and transcriptomic variability between genetically identical human B-lymphoblastoid cells with implications in pharmacogenomics research. *Sci Rep,* 9**,** 4889.

PALSER, A. L., GRAYSON, N. E., WHITE, R. E., CORTON, C., CORREIA, S., BA ABDULLAH, M. M., WATSON, S. J., COTTEN, M., ARRAND, J. R., MURRAY, P. G., ALLDAY, M. J., RICKINSON, A. B., YOUNG, L. S., FARRELL, P. J. & KELLAM, P. 2015. Genome diversity of Epstein-Barr virus from multiple tumor types and normal infection. *J Virol,* 89**,** 5222–37.

PAN, S., ZHAO, W., LI, Y., YING, Z., LUO, Y., WANG, Q., LI, X., LU, W., DONG, X., WU, Y. & WU, X. 2023. Prediction of risk and overall survival of pancreatic cancer from blood soluble immune checkpoint-related proteins. *Front Immunol,* 14**,** 1189161.

PAN, Y., JIANG, X., YANG, L., CHEN, L., ZENG, X., LIU, G., TANG, Y., QIAN, C., WANG, X., CHENG, F., LIN, J., WANG, X. & LI, Y. 2021. SARS-CoV-2-specific immune response in COVID-19 convalescent individuals. *Signal Transduct Target Ther,* 6**,** 256.

PAPA, G., MALLERY, D. L., ALBECKA, A., WELCH, L. G., CATTIN-ORTOLÁ, J., LUPTAK, J., PAUL, D., MCMAHON, H. T., GOODFELLOW, I. G., CARTER, A., MUNRO, S. & JAMES, L. C. 2021. Furin cleavage of SARS-CoV-2 Spike promotes but is not essential for infection and cell-cell fusion. *PLoS Pathog,* 17**,** e1009246.

PAPADOPOULOS, E. B., LADANYI, M., EMANUEL, D., MACKINNON, S., BOULAD, F., CARABASI, M. H., CASTRO-MALASPINA, H., CHILDS, B. H., GILLIO, A. P., SMALL, T. N. & ET AL. 1994. Infusions of donor leukocytes to treat Epstein-Barr virus-associated lymphoproliferative disorders after allogeneic bone marrow transplantation. *N Engl J Med,* 330**,** 1185–91.

PAPADOPOULOU, A., KARAVALAKIS, G., PAPADOPOULOU, E., XOCHELLI, A., BOUSIOU, Z., VOGIATZOGLOU, A., PAPAYANNI, P. G., GEORGAKOPOULOU, A., GIANNAKI, M., STAVRIDOU, F., VALLIANOU, I., KAMMENOU, M., VARSAMOUDI, E., PAPADIMITRIOU, V., GIANNAKI, C., SILELI, M., STERGIOUDA, Z., STEFANOU, G., KOURLABA, G., GOUNELAS, G., TRIANTAFYLLIDOU, M., SIOTOU, E., KARAGLANI, A., ZOTOU, E., CHATZIKA, G., BOUKLA, A., PAPALEXANDRI, A., KOUTRA, M. G., APOSTOLOU, D., PITSIOU, G., MORFESIS, P., DOUMAS, M., KARAMPATAKIS, T., KAPRAVELOS, N., BITZANI, M., THEODORAKOPOULOU, M., SERASLI, E., GEORGOLOPOULOS, G., SAKELLARI, I., FYLAKTOU, A., TRYFON, S., ANAGNOSTOPOULOS, A. & YANNAKI, E. 2023. SARS-CoV-2-specific T cell therapy for severe COVID-19: a randomized phase 1/2 trial. *Nat Med,* 29**,** 2019–2029.

PAPAYANNI, P. G., CHASIOTIS, D., KOUKOULIAS, K., GEORGAKOPOULOU, A., IATROU, A., GAVRIILAKI, E., GIANNAKI, C., BITZANI, M., GEKA, E., TASIOUDIS, P., CHLOROS, D., FYLAKTOU, A., KIOUMIS, I., TRIANTAFYLLIDOU, M., DIMOU-BESIKLI, S., KARAVALAKIS, G., BOUTOU, A. K., SIOTOU, E., ANAGNOSTOPOULOS, A., PAPADOPOULOU, A. & YANNAKI, E. 2021. Vaccinated and Convalescent Donor-Derived Severe Acute Respiratory Syndrome Coronavirus 2-Specific T Cells as Adoptive Immunotherapy for High-Risk Coronavirus Disease 2019 Patients. *Clin Infect Dis,* 73**,** 2073–2082.

PARAMITA, D. K., FATMAWATI, C., JUWANA, H., VAN SCHAIJK, F. G., FACHIROH, J., HARYANA, S. M. & MIDDELDORP, J. M. 2011. Humoral immune responses to Epstein-Barr virus encoded tumor associated proteins and their putative extracellular domains in nasopharyngeal carcinoma patients and regional controls. *J Med Virol,* 83**,** 665–78.

PARASHER, A. 2021. COVID-19: Current understanding of its Pathophysiology, Clinical presentation and Treatment. *Postgrad Med J,* 97**,** 312–320.

PARKER, B. D., BANKIER, A., SATCHWELL, S., BARRELL, B. & FARRELL, P. J. 1990. Sequence and transcription of Raji Epstein-Barr virus DNA spanning the B95-8 deletion region. *Virology,* 179**,** 339–46.

PAROLINI, S., BOTTINO, C., FALCO, M., AUGUGLIARO, R., GILIANI, S., FRANCESCHINI, R., OCHS, H. D., WOLF, H., BONNEFOY, J. Y., BIASSONI, R., MORETTA, L., NOTARANGELO, L. D. & MORETTA, A. 2000. X-linked

lymphoproliferative disease. 2B4 molecules displaying inhibitory rather than activating function are responsible for the inability of natural killer cells to kill Epstein-Barr virus-infected cells. *J Exp Med,* 192**,** 337–46.

PARRY, R. V., CHEMNITZ, J. M., FRAUWIRTH, K. A., LANFRANCO, A. R., BRAUNSTEIN, I., KOBAYASHI, S. V., LINSLEY, P. S., THOMPSON, C. B. & RILEY, J. L. 2005. CTLA-4 and PD-1 receptors inhibit T-cell activation by distinct mechanisms. *Mol Cell Biol,* 25**,** 9543–53.

PARSONAGE, G., MACHADO, L. R., HUI, J. W., MCLARNON, A., SCHMALER, T., BALASOTHY, M., TO, K. F., VLANTIS, A. C., VAN HASSELT, C. A., LO, K. W., WONG, W. L., HUI, E. P., CHAN, A. T. C. & LEE, S. P. 2012. CXCR6 and CCR5 localize T lymphocyte subsets in nasopharyngeal carcinoma. *Am J Pathol,* 180**,** 1215–1222.

PASCHOS, K., SMITH, P., ANDERTON, E., MIDDELDORP, J. M., WHITE, R. E. & ALLDAY, M. J. 2009. Epstein-barr virus latency in B cells leads to epigenetic repression and CpG methylation of the tumour suppressor gene Bim. *PLoS Pathog,* 5**,** e1000492.

PAVLOVA, S., FEEDERLE, R., GÄRTNER, K., FUCHS, W., GRANZOW, H. & DELECLUSE, H. J. 2013. An Epstein-Barr virus mutant produces immunogenic defective particles devoid of viral DNA. *J Virol,* 87**,** 2011–22.

PEDDIBHOTLA, S., HERSHBERGER, P. M., JASON KIRBY, R., SUGARMAN, E., MALONEY, P. R., HAMPTON SESSIONS, E., DIVLIANSKA, D., MORFA, C. J., TERRY, D., PINKERTON, A. B., SMITH, L. H. & MALANY, S. 2020. Discovery of small molecule antagonists of chemokine receptor CXCR6 that arrest tumor growth in SK-HEP-1 mouse xenografts as a model of hepatocellular carcinoma. *Bioorg Med Chem Lett,* 30**,** 126899.

PEGGS, K. S., VERFUERTH, S., PIZZEY, A., KHAN, N., GUIVER, M., MOSS, P. A. & MACKINNON, S. 2003. Adoptive cellular therapy for early cytomegalovirus infection after allogeneic stem-cell transplantation with virus-specific T-cell lines. *Lancet,* 362**,** 1375–7.

PEGTEL, D. M., MIDDELDORP, J. & THORLEY-LAWSON, D. A. 2004. Epstein-Barr virus infection in ex vivo tonsil epithelial cell cultures of asymptomatic carriers. *J Virol,* 78**,** 12613–24.

PELLICCI, D. G., KOAY, H. F. & BERZINS, S. P. 2020. Thymic development of unconventional T cells: how NKT cells, MAIT cells and γδ T cells emerge. *Nat Rev Immunol,* 20**,** 756–770.

PENDER, M. P., CSURHES, P. A., SMITH, C., DOUGLAS, N. L., NELLER, M. A., MATTHEWS, K. K., BEAGLEY, L., REHAN, S., CROOKS, P., HOPKINS, T. J., BLUM, S., GREEN, K. A., IOANNIDES, Z. A., SWAYNE, A., AFTAB, B. T., HOOPER, K. D., BURROWS, S. R., THOMPSON, K. M., COULTHARD, A. & KHANNA, R. 2018. Epstein-Barr virus-specific T cell therapy for progressive multiple sclerosis. *JCI Insight,* 3.

PENG, Y., MENTZER, A. J., LIU, G., YAO, X., YIN, Z., DONG, D., DEJNIRATTISAI, W., ROSTRON, T., SUPASA, P., LIU, C., LÓPEZ-CAMACHO, C., SLON-CAMPOS, J., ZHAO, Y., STUART, D. I., PAESEN, G. C., GRIMES, J. M., ANTSON, A. A., BAYFIELD, O. W., HAWKINS, D., KER, D. S., WANG, B., TURTLE, L., SUBRAMANIAM, K., THOMSON, P., ZHANG, P., DOLD, C., RATCLIFF, J., SIMMONDS, P., DE SILVA, T., SOPP, P., WELLINGTON, D., RAJAPAKSA, U., CHEN, Y. L., SALIO, M., NAPOLITANI, G., PAES, W., BORROW, P., KESSLER, B. M., FRY, J. W., SCHWABE, N. F., SEMPLE, M. G., BAILLIE, J. K., MOORE, S. C., OPENSHAW, P. J. M., ANSARI, M. A., DUNACHIE, S., BARNES, E., FRATER, J., KERR, G., GOULDER, P., LOCKETT, T., LEVIN, R., ZHANG, Y., JING, R., HO, L. P., CORNALL, R. J., CONLON, C. P., KLENERMAN, P., SCREATON, G. R., MONGKOLSAPAYA, J.,

MCMICHAEL, A., KNIGHT, J. C., OGG, G. & DONG, T. 2020. Broad and strong memory CD4(+) and CD8(+) T cells induced by SARS-CoV-2 in UK convalescent individuals following COVID-19. *Nat Immunol,* 21**,** 1336–1345.

PEPPA, D., PEDROZA-PACHECO, I., PELLEGRINO, P., WILLIAMS, I., MAINI, M. K. & BORROW, P. 2018. Adaptive Reconfiguration of Natural Killer Cells in HIV-1 Infection. *Front Immunol,* 9**,** 474.

PÉREZ-MARTÍNEZ, A., MORA-RILLO, M., FERRERAS, C., GUERRA-GARCÍA, P., PASCUAL-MIGUEL, B., MESTRE-DURÁN, C., BOROBIA, A. M., CARCAS, A. J., QUEIRUGA-PARADA, J., GARCÍA, I., SÁNCHEZ-ZAPARDIEL, E., GASIOR, M., DE PAZ, R., MARCOS, A., VICARIO, J. L., BALAS, A., MORENO, M. A., EGUIZABAL, C., SOLANO, C., ARRIBAS, J. R., BUCKLEY, R. M., MONTEJANO, R. & SORIA, B. 2021. Phase I dose-escalation single centre clinical trial to evaluate the safety of infusion of memory T cells as adoptive therapy in COVID-19 (RELEASE). *EClinicalMedicine,* 39**,** 101086.

PETER, L., WENDERING, D. J., SCHLICKEISER, S., HOFFMANN, H., NOSTER, R., WAGNER, D. L., ZARRINRAD, G., MÜNCH, S., PICHT, S., SCHULENBERG, S., MORADIAN, H., MASHREGHI, M. F., KLEIN, O., GOSSEN, M., ROCH, T., BABEL, N., REINKE, P., VOLK, H. D., AMINI, L. & SCHMUECK-HENNERESSE, M. 2022. Tacrolimus-resistant SARS-CoV-2-specific T cell products to prevent and treat severe COVID-19 in immunosuppressed patients. *Mol Ther Methods Clin Dev,* 25**,** 52–73.

PETERS, A. C., AKINWUMI, M. S., CERVERA, C., MABILANGAN, C., GHOSH, S., LAI, R., IAFOLLA, M., DOUCETTE, K. & PREIKSAITIS, J. K. 2018. The Changing Epidemiology of Posttransplant Lymphoproliferative Disorder in Adult Solid Organ Transplant Recipients Over 30 Years: A Single-center Experience. *Transplantation,* 102**,** 1553–1562.

PETITDEMANGE, C., BECQUART, P., WAUQUIER, N., BÉZIAT, V., DEBRÉ, P., LEROY, E. M. & VIEILLARD, V. 2011. Unconventional repertoire profile is imprinted during acute chikungunya infection for natural killer cells polarization toward cytotoxicity. *PLoS Pathog,* 7**,** e1002268.

PETITDEMANGE, C., WAUQUIER, N., DEVILLIERS, H., YSSEL, H., MOMBO, I., CARON, M., NKOGHÉ, D., DEBRÉ, P., LEROY, E. & VIEILLARD, V. 2016. Longitudinal Analysis of Natural Killer Cells in Dengue Virus-Infected Patients in Comparison to Chikungunya and Chikungunya/Dengue Virus-Infected Patients. *PLoS Negl Trop Dis,* 10**,** e0004499.

PHONG, B. L., AVERY, L., SUMPTER, T. L., GORMAN, J. V., WATKINS, S. C., COLGAN, J. D. & KANE, L. P. 2015. Tim-3 enhances FcεRI-proximal signaling to modulate mast cell activation. *J Exp Med,* 212**,** 2289–304.

PICH, D., MROZEK-GORSKA, P., BOUVET, M., SUGIMOTO, A., AKIDIL, E., GRUNDHOFF, A., HAMPERL, S., LING, P. D. & HAMMERSCHMIDT, W. 2019. First Days in the Life of Naive Human B Lymphocytes Infected with Epstein-Barr Virus. *mBio,* 10.

PINCHUK, L. M., KLAUS, S. J., MAGALETTI, D. M., PINCHUK, G. V., NORSEN, J. P. & CLARK, E. A. 1996. Functional CD40 ligand expressed by human blood dendritic cells is up-regulated by CD40 ligation. *J Immunol,* 157**,** 4363–70.

PISANO, G., ROY, A., AHMED ANSARI, M., KUMAR, B., CHIKOTI, L. & CHANDRAN, B. 2017. Interferon-γ-inducible protein 16 (IFI16) is required for the maintenance of Epstein-Barr virus latency. *Virol J,* 14**,** 221.

PISHESHA, N., HARMAND, T. J. & PLOEGH, H. L. 2022. A guide to antigen processing and presentation. *Nat Rev Immunol,* 22**,** 751–764.

POLING, B. C., PRICE, A. M., LUFTIG, M. A. & CULLEN, B. R. 2017. The Epstein-Barr virus miR-BHRF1 microRNAs regulate viral gene expression in cis. *Virology,* 512**,** 113–123.

POLONI, C., SCHONHOFER, C., IVISON, S., LEVINGS, M. K., STEINER, T. S. & COOK, L. 2023. T-cell activation-induced marker assays in health and disease. *Immunol Cell Biol,* 101**,** 491–503.

PONNUSAMY, R., KHATRI, R., CORREIA, P. B., WOOD, C. D., MANCINI, E. J., FARRELL, P. J. & WEST, M. J. 2019. Increased association between Epstein-Barr virus EBNA2 from type 2 strains and the transcriptional repressor BS69 restricts EBNA2 activity. *PLoS Pathog,* 15**,** e1007458.

PORCIELLO, N., FRANZESE, O., D'AMBROSIO, L., PALERMO, B. & NISTICÒ, P. 2022. T-cell repertoire diversity: friend or foe for protective antitumor response? *J Exp Clin Cancer Res,* 41**,** 356.

PORMOHAMMAD, A., ZAREI, M., GHORBANI, S., MOHAMMADI, M., RAZIZADEH, M. H., TURNER, D. L. & TURNER, R. J. 2021. Efficacy and Safety of COVID-19 Vaccines: A Systematic Review and Meta-Analysis of Randomized Clinical Trials. *Vaccines (Basel),* 9.

PORTER, D. L., COLLINS, R. H., JR., SHPILBERG, O., DROBYSKI, W. R., CONNORS, J. M., SPROLES, A. & ANTIN, J. H. 1999. Long-term follow-up of patients who achieved complete remission after donor leukocyte infusions. *Biol Blood Marrow Transplant,* 5**,** 253–61.

PRATO, M., TIBERTI, N., MAZZI, C., GOBBI, F., PIUBELLI, C. & LONGONI, S. S. 2024. The Renin-Angiotensin System (RAS) in COVID-19 Disease: Where We Are 3 Years after the Beginning of the Pandemic. *Microorganisms,* 12.

PREIKSAITIS, J., ALLEN, U., BOLLARD, C. M., DHARNIDHARKA, V. R., DULEK, D. E., GREEN, M., MARTINEZ, O. M., METES, D. M., MICHAELS, M. G., SMETS, F., CHINNOCK, R. E., COMOLI, P., DANZIGER-ISAKOV, L., DIPCHAND, A. I., ESQUIVEL, C. O., FERRY, J. A., GROSS, T. G., HAYASHI, R. J., HÖCKER, B., L'HUILLIER, A. G., MARKS, S. D., MAZARIEGOS, G. V., SQUIRES, J., SWERDLOW, S. H., TRAPPE, R. U., VISNER, G., WEBBER, S. A., WILKINSON, J. D. & MAECKER-KOLHOFF, B. 2024. The IPTA Nashville Consensus Conference on Post-Transplant lymphoproliferative disorders after solid organ transplantation in children: III - Consensus guidelines for Epstein-Barr virus load and other biomarker monitoring. *Pediatr Transplant,* 28**,** e14471.

PROCKOP, S., DOUBROVINA, E., SUSER, S., HELLER, G., BARKER, J., DAHI, P., PERALES, M. A., PAPADOPOULOS, E., SAUTER, C., CASTRO-MALASPINA, H., BOULAD, F., CURRAN, K. J., GIRALT, S., GYURKOCZA, B., HSU, K. C., JAKUBOWSKI, A., HANASH, A. M., KERNAN, N. A., KOBOS, R., KOEHNE, G., LANDAU, H., PONCE, D., SPITZER, B., YOUNG, J. W., BEHR, G., DUNPHY, M., HAQUE, S., TERUYA-FELDSTEIN, J., ARCILA, M., MOUNG, C., HSU, S., HASAN, A. & O'REILLY, R. J. 2020. Off-the-shelf EBV-specific T cell immunotherapy for rituximab-refractory EBV-associated lymphoma following transplantation. *J Clin Invest,* 130**,** 733–747.

PUDNEY, V. A., LEESE, A. M., RICKINSON, A. B. & HISLOP, A. D. 2005. CD8+ immunodominance among Epstein-Barr virus lytic cycle antigens directly reflects the efficiency of antigen presentation in lytically infected cells. *J Exp Med,* 201**,** 349–60.

QASIM, W., ZHAN, H., SAMARASINGHE, S., ADAMS, S., AMROLIA, P., STAFFORD, S., BUTLER, K., RIVAT, C., WRIGHT, G., SOMANA, K., GHORASHIAN, S., PINNER, D., AHSAN, G., GILMOUR, K., LUCCHINI, G., INGLOTT, S., MIFSUD, W., CHIESA, R., PEGGS, K. S., CHAN, L., FARZENEH, F., THRASHER, A. J., VORA, A., PULE, M. & VEYS, P. 2017. Molecular remission of infant B-ALL after infusion of universal TALEN gene-edited CAR T cells. *Sci Transl Med,* 9.

QI, Q., LIU, Y., CHENG, Y., GLANVILLE, J., ZHANG, D., LEE, J. Y., OLSHEN, R. A., WEYAND, C. M., BOYD, S. D. & GORONZY, J. J. 2014. Diversity and clonal selection in the human T-cell repertoire. *Proc Natl Acad Sci U S A,* 111**,** 13139–44.

QIN, C., ZHOU, L., HU, Z., ZHANG, S., YANG, S., TAO, Y., XIE, C., MA, K., SHANG, K., WANG, W. & TIAN, D. S. 2020. Dysregulation of Immune Response in Patients With Coronavirus 2019 (COVID-19) in Wuhan, China. *Clin Infect Dis,* 71**,** 762–768.

QUACH, D. H., BECERRA-DOMINGUEZ, L., ROUCE, R. H. & ROONEY, C. M. 2019. A strategy to protect off-the-shelf cell therapy products using virus-specific T-cells engineered to eliminate alloreactive T-cells. *J Transl Med,* 17**,** 240.

QUACH, D. H., GANESH, H. R., BRIONES, Y. D., NOURAEE, N., MA, A., HADIDI, Y. F., SHARMA, S. & ROONEY, C. M. 2024. Rejection resistant CD30.CAR-modified Epstein-Barr virus-specific T cells as an off-the-shelf platform for CD30(+) lymphoma. *Mol Ther Oncol,* 32**,** 200814.

QUACH, D. H., LULLA, P. & ROONEY, C. M. 2023. Banking on virus-specific T cells to fulfill the need for off-the-shelf cell therapies. *Blood,* 141**,** 877–885.

RAAB-TRAUB, N., DAMBAUGH, T. & KIEFF, E. 1980. DNA of Epstein-Barr virus VIII: B95-8, the previous prototype, is an unusual deletion derivative. *Cell,* 22**,** 257–67.

RAHIMI, R. A. & LUSTER, A. D. 2018. Chemokines: Critical Regulators of Memory T Cell Development, Maintenance, and Function. *Adv Immunol,* 138**,** 71–98.

RAMOS, C. A., GROVER, N. S., BEAVEN, A. W., LULLA, P. D., WU, M. F., IVANOVA, A., WANG, T., SHEA, T. C., ROONEY, C. M., DITTUS, C., PARK, S. I., GEE, A. P., ELDRIDGE, P. W., MCKAY, K. L., MEHTA, B., CHENG, C. J., BUCHANAN, F. B., GRILLEY, B. J., MORRISON, K., BRENNER, M. K., SERODY, J. S., DOTTI, G., HESLOP, H. E. & SAVOLDO, B. 2020. Anti-CD30 CAR-T Cell Therapy in Relapsed and Refractory Hodgkin Lymphoma. *J Clin Oncol,* 38**,** 3794–3804.

RANGACHARI, M., ZHU, C., SAKUISHI, K., XIAO, S., KARMAN, J., CHEN, A., ANGIN, M., WAKEHAM, A., GREENFIELD, E. A., SOBEL, R. A., OKADA, H., MCKINNON, P. J., MAK, T. W., ADDO, M. M., ANDERSON, A. C. & KUCHROO, V. K. 2012. Bat3 promotes T cell responses and autoimmunity by repressing Tim-3–mediated cell death and exhaustion. *Nat Med,* 18**,** 1394–400.

RAUSER, G., EINSELE, H., SINZGER, C., WERNET, D., KUNTZ, G., ASSENMACHER, M., CAMPBELL, J. D. & TOPP, M. S. 2004. Rapid generation of combined CMV-specific CD4+ and CD8+ T-cell lines for adoptive transfer into recipients of allogeneic stem cell transplants. *Blood,* 103**,** 3565–72.

READ, S., GREENWALD, R., IZCUE, A., ROBINSON, N., MANDELBROT, D., FRANCISCO, L., SHARPE, A. H. & POWRIE, F. 2006. Blockade of CTLA-4 on CD4+CD25+ regulatory T cells abrogates their function in vivo. *J Immunol,* 177**,** 4376–83.

RECHSTEINER, M. P., BERGER, C., ZAUNER, L., SIGRIST, J. A., WEBER, M., LONGNECKER, R., BERNASCONI, M. & NADAL, D. 2008. Latent membrane protein 2B regulates susceptibility to induction of lytic Epstein-Barr virus infection. *J Virol,* 82**,** 1739–47.

REDMOND, W. L., RUBY, C. E. & WEINBERG, A. D. 2009. The role of OX40-mediated co-stimulation in T-cell activation and survival. *Crit Rev Immunol,* 29**,** 187–201.

REGAN, F. & TAYLOR, C. 2002. Blood transfusion medicine. *Bmj,* 325**,** 143–7.

REN, J., LIU, X., FANG, C., JIANG, S., JUNE, C. H. & ZHAO, Y. 2017. Multiplex Genome Editing to Generate Universal CAR T Cells Resistant to PD1 Inhibition. *Clin Cancer Res,* 23**,** 2255–2266.

RESHEF, R., VARDHANABHUTI, S., LUSKIN, M. R., HEITJAN, D. F., HADJILIADIS, D., GORAL, S., KROK, K. L., GOLDBERG, L. R., PORTER, D. L., STADTMAUER, E. A. & TSAI, D. E. 2011. Reduction of immunosuppression as initial therapy for posttransplantation lymphoproliferative disorder(★). *Am J Transplant,* 11**,** 336–47.

REYNALDI, A., SCHLUB, T. E., PIRIOU, E., OGOLLA, S., SUMBA, O. P., MOORMANN, A. M., ROCHFORD, R. & DAVENPORT, M. P. 2016. Modeling of EBV Infection and Antibody Responses in Kenyan Infants With Different Levels of Malaria Exposure Shows Maternal Antibody Decay is a Major Determinant of Early EBV Infection. *J Infect Dis,* 214**,** 1390–1398.

RICCIARDELLI, I., BREWIN, J., LUGTHART, G., ALBON, S. J., PULE, M. & AMROLIA, P. J. 2013. Rapid generation of EBV-specific cytotoxic T lymphocytes resistant to calcineurin inhibitors for adoptive immunotherapy. *Am J Transplant,* 13**,** 3244–52.

RICKINSON, A. B., YOUNG, L. S. & ROWE, M. 1987. Influence of the Epstein-Barr virus nuclear antigen EBNA 2 on the growth phenotype of virus-transformed B cells. *J Virol,* 61**,** 1310–7.

RIDDELL, S. R., WATANABE, K. S., GOODRICH, J. M., LI, C. R., AGHA, M. E. & GREENBERG, P. D. 1992. Restoration of viral immunity in immunodeficient humans by the adoptive transfer of T cell clones. *Science,* 257**,** 238–41.

ROBINS, H., DESMARAIS, C., MATTHIS, J., LIVINGSTON, R., ANDRIESEN, J., REIJONEN, H., CARLSON, C., NEPOM, G., YEE, C. & CEROSALETTI, K. 2012. Ultra-sensitive detection of rare T cell clones. *J Immunol Methods,* 375**,** 14–9.

ROBINSON, W. H., YOUNIS, S., LOVE, Z. Z., STEINMAN, L. & LANZ, T. V. 2024. Epstein-Barr virus as a potentiator of autoimmune diseases. *Nat Rev Rheumatol,* 20**,** 729–740.

RODDA, L. B., MORAWSKI, P. A., PRUNER, K. B., FAHNING, M. L., HOWARD, C. A., FRANKO, N., LOGUE, J., EGGENBERGER, J., STOKES, C., GOLEZ, I., HALE, M., GALE, M., JR., CHU, H. Y., CAMPBELL, D. J. & PEPPER, M. 2022. Imprinted SARS-CoV-2-specific memory lymphocytes define hybrid immunity. *Cell,* 185**,** 1588–1601.e14.

RODDA, L. B., NETLAND, J., SHEHATA, L., PRUNER, K. B., MORAWSKI, P. A., THOUVENEL, C. D., TAKEHARA, K. K., EGGENBERGER, J., HEMANN, E. A., WATERMAN, H. R., FAHNING, M. L., CHEN, Y., HALE, M., RATHE, J., STOKES, C., WRENN, S., FIALA, B., CARTER, L., HAMERMAN, J. A., KING, N. P., GALE, M., JR., CAMPBELL, D. J., RAWLINGS, D. J. & PEPPER, M. 2021. Functional SARS-CoV-2-Specific Immune Memory Persists after Mild COVID-19. *Cell,* 184**,** 169–183.e17.

RONIT, A., BERG, R. M. G., BAY, J. T., HAUGAARD, A. K., AHLSTRÖM, M. G., BURGDORF, K. S., ULLUM, H., RØRVIG, S. B., TJELLE, K., FOSS, N. B., BENFIELD, T., MARQUART, H. V. & PLOVSING, R. R. 2021. Compartmental immunophenotyping in COVID-19 ARDS: A case series. *J Allergy Clin Immunol,* 147**,** 81–91.

ROONEY, C. M., ROSKROW, M. A., SMITH, C. A., BRENNER, M. K. & HESLOP, H. E. 1998. Immunotherapy for Epstein-Barr virus-associated cancers. *J Natl Cancer Inst Monogr***,** 89–93.

ROONEY, C. M., SMITH, C. A., NG, C. Y., LOFTIN, S., LI, C., KRANCE, R. A., BRENNER, M. K. & HESLOP, H. E. 1995. Use of gene-modified virus-specific

T lymphocytes to control Epstein-Barr-virus-related lymphoproliferation. *Lancet,* 345**,** 9–13.

ROSSIGNOL, J., TERRIOU, L., ROBU, D., WILLEKENS, C., HIVERT, B., PASCAL, L., GUIEZE, R., TRAPPE, R., BAILLET, C., HUGLO, D. & MORSCHHAUSER, F. 2015. Radioimmunotherapy ((90) Y-Ibritumomab Tiuxetan) for Posttransplant Lymphoproliferative Disorders After Prior Exposure to Rituximab. *Am J Transplant,* 15**,** 1976–81.

ROVITO, R., AUGELLO, M., BEN-HAIM, A., BONO, V., D'ARMINIO MONFORTE, A. & MARCHETTI, G. 2022. Hallmarks of Severe COVID-19 Pathogenesis: A Pas de Deux Between Viral and Host Factors. *Front Immunol,* 13**,** 912336.

RUBINSTEIN, J. D., ZHU, X., LEEMHUIS, T., PHAM, G., RAY, L., EMBERESH, S., JODELE, S., THOMAS, S., CANCELAS, J. A., BOLLARD, C. M., HANLEY, P. J., KELLER, M. D., GRIMLEY, O., CLARK, D., CLARK, T., LINDESTAM ARLEHAMN, C. S., SETTE, A., DAVIES, S. M., NELSON, A. S., GRIMLEY, M. S. & LUTZKO, C. 2021. Virus-specific T cells for adenovirus infection after stem cell transplantation are highly effective and class II HLA restricted. *Blood Adv,* 5**,** 3309–3321.

RUBIO, V., STUGE, T. B., SINGH, N., BETTS, M. R., WEBER, J. S., ROEDERER, M. & LEE, P. P. 2003. Ex vivo identification, isolation and analysis of tumor-cytolytic T cells. *Nat Med,* 9**,** 1377–82.

RÜHL, H., BEIN, G. & SACHS, U. J. 2009. Transfusion-associated graft-versus-host disease. *Transfus Med Rev,* 23**,** 62–71.

RUMPRET, M., DRYLEWICZ, J., ACKERMANS, L. J. E., BORGHANS, J. A. M., MEDZHITOV, R. & MEYAARD, L. 2020. Functional categories of immune inhibitory receptors. *Nat Rev Immunol,* 20**,** 771–780.

RUTERBUSCH, M., PRUNER, K. B., SHEHATA, L. & PEPPER, M. 2020. In Vivo CD4(+) T Cell Differentiation and Function: Revisiting the Th1/Th2 Paradigm. *Annu Rev Immunol,* 38**,** 705–725.

RYAN, F. J., HOPE, C. M., MASAVULI, M. G., LYNN, M. A., MEKONNEN, Z. A., YEOW, A. E. L., GARCIA-VALTANEN, P., AL-DELFI, Z., GUMMOW, J., FERGUSON, C., O'CONNOR, S., REDDI, B. A. J., HISSARIA, P., SHAW, D., KOK-LIM, C., GLEADLE, J. M., BEARD, M. R., BARRY, S. C., GRUBOR-BAUK, B. & LYNN, D. J. 2022. Long-term perturbation of the peripheral immune system months after SARS-CoV-2 infection. *BMC Med,* 20**,** 26.

RYDYZNSKI MODERBACHER, C., RAMIREZ, S. I., DAN, J. M., GRIFONI, A., HASTIE, K. M., WEISKOPF, D., BELANGER, S., ABBOTT, R. K., KIM, C., CHOI, J., KATO, Y., CROTTY, E. G., KIM, C., RAWLINGS, S. A., MATEUS, J., TSE, L. P. V., FRAZIER, A., BARIC, R., PETERS, B., GREENBAUM, J., OLLMANN SAPHIRE, E., SMITH, D. M., SETTE, A. & CROTTY, S. 2020. Antigen-Specific Adaptive Immunity to SARS-CoV-2 in Acute COVID-19 and Associations with Age and Disease Severity. *Cell,* 183**,** 996–1012.e19.

SAGGAU, C., BACHER, P., ESSER, D., RASA, M., MEISE, S., MOHR, N., KOHLSTEDT, N., HUTLOFF, A., SCHACHT, S. S., DARGVAINIENE, J., MARTINI, G. R., STÜRNER, K. H., SCHRÖDER, I., MARKEWITZ, R., HARTL, J., HASTERMANN, M., DUCHOW, A., SCHINDLER, P., BECKER, M., BAUTISTA, C., GOTTFREUND, J., WALTER, J., POLANSKY, J. K., YANG, M., NAGHAVIAN, R., WENDORFF, M., SCHUSTER, E. M., DAHL, A., PETZOLD, A., REINHARDT, S., FRANKE, A., WIECZOREK, M., HENSCHEL, L., BERGER, D., HEINE, G., HOLTSCHE, M., HÄUßLER, V., PETERS, C., SCHMIDT, E., FILLATREAU, S., BUSCH, D. H., WANDINGER, K. P., SCHOBER, K., MARTIN, R., PAUL, F., LEYPOLDT, F. & SCHEFFOLD, A. 2024. Autoantigen-specific CD4(+) T cells acquire an exhausted phenotype and persist in human antigen-specific autoimmune diseases. *Immunity,* 57**,** 2416–2432.e8.

SAINATHAM, C., YADAV, D., DILLI BABU, A., TALLAPALLI, J. R., KANAGALA, S. G., FILIPPOV, E., MURILLO CHAVEZ, F., AHMED, N. & LUTFI, F. 2024. The current socioeconomic and regulatory landscape of immune effector cell therapies. *Front Med (Lausanne),* 11**,** 1462307.

SALAHUDEEN, A. A., CHOI, S. S., RUSTAGI, A., ZHU, J., VAN UNEN, V., DE LA, O. S., FLYNN, R. A., MARGALEF-CATALÀ, M., SANTOS, A. J. M., JU, J., BATISH, A., USUI, T., ZHENG, G. X. Y., EDWARDS, C. E., WAGAR, L. E., LUCA, V., ANCHANG, B., NAGENDRAN, M., NGUYEN, K., HART, D. J., TERRY, J. M., BELGRADER, P., ZIRALDO, S. B., MIKKELSEN, T. S., HARBURY, P. B., GLENN, J. S., GARCIA, K. C., DAVIS, M. M., BARIC, R. S., SABATTI, C., AMIEVA, M. R., BLISH, C. A., DESAI, T. J. & KUO, C. J. 2020. Progenitor identification and SARS-CoV-2 infection in human distal lung organoids. *Nature,* 588**,** 670–675.

SALAS, M. Q., PREM, S., REMBERGER, M., LAM, W., KIM, D. D. H., MICHELIS, F. V., AL-SHAIBANI, Z., GERBITZ, A., LIPTON, J. H., VISWABANDYA, A., KUMAR, R., KUMAR, D., MATTSSON, J. & LAW, A. D. 2020. High incidence but low mortality of EBV-reactivation and PTLD after alloHCT using ATG and PTCy for GVHD prophylaxis. *Leuk Lymphoma,* 61**,** 3198–3208.

SALZER, E., DASCHKEY, S., CHOO, S., GOMBERT, M., SANTOS-VALENTE, E., GINZEL, S., SCHWENDINGER, M., HAAS, O. A., FRITSCH, G., PICKL, W. F., FÖRSTER-WALDL, E., BORKHARDT, A., BOZTUG, K., BIENEMANN, K. & SEIDEL, M. G. 2013. Combined immunodeficiency with life-threatening EBV-associated lymphoproliferative disorder in patients lacking functional CD27. *Haematologica,* 98**,** 473–8.

SAMARASINGHE, S., MANCAO, C., PULE, M., NAWROLY, N., KARLSSON, H., BREWIN, J., OPENSHAW, P., GASPAR, H. B., VEYS, P. & AMROLIA, P. J. 2010. Functional characterization of alloreactive T cells identifies CD25 and CD71 as optimal targets for a clinically applicable allodepletion strategy. *Blood,* 115**,** 396–407.

SAMAVATI, L. & UHAL, B. D. 2020. ACE2, Much More Than Just a Receptor for SARS-COV-2. *Front Cell Infect Microbiol,* 10**,** 317.

SAMPAIO, N. G., CHAUVEAU, L., HERTZOG, J., BRIDGEMAN, A., FOWLER, G., MOONEN, J. P., DUPONT, M., RUSSELL, R. A., NOERENBERG, M. & REHWINKEL, J. 2021. The RNA sensor MDA5 detects SARS-CoV-2 infection. *Sci Rep,* 11**,** 13638.

SAMPLE, J., YOUNG, L., MARTIN, B., CHATMAN, T., KIEFF, E., RICKINSON, A. & KIEFF, E. 1990. Epstein-Barr virus types 1 and 2 differ in their EBNA-3A, EBNA-3B, and EBNA-3C genes. *J Virol,* 64**,** 4084–92.

SANJUÁN, R., NEBOT, M. R., CHIRICO, N., MANSKY, L. M. & BELSHAW, R. 2010. Viral mutation rates. *J Virol,* 84**,** 9733–48.

SANSONI, P., VESCOVINI, R., FAGNONI, F., BIASINI, C., ZANNI, F., ZANLARI, L., TELERA, A., LUCCHINI, G., PASSERI, G., MONTI, D., FRANCESCHI, C. & PASSERI, M. 2008. The immune system in extreme longevity. *Exp Gerontol,* 43**,** 61–5.

SANTPERE, G., DARRE, F., BLANCO, S., ALCAMI, A., VILLOSLADA, P., MAR ALBÀ, M. & NAVARRO, A. 2014. Genome-wide analysis of wild-type Epstein-Barr virus genomes derived from healthy individuals of the 1,000 Genomes Project. *Genome Biol Evol,* 6**,** 846–60.

SATHIYAMOORTHY, K., HU, Y. X., MÖHL, B. S., CHEN, J., LONGNECKER, R. & JARDETZKY, T. S. 2016. Structural basis for Epstein-Barr virus host cell tropism mediated by gp42 and gHgL entry glycoproteins. *Nat Commun,* 7**,** 13557.

SATO, Y., BANDO, H., DI PIAZZA, M., GOWING, G., HERBERTS, C., JACKMAN, S., LEONI, G., LIBERTINI, S., MACLACHLAN, T., MCBLANE, J. W., PEREIRA MOURIÈS, L., SHARPE, M., SHINGLETON, W., SURMACZ-CORDLE, B., YAMAMOTO, K. & VAN DER LAAN, J. W. 2019. Tumorigenicity assessment of cell therapy products: The need for global consensus and points to consider. *Cytotherapy,* 21**,** 1095–1111.

SAVARD, M., BÉLANGER, C., TARDIF, M., GOURDE, P., FLAMAND, L. & GOSSELIN, J. 2000. Infection of primary human monocytes by Epstein-Barr virus. *J Virol,* 74**,** 2612–9.

SAVOLDO, B., GOSS, J. A., HAMMER, M. M., ZHANG, L., LOPEZ, T., GEE, A. P., LIN, Y. F., QUIROS-TEJEIRA, R. E., REINKE, P., SCHUBERT, S., GOTTSCHALK, S., FINEGOLD, M. J., BRENNER, M. K., ROONEY, C. M. & HESLOP, H. E. 2006. Treatment of solid organ transplant recipients with autologous Epstein Barr virus-specific cytotoxic T lymphocytes (CTLs). *Blood,* 108**,** 2942–9.

SCHLUMS, H., CICHOCKI, F., TESI, B., THEORELL, J., BEZIAT, V., HOLMES, T. D., HAN, H., CHIANG, S. C., FOLEY, B., MATTSSON, K., LARSSON, S., SCHAFFER, M., MALMBERG, K. J., LJUNGGREN, H. G., MILLER, J. S. & BRYCESON, Y. T. 2015. Cytomegalovirus infection drives adaptive epigenetic diversification of NK cells with altered signaling and effector function. *Immunity,* 42**,** 443–56.

SCHMIED, S., GOSTICK, E., PRICE, D. A., ABKEN, H., ASSENMACHER, M. & RICHTER, A. 2015. Analysis of the functional WT1-specific T-cell repertoire in healthy donors reveals a discrepancy between CD4(+) and CD8(+) memory formation. *Immunology,* 145**,** 558–69.

SCHNELL, A., BOD, L., MADI, A. & KUCHROO, V. K. 2020. The yin and yang of co-inhibitory receptors: toward anti-tumor immunity without autoimmunity. *Cell Res,* 30**,** 285–299.

SCHULTHEIß, C., PASCHOLD, L., SIMNICA, D., MOHME, M., WILLSCHER, E., VON WENSERSKI, L., SCHOLZ, R., WIETERS, I., DAHLKE, C., TOLOSA, E., SEDDING, D. G., CIESEK, S., ADDO, M. & BINDER, M. 2020. Next-Generation Sequencing of T and B Cell Receptor Repertoires from COVID-19 Patients Showed Signatures Associated with Severity of Disease. *Immunity,* 53**,** 442–455.e4.

SCHULTZE, J. L. & ASCHENBRENNER, A. C. 2021. COVID-19 and the human innate immune system. *Cell,* 184**,** 1671–1692.

SCHULZE LAMMERS, F. C., BONIFACIUS, A., TISCHER-ZIMMERMANN, S., GOUDEVA, L., MARTENS, J., LEPENIES, B., VON KARPOWITZ, M., EINECKE, G., BEUTEL, G., SKRIPULETZ, T., BLASCZYK, R., BEIER, R., MAECKER-KOLHOFF, B. & EIZ-VESPER, B. 2022. Antiviral T-Cell Frequencies in a Healthy Population: Reference Values for Evaluating Antiviral Immune Cell Profiles in Immunocompromised Patients. *J Clin Immunol,* 42**,** 546–558.

SEKINE, T., PEREZ-POTTI, A., RIVERA-BALLESTEROS, O., STRÅLIN, K., GORIN, J. B., OLSSON, A., LLEWELLYN-LACEY, S., KAMAL, H., BOGDANOVIC, G., MUSCHIOL, S., WULLIMANN, D. J., KAMMANN, T., EMGÅRD, J., PARROT, T., FOLKESSON, E., ROOYACKERS, O., ERIKSSON, L. I., HENTER, J. I., SÖNNERBORG, A., ALLANDER, T., ALBERT, J., NIELSEN, M., KLINGSTRÖM, J., GREDMARK-RUSS, S., BJÖRKSTRÖM, N. K., SANDBERG, J. K., PRICE, D. A., LJUNGGREN, H. G., ALEMAN, S. & BUGGERT, M. 2020. Robust T Cell Immunity in Convalescent Individuals with Asymptomatic or Mild COVID-19. *Cell,* 183**,** 158–168.e14.

SHAH, P., FORGET, M. A., FRANK, M. L., JIANG, P., SAKELLARIOU-THOMPSON, D., FEDERICO, L., KHAIRULLAH, R., NEUTZLER, C. A., WISTUBA, I., CHOW,

C. B., LONG, Y., FUJIMOTO, J., LIN, S. Y., MAITRA, A., NEGRAO, M. V., MITCHELL, K. G., WEISSFERDT, A., VAPORCIYAN, A. A., CASCONE, T., ROTH, J. A., ZHANG, J., SEPESI, B., GIBBONS, D. L., HEYMACH, J. V., HAYMAKER, C. L., MCGRAIL, D. J., REUBEN, A. & BERNATCHEZ, C. 2022. Combined IL-2, agonistic CD3 and 4-1BB stimulation preserve clonotype hierarchy in propagated non-small cell lung cancer tumor-infiltrating lymphocytes. *J Immunother Cancer,* 10.

SHANNON-LOWE, C. & RICKINSON, A. 2019. The Global Landscape of EBV-Associated Tumors. *Front Oncol,* 9**,** 713.

SHEAFFER, A. K., NEWCOMB, W. W., GAO, M., YU, D., WELLER, S. K., BROWN, J. C. & TENNEY, D. J. 2001. Herpes simplex virus DNA cleavage and packaging proteins associate with the procapsid prior to its maturation. *J Virol,* 75**,** 687–98.

SHERINA, N., PIRALLA, A., DU, L., WAN, H., KUMAGAI-BRAESCH, M., ANDRÉLL, J., BRAESCH-ANDERSEN, S., CASSANITI, I., PERCIVALLE, E., SARASINI, A., BERGAMI, F., DI MARTINO, R., COLANERI, M., VECCHIA, M., SAMBO, M., ZUCCARO, V., BRUNO, R., SACHS, M., OGGIONNI, T., MELONI, F., ABOLHASSANI, H., BERTOGLIO, F., SCHUBERT, M., BYRNE-STEELE, M., HAN, J., HUST, M., XUE, Y., HAMMARSTRÖM, L., BALDANTI, F., MARCOTTE, H. & PAN-HAMMARSTRÖM, Q. 2021. Persistence of SARS-CoV-2-specific B and T cell responses in convalescent COVID-19 patients 6-8 months after the infection. *Med,* 2**,** 281–295.e4.

SHI, H., LI, A., DAI, Z., XUE, J., ZHAO, Q., TIAN, J., SONG, D., WANG, H., CHEN, J., ZHANG, X., ZHOU, K., WEI, H. & QIN, S. 2023. IL-15 armoring enhances the antitumor efficacy of claudin 18.2-targeting CAR-T cells in syngeneic mouse tumor models. *Front Immunol,* 14**,** 1165404.

SHI, Y., WU, W., WAN, T., LIU, Y., PENG, G., CHEN, Z. & ZHU, H. 2013. Impact of polyclonal anti-CD3/CD28-coated magnetic bead expansion methods on T cell proliferation, differentiation and function. *Int Immunopharmacol,* 15**,** 129–37.

SHIBUYA, K., LANIER, L. L., PHILLIPS, J. H., OCHS, H. D., SHIMIZU, K., NAKAYAMA, E., NAKAUCHI, H. & SHIBUYA, A. 1999. Physical and functional association of LFA-1 with DNAM-1 adhesion molecule. *Immunity,* 11**,** 615–23.

SHOMURADOVA, A. S., VAGIDA, M. S., SHEETIKOV, S. A., ZORNIKOVA, K. V., KIRYUKHIN, D., TITOV, A., PESHKOVA, I. O., KHMELEVSKAYA, A., DIANOV, D. V., MALASHEVA, M., SHMELEV, A., SERDYUK, Y., BAGAEV, D. V., PIVNYUK, A., SHCHERBININ, D. S., MALEEVA, A. V., SHAKIROVA, N. T., PILUNOV, A., MALKO, D. B., KHAMAGANOVA, E. G., BIDERMAN, B., IVANOV, A., SHUGAY, M. & EFIMOV, G. A. 2020. SARS-CoV-2 Epitopes Are Recognized by a Public and Diverse Repertoire of Human T Cell Receptors. *Immunity,* 53**,** 1245–1257.e5.

SHUM, T., OMER, B., TASHIRO, H., KRUSE, R. L., WAGNER, D. L., PARIKH, K., YI, Z., SAUER, T., LIU, D., PARIHAR, R., CASTILLO, P., LIU, H., BRENNER, M. K., METELITSA, L. S., GOTTSCHALK, S. & ROONEY, C. M. 2017. Constitutive Signaling from an Engineered IL7 Receptor Promotes Durable Tumor Elimination by Tumor-Redirected T Cells. *Cancer Discov,* 7**,** 1238–1247.

SIDHOM, J. W. & BARAS, A. S. 2021. Deep learning identifies antigenic determinants of severe SARS-CoV-2 infection within T-cell repertoires. *Sci Rep,* 11**,** 14275.

SILINS, S. L., SHERRITT, M. A., SILLERI, J. M., CROSS, S. M., ELLIOTT, S. L., BHARADWAJ, M., LE, T. T., MORRISON, L. E., KHANNA, R., MOSS, D. J.,

SUHRBIER, A. & MISKO, I. S. 2001. Asymptomatic primary Epstein-Barr virus infection occurs in the absence of blood T-cell repertoire perturbations despite high levels of systemic viral load. *Blood,* 98**,** 3739–44.

SILVA, L. T. D., ORTEGA, M. M., TIYO, B. T., VIANA, I. F. T., LIMA, T. E., TOZETTO-MENDOZA, T. R., OLIVEIRA, L., TEIXEIRA, F. M. E., LINS, R. D., ALMEIDA, A., MENDES-CORREA, M. C., DUARTE, A. & OSHIRO, T. M. 2021. SARS-CoV-2 recombinant proteins stimulate distinct cellular and humoral immune response profiles in samples from COVID-19 convalescent patients. *Clinics (Sao Paulo),* 76**,** e3548.

SIMARA, P., TESAROVA, L., TAPUCHOVA, I., CELEROVA, J. & KOUTNA, I. 2021. T-Cell Activation: Post-Infection Diagnostic Tool for COVID-19. *Folia Biol (Praha),* 67**,** 16–27.

SIMÕES E SILVA, A. C., SILVEIRA, K. D., FERREIRA, A. J. & TEIXEIRA, M. M. 2013. ACE2, angiotensin-(1-7) and Mas receptor axis in inflammation and fibrosis. *Br J Pharmacol,* 169**,** 477–92.

SIMS, A. C., BARIC, R. S., YOUNT, B., BURKETT, S. E., COLLINS, P. L. & PICKLES, R. J. 2005. Severe acute respiratory syndrome coronavirus infection of human ciliated airway epithelia: role of ciliated cells in viral spread in the conducting airways of the lungs. *J Virol,* 79**,** 15511–24.

SKALSKA, L., WHITE, R. E., FRANZ, M., RUHMANN, M. & ALLDAY, M. J. 2010. Epigenetic repression of p16(INK4A) by latent Epstein-Barr virus requires the interaction of EBNA3A and EBNA3C with CtBP. *PLoS Pathog,* 6**,** e1000951.

SMATTI, M. K., AL-SADEQ, D. W., ALI, N. H., PINTUS, G., ABOU-SALEH, H. & NASRALLAH, G. K. 2018. Epstein-Barr Virus Epidemiology, Serology, and Genetic Variability of LMP-1 Oncogene Among Healthy Population: An Update. *Front Oncol,* 8**,** 211.

SMITH, C. & KHANNA, R. 2017. Adoptive cellular immunotherapy for virus-associated cancers: a new paradigm in personalized medicine. *Immunol Cell Biol,* 95**,** 364–371.

SMITH, C., LEE, V., SCHUESSLER, A., BEAGLEY, L., REHAN, S., TSANG, J., LI, V., TIU, R., SMITH, D., NELLER, M. A., MATTHEWS, K. K., GOSTICK, E., PRICE, D. A., BURROWS, J., BOYLE, G. M., CHUA, D., PANIZZA, B., PORCEDDU, S. V., NICHOLLS, J., KWONG, D. & KHANNA, R. 2017. Pre-emptive and therapeutic adoptive immunotherapy for nasopharyngeal carcinoma: Phenotype and effector function of T cells impact on clinical response. *Oncoimmunology,* 6**,** e1273311.

SMITH, E. C., SEXTON, N. R. & DENISON, M. R. 2014. Thinking Outside the Triangle: Replication Fidelity of the Largest RNA Viruses. *Annu Rev Virol,* 1**,** 111–32.

SMITH, N. A., BARESEL, P. C., JACKSON, C. L., OGOLLA, S., TOKO, E. N., HEIT, S., PIRIOU, E., SUMBA, O. P., MIDDELDORP, J. M., COLBORN, K. L. & ROCHFORD, R. 2019. Differences in the Epstein-Barr Virus gp350 IgA Antibody Response Are Associated With Increased Risk for Coinfection With a Second Strain of Epstein-Barr Virus. *J Infect Dis,* 219**,** 955–963.

SMITH, N. A., COLEMAN, C. B., GEWURZ, B. E. & ROCHFORD, R. 2020a. CD21 (Complement Receptor 2) Is the Receptor for Epstein-Barr Virus Entry into T Cells. *J Virol,* 94.

SMITH, N. L., NAHRENDORF, W., SUTHERLAND, C., MOONEY, J. P., THOMPSON, J., SPENCE, P. J. & COWAN, G. J. M. 2020b. A Conserved TCRβ Signature Dominates a Highly Polyclonal T-Cell Expansion During the Acute Phase of a Murine Malaria Infection. *Front Immunol,* 11**,** 587756.

SOERENS, A. G., KÜNZLI, M., QUARNSTROM, C. F., SCOTT, M. C., SWANSON, L., LOCQUIAO, J. J., GHONEIM, H. E., ZEHN, D., YOUNGBLOOD, B., VEZYS, V. & MASOPUST, D. 2023. Functional T cells are capable of supernumerary cell division and longevity. *Nature,* 614**,** 762–766.

SOLOMON, S. R., MIELKE, S., SAVANI, B. N., MONTERO, A., WISCH, L., CHILDS, R., HENSEL, N., SCHINDLER, J., GHETIE, V., LEITMAN, S. F., MAI, T., CARTER, C. S., KURLANDER, R., READ, E. J., VITETTA, E. S. & BARRETT, A. J. 2005. Selective depletion of alloreactive donor lymphocytes: a novel method to reduce the severity of graft-versus-host disease in older patients undergoing matched sibling donor stem cell transplantation. *Blood,* 106**,** 1123–9.

SOLOMON, S. R., TRAN, T., CARTER, C. S., DONNELLY, S., HENSEL, N., SCHINDLER, J., BAHCECI, E., GHETIE, V., MICHÁLEK, J., MAVROUDIS, D., READ, E. J., VITETTA, E. S. & BARRETT, A. J. 2002. Optimized clinical-scale culture conditions for ex vivo selective depletion of host-reactive donor lymphocytes: a strategy for GvHD prophylaxis in allogeneic PBSC transplantation. *Cytotherapy,* 4**,** 395–406.

SONG, K. A., YANG, S. D., HWANG, J., KIM, J. I. & KANG, M. S. 2015. The full-length DNA sequence of Epstein Barr virus from a human gastric carcinoma cell line, SNU-719. *Virus Genes,* 51**,** 329–37.

SONG, W., GUI, M., WANG, X. & XIANG, Y. 2018. Cryo-EM structure of the SARS coronavirus spike glycoprotein in complex with its host cell receptor ACE2. *PLoS Pathog,* 14**,** e1007236.

SPOERL, S., KREMER, A. N., AIGNER, M., EISENHAUER, N., KOCH, P., MERETUK, L., LÖFFLER, P., TENBUSCH, M., MAIER, C., ÜBERLA, K., HEINZERLING, L., FREY, B., LUTZNY-GEIER, G., WINKLER, T. H., KRÖNKE, G., VETTER, M., BRUNS, H., NEURATH, M. F., MACKENSEN, A., KREMER, A. E. & VÖLKL, S. 2021. Upregulation of CCR4 in activated CD8(+) T cells indicates enhanced lung homing in patients with severe acute SARS-CoV-2 infection. *Eur J Immunol,* 51**,** 1436–1448.

STANIETSKY, N., SIMIC, H., ARAPOVIC, J., TOPORIK, A., LEVY, O., NOVIK, A., LEVINE, Z., BEIMAN, M., DASSA, L., ACHDOUT, H., STERN-GINOSSAR, N., TSUKERMAN, P., JONJIC, S. & MANDELBOIM, O. 2009. The interaction of TIGIT with PVR and PVRL2 inhibits human NK cell cytotoxicity. *Proc Natl Acad Sci U S A,* 106**,** 17858–63.

STEFFIN, D., GHATWAI, N., MONTALBANO, A., RATHI, P., COURTNEY, A. N., ARNETT, A. B., FLEURENCE, J., SWEIDAN, R., WANG, T., ZHANG, H., MASAND, P., MARIS, J. M., MARTINEZ, D., POGORILER, J., VARADARAJAN, N., THAKKAR, S. G., LYON, D., LAPTEVA, N., ZHUYONG, M., PATEL, K., LOPEZ-TERRADA, D., RAMOS, C. A., LULLA, P., ARMAGHANY, T., GRILLEY, B. J., GOTTSCHALK, S., DOTTI, G., METELITSA, L. S., HESLOP, H. E., BRENNER, M. K., SUMAZIN, P. & HECZEY, A. 2025. Interleukin-15-armoured GPC3 CAR T cells for patients with solid cancers. *Nature,* 637**,** 940–946.

STENGER, D., STIEF, T. A., KAEUFERLE, T., WILLIER, S., RATAJ, F., SCHOBER, K., VICK, B., LOTFI, R., WAGNER, B., GRÜNEWALD, T. G. P., KOBOLD, S., BUSCH, D. H., JEREMIAS, I., BLAESCHKE, F. & FEUCHTINGER, T. 2020. Endogenous TCR promotes in vivo persistence of CD19-CAR-T cells compared to a CRISPR/Cas9-mediated TCR knockout CAR. *Blood,* 136**,** 1407–1418.

STEVEN, N. M., ANNELS, N. E., KUMAR, A., LEESE, A. M., KURILLA, M. G. & RICKINSON, A. B. 1997. Immediate early and early lytic cycle proteins are

frequent targets of the Epstein-Barr virus-induced cytotoxic T cell response. *J Exp Med,* 185**,** 1605–17.

STOJANOVIC, A., FIEGLER, N., BRUNNER-WEINZIERL, M. & CERWENKA, A. 2014. CTLA-4 is expressed by activated mouse NK cells and inhibits NK Cell IFN-γ production in response to mature dendritic cells. *J Immunol,* 192**,** 4184–91.

STRAUS, S. E., COHEN, J. I., TOSATO, G. & MEIER, J. 1993. NIH conference. Epstein-Barr virus infections: biology, pathogenesis, and management. *Ann Intern Med,* 118**,** 45–58.

STYCZYNSKI, J., GIL, L., TRIDELLO, G., LJUNGMAN, P., DONNELLY, J. P., VAN DER VELDEN, W., OMAR, H., MARTINO, R., HALKES, C., FARACI, M., THEUNISSEN, K., KALWAK, K., HUBACEK, P., SICA, S., NOZZOLI, C., FAGIOLI, F., MATTHES, S., DIAZ, M. A., MIGLIAVACCA, M., BALDUZZI, A., TOMASZEWSKA, A., CAMARA RDE, L., VAN BIEZEN, A., HOEK, J., IACOBELLI, S., EINSELE, H. & CESARO, S. 2013. Response to rituximab-based therapy and risk factor analysis in Epstein Barr Virus-related lymphoproliferative disorder after hematopoietic stem cell transplant in children and adults: a study from the Infectious Diseases Working Party of the European Group for Blood and Marrow Transplantation. *Clin Infect Dis,* 57**,** 794–802.

SUDARSANAM, H., BUHMANN, R. & HENSCHLER, R. 2022. Influence of Culture Conditions on Ex Vivo Expansion of T Lymphocytes and Their Function for Therapy: Current Insights and Open Questions. *Front Bioeng Biotechnol,* 10**,** 886637.

SUGIMOTO, A., KANDA, T., YAMASHITA, Y., MURATA, T., SAITO, S., KAWASHIMA, D., ISOMURA, H., NISHIYAMA, Y. & TSURUMI, T. 2011. Spatiotemporally different DNA repair systems participate in Epstein-Barr virus genome maturation. *J Virol,* 85**,** 6127–35.

SUN, J. C., BEILKE, J. N. & LANIER, L. L. 2009. Adaptive immune features of natural killer cells. *Nature,* 457**,** 557–61.

SUN, Q., BURTON, R., REDDY, V. & LUCAS, K. G. 2002a. Safety of allogeneic Epstein-Barr virus (EBV)-specific cytotoxic T lymphocytes for patients with refractory EBV-related lymphoma. *Br J Haematol,* 118**,** 799–808.

SUN, Q., BURTON, R. L. & LUCAS, K. G. 2002b. Cytokine production and cytolytic mechanism of CD4(+) cytotoxic T lymphocytes in ex vivo expanded therapeutic Epstein-Barr virus-specific T-cell cultures. *Blood,* 99**,** 3302–9.

TAI, X., VAN LAETHEM, F., POBEZINSKY, L., GUINTER, T., SHARROW, S. O., ADAMS, A., GRANGER, L., KRUHLAK, M., LINDSTEN, T., THOMPSON, C. B., FEIGENBAUM, L. & SINGER, A. 2012. Basis of CTLA-4 function in regulatory and conventional CD4(+) T cells. *Blood,* 119**,** 5155–63.

TAJIMA, T., MARTINEZ, O. M., BERNSTEIN, D., BOYD, S. D., GRATZINGER, D., LUM, G., SASAKI, K., TAN, B., TWIST, C. J., WEINBERG, K., ARMSTRONG, B., DESAI, D. M., MAZARIEGOS, G. V., CHIN, C., FISHBEIN, T. M., TEKIN, A., VENICK, R. S., KRAMS, S. M. & ESQUIVEL, C. O. 2024. Epstein-Barr virus-associated post-transplant lymphoproliferative disorders in pediatric transplantation: A prospective multicenter study in the United States. *Pediatr Transplant,* 28**,** e14763.

TAN, Q., KU, W., ZHANG, C., HEYILIMU, P., TIAN, Y., KE, Y. & LU, Z. 2018. Mutation analysis of the EBV-lymphoblastoid cell line cautions their use as antigen-presenting cells. *Immunol Cell Biol,* 96**,** 204–211.

TANG, N., LI, D., WANG, X. & SUN, Z. 2020. Abnormal coagulation parameters are associated with poor prognosis in patients with novel coronavirus pneumonia. *J Thromb Haemost,* 18**,** 844–847.

TAUS, E., HOFMANN, C., IBARRONDO, F. J., HAUSNER, M. A., FULCHER, J. A., KROGSTAD, P., FERBAS, K. G., TOBIN, N. H., RIMOIN, A. W., ALDROVANDI, G. M. & YANG, O. O. 2022. Dominant CD8(+) T Cell Nucleocapsid Targeting in SARS-CoV-2 Infection and Broad Spike Targeting From Vaccination. *Front Immunol,* 13**,** 835830.

TAWBI, H. A., SCHADENDORF, D., LIPSON, E. J., ASCIERTO, P. A., MATAMALA, L., CASTILLO GUTIÉRREZ, E., RUTKOWSKI, P., GOGAS, H. J., LAO, C. D., DE MENEZES, J. J., DALLE, S., ARANCE, A., GROB, J. J., SRIVASTAVA, S., ABASKHAROUN, M., HAMILTON, M., KEIDEL, S., SIMONSEN, K. L., SOBIESK, A. M., LI, B., HODI, F. S. & LONG, G. V. 2022. Relatlimab and Nivolumab versus Nivolumab in Untreated Advanced Melanoma. *N Engl J Med,* 386**,** 24–34.

TAY, M. Z., POH, C. M., RÉNIA, L., MACARY, P. A. & NG, L. F. P. 2020. The trinity of COVID-19: immunity, inflammation and intervention. *Nat Rev Immunol,* 20**,** 363–374.

TAYLOR, G. S., LONG, H. M., BROOKS, J. M., RICKINSON, A. B. & HISLOP, A. D. 2015. The immunology of Epstein-Barr virus-induced disease. *Annu Rev Immunol,* 33**,** 787–821.

TEN BRINKE, A., MAREK-TRZONKOWSKA, N., MANSILLA, M. J., TURKSMA, A. W., PIEKARSKA, K., IWASZKIEWICZ-GRZEŚ, D., PASSERINI, L., LOCAFARO, G., PUÑET-ORTIZ, J., VAN HAM, S. M., HERNANDEZ-FUENTES, M. P., MARTÍNEZ-CÁCERES, E. M. & GREGORI, S. 2017. Monitoring T-Cell Responses in Translational Studies: Optimization of Dye-Based Proliferation Assay for Evaluation of Antigen-Specific Responses. *Front Immunol,* 8**,** 1870.

TEN HAM, R. M. T., HÖVELS, A. M., HOEKMAN, J., FREDERIX, G. W. J., LEUFKENS, H. G. M., KLUNGEL, O. H., JEDEMA, I., VELD, S. A. J., NIKOLIC, T., VAN PEL, M., ZWAGINGA, J. J., LIN, F., DE GOEDE, A. L., SCHREIBELT, G., BUDDE, S., DE VRIES, I. J. M., WILKIE, G. M., DOLSTRA, H., OVELGÖNNE, H., MEIJ, P., MOUNTFORD, J. C., TURNER, M. L. & HOEFNAGEL, M. H. N. 2020. What does cell therapy manufacturing cost? A framework and methodology to facilitate academic and other small-scale cell therapy manufacturing costings. *Cytotherapy,* 22**,** 388–397.

TEN HAM, R. M. T., NIEVAART, J. C., HOEKMAN, J., COOPER, R. S., FREDERIX, G. W. J., LEUFKENS, H. G. M., KLUNGEL, O. H., OVELGÖNNE, H., HOEFNAGEL, M. H. N., TURNER, M. L. & MOUNTFORD, J. C. 2021. Estimation of manufacturing development costs of cell-based therapies: a feasibility study. *Cytotherapy,* 23**,** 730–739.

THE LANCET, M. 2023. Searching for SARS-CoV-2 origins: confidence versus evidence. *Lancet Microbe,* 4**,** e200.

THIEME, C. J., ANFT, M., PANISKAKI, K., BLAZQUEZ-NAVARRO, A., DOEVELAAR, A., SEIBERT, F. S., HOELZER, B., KONIK, M. J., BERGER, M. M., BRENNER, T., TEMPFER, C., WATZL, C., MEISTER, T. L., PFAENDER, S., STEINMANN, E., DOLFF, S., DITTMER, U., WESTHOFF, T. H., WITZKE, O., STERVBO, U., ROCH, T. & BABEL, N. 2020. Robust T Cell Response Toward Spike, Membrane, and Nucleocapsid SARS-CoV-2 Proteins Is Not Associated with Recovery in Critical COVID-19 Patients. *Cell Rep Med,* 1**,** 100092.

THOMPSON, J., VERMA, D., LI, D., MOSBRUGER, T. & SWAMINATHAN, S. 2016. Identification and Characterization of the Physiological Gene Targets of the Essential Lytic Replicative Epstein-Barr Virus SM Protein. *J Virol,* 90**,** 1206–21.

THOMS, M., BUSCHAUER, R., AMEISMEIER, M., KOEPKE, L., DENK, T., HIRSCHENBERGER, M., KRATZAT, H., HAYN, M., MACKENS-KIANI, T.,

CHENG, J., STRAUB, J. H., STÜRZEL, C. M., FRÖHLICH, T., BERNINGHAUSEN, O., BECKER, T., KIRCHHOFF, F., SPARRER, K. M. J. & BECKMANN, R. 2020. Structural basis for translational shutdown and immune evasion by the Nsp1 protein of SARS-CoV-2. *Science,* 369**,** 1249–1255.

THORLEY-LAWSON, D. A. & GROSS, A. 2004. Persistence of the Epstein-Barr virus and the origins of associated lymphomas. *N Engl J Med,* 350**,** 1328–37.

TIERNEY, R. J., EDWARDS, R. H., SITKI-GREEN, D., CROOM-CARTER, D., ROY, S., YAO, Q. Y., RAAB-TRAUB, N. & RICKINSON, A. B. 2006. Multiple Epstein-Barr virus strains in patients with infectious mononucleosis: comparison of ex vivo samples with in vitro isolates by use of heteroduplex tracking assays. *J Infect Dis,* 193**,** 287–97.

TIKHMYANOVA, N., PAPAROIDAMIS, N., ROMERO-MASTERS, J., FENG, X., MOHAMMED, F. S., REDDY, P. A. N., KENNEY, S. C., LIEBERMAN, P. M. & SALVINO, J. M. 2019. Development of a novel inducer for EBV lytic therapy. *Bioorg Med Chem Lett,* 29**,** 2259–2264.

TITOV, A., SHAYKHUTDINOVA, R., SHCHERBAKOVA, O. V., SERDYUK, Y. V., SHEETIKOV, S. A., ZORNIKOVA, K. V., MALEEVA, A. V., KHMELEVSKAYA, A., DIANOV, D. V., SHAKIROVA, N. T., MALKO, D. B., SHKURNIKOV, M., NERSISYAN, S., TONEVITSKY, A., KHAMAGANOVA, E., ERSHOV, A. V., OSIPOVA, E. Y., NIKOLAEV, R. V., PERSHIN, D. E., VEDMEDSKIA, V. A., MASCHAN, M., GINANOVA, V. R. & EFIMOV, G. A. 2022. Immunogenic epitope panel for accurate detection of non-cross-reactive T cell response to SARS-CoV-2. *JCI Insight,* 7.

TO, K. K., TSANG, O. T., LEUNG, W. S., TAM, A. R., WU, T. C., LUNG, D. C., YIP, C. C., CAI, J. P., CHAN, J. M., CHIK, T. S., LAU, D. P., CHOI, C. Y., CHEN, L. L., CHAN, W. M., CHAN, K. H., IP, J. D., NG, A. C., POON, R. W., LUO, C. T., CHENG, V. C., CHAN, J. F., HUNG, I. F., CHEN, Z., CHEN, H. & YUEN, K. Y. 2020. Temporal profiles of viral load in posterior oropharyngeal saliva samples and serum antibody responses during infection by SARS-CoV-2: an observational cohort study. *Lancet Infect Dis,* 20**,** 565–574.

TOMBLYN, M., CHILLER, T., EINSELE, H., GRESS, R., SEPKOWITZ, K., STOREK, J., WINGARD, J. R., YOUNG, J. A. & BOECKH, M. J. 2009. Guidelines for preventing infectious complications among hematopoietic cell transplantation recipients: a global perspective. *Biol Blood Marrow Transplant,* 15**,** 1143–238.

TOMKINSON, B. & KIEFF, E. 1992. Use of second-site homologous recombination to demonstrate that Epstein-Barr virus nuclear protein 3B is not important for lymphocyte infection or growth transformation in vitro. *J Virol,* 66**,** 2893–903.

TOMKINSON, B., ROBERTSON, E. & KIEFF, E. 1993. Epstein-Barr virus nuclear proteins EBNA-3A and EBNA-3C are essential for B-lymphocyte growth transformation. *J Virol,* 67**,** 2014–25.

TOOMER, K. H., GERBER, G. F., ZHANG, Y., DAOU, L., TUSHEK, M., HOOPER, J. E. & FRANCISCHETTI, I. M. B. 2023. SARS-CoV-2 infection results in upregulation of Plasminogen Activator Inhibitor-1 and Neuroserpin in the lungs, and an increase in fibrinolysis inhibitors associated with disease severity. *EJHaem,* 4**,** 324–338.

TOUSSI, S. S., HAMMOND, J. L., GERSTENBERGER, B. S. & ANDERSON, A. S. 2023. Therapeutics for COVID-19. *Nat Microbiol,* 8**,** 771–786.

TRAPPE, R. U., DIERICKX, D., ZIMMERMANN, H., MORSCHHAUSER, F., MOLLEE, P., ZAUCHA, J. M., DREYLING, M. H., DÜHRSEN, U., REINKE, P., VERHOEF, G.,

SUBKLEWE, M., HÜTTMANN, A., TOUSSEYN, T., SALLES, G., KLIEM, V., HAUSER, I. A., TARELLA, C., VAN DEN NESTE, E., GHEYSENS, O., ANAGNOSTOPOULOS, I., LEBLOND, V., RIESS, H. & CHOQUET, S. 2017. Response to Rituximab Induction Is a Predictive Marker in B-Cell Post-Transplant Lymphoproliferative Disorder and Allows Successful Stratification Into Rituximab or R-CHOP Consolidation in an International, Prospective, Multicenter Phase II Trial. *J Clin Oncol,* 35**,** 536–543.

TRIANA, S., METZ-ZUMARAN, C., RAMIREZ, C., KEE, C., DOLDAN, P., SHAHRAZ, M., SCHRAIVOGEL, D., GSCHWIND, A. R., SHARMA, A. K., STEINMETZ, L. M., HERRMANN, C., ALEXANDROV, T., BOULANT, S. & STANIFER, M. L. 2021. Single-cell analyses reveal SARS-CoV-2 interference with intrinsic immune response in the human gut. *Mol Syst Biol,* 17**,** e10232.

TRIPLETT, B. M., MULLER, B., KANG, G., LI, Y., CROSS, S. J., MOEN, J., CUNNINGHAM, L., JANSSEN, W., MAMCARZ, E., SHOOK, D. R., SRINIVASAN, A., CHOI, J., HAYDEN, R. T. & LEUNG, W. 2018. Selective T-cell depletion targeting CD45RA reduces viremia and enhances early T-cell recovery compared with CD3-targeted T-cell depletion. *Transpl Infect Dis,* 20.

TSAI, D. E., HARDY, C. L., TOMASZEWSKI, J. E., KOTLOFF, R. M., OLTOFF, K. M., SOMER, B. G., SCHUSTER, S. J., PORTER, D. L., MONTONE, K. T. & STADTMAUER, E. A. 2001. Reduction in immunosuppression as initial therapy for posttransplant lymphoproliferative disorder: analysis of prognostic variables and long-term follow-up of 42 adult patients. *Transplantation,* 71**,** 1076–88.

TSAI, M. H., LIN, X., SHUMILOV, A., BERNHARDT, K., FEEDERLE, R., POIREY, R., KOPP-SCHNEIDER, A., PEREIRA, B., ALMEIDA, R. & DELECLUSE, H. J. 2017. The biological properties of different Epstein-Barr virus strains explain their association with various types of cancers. *Oncotarget,* 8**,** 10238–10254.

TSAI, M. H., RAYKOVA, A., KLINKE, O., BERNHARDT, K., GÄRTNER, K., LEUNG, C. S., GELETNEKY, K., SERTEL, S., MÜNZ, C., FEEDERLE, R. & DELECLUSE, H. J. 2013a. Spontaneous lytic replication and epitheliotropism define an Epstein-Barr virus strain found in carcinomas. *Cell Rep,* 5**,** 458–70.

TSAI, S. C., LIN, S. J., LIN, C. J., CHOU, Y. C., LIN, J. H., YEH, T. H., CHEN, M. R., HUANG, L. M., LU, M. Y., HUANG, Y. C., CHEN, H. Y. & TSAI, C. H. 2013b. Autocrine CCL3 and CCL4 induced by the oncoprotein LMP1 promote Epstein-Barr virus-triggered B cell proliferation. *J Virol,* 87**,** 9041–52.

TSUDA, K., YAMANAKA, K., KITAGAWA, H., AKEDA, T., NAKA, M., NIWA, K., NAKANISHI, T., KAKEDA, M., GABAZZA, E. C. & MIZUTANI, H. 2012. Calcineurin inhibitors suppress cytokine production from memory T cells and differentiation of naïve T cells into cytokine-producing mature T cells. *PLoS One,* 7**,** e31465.

UEDA, K., UEMURA, K., ITO, N., SAKAI, Y., OHNISHI, S., SUEKANE, H., KUROSE, H., HIROSHIGE, T., CHIKUI, K., NISHIHARA, K., NAKIRI, M., SUEKANE, S., OGASAWARA, S., YANO, H. & IGAWA, T. 2024. Soluble Immune Checkpoint Molecules as Predictors of Efficacy in Immuno-Oncology Combination Therapy in Advanced Renal Cell Carcinoma. *Curr Oncol,* 31**,** 1701–1712.

UGOLINI, A. & NUTI, M. 2021. CD137(+) T-Cells: Protagonists of the Immunotherapy Revolution. *Cancers (Basel),* 13.

UHLIN, M., GERTOW, J., UZUNEL, M., OKAS, M., BERGLUND, S., WATZ, E., BRUNE, M., LJUNGMAN, P., MAEURER, M. & MATTSSON, J. 2012. Rapid salvage treatment with virus-specific T cells for therapy-resistant disease. *Clin Infect Dis,* 55**,** 1064–73.

V'KOVSKI, P., KRATZEL, A., STEINER, S., STALDER, H. & THIEL, V. 2021. Coronavirus biology and replication: implications for SARS-CoV-2. *Nat Rev Microbiol,* 19**,** 155–170.

VAN DEN BERG, A., VISSER, L. & POPPEMA, S. 1999. High expression of the CC chemokine TARC in Reed-Sternberg cells. A possible explanation for the characteristic T-cell infiltratein Hodgkin's lymphoma. *Am J Pathol,* 154**,** 1685–91.

VAN DIJK, A. M., KESSLER, F. L., STADHOUDERS-KEET, S. A., VERDONCK, L. F., DE GAST, G. C. & OTTEN, H. G. 1999. Selective depletion of major and minor histocompatibility antigen reactive T cells: towards prevention of acute graft-versus-host disease. *Br J Haematol,* 107**,** 169–75.

VAN GENT, M., BRAEM, S. G., DE JONG, A., DELAGIC, N., PEETERS, J. G., BOER, I. G., MOYNAGH, P. N., KREMMER, E., WIERTZ, E. J., OVAA, H., GRIFFIN, B. D. & RESSING, M. E. 2014. Epstein-Barr virus large tegument protein BPLF1 contributes to innate immune evasion through interference with toll-like receptor signaling. *PLoS Pathog,* 10**,** e1003960.

VAN MONTFRANS, J. M., HOEPELMAN, A. I., OTTO, S., VAN GIJN, M., VAN DE CORPUT, L., DE WEGER, R. A., MONACO-SHAWVER, L., BANERJEE, P. P., SANDERS, E. A., JOL-VAN DER ZIJDE, C. M., BETTS, M. R., ORANGE, J. S., BLOEM, A. C. & TESSELAAR, K. 2012. CD27 deficiency is associated with combined immunodeficiency and persistent symptomatic EBV viremia. *J Allergy Clin Immunol,* 129**,** 787–793.e6.

VANKADARI, N. 2020. Structure of Furin Protease Binding to SARS-CoV-2 Spike Glycoprotein and Implications for Potential Targets and Virulence. *J Phys Chem Lett,* 11**,** 6655–6663.

VASE, M., MAKSTEN, E. F., BENDIX, K., HAMILTON-DUTOIT, S., ANDERSEN, C., MØLLER, M. B., SØRENSEN, S. S., JESPERSEN, B., KAMPMANN, J., SØNDERGÅRD, E., NIELSEN, P. S. & D'AMORE, F. 2015. Occurrence and prognostic relevance of CD30 expression in post-transplant lymphoproliferative disorders. *Leuk Lymphoma,* 56**,** 1677–85.

VASILEIOU, S., HILL, L., KUVALEKAR, M., WORKINEH, A. G., WATANABE, A., VELAZQUEZ, Y., LULLA, S., MOONEY, K., LAPTEVA, N., GRILLEY, B. J., HESLOP, H. E., ROONEY, C. M., BRENNER, M. K., EAGAR, T. N., CARRUM, G., GRIMES, K. A., LEEN, A. M. & LULLA, P. 2023. Allogeneic, off-the-shelf, SARS-CoV-2-specific T cells (ALVR109) for the treatment of COVID-19 in high-risk patients. *Haematologica,* 108**,** 1840–1850.

VASILEIOU, S., TURNEY, A. M., KUVALEKAR, M., MUKHI, S. S., WATANABE, A., LULLA, P., RAMOS, C. A., NAIK, S., VERA, J. F., TZANNOU, I. & LEEN, A. M. 2020. Rapid generation of multivirus-specific T lymphocytes for the prevention and treatment of respiratory viral infections. *Haematologica,* 105**,** 235–243.

VEREIDE, D. T., SETO, E., CHIU, Y. F., HAYES, M., TAGAWA, T., GRUNDHOFF, A., HAMMERSCHMIDT, W. & SUGDEN, B. 2014. Epstein-Barr virus maintains lymphomas via its miRNAs. *Oncogene,* 33**,** 1258–64.

VERMA, D., THOMPSON, J. & SWAMINATHAN, S. 2016. Spironolactone blocks Epstein-Barr virus production by inhibiting EBV SM protein function. *Proc Natl Acad Sci U S A,* 113**,** 3609–14.

VICKERS, M. A., WILKIE, G. M., ROBINSON, N., RIVERA, N., HAQUE, T., CRAWFORD, D. H., BARRY, J., FRASER, N., TURNER, D. M., ROBERTSON, V., DYER, P., FLANAGAN, P., NEWLANDS, H. R., CAMPBELL, J. & TURNER, M. L. 2014. Establishment and operation of a Good Manufacturing Practice-compliant allogeneic Epstein-Barr virus (EBV)-specific cytotoxic

cell bank for the treatment of EBV-associated lymphoproliferative disease. *Br J Haematol,* 167**,** 402–10.
VIOLA, A., SARUKHAN, A., BRONTE, V. & MOLON, B. 2012. The pros and cons of chemokines in tumor immunology. *Trends Immunol,* 33**,** 496–504.
VIRTANEN, P., GOMMERS, R., OLIPHANT, T. E., HABERLAND, M., REDDY, T., COURNAPEAU, D., BUROVSKI, E., PETERSON, P., WECKESSER, W., BRIGHT, J., VAN DER WALT, S. J., BRETT, M., WILSON, J., MILLMAN, K. J., MAYOROV, N., NELSON, A. R. J., JONES, E., KERN, R., LARSON, E., CAREY, C. J., POLAT, İ., FENG, Y., MOORE, E. W., VANDERPLAS, J., LAXALDE, D., PERKTOLD, J., CIMRMAN, R., HENRIKSEN, I., QUINTERO, E. A., HARRIS, C. R., ARCHIBALD, A. M., RIBEIRO, A. H., PEDREGOSA, F. & VAN MULBREGT, P. 2020. Author Correction: SciPy 1.0: fundamental algorithms for scientific computing in Python. *Nat Methods,* 17**,** 352.
WAGNER, H. J., BOLLARD, C. M., VIGOUROUX, S., HULS, M. H., ANDERSON, R., PRENTICE, H. G., BRENNER, M. K., HESLOP, H. E. & ROONEY, C. M. 2004. A strategy for treatment of Epstein-Barr virus-positive Hodgkin's disease by targeting interleukin 12 to the tumor environment using tumor antigen-specific T cells. *Cancer Gene Ther,* 11**,** 81–91.
WALKER, L. S. K. 2017. EFIS Lecture: Understanding the CTLA-4 checkpoint in the maintenance of immune homeostasis. *Immunol Lett,* 184**,** 43–50.
WALLS, A. C., PARK, Y. J., TORTORICI, M. A., WALL, A., MCGUIRE, A. T. & VEESLER, D. 2020. Structure, Function, and Antigenicity of the SARS-CoV-2 Spike Glycoprotein. *Cell,* 181**,** 281–292.e6.
WALTER, E. A., GREENBERG, P. D., GILBERT, M. J., FINCH, R. J., WATANABE, K. S., THOMAS, E. D. & RIDDELL, S. R. 1995. Reconstitution of cellular immunity against cytomegalovirus in recipients of allogeneic bone marrow by transfer of T-cell clones from the donor. *N Engl J Med,* 333**,** 1038–44.
WALTI, C. S., KHANNA, N., AVERY, R. K. & HELANTERÄ, I. 2023. New Treatment Options for Refractory/Resistant CMV Infection. *Transpl Int,* 36**,** 11785.
WAN, S., YI, Q., FAN, S., LV, J., ZHANG, X., GUO, L., LANG, C., XIAO, Q., XIAO, K., YI, Z., QIANG, M., XIANG, J., ZHANG, B., CHEN, Y. & GAO, C. 2020a. Relationships among lymphocyte subsets, cytokines, and the pulmonary inflammation index in coronavirus (COVID-19) infected patients. *Br J Haematol,* 189**,** 428–437.
WAN, Y., SHANG, J., GRAHAM, R., BARIC, R. S. & LI, F. 2020b. Receptor Recognition by the Novel Coronavirus from Wuhan: an Analysis Based on Decade-Long Structural Studies of SARS Coronavirus. *J Virol,* 94.
WANG, D., HU, B., HU, C., ZHU, F., LIU, X., ZHANG, J., WANG, B., XIANG, H., CHENG, Z., XIONG, Y., ZHAO, Y., LI, Y., WANG, X. & PENG, Z. 2020a. Clinical Characteristics of 138 Hospitalized Patients With 2019 Novel Coronavirus-Infected Pneumonia in Wuhan, China. *Jama,* 323**,** 1061–1069.
WANG, F., HOU, H., YAO, Y., WU, S., HUANG, M., RAN, X., ZHOU, H., LIU, Z. & SUN, Z. 2020b. Systemically comparing host immunity between survived and deceased COVID-19 patients. *Cell Mol Immunol,* 17**,** 875–877.
WANG, F., NIE, J., WANG, H., ZHAO, Q., XIONG, Y., DENG, L., SONG, S., MA, Z., MO, P. & ZHANG, Y. 2020c. Characteristics of Peripheral Lymphocyte Subset Alteration in COVID-19 Pneumonia. *J Infect Dis,* 221**,** 1762–1769.
WANG, G., MUDGAL, P., WANG, L., SHUEN, T. W. H., WU, H., ALEXANDER, P. B., WANG, W. W., WAN, Y., TOH, H. C., WANG, X. F. & LI, Q. J. 2021. TCR repertoire characteristics predict clinical response to adoptive CTL therapy against nasopharyngeal carcinoma. *Oncoimmunology,* 10**,** 1955545.

WANG, H. B., ZHANG, H., ZHANG, J. P., LI, Y., ZHAO, B., FENG, G. K., DU, Y., XIONG, D., ZHONG, Q., LIU, W. L., DU, H., LI, M. Z., HUANG, W. L., TSAO, S. W., HUTT-FLETCHER, L., ZENG, Y. X., KIEFF, E. & ZENG, M. S. 2015. Neuropilin 1 is an entry factor that promotes EBV infection of nasopharyngeal epithelial cells. *Nat Commun,* 6**,** 6240.

WANG, J., SANMAMED, M. F., DATAR, I., SU, T. T., JI, L., SUN, J., CHEN, L., CHEN, Y., ZHU, G., YIN, W., ZHENG, L., ZHOU, T., BADRI, T., YAO, S., ZHU, S., BOTO, A., SZNOL, M., MELERO, I., VIGNALI, D. A. A., SCHALPER, K. & CHEN, L. 2019. Fibrinogen-like Protein 1 Is a Major Immune Inhibitory Ligand of LAG-3. *Cell,* 176**,** 334–347.e12.

WANG, S., WANG, J., YU, X., JIANG, W., CHEN, S., WANG, R., WANG, M., JIAO, S., YANG, Y., WANG, W., CHEN, H., CHEN, B., GU, C., LIU, C., WANG, A., WANG, M., LI, G., GUO, C., LIU, D., ZHANG, J., ZHANG, M., WANG, L. & GUI, X. 2022. Antibody-dependent enhancement (ADE) of SARS-CoV-2 pseudoviral infection requires FcγRIIB and virus-antibody complex with bivalent interaction. *Commun Biol,* 5**,** 262.

WANG, X., BERGER, C., WONG, C. W., FORMAN, S. J., RIDDELL, S. R. & JENSEN, M. C. 2011. Engraftment of human central memory-derived effector CD8+ T cells in immunodeficient mice. *Blood,* 117**,** 1888–98.

WATANABE, K., SUZUKI, S., KAMEI, M., TOJI, S., KAWASE, T., TAKAHASHI, T., KUZUSHIMA, K. & AKATSUKA, Y. 2008. CD137-guided isolation and expansion of antigen-specific CD8 cells for potential use in adoptive immunotherapy. *Int J Hematol,* 88**,** 311–320.

WATANABE, Y., ALLEN, J. D., WRAPP, D., MCLELLAN, J. S. & CRISPIN, M. 2020. Site-specific glycan analysis of the SARS-CoV-2 spike. *Science,* 369**,** 330–333.

WATTS, T. H. 2005. TNF/TNFR family members in costimulation of T cell responses. *Annu Rev Immunol,* 23**,** 23–68.

WEBER, E. W., MAUS, M. V. & MACKALL, C. L. 2020. The Emerging Landscape of Immune Cell Therapies. *Cell,* 181**,** 46–62.

WEHLER, T. C., KARG, M., DISTLER, E., KONUR, A., NONN, M., MEYER, R. G., HUBER, C., HARTWIG, U. F. & HERR, W. 2008. Rapid identification and sorting of viable virus-reactive CD4(+) and CD8(+) T cells based on antigen-triggered CD137 expression. *J Immunol Methods,* 339**,** 23–37.

WEHLER, T. C., NONN, M., BRANDT, B., BRITTEN, C. M., GRÖNE, M., TODOROVA, M., LINK, I., KHAN, S. A., MEYER, R. G., HUBER, C., HARTWIG, U. F. & HERR, W. 2007. Targeting the activation-induced antigen CD137 can selectively deplete alloreactive T cells from antileukemic and antitumor donor T-cell lines. *Blood,* 109**,** 365–73.

WHERRY, E. J. & AHMED, R. 2004. Memory CD8 T-cell differentiation during viral infection. *J Virol,* 78**,** 5535–45.

WHITE, R. E., GROVES, I. J., TURRO, E., YEE, J., KREMMER, E. & ALLDAY, M. J. 2010. Extensive co-operation between the Epstein-Barr virus EBNA3 proteins in the manipulation of host gene expression and epigenetic chromatin modification. *PLoS One,* 5**,** e13979.

WHITE, R. E., RÄMER, P. C., NARESH, K. N., MEIXLSPERGER, S., PINAUD, L., ROONEY, C., SAVOLDO, B., COUTINHO, R., BÖDÖR, C., GRIBBEN, J., IBRAHIM, H. A., BOWER, M., NOURSE, J. P., GANDHI, M. K., MIDDELDORP, J., CADER, F. Z., MURRAY, P., MÜNZ, C. & ALLDAY, M. J. 2012. EBNA3B-deficient EBV promotes B cell lymphomagenesis in humanized mice and is found in human tumors. *J Clin Invest,* 122**,** 1487–502.

WICHMANN, D., SPERHAKE, J. P., LÜTGEHETMANN, M., STEURER, S., EDLER, C., HEINEMANN, A., HEINRICH, F., MUSHUMBA, H., KNIEP, I., SCHRÖDER, A.

S., BURDELSKI, C., DE HEER, G., NIERHAUS, A., FRINGS, D., PFEFFERLE, S., BECKER, H., BREDEREKE-WIEDLING, H., DE WEERTH, A., PASCHEN, H. R., SHEIKHZADEH-EGGERS, S., STANG, A., SCHMIEDEL, S., BOKEMEYER, C., ADDO, M. M., AEPFELBACHER, M., PÜSCHEL, K. & KLUGE, S. 2020. Autopsy Findings and Venous Thromboembolism in Patients With COVID-19: A Prospective Cohort Study. *Ann Intern Med,* 173**,** 268–277.

WIECZOREK, M., ABUALROUS, E. T., STICHT, J., ÁLVARO-BENITO, M., STOLZENBERG, S., NOÉ, F. & FREUND, C. 2017. Major Histocompatibility Complex (MHC) Class I and MHC Class II Proteins: Conformational Plasticity in Antigen Presentation. *Front Immunol,* 8**,** 292.

WILK, A. J., RUSTAGI, A., ZHAO, N. Q., ROQUE, J., MARTÍNEZ-COLÓN, G. J., MCKECHNIE, J. L., IVISON, G. T., RANGANATH, T., VERGARA, R., HOLLIS, T., SIMPSON, L. J., GRANT, P., SUBRAMANIAN, A., ROGERS, A. J. & BLISH, C. A. 2020. A single-cell atlas of the peripheral immune response in patients with severe COVID-19. *Nat Med,* 26**,** 1070–1076.

WILKIE, G. M., TAYLOR, C., JONES, M. M., BURNS, D. M., TURNER, M., KILPATRICK, D., AMLOT, P. L., CRAWFORD, D. H. & HAQUE, T. 2004. Establishment and characterization of a bank of cytotoxic T lymphocytes for immunotherapy of epstein-barr virus-associated diseases. *J Immunother,* 27**,** 309–16.

WILLIAMS, H., MCAULAY, K., MACSWEEN, K. F., GALLACHER, N. J., HIGGINS, C. D., HARRISON, N., SWERDLOW, A. J. & CRAWFORD, D. H. 2005. The immune response to primary EBV infection: a role for natural killer cells. *Br J Haematol,* 129**,** 266–74.

WISTINGHAUSEN, B., TONER, K., BARKAUSKAS, D. A., JERKINS, L. P., KINOSHITA, H., CHANSKY, P., PEZZELLA, G., SAGUILIG, L., HAYASHI, R. J., ABHYANKAR, H., SCULL, B., KARRI, V., TANNA, J., HANLEY, P., HERMISTON, M. L., ALLEN, C. E. & BOLLARD, C. M. 2024. Durable immunity to EBV after rituximab and third-party LMP-specific T cells: a Children's Oncology Group study. *Blood Adv,* 8**,** 1116–1127.

WITHERS, B., BLYTH, E., CLANCY, L. E., YONG, A., FRASER, C., BURGESS, J., SIMMS, R., BROWN, R., KLIMAN, D., DUBOSQ, M. C., BISHOP, D., SUTRAVE, G., MA, C. K. K., SHAW, P. J., MICKLETHWAITE, K. P. & GOTTLIEB, D. J. 2017. Long-term control of recurrent or refractory viral infections after allogeneic HSCT with third-party virus-specific T cells. *Blood Adv,* 1**,** 2193–2205.

WITKOWSKI, M., TIZIAN, C., FERREIRA-GOMES, M., NIEMEYER, D., JONES, T. C., HEINRICH, F., FRISCHBUTTER, S., ANGERMAIR, S., HOHNSTEIN, T., MATTIOLA, I., NAWRATH, P., MCEWEN, S., ZOCCHE, S., VIVIANO, E., HEINZ, G. A., MAURER, M., KÖLSCH, U., CHUA, R. L., ASCHMAN, T., MEISEL, C., RADKE, J., SAWITZKI, B., ROEHMEL, J., ALLERS, K., MOOS, V., SCHNEIDER, T., HANITSCH, L., MALL, M. A., CONRAD, C., RADBRUCH, H., DUERR, C. U., TRAPANI, J. A., MARCENARO, E., KALLINICH, T., CORMAN, V. M., KURTH, F., SANDER, L. E., DROSTEN, C., TRESKATSCH, S., DUREK, P., KRUGLOV, A., RADBRUCH, A., MASHREGHI, M. F. & DIEFENBACH, A. 2021. Untimely TGFß responses in COVID-19 limit antiviral functions of NK cells. *Nature,* 600**,** 295–301.

WOLF, Y., ANDERSON, A. C. & KUCHROO, V. K. 2020. TIM3 comes of age as an inhibitory receptor. *Nat Rev Immunol,* 20**,** 173–185.

WOLFF, G., LIMPENS, R., ZEVENHOVEN-DOBBE, J. C., LAUGKS, U., ZHENG, S., DE JONG, A. W. M., KONING, R. I., AGARD, D. A., GRÜNEWALD, K., KOSTER, A. J., SNIJDER, E. J. & BÁRCENA, M. 2020. A molecular pore spans the

double membrane of the coronavirus replication organelle. *Science,* 369**,** 1395–1398.

WOLFL, M., KUBALL, J., HO, W. Y., NGUYEN, H., MANLEY, T. J., BLEAKLEY, M. & GREENBERG, P. D. 2007. Activation-induced expression of CD137 permits detection, isolation, and expansion of the full repertoire of CD8+ T cells responding to antigen without requiring knowledge of epitope specificities. *Blood,* 110**,** 201–10.

WOODBERRY, T., SUSCOVICH, T. J., HENRY, L. M., DAVIS, J. K., FRAHM, N., WALKER, B. D., SCADDEN, D. T., WANG, F. & BRANDER, C. 2005. Differential targeting and shifts in the immunodominance of Epstein-Barr virus--specific CD8 and CD4 T cell responses during acute and persistent infection. *J Infect Dis,* 192**,** 1513–24.

WOOLDRIDGE, L., LISSINA, A., COLE, D. K., VAN DEN BERG, H. A., PRICE, D. A. & SEWELL, A. K. 2009. Tricks with tetramers: how to get the most from multimeric peptide-MHC. *Immunology,* 126**,** 147–64.

WORKMAN, C. J., DUGGER, K. J. & VIGNALI, D. A. 2002. Cutting edge: molecular analysis of the negative regulatory function of lymphocyte activation gene-3. *J Immunol,* 169**,** 5392–5.

WU, F., ZHAO, S., YU, B., CHEN, Y. M., WANG, W., SONG, Z. G., HU, Y., TAO, Z. W., TIAN, J. H., PEI, Y. Y., YUAN, M. L., ZHANG, Y. L., DAI, F. H., LIU, Y., WANG, Q. M., ZHENG, J. J., XU, L., HOLMES, E. C. & ZHANG, Y. Z. 2020. A new coronavirus associated with human respiratory disease in China. *Nature,* 579**,** 265–269.

WU, H., WITZL, A. & UENO, H. 2019. Assessment of TCR signal strength of antigen-specific memory CD8(+) T cells in human blood. *Blood Adv,* 3**,** 2153–2163.

WU, Y., MARUO, S., YAJIMA, M., KANDA, T. & TAKADA, K. 2007. Epstein-Barr virus (EBV)-encoded RNA 2 (EBER2) but not EBER1 plays a critical role in EBV-induced B-cell growth transformation. *J Virol,* 81**,** 11236–45.

WYNN, R. F., ARKWRIGHT, P. D., HAQUE, T., GHARIB, M. I., WILKIE, G., MORTON-JONES, M. & CRAWFORD, D. H. 2005. Treatment of Epstein-Barr-virus-associated primary CNS B cell lymphoma with allogeneic T-cell immunotherapy and stem-cell transplantation. *Lancet Oncol,* 6**,** 344–6.

XIAO, J., PALEFSKY, J. M., HERRERA, R., BERLINE, J. & TUGIZOV, S. M. 2008. The Epstein-Barr virus BMRF-2 protein facilitates virus attachment to oral epithelial cells. *Virology,* 370**,** 430–42.

XIAO, K., ZHAI, J., FENG, Y., ZHOU, N., ZHANG, X., ZOU, J. J., LI, N., GUO, Y., LI, X., SHEN, X., ZHANG, Z., SHU, F., HUANG, W., LI, Y., ZHANG, Z., CHEN, R. A., WU, Y. J., PENG, S. M., HUANG, M., XIE, W. J., CAI, Q. H., HOU, F. H., CHEN, W., XIAO, L. & SHEN, Y. 2020a. Isolation of SARS-CoV-2-related coronavirus from Malayan pangolins. *Nature,* 583**,** 286–289.

XIAO, L., CHEN, C., LI, Z., ZHU, S., TAY, J. C., ZHANG, X., ZHA, S., ZENG, J., TAN, W. K., LIU, X., CHNG, W. J. & WANG, S. 2018. Large-scale expansion of Vγ9Vδ2 T cells with engineered K562 feeder cells in G-Rex vessels and their use as chimeric antigen receptor-modified effector cells. *Cytotherapy,* 20**,** 420–435.

XIAO, S., BOD, L., POCHET, N., KOTA, S. B., HU, D., MADI, A., KILPATRICK, J., SHI, J., HO, A., ZHANG, H., SOBEL, R., WEINER, H. L., STROM, T. B., QUINTANA, F. J., JOLLER, N. & KUCHROO, V. K. 2020b. Checkpoint Receptor TIGIT Expressed on Tim-1(+) B Cells Regulates Tissue Inflammation. *Cell Rep,* 32**,** 107892.

XIAO, Z., MESCHER, M. F. & JAMESON, S. C. 2007. Detuning CD8 T cells: down-regulation of CD8 expression, tetramer binding, and response during CTL activation. *J Exp Med,* 204**,** 2667–77.

XU, F., LIU, J., LIU, D., LIU, B., WANG, M., HU, Z., DU, X., TANG, L. & HE, F. 2014. LSECtin expressed on melanoma cells promotes tumor progression by inhibiting antitumor T-cell responses. *Cancer Res,* 74**,** 3418–28.

XUE, W. Q., WANG, T. M., HUANG, J. W., ZHANG, J. B., HE, Y. Q., WU, Z. Y., LIAO, Y., YUAN, L. L., MU, J. & JIA, W. H. 2021. A comprehensive analysis of genetic diversity of EBV reveals potential high-risk subtypes associated with nasopharyngeal carcinoma in China. *Virus Evol,* 7**,** veab010.

YAJIMA, M., KANDA, T. & TAKADA, K. 2005. Critical role of Epstein-Barr Virus (EBV)-encoded RNA in efficient EBV-induced B-lymphocyte growth transformation. *J Virol,* 79**,** 4298–307.

YAKOUB-AGHA, I., SAULE, P., DEPIL, S., MICOL, J. B., GRUTZMACHER, C., BOULANGER-VILLARD, F., BAUTERS, F., JOUET, J. P., DESSAINT, J. P. & LABALETTE, M. 2006. A high proportion of donor CD4+ T cells expressing the lymph node-homing chemokine receptor CCR7 increases incidence and severity of acute graft-versus-host disease in patients undergoing allogeneic stem cell transplantation for hematological malignancy. *Leukemia,* 20**,** 1557–65.

YAMADA, T., TATEMATSU, M., TAKASUGA, S., FUCHIMUKAI, A., YAMAGATA, K., SEKI, S., KUBA, K., YOSHIDA, H., TANIUCHI, I., BERNHARDT, G., SHIBUYA, K., SHIBUYA, A., YAMADA, T. & EBIHARA, T. 2023. TIGIT mediates activation-induced cell death of ILC2s during chronic airway allergy. *J Exp Med,* 220.

YAMAGUCHI, T., HOSHIZAKI, M., MINATO, T., NIRASAWA, S., ASAKA, M. N., NIIYAMA, M., IMAI, M., UDA, A., CHAN, J. F., TAKAHASHI, S., AN, J., SAKU, A., NUKIWA, R., UTSUMI, D., KISO, M., YASUHARA, A., POON, V. K., CHAN, C. C., FUJINO, Y., MOTOYAMA, S., NAGATA, S., PENNINGER, J. M., KAMADA, H., YUEN, K. Y., KAMITANI, W., MAEDA, K., KAWAOKA, Y., YASUTOMI, Y., IMAI, Y. & KUBA, K. 2021. ACE2-like carboxypeptidase B38-CAP protects from SARS-CoV-2-induced lung injury. *Nat Commun,* 12**,** 6791.

YANG, H. & RAO, Z. 2021. Structural biology of SARS-CoV-2 and implications for therapeutic development. *Nat Rev Microbiol,* 19**,** 685–700.

YANG, L., LIU, S., LIU, J., ZHANG, Z., WAN, X., HUANG, B., CHEN, Y. & ZHANG, Y. 2020. COVID-19: immunopathogenesis and Immunotherapeutics. *Signal Transduct Target Ther,* 5**,** 128.

YANG, Y., LI, X., MA, Z., WANG, C., YANG, Q., BYRNE-STEELE, M., HONG, R., MIN, Q., ZHOU, G., CHENG, Y., QIN, G., YOUNGYUNPIPATKUL, J. V., WING, J. B., SAKAGUCHI, S., TOONSTRA, C., WANG, L. X., VILCHES-MOURE, J. G., WANG, D., SNYDER, M. P., WANG, J. Y., HAN, J. & HERZENBERG, L. A. 2021. CTLA-4 expression by B-1a B cells is essential for immune tolerance. *Nat Commun,* 12**,** 525.

YANG, Y. & XU, F. 2022. Evolving understanding of antibody-dependent enhancement (ADE) of SARS-CoV-2. *Front Immunol,* 13**,** 1008285.

YAO, Q. Y., TIERNEY, R. J., CROOM-CARTER, D., COOPER, G. M., ELLIS, C. J., ROWE, M. & RICKINSON, A. B. 1996. Isolation of intertypic recombinants of Epstein-Barr virus from T-cell-immunocompromised individuals. *J Virol,* 70**,** 4895–903.

YE, J., GRADOVILLE, L. & MILLER, G. 2010. Cellular immediate-early gene expression occurs kinetically upstream of Epstein-Barr virus bzlf1 and

brlf1 following cross-linking of the B cell antigen receptor in the Akata Burkitt lymphoma cell line. *J Virol,* 84**,** 12405–18.

YELLIN, M. J., SIPPEL, K., INGHIRAMI, G., COVEY, L. R., LEE, J. J., SINNING, J., CLARK, E. A., CHESS, L. & LEDERMAN, S. 1994. CD40 molecules induce down-modulation and endocytosis of T cell surface T cell-B cell activating molecule/CD40-L. Potential role in regulating helper effector function. *J Immunol,* 152**,** 598–608.

YIN, X., RIVA, L., PU, Y., MARTIN-SANCHO, L., KANAMUNE, J., YAMAMOTO, Y., SAKAI, K., GOTOH, S., MIORIN, L., DE JESUS, P. D., YANG, C. C., HERBERT, K. M., YOH, S., HULTQUIST, J. F., GARCÍA-SASTRE, A. & CHANDA, S. K. 2021. MDA5 Governs the Innate Immune Response to SARS-CoV-2 in Lung Epithelial Cells. *Cell Rep,* 34**,** 108628.

YIN, Z., CHEN, J. L., LU, Y., WANG, B., GODFREY, L., MENTZER, A. J., YAO, X., LIU, G., WELLINGTON, D., ZHAO, Y., WING, P. A. C., DEJNIRATTISA, W., SUPASA, P., LIU, C., HUBLITZ, P., BEVERIDGE, R., WAUGH, C., CLARK, S. A., CLARK, K., SOPP, P., ROSTRON, T., MONGKOLSAPAYA, J., SCREATON, G. R., OGG, G., EWER, K., POLLARD, A. J., GILBERT, S., KNIGHT, J. C., LAMBE, T., SMITH, G. L., DONG, T. & PENG, Y. 2023. Evaluation of T cell responses to naturally processed variant SARS-CoV-2 spike antigens in individuals following infection or vaccination. *Cell Rep,* 42**,** 112470.

YOSHIDA, M., WORLOCK, K. B., HUANG, N., LINDEBOOM, R. G. H., BUTLER, C. R., KUMASAKA, N., DOMINGUEZ CONDE, C., MAMANOVA, L., BOLT, L., RICHARDSON, L., POLANSKI, K., MADISSOON, E., BARNES, J. L., ALLEN-HYTTINEN, J., KILICH, E., JONES, B. C., DE WILTON, A., WILBREY-CLARK, A., SUNGNAK, W., PETT, J. P., WELLER, J., PRIGMORE, E., YUNG, H., MEHTA, P., SALEH, A., SAIGAL, A., CHU, V., COHEN, J. M., CANE, C., IORDANIDOU, A., SHIBUYA, S., REUSCHL, A. K., HERCZEG, I. T., ARGENTO, A. C., WUNDERINK, R. G., SMITH, S. B., POOR, T. A., GAO, C. A., DEMATTE, J. E., REYNOLDS, G., HANIFFA, M., BOWYER, G. S., COATES, M., CLATWORTHY, M. R., CALERO-NIETO, F. J., GÖTTGENS, B., O'CALLAGHAN, C., SEBIRE, N. J., JOLLY, C., DE COPPI, P., SMITH, C. M., MISHARIN, A. V., JANES, S. M., TEICHMANN, S. A., NIKOLIĆ, M. Z. & MEYER, K. B. 2022. Local and systemic responses to SARS-CoV-2 infection in children and adults. *Nature,* 602**,** 321–327.

YOUK, J., KIM, T., EVANS, K. V., JEONG, Y. I., HUR, Y., HONG, S. P., KIM, J. H., YI, K., KIM, S. Y., NA, K. J., BLEAZARD, T., KIM, H. M., FELLOWS, M., MAHBUBANI, K. T., SAEB-PARSY, K., KIM, S. Y., KIM, Y. T., KOH, G. Y., CHOI, B. S., JU, Y. S. & LEE, J. H. 2020. Three-Dimensional Human Alveolar Stem Cell Culture Models Reveal Infection Response to SARS-CoV-2. *Cell Stem Cell,* 27**,** 905–919.e10.

YOUNES, A., SANTORO, A., SHIPP, M., ZINZANI, P. L., TIMMERMAN, J. M., ANSELL, S., ARMAND, P., FANALE, M., RATANATHARATHORN, V., KURUVILLA, J., COHEN, J. B., COLLINS, G., SAVAGE, K. J., TRNENY, M., KATO, K., FARSACI, B., PARKER, S. M., RODIG, S., ROEMER, M. G., LIGON, A. H. & ENGERT, A. 2016. Nivolumab for classical Hodgkin's lymphoma after failure of both autologous stem-cell transplantation and brentuximab vedotin: a multicentre, multicohort, single-arm phase 2 trial. *Lancet Oncol,* 17**,** 1283–94.

YOUNG, L. S., YAP, L. F. & MURRAY, P. G. 2016. Epstein-Barr virus: more than 50 years old and still providing surprises. *Nat Rev Cancer,* 16**,** 789–802.

YU, X., HARDEN, K., GONZALEZ, L. C., FRANCESCO, M., CHIANG, E., IRVING, B., TOM, I., IVELJA, S., REFINO, C. J., CLARK, H., EATON, D. & GROGAN, J. L. 2009. The surface protein TIGIT suppresses T cell activation by promoting

the generation of mature immunoregulatory dendritic cells. *Nat Immunol,* 10**,** 48–57.

YULING, H., RUIJING, X., LI, L., XIANG, J., RUI, Z., YUJUAN, W., LIJUN, Z., CHUNXIAN, D., XINTI, T., WEI, X., LANG, C., YANPING, J., TAO, X., MENGJUN, W., JIE, X., YOUXIN, J. & JINQUAN, T. 2009. EBV-induced human CD8+ NKT cells suppress tumorigenesis by EBV-associated malignancies. *Cancer Res,* 69**,** 7935–44.

ZAFFIRI, L., LONG, A., NEELY, M. L., CHERIKH, W. S., CHAMBERS, D. C. & SNYDER, L. D. 2020. Incidence and outcome of post-transplant lymphoproliferative disorders in lung transplant patients: Analysis of ISHLT Registry. *J Heart Lung Transplant,* 39**,** 1089–1099.

ZAJAC, A. J., BLATTMAN, J. N., MURALI-KRISHNA, K., SOURDIVE, D. J., SURESH, M., ALTMAN, J. D. & AHMED, R. 1998. Viral immune evasion due to persistence of activated T cells without effector function. *J Exp Med,* 188**,** 2205–13.

ZAJONC, D. M. 2020. Unconventional Peptide Presentation by Classical MHC Class I and Implications for T and NK Cell Activation. *Int J Mol Sci,* 21.

ZANDVLIET, M. L., VAN LIEMPT, E., JEDEMA, I., KRUITHOF, S., KESTER, M. G., GUCHELAAR, H. J., FALKENBURG, J. H. & MEIJ, P. 2011. Simultaneous isolation of CD8(+) and CD4(+) T cells specific for multiple viruses for broad antiviral immune reconstitution after allogeneic stem cell transplantation. *J Immunother,* 34**,** 307–19.

ZENG, M. S., LI, D. J., LIU, Q. L., SONG, L. B., LI, M. Z., ZHANG, R. H., YU, X. J., WANG, H. M., ERNBERG, I. & ZENG, Y. X. 2005. Genomic sequence analysis of Epstein-Barr virus strain GD1 from a nasopharyngeal carcinoma patient. *J Virol,* 79**,** 15323–30.

ZENG, Y., MIDDELDORP, J., MADJAR, J. J. & OOKA, T. 1997. A major DNA binding protein encoded by BALF2 open reading frame of Epstein-Barr virus (EBV) forms a complex with other EBV DNA-binding proteins: DNAase, EA-D, and DNA polymerase. *Virology,* 239**,** 285–95.

ZHANG, B., KRACKER, S., YASUDA, T., CASOLA, S., VANNEMAN, M., HÖMIG-HÖLZEL, C., WANG, Z., DERUDDER, E., LI, S., CHAKRABORTY, T., COTTER, S. E., KOYAMA, S., CURRIE, T., FREEMAN, G. J., KUTOK, J. L., RODIG, S. J., DRANOFF, G. & RAJEWSKY, K. 2012. Immune surveillance and therapy of lymphomas driven by Epstein-Barr virus protein LMP1 in a mouse model. *Cell,* 148**,** 739–51.

ZHANG, F., GAN, R., ZHEN, Z., HU, X., LI, X., ZHOU, F., LIU, Y., CHEN, C., XIE, S., ZHANG, B., WU, X. & HUANG, Z. 2020. Adaptive immune responses to SARS-CoV-2 infection in severe versus mild individuals. *Signal Transduct Target Ther,* 5**,** 156.

ZHANG, J., SOMMERMANN, T., LI, X., GIESELMANN, L., DE LA ROSA, K., STECKLUM, M., KLEIN, F., KOCKS, C. & RAJEWSKY, K. 2023. LMP1 and EBNA2 constitute a minimal set of EBV genes for transformation of human B cells. *Front Immunol,* 14**,** 1331730.

ZHANG, N., ZUO, Y., JIANG, L., PENG, Y., HUANG, X. & ZUO, L. 2021. Epstein-Barr Virus and Neurological Diseases. *Front Mol Biosci,* 8**,** 816098.

ZHANG, Z., NOMURA, N., MURAMOTO, Y., EKIMOTO, T., UEMURA, T., LIU, K., YUI, M., KONO, N., AOKI, J., IKEGUCHI, M., NODA, T., IWATA, S., OHTO, U. & SHIMIZU, T. 2022. Structure of SARS-CoV-2 membrane protein essential for virus assembly. *Nat Commun,* 13**,** 4399.

ZHAO, F., MA, Q., YUE, Q. & CHEN, H. 2022a. SARS-CoV-2 Infection and Lung Regeneration. *Clin Microbiol Rev,* 35**,** e0018821.

ZHAO, M. M., ZHU, Y., ZHANG, L., ZHONG, G., TAI, L., LIU, S., YIN, G., LU, J., HE, Q., LI, M. J., ZHAO, R. X., WANG, H., HUANG, W., FAN, C., SHUAI, L., WEN, Z., WANG, C., HE, X., CHEN, Q., LIU, B., XIONG, X., BU, Z., WANG, Y., SUN, F. & YANG, J. K. 2022b. Novel cleavage sites identified in SARS-CoV-2 spike protein reveal mechanism for cathepsin L-facilitated viral infection and treatment strategies. *Cell Discov,* 8**,** 53.

ZHENG, H. Y., ZHANG, M., YANG, C. X., ZHANG, N., WANG, X. C., YANG, X. P., DONG, X. Q. & ZHENG, Y. T. 2020a. Elevated exhaustion levels and reduced functional diversity of T cells in peripheral blood may predict severe progression in COVID-19 patients. *Cell Mol Immunol,* 17**,** 541–543.

ZHENG, M., GAO, Y., WANG, G., SONG, G., LIU, S., SUN, D., XU, Y. & TIAN, Z. 2020b. Functional exhaustion of antiviral lymphocytes in COVID-19 patients. *Cell Mol Immunol,* 17**,** 533–535.

ZHENG, M., KARKI, R., WILLIAMS, E. P., YANG, D., FITZPATRICK, E., VOGEL, P., JONSSON, C. B. & KANNEGANTI, T. D. 2021. TLR2 senses the SARS-CoV-2 envelope protein to produce inflammatory cytokines. *Nat Immunol,* 22**,** 829–838.

ZHENG, Y., QIN, Z., YE, Q., CHEN, P., WANG, Z., YAN, Q., LUO, Z., LIU, X., ZHOU, Y., XIONG, W., MA, J. & LI, G. 2014. Lactoferrin suppresses the Epstein-Barr virus-induced inflammatory response by interfering with pattern recognition of TLR2 and TLR9. *Lab Invest,* 94**,** 1188–99.

ZHONG, H., HU, X., JANOWSKI, A. B., STORCH, G. A., SU, L., CAO, L., YU, J. & XU, J. 2017. Whole transcriptome profiling reveals major cell types in the cellular immune response against acute and chronic active Epstein-Barr virus infection. *Sci Rep,* 7**,** 17775.

ZHOU, F., YU, T., DU, R., FAN, G., LIU, Y., LIU, Z., XIANG, J., WANG, Y., SONG, B., GU, X., GUAN, L., WEI, Y., LI, H., WU, X., XU, J., TU, S., ZHANG, Y., CHEN, H. & CAO, B. 2020a. Clinical course and risk factors for mortality of adult inpatients with COVID-19 in Wuhan, China: a retrospective cohort study. *Lancet,* 395**,** 1054–1062.

ZHOU, J., AMRAN, F. S., KRAMSKI, M., ANGELOVICH, T. A., ELLIOTT, J., HEARPS, A. C., PRICE, P. & JAWOROWSKI, A. 2015. An NK Cell Population Lacking FcRγ Is Expanded in Chronically Infected HIV Patients. *J Immunol,* 194**,** 4688–97.

ZHOU, J., JIN, L., WANG, F., ZHANG, Y., LIU, B. & ZHAO, T. 2019. Chimeric antigen receptor T (CAR-T) cells expanded with IL-7/IL-15 mediate superior antitumor effects. *Protein Cell,* 10**,** 764–769.

ZHOU, P., YANG, X. L., WANG, X. G., HU, B., ZHANG, L., ZHANG, W., SI, H. R., ZHU, Y., LI, B., HUANG, C. L., CHEN, H. D., CHEN, J., LUO, Y., GUO, H., JIANG, R. D., LIU, M. Q., CHEN, Y., SHEN, X. R., WANG, X., ZHENG, X. S., ZHAO, K., CHEN, Q. J., DENG, F., LIU, L. L., YAN, B., ZHAN, F. X., WANG, Y. Y., XIAO, G. F. & SHI, Z. L. 2020b. A pneumonia outbreak associated with a new coronavirus of probable bat origin. *Nature,* 579**,** 270–273.

ZHOU, Y., FU, B., ZHENG, X., WANG, D., ZHAO, C., QI, Y., SUN, R., TIAN, Z., XU, X. & WEI, H. 2020c. Pathogenic T-cells and inflammatory monocytes incite inflammatory storms in severe COVID-19 patients. *Natl Sci Rev,* 7**,** 998–1002.

ZHU, N., ZHANG, D., WANG, W., LI, X., YANG, B., SONG, J., ZHAO, X., HUANG, B., SHI, W., LU, R., NIU, P., ZHAN, F., MA, X., WANG, D., XU, W., WU, G., GAO, G. F. & TAN, W. 2020. A Novel Coronavirus from Patients with Pneumonia in China, 2019. *N Engl J Med,* 382**,** 727–733.

ZHU, Y., SHARMA, L. & CHANG, D. 2023. Pathophysiology and clinical management of coronavirus disease (COVID-19): a mini-review. *Front Immunol,* 14**,** 1116131.

ZIEGLER, C. G. K., ALLON, S. J., NYQUIST, S. K., MBANO, I. M., MIAO, V. N., TZOUANAS, C. N., CAO, Y., YOUSIF, A. S., BALS, J., HAUSER, B. M., FELDMAN, J., MUUS, C., WADSWORTH, M. H., 2ND, KAZER, S. W., HUGHES, T. K., DORAN, B., GATTER, G. J., VUKOVIC, M., TALIAFERRO, F., MEAD, B. E., GUO, Z., WANG, J. P., GRAS, D., PLAISANT, M., ANSARI, M., ANGELIDIS, I., ADLER, H., SUCRE, J. M. S., TAYLOR, C. J., LIN, B., WAGHRAY, A., MITSIALIS, V., DWYER, D. F., BUCHHEIT, K. M., BOYCE, J. A., BARRETT, N. A., LAIDLAW, T. M., CARROLL, S. L., COLONNA, L., TKACHEV, V., PETERSON, C. W., YU, A., ZHENG, H. B., GIDEON, H. P., WINCHELL, C. G., LIN, P. L., BINGLE, C. D., SNAPPER, S. B., KROPSKI, J. A., THEIS, F. J., SCHILLER, H. B., ZARAGOSI, L. E., BARBRY, P., LESLIE, A., KIEM, H. P., FLYNN, J. L., FORTUNE, S. M., BERGER, B., FINBERG, R. W., KEAN, L. S., GARBER, M., SCHMIDT, A. G., LINGWOOD, D., SHALEK, A. K. & ORDOVAS-MONTANES, J. 2020. SARS-CoV-2 Receptor ACE2 Is an Interferon-Stimulated Gene in Human Airway Epithelial Cells and Is Detected in Specific Cell Subsets across Tissues. *Cell,* 181**,** 1016–1035.e19.

ZIMBER, U., ADLDINGER, H. K., LENOIR, G. M., VUILLAUME, M., KNEBEL-DOEBERITZ, M. V., LAUX, G., DESGRANGES, C., WITTMANN, P., FREESE, U. K., SCHNEIDER, U. & ET AL. 1986. Geographical prevalence of two types of Epstein-Barr virus. *Virology,* 154**,** 56–66.

ZIMMERMANN, H., KOENECKE, C., DREYLING, M. H., POTT, C., DÜHRSEN, U., HAHN, D., MEIDENBAUER, N., HAUSER, I. A., RUMMEL, M. J., WOLF, D., HEUSER, M., SCHMIDT, C., SCHLATTMANN, P., RITGEN, M., SIEBERT, R., OSCHLIES, I., ANAGNOSTOPOULOS, I. & TRAPPE, R. U. 2022. Modified risk-stratified sequential treatment (subcutaneous rituximab with or without chemotherapy) in B-cell Post-transplant lymphoproliferative disorder (PTLD) after Solid organ transplantation (SOT): the prospective multicentre phase II PTLD-2 trial. *Leukemia,* 36**,** 2468–2478.

ZIMMERMANN, H. & TRAPPE, R. U. 2013. EBV and posttransplantation lymphoproliferative disease: what to do? *Hematology Am Soc Hematol Educ Program,* 2013**,** 95–102.

ZIZZO, G., TAMBURELLO, A., CASTELNOVO, L., LARIA, A., MUMOLI, N., FAGGIOLI, P. M., STEFANI, I. & MAZZONE, A. 2022. Immunotherapy of COVID-19: Inside and Beyond IL-6 Signalling. *Front Immunol,* 13**,** 795315.

ZOU, X., CHEN, K., ZOU, J., HAN, P., HAO, J. & HAN, Z. 2020. Single-cell RNA-seq data analysis on the receptor ACE2 expression reveals the potential risk of different human organs vulnerable to 2019-nCoV infection. *Front Med,* 14**,** 185–192.

ZUHAIR, M., SMIT, G. S. A., WALLIS, G., JABBAR, F., SMITH, C., DEVLEESSCHAUWER, B. & GRIFFITHS, P. 2019. Estimation of the worldwide seroprevalence of cytomegalovirus: A systematic review and meta-analysis. *Rev Med Virol,* 29**,** e2034.

ZUO, Y., WARNOCK, M., HARBAUGH, A., YALAVARTHI, S., GOCKMAN, K., ZUO, M., MADISON, J. A., KNIGHT, J. S., KANTHI, Y. & LAWRENCE, D. A. 2021. Plasma tissue plasminogen activator and plasminogen activator inhibitor-1 in hospitalized COVID-19 patients. *Sci Rep,* 11**,** 1580.

ZVEJNIECE, L., KOZIREVA, S., RUDEVICA, Z., LEONCIKS, A., EHLIN-HENRIKSSON, B., KASHUBA, E. & KHOLODNYUK, I. 2022. Expression of the Chemokine Receptor CCR1 in Burkitt Lymphoma Cell Lines Is Linked to the CD10-

Negative Cell Phenotype and Co-Expression of the EBV Latent Genes EBNA2, LMP1, and LMP2. *Int J Mol Sci,* 23.

Associated Publications

Cooper RS, Kowalczuk A, Wilkie G, Vickers MA, Turner ML, Campbell JDM, Fraser AR. Cytometric analysis of T cell phenotype using cytokine profiling for improved manufacturing of an EBV-specific T cell therapy. Clin Exp Immunol. 2021 Oct;206(1):68-81. doi: 10.1111/cei.13640. Epub 2021 Jul 14. PMID: 34146397; PMCID: PMC8446406.

Cooper RS, Fraser AR, Smith L, Burgoyne P, Imlach SN, Jarvis LM, Turner DM, Zahra S, Turner ML, Campbell JDM. Rapid GMP-Compliant Expansion of SARS-CoV-2-Specific T Cells From Convalescent Donors for Use as an Allogeneic Cell Therapy for COVID-19. Front Immunol. 2021 Jan 8;11:598402. doi: 10.3389/fimmu.2020.598402. PMID: 33488592; PMCID: PMC7819874.

Ten Ham RMT, Nievaart JC, Hoekman J, Cooper RS, Frederix GWJ, Leufkens HGM, Klungel OH, Ovelgönne H, Hoefnagel MHN, Turner ML, Mountford JC. Estimation of manufacturing development costs of cell-based therapies: a feasibility study. Cytotherapy. 2021 Aug;23(8):730-739. doi: 10.1016/j.jcyt.2020.12.014. Epub 2021 Feb 13. PMID: 33593688.

Cooper RS, Sutherland C, Smith LM, Cowan G, Barnett M, Mitchell D, McLean C, Imlach S, Hayes A, Zahra S, Manchanayake C, Vickers MA, Graham G, McGowan NWA, Turner ML, Campbell JDM, Fraser AR. EBV T-cell immunotherapy generated by peptide selection has enhanced effector functionality compared to LCL stimulation. Front Immunol. 2024 Jul 1;15:1412211. doi: 10.3389/fimmu.2024.1412211. PMID: 39011042; PMCID: PMC11246990.